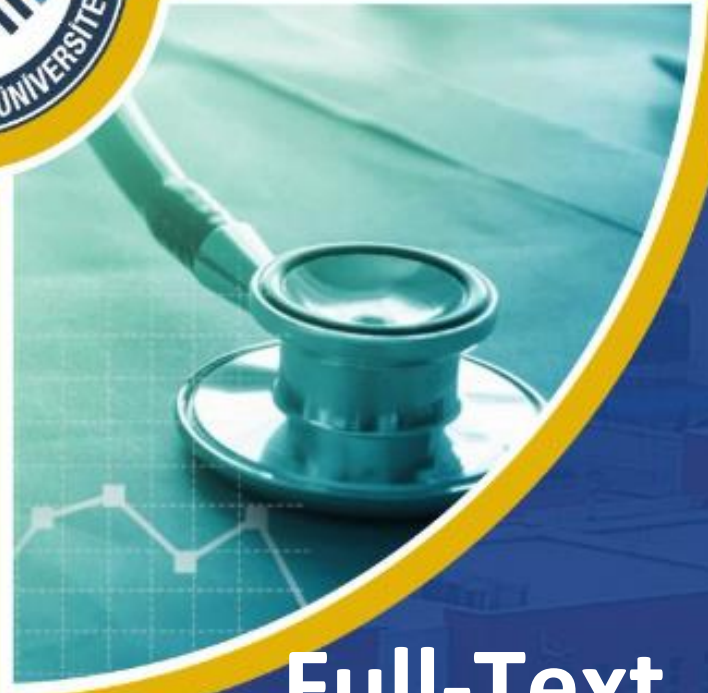
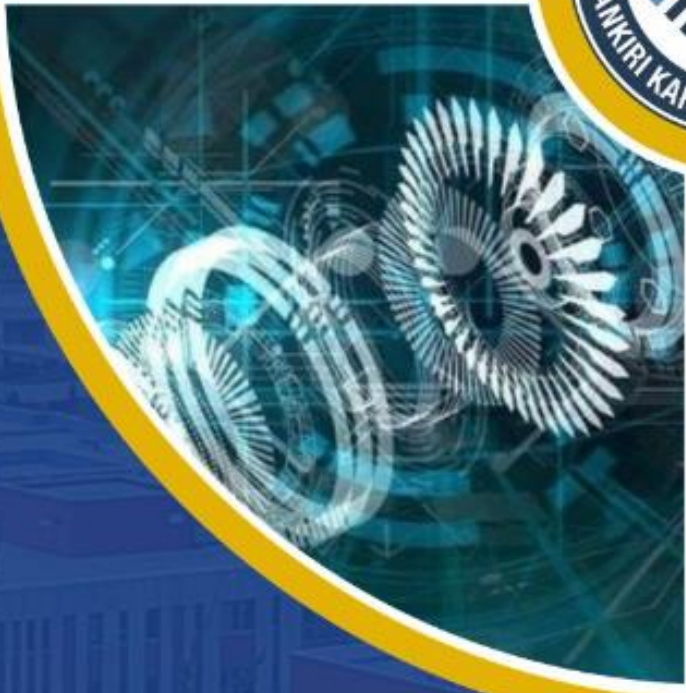


# 1<sup>st</sup> INTERNATIONAL KARATEKIN SCIENCE AND TECHNOLOGY CONFERENCE

1-3 SEPTEMBER 2022

ÇANKIRI, TURKEY



## Full-Text Proceeding Book

Science from Çankırı to the World

[www.karatekin.edu.tr](http://www.karatekin.edu.tr)



IKSTC1<sup>st</sup>

**1<sup>st</sup> International Karatekin Science and Technology Conference**

# **FULL-TEXT PROCEEDING BOOK**

**September 1-3, 2022 – Çankırı, Türkiye**

## **Editors**

Asst. Prof. Dr. Muhammed Bora AKIN

Asst. Prof. Dr. Zehra Gülten YALÇIN

Dr. Caner TANIŞ

ISBN: 978-605-82910-6-5





# IKSTC1<sup>st</sup> 2022

**1st International Karatekin Science and Technology Conference**

**Full-Text Proceedings Book**

**ISBN: 978-605-82910-6-5**

**ÇANKIRI KARATEKİN UNIVERSITY PUBLICATION®**

**TURKIYE**

**TR: +90 376 218 95 00**

**<https://www.ikstc.org/>**

**All rights reserved to Çankırı Karatekin University.**

**It can not be copied or reproduced without permission.**

**Whole legal and ethical responsibilities belongs to the authors.**

**ÇAKU Publications - 2022©**

**Publish Date: October 24th, 2022**

**ISBN: 978-605-82910-6-5**

## **ABOUT THE CONFERENCE**

### **CONFERENCE NAME**

**1<sup>st</sup> International Karatekin Science and Technology Conference**

### **DATE AND PLACE**

**September 1-3, 2022 Çankırı – Türkiye**

### **ORGANIZING AGENCY**

**ÇAKU – Çankırı Karatekin University**

### **CHAIRMAN OF THE CONFERENCE**

**Prof. Dr. Harun ÇİFTÇİ**

### **GENERAL COORDINATOR**

**Prof. Dr. Volkan EYÜPOĞLU**

### **OFFICIAL LANGUAGE OF THE CONFERENCE**

**English**

### **PARTICIPANT COUNTRIES**

**Türkiye, Iraq, Pakistan, Bangladesh, India, Portugal, Saudi Arabia, Sudan, Egypt, Lebanon, Iran, Bulgaria, Libya, Kosovo, Austria, United Kingdom, Turkish Republic of Northern Cyprus**



# IKSTC1<sup>st</sup> 2022

## **Conference Chairman**

Prof. Dr. Harun Çiftçi, Çankırı Karatekin University, Türkiye

## **Vice Conference Chairman**

Prof. Dr. Hüseyin Odabaş, Çankırı Karatekin University, Türkiye

Prof. Dr. Mehmet Erdem, Çankırı Karatekin University, Türkiye

## **Organization Chairman**

Prof. Dr. Volkan Eyüpoğlu, Çankırı Karatekin University, Türkiye





# IKSTC1<sup>st</sup> 2022

## Organization Committee

Prof. Dr. Ali Yiğit, Çankırı Karatekin University, Türkiye  
Assoc. Prof. Dr. Ender Budgay, Çankırı Karatekin University, Türkiye  
Assoc. Prof. Dr. Faruk Karaaslan, Çankırı Karatekin University, Türkiye  
Assoc. Prof. Dr. Gonca Durmaz Güngör, Çankırı Karatekin University, Türkiye  
Assoc. Prof. Dr. Oğuz Aydemir, Çankırı Karatekin University, Türkiye  
Assoc. Prof. Dr. Ömer Faruk Dilmaç, Çankırı Karatekin University, Türkiye  
Assoc. Prof. Dr. Şevki Adem, Çankırı Karatekin University, Türkiye  
Assoc. Prof. Dr. Şinasi Aşkar, Çankırı Karatekin University, Türkiye  
Assoc. Prof. Dr. Tolga Zaman, Çankırı Karatekin University, Türkiye  
Assoc. Prof. Dr. Ufuk Öztürk, Çankırı Karatekin University, Türkiye  
Asst. Prof. Dr. Ceyhun Türkmen, Çankırı Karatekin University, Türkiye  
Asst. Prof. Dr. Ercan Aydoğmuş, Fırat University, Türkiye  
Asst. Prof. Dr. Fuat Türk, Çankırı Karatekin University, Türkiye  
Asst. Prof. Dr. Göksu Görel, Çankırı Karatekin University, Türkiye  
Asst. Prof. Dr. Gülay Karahan, Çankırı Karatekin University, Türkiye  
Asst. Prof. Dr. Hüseyin Gökçe, Çankırı Karatekin University, Türkiye  
Asst. Prof. Dr. Kahraman Esen Özen, Çankırı Karatekin University, Türkiye  
Asst. Prof. Dr. Muhammed Bora Akin, Çankırı Karatekin University, Türkiye  
Asst. Prof. Dr. Mustafa Karhan, Çankırı Karatekin University, Türkiye  
Asst. Prof. Dr. Pembe Merve Karabulut, Çankırı Karatekin University, Türkiye  
Asst. Prof. Dr. Pınar Arslan, Çankırı Karatekin University, Türkiye  
Asst. Prof. Dr. Sakine Kiratli, Çankırı Karatekin University, Türkiye  
Asst. Prof. Dr. Selma Akçay, Çankırı Karatekin University, Türkiye  
Asst. Prof. Dr. Selim Buyrukoğlu, Çankırı Karatekin University, Türkiye  
Asst. Prof. Dr. Serap Kocabiyik Çaşkurlu, İstanbul University-Cerrahpasa, Türkiye  
Asst. Prof. Dr. Serdar Aykut, Çankırı Karatekin University, Türkiye  
Asst. Prof. Dr. Sevcan Toptaş, Çankırı Karatekin University, Türkiye  
Asst. Prof. Dr. Zehra Gülten Yalçın, Çankırı Karatekin University, Türkiye  
Dr. Caner Tanış, Çankırı Karatekin University, Türkiye  
Dr. Funda Aslan, Çankırı Karatekin University, Türkiye  
Dr. Murat Konca, Çankırı Karatekin University, Türkiye  
Dr. Mustafa Dağ, Çankırı Karatekin University, Türkiye  
Dr. Vedat Arda Küçük, Çankırı Karatekin University, Türkiye  
Lec. Dr. Asuman Ünal, Çankırı Karatekin University, Türkiye  
Lec. Furkan Özdemir, Çankırı Karatekin University, Türkiye



# IKSTC1<sup>st</sup> 2022

## Scientific Committee

- Prof. Dr. Abdullah Emin Akay, Bursa Technical University, Türkiye  
Prof. Dr. Abdülkerim Yörükoğlu, Sivas Cumhuriyet University, Türkiye  
Prof. Dr. Ahmet Emin Eroğlu, İzmir Institute of Technology, Türkiye  
Prof. Dr. Ali Karaiepli, Çankırı Karatekin University, Türkiye  
Prof. Dr. Ali Yiğit, Çankırı Karatekin University, Türkiye  
Prof. Dr. Aysel Çağlan Günel, Gazi University, Türkiye  
Prof. Dr. Ayşe Şahin Yağlıoğlu, Amasya University, Türkiye  
Prof. Dr. Beytullah Afşin, Ondokuz Mayıs University, Türkiye  
Prof. Dr. Birnur Akkaya, Sivas Cumhuriyet University, Türkiye  
Prof. Dr. Bülent Dede, Süleyman Demirel University, Türkiye  
Prof. Dr. Carlos Manuel Agra Coelho, Universidade Nova De Lisboa, Portugal  
Prof. Dr. Çiğdem Yüksektepe Ataol, Çankırı Karatekin University, Türkiye  
Prof. Dr. Emine Hilal Mert, Yalova University, Türkiye  
Prof. Dr. Ender Sarifakioğlu, Çankırı Karatekin University, Türkiye  
Prof. Dr. Faruk Polat, Çankırı Karatekin University, Türkiye  
Prof. Dr. Fatma Karaca Albayrak, Marmara University, Türkiye  
Prof. Dr. Fethiye Göde, Süleyman Demirel University, Türkiye  
Prof. Dr. Halit Altuntaş, Çankırı Karatekin University, Türkiye  
Prof. Dr. Hamit Alyar, Çankırı Karatekin University, Türkiye  
Prof. Dr. Harun Karsli, Bolu Abant İzzet Baysal University, Türkiye  
Prof. Dr. İbrahim Çiftçi, Çankırı Karatekin University, Türkiye  
Prof. Dr. İlkey Şisman, Sakarya University, Türkiye  
Prof. Dr. İsa Çömez, Karadeniz Technical University, Türkiye  
Prof. Dr. İshak Altun, Kırıkkale University, Türkiye  
Prof. Dr. Jale Gülen, Yıldız Technical University, Türkiye  
Prof. Dr. Kazım İlarslan, Kırıkkale University, Türkiye  
Prof. Dr. Kudret Yıldırım, Sakarya University, Türkiye  
Prof. Dr. Levent Kula, Kırşehir Ahi Evran University, Türkiye  
Prof. Dr. Mehmet Ali Cengiz, Ondokuz Mayıs University, Türkiye  
Prof. Dr. Mehmet Ali Güngör, Sakarya University, Türkiye  
Prof. Dr. Mehmet Çiftçi, Bingöl University, Türkiye  
Prof. Dr. Mehmet Nebioğlu, Sakarya University, Türkiye  
Prof. Dr. Mehmet Şahin, Abdullah Gül University, Türkiye  
Prof. Dr. Meryem Nilüfer Yaraşır, Sakarya University, Türkiye  
Prof. Dr. Naim Çağman, Gaziosmanpaşa University, Türkiye  
Prof. Dr. Oktay Muhtaroglu, Gaziosmanpaşa University, Türkiye  
Prof. Dr. Özcan Özkan, Çankırı Karatekin University, Türkiye  
Prof. Dr. Özkan Adigüzel, Dicle University, Türkiye





# IKSTC1<sup>st</sup> 2022

## Scientific Committee (Continued)

- Prof. Dr. Recep Akkaya, Sivas Cumhuriyet University, Türkiye  
Prof. Dr. Robert Hillman, University of Leicester, United Kingdom  
Prof. Dr. S.M. Mostafa Kamal, Islamic University, Bangladesh  
Prof. Dr. Sadık Kakaç, University of Economics & Technology, Türkiye  
Prof. Dr. Seçil Akilli Şimşek, Çankırı Karatekin University, Türkiye  
Prof. Dr. Seda Akkerman, Çankırı Karatekin University, Türkiye  
Prof. Dr. Seyfettin Erturan, Yıldız Technical University, Türkiye  
Prof. Dr. Soley Ersoy, Sakarya University, Türkiye  
Prof. Dr. Şadan Özcan, Hacettepe University, Türkiye  
Prof. Dr. Şemsettin Altındal, Gazi University, Türkiye  
Prof. Dr. Tayfun Uygunoglu, Afyon Kocatepe University, Türkiye  
Prof. Dr. Tevfik Özen, Ondokuz Mayıs University, Türkiye  
Prof. Dr. Tünay Konaş Aşkar, Çankırı Karatekin University, Türkiye  
Prof. Dr. Ülkü Nihan Yazgan Tavşanoğlu, Çankırı Karatekin University, Türkiye  
Prof. Dr. Ünal Akdağ, Aksaray University, Türkiye  
Prof. Dr. Veysel Çomaklı, Ağrı İbrahim Çeçen University, Türkiye  
Prof. Dr. Volkan Eyüpoğlu, Çankırı Karatekin University, Türkiye  
Prof. Dr. Yusuf Yaylı, Ankara University, Türkiye  
Prof. Dr. Zeliha Selek, Gazi University, Türkiye  
Assoc. Prof. Dr. Abdelhafeez M. A. Mohammed, King Abdulaziz University, Saudi Arabia  
Assoc. Prof. Dr. Abdo A Elfiky, Cairo University, Egypt  
Assoc. Prof. Dr. Abdulcabbar Yavuz, Gaziantep University, Türkiye  
Assoc. Prof. Dr. Ahmet Turgut Bilgicli, Sakarya University, Türkiye  
Assoc. Prof. Dr. Azmi Seyhun Kipçak, Yıldız Technical University, Türkiye  
Assoc. Prof. Dr. Bengi Özkahraman, Hitit University, Türkiye  
Assoc. Prof. Dr. Burak Tüzün, Sivas Cumhuriyet University, Türkiye  
Assoc. Prof. Dr. Bülent Altunkaya, Kırşehir Ahi Evran University, Türkiye  
Assoc. Prof. Dr. Celal Tuğrul Zeyrek, Çankırı Karatekin University, Türkiye  
Assoc. Prof. Dr. Çetin Camci, Çanakkale Onsekiz Mart University, Türkiye  
Assoc. Prof. Dr. Ebru Akkemik, Siirt University, Türkiye  
Assoc. Prof. Dr. Efehan Ulaş, Çankırı Karatekin University, Türkiye  
Assoc. Prof. Dr. Elsir Adam Omer Salih, Alzaeim Alazhari University, Sudan  
Assoc. Prof. Dr. Emel Akyol, Yıldız Technical University, Türkiye  
Assoc. Prof. Dr. Emin Aygün, Erciyes University, Türkiye  
Assoc. Prof. Dr. Emre Dünder, Ondokuz Mayıs University, Türkiye  
Assoc. Prof. Dr. Ender Buğday, Çankırı Karatekin University, Türkiye  
Assoc. Prof. Dr. Erhan Güler, Bartın University, Türkiye



# IKSTC1<sup>st</sup> 2022

## Scientific Committee (Continued)

- Assoc. Prof. Dr. Esra Betül Koç Öztürk, Bolu Abant İzzet Baysal University, Türkiye  
Assoc. Prof. Dr. Faruk Karaaslan, Çankırı Karatekin University, Türkiye  
Assoc. Prof. Dr. Fatih Karayürek, Çankırı Karatekin University, Türkiye  
Assoc. Prof. Dr. Fatih Korkmaz, Çankırı Karatekin University, Türkiye  
Assoc. Prof. Dr. Figen Çilingir, Iğdır University, Türkiye  
Assoc. Prof. Dr. Gonca Durmaz Güngör, Çankırı Karatekin University, Türkiye  
Assoc. Prof. Dr. Gülsüm Ulusoy Ada, Çankırı Karatekin University, Türkiye  
Assoc. Prof. Dr. Hakan Çolak, Çankırı Karatekin University  
Assoc. Prof. Dr. Hakan Yoğurtçu, Munzur University, Türkiye  
Assoc. Prof. Dr. Hasan Bulut, Ondokuz Mayıs University, Türkiye  
Assoc. Prof. Dr. Hatice Hande Mert, Yalova University, Türkiye  
Assoc. Prof. Dr. Hüdayi Ercoşkun, Çankırı Karatekin University, Türkiye  
Assoc. Prof. Dr. İlyas İnci, Çankırı Karatekin University, Türkiye  
Assoc. Prof. Dr. Mehmet Kalender, Fırat University, Türkiye  
Assoc. Prof. Dr. Mehmet Selçuk Mert, Yalova University, Türkiye  
Assoc. Prof. Dr. Melike Bilgi Kamaç, Çankırı Karatekin University, Türkiye  
Assoc. Prof. Dr. Murat Yaylaci, Recep Tayyip Erdoğan University, Türkiye  
Assoc. Prof. Dr. Müslüm Kuzu, Karabuk University, Türkiye  
Assoc. Prof. Dr. Oğuz Aydemir, Çankırı Karatekin University, Türkiye  
Assoc. Prof. Dr. Osman Şimşek, Gazi University, Türkiye  
Assoc. Prof. Dr. Ömer Faruk Dilmaç, Çankırı Karatekin University, Türkiye  
Assoc. Prof. Dr. Özlem Doğan Aydeniz, Yıldız Technical University, Türkiye  
Assoc. Prof. Dr. Saif Athamneh, Yarmouk University, Jordan  
Assoc. Prof. Dr. Sebahaddin Alptekin, Çankırı Karatekin University, Türkiye  
Assoc. Prof. Dr. Sibel Demir Kanmazalp, Gaziantep University, Türkiye  
Assoc. Prof. Dr. Suzan Cangül, Dicle University, Türkiye  
Assoc. Prof. Dr. Şevki Adem, Çankırı Karatekin University, Türkiye  
Assoc. Prof. Dr. Tolga Zaman, Çankırı Karatekin University, Türkiye  
Assoc. Prof. Dr. Ufuk Öztürk, Çankırı Karatekin University, Türkiye  
Assoc. Prof. Dr. Zehra Özbaş, Çankırı Karatekin University, Türkiye  
Asst. Prof. Dr. Ayça Bal Öztürk, Instinye University, Türkiye  
Asst. Prof. Dr. Ayşin Zülfikaroğlu, Amasya University, Türkiye  
Asst. Prof. Dr. Azhar Rasul, Government College University Faisalabad, Pakistan  
Asst. Prof. Dr. Başak Karasu, Çankırı Karatekin University, Türkiye  
Asst. Prof. Dr. Beytullah Eren, Sakarya University, Türkiye  
Asst. Prof. Dr. Celalettin Kaya, Çankırı Karatekin University, Türkiye  
Asst. Prof. Dr. Ercan Aydoğmuş, Fırat University, Türkiye  
Asst. Prof. Dr. Erdal Öner, Bayburt University, Türkiye





# IKSTC1<sup>st</sup> 2022

## Scientific Committee (Continued)

- Asst. Prof. Dr. Fazlı Akyüz, İstanbul University-Cerrahpasa, Türkiye  
Asst. Prof. Dr. Gül Ateş, Çankırı Karatekin University, Türkiye  
Asst. Prof. Dr. Gülay Karahan, Çankırı Karatekin University, Türkiye  
Asst. Prof. Dr. Günal Bilek, İzmir Democracy University, Türkiye  
Asst. Prof. Dr. Haydar Koç, Çankırı Karatekin University, Türkiye  
Asst. Prof. Dr. Kahraman Esen Özen, Çankırı Karatekin University, Türkiye  
Asst. Prof. Dr. Korkut Açıkalin, Yalova University, Türkiye  
Asst. Prof. Dr. Mahmut Mak, Kırşehir Ahi Evran University, Türkiye  
Asst. Prof. Dr. Muhammed Bora Akin, Çankırı Karatekin University, Türkiye  
Asst. Prof. Dr. Musa Acartürk, Çankırı Karatekin University, Türkiye.  
Asst. Prof. Dr. Mustafa Aslantaş, Çankırı Karatekin University, Türkiye  
Asst. Prof. Dr. Mustafa Karhan, Çankırı Karatekin University, Türkiye  
Asst. Prof. Dr. Mustafa Teke, Çankırı Karatekin University, Türkiye  
Asst. Prof. Dr. Orhan Keklikçioğlu, Erciyes University, Türkiye  
Asst. Prof. Dr. Özgün Yıldırım, Çankırı Karatekin University, Türkiye  
Asst. Prof. Dr. Pembe Merve Karabulut, Çankırı Karatekin University, Türkiye  
Asst. Prof. Dr. Pınar Arslan, Çankırı Karatekin University, Türkiye  
Asst. Prof. Dr. Ravi Ravat, Mvn University, India  
Asst. Prof. Dr. Remzi Orkun Akgün, Çankırı Karatekin University, Türkiye  
Asst. Prof. Dr. Sakine Kiratli, Çankırı Karatekin University, Türkiye  
Asst. Prof. Dr. Salih Cihangir, Munzur University, Türkiye  
Asst. Prof. Dr. Seda Şahin, Çankırı Karatekin University, Türkiye  
Asst. Prof. Dr. Selim Buyrukoğlu, Çankırı Karatekin University, Türkiye  
Asst. Prof. Dr. Serap Çetinkaya, Sivas Cumhuriyet University, Türkiye  
Asst. Prof. Dr. Serap Kocabiyik Çaşkurlu, İstanbul University-Cerrahpasa, Türkiye  
Asst. Prof. Dr. Selma Akçay, Çankırı Karatekin University, Türkiye  
Asst. Prof. Dr. Serdar Aykut, Çankırı Karatekin University, Türkiye  
Asst. Prof. Dr. Serpil Aydın, Ondokuz Mayıs University, Türkiye  
Asst. Prof. Dr. Songül Şahin, Çankırı Karatekin University, Türkiye  
Asst. Prof. Dr. Tuba Koç, Çankırı Karatekin University, Türkiye  
Asst. Prof. Dr. Ümit Yirtici, Kırıkkale University, Türkiye  
Asst. Prof. Dr. Yıldırım Yılmaz, Recep Tayyip Erdoğan University, Türkiye  
Asst. Prof. Dr. Zehra Gülten Yalçın, Çankırı Karatekin University, Türkiye  
Res. Asst. Dr. Ayşenur Kayabaş, Çankırı Karatekin University, Türkiye  
Res. Asst. Dr. Caner Tanış, Çankırı Karatekin University, Türkiye  
Res. Asst. Dr. Eyüp Canlı, Selçuk University, Türkiye  
Res. Asst. Dr. Göksu Görel, Çankırı Karatekin University, Türkiye  
Res. Asst. Dr. Mustafa Dağ, Çankırı Karatekin University, Türkiye  
Res. Asst. Dr. Vedat Arda Küçük, Çankırı Karatekin University, Türkiye



# IKSTC1<sup>st</sup> 2022

## **Scientific Committee (Continued)**

Res. Asst. Enis Sert, Çankırı Karatekin University, Türkiye

Res. Asst. Murat Konca, Çankırı Karatekin University, Türkiye

Lec. Dr. Asuman Ünal, Çankırı Karatekin University, Türkiye

Lec. Dr. Gonca Buyrukoğlu, Çankırı Karatekin University, Türkiye

Lec. Dr. Göktuğ Gül, Gazi University, Türkiye

Lec. Dr. Harun Baldemir, Çankırı Karatekin University, Türkiye

Lec. Dr. Meliz Akyol Alay, İstanbul Technical University, Türkiye

Dr. Ayşe Günay, Dicle University, Türkiye





# IKSTC1<sup>st</sup> 2022

## Conference Secretariat

Asst. Prof. Dr. Muhammed Bora Akin, Çankırı Karatekin University, Türkiye

Asst. Prof. Dr. Zehra Gülten Yalçın, Çankırı Karatekin University, Türkiye

Res. Asst. Dr. Bircan Taşkıran, Çankırı Karatekin University, Türkiye

Res. Asst. Dr. Caner Tanış, Çankırı Karatekin University, Türkiye

Res. Asst. Dr. Enis Sert, Çankırı Karatekin University, Türkiye

Res. Asst. Dr. Mustafa Dağ, Çankırı Karatekin University, Türkiye

Res. Asst. Dr. Serkan Koldaş, Çankırı Karatekin University, Türkiye

Res. Asst. Dr. Vedat Arda Küçük, Çankırı Karatekin University, Türkiye

Res. Asst. Eren Yurdakul, Çankırı Karatekin University, Türkiye

Res. Asst. Fadime Baldemir, Çankırı Karatekin University, Türkiye

Res. Asst. Mehmet Ali Boz, Çankırı Karatekin University, Türkiye

Lec. Dr. Asuman Ünal, Çankırı Karatekin University, Türkiye



# IKSTC1<sup>st</sup> 2022

## Conference Moderators

Assoc. Prof. Dr. Ender Budgay, Çankırı Karatekin University, Türkiye  
Asst. Prof. Dr. Ceyhun Türkmen, Çankırı Karatekin University, Türkiye  
Asst. Prof. Dr. Gülay Karahan, Çankırı Karatekin University, Türkiye  
Asst. Prof. Dr. Muhammed Bora Akin, Çankırı Karatekin University, Türkiye  
Asst. Prof. Dr. Mustafa Karhan, Çankırı Karatekin University, Türkiye  
Asst. Prof. Dr. Selim Buyrukoğlu, Çankırı Karatekin University, Türkiye  
Asst. Prof. Dr. Zehra Gülten Yalçın, Çankırı Karatekin University, Türkiye  
Res. Asst. Dr. Mustafa Dağ, Çankırı Karatekin University, Türkiye  
Res. Asst. Dr. Serkan Koldaş, Çankırı Karatekin University, Türkiye  
Res. Asst. Dr. Vedat Arda Küçük, Çankırı Karatekin University, Türkiye  
Res. Asst. Eren Yurdakul, Çankırı Karatekin University, Türkiye  
Lec. Dr. Asuman Ünal, Çankırı Karatekin University, Türkiye  
Lec. Dr. Gonca Buyrukoğlu, Çankırı Karatekin University, Türkiye  
Dr. Murat Konca, Çankırı Karatekin University, Türkiye



# IKSTC1<sup>st</sup> 2022

## Invited Speakers

- Prof. Dr. Abdülkerim Yörükoğlu, Sivas Cumhuriyet University, Türkiye.
- Prof. Dr. Ahmet Can Altunişik, Karadeniz Technical University, Türkiye
- Prof. Dr. Ahmet Emin Eroğlu, Izmir Institute of Technology, Türkiye
- Prof. Dr. Birnur Akkaya, Sivas Cumhuriyet University, Türkiye
- Prof. Dr. Carlos Manuel Agra Coelho, Universidade Nova De Lisboa, Portugal
- Prof. Dr. Mehmet Şahin, Abdullah Gül University, Türkiye
- Prof. Dr. Recep Akkaya, Sivas Cumhuriyet University, Türkiye
- Prof. Dr. Robert Hillman, University of Leicester, United Kingdom
- Prof. Dr. S. M. Mostafa Kamal, Islamic University, Bangladesh
- Prof. Dr. Sadık Kakaç, University of Economics & Technology, Türkiye
- Assoc. Prof. Dr. Abdelhafeez M. A. Mohammed, King Abdulaziz University, Saudi Arabia
- Assoc. Prof. Dr. Abdo A Elfiky Cairo University, Egypt
- Assoc. Prof. Dr. Elsir Adam Omer Salih, Alazhari University, Sudan
- Assoc. Prof. Dr. Emel Akyol, Yıldız Technical University, Türkiye
- Asst. Prof. Dr. Ravi Ravat, Mvn University, India
- Asst. Prof. Dr. Azhar Rasul, Government College University Faisalabad, Pakistan
- Asst. Prof. Dr. Yıldırım Yılmaz, Recep Tayyip Erdoğan University, Türkiye
- Lecturer Dr. Yunus Kökver, Ankara University, Türkiye



# IKSTC1<sup>st</sup> 2022

## **Conference Topics**

Audiology  
Biology  
Chemical Engineering  
Chemistry  
Civil Engineering  
Computer Engineering  
Dentistry  
Electrical and Electronic Engineering  
Emergency Aid and Disaster Management  
Food Engineering  
Forest Engineering  
Gerontology  
Health Management  
Landscape Architecture  
Mathematics  
Mechanical Engineering  
Midwifery  
Nursing  
Nutrition and Dietetics  
Orthotic-Prosthetic  
Physics  
Physiotherapy and Rehabilitation  
Social Work  
Statistics





## Index

CLASSIFICATION OF BREAST LESIONS ON MAMMOGRAM IMAGES USING MONARCH BUTTERFLY OPTIMIZATION AND SUPPORT VECTOR MACHINE .....	1
ON INTUITIONISTIC FUZZY SOFT MULTISSETS .....	7
NUMERICAL STUDY OF FLOW AND HEAT TRANSFER OF NANOFLUIDS IN A RIBBED CHANNEL WITH WINGLETS.....	13
FABRICATION AND CHARACTERIZATION OF MOLYBDENUM DOPED ZNO NANORODS VIA ULTRASONIC SPRAY PYROLYSIS.....	19
PRODUCTION OF DIATOMITE REINFORCED POLYESTER COMPOSITE AND INVESTIGATION OF ITS THERMOPHYSICAL PROPERTIES .....	24
RETROSPECTIVE ANALYSIS OF MEDICAL PATHOLOGY QUESTIONS ASKED IN THE ENTRANCE EXAMINATION TO SPECIALTY EDUCATION IN DENTISTRY .....	29
NIOBIUM DOPING EFFECT ON ZNO NANORODS.....	33
REMOVAL OF ZN(II) ION FROM AQUEOUS SOLUTIONS BY GELLAN GAM-CHITOSAN COMPLEX ADSORBENT .....	38
MODELLING EARTHQUAKE DATA USING SOME LIFETIME DISTRIBUTIONS .....	44
INVESTIGATION OF A GRID-CONNECTED SYSTEM DESIGN ON A ROOFTOP IN ÇAKU.....	51
A SUCCESSFUL FALCIPARUM MALARIA TREATMENT WITH HEMODIAFILTRATION IN AN AFRICAN PATIENT .....	57
PRODUCTION AND CHARACTERIZATION OF DIATOMITE REINFORCED MDI BASED COMPOSITES .....	61
INVESTIGATION OF MG+2 ION BEHAVIOR IN COLEMANITE PROPIONIC ACID SOLUTIONS.....	66
EVALUATION OF THE PERFORMANCE OF REDUCED GRAPHENE OXIDE SAMPLES SYNTHESIZED USING HUMMERS AND CHEMICAL REDUCTION METHOD USING DIFFERENT PURITY GRAPHITE ON CEMENT MORTAR .....	71
THE EFFECT OF THICKNESS ON THE MORPHOLOGICAL AND OPTICAL PROPERTIES OF ZNSE THIN FILMS .....	76
A COMPARISON STUDY ON FIVE ESTIMATION METHODS FOR POWER SHANKER DISTRIBUTION .....	83
RAM PUMP APPLICATION FOR AGRICULTURAL IRRIGATION IN ÇANKIRI .....	87
CLASSIFICATION OF NETWORK ATTACKS WITH LSTM ARCHITECTURE METHOD .....	93
HORMONAL AND BIOCHEMICAL STUDY OF THE EFFECT OF VITAMIN D ON POLYCYSTIC OVARIES IN WOMEN.....	97
OPTIMIZATION APPROACH TO THE DESIGN OF DUAL BAND SLOTTED CIRCULAR MICROSTRIP ANTENNA.....	101
CIRCULARLY POLARIZED PATCH ANTENNA USING METAMATERIAL FOR 5G APPLICATIONS .....	107



---

THE STUDY RELATION OF ENDOTHELIN-1 AND MALONDIALDEHYDE WITH CHRONIC KIDNEY DISEASE .....	112
EXAMINING THE LEVELS OF ANXIETY AND DEPRESSION AMONG NURSES WORKING AT AL-DIWANIYAH TEACHING HOSPITAL DURING COVID-19 PANDEMIC .....	116
WHAT IS OSTEOMYELITIS OF THE JAW BONES? ITS HISTORY AND CLASSIFICATION.....	120
MENOPAUSAL HORMONES DISTURBANCE IN YOUNG AND ELDER BREAST CANCER PATIENTS IN IRAQ.....	126
STUDY OF THE CHANGES THAT OCCUR IN SOME BIOCHEMICAL VARIABLES AFTER CHOLECYSTECTOMY FOR PATIENTS IN AL-ANBAR GOVERNORATE/ IRAQ .....	133
STUDY OF RELATIONSHIP BETWEEN LEVELS OF HEPcidine HORMONE AND GDF15 FOR PATIENTS WITH PROSTATIC CANCER AND THEIR CLINICAL IMPORTANCE.....	142
THE INSECTICIDAL AND ACHE INHIBITORY ACTIVITIES OF DILOTAXIS TENUIFOLIA ESSENTIAL OILS PLANT EXTRACTS AND THEIR DETERMINATION OF CHEMICAL CONTENT OF EXTRACTS .....	149
THE INHIBITION EFFECTS INVESTIGATION OF METAL COMPLEXES WITH COUMARIN SCHIFF BASE ON G6PD ACTIVITY .....	155
PRODUCTION AND CHARACTERIZATION OF NANO-SIZED CALCIUM CARBONATE-ZINC OXIDE COMPOSITES .....	160
USING TRANSDERMAL PATCHES ON CONTROLLED DRUG RELEASE .....	165
SYNTHESIS, CHARACTERIZATION AND ANTIOXIDANT ACTIVITY OF N1-(5-CHLORO-2-OXOINDOLINE-3-YLIDENE) THIOCARBOHYDRAZONE SCHIFF BASES .....	169
FLEXIBLE ALTERNATING CURRENT TRANSMISSION SYSTEM.....	175
SEPARATION OF RHODIUM FROM SIMULATED RHODIUM PLATING SOLUTIONS WITH IMIDAZOLIUM DERIVATIVE IONIC LIQUIDS .....	181
SELF-ASSEMBLING PEPTIDES IN ORAL AND MAXILLOFACIAL SURGERY.....	186
SELECTIVE TRANSPORT OF CADMIUM FROM ACIDIC LEACH SOLUTIONS BY EMULSION LIQUID MEMBRANE USING TIOA AS THE CARRIER.....	189
PLANNING OPTIMAL FOREST ROAD NETWORK USING UNMANNED AERIAL VEHICLE (ELDIVAN SAMPLE) .....	199
THE POTENTIAL USE OF SALIVARY CYTOKINES IN DIAGNOSIS OF PERIODONTAL DISEASES .....	205
THE RELATION OF SERUM URIC ACID WITH A RISK MARKERS OF CARDIOVASCULAR DISEASE PATIENTS .....	210
ELECTROCOATING OF POLYANILINE AND POLYPYRROLE FROM DEEP EUTECTIC SOLUTION .....	217
MORPHOLOGY AND FUNCTIONS OF CUP CELLS IN THE EPITHELIUM OF SMALL INTESTINE.....	224
IN VITRO EFFECTS OF CLINDAMYCIN ANTIBIOTIC ON GLUCOSE-6-PHOSPHATE DEHYDROGENASE ENZYME PURIFIED FROM SHEEP SPLEEN TISSUE .....	228



---

PATHOLOGICAL FRACTURE OF THE MANDIBLE DUE TO ACTINOMYCOSIS OSTEOMYELITIS: CASE REPORT .....	235
THE IMPORTANCE OF SEDIMENTATION POOL IN SEDIMENT DYNAMISM: EXAMPLE OF KIZILIRMAK BASIN (CANKIRI)– TIMARLI LOCATION .....	238
INVESTIGATION IN TERMS OF SOIL CHARACTERISTICS OF INANDIK (CANKIRI,TURKIYE) SINKHOLES DUE TO GYPSUM KARSTIFICATION .....	245
REGENERATIVE LOAD GAIN WITH BRAKING SYSTEMS İN ELEVATORS.....	252
PREVALENCE OF DIARRHEA DUE TO CLOSTRIDIUM DIFFICILE A-B TOXINS IN A UNIVERSITY HOSPITAL IN NORTHERN CYPRUS .....	258
FINITE ELEMENT SOLUTION OF CONTACT PROBLEM FOR THE FUNCTIONALLY GRADED ORTHOTROPIC LAYER RESTING ON A HALF PLANE.....	264
INVESTIGATION OF THE EFFECTS OF SOME METALS ON GLUTATHIONE REDUCTASE ACTIVITY PURIFIED OF FROM RAINBOW TROUT (ONCORHYNCHUS MYKISS) ERYTHROCYTES.....	269
IN VITRO EFFECTS OF SOME DRUGS ON GLUTATHIONE REDUCTASE ENZYME PURIFIED FROM SHEEP SPLEEN TISSUE.....	274
DESIGN MULTI INPUT SINGLE OUTPUT DC TO DC CONVERTER FOR MOBILE DEVICES .....	281
EXCISION OF RESIDUAL CYST SEEN WITH ODONTOMA FROM RAMUS OF MANDIBLE: A CASE REPORT .....	287
CREATINE KINASE ELEVATION IN COVID-19 PATIENTS ON STATIN .....	292
EXAMINING THE RELATIONSHIP BETWEEN QUALITY OF LIFE AND PHYSICAL ACTIVITY, EXERCISE PERCEPTION IN MIDDLE ADULTHOOD .....	299
ELECTROCHEMICAL DETECTION OF DOPAMINE USING A SIMPLE REDOX CYCLING-BASED DEVICE ..	304
THE INVESTIGATION OF THE INHIBITORY POTENTIALS OF SOME POLYPHENOLS FOR ACETYLCHOLINESTERASE ACTIVITY .....	308
RELATIONSHIP BETWEEN GROWTH HORMONE AND JUVENILE IDIOPATHIC ARTHRITIS IN IRAQI PATIENTS .....	314
EFFECT OF PARAMETERS ON THE CALCIUM SULFATE CRYSTALLIZATION.....	317
INVESTIGATION OF THE PHOTOVOLTAIC, STRUCTURAL, ELECTRONIC AND SPECTROSCOPIC PROPERTIES OF SOME MOLECULES CONTAINING DIMETHYLANILINE .....	321
STUDY OF THE ASSOCIATION OF GENES AND PROTEINS OF RESISTANCE TO MULTIPLE DRUGS WITH MOLECULAR MARKERS IN PATIENTS WITH ACUTE LEUKAEMIA.....	327
THE EFFECT OF MATERIAL PREFERENCE ON ENGINE PERFORMANCE IN OTTO CYCLE ENGINE .....	332
EVALUATION OF SOME BIOLOGICAL PARAMETERS AND TRACE ELEMENTS IN PROSTATIC TUMORS AMONG IRAQI PATIENTS WITH DMII .....	337
IMPROVED SPEED AND TORQUE EFFICIENCY FOR DTC CONTROLLED ASYNCHRONOUS MACHINE USING FUZZY SWITCHING ALGORITHM .....	340



---

STUDY CHANGE IN LIVER ENZYMES AND HEPCIDIN HORMONE AS A POSSIBLE RISK FACTOR TO JUVENILE IDIOPATHIC ARTHRITIS.....	346
THE RELATIONSHIP BETWEEN GROWTH DIFFERENTIATION FACTOR-15 AND TESTOSTERONE HORMONE LEVEL IN PROSTATE CANCER PATIENTS.....	349
ROLE OF TRANSCRIPTION FACTOR 7 LIKE RS7903146 AND RS12255372 GENE POLYMORPHISMS AND SELECTIVE BIOCHEMICAL TESTS IN TYPE II IRAQI DIABETIC PATIENTS .....	357
LUNG OPACITY CLASSIFICATION WITH CONVOLUTIONAL NEURAL NETWORK .....	360
THE INHIBITION EFFECTS INVESTIGATION OF METAL COMPLEXES WITH COUMARIN SCHIFF BASE ON 6PGD ACTIVITY .....	364
INVESTIGATION OF EFFECT OF THE PARAMETERS ON CALCIUM CARBONATE CRYSTALLIZATION.....	369



# Classification of Breast Lesions on Mammogram Images using Monarch Butterfly Optimization and Support Vector Machine

Erkan AKKUR<sup>1,\*</sup> , Fuat TÜRK<sup>2</sup> , Osman EROĞUL<sup>3</sup> 

<sup>1</sup>Faculty of Engineering, Department of Biomedical Engineering, TOBB University of Economics and Technology, Ankara, Turkey

<sup>2</sup>Faculty of Engineering, Computer Engineering, Çankırı Karatekin University, Çankırı, Turkey

## Abstract

Currently, breast cancer affects many women worldwide. In recent years, many Computer-aided diagnosis (CAD) model have been developed for early diagnosis of breast cancer. An efficient CAD model is suggested to identify mammogram images as benign versus malignant in this study. The suggested CAD model constitutes four stages which are image acquisition, segmentation, feature extraction, feature selection and classification process. Gray level run matrix (GLRM) approach is used for feature extraction, while monarch butterfly optimization (MBO) for feature selection process. Support vector machine (SVM) algorithm is preferred for classification process. The suggested model has been tested on a private mammographic dataset. The suggested model (GLRM+MBO+SVM) shows an 0.944 of accuracy for breast lesion classification. Compared with similar studies, our proposed model showed good classification results for the breast lesion classification process.

**Keywords:** Breast cancer, Gray level run matrix, Monarch Butterfly optimization, Support vector machine

## 1. Introduction

Currently, breast cancer (BC) is one of leading cause of death among women worldwide. Early diagnosis of breast cancer is key functionality to reduce the mortality rates. Screening mammography is recommended imaging tool for early diagnosis [1]. Generally, radiologists use mammogram images to classify breast lesions as malignant versus benign. This classification process can be challenging task for radiologists as they interpret many mammogram images daily. In recent years, computer-aided (CAD) systems have been used to assist radiologists when decision making. Typical a CAD system includes four main parts; (1) segmenting of breast lesion (2) feature extraction (3) feature selection (4) classification. The performance of a CAD system mainly relies on three issues: extraction of features from an image, selection of optimal features from the extracted features and classification [2]. Therefore, this study focuses on feature extraction (FE), feature selection (FS) and classification. This study proposes Gray Level Run Matrix(GLRM) for FE, Monarch butterfly optimization (MBO) for FS and Support Vector Machine (SVM) for classification. This combination methods (GLRM/WOA/SVM) are the novelty of this study. The main aim of this study is to investigate whether the proposed MBO feature selection improves the performance of the SVM algorithm.

## 2. Literature Survey

Bajsci et al. [3] used GLRM for FE. The study used decision tree and random forest for classification. The experiments conducted on The Mammographic Image Analysis (MIAS) dataset and they achieved 100% of accuracy.

Punitha et al. [4] utilized a neural network to classify malign and benign breast lesions. The study used GLCM and GLRM features. Their study achieved 98% of accuracy for Digital Database for Screening Mammography (DDSM).

Mohanty et al. [5] suggested a hybrid model for BC classification. They used 2-D wavelet transform and gray level co-occurrence matrix (GLCM) for FE. Forest optimization algorithm was used for feature selection. Several algorithms were used for classification. The experiments were conducted on MIAS and DDSM datasets. Decision Tree-based model achieved the best performance with 100% of accuracy compared to other models.

\* Corresponding author. e-mail address: eakkur@gmail.com

Jona and Navegeni [6] suggested Genetical swarm optimization (GSO)-SVM based model for BC classification. Gray Level Co-occurrence Matrix (GLCM) approach is utilized for FE. The experiments are conducted on MiniMIAS database. The suggested model achieved 94% of accuracy.

Candra [7] et al. suggested an CAD system for BC prediction. They used GLRM and GLCM approach FE. The experiments are conducted on MiniMIAS database. The best performance demonstrated 93.97% of accuracy using polynomial kernel.

Dheeba et al. [8] proposed an CAD model for breast microcalcification classification. They used the combination particle swarm optimization (PSO)-feed forward neural network (FFNN). Laws texture approach is used for FE. The experiments are conducted on MiniMIAS database and clinical database. The suggested model showed 0.97 of accuracy for MIAS and 0.913 of accuracy for clinical database.

### 3. Materials and Methods

The suggested CAD approach includes four main parts namely, data acquisition of mammogram images dataset, FE, FS and classification. The suggested of CAD approach is shown in Figure 1.

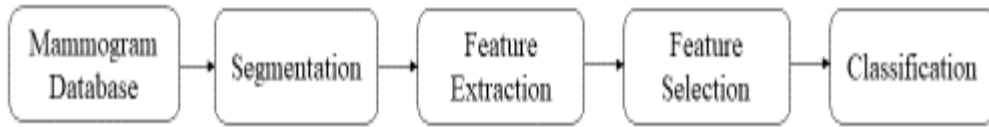


**Figure 1.** The framework of the suggested model

#### 3.1 Mammogram Database

The proposed methodology was evaluated on a mammography dataset provided by the Department of Radiology at Ankara Education and Research Hospital. This dataset was approved by the ethics committee of Ankara Training and Research Hospital. Due to the retrospective nature of this study, informed consent was waived. All patients who underwent digital mammography were retrieved from the Picture Archiving and Communication System (PACS) between April 2015 and April 2020. All patients underwent mammography using IMS Giotto (Bologna-Italy). The datasets consist of 195 mammogram images (116 images (59%) for malign, 79 images (41%) for benign). The mammogram images were segmented to identify breast lesions. The stages of the segmentation process are demonstrated in Figure 2. First, the mammogram images were retrieved (Figure 2-a). Then, the borders of the breast lesions were determined by the green contour with the radiologists. (Figure 2-b). Finally, the breast lesions were extracted from the image, using the gray level thresholding and morphological operations (Figure 2-c).

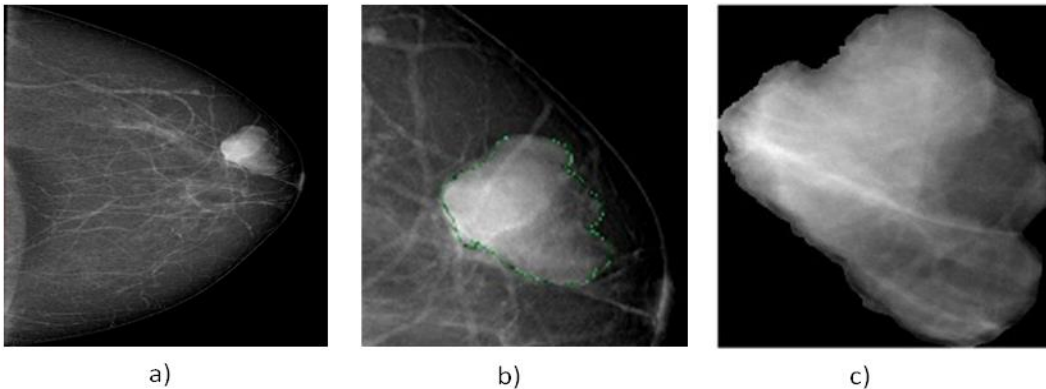


**Figure 2.** a) Original mammogram image, b) Marking of ROI with green contours



### 3.2. Feature Extraction

Mammogram images contain a lot of confidential information based on pixels that the human eye cannot see. Feature extraction is the process of extracting measurable pixel-based information from images. This study, GLRM approach is used for FE. GLRM approach provides about gray level runs (number of pixels with the same intensity in a given direction), describing the texture of an image. These features characterize the distribution of short and long runs of an image in a specific direction. *Short run emphasis (SRE)*, *long run emphasis (LRE)*, *gray-level nonuniformity (GLN)*, *run length nonuniformity (RLN)*, *run percentage (RP)*, *low gray-level run emphasis (LGRE)*, *high gray-level run emphasis (HGRE)*, *short run low gray-level emphasis (SRLGE)*, *short run high gray-level emphasis (SRHGE)*, *long run low gray-level emphasis (LRLGE)* and *long run high gray level emphasis (LRHGE)*; 11 GLRM features were extracted [3].

### 3.3. Feature Selection

The size of features can affect the performance of classification process due to high computational cost. Therefore, FS approaches are used to eliminate redundant and irrelevant features to improve the performance of classification process and reduces the computational cost. In this study, monarch butterfly optimization (MBO) method is used for FS. MBO is a swarm-based algorithm which is developed by Wang et al. [9]. This mimics by monarch butterfly migration behavior. MBO algorithm consists of two main equal-sized subpopulation which are subpopulation 1 and subpopulation 2. The migration operator and butterfly adjusting operator generate of two main strategies of this algorithm. The strategies are based on iteration. The global optimal information is separated during iterations and the subpopulations are revised into population again. According to the determining new fitness value, the whole population is divided by two subpopulations. When the termination condition is met, this process is ended [10]. The mathematical formulation of MBO algorithm is explained in details in ref. 10.

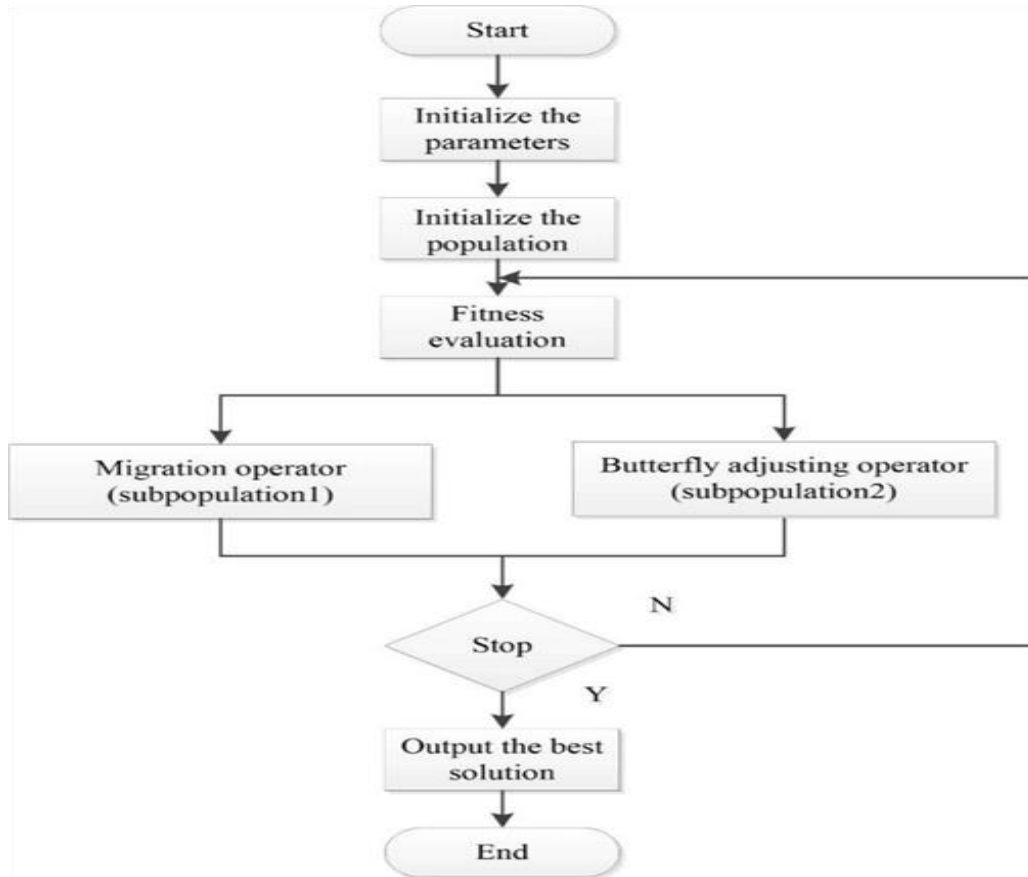


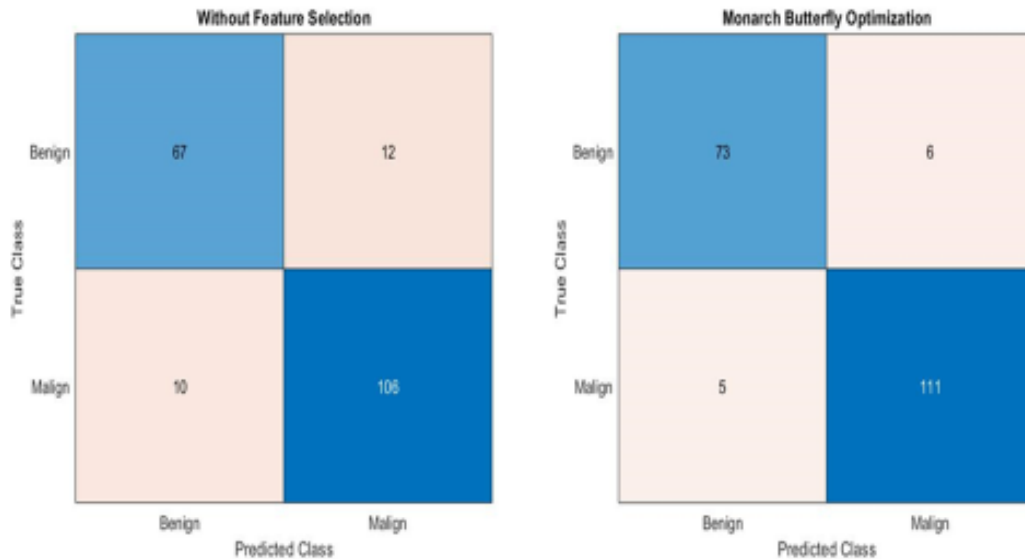
**Figure 3.** The framework of Monarch butterfly optimization [10]

### 3.4 Classification

Classification is the process of assigning unclassified images to their own classes within categories. With the high discriminating ability, machine learning algorithms have been used for breast lesion classification in recent years. In this study, support vector machine algorithm is used to classify breast lesion as malignant versus benign. SVM is a popular machine learning algorithm which uses generally regression and classification process. The primary aim of this algorithm is to build a line or hyperplane which splits the data into classes. Support vectors are defined as data points near the hyperplane, while data points are called margin [2].

## 4. Experimental Results and Discussion

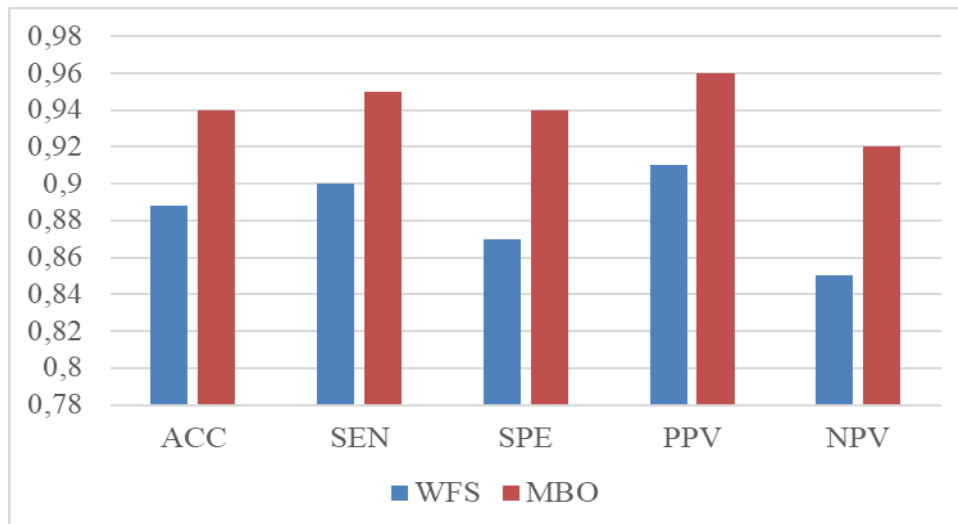
This section of the study presents the results of experiments. Experiments were carried out using the MATLAB 2020a program to validate the predictive model. 10-fold cross validation is used for evaluation of suggested model. SVM algorithm is used to classify breast lesions malignant versus benign. The performance results of SVM are evaluated within the framework of two different scenarios. In the first scenario, the performance of SVM is analyzed without using feature selection method. In the second scenario, the performance of SVM is analyzed after applying the MBO-based method. The parameters for MBO are set as follows: *population size=50, max step=1.0, butterfly adjusting rate=5/12, migration period=1.2, migration ratio=5/12 and maximum generation=50* [10]. Experimental results were evaluated in terms of accuracy (ACC), sensitivity (SEN), specificity (SPE), positive predictive value (PPV) and negative predictive value (NPV) performance metrics calculated using the confusion matrix shown in Figure 4. The results of both scenarios are summarized in Table 1. After applying MBO based feature selection, two features are rest which are SRE and RP. Without applying the feature selection method (WFS), the SVM algorithm shows 0.888 of accuracy, 0.899 of sensitivity, 0.87 of specificity, 0.914 of PPV, and 0.849 of NPV. After applying the MBO feature selection method, the SVM algorithm shows 0.944 of accuracy, 0.949 of sensitivity, 0.936 of specificity, 0.957 of PPV, and 0.924 of NPV. After using the MBO feature method, 2 of the 11 GLRM features are selected as distinctive features which are SRE and RP. After the predictive model is created, the efficiency of the model can be checked. For that, the results of without feature selection (WFS) and MBO based method are compared in Figure 5. As analyzed Figure 5, MBO based method enhances the performance of SVM algorithm in terms of ACC, SEN, SPE, PPV and NPV.



**Figure 4.** Confusion matrix of suggested model

**Table 1.** Comparison of WFS and MBOA methods

Classification	Method	Selected Features	ACC	SEN	SPE	PPV	NPV
SVM	WFS	11	0.888	0.899	0.87	0.914	0.849
	MBO	2	0.944	0.949	0.936	0.957	0.924

**Figure 5.** Comparison of WFS and MBO model

## 5. Conclusion

An efficient CAD scheme for mammographic breast lesion classification has been suggested in this study. GLRM approach is used for FE. Further, the most discriminating features are selected using monarch butterfly optimization (MBOA). SVM algorithm is used for breast lesion classification. The experimental analyzes are conducted on a private mammographic dataset. The proposed scheme (GLRM+MBO+SVM) shows 0.944 of accuracy. Our proposed method yields similar results when compared with similar recent studies, as shown in Table 2. As a result, we believe that the suggested method shows a good result in the diagnosis of breast cancer. In the future, other feature selection methods and classification methods can be considered as potential alternatives to the proposed scheme.

**Table 2.** Comparison of suggested with some recent similar studies

References	Proposed Method	Dataset	ACC
[6]	GLCM+GSO+SVM	MIAS	0.94
[7]	GLRM+SVM	MIAS	0.939
[8]	PSO-FFNN	MIAS	0.976
		Private Dataset	0.913
Suggested method	GLRM+MBO+SVM	Private Dataset	0.944

## References

- [1] Sung, H., Ferlay, J., Siegel, R. L., Laversanne, M., Soerjomataram, I., Jemal, A., & Bray, F. (2021). Global cancer statistics 2020: GLOBOCAN estimates of incidence and mortality worldwide for 36 cancers in 185 countries. *CA: a cancer journal for clinicians*, 71(3), 209-249.
- [2] Hassan, N. M., Hamad, S., & Mahar, K. (2022). Mammogram breast cancer CAD systems for mass detection and classification: a review. *Multimedia Tools and Applications*, 1-
- [3] Bajcsi, A., Andreica, A., & Chira, C. (2021). Towards feature selection for digital mammogram

classification. *Procedia Computer Science*, 192, 632-641.

- [4] Punitha, S., Amuthan, A., & Joseph, K. S. (2018). Benign and malignant breast cancer segmentation using optimized region growing technique. *Future Computing and Informatics Journal*, 3(2), 348-358.
- [5] Mohanty, F., Rup, S., Dash, B., Majhi, B., & Swamy, M. N. S. (2020). Digital mammogram classification using 2D-BDWT and GLCM features with FOA-based feature selection approach. *Neural Computing and Applications*, 32(11), 7029-7043.
- [6] Jona, J., & Nagaveni, N. (2012). A hybrid swarm optimization approach for feature set reduction in digital mammograms. *WSEAS Trans Inf Sci Appl*, 9(11), 340-349.
- [7] Candra, D., Novitasari, R., Lubab, A., Sawiji, A., Asyhar, A.H., 2019. Application of feature extraction for breast cancer using one order statistic, GLCM, GLRLM, and GLDM. *Advances in Science, Technology and Engineering Systems Journal* 4, 115–120.
- [8] Dheeba, J., & Selvi, S. (2012). A swarm optimized neural network system for classification of microcalcification in mammograms. *Journal of medical systems*, 36(5).
- [9] Wang, G. G., Deb, S., & Cui, Z. (2019). Monarch butterfly optimization. *Neural computing and applications*, 31(7), 1995-2014.
- [10] Feng, Y., Deb, S., Wang, G. G., & Alavi, A. H. (2021). Monarch butterfly optimization: a comprehensive review. *Expert Systems with Applications*, 168, 114418.



## On Intuitionistic Fuzzy Soft Multisets

Fatih KARAMAZ<sup>1,\*</sup> , Faruk KARAASLAN<sup>1</sup> 

<sup>1</sup>Department of Mathematics, Faculty of Sciences, Çankırı Karatekin University, Çankırı, Turkey

### Abstract

An intuitionistic fuzzy set is characterized by membership and non-membership functions. The notions of the soft set and multiset are other useful instruments in the modeling of some problems. In this paper, the concept of intuitionistic fuzzy soft multisets (IFSMSs) and set-theoretical operations of IFSMSs are defined. Fundamental definitions and operations are supported with examples to make the concepts more understandable.

**Keywords:** Intuitionistic fuzzy set, Soft sets, Intuitionistic fuzzy soft set, Multiset, Intuitionistic fuzzy soft multisets

### 1. Introduction

In real life, human being encounters some situations involving uncertainty and incomplete information. Researchers seek constantly new ways to cope with such situations. As a result of this search, new mathematical theories have emerged. The well-knowns of these are fuzzy set theory [1], intuitionistic fuzzy set theory [2], rough set theory [3], soft set theory [4], neutrosophic set theory [5], and multiset theory [6]. Recently, the properties and applications of the intuitionistic fuzzy sets and multisets have been studied extensively.

The concept of the soft set was introduced by Molodtsov [4] as a mathematical tool to deal with some uncertainties. Then, Maji et al. [7] defined several operations between two soft sets and derived some properties of soft set operations. The soft set theory has a rich application area in solving practical problems in economics, social science, medical science etc. Many interesting results of soft set theory have been studied by embedding the ideas of fuzzy sets and intuitionistic fuzzy set.

In the solving of the decision-making problems multisets, intuitionistic fuzzy sets, and soft sets have individual advantages. In this paper, to utilize by integrating the advantages of mentioned sets in the modeling of the decision-making problems, we define the concept of intuitionistic fuzzy soft multiset. we define the concept of intuitionistic fuzzy soft multisets (IFSMSs). We also define the set theoretical operations of IFSMSs and obtain some of their properties.

### 2. Preliminaries

In this section, some definitions and operations which they will be required in the next sections are given.

**Definition 2.1.** [1] Let  $U$  be a nonempty set called initial universe. Then, a fuzzy set  $\Omega$  is defined by its membership function  $\kappa_{\Omega}$  as follows:

$$\kappa_{\Omega}: U \rightarrow [0,1]$$

the value  $\kappa_{\Omega}(\alpha)$  is called the membership degree of  $\alpha \in U$ . This numerical value  $\kappa_{\Omega}(\alpha)$  expresses the degree of  $\alpha$  belonging to the fuzzy set  $\Omega$ . Also, fuzzy set  $\Omega$  on  $U$  can be written as follows:

$$\Omega = \{(\kappa_{\Omega}(\alpha)/\alpha): \alpha \in U, \kappa_{\Omega}(\alpha) \in [0,1]\}.$$

From now onward  $\mathcal{F}(U)$  will be denote the family of all fuzzy sets  $U$ .

**Definition 2.2.** [8] Let  $U$  be a nonempty set,  $J$  be an indexing set and  $\{L_j: j \in J\}$  a family of partially ordered sets. A fuzzy multiset  $\mathcal{FMS}(U)$  in  $U$  is a set:

\* Corresponding author. e-mail address: karamaz@karamaz.com

$$\mathcal{FMS}(U) = \left\{ \left( \alpha, \left( \kappa_{\Omega_j}(\alpha) \right)_{j \in J} \right) : \alpha \in U, \kappa_{\Omega_j} \in L_j^U, j \in J \right\}.$$

**Definition 2.3. [2]** An intuitionistic fuzzy set (IFS)  $X$  over  $U$  is defined as an object of the following form  $X = \{(\alpha, \mu_X(\alpha), \nu_X(\alpha)) : \alpha \in U\}$  where the functions  $\mu_X : U \rightarrow [0,1]$  and  $\nu_X : U \rightarrow [0,1]$  define the degree of membership and the degree of non-membership of the element  $\alpha \in U$ , respectively, and for every  $\alpha \in U$ ,  $0 \leq \mu_X(\alpha) + \nu_X(\alpha) \leq 1$ .

In addition, for all  $\alpha \in U$ ,  $U = \{(\alpha, 1, 0) : \alpha \in U\}$ ,  $\emptyset = \{(\alpha, 0, 1) : \alpha \in U\}$  are intuitionistic fuzzy universal and intuitionistic fuzzy empty set, respectively.

**Definition 2.4. [2]** For every two IFS's  $X_1$  and  $X_2$  the following operations and relations are valid:

1. **Inclusion:**  $X_1 \subset X_2 \Leftrightarrow (\forall \alpha \in U)(\mu_{X_1}(\alpha) \leq \mu_{X_2}(\alpha) \text{ and } \nu_{X_2}(\alpha) \leq \nu_{X_1}(\alpha))$
2. **Equality:**  $X_1 = X_2 \Leftrightarrow X_1 \subset X_2 \text{ and } X_2 \subset X_1$
3. **Complement:**  $X^C = \{(x, \nu_X(\alpha), \mu_X(\alpha)) : \alpha \in U\}$
4. **Intersection:**  $X_1 \cap X_2 = \{(x, \min(\mu_{X_1}(\alpha), \mu_{X_2}(\alpha)), \max(\nu_{X_1}(\alpha), \nu_{X_2}(\alpha))) : \alpha \in U\}$
5. **Union:**  $X_1 \cup X_2 = \{(x, \max(\mu_{X_1}(\alpha), \mu_{X_2}(\alpha)), \min(\nu_{X_1}(\alpha), \nu_{X_2}(\alpha))) : \alpha \in U\}$
6. **Addition:**  $X_1 \oplus X_2 = \{(x, \mu_{X_1}(\alpha) + \mu_{X_2}(\alpha) - \mu_{X_1}(\alpha) \cdot \mu_{X_2}(\alpha), \nu_{X_1}(\alpha) \cdot \nu_{X_2}(\alpha)) : \alpha \in U\}$
7. **Multiplication:**  $X_1 \otimes X_2 = \{(x, \mu_{X_1}(\alpha) \cdot \mu_{X_2}(\alpha), \nu_{X_1}(\alpha) + \nu_{X_2}(\alpha) - \nu_{X_1}(\alpha) \cdot \nu_{X_2}(\alpha)) : \alpha \in U\}$

**Definition 2.5. [9]** Let  $A$  be an IFS. Then,  $\forall \alpha \in U$ ,  $S_A(\alpha) = \frac{1 - \nu_A(\alpha)}{2 - \mu_A(\alpha) - \nu_A(\alpha)}$  is called the score function of intuitionistic fuzzy elements of  $A$ .

**Definition 2.6. [10]** A triangular norm (t-norm, for short)  $\mathcal{T}$  is a  $[0,1]^2 \rightarrow [0,1]$  map which satisfies:

$$\mathcal{T}_1: (\forall x \in [0,1])(x\mathcal{T}1 = x),$$

$$\mathcal{T}_2: (\forall (x, y) \in [0,1]^2)(x\mathcal{T}y = y\mathcal{T}x),$$

$$\mathcal{T}_3: (\forall (x, y, z) \in [0,1]^3)((x\mathcal{T}(y\mathcal{T}z)) = ((x\mathcal{T}y)\mathcal{T}z)),$$

$$\mathcal{T}_4: (\forall (x_1, y_1, x_2, y_2) \in [0,1]^4)(x_1 \leq y_1 \wedge x_2 \leq y_2 (x_1\mathcal{T}x_2) \leq (y_1\mathcal{T}y_2)).$$

**Definition 2.7. [10]** A triangular norm (t-conorm, for short)  $\mathcal{S}$  is a  $[0,1]^2 \rightarrow [0,1]$  map which satisfies:

$$\mathcal{S}_1: (\forall x \in [0,1])(x\mathcal{S}0 = x),$$

$$\mathcal{S}_2: (\forall (x, y) \in [0,1]^2)(x\mathcal{S}y = y\mathcal{S}x),$$

$$\mathcal{S}_3: (\forall (x, y, z) \in [0,1]^3)((x\mathcal{S}(y\mathcal{S}z)) = ((x\mathcal{S}y)\mathcal{S}z)),$$

$$\mathcal{S}_4: (\forall (x_1, y_1, x_2, y_2) \in [0,1]^4)(x_1 \leq y_1 \wedge x_2 \leq y_2 (x_1\mathcal{S}x_2) \leq (y_1\mathcal{S}y_2)).$$

**Definition 2.8. [10]** For two intuitionistic fuzzy sets  $A$  and  $B$  in  $U$ , we define the generalised intersection and union as:

$$A \sqcap_{\mathcal{T}, \mathcal{S}} B = \left\{ \left( \alpha, (\mu_A(\alpha)\mathcal{T}\mu_B(\alpha)), (\nu_A(\alpha)\mathcal{S}\nu_B(\alpha)) \right) \mid \alpha \in U \right\},$$

$$A \sqcup_{\mathcal{T}, \mathcal{S}} B = \left\{ \left( \alpha, (\mu_A(\alpha)\mathcal{S}\mu_B(\alpha)), (\nu_A(\alpha)\mathcal{T}\nu_B(\alpha)) \right) \mid \alpha \in U \right\}.$$

where  $\mathcal{T}$  denotes a t-norm and  $\mathcal{S}$  a t-conorm.

**Definition 2.9. [11]** Let  $X$  be a nonempty set. An Intuitionistic Fuzzy Multiset  $A$  denoted by IFMS drawn from  $X$  is characterized by two functions: 'count membership' of  $A(CM_A)$  and 'count non membership' of  $A(CN_A)$  given respectively by  $CM_A : X \rightarrow Q$  and  $CN_A : X \rightarrow Q$  where  $Q$  is the set of all crisp multisets drawn from the unit interval  $[0,1]$  such that for each  $x \in X$ , the membership sequence is defined as a decreasingly ordered sequence of elements in  $CM_A(x)$  which is denoted by  $(\mu_A^1(x), \mu_A^2(x), \dots, \mu_A^p(x))$  where  $(\mu_A^1(x) \geq \mu_A^2(x) \geq \dots \geq \mu_A^p(x))$  and the corresponding non membership sequence will be denoted by  $(\nu_A^1(x) \geq \nu_A^2(x) \geq \dots \geq \nu_A^p(x))$  such that  $0 \leq \mu_A^i(x) + \nu_A^i(x) \leq 1$  for every  $x \in X$  and  $i = 1, 2, \dots, p$ .

An IFMS  $A$  is denoted by  $A = \{ \langle x : (\mu_A^1(x), \mu_A^2(x), \dots, \mu_A^p(x)), (\nu_A^1(x), \nu_A^2(x), \dots, \nu_A^p(x)) \rangle : x \in X \}$ .



**Definition 2.10.** [4,7,12] Let  $\mathfrak{E}$  be a set of parameters,  $\emptyset \neq \mathcal{A} \subset \mathfrak{E}$  and  $U$  be the universal set of objects. A soft set  $\mathcal{F}_{\mathcal{A}}$  over  $U$  is a set of pairs defined as follows:  $\mathcal{F}_{\mathcal{A}} = \{(\sigma, \delta_{\mathcal{A}}(\sigma)) : \sigma \in \mathfrak{E}, \delta_{\mathcal{A}}(\sigma) \in \mathfrak{P}(U)\}$  where  $\delta_{\mathcal{A}}: \mathfrak{E} \rightarrow \mathfrak{P}(U)$  such that  $\delta_{\mathcal{A}}(\sigma) = \emptyset$  if  $\sigma \notin \mathcal{A}$  and  $\delta_{\mathcal{A}}$  is called approximate function of the soft set  $\mathcal{F}_{\mathcal{A}}$ . The image of  $\sigma \in \mathfrak{E}$  under mapping  $\delta_{\mathcal{A}}$  is called  $\sigma$ -element.

After this time, the set of all soft sets over  $U$  and parameter sets  $\mathfrak{E}$  will be denoted by  $\mathfrak{S}_{\mathfrak{E}}(U)$ .

**Definition 2.11.**[12] For every two soft sets  $\mathcal{F}_{\mathcal{A}}$  and  $\mathcal{F}_{\mathcal{B}}$  the following operations and relations are valid:

1. **Inclusion:**  $\mathcal{F}_{\mathcal{A}} \subseteq \mathcal{F}_{\mathcal{B}} \Rightarrow \delta_{\mathcal{A}}(\sigma) \subseteq \delta_{\mathcal{B}}(\sigma)$  for all  $\sigma \in \mathfrak{E}$
2. **Equality:**  $\mathcal{F}_{\mathcal{A}} = \mathcal{F}_{\mathcal{B}} \Rightarrow \delta_{\mathcal{A}}(\sigma) = \delta_{\mathcal{B}}(\sigma)$  for all  $\sigma \in \mathfrak{E}$
3. **Complement:**  $\mathcal{F}_{\mathcal{A}}^c \Rightarrow \delta_{\mathcal{A}^c}(\sigma) = \delta_{\mathcal{A}}^c(\sigma)$   
for all  $\sigma \in \mathfrak{E}$  where  $\delta_{\mathcal{A}}^c(\sigma)$  is complement of the set  $\delta_{\mathcal{A}}(\sigma)$  that is  $\delta_{\mathcal{A}}^c(\sigma) = U \setminus \delta_{\mathcal{A}}(\sigma)$  for all  $\sigma \in \mathfrak{E}$
4. **Intersection:**  $\mathcal{F}_{\mathcal{A}} \tilde{\cap} \mathcal{F}_{\mathcal{B}} \Rightarrow \delta_{\mathcal{A} \tilde{\cap} \mathcal{B}}(\sigma) = \delta_{\mathcal{A}}(\sigma) \cap \delta_{\mathcal{B}}(\sigma)$  for all  $\sigma \in \mathfrak{E}$
5. **Union:**  $\mathcal{F}_{\mathcal{A}} \tilde{\cup} \mathcal{F}_{\mathcal{B}} \Rightarrow \delta_{\mathcal{A} \tilde{\cup} \mathcal{B}}(\sigma) = \delta_{\mathcal{A}}(\sigma) \cup \delta_{\mathcal{B}}(\sigma)$  for all  $\sigma \in \mathfrak{E}$

**Definition 2.12.** [13,14] Let  $U$  be an initial universe,  $\mathcal{IF}(U)$  be the set of all intuitionistic fuzzy set over  $U$ ,  $\mathfrak{E}$  be a set of all parameters and  $A \in \mathfrak{E}$ . Then an intuitionistic fuzzy soft set (IFS-set)  $\gamma_A$  over  $U$  is a function from  $\mathfrak{E}$  into  $\mathcal{IF}(U)$ .

Where, the value  $\gamma_A(\alpha)$  is an intuitionistic fuzzy set over  $U$ . That is,  $\gamma_A(\sigma) = \{(\alpha, \mu(\alpha), \nu(\alpha)) : \sigma \in \mathfrak{E}, \alpha \in U\}$ , where  $\mu(\alpha)$  and  $\nu(\alpha)$  are the membership and non-membership degrees of  $\alpha$  to the parameter  $\sigma$ , respectively.

Note that, the set of all intuitionistic fuzzy soft sets over  $U$  is denoted by  $\mathcal{IFS}(U)$ .

### 3. Intuitionistic Fuzzy Soft Multisets

Let  $U$  be a universal set and  $A \subset \mathfrak{E}$  be a parameter set. Then, an intuitionistic fuzzy soft multiset (IFSMS) is a set defined as follows:

$$\dot{\mathcal{M}} = \left\{ \left( \sigma_i \left\{ \left( \alpha_j, \sum_{k \in \{1,2,\dots,n\}} (\mu_k(\alpha_j), \nu_k(\alpha_j)) / m_k \right) : m_k \in \mathbb{N}, \alpha_j \in U \right\} \right) : \sigma_i \in \mathfrak{E} \right\}$$

such that for  $\sigma_i \in \mathfrak{E} \setminus A$ ,  $(\sigma_i \{(\alpha_j, \sum_{k \in \{1,2,\dots,n\}} (0,1)/m_k (0,1)/0) : m_k \in \mathbb{N}, \alpha_j \in U\})$ . In generally, such elements are not displayed in IFSMS. Here,  $\{\sum_{k \in \{1,2,\dots,n\}} (\mu_k(\alpha_j), \nu_k(\alpha_j)) / m_k : m_k \in \mathbb{N}, \alpha_j \in U\}$  is called intuitionistic fuzzy multi element (IFME) and  $n$  denotes number of different intuitionistic fuzzy element (IFE) in IFME corresponding to  $\alpha_j$ .

Here,  $m_k$  denotes the repeating number of IFEs in  $\alpha_j$  evaluated with parameter  $\sigma_i$ .

**Example 3.1.** Consider universal set  $U = \{\alpha_1, \alpha_2, \alpha_3\}$  and parameter set  $\mathfrak{E} = \{\sigma_1, \sigma_2\}$ . Then, an IFSMS  $\dot{\mathcal{M}}$  can be written as

$$\dot{\mathcal{M}} = \{(\sigma_1\{(\alpha_1, (0.2,0.4)/2 + (0.3,0.5)/3 + (0.4,0.5)/1), (\alpha_2, (0.4,0.6)/1 + (0.5,0.5)/2 + (0.3,0.4)/1 + (0.7,0.3)/2), (\alpha_3, (0.3,0.7)/2 + (0.3,0.5)/3 + (0.4,0.6)/3 + (0.6,0.4)/1\}), (\sigma_2\{(\alpha_1, (0.3,0.6)/3 + (0.2,0.7)/1 + (0.3,0.5)/2), (\alpha_2, (0.3,0.3)/2 + (0.5,0.5)/3 + (0.1,0.3)/2), (\alpha_3, (0.3,0.6)/2 + (0.1,0.9)/1 + (0.1,0.7)/2 + (0.2,0.8)/3\})\}.$$

**Definition 3.1.** Let  $\dot{\mathcal{M}}$  be an IFSMS on  $U$  and parameter set  $\mathfrak{E}$ . Then, cardinality of  $\alpha_j$  according to parameter  $\sigma_i$  denoted by  $\mathcal{L}_{\sigma_i}(\alpha_j, \dot{\mathcal{M}})$  is defined as follows:  $\mathcal{L}_{\sigma_i}(\alpha_j, \dot{\mathcal{M}}) = \sum_{k \in \{1,2,\dots,n\}} m_k$ .

From now on set of all IFSMS over  $U$  and parameter set  $\mathfrak{E}$  will be denoted by  $\mathcal{IFSMS}_{\mathfrak{E}}^U$ . Throughout the paper, IFMS will be denoted by  $\dot{\mathcal{M}}_{\sigma_i}$  and IFME will be denoted by  $\dot{\mathcal{M}}_{\sigma_i}^{(\alpha_j)}$ .

If  $\sigma \notin A$ , then  $\dot{\mathcal{M}}_{\sigma}^{(\alpha)} = \{(0,1)/0\}$ .

**Definition 3.2.** Let  $\check{\mathcal{M}} \in \text{IFSMS}_{\mathfrak{E}}^U$ . Then,  $\forall \sigma_i \in \mathfrak{E}$  and  $\alpha_j \in U$ , decreasing sequence of the elements in  $\check{\mathcal{M}}_{\sigma_i}^{(\alpha_j)}$  according to score function of IFE is denoted by  $\check{\mathcal{M}}_{\sigma_i}^{(\alpha_j)} = (\gamma_{ij_1}, \gamma_{ij_2}, \dots, \gamma_{ij_n})$ . Here  $\gamma_{ij_l}$  ( $l = 1, 2, \dots, n$ ) denotes IFEs such that  $(S(\gamma_{ij_1}) > S(\gamma_{ij_2}) > \dots > S(\gamma_{ij_n}))$ . This sequence is called ordered sequence of  $\check{\mathcal{M}}_{\sigma_i}^{(\alpha_j)}$ . Also,  $(m_{ij_1}, m_{ij_2}, \dots, m_{ij_n})$  denotes sequence of repetition number corresponding to elements of the ordered sequence  $(\gamma_{ij_1}, \gamma_{ij_2}, \dots, \gamma_{ij_n})$ .

After that,  $\{(\sigma_i\{(\alpha_j, \sum_{k \in \{1,2,\dots,n\}} \gamma_{ijk}/m_{ijk}) : m_{ijk} \in \mathbb{N}, \alpha_j \in U\}) : \sigma_i \in \mathfrak{E}\}$  is called ordered IFSMS (OIFSMS) and is denoted by  $\check{\mathcal{M}}$ . Set of all OIFSMSs on  $U$  and  $\mathfrak{E}$  is denoted by  $\text{OIFSMS}_{\mathfrak{E}}^U$ .

**Definition 3.3.** Let  $\check{\mathcal{M}}_1 = \{(\sigma_i\{(\alpha_j, \sum_{k \in \{1,2,\dots,s\}} \gamma_{ijk}^1/m_{ijk}^1) : m_{ijk}^1 \in \mathbb{N}, \alpha_j \in U\}) : \sigma_i \in \mathfrak{E}\}$ ,  $\check{\mathcal{M}}_2 = \{(\sigma_i\{(\alpha_j, \sum_{k \in \{1,2,\dots,r\}} \gamma_{ijk}^2/m_{ijk}^2) : m_{ijk}^2 \in \mathbb{N}, \alpha_j \in U\}) : \sigma_i \in \mathfrak{E}\} \in \text{OIFSMS}_{\mathfrak{E}}^U$ . Then, it is said to be  $\check{\mathcal{M}}_1$  is subset of  $\check{\mathcal{M}}_2$ , if  $\check{\mathcal{M}}_{1\sigma_i}^{(\alpha_j)} \leq \check{\mathcal{M}}_{2\sigma_i}^{(\alpha_j)}$  for  $s = r$ , and denoted by  $\check{\mathcal{M}}_1 \subseteq \check{\mathcal{M}}_2$ .

**Remark 3.1.** Sometimes it may be  $s > r$  or  $s < r$ . If  $s > r$ ,  $s$  and  $r$  are equalized by adding  $s - r$  times  $(0,1)/0$  to  $\check{\mathcal{M}}_{2\sigma_i}^{(\alpha_j)}$ . Set of all equalized OIFSMSs on  $U$  and  $\mathfrak{E}$  is denoted by  $\text{EOIFSMS}_{\mathfrak{E}}^U$ . Then, subethood relation is checked. If  $s < r$ , then subethood relation doesn't exist.

**Note 3.1.** Equalization method mentioned above will be used in other set operations such as union, intersection, and so on.

**Example 3.2.** Let us consider the universal set  $U = \{\alpha_1, \alpha_2, \alpha_3\}$  and parameter set  $\mathfrak{E} = \{\sigma_1, \sigma_2\}$ . Assume that  $\text{EOIFSMS}_{\mathfrak{E}}^U$   $\check{\mathcal{M}}_1$  and  $\check{\mathcal{M}}_2$  are given as follows:

$$\begin{aligned} \check{\mathcal{M}}_1 = & \{(\sigma_1\{(\alpha_1, (0.3,0.6)/1 + (0.1,0.5)/2 + (0.2,0.7)/3), (\alpha_2, (0.6,0.4)/2 + (0.5,0.5)/2 + (0.1,0.5)/1 + (0.2,0.7)/1), \\ & (\alpha_3, (0.3,0.6)/1 + (0.1,0.6)/3 + (0.3,0.7)/3 + (0.1,0.8)/2\}), (\sigma_2\{(\alpha_1, (0.2,0.7)/3 + (0.2,0.8)/1 + (0.1,0.8)/2), \\ & (\alpha_2, (0.2,0.5)/2 + (0.3,0.6)/3 + (0.1,0.5)/2 + (0.2,0.8)/4), (\alpha_3, (0.2,0.6)/3 + (0.2,0.8)/2 + (0.1,0.8)/2 + (0.1,0.9)/1\})\} \text{ and} \\ \check{\mathcal{M}}_2 = & \{(\sigma_1\{(\alpha_1, (0.4,0.5)/1 + (0.2,0.4)/2 + (0.3,0.5)/3), (\alpha_2, (0.7,0.2)/3 + (0.5,0.4)/2 + (0.1)/0 + (0.1)/0), \\ & (\alpha_3, (0.3,0.5)/3 + (0.4,0.6)/3 + (0.3,0.7)/2 + (0.1)/0\}), (\sigma_2\{(\alpha_1, (0.3,0.5)/2 + (0.3,0.6)/3 + (0.2,0.7)/1), \\ & (\alpha_2, (0.3,0.3)/2 + (0.5,0.6)/3 + (0.1,0.3)/2 + (0.3,0.7)/4), (\alpha_3, (0.3,0.6)/2 + (0.1)/0 + (0.1)/0 + (0.1)/0\})\}. \end{aligned}$$

Since, for all  $\alpha \in U$   $\check{\mathcal{M}}_{1\sigma_i}^{(\alpha_j)} \leq \check{\mathcal{M}}_{2\sigma_i}^{(\alpha_j)}$ ,  $\check{\mathcal{M}}_1$  subset  $\check{\mathcal{M}}_2$ , i.e.  $\check{\mathcal{M}}_1 \subseteq \check{\mathcal{M}}_2$ .

**Definition 3.4.** Let  $\check{\mathcal{M}} \in \text{OIFSMS}_{\mathfrak{E}}^U$ . If  $\forall \sigma \in \mathfrak{E}$  and  $\forall \alpha \in U$ ,  $\check{\mathcal{M}}_{\sigma_i}^{(\alpha_j)} = (0,1)/1$ , then it is called an empty IFSMS, and denoted by  $\check{\emptyset}_{\mathfrak{E}}$ .

**Definition 3.5.** Let  $\check{\mathcal{M}} \in \text{OIFSMS}_{\mathfrak{E}}^U$ . If  $\forall \sigma \in \mathfrak{E}$  and  $\forall \alpha \in U$ ,  $\check{\mathcal{M}}_{\sigma_i}^{(\alpha_j)} = (1,0)/1$ , then it is called an universal IFSMS, and denoted by  $\check{U}_{\mathfrak{E}}$ .

**Definition 3.6.** Let  $\check{\mathcal{M}}_1, \check{\mathcal{M}}_2 \in \text{OIFSMS}_{\mathfrak{E}}^U$ . If  $\forall \sigma \in \mathfrak{E}$  and  $\forall \alpha \in U$ ,  $\check{\mathcal{M}}_{1\sigma_i}^{(\alpha_j)} = \check{\mathcal{M}}_{2\sigma_i}^{(\alpha_j)}$ , then it is said that  $\check{\mathcal{M}}_1$  equal to  $\check{\mathcal{M}}_2$  and denoted by  $\check{\mathcal{M}}_1 = \check{\mathcal{M}}_2$ .

**Proposition 3.1.** Let  $\check{\mathcal{M}}_1, \check{\mathcal{M}}_2$ , and  $\check{\mathcal{M}}_3 \in \text{OIFSMS}_{\mathfrak{E}}^U$ . Then

1.  $\check{\mathcal{M}}_1 \subseteq \check{U}_{\mathfrak{E}}$
2.  $\check{\emptyset}_{\mathfrak{E}} \subseteq \check{\mathcal{M}}_1$
3.  $\check{\mathcal{M}}_1 \subseteq \check{\mathcal{M}}_1$
4. If  $\check{\mathcal{M}}_1 \subseteq \check{\mathcal{M}}_2$  and  $\check{\mathcal{M}}_2 \subseteq \check{\mathcal{M}}_3$  then  $\check{\mathcal{M}}_1 \subseteq \check{\mathcal{M}}_3$ .

*Proof.* The proofs are clear from Definition 3.3.

**Corollary 3.1.** Let  $\check{\mathcal{M}}_1, \check{\mathcal{M}}_2$ , and  $\check{\mathcal{M}}_3 \in \text{OIFSMS}_{\mathfrak{E}}^U$ . Then,

1. If  $\check{\mathcal{M}}_1 = \check{\mathcal{M}}_2$  and  $\check{\mathcal{M}}_2 = \check{\mathcal{M}}_3$ , then  $\check{\mathcal{M}}_1 = \check{\mathcal{M}}_3$
2. If  $\check{\mathcal{M}}_1 \subseteq \check{\mathcal{M}}_2$  and  $\check{\mathcal{M}}_2 \subseteq \check{\mathcal{M}}_1$ , then  $\check{\mathcal{M}}_1 = \check{\mathcal{M}}_2$ .

**Definition 3.7.** Let  $\dot{\mathcal{M}} \in IFSMS_{\mathfrak{E}}^U$ . Then the complement of  $\dot{\mathcal{M}}$  denoted by  $\dot{\mathcal{M}}^c$ , is defined as follows:

$$\dot{\mathcal{M}}^c = \{(\sigma_i\{(\alpha_j, \sum_{k \in \{1,2,\dots,n\}} (\nu_k(\alpha_j), (\mu_k(\alpha_j))/m_k : m_k \in \mathbb{N}, \alpha_j \in U\}): \sigma_i \in \mathfrak{E}\}.$$

**Example 3.3.** Consider universal set  $U = \{\alpha_1, \alpha_2, \alpha_3\}$  and parameter set  $\mathfrak{E} = \{\sigma_1, \sigma_2\}$ . Assume that IFSMS  $\dot{\mathcal{M}}$  is given as follows:

$$\begin{aligned} \dot{\mathcal{M}} = \{ & (\sigma_1\{(\alpha_1, (0.2,0.4)/2 + (0.3,0.5)/3 + (0.4,0.5)/1), (\alpha_2, (0.4,0.6)/1 + (0.5,0.5)/2 + (0.3,0.4)/1 + (0.7,0.3)/2), \\ & (\alpha_3, (0.3,0.7)/2 + (0.3,0.5)/3 + (0.4,0.6)/3 + (0.6,0.4)/1\}), (\sigma_2\{(\alpha_1, (0.3,0.6)/3 + (0.2,0.7)/1 + (0.3,0.5)/2), \\ & (\alpha_2, (0.3,0.3)/2 + (0.5,0.5)/3 + (0.1,0.3)/2), (\alpha_3, (0.3,0.6)/2 + (0.1,0.9)/1 + (0.1,0.7)/2 + (0.2,0.8)/3\})\}. \end{aligned}$$

Then, the complement of  $\dot{\mathcal{M}}$  can be written as

$$\begin{aligned} \dot{\mathcal{M}}^c = \{ & (\sigma_1\{(\alpha_1, (0.4,0.2)/2 + (0.5,0.3)/3 + (0.5,0.4)/1), (\alpha_2, (0.6,0.4)/1 + (0.5,0.5)/2 + (0.4,0.3)/1 + (0.3,0.7)/2), \\ & (\alpha_3, (0.7,0.3)/2 + (0.5,0.3)/3 + (0.6,0.4)/3 + (0.4,0.6)/1\}), (\sigma_2\{(\alpha_1, (0.6,0.3)/3 + (0.7,0.2)/1 + (0.5,0.3)/2), \\ & (\alpha_2, (0.3,0.3)/2 + (0.5,0.5)/3 + (0.3,0.1)/2), (\alpha_3, (0.6,0.3)/2 + (0.9,0.1)/1 + (0.7,0.1)/2 + (0.8,0.2)/3\})\}. \end{aligned}$$

**Proposition 3.2.** Let  $\dot{\mathcal{M}} \in IFSMS_{\mathfrak{E}}^U$ . Then,

1.  $(\dot{\mathcal{M}}^c)^c = \dot{\mathcal{M}}$
2.  $\dot{\emptyset}_{\mathfrak{E}}^c = \dot{U}_{\mathfrak{E}}^c$

*Proof.* The proofs are clear from Definition 3.7.

**Definition 3.8.** Let  $\ddot{\mathcal{M}}_1 = \{(\sigma_i\{(\alpha_j, \sum_{k \in \{1,2,\dots,s\}} \gamma_{ijk}^1/m_{ijk}^1): m_{ijk}^1 \in \mathbb{N}, \alpha_j \in U\}): \sigma_i \in \mathfrak{E}\}$ ,  $\ddot{\mathcal{M}}_2 = \{(\sigma_i\{(\alpha_j, \sum_{k \in \{1,2,\dots,s\}} \gamma_{ijk}^2/m_{ijk}^2): m_{ijk}^2 \in \mathbb{N}, \alpha_j \in U\}): \sigma_i \in \mathfrak{E}\} \in \mathcal{OIFSMS}_{\mathfrak{E}}^U$ . Intersection of  $\ddot{\mathcal{M}}_1$  and  $\ddot{\mathcal{M}}_2$ , denoted by  $\ddot{\mathcal{M}}_1 \dot{\cap} \ddot{\mathcal{M}}_2$ , is defined as follows:

$$\ddot{\mathcal{M}}_1 \dot{\cap} \ddot{\mathcal{M}}_2 = \{(\sigma_i, \{(\alpha_j, \sum_{k \in \{1,2,\dots,s\}} (\gamma_{ijk}^1 \mathcal{T} \gamma_{ijk}^2) / \min\{m_{ijk}^1, m_{ijk}^2\}: m_{ijk}^1, m_{ijk}^2 \in \mathbb{N}, \alpha_j \in U\}): \sigma_i \in \mathfrak{E}\}.$$

**Proposition 3.3.** Let  $\ddot{\mathcal{M}}_1, \ddot{\mathcal{M}}_2$ , and  $\ddot{\mathcal{M}}_3 \in \mathcal{OIFSMS}_{\mathfrak{E}}^U$ . Then,

1.  $\ddot{\mathcal{M}}_1 \dot{\cap} \ddot{\mathcal{M}}_1 = \ddot{\mathcal{M}}_1$
2.  $\dot{\emptyset}_{\mathfrak{E}} \dot{\cap} \ddot{\mathcal{M}}_1 = \dot{\emptyset}_{\mathfrak{E}}$
3.  $\ddot{\mathcal{M}}_1 \dot{\cap} \dot{U}_{\mathfrak{E}} = \ddot{\mathcal{M}}_1$
4.  $\ddot{\mathcal{M}}_1 \dot{\cap} \ddot{\mathcal{M}}_2 = \ddot{\mathcal{M}}_2 \dot{\cap} \ddot{\mathcal{M}}_1$
5.  $(\ddot{\mathcal{M}}_1 \dot{\cap} \ddot{\mathcal{M}}_2) \dot{\cap} \ddot{\mathcal{M}}_3 = \ddot{\mathcal{M}}_1 \dot{\cap} (\ddot{\mathcal{M}}_2 \dot{\cap} \ddot{\mathcal{M}}_3)$

*Proof.* The proofs are clear from Definition 3.8.

**Definition 3.9.** Let  $\ddot{\mathcal{M}}_1 = \{(\sigma_i\{(\alpha_j, \sum_{k \in \{1,2,\dots,s\}} \gamma_{ijk}^1/m_{ijk}^1): m_{ijk}^1 \in \mathbb{N}, \alpha_j \in U\}): \sigma_i \in \mathfrak{E}\}$ ,  $\ddot{\mathcal{M}}_2 = \{(\sigma_i\{(\alpha_j, \sum_{k \in \{1,2,\dots,s\}} \gamma_{ijk}^2/m_{ijk}^2): m_{ijk}^2 \in \mathbb{N}, \alpha_j \in U\}): \sigma_i \in \mathfrak{E}\} \in \mathcal{OIFSMS}_{\mathfrak{E}}^U$ . Union of  $\ddot{\mathcal{M}}_1$  and  $\ddot{\mathcal{M}}_2$ , denoted by  $\ddot{\mathcal{M}}_1 \dot{\cup} \ddot{\mathcal{M}}_2$ , is defined as follows:

$$\ddot{\mathcal{M}}_1 \dot{\cup} \ddot{\mathcal{M}}_2 = \{(\sigma_i, \{(\alpha_j, \sum_{k \in \{1,2,\dots,s\}} (\gamma_{ijk}^1 \mathcal{S} \gamma_{ijk}^2) / \max\{m_{ijk}^1, m_{ijk}^2\}: m_{ijk}^1, m_{ijk}^2 \in \mathbb{N}, \alpha_j \in U\}): \sigma_i \in \mathfrak{E}\}.$$

**Proposition 3.3.** Let  $\ddot{\mathcal{M}}_1, \ddot{\mathcal{M}}_2$ , and  $\ddot{\mathcal{M}}_3 \in \mathcal{OIFSMS}_{\mathfrak{E}}^U$ . Then,

1.  $\ddot{\mathcal{M}}_1 \dot{\cup} \ddot{\mathcal{M}}_1 = \ddot{\mathcal{M}}_1$
2.  $\dot{\emptyset}_{\mathfrak{E}} \dot{\cup} \ddot{\mathcal{M}}_1 = \ddot{\mathcal{M}}_1$
3.  $\ddot{\mathcal{M}}_1 \dot{\cup} \dot{U}_{\mathfrak{E}} = \dot{U}_{\mathfrak{E}}$
4.  $\ddot{\mathcal{M}}_1 \dot{\cup} \ddot{\mathcal{M}}_2 = \ddot{\mathcal{M}}_2 \dot{\cup} \ddot{\mathcal{M}}_1$
5.  $(\ddot{\mathcal{M}}_1 \dot{\cup} \ddot{\mathcal{M}}_2) \dot{\cup} \ddot{\mathcal{M}}_3 = \ddot{\mathcal{M}}_1 \dot{\cup} (\ddot{\mathcal{M}}_2 \dot{\cup} \ddot{\mathcal{M}}_3)$

*Proof.* The proofs are clear from Definition 3.9.

**Example 3.4.** Let us consider the universal set  $U = \{\alpha_1, \alpha_2, \alpha_3\}$  and parameter set  $\mathfrak{E} = \{\sigma_1, \sigma_2\}$ . Assume that  $\mathcal{EOIFSMS}$ s  $\tilde{\mathcal{M}}_1$  and  $\tilde{\mathcal{M}}_2$  are given as follows:

$$\begin{aligned} \tilde{\mathcal{M}}_1 = & \{(\sigma_1\{(\alpha_1, (0.3, 0.6)/1 + (0.1, 0.5)/2 + (0.2, 0.7)/3), (\alpha_2, (0.6, 0.4)/2 + (0.5, 0.5)/2 + (0.1, 0.5)/1 + (0.2, 0.7)/1), \\ & (\alpha_3, (0.3, 0.6)/1 + (0.1, 0.6)/3 + (0.3, 0.7)/3 + (0.1, 0.8)/2)\}, (\sigma_2\{(\alpha_1, (0.2, 0.7)/3 + (0.2, 0.8)/1 + (0.1, 0.8)/2), \\ & (\alpha_2, (0.2, 0.5)/2 + (0.3, 0.6)/3 + (0.1, 0.5)/2 + (0.2, 0.8)/4), (\alpha_3, (0.2, 0.6)/3 + (0.2, 0.8)/2 + (0.1, 0.8)/2 + (0.1, 0.9)/1)\}) \text{ and} \\ \tilde{\mathcal{M}}_2 = & \{(\sigma_1\{(\alpha_1, (0.4, 0.5)/1 + (0.2, 0.4)/2 + (0.3, 0.5)/3), (\alpha_2, (0.7, 0.2)/3 + (0.5, 0.4)/2 + (0.1)/0 + (0.1)/0), \\ & (\alpha_3, (0.3, 0.5)/3 + (0.4, 0.6)/3 + (0.3, 0.7)/2 + (0.1)/0)\}, (\sigma_2\{(\alpha_1, (0.3, 0.5)/2 + (0.3, 0.6)/3 + (0.2, 0.7)/1), \\ & (\alpha_2, (0.3, 0.3)/2 + (0.5, 0.6)/3 + (0.1, 0.3)/2 + (0.3, 0.7)/4), (\alpha_3, (0.3, 0.6)/2 + (0.1)/0 + (0.1)/0 + (0.1)/0)\}). \text{ Then} \\ \tilde{\mathcal{M}}_1 \tilde{\cap} \tilde{\mathcal{M}}_2 = & \{(\sigma_1\{(\alpha_1, (0.3, 0.6)/1 + (0.1, 0.5)/2 + (0.2, 0.7)/3), (\alpha_2, (0.6, 0.4)/2 + (0.5, 0.5)/2 + (0.1)/0 + (0.1)/0), \\ & (\alpha_3, (0.3, 0.6)/1 + (0.1, 0.6)/3 + (0.3, 0.7)/3 + (0.1)/0)\}, (\sigma_2\{(\alpha_1, (0.2, 0.7)/3 + (0.2, 0.8)/1 + (0.1, 0.8)/2), \\ & (\alpha_2, (0.2, 0.5)/2 + (0.3, 0.6)/3 + (0.1, 0.5)/2 + (0.2, 0.8)/4), (\alpha_3, (0.2, 0.6)/3 + (0.1)/0 + (0.1)/0 + (0.1)/0)\}) \text{ and} \\ \tilde{\mathcal{M}}_1 \tilde{\cup} \tilde{\mathcal{M}}_2 = & \{(\sigma_1\{(\alpha_1, (0.4, 0.5)/1 + (0.2, 0.4)/2 + (0.3, 0.5)/3), (\alpha_2, (0.7, 0.2)/3 + (0.5, 0.4)/2 + (0.1, 0.5)/1 + (0.2, 0.7)/1), \\ & (\alpha_3, (0.3, 0.5)/3 + (0.4, 0.6)/3 + (0.3, 0.7)/2 + (0.1, 0.8)/2)\}, (\sigma_2\{(\alpha_1, (0.3, 0.5)/2 + (0.3, 0.6)/3 + (0.2, 0.7)/1), \\ & (\alpha_2, (0.3, 0.3)/2 + (0.5, 0.6)/3 + (0.1, 0.3)/2 + (0.3, 0.7)/4), (\alpha_3, (0.3, 0.6)/2 + (0.2, 0.8)/2 + (0.3, 0.7)/3 + (0.1, 0.8)/2)\}). \end{aligned}$$

**Remark 3.2.** Let  $\tilde{\mathcal{M}} \in \mathcal{EOIFSMS}_{\mathfrak{E}}^U$ . If  $\tilde{\mathcal{M}} \neq \tilde{U}_{\mathfrak{E}}$  or  $\tilde{\mathcal{M}} = \tilde{\emptyset}_{\mathfrak{E}}$ , then  $\tilde{\mathcal{M}} \tilde{\cup} \tilde{\mathcal{M}}^c \neq \tilde{U}_{\mathfrak{E}}$  and  $\tilde{\mathcal{M}} \tilde{\cap} \tilde{\mathcal{M}}^c \neq \tilde{\emptyset}_{\mathfrak{E}}$ .

## Acknowledgment

In this study, the financial support was provided by The Scientific and Technological Research Council of Turkey (TUBITAK), 2211/A - Domestic Doctorate Scholarship Program. The author would like to thanks to all supporters due to their precious contributions.

## References

- [1] Zadeh, L. A. (1965). Fuzzy Sets, *Information and Control*, 8, 338-353.
- [2] Atanassov, K. (1986). Intuitionistic fuzzy sets, *Fuzzy Set and Systems*, 20, 87-96.
- [3] Pawlak, Z. (1982). Rough sets. *Int J Comput Inform Sci*, 11(5), 341-356.
- [4] Molodtsov, D. A. (1999). Soft set theory-First results, *Computer and Mathematics with Applications*, 37, 19-31.
- [5] Smarandache, F. (1999). *A unifying feld in logics. Neutrosophy: neutrosophic probability, set and logic*, American Research Press, Rehoboth.
- [6] Yager, R. R. (1986). On the theory of bags, *Int. J. General Systems*, 13, 23-37.
- [7] Maji, P.K., Biswas, R., & Roy, A.R. (2003). Soft set theory. *Computers and Mathematics with Applications*, 41(4), 555-562.
- [8] Miyamoto, S. (2001). Fuzzy Multisets and Their Generalizations. In: Calude, C.S., Păun, G., Rozenberg, G., Salomaa, A. (eds) Multiset Processing. WMC 2000. Lecture Notes in Computer Science, vol 2235. Springer, Berlin, Heidelberg.
- [9] Zhang, Z., Yang, J., Ye, Y., Hu, Y., & Zhang, Q. (2013). Intuitionistic fuzzy soft set theory and its decision making, *Journal of Intelligent Fuzzy Systems*, 24(4), 829-836.
- [10] Deschrijver, D., & Kerre, E. (2002). A generalisation of operators on intuitionistic fuzzy sets using triangular norms and conorms. Notes on Intuitionistic Fuzzy Sets. 1.
- [11] Shinoj, T.K., & Sunil, J.J. (2012). Intuitionistic fuzzy multisets and its application in medical diagnosis, *International Journal of Mathematical and Computational Sciences*, 6, 34-37.
- [12] Çağman, N., & Enginoğlu, S. (2010). Soft set theory and uni-int decision making. *European J. Oper. Res.*, 207, 848-855.
- [13] Maji, P. K., Biswas, R., & Roy, A. R. (2001) Intuitionistic fuzzy soft sets, *J. Fuzzy Math.*, 9(3) 677-692.
- [14] Çağman, N., & Karataş, S. (2013). Intuitionistic fuzzy soft set theory and its decision making, *Journal of Intelligent Fuzzy Systems*, 24(4), 829-836.



# Numerical study of flow and heat transfer of nanofluids in a ribbed channel with winglets

Selma AKCAY<sup>1,\*</sup> 

<sup>1</sup>Engineering Faculty, Mechanical Engineering Department, Cankiri Karatekin University, Cankiri, Turkey

## Abstract

This study numerically investigates the flow and heat transfer of CuO-water nanofluid in a ribbed channel with winglets at its center. Analyses are performed with the Computational Fluid Dynamics (CFD) based ANSYS Fluent program. Governing equations are solved with the SIMPLE algorithm. The upper and lower surfaces of the channel consist of V-shaped ribs, and discrete V-shaped winglets are placed in the center of the channel. In the study, the nanoparticle volume fraction is kept constant at  $\phi = 5\%$ , and the Reynolds number (Re) varied between 100 and 600. The upper and lower ribbed surfaces are protected at a constant temperature of  $T_w = 360$  K. The study results are given in terms of Nusselt number (Nu), and relative friction factor (r). In addition, the solutions are compared to the ribbed channel without winglets for the base fluid. The flow and temperature distributions are obtained at different Re for the ribbed channel with/without winglets. The results show that the CuO-water nanofluid and winglets contribute significantly to the heat transfer, but the friction factor is slightly increased. Nusselt number increases with increasing Reynolds number. In the channel with winglets for nanofluid flow, the heat transfer improvement is 1.32 times higher than the base fluid flow of the channel without winglets.

**Keywords:** Ribbed channel, Winglet, Nanofluids, Heat transfer, Friction factor

## 1. Introduction

Passive methods are often used to increase heat transfer without reducing the overall efficiency of thermal devices. These methods are applications such as baffles, fins, winglets, vortex generators and ribbed/grooved surfaces in different configurations. These applications are preferred in refrigeration and air conditioning systems, transportation, nuclear reactors, heat exchangers, solar air heaters, chemical or food processing such as many fields. This method is economical compared to other techniques as it does not require external power [1-5].

Grooved channels are preferred in many engineering applications. These surfaces both increase surface area and cause self-flow oscillation. Thus, these channels have an important role in increasing thermal performance. This enhancement substantially depends on the channel geometry [6,7]. Several passive methods are used simultaneously to further improve heat transfer. Extended surfaces such as ribs/fins are generally used to increase the heat transfer area. Many studies investigated the flow and heat transfer in channel with baffles [8-10]. Promvonge et al. [11] examined heat transfer in a channel with horseshoe baffles. They declared that the heat transfer increased by approximately 92-208% and the pressure drop increased by 1.76-6.37 compared to straight channels. Kumar et al. [12] studied heat transfer of the solar air duct using multiple V-type baffles. Menni et al. [13] examined the flow and heat transfer of S-shaped baffles in the solar air duct. They reported that the highest thermal enhancement was found about 1.513 at  $Re = 32000$  and S-downstream. Luan and Phu [14] suggested correlations for flow and heat transfer of an air heater duct with curved baffles. Bensaci et al. [15] investigated heat transfer of air heater with different baffle positions. The results shown that the highest heat transfer was obtained when the baffles were placed in the first half of the duct. Wang et al. [16] studied the effects on heat transfer of parameters such as different rib parameters, radiation intensity, mass flow rate in the solar air heater. They reported that the thermal performance of the duct with S-shaped rib increased up to 48% compared to the straight duct. Modi and Rathod [17] examined the effects of vortex generator on heat transfer in the wavy channels for  $400 \leq Re \leq 1000$ . They declared that vortex shapes significantly affected the flow and thermal performance. Promvonge et al. [18] experimentally and numerically investigated the heat transfer at  $4200 \leq Re \leq 25800$  in a heat exchanger with discrete V winglets. The results reported that at a specific winglet height, the smallest pitch length ensured the highest Nu and pressure drop.

\*Corresponding author. e-mail address: selma.352@hotmail.com

On the other hand, conventional fluids (water, ethylene glycol, and oil etc.) have low thermal properties. Nanoparticles use to increase the thermal conductivity of these fluids. Some researchers have used nanofluids together with other passive techniques [19-21]. Manca et al. [22] studied the flow and heat transfer for  $20000 \leq Re \leq 60000$  of  $Al_2O_3$ -water nanofluid at different rib heights and nanoparticle volume ratios ( $0\% \leq \phi \leq 4\%$ ) in a channel. As a result, they reported that as  $Re$  and particle volume ratio increased, the heat transfer improved, and the pumping power increased. Menni et al. [23] investigated the hydraulic and thermal performance of nanofluids in turbulent flow conditions by using baffles at different angles in the channel and reported that the highest thermal improvement was obtained when vertical baffles were used at high  $Re$ . Qi et al. [24] numerically and experimentally researched the flow and heat transfer of  $TiO_2$ -water nanofluid in a wavy channel. Pordanjani et al. [25] carried out a review study examining the effects of nanofluid applications on energy savings in heat exchangers. Kaood and Hassan [26] numerically investigated the flow and heat transfer improvement and energy performance of different nanofluids in different wavy channels. They reported that nanofluids increased heat transfer according to smooth channel, and all performance improvement decreased at  $Re \geq 10000$  for all fluids and channel configurations. The thermal, frictional and exergy behavior of triangular vortex generator in a channel with different cross-sectional areas were examined by Tian et al. [27]. In their study, air, water and two different nanofluids ( $Al_2O_3$ -water and  $CuO$ -water) were used. They declared that the most thermal enhancement was obtained the circular cross section and the vortex generators enhanced significantly the  $Nu$  when the nanofluids are employed as the working fluid. However, nanofluids caused more exergy destruction as well.

As seen from previous studies, there are many experimental and numerical studies investigating the combined impact of passive heat transfer applications. However, the large number of investigated parameters increases the efforts to find the optimum parameters. As shown above, further studies on nanofluid flow in a ribbed channel with winglets are needed. Effect of discrete V-shaped winglets in a V-shaped ribbed channel geometry was not investigated. In the presented study, the effects of both ribbed channel and winglets on the nanofluid flow and heat transfer were investigated together. The effects on flow and heat transfer of  $CuO$ -water nanofluid at constant particle volume fraction ( $\phi = 0.05$ ) under laminar flow condition ( $100 \leq Re \leq 600$ ) in this channel were numerically examined.

## 2. Materials and Methods

### 2.1. Numerical Model

Figure 1 shows the geometry (a) and mesh structure (b) of the ribbed channel with winglets. The height of channel is  $D = 19$  mm. At the inlet and outlet of channel, there are the unheated flat sections  $L_1 = 5D$  and  $L_2 = 10D$ , respectively.

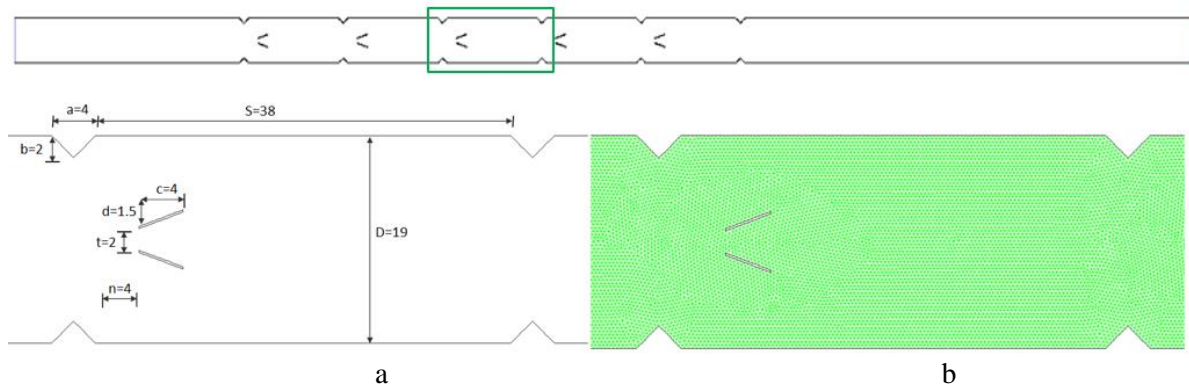


**Figure 1.** (a) Geometry of the numerical model (dimensions are mm), and (b) mesh structure of the ribbed channel with winglets.

Fluid is incompressible, single phase and Newtonian type. The flow is steady, 2-d, and laminar regime. Gravity and heat transfer with radiation are ignored. The governing equations are given as follows.

$$\frac{\partial u}{\partial x} + \frac{\partial v}{\partial y} = 0 \quad (1)$$



$$u \frac{\partial u}{\partial x} + v \frac{\partial u}{\partial y} = -\frac{1}{\rho_{nf}} \frac{\partial P}{\partial x} + \vartheta_{nf} \left( \frac{\partial^2 u}{\partial x^2} + \frac{\partial^2 u}{\partial y^2} \right) \quad (2)$$

$$u \frac{\partial v}{\partial x} + v \frac{\partial v}{\partial y} = -\frac{1}{\rho_{nf}} \frac{\partial P}{\partial y} + \vartheta_{nf} \left( \frac{\partial^2 v}{\partial x^2} + \frac{\partial^2 v}{\partial y^2} \right) \quad (3)$$

$$u \frac{\partial T}{\partial x} + v \frac{\partial T}{\partial y} = \alpha_{nf} \left( \frac{\partial^2 T}{\partial x^2} + \frac{\partial^2 T}{\partial y^2} \right) \quad (4)$$

## 2.2. Numerical Procedure

The numerical solutions are carried out with the FLUENT 15.0 program [28]. The simulations are solved with the SIMPLE algorithm. 176144 element numbers were adopted to the numerical model. The inlet temperature of fluid is  $T_{in} = 300$  K. The upper and lower ribbed surfaces are maintained at a constant temperature of  $T_w = 360$  K and the winglets are defined adiabatic wall conditions. A non-slip and adiabatic boundary condition are applied for the straight section at inlet and outlet of the channel. For the validity of the solutions, the numerical results of this study are compared with the experimental study conducted by Meyer and Abolarin [29]. The agreement between the results of both studies in Ref. [30] was given.

The Nusselt number is calculated given by

$$Nu = \frac{hD_h}{k_f} \quad (5)$$

where  $D_h$  is the hydraulic diameter,  $k_f$  is the thermal conductivity,  $h$  is heat convective coefficient.

The average Nusselt number is calculated as follows

$$Nu = \frac{1}{L} \int_0^L Nu_x dx \quad (6)$$

The friction factor ( $f$ ) is defined as

$$f = \frac{\Delta P D_h}{0.5 L \rho u^2} \quad (7)$$

where,  $\Delta P$  is the pressure difference at the inlet and outlet of the channel. Relative friction factor is defined as

$$r = \frac{f_{(r,w,n)}}{f_{(r)}} \quad (8)$$

where  $f_{(r,w,n)}$  and  $f_{(r)}$  are friction factor for the nanofluids flow in the ribbed channel with winglets and friction factor for the base fluid in the ribbed channel without winglet, respectively.  $f_{(r,w)}$  is friction factor for the base fluid in the ribbed channel with winglets. The CuO nanoparticles with the volume fraction of  $\phi = 5\%$  in pure water was used as the nanofluid. The thermo-physical properties of the nanofluid were calculated with the Ref. [27].

## 3. Results and Discussion

In this section, the velocity, temperature and vorticity contours were obtained in the ribbed channel with/without winglets to explain the flow and heat transfer mechanism. Figure 2 shows the velocity, temperature and vorticity contours for the base fluid in the ribbed channel without winglets at  $Re = 100$  (a) and  $Re = 600$  (b). It was seen that the ribbed channel structure affected the flow and temperature fields depending on  $Re$ . It was observed that with increasing  $Re$ , the fluid velocity increased, the surface temperature of the channel decreased, and the longitudinal vortex structures increased due to the cross-section narrowing in the grooved sections.

Figure 3 indicates the velocity, temperature, and vorticity contours in the CuO-water nanofluid at  $\phi = 0.05$  in the ribbed channel with winglets for  $Re = 100$  (a), and  $Re = 600$  (b). The winglets have changed the flow and temperature fields depending on  $Re$ . The winglets directed the cold fluid towards the channel surfaces and flow oscillations occurred in the channel. Due to the winglets, the temperature gradient on the channel surfaces decreased considerably with increasing  $Re$ , the seconder flow loops were concentrated throughout the channel, and the heat transfer was improved due to a homogeneous flow mixing.

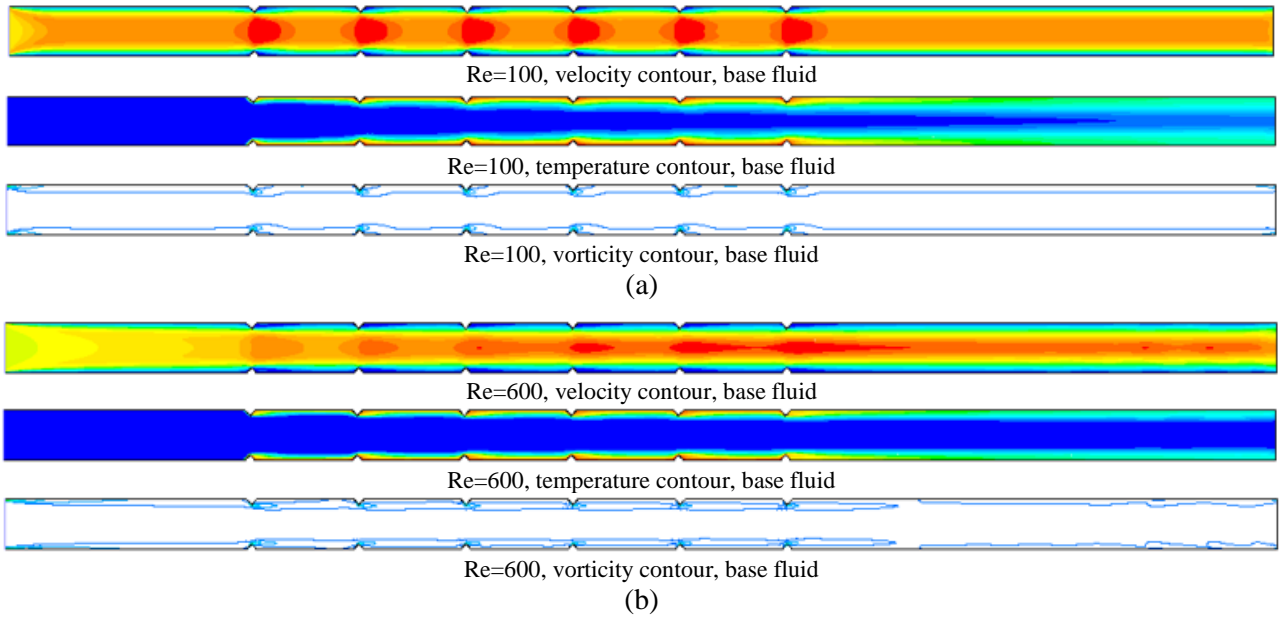


**Figure 2.** The velocity, temperature and vorticity contours for base fluid in the ribbed channel without winglets, a)  $Re=100$ , b)  $Re=600$ .

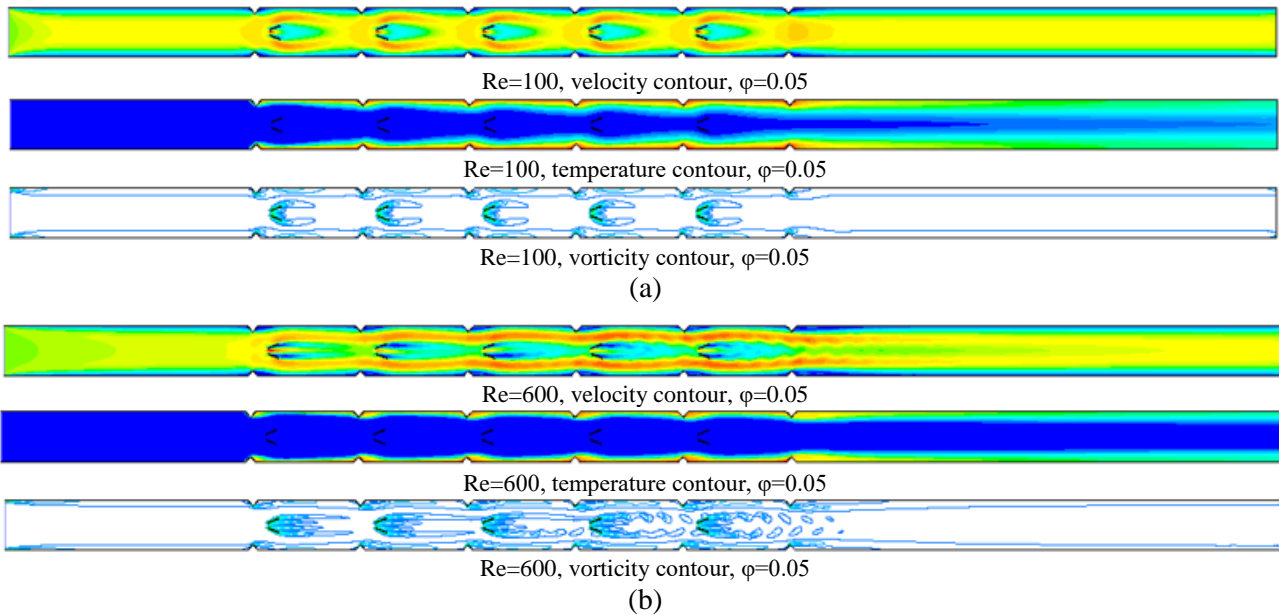


**Figure 3.** The velocity, temperature and vorticity contours for CuO-water nanofluid at  $\phi=0.05$  in the ribbed channel with winglets, a)  $Re=100$ , b)  $Re=600$ .

Figures 4a and 4b show  $Nu$  (a) and the relative friction factor (b) with  $Re$  in the ribbed channel with/without winglets for the nanofluid and base fluid flow, respectively. The dashed line represents the base fluid for the ribbed channel without winglets.  $Nu_{(r,w,n)}$  is  $Nu$  for the nanofluids flow in the ribbed channel with winglets,  $Nu_{(r,w)}$  is  $Nu$  for the base fluid in the ribbed channel with winglets, and  $Nu_{(r)}$  is  $Nu$  for the base fluid in the ribbed channel without winglet. From Figure 4a, it is visible that the Nusselt number increases with increasing  $Re$  for all channel structures. The highest  $Nu$  was found to be about  $Nu = 5.38$  in the ribbed channel with winglets for  $Re = 600$  and  $\phi=0.05$ . In the ribbed channel with winglets for CuO-water nanofluid flow, the heat transfer improved by about 1.32 compared to the ribbed channel without winglets for base fluid. Although heat transfer is increased with the addition of winglets, the pressure drop within the channel also increases due to the decreasing flow field effects. It can be visible in Figure 4b that the relative friction factor increases as the  $Re$

increases compared to the channel without winglets. The highest relative friction factor was obtained to be about 1.42 for  $Re = 600$  and  $\phi = 0.05$ .

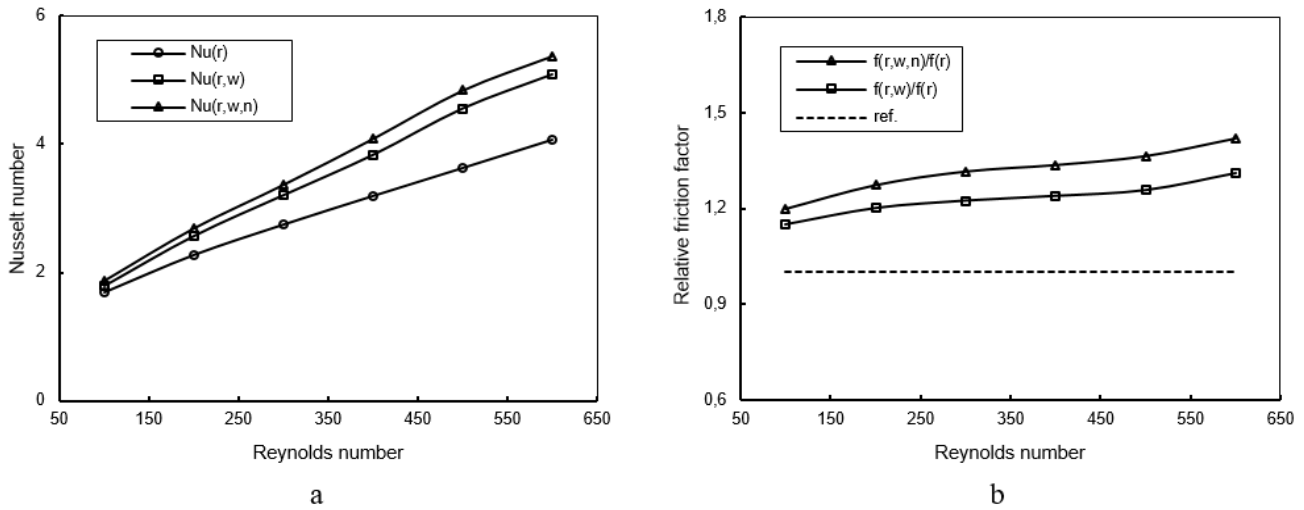


**Figure 4.** a) Nusselt number, b) Relative friction factor with  $Re$ .

#### 4. Conclusion

In the present study, the heat transfer and friction factor of CuO-water nanofluids flow in a ribbed channel with/without winglets were investigated numerically. The study was also compared to the base fluid of the ribbed channel without winglets. The velocity, temperature, and vorticity contours were presented in the channel to understand the flow and heat transfer behaviors. The results of the study indicated that the contours were highly influenced by channel geometry. There is a significant effect of winglets and CuO-water nanofluid on heat transfer improvement. In the channel with winglets for nanofluid flow, the heat transfer is 1.32 times higher than the base fluid of the channel without winglets. The relative friction factor increased with  $Re$ . CuO-water nanofluid in the ribbed channel with winglets provided considerable improvement in heat transfer, while an acceptable increase in friction factor was seen. The highest  $Nu$  was obtained as 5.38 at  $Re = 600$  and  $\phi = 0.05$ . The highest relative friction factor was found to be 1.42 at  $Re = 600$  and  $\phi = 0.05$ .

#### References

- [1] Skullong, S., Promvong, P., Thianpong, C., & Pimsarn, M. (2016). Thermal performance in solar air heater channel with combined wavy-groove and perforated-delta wing vortex generators. *Applied Thermal Engineering*, 100, 611–620.
- [2] Menasria, F., Zedairia, M., & Moummi, A. (2017). Numerical study of thermohydraulic performance of solar air heater duct equipped with novel continuous rectangular baffles with high aspect ratio. *Energy*, 133, 593–608.
- [3] Promvong, P., & Skullong, S. (2020). Thermo-hydraulic performance in heat exchanger tube with V-shaped winglet vortex generator. *Applied Thermal Engineering*, 164, 114424.
- [4] Sun, Z., Zhang, K., Li, W., Chen, Q., & Zheng, N. (2020). Investigations of the turbulent thermal-hydraulic performance in circular heat exchanger tubes with multiple rectangular winglet vortex generators. *Applied Thermal Engineering*, 168, 114838.
- [5] Nakhchi, M.E., Hatami, M., & Rahmati, M. (2021). Experimental investigation of performance improvement of double-pipe heat exchangers with novel perforated elliptic turbulators. *International Journal of Thermal Sciences*, 168, 107057.
- [6] Nakhchi, M.E. (2019). Experimental optimization of geometrical parameters on heat transfer and pressure drop inside sinusoidal wavy channels. *Thermal Science and Engineering Progress*, 9, 121–31.
- [7] Tokgoz, N., Tunay, T., & Sahin, B. (2018). Effect of corrugated channel phase shifts on flow structures and heat transfer rate. *Experimental Thermal and Fluid Science*, 99, 374–391.
- [8] Sripattanapipat, S., & Promvong, P. (2009). Numerical analysis of laminar heat transfer in a channel with diamond-shaped baffles. *International Communications in Heat and Mass Transfer*, 36 (1), 32–38.

- [9] Kwankaomeng, S., & Promvonge, P. (2010). Numerical prediction on laminar heat transfer in square duct with 30° angled baffle on one wall. *International Communications in Heat and Mass Transfer*, 37, 857-866.
- [10] Surendhar, G., Srinivasan, G., Muthukumar, P., & Senthilmurugan, S. (2021). Performance analysis of arc rib fin embedded in a solar air heater. *Thermal Science and Engineering Progress*, 23, 100891.
- [11] Promvonge, P., Tamna, S., Pimsarn, M., & Thianpong, C. (2015). Thermal characterization in a circular tube fitted with inclined horseshoe baffles. *Applied Thermal Engineering*, 75, 1147–1155.
- [12] Kumar, R., Kumar, A., Chauhan, R., & Sethi, M. (2016). Heat transfer enhancement in solar air channel with broken multiple V-type baffle. *Case Studies in Thermal Engineering*, 8, 187–197.
- [13] Menni, Y., Azzi, A., Chamkha, A.J., & Harmand, S. (2019). Analysis of fluid dynamics and heat transfer in a rectangular duct with staggered baffles. *Journal of Applied and Computational Mechanics*, 5(2), 231-248.
- [14] Luan, N.T., & Phu, N.M. (2020). Thermohydraulic correlations and exergy analysis of a solar air heater duct with inclined baffles. *Case Studies in Thermal Engineering*, 21, 100672.
- [15] Bensaci, C.E., Moummi, A., Sanchez de la Flor, F.J., Rodriguez Jara, E.A., Rincon-Casado, A., & Ruiz-Pardo, A. (2020). Numerical and experimental study of the heat transfer and hydraulic performance of solar air heaters with different baffle positions. *Renewable Energy*, 155, 1231–1244.
- [16] Wang, D., Liu, J., Liu, Y., Wang, Y., Li, B., & Liu, J. (2020). Evaluation of the performance of an improved solar air heater with “S” shaped ribs with gap. *Solar Energy*, 195, 89–101.
- [17] Modi, J.A., & Rathod, M.K. (2019). Comparative study of heat transfer enhancement and pressure drop for fin-and-circular tube compact heat exchangers with sinusoidal wavy and elliptical curved rectangular winglet vortex generator. *International Journal of Heat and Mass Transfer*, 141, 310- 326.
- [18] Promvonge, P., Promthaisong, P., & Skullong, S. (2020). Experimental and numerical heat transfer study of turbulent tube flow through discrete V-winglets. *International Journal of Heat and Mass Transfer*, 151, 119351.
- [19] Kakac, S., & Pramuanjaroenkij, A. (2009). Review of convective heat transfer enhancement with nanofluids. *International Journal of Heat and Mass Transfer*, 52, 3187–3196.
- [20] Karoui, S.H.H., Ajarostaghi, S.S.M., Bandpy, M.G., & Fard, S.R.H. (2021). Laminar heat transfer and fluid flow of two various hybrid nanofluids in a helical double pipe heat exchanger equipped with an innovative curved conical turbulator. *Journal of Thermal Analysis and Calorimetry*, 143, 1455–1466.
- [21] Ajeel, R.K., Sopian, K., & Zulkifli, R. (2021). Thermal-hydraulic performance and design parameters in a curved-corrugated channel with L-shaped baffles and nanofluid. *Journal of Energy Storage*, 34, 101996.
- [22] Manca, O., Nardini, S., & Ricci, D. (2012). A numerical study of nanofluid forced convection in ribbed channels. *Applied Thermal Engineering*, 37, 280-297.
- [23] Menni, Y., Chamkha, A.J., Ghazvini, M., Ahmadi, M.H., Ameer, H., Issakhov, A., & Inc, M. (2021). Enhancement of the turbulent convective heat transfer in channels through the baffling technique and oil/multiwalled carbon nanotube nanofluids. *Numerical Heat Transfer, Part A: Applications*, 79 (4), 311-351.
- [24] Qi, C., Wan, Y.L., Li, C.Y., Han, D.T., & Rao, Z.H. (2017). Experimental and numerical research on the flow and heat transfer characteristics of TiO<sub>2</sub>-water nanofluids in a corrugated tube. *International Journal of Heat and Mass Transfer*, 115: 1072–1084.
- [25] Pordanjani, A. H., Aghakhani, S., Afrand, M., Mahmoudi, B., Mahian, O., & Wongwises, S. (2019). An updated review on application of nanofluids in heat exchangers for saving energy. *Energy Conversion Management*, 198, 111886.
- [26] Kaood, A., & Hassan, M.A. (2020). Thermo-hydraulic performance of nanofluids flow in various internally corrugated tubes. *Chemical Engineering & Processing: Process Intensification*, 154, 08043.
- [27] Tian, M.-W., Khorasani, S., Moria, H., Pourhedayat, S., & Dizaji, H.S. (2020). Profit and efficiency boost of triangular vortex-generators by novel techniques. *International Journal of Heat and Mass Transfer*, 156, 119842.
- [28] ANSYS Inc., (2015). ANSYS Fluent user guide & theory guide- Release 15.0. USA.
- [29] Meyer, J.P., & Abolarin, S.M. (2018). Heat transfer and pressure drop in the transitional flow regime for a smooth circular tube with twisted tape inserts and a square-edged inlet. *Int. Journal of Heat and Mass Transfer*, 117, 11-29.
- [30] Akcay S. (2023). Numerical analysis of hydraulic and thermal performance of Al<sub>2</sub>O<sub>3</sub>-water nanofluid in a zigzag channel with central winglets. *Gazi University Journal of Science*, 36 (2), (in press) DOI: 10.35378/gujs.1012201.



# Fabrication and Characterization of Molybdenum Doped ZnO Nanorods via Ultrasonic Spray Pyrolysis

**Hakan ÇOLAK**<sup>1,2\*</sup> 

<sup>1</sup>Science Faculty, Chemistry Department, Çankırı Karatekin University, Çankırı, Türkiye

<sup>2</sup> Central Research Laboratory (ÇANKAM), Çankırı Karatekin University, Çankırı, Türkiye

## Abstract

Molybdenum metal doped ZnO nanorods were fabricated on a glass substrate via ultrasonic spray pyrolysis technique. The doping concentrations were in the range of 1 and 10 mol %. The crystallographic properties of the resulting ZnO samples were analyzed by the x-ray diffraction (XRD) method. According to the XRD analysis, it was determined that the lattice structure of the samples belonged to the hexagonal (wurtzite) unit cell. According to the XRD peaks it was understood that the crystals grow in the c-axis (002) direction. The morphological characteristics of the obtained thin films were analyzed by scanning electron microscopy (SEM). The presence of Mo ions in the samples was confirmed via energy dispersive x-ray spectroscopy (EDX) analysis. The optical transmittances of the samples were measured by ultraviolet / visible spectrophotometer (UV/VIS) at a wavelength of 300-1000 nm. It was observed that the produced films had high optical transparency.

**Keywords:** 1D nanostructure, ZnO, Metal doping, Ultrasonic spray pyrolysis method.

## 1. Introduction

One of the most important problems in our world is meeting the need for environmentally friendly and sustainable energy. One of the best approaches to solving this important problem is to obtain electrical energy from solar energy. Photovoltaic (PV) solar cells are best practices for converting solar energy into electrical energy. Optoelectronic devices in systems with technological and industrial application areas, especially photovoltaic cells, generally require the use of a transparent electrode. For this purpose, n-type transparent conductive oxide (TCO) semiconductors with high optical transmittance and electrical conductivity and high chemical and thermal stability are preferred [1]. Tin-doped indium oxide (ITO) and fluorine-doped tin oxide (FTO) are the most known and preferred TCO materials. However, ITO has some disadvantages such as low stability, toxicity, limited indium sources, as well as high cost. On the other hand, the use of indium-free FTO films is more limited due to the low conductivity and chemical stability of this material compared to ITO. Other than these, zinc oxide (ZnO)-based materials, which can be produced more economically and easily, have attracted attention recently. ZnO is chemically and thermally stable, as well as suitable for use in optoelectronic devices [2]. ZnO is a semiconductor material with a wide band gap (3.37 eV) and large exciton binding energy (60 meV) at room temperature. Many technological application areas are foreseen for ZnO materials with their structural, optical, and piezoelectric properties. Recently, the investigation of 1D nanostructures has been one of the most interesting topics in physics, chemistry, and materials science. These structures offer new opportunities for designing new generation, high-efficiency solar cells, especially with large surface areas [3]. However, these properties are not stable because atmospheric oxygen adsorbs onto the ZnO surface. It is necessary the metallic doping to stabilize ZnO against these changes, and to further develop its properties [4]. The doping process happens in the form of the displacement of the ions of the doping element with  $Zn^{2+}$  ions which are in the unit cell of the ZnO. When ions that have higher valance than  $Zn^{2+}$  enter the unit cell, there is an increase in electron concentration in the ZnO crystal lattice and, as a result, an increase in electrical conductivity [5].

In the present study, with the motivation that optical transmittance and high electrical conductivity are important for TCO materials, molybdenum (Mo)-doped ZnO NRs were produced via an ultrasonic spray pyrolysis system. Mo is a group VI-B element, and the valence state is  $5s^1 4d^5$ . Therefore, Mo is thought to be a suitable dopant for ZnO.

\* Corresponding author. e-mail address: hakancolak@karatekin.edu.tr

## 2. Materials and Methods

### 2.1. Producing the samples

Production of ZnO nanorod structures on glass substrate was carried out in two steps. In the first step, ZnO seed layer was produced on the cleaned glass substrate with an ultrasonic spray pyrolysis system (USP, HO-TH-04, HOLMARC, India). The produced seed layer acts as nucleation in the growth of nanorod structures. At this stage, the stock solution with a concentration of 0.5 M was used as the coating solution. The stock solution was prepared by dissolving  $\text{Zn}(\text{CH}_3\text{COO})_2 \cdot 2\text{H}_2\text{O}$  (Sigma-Aldrich, 99-102 %) in 2-methoxyethanol (Sigma-Aldrich,  $\geq 99.3$  %). Monoethanolamine (MEA, Merck,  $\geq 99.5\%$ ) was added to the solution as a stabilizer (molar ratio of  $\text{Zn}^{2+}/\text{MEA}$  was 1:1). The USP process parameters used for seed layer production are listed in table 1. In the second step, undoped and Mo-doped ZnO nanorod structures were produced on ZnO seeded glass substrates by the USP technique. For the production of undoped ZnO nanorod structures, 0.1 M  $\text{Zn}(\text{NO}_3)_2 \cdot 6\text{H}_2\text{O}$  (Sigma-Aldrich,  $\geq 99.0$  %) aqueous solution was prepared, and hexamethylenetetramine (HMT, Sigma-Aldrich,  $\geq 99.5$  %) was added into the solution as a stabilizer (molar ratio of  $\text{Zn}^{2+}/\text{HMT}$  was 1:1). For the production of Mo-doped ZnO nanorod structures, 0.5 M  $\text{Zn}(\text{NO}_3)_2 \cdot 6\text{H}_2\text{O}$  aqueous solution was prepared, and  $\text{MoCl}_5$  (Sigma-Aldrich,  $\geq 99.9$  %) was added to this solution at stoichiometric ratios of 1-10 mol %. The USP process parameters used in the production of undoped and Mo-doped ZnO nanorods are given in Table 1.

**Table 1.** The USP process parameters for ZnO nanorod structures production.

Parameters	Produced Samples		
	ZnO seed layer	Undoped ZnO nanostructures	Mo-doped ZnO nanorod structures
Distance between nozzle and substrate (cm):	15	15	25
Spraying precursor volume (mL):	15	10	50
Spraying speed (mL/min):	5	5	1
Substrate temperature ( $^{\circ}\text{C}$ ):	500	400	475

### 2.2. Characterizations

The samples were characterized as structurally and morphologically by an x-ray diffractometer system (Bruker AXS D8), a field emission scanning electron microscope with EDX (Zeiss, EVO LS 10), respectively.

## 3. Results and Discussion

### 3.1. Structural analysis

Figure 1 exhibits the XRD patterns of the produced samples. All the patterns were indexed in the type of wurtzite (hexagonal) unit cell. The XRD results were found to be in good agreement with JCPDS card No. 36-1451 corresponding to hexagonal ZnO. The (002) diffraction peaks indicate the c-axis orientation of hexagonal ZnO. Any impurity peak was not observed.

The results indicated that all ZnO samples have a wurtzite (hexagonal) structure. Any impurity peak was not observed in the patterns due to niobium metal, niobium/other oxides, or any zinc niobium phase, exhibiting that the as-synthesized samples have single phase. The  $\text{Nb}^{5+}$  ions were understood to have substituted the  $\text{Zn}^{2+}$  site without changing the hexagonal structure. But, from the patterns of 10 mol %, the  $\text{Nb}^{5+}$  ions have difficulty in entering the ZnO lattice. The undoped and Nb-doped ZnO structures have single crystalline (1D) structure owing to have single peak (002). The very strong (002) peak indicates that the c-axis is the fastest growth direction, and the film has rod shape structure.

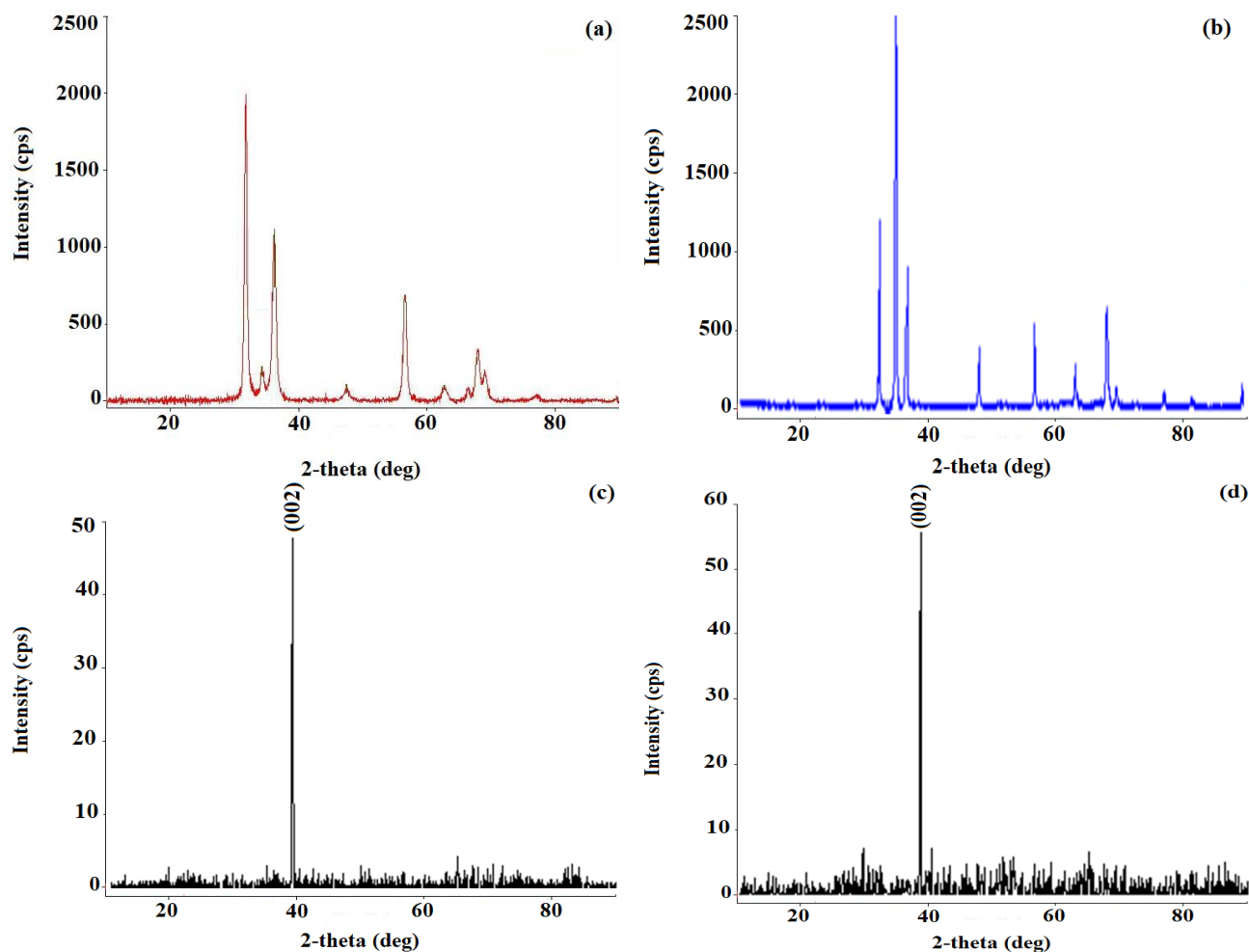
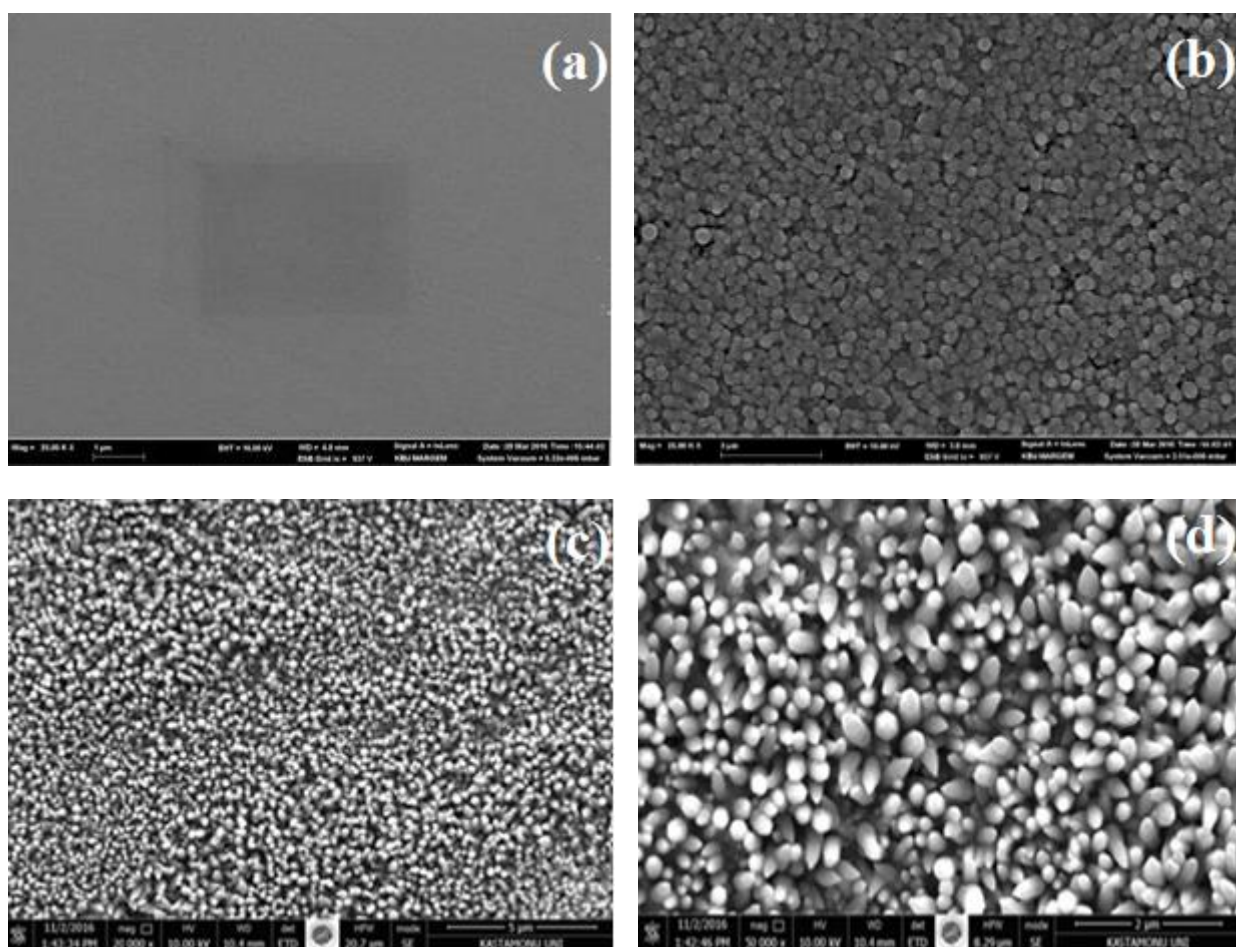


**Figure 1.** XRD patterns of the samples: (a) ZnO seed layer, (b) undoped ZnO nanorod structures, (c) 1 mol % Mo-doped ZnO nanorod structures, (d) 10 mol % Mo-doped ZnO nanorod structures.

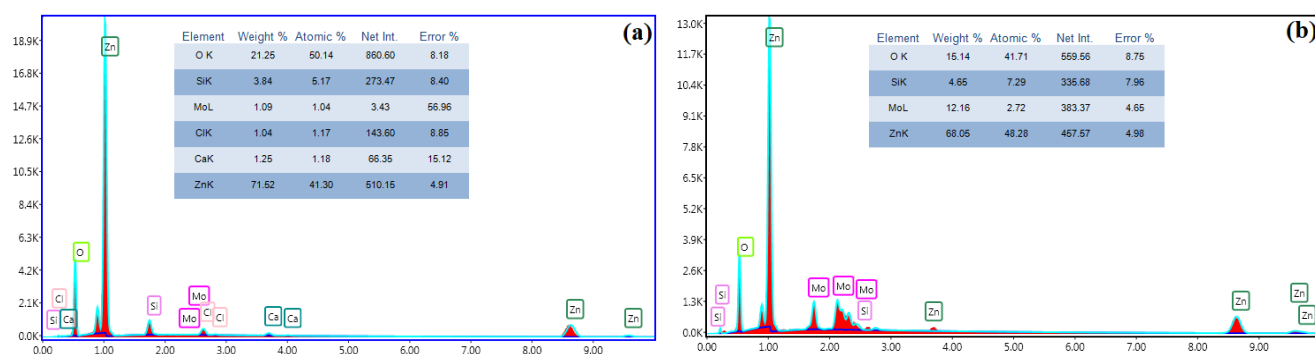
### 3.2. Morphological and compositional analysis

Figure 2 shows the FE-SEM micrographs of produced samples. All the samples have homogeneous distribution. The more homogeneous the seed layer is, the more homogeneous the structures of the nanorods produced are understood from the micrographs. On the other hand, it is seen that the rod-shaped nanoparticles are very close to each other and there is almost no space between them, that is, they have a very dense structure. The nanorod diameters were measured at approximately 90 nm. The EDX spectra shown in Figure 3 confirm that the molybdenum metal enters into the ZnO crystal lattice.





**Figure 2.** FE-SEM micrographs of the produced samples: (a) ZnO seed layer, (b) undoped ZnO nanorod structure, (c) and (d) 10 mol % Mo-doped ZnO nanostructures.



**Figure 3.** EDX spectra of the ZnO nanorod structures: (a) 1 mol % Mo doped, (b) 10 mol % Mo-doped.

## Acknowledgment

This research was financially supported by Çankırı Karatekin University Scientific Research Projects Coordinatorship (ÇAKÜ BAP), Project No. FF031114B05.

## References

- [1] Sohn, S., & Kim, H. M. (2011). Organic light emitting diode- material, process and devices, Chapter 9:

Transparent conductive oxide (TCO) films for organic light emissive devices (OLEDs). *InTech Publication, Korea South*, 233-274.

- [2] Liao, Y., Zhou X., Xie X., & Yu Q. (2013). The effects of solvents on the highly oriented ZnO films prepared using sol–gel method. *Journal of Materials Science: Materials in Electronics*, 24, 4427-4432.
- [3] Rajeswari Yogamalar, N., & Chandra Bose A. (2013). Synthesis, dopant study and device fabrication of zinc oxide nanostructures. *Progress in Nanotechnology and Nanomaterials*, 2 (1), 1-20.
- [4] Çolak, H., & Türkoğlu, O. (2012). Studies on structural and electrical properties of copper-doped zinc oxide powders prepared by a solid state method at high temperatures. *Materials at High Temperatures*, 29, 344–350.
- [5] Kumari, V., Kumar, V., Malik, B. P., Mehra, R. M., Mohan, D., & Mohan, D. (2012). Nonlinear optical properties of erbium doped zinc oxide (EZO) thin films. *Optics Communications*, 285, 2182–2188.



# Production of Diatomite Reinforced Polyester Composite and Investigation of Its Thermophysical Properties

Mustafa DAĞ<sup>1</sup> , Zehra Gülten YALÇIN<sup>1</sup> , Ercan AYDOĞMUS<sup>2\*</sup>

<sup>1</sup>Chemical Engineering, Engineering Faculty, Çankırı Karatekin University, Çankırı, Türkiye

<sup>2</sup>Chemical Engineering, Engineering Faculty, Fırat University, Elazığ, Türkiye

## Abstract

In this study, composite materials have been improved by reinforcing diatomite soil into unsaturated polyester. Diatomite in the particle size range of 297 to 149 microns is used as a filler after drying at 105 °C. Diatomite reinforced polyester composites at different ratios by mass (0 %, 1 %, 3 %, 5 %, and 7 %) are produced at room temperature under open conditions to the atmosphere. In the experimental studies, the homogeneity of unsaturated polyester (UP) and the filler is provided first. Then, after methyl ethyl ketone peroxide (MEKP) and cobalt octoate (Co Oc) catalysts are added to the mixture, mixing is done at 1000 rpm for 2 min [1-3]. After the polyester composite is cured for 24 hours under laboratory conditions, necessary tests and analyzes are performed. The chemical bond structure of the obtained polyester composite is determined by Fourier transform infrared (FTIR) spectroscopy. The surface morphology of the composite material is examined by scanning electron microscopy (SEM). As the mass ratio of diatomite soil in the mixture raises, the porosity of the obtained composite increases. In the results, it has been observed that the density of the polyester composite decreases as the ratio of diatomite in the mixture by mass increases. Diatomite reinforcement changes the thermal conductivity coefficient of the polyester composite between 0.056 W/m·K and 0.079 W/m·K. Besides, Shore D hardness of the polyester composite varies between 78.0 and 81.5. It is observed that diatomite reinforcement tends to increase both the thermal conductivity and Shore D hardness of the polyester composite. Also, thermal decomposition experiments are carried out in a PID-controlled system in an inert environment between 25 °C and 605 °C. In the thermal decomposition experiments of polyester composites, it has been determined that the filler reinforcement increases the activation energy. Activation energy values are calculated using Coats-Redfern method when the temperature rise is 10 °C/min and the conversion rate ( $\alpha$ ) is between 0.1 and 0.9. Therefore, increasing the activation energy improves the thermal stability of the composite [4-6].

**Keywords:** Diatomite, Polyester Composite, Density, Hardness, Thermal Conductivity

## 1. Introduction

Due to the excellent strength, hardness, and suitable mechanical properties of composite materials, their use in industry is becoming more and more widespread. Despite their superior properties, their weak properties such as limited ductility can also be seen [7-9]. Composite materials consist of matrix, additive, and filler materials. Many materials can be used as a matrix in industrial applications. Aliphatic and aromatic polyesters can be given as examples of these materials that are commonly used. Polyester materials, which have thermoplastic properties at high temperatures, have good impact resistance, are lightweight and recyclable, and can be an alternative to many rubbers. In addition, its elastomeric behavior at room temperature is one of its other superior features. Among the reasons for its widespread use in industry, it can be said that its chemical resistance is high, and its cost is low [10-14].

In addition to the importance of matrix materials, the importance of the contributions involved in it is also noteworthy. By adding the properties of the additives to the composite, it is possible to produce composites with new and superior properties. For this purpose, it is possible to develop a composite material with new properties by adding polyester resin to diatomite from various additives. When the properties of diatomite are examined, it is known from the literature that it has a composition in the form of  $\text{SiO}_2 \cdot n\text{H}_2\text{O}$  and has a very high water absorption capacity due to its porous structure. Diatomite, which has a hardness of 1.5-6 mohr and has abrasive properties, originated from the fossilization of algae millions of years ago. Also, the high chemical resistance of diatomites encourages their use as additives in composite materials [15-18].

\* Corresponding author. e-mail address: ercanaydogmus@firat.edu.tr

In this study, diatomite reinforced polyester composite production has been carried out for composite production with new properties and its properties are examined. Certain amounts of diatomite filler can be used to produce a low density, economical, thermally stable, and tough polyester composite.

## 2. Materials and Methods

### 2.1. Materials used in the experimental study

UP, MEKP, and cobalt octoate (Co Oc) components used in experimental studies were supplied by Turkuaz Polyester company. In addition, diatomite used as a filler was purchased from Türk Diatom Company.

### 2.2. Method used in polyester synthesis

In Figure 1, the polyester composite production scheme in experimental studies is expressed. Here, both the quantities of the ingredients and the order of use are very important. Also, the fillers should provide a homogeneous distribution to the synthesized composite.

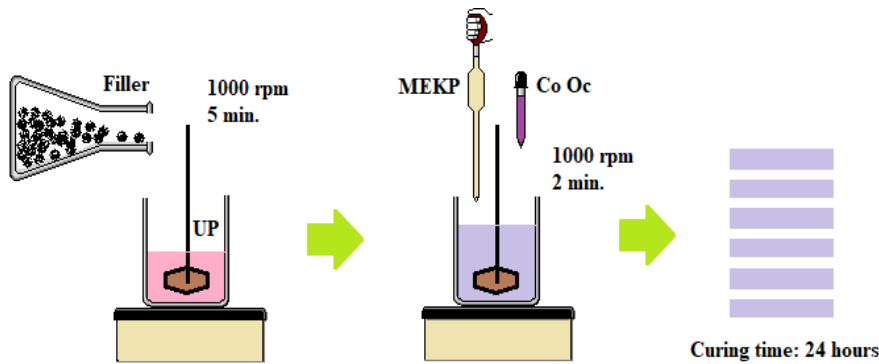


**Figure 1.** Production scheme of diatomite reinforced polyester composite.

The amounts of each ingredient used are expressed in Table 1. The amounts of other components are kept constant, except for the filler (diatomite) used here.

**Table 1.** Production plan of diatomite reinforced polyester composite.

UP (g)	MEKP (g)	Co Oc (g)	Filler (g)
98	1.4	0.6	0
98	1.4	0.6	1
98	1.4	0.6	3
98	1.4	0.6	5
98	1.4	0.6	7

## 3. Results and Discussions

### 3.1. Density of produced polyester composites

The variation of the density of the obtained polyester composites is shown in Figure 2 depending on the diatomite ratio by mass. It is understood from the graph that diatomite reduces the density of the polyester composite.

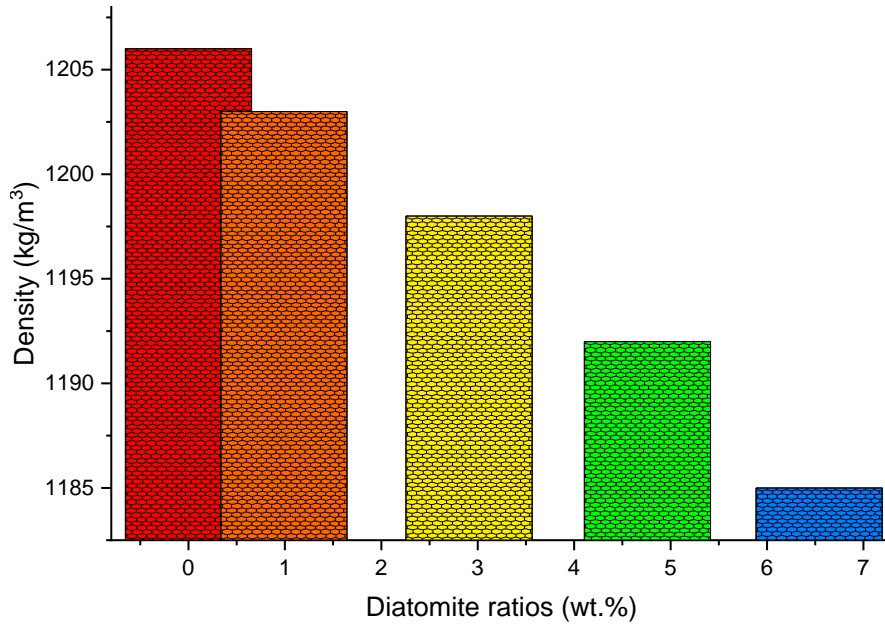


**Figure 2.** The effect of diatomite reinforcement on the density of polyester composite.

### 3.2. Hardness of the polyester composites

In the graphs shown in Figure 3, it is seen that the hardness of the synthesized polyester composites increased with diatomite reinforcement.

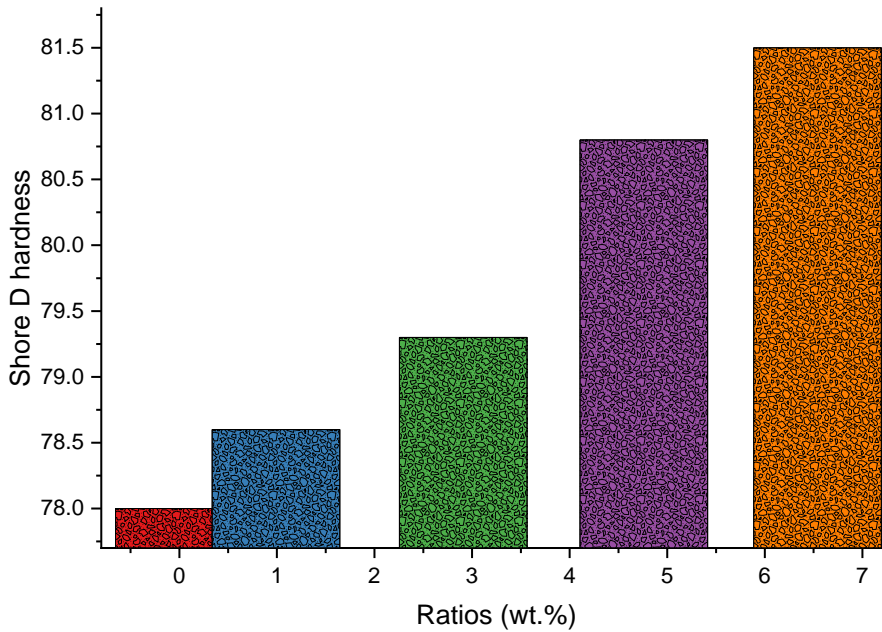


**Figure 3.** The effect of diatomite reinforcement on the hardness of the polyester composite.

### 3.3. Thermal conductivity of the polyester composites

In Figure 4, it is seen that as the mass of diatomite raises in the composite, the thermal conductivity coefficient increases, albeit slightly.



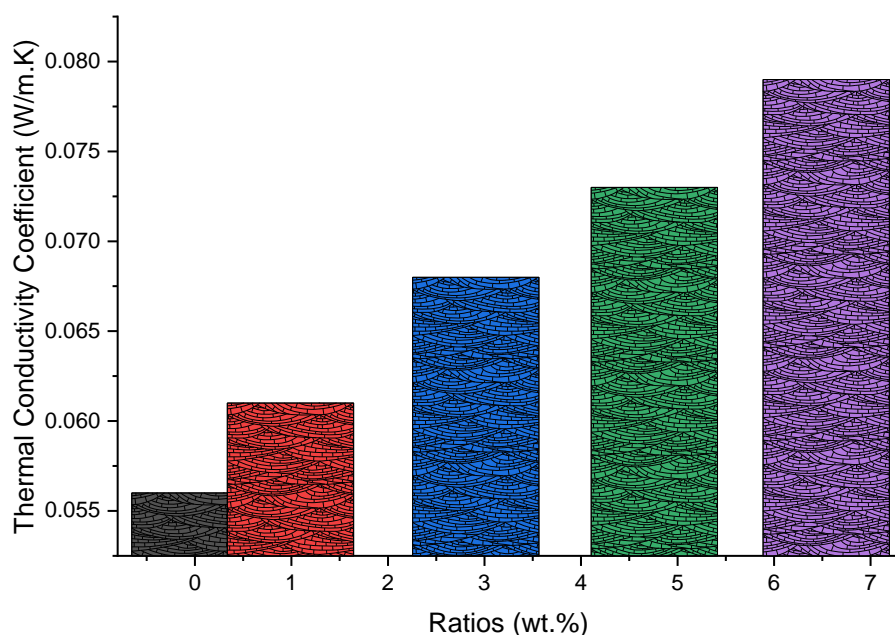


**Figure 4.** The effect of diatomite reinforcement on the thermal conductivity of the polyester composite.

### 3.4. Activation energy of the polyester composites

Activation energy ( $E_a$ ) values are calculated according to Coats-Redfern (Table 2). In this method, the highest correlation coefficient was obtained with three-dimensional diffusion equation. Activation energies of the pure polyester and polyester composites reinforced with fillers are calculated in thermal decomposition experiments carried out at a heating rate of about 10 °C/min at 605 °C.

**Table 2.** Activation energies of the polyester composites

Ratio (wt.%)	Activation Energy (kJ/mol)
0	115.43
0.99	117.56
2.91	123.05
4.76	126.18
6.54	129.74

### Acknowledgment

We would like to thank Fırat University Chemical Engineering Department and Çankırı Karatekin University Chemical Engineering Department for their support in laboratory studies.

### References

- [1] Orhan, R., Aydoğmuş, E., Topuz, S., & Arslanoğlu, H. (2021). Investigation of thermo-mechanical characteristics of borax reinforced polyester composites. *Journal of Building Engineering*, 42, 103051.
- [2] Aydoğmuş, E., Arslanoğlu, H., & Dağ, M. (2021). Production of waste polyethylene terephthalate reinforced biocomposite with RSM design and evaluation of thermophysical properties by ANN. *Journal of Building Engineering*, 44, 103337.
- [3] Aydoğmuş, E., & Arslanoğlu, H. (2021). Kinetics of thermal decomposition of the polyester nanocomposites. *Petroleum Science and Technology*, 39(13–14), 484–500.
- [4] Aydoğmuş, E. (2022) Biohybrid nanocomposite production and characterization by RSM investigation of thermal decomposition kinetics with ANN. *Biomass Conversion and Biorefinery*.
- [5] Aydoğmuş, E., Dağ, M., Yalçın, Z. G., & Arslanoğlu, H. (2022). Synthesis and characterization of waste polyethylene reinforced modified castor oil-based polyester biocomposite. *Journal of Applied Polymer*

*Science*, 139, e525256.

- [6] Yanen, C., Dağ, M., & Aydoğmuş, E. (2022). Investigation of Thermophysical Properties of Colemanite, Ulexite, and Tincal Reinforced Polyester Composites. *European Journal of Science and Technology*, 36, 155–159.
- [7] J. George, D. Bhattacharyya Biocarbon reinforced polypropylene composite: an investigation of mechanical and filler behavior through advanced dynamic atomic force microscopy and X-ray micro CT Express Polym. Lett., 15 (2021), pp. 224-235
- [8] A. Khan, D. Dragatogiannis, P. Jagdale, M. Rovere, C. Rosso, A. Tagliaferro, et al. Novel carbon fibres synthesis, plasma functionalization, and application to polymer composites Express Polym. Lett., 15 (2021), pp. 361-374
- [9] D. Sethy, S. Makireddi, F.V. Varghese, K. Balasubramaniam Piezoresistive behaviour of graphene nanoplatelet (GNP)/PMMA spray coated sensors on a polymer matrix composite beam Express Polym. Lett., 13 (2019), pp. 1018-1025
- [10] L. Averous, C. Fringant, “Association between plasticized starch and polyesters: processing and performances of injected biodegradable systems,” Polym. Eng. Sci., 41, pp. 727–734, 2001.
- [11] J.L. Willet, F.C. Felker, “Tensile yield properties of starch-filled poly(ester amide) materials,” Journal Polymer, vol. 46, pp. 3035–3042, 2005.
- [12] X. Cao, L.J. Lee, “Control of shrinkage and residual styrene of unsaturated polyester resins cured at low temperatures: I. Effect of curing agents,” J. Polymer, vol. 44, pp. 1893–1902, 2003.
- [13] A.C. Fonseca, I.M. Lopes, J.F.J. Coelho, A.C. Serra, “Synthesis of unsaturated polyesters based on renewable monomers: structure/properties relationship and crosslinking with 2-hydroxyethyl methacrylate,” React. Funct. Polym., vol. 97, pp. 1–11, 2015.
- [14] J.M.L. Reis, “Effect of aging on the fracture mechanics of unsaturated polyester based on recycled PET polymer concrete” Mater. Sci. Eng., A, vol. 528, pp. 3007–3009, 2011.
- [15] Kaya, A. İ. (2016). Kompozit malzemeler ve özellikleri. Putech & Composite Poliüretan ve Kompozit Sanayi Dergisi, 29, 38-45.
- [16] Bulut, Y., & Erdoğan, Ü. H. (2011). Selüloz Esaslı Doğal Liflerin Kompozit Üretiminde Takviye Materyali Olarak Kullanımı. Tekstil ve Mühendis, 18(82), 26-35.
- [17] Arat, A. Y., Kaya, H., & Çep, E. B. Grafenli ve Geri Dönüştürülmüş Karbon Fiberli Polimer Kompozit Malzemenin Üretilerek Mekanik Deney Çubuklarının Üretimi ve İncelenmesi, International Marmara Sciences Congress (Imascon Spring) 2022 Proceedings Book, Kocaeli, 2022, 323-329
- [18] Taş, B., & Çetin, M. (2012). Biyolojik orijinli tek doğal mineral: diyatomit. Tübav Bilim Dergisi, 5(2), 28-46.





# Retrospective Analysis of Medical Pathology Questions Asked in the Entrance Examination to Specialty Education in Dentistry

**Songül SAHİN\*** 

*Dentistry Faculty, Basic Sciences, Pathology, Karatekin University, Çankırı, Turkey*

## Abstract

Those who graduated from or continue their education from Faculties of Dentistry, in case they want to receive specialization training, must take the Dentistry Specialization Education Entrance Exam (DUS). In DUS, questions arise from basic and clinical sciences. In the Basic Sciences test, candidates face medical pathology questions along with other basic sciences. Our study evaluated the total 52 pathology questions found in 13 dental specialty education entrance exams held from 2012-2021. While 31 (59.6%) questions related to general pathology were asked, 21 (40.4%) questions included oral pathology. As a result of the study, it was determined that the most frequently asked questions from oral pathology were diseases and tumors of the soft and bone tissue in the jaw (n: 13, 25%), while the general pathology was the acute and chronic inflammation (n:8, 15.3%).

In the distribution of subjects according to years, general pathology and oral pathology were found to be equally distributed. Some issues are common to both general and oral pathology. Oral pathology questions are given with clinical information. Some questions are also intertwined with other basic sciences. The fact that pathology is a bridge between basic and clinical sciences has made it difficult to clearly distinguish the questions. We think that the data obtained as a result of the study will be useful for candidates preparing for the specialty exam in dentistry.

**Keywords:** *Dentistry, Pathology, Test ,Examination,DUS*

## 1. Introduction

Those who graduated from or continue their education from Faculties of Dentistry, in case they want to receive specialization training, must take the Dentistry Specialization Education Entrance Exam (DUS).

DUS is a central examination held every year since 2012 by ÖSYM in line with the Regulation on Specialization Education in Medicine and Dentistry. The exam, which was held twice a year in the first 3 years, in spring and autumn, has continued to be held once a year since 2015. The exam consists of two parts as Basic Sciences and Clinical Sciences. There are 40 questions in the Basic Sciences test and 80 questions in the Clinical Sciences test.

In the Basic Sciences test, candidates are evaluated with questions from basic medical sciences such as Anatomy, Histology and Embryology, Physiology, Medical Biochemistry, Medical Pathology, Medical Pharmacology, Medical Biology and Genetics (Table1). The Clinical Sciences test is consists of 10 questions from each of the dentistry specialties (1).

Medical Pathology is a branch of science that is a bridge between basic and clinical sciences and examines the cause, mechanism and consequences of diseases. Pathology education is generally divided into two main sections. General pathology covers the basic responses of cells and tissues to harmful factors underlying diseases (2). Systemic (specific) pathology, on the other hand, examines the tissue-specific responses of specialized tissues and organs to certain stimuli. Oral pathology is gaining importance for dentistry (3).

\*Corresponding author. e-mail address: songulsahin@karatekin.edu.tr

This study aims to retrospectively examine the distribution of pathology questions asked in the entrance examination to specialty education in dentistry according to subjects and years.

**Table 1.** Distribution of the basic sciences test by dentistry specialization

Basic Sciences	Number of questions in the test	Percentage of the test - %
Anatomy	6	15
Medical Microbiology	6	15
Physiology	6	15
Medical Biochemistry	6	15
Medical Pathology	4	10
Medical Pharmacology	4	10
Medical Biology And Genetics	4	10
Histology And Embryology	4	10

## 2. Materials and Methods

Our study was based on 13 dental specialty education entrance exams held in 2012-2021. In each exam, 4 questions were asked from the field of pathology, and a total of 52 pathology questions were included in the study. Exam questions were obtained from the OSYM website (1). The distribution of the questions according to the subjects and the distribution of the subjects according to the years were examined. Subject headings have been created with reference to the book "*Robbins and Cotran, Pathological Basis of Disease*"(2) and "*Oral Pathology, Clinic Pathologic Correlations*"(3), which is the main source book of pathology.

## 3. Results and Discussion

When we look at the topics of the questions in the exam (Table 2); 31 (59.6%) questions related to general pathology were asked, and the remaining 21 (40.4%) questions included oral pathology. As a result of the study, most questions were asked about soft and bone tissue diseases and tumors in the jaw (n:13, 25%) from oral pathology. Oral mucosal lesions (n:7, 13.4%) are the second most frequently asked issue. The least question is about salivary gland tumors (n:1, 1.9%).

Acute and chronic inflammation (n:8, 15.3%) are the most frequently asked subjects from general pathology, and cell adaptation - cell injury and cell death (n:7 13.6%), immune system and its diseases (n:6, 11.5%) , infections (n:4, 7.7%) and neoplasia (n:3, 5.7%). The least questions were asked about wound healing (n:2, 3.8%) and hemodynamic disorders and thromboembolic diseases (n:1, 1.9%).

No questions asked during all exams (2012-2021), from general pathology to environmental and nutrition-related diseases, from oral pathology to red lesions of the mucosa and lymphoid lesions.

In general, 2 of the 4 questions belong to general pathology, while 2 of them include oral pathology. It was not possible to separate some questions as general or oral pathology.

It was determined that at least 1 question was asked from bone-soft tissue diseases and tumors in each exam. Squamous cell carcinoma and its developmental stages (n:5, 9.6%) are among the tumor types that are frequently asked about both oral pathology and general pathology. Pemphigus disease was asked twice as (2012-1,2019) a question as the subject of both oral mucosal lesions and immune system diseases (2,3). Immune system diseases and neoplasms have been questioned in both general pathology and oral mucosal lesions.

However, some questions may contain common areas for both pathologies and other basic sciences such as microbiology and histology (2). Infectious diseases-bacteria, viruses, fungal and immune system are also explained in the branch of microbiology (4). Among the infectious diseases (n:4, 7.6%), HPV types and their mechanisms of action in neoplasia were mostly asked.

In 11 of the questions, clinical and radiological information accompanied the pathology information.

Basic sciences and clinical sciences together interpretation is very important to pathology. Clinically informed questions are the exam dates in Table 2, written in font bold.

**Table 2.** Distribution of subjects by years

SUBJECTS	Years of questions asked
<b>General Pathology</b>	
Cellular Adaptation, Cell Injury, and Cell Death	2012-2**,2014-2,2015, 2016,2017, <b>2018</b> ,2021
Acute And Chronic Inflammation	2012-1*, 2012-2, 2013-1,2013-2,2017,2019,2020,2020
Tissue Regeneration and Repair	2013-2,2019
Hemodynamic Disorders, Thromboembolic Diseases	2020
Genetic Diseases	-
Immune System Diseases	2012-1,2013-1,2014-1,2014-2, <b>2016</b> ,2021
Infectious Diseases	2013-1,2014-1,2015, 2021
Neoplasia	2012-2, 2013-2, <b>2018</b>
<b>Oral Pathology</b>	
<b>Oral mucosa lesions(n:7)</b>	
• Vesiculobullous Diseases	2012-1,2019
• Ulcerative Conditions	2014-2
• White Lesions	2012-1,2017
• Red Blue Lesions	-
• Pigmented Lesions	2018
• Verrucal-Papillary Lesions	<b>2016</b>
<b>Salivary Gland Diseases</b>	<b>2021</b>
<b>Lymphoid Lesions</b>	-
<b>Soft And Bone Tissue Diseases And Tumors In The Jaw(n:11)</b>	
• Cysts of the Jaws and Neck	<b>2012-2</b> , 2014-1
• Odontogenic Tumors	2013-1, 2013-1, <b>2016</b>
• Benign Nonodontogenic Tumors	2013-2
• Inflammatory Jaw Lesions	2014-2, <b>2018</b>
• Malignancies of the Jaws	<b>2017,2019</b> ,2020
• Metabolic and Genetic Diseases	<b>2015</b>
• Connective Tissue Lesions	<b>2015</b>

\*-1: the exam in the spring semester, \*\*-2: the exam in the autumn semester

## Acknowledgment

In the distribution of subjects according to years, general pathology and oral pathology were found to be equally distributed. Some issues are common to both general and oral pathology. Some questions are given with clinical knowledge, some questions are intertwined with other basic sciences. The fact that pathology is a bridge between basic and clinical sciences has made it difficult to distinguish the questions clearly. In the light of basic information, correlation with clinic is very important for pathology science. We think that the data obtained as a result of the study will be useful for candidates preparing for the specialty exam in dentistry.

## References

- [1] DUS Geçmiş Yıllarda Çıkış Sorular at: [http:// https://www.osym.gov.tr/TR,15070/dus-cikmis-sorular.html](http://https://www.osym.gov.tr/TR,15070/dus-cikmis-sorular.html). Retrieved August 2, 2022.
- [2] Mitchell, R. , Kumar, V. , Abbas, A.K. , Fausto,N. (2008). Robbins And Cotran, Pathologic Basis Of Disease, Eighth Edition, Saunders
- [3] Regezi, Sciubba, Jordan (2017). Oral Pathology: Clinical Pathologic Correlations, Seventh Edition, Elsevier
- [4] AK Abbas, AH Lichtman, JS Pober ,Temel İmmünoloji İmmun Sistemin Fonksiyonları ve Bozuklukları,İstanbul Medikal Yayıncılık, İstanbul, 2007



## Niobium Doping Effect on ZnO Nanorods

**Hakan ÇOLAK**<sup>1,2\*</sup> 

<sup>1</sup>Science Faculty, Chemistry Department, Çankırı Karatekin University, Çankırı, Türkiye

<sup>2</sup> Central Research Laboratory (ÇANKAM), Çankırı Karatekin University, Çankırı, Türkiye

### Abstract

Niobium metal doped ZnO nanorods were synthesized on a glass substrate by ultrasonic spray pyrolysis technique in two steps. The structural, morphological, and optical properties of the produced samples were investigated via x-ray diffractometer (XRD), a field emission scanning electron microscopy (FE-SEM) combined with energy dispersive x-ray spectroscopy (EDX), and an ultraviolet/visible spectrophotometer (UV/VIS). The XRD patterns were indexed in the hexagonal (wurtzite) unit cell for all the ZnO samples. Also, according to the XRD peaks it was understood that the crystals grow in the c-axis (002) direction. The morphological characteristics of the obtained thin films were analyzed by. From the SEM micrographs, it was observed that ZnO thin films doped with Nb had a nanorod structure in the c-axis direction. The presence of Nb ions in the samples was confirmed via EDX analysis. The optical transmittances of the samples were measured at a wavelength of 300-1000 nm. It was observed that the produced films had high optical transparency. The average optical transmittance value of the samples is 90 %.

**Keywords:** Zinc oxide, Nanorod structure, Doping process, Ultrasonic spray pyrolysis system.

### 1. Introduction

ZnO is an II-VI semiconductor compound located at the border of covalent and ionic characters. Semiconductor ZnO crystals, formed by the combination of zinc and oxygen, have the appearance of a tetrahedral geometric structure formed by the surrounding of each zinc atom with 4 oxygen atoms [1]. The crystal structure of ZnO may be in the wurtzite (hexagonal), zinc-blend (cubic), or rock salt structures. The thermodynamically stable phase under normal conditions is the wurtzite. The zinc-blend phase becomes stable with the growth of cubic structures. The rock salt phase can be formed under high pressure [2]. In the hexagonal structure of the ZnO unit cell, each Zn atom is surrounded by four O atoms in the first shell and twelve Zn atoms in the second shell. As a result, the ZnO structure is quite open, and all octahedral positions are empty, while half of the tetrahedral positions are empty. For this reason, doping atoms can settle into the ZnO crystal lattice quite easily. This open structure also affects the type of defects and diffusion mechanism [2]. When dopants enter the crystal lattice of ZnO, they cause changes in the lattice structure. Some properties such as electrical and optical properties can be enhanced by using suitable dopants with the required amounts. Nanotechnology is an important research area of materials science. Nanostructured materials have different physical and chemical properties from bulk materials. Nanostructured materials exhibit atom-like behaviors due to their large surface area [3]. Due to its superior properties, semiconductor materials such as ZnO attract great attention. ZnO has a wide band gap of 3.3 eV at room temperature, is abundant in nature and is an environmentally friendly material [4]. ZnO semiconductor material is used in light emitting diodes (LED), optoelectronic devices, solar cells, liquid crystal displays (LCD), gas sensors ...etc. It is widely used in many device applications such as [5-7]. ZnO nanoparticles can be produced by different methods such as sol-gel, hydrothermal, spray pyrolysis, chemical precipitation, and thermal degradation [8]. Traditional chemical synthesis methods, on the other hand, can cause the formation of toxic wastes [9].

In this study, niobium (Nb)-doped ZnO nanorods were fabricated. Nb is a group V-B element, and the valence state is  $5s^2 4d^3$ . The Tl metal enters into the ZnO crystal lattice as  $Nb^{5+}$  and has three more oxidation state than  $Zn^{2+}$ . Therefore, Nb is thought to be a suitable dopant for ZnO.

\*Corresponding author. e-mail address: hakancolak@karatekin.edu.tr

## 2. Materials and Methods

### 2.1. Fabricating the ZnO nanorods

Nb-doped ZnO nanorods were produced on a glass substrate via ultrasonic spray pyrolysis technique (USP, HO-TH-04, HOLMARC, India) in two steps. The USP technique is represented as a schematic diagram in figure 1. Firstly, ZnO seed layer was produced on the cleaned glass substrate. At this stage, the aqueous stock solution with a concentration of 0.5 M was used. For this aim,  $\text{Zn}(\text{Ac})_2 \cdot 2\text{H}_2\text{O}$  (Sigma-Aldrich, 99-102 %), 2-methoxyethanol ( $\text{C}_3\text{H}_8\text{O}_2$ , Sigma-Aldrich,  $\geq 99.3\%$ ), and monoethanolamine (MEA,  $\text{C}_2\text{H}_7\text{NO}$ , Merck,  $\geq 99.5\%$ ) were used as a zinc source, a solvent, and a stabilizer, respectively. The molar ratio of  $\text{Zn}^{2+}/\text{MEA}$  was 1:1. In the second step, undoped and Nb-doped ZnO nanorod structures were produced on ZnO seeded glass substrates by the USP system. For the second step, 0.1 M  $\text{Zn}(\text{NO}_3)_2 \cdot 6\text{H}_2\text{O}$  (Sigma-Aldrich,  $\geq 99.0\%$ ) solution was prepared in deionized water as a coating solution. Then, hexamethylenetetramine (HMT,  $\text{C}_6\text{H}_{12}\text{N}_4$ , Sigma-Aldrich,  $\geq 99.5\%$ ) was added into the solution as a stabilizer with 1:1 molar ratio of  $\text{Zn}^{2+}/\text{HMT}$ . For the Nb-doped ZnO nanorod structures, 0.5 M  $\text{Zn}(\text{NO}_3)_2 \cdot 6\text{H}_2\text{O}$  aqueous solution was used, and  $\text{NbCl}_5$  (Sigma-Aldrich,  $\geq 99.9\%$ ) was added into the solution. The dopant concentrations were 1-10 mol %.

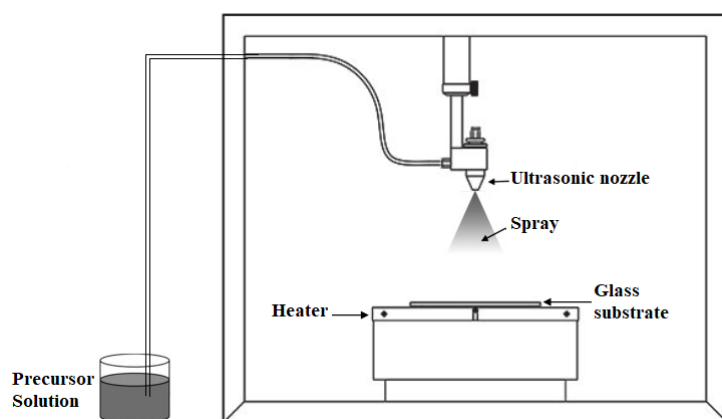


**Figure 1.** Schematic representation of the ultrasonic spray system.

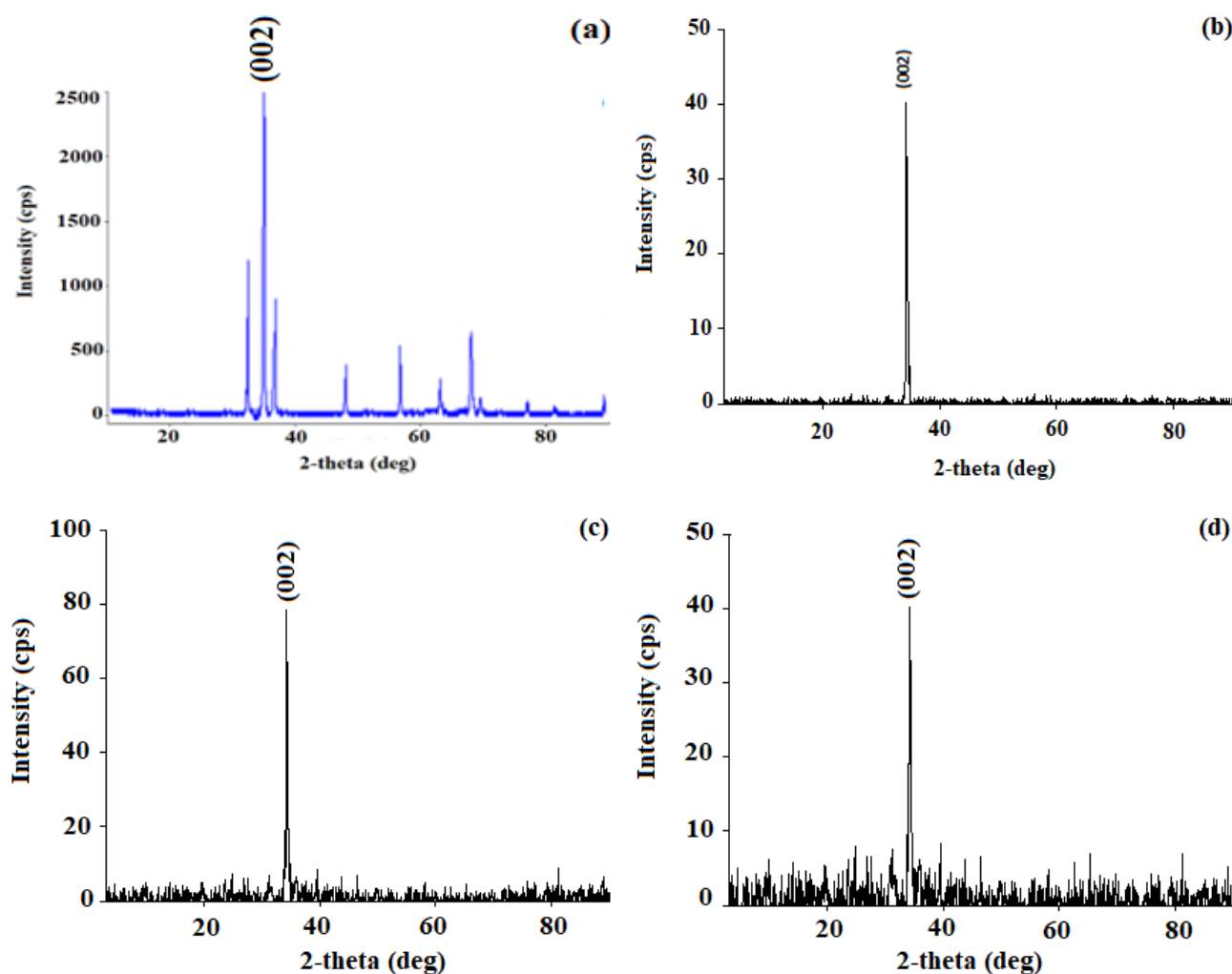
### 2.1. Characterizations

The produced ZnO samples were characterized structurally and morphologically by an x-ray diffractometer system (Bruker AXS D8), a field emission scanning electron microscope with EDX (Zeiss, EVO LS 10), and a Uv/vis spectrophotometer (Rayleigh UV-2601).

## 3. Results and Discussion

### 3.1. XRD analysis

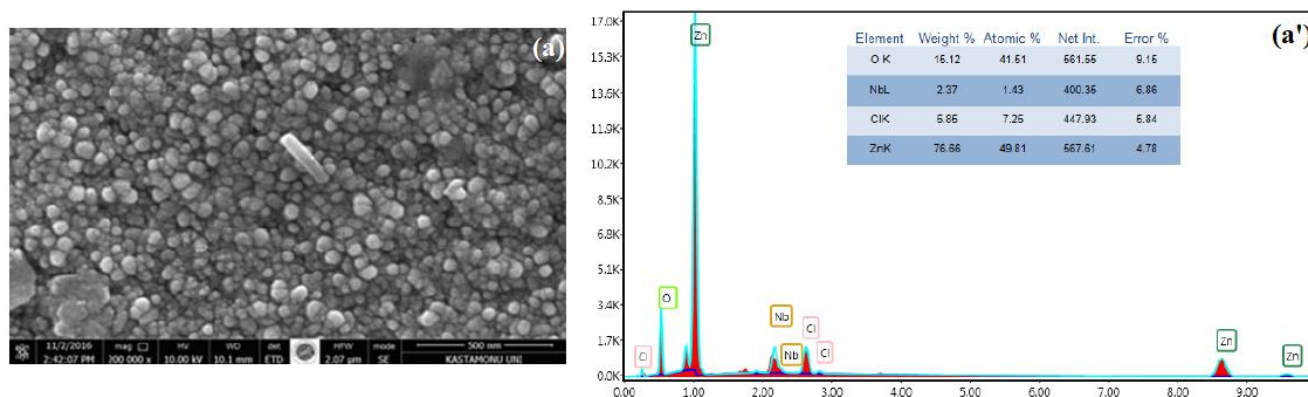
The XRD patterns of some samples are shown in figure 2. The results indicated that all ZnO samples have a wurtzite (hexagonal) structure. Any impurity peak was not observed in the patterns due to niobium metal, niobium/other oxides, or any zinc niobium phase, exhibiting that the as-synthesized samples have single phase. The  $\text{Nb}^{5+}$  ions were understood to have substituted the  $\text{Zn}^{2+}$  site without changing the hexagonal structure. But, from the patterns of 10 mol %, the  $\text{Nb}^{5+}$  ions have difficulty in entering the ZnO lattice. The undoped and Nb-doped ZnO structures have single crystalline (1D) structure owing to have single peak (002). The very strong (002) peak indicates that the c-axis is the fastest growth direction, and the film has rod shape structure.



**Figure 2.** XRD patterns of the samples: (a) u doped ZnO nanorod, (b) 1 mol % Nb-doped ZnO nanorod, (c) 5 mol % Nb-doped ZnO nanorod, (d) 10 mol % Nb-doped ZnO nanorod.

### 3.2. FE-SEM analysis

Figure 3 shows the top view SEM micrographs of undoped and Nb-doped ZnO nanorod samples. All the samples are of wurtzite structure and have a nanorod shape. From the SEM images, it is clear that the undoped and Nb-doped ZnO nanorod samples have homogeneous distribution on the glass substrate. The Nb composition of the doped ZnO nanorod samples was investigated by EDX, and the graphs are shown in figure 3. The EDX results confirm that Nb ions enter the crystal structure.





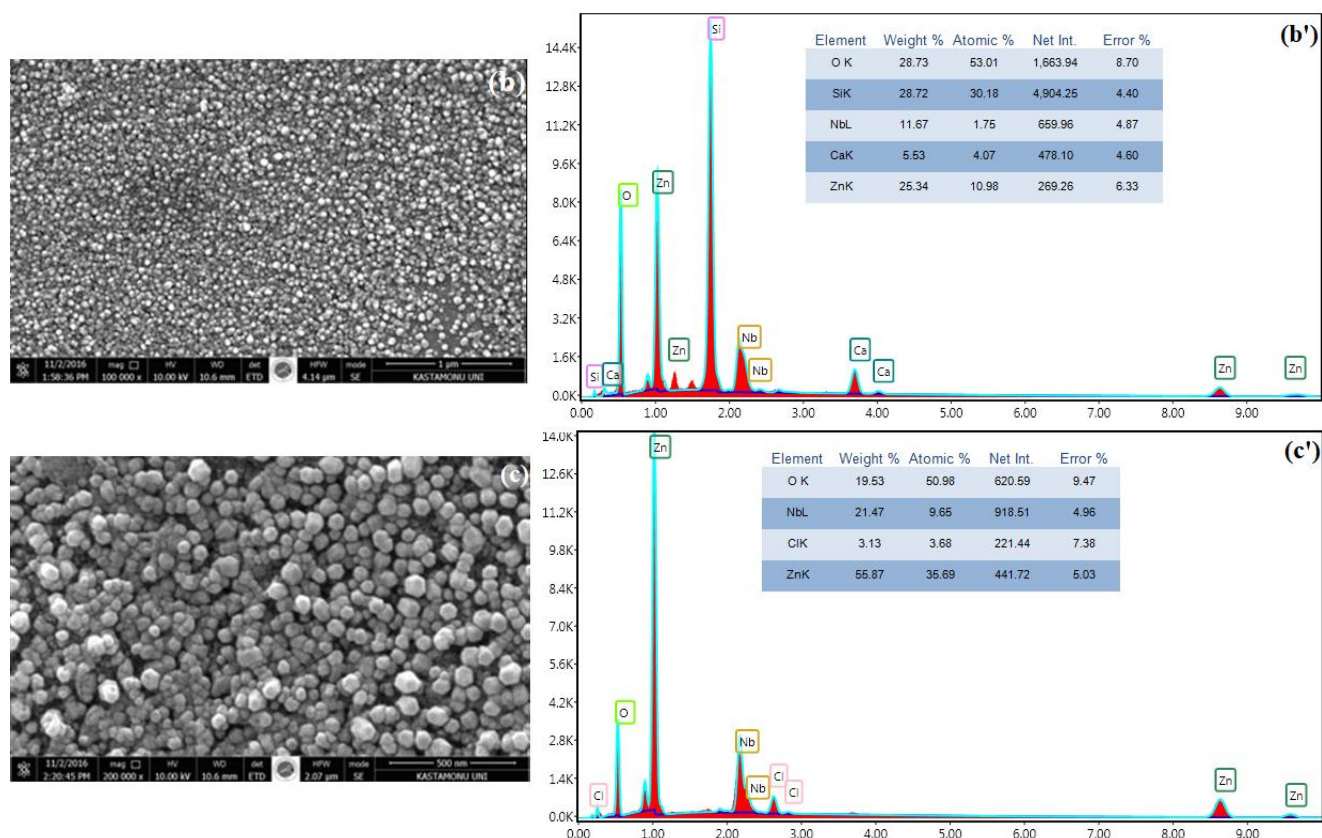


**Figure 3.** Top view FE-SEM images and EDX spectra of the ZnO samples: a-a' 1 mol %; b-b' 5 mol %; c-c' 10 mol % Nb-doped.

### 3.3. Optical analysis

In figure 4, the optical transmittance spectra of 1-10 mol % Nb<sup>5+</sup>-doped ZnO samples are shown. The optical transmittance values of Nb<sup>5+</sup>-doped samples are higher than those of undoped ZnO sample. The optical transmittance values of 1, 3, and 5 mol % Nb<sup>5+</sup>-doped samples are over 90 %. 1 mol % Nb<sup>5+</sup>-doped sample has the highest optical transmittance. For the doped samples with more than 1 mol %, the Nb<sup>5+</sup> doping decreases the optical transmittance value.

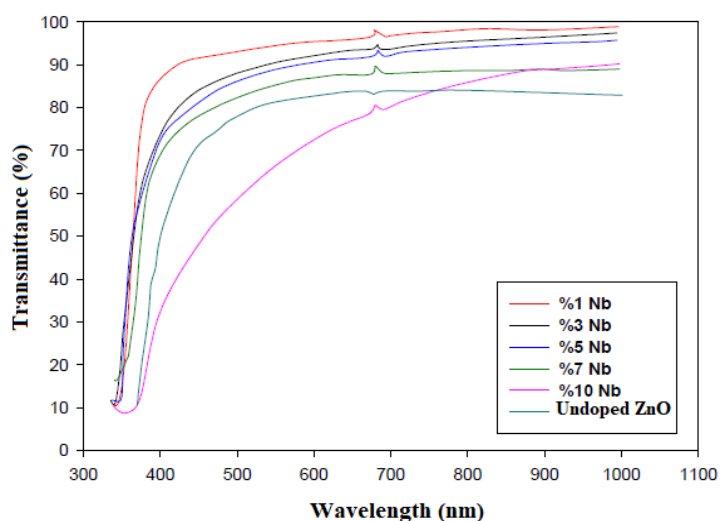


**Figure 4.** Optical transmittance graphs of the ZnO samples.



## Acknowledgment

This research was financially supported by Çankırı Karatekin University Scientific Research Projects Coordinatorship (ÇAKÜ BAP), Project No. FF031114B05.

## References

- [1] Pearton, S.J., Norton, D.P., Ip, K., Heo, Y.W., & Steiner, T. (2003). Recent progress in processing and properties of ZnO. *Superlattices and Microstructures*, 34 (1-2), 3-32.
- [2] Grzanka, E., Gierlotka, S., Stelmakh, S., Palos, B., Strachowski, T., Sroda, A.S., Kalisz, G., Lojkowski, W., & Porsch, F. (2006). Phase transition in nanocrystalline ZnO. *Zeitschrift für Kristallographie Supplements*, 23, 337-342.
- [3] Sirelkhatim, A., Mahmud, S., Seeni, A., Kaus, N.H.M., Ann, L.C., Bakhori, S.K.M., Hasan, H., & Mohamad, D. (2015). Review on zinc oxide nanoparticles: antibacterial activity and toxicity mechanism. *Nano-Micro Letters*, 7(3), 219–242.
- [4] Lee, J.B., Le, H.J., Seo, S.H., & Park, J.S. (2001). Characterization of undoped and Cu-doped ZnO films for surface Acoustic wave applications. *Thin Solid Films*, 398-399, 641-646.
- [5] Bagnall, D., Chen, Y., Zhu, Z., Yao, T., Koyama, S., Shen, M., & Goto, T., (1997). Optically pumped lasing of ZnO at room temperature. *Applied Physics Letters*, 70 (17), 2230-2232.
- [6] Tang, Z., Wong, G., Yu, P., Kawasaki, M., Ohtomo, A., Koinmura, H., & Segawa, Y. (1998). Room-temperature ultraviolet laser emission from self-assembled ZnO microcrystallite thin films. *Applied Physics Letters*, 72 (25), 3270-3272.
- [7] Lee, W., Kang, J., & Chang K. (2006). Electronic structure of phosphorus in ZnO. *Physica B: Condensed Matter*, 376-377, 699-702.
- [8] Çolak, H., & Karaköse, E. (2017). Green synthesis and characterization of nanostructured ZnO thin films using Citrus aurantifolia (lemon) peel extract by spin coating method. *Journal of Alloys and Compounds*, 690, 658-662.
- [9] Sangeetha, G., Rajeshwari, S., & Venkatesh, R. (2011). Green synthesis of zinc oxide nanoparticles by Aloe barbadensis miller leaf extract: structure and optical properties. *Materials Research Bulletin*, 46 (12), 2560-2566.



## Removal of Zn(II) Ion from Aqueous Solutions by Gellan Gam-Chitosan Complex Adsorbent

Nazife DOĞAN<sup>1</sup> , Bengi ÖZKAHRAMAN<sup>2</sup> , Zehra ÖZBAS<sup>1,\*</sup>

<sup>1</sup>Institute of Natural Sciences, Faculty of Engineering, Department of Chemical Engineering, Çankırı Karatekin University, Çankırı, Turkey

<sup>2</sup>Institute of Graduate Education, Faculty of Engineering, Department of Polymer Materials Engineering, Hitit University, Çorum, Turkey

### Abstract

In this study, the cross-linked gellan gum (GG) beads were kept in the chitosan (CS) solution for the formation of the polyelectrolyte complex, later the beads were purified and removed from the solution before the second crosslinking [1]. The potential of these complex beads to remove Zn(II) ions from wastewater was investigated. The analysis of FT-IR and SEM/EDX was performed to characterize the obtained polyelectrolyte complex. In the adsorption studies performed with the polyelectrolyte complex, the most appropriate pH value was 6. When the experimental conditions were applied at temperature: 25°C, pH: 6, the initial concentration of the solution: 200 ppm, and the adsorption time: 10 hours, the adsorption capacity was found to be approximately 42.05 mg/g. Kinetic studies demonstrated that the experimental results were consistent with the pseudo-second-order kinetic model. The Langmuir isotherm model was also found to be compatible with the equilibrium adsorption results. It has also been determined that the complex adsorbent can be used at least five times without a serious reduction in the adsorption capacity. As a result, the prepared polyelectrolyte complex may be a proper adsorbent for the adsorption of Zn(II) ions to treat wastewater containing a low metal concentration.

**Keywords:** Chitosan, Gellan gum, Polyelectrolyte complex, Zn(II)

## 1. Introduction

Zinc is widely used in many industrial applications such as dry cell, electroplating industry, pesticides, foundry, metallurgy, pigments, and explosives manufacturing. Zinc is often present in high levels in the wastewater from many sources, including galvanizing plants, mine drainage, pharmaceutical production, and pigment production [1]. Known as an inorganic pollutant, zinc is not biodegradable and can bioaccumulate through the food chain. Zinc is considered an essential trace element for life, but it is harmful to health in high concentrations. The WHO recommends that the maximum acceptable concentration of zinc in drinking water be 5 mg/L [2]. The conventional technologies use to remove Zn(II) from wastewater include ion exchange, chemical precipitation, electrolysis, membrane separation, and adsorption. The adsorption is the preferred method under being a cheap, effective, and easy-to-apply process [1, 2].

In the present study, we aimed to prepare a polyelectrolyte complex consisting of GG and CS for Zn(II) adsorption. The complex was characterized by FTIR and SEM/EDX analysis before and after adsorption process. pH, adsorption time, temperature, and initial Zn(II) concentration were examined for the adsorption process. In addition, the desorption process was performed with HCl.

## 2. Materials and Methods

### 2.1. Materials

Gellan gum (GG), CaCl<sub>2</sub>, chitosan (CS), glutaraldehyde (GA), CH<sub>3</sub>COOH, zinc acetate dihydrate (Zn(CH<sub>3</sub>COO)<sub>2</sub>·2H<sub>2</sub>O), NaOH and HCl used in the study were Sigma-Aldrich products and used without purification.

\*Corresponding author. e-mail address: zehraozbas@karatekin.edu.tr

## 2.2. Methods

The adsorbent particles in spherical form were prepared in three steps: bead formation-combination-crosslinking [3].

**Bead formation:** 1.5 g of GG was dissolved in 100 mL of distilled water to prepare a 1.5% GG solution. Then, GG solution was dropped dropwise into 7%  $\text{CaCl}_2$  solution using a syringe pump (New Era Pump System, Inc.) and cross-linked GG gel beads were obtained. After these beads were kept in the crosslinker solution for 3 hours, they were washed in distilled water for 1 hour to remove the chloride ions on the surface.

**Combination:** 1 g of CS was dissolved in 100 mL of 1%  $\text{CH}_3\text{COOH}$  solution to prepare a 1% CS solution. The GG beads washed in the previous step were transferred to this CS solution and kept for 24 hours.

**Crosslinking:** The combined beads were kept in 1% GA solution for 2 hours at room temperature to ensure crosslinking. The GA remaining on the surface of the complex beads was removed by washing with distilled water. The obtained complex beads (CS-GG) were used in adsorption studies after drying in an oven.

**Adsorption studies:** The batch system was applied in the adsorption studies of  $\text{Zn(II)}$  ions by the complex beads. First of all, in the presence of 100 ppm initial concentration and 0.15 g adsorbent, the initial pH value of the solution was changed in the range of 2-8, and the appropriate pH value for adsorption was determined. The solutions of HCl and NaOH were used for pH adjustment of the solution. The suitable conditions for  $\text{Zn(II)}$  adsorption were determined by changing the experimental conditions such as the contact time (0-28 h), the initial concentration of the solution (100-500 ppm), and the temperature (25-45°C). The experiments were conducted in a shaking water bath at 100 rpm and at specific temperatures. At the end of the time, the adsorbent was filtered off and the  $\text{Zn(II)}$  concentration in the solution was determined using AAS (atomic absorption spectrophotometer). Equation (1) was used to estimate  $q_e$  (mg/g, the sorption capacity at equilibrium). For desorption studies, 1 g  $\text{Zn(II)}$  adsorbed complex adsorbent was mixed with 1 M HCl solution at 25°C at 100 rpm for 4 hours. After desorption, the same adsorbent sample was dried and the reusability of the complex adsorbent was evaluated through the adsorption-desorption cycle repeated 5 times. The desorption percentage was determined with Equation (2):

$$q_e = \frac{(C_i - C_e) \cdot V}{m} \quad (1)$$

$$\text{Desorption \%} = \frac{\text{metal ions desorbed to the solution}}{\text{metal ions adsorbed onto adsorbent}} \cdot 100 \quad (2)$$

## 3. Results and Discussion

### 3.1. The characterization of the complex beads

The structural characterization of the beads obtained in the study was carried out by FT-IR analysis. The FT-IR spectrum of cross-linked GG and the complex beads CS-GG were given in Figure 1. The FT-IR spectrum of the complex adsorbent after  $\text{Zn(II)}$  adsorption was also presented in Figure 1.

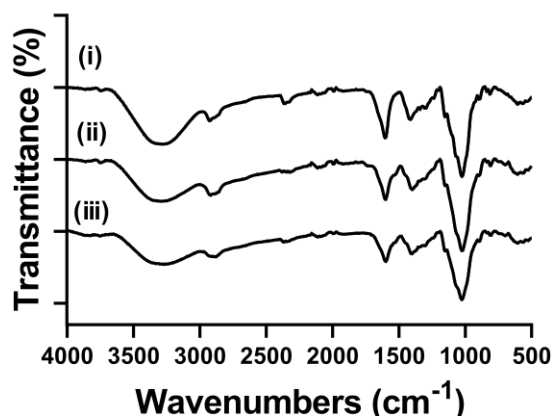


**Figure 1.** FTIR spectrum of crosslinked (i) GG, (ii) CS-GG (before adsorption), and (iii) CS-GG (after adsorption).

The SEM images obtained before and after adsorption to elucidate the morphological structure of CS-GG complex adsorbent were given in Figure 2 (a) and (b). EDX analysis after adsorption confirmed the existence of Zn(II) (Figure 2 (c)).

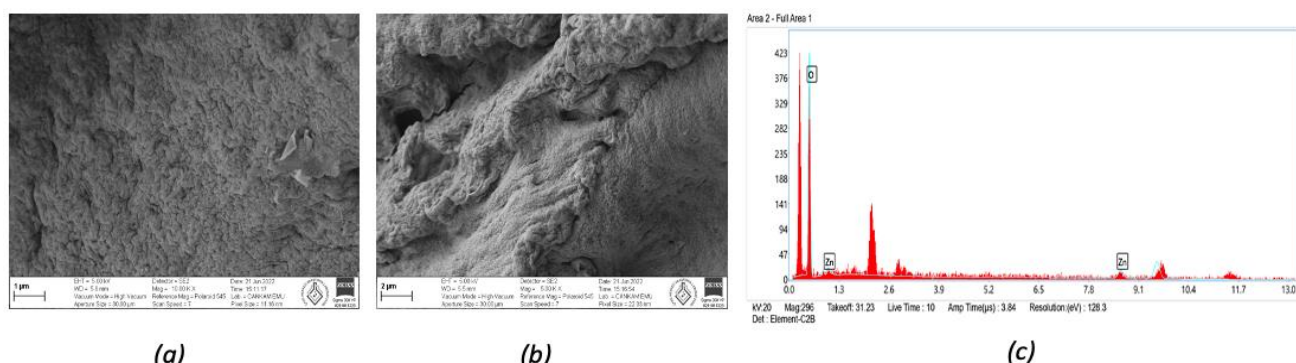


**Figure 2.** SEM images: a) CS-GG (before adsorption), b) CS-GG (after adsorption), and EDX analysis: c) CS-GG (after adsorption).

### 3.2. Adsorption studies

The pH of the initial solution is one of the most important parameters governing the adsorption of metal ions to adsorbents [3]. The effect of pH on Zn(II) adsorption with the complex adsorbent was investigated at different pH values ranging from 2 to 8 (initial concentration: 200 ppm, adsorption time: 24 h, and adsorbent dose: 0.15 g), and the results obtained was shown in Figure 3 (a). pH 6 was determined as the appropriate pH value for the adsorption of Zn(II) ions.

The adsorption of Zn(II) with CS-GG was investigated as a function of time at initial concentration: 200 ppm, adsorbent dose: 0.15 g, and pH: 6, and the results were shown in Figure 3 (b). As observed in the figure,  $q_e$  increased with the increase of contact time and reached the highest value at 10 h. After this period, no increase in adsorption capacity was observed. The experimental kinetic data was tested using pseudo-first-order and pseudo-second-order kinetic models. The kinetic model parameters were presented in Table 1. The experimental results were consistent with the pseudo-second-order kinetic model.

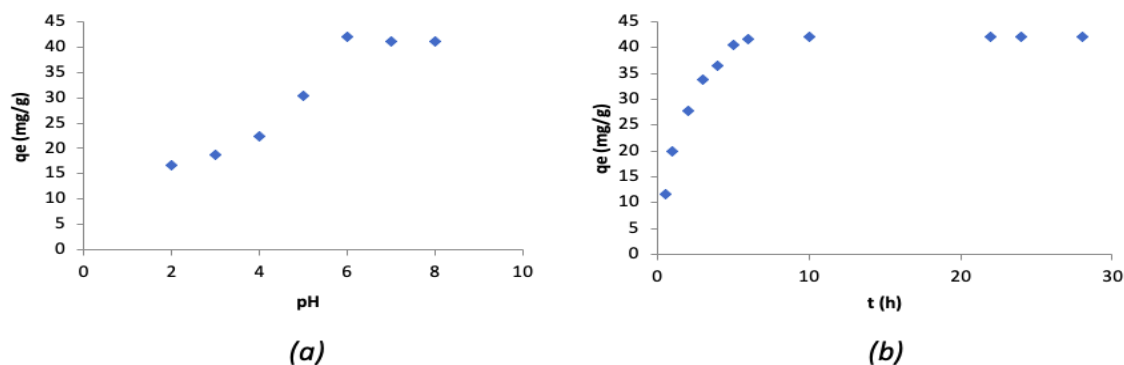


**Figure 3.** The effect of pH (a) and contact time (b).

**Table 1.** Kinetic parameters.

Kinetic models	Pseudo-first-order [4]	Pseudo-second-order [4]
Equations*	$\ln(q_e - q_t) = \ln q_e - k_1 t$	$\frac{t}{q_t} = \frac{1}{k_2 q_e^2} + \frac{1}{q_e} t$
Plots	$\ln(q_e - q_t)$ vs. $t$	$t/q_t$ vs. $t$
	$k_1 = 0.7341$ 1/h	$k_2 = 0.014$ g/mg.h
Parameters	$q_e = 53.18$ mg/g	$q_e = 49.50$ mg/g
	$R^2 = 0.9308$	$R^2 = 0.9945$

\* $k_1$ ,  $k_2$ : rate constants,  $q_t$ : adsorbent capacity at time  $t$

Adsorption isotherms express the specific relation between the concentration of adsorbate and the quantity adsorbed on the adsorbent surface at a constant temperature. Figure 4 showed the amount of adsorbed Zn(II) ( $q_e$ ) as a function of the equilibrium Zn(II) ion concentrations ( $C_e$ ) in the solutions (at 25°C, pH: 6, contact time: 10 h). Obviously,  $q_e$  values tend to increase with increasing initial Zn(II) ion concentration. The isotherm data had analyzed for Langmuir and Freundlich isotherms (Table 2), and Langmuir isotherm model was also found to be compatible with the equilibrium adsorption results.

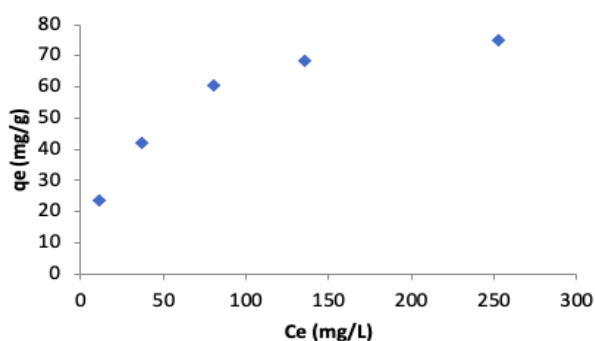


**Figure 4.** The equilibrium adsorption of CS-GG ( $q_e$  vs.  $C_e$ ).

**Table 2.** Parameters for the isotherm.

Models	Langmuir [5]	Freundlich [5]
Equations*	$1/q_e = \frac{1}{b \cdot q_{max} \cdot C_e} + \frac{1}{q_{max}}$	$\ln q_e = \ln K_F + \frac{1}{n} \ln C_e$
Plots	$C_e/q_e$ vs. $C_e$	$\ln q_e$ vs. $\ln C_e$
Parameters	$b = 0.037$ L/mg	$K_F ((\text{mg/g}) \cdot (\text{L/mg})^{1/n}) = 10.09$
	$q_{max} = 79.36$ mg/g	$1/n = 0.3833$
	$R_L = 0.051$	$R^2 = 0.9622$
	$R^2 = 0.9918$	

\*b: Langmuir constant,  $q_{max}$ : monolayer capacity,  $R_L$ : separation factor,  $K_F$ : Freundlich constant, n: Freundlich exponent

For an adsorption process, the evaluation of thermodynamics parameters provides useful information to identify processes that may occur spontaneously. These parameters were calculated by the following equations 3-5 [4].

$$K_d = \frac{q_e}{C_e} \quad (3)$$

$$\ln K_d = \frac{-\Delta H^0}{RT} + \frac{\Delta S^0}{R} \quad (4)$$

$$\Delta G^0 = \Delta H^0 - T \cdot \Delta S^0 \quad (5)$$

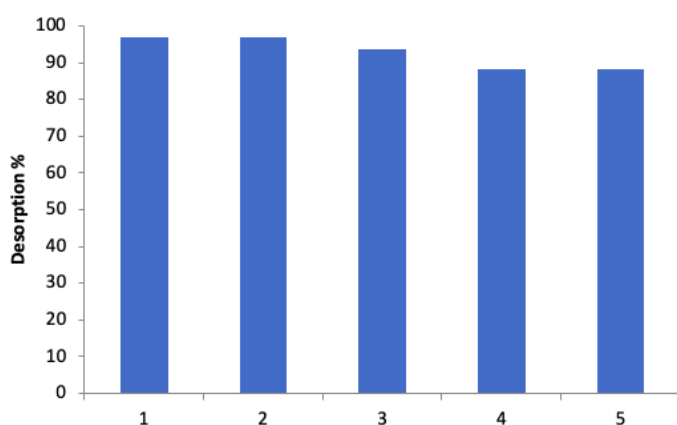
**Table 3.** Thermodynamic parameters.

Temperature	$\Delta H^0$ (kJ/mol)*	$\Delta S^0$ (kJ/mol.K)*	$\Delta G^0$ (kJ/mol)*
293.15	9.62	0.057	-7.37
303.15			-7.94
313.15			-8.51

\* $\Delta H^0$ : change in enthalpy,  $\Delta S^0$ : change in entropy,  $\Delta G^0$ : change in free energy

The positive value of  $\Delta H^0$  was an indication that the adsorption process has an endothermic character. The positive  $\Delta S^0$  value indicated a randomness in the solid-solution interface during the Zn(II) ion removal process. Negative  $\Delta G^0$  values meant that the ion removal process was spontaneous and feasible.

Good desorption performance and regeneration of an adsorbent is an essential parameter for practical applications. As seen in Figure 5, a loss of approximately 11% was observed in the capacity of the adsorbent after the first and fifth adsorption. Therefore, it is predicted that the complex adsorbent can be reused without a serious reduction in adsorption capacity.

**Figure 5.** The desorption rates of the adsorbent CS-GG.

## Acknowledgment.

The financial support from the Scientific Research Projects Unit of Çankırı Karatekin University under the project number MF210621L11 is gratefully acknowledged.

## References

- [1] Zhang, H., Tong, Z., Wei, T. & Tang, Y. (2011). Removal characteristics of Zn(II) from aqueous solution by alkaline Ca-bentonite. *Desalination*, 276, 103-108.
- [2] Wang, H., Yuan, X., Wu, Y., Huang, H., Zeng, G., Liu, Y., Wang, X., Lin, N. & Qi, Y. (2013). Adsorption characteristics and behaviours of graphene oxide for Zn(II) removal from aqueous solution. *Applied Surface Science*, 279, 432-440.
- [3] Zhang, W., Yun, M., Yu, Z., Chen, D. & Li, X. (2019). A novel Cu(II) ion-imprinted alginate-chitosan complex adsorbent for selective separation of Cu(II) from aqueous solution. *Polymer Bulletin*, 76, 1861-1876.
- [4] Özkahraman, B. & Özbaş, Z. (2020). Removal of Al(III) ions using gellan gum-acrylic acid double network hydrogel. *Journal of Polymers and the Environment*, 28, 689-698.
- [5] Emik, S. (2014). Preparation and characterization of an IPN type chelating resin containing amino and carboxyl groups for removal of Cu(II) from aqueous solutions. *Reactive and Functional Polymers*, 75, 63-74.



# Modelling Earthquake Data Using Some Lifetime Distributions

**Caner TANIŞ<sup>1,\*</sup>** 

<sup>1</sup> Science Faculty, Department of Statistics, Çankırı Karatekin University, Çankırı, Turkey

## Abstract

In this study, we provide statistical inferences about earthquake data by modelling some lifetime distributions. We consider five lifetime distributions (Weibull, exponentiated Exponential [1], exponentiated Weibull [2], generalized Lindley [3], and Power Lindley [4]) to model earthquake data. We consider two earthquake data sets in this paper. The first data consists of 20 observations denoting the magnitudes of earthquakes in the Kuşadası bay on 23 November 2020 while the second data set includes the magnitudes of earthquakes in the Kuşadası bay on 24 November 2020. The maximum likelihood method is used to estimate the unknown parameters of these distributions. We estimate the average magnitude of earthquakes via the maximum likelihood estimates of the parameters of five lifetime distributions.

**Keywords:** Weibull distribution, Exponentiated Exponential distribution, Maximum likelihood estimation, Real data analysis.

## 1. Introduction

On October 30, 2020, an earthquake occurred in Kuşadası Bay with a magnitude calculated as 6.9 by the Kandilli Observatory and Earthquake Research Institute. Hundreds of aftershocks occurred after the earthquake [5,6]. As a result of this earthquake, a total of 117 people lost their lives and 1,034 people were injured [7]. Many buildings were destroyed in Bayraklı and Bornova districts of İzmir [8].

In the literature, many statistical distributions are used to model real-life data in many fields such as biology, chemistry, engineering, and medical sciences, etc. Some of the commonly used lifetime distributions are Weibull, Lindley, and various modified versions of these distributions. In this study, unlike other studies in the literature, estimates of the mean magnitude of earthquakes will be provided using some known lifetime distributions such as Weibull, exponential Exponential [1], exponentiated Weibull [2], generalized Lindley [3] and Power Lindley distribution [4]. The main aim of this paper is to model earthquake data via these lifetime distributions and estimate the average magnitude of the earthquakes.

The rest of this study is organized as follows: In the second section, we present the mentioned lifetime distributions. In Section 3, the maximum likelihood estimators (MLEs) of the parameters of the examined distributions are obtained. In Section 4, we present two data applications to determine the optimal model for each dataset and compute the estimated average magnitude of earthquakes. Also, the selection criteria to compare the fits of the models to data sets are given in same section. The results are given in Section 5.

## 2. Modelling Methodology

### 2.1. Weibull distribution

The Weibull distribution is one of the popular lifetime distributions. The Weibull is very useful in modeling lifetime data obtained in various fields. The cumulative distribution function (CDF) and probability density function (PDF) of the Weibull distribution are given by

---

\*Corresponding author. e-mail address: canertanis@karatekin.edu.tr



$$F_{Weibull}(x) = 1 - \exp\left\{-\left(\frac{x}{\beta}\right)^\alpha\right\}, \quad (1)$$

$$f_{Weibull}(x) = \frac{\alpha}{\beta} \left(\frac{x}{\beta}\right)^{\alpha-1} \exp\left\{-\left(\frac{x}{\beta}\right)^\alpha\right\}, \quad (2)$$

respectively, where,  $\alpha > 0$  is the shape parameter,  $\beta > 0$  is the scale parameter and  $x > 0$ .

## 2.2. Exponentiated Exponential distribution

Exponentiated Exponential (EE) distribution was introduced by Gupta and Kundu [1]. The CDF and PDF of the EE distribution are given as follows:

$$F_{EE}(x) = (1 - e^{-\alpha x})^\beta, \quad (3)$$

$$f_{EE}(x) = \alpha\beta(1 - e^{-\alpha x})^{\beta-1} e^{-\alpha x}, \quad (4)$$

respectively, where  $\alpha, \beta > 0$  and  $x > 0$ .

## 2.3. Exponentiated Weibull distribution

Exponentiated Weibull (EW) distribution was proposed by Pal et al. [2]. The EW distribution is a generalization of the Weibull distribution. The CDF and PDF of the EW distribution are given by

$$F_{EW}(x) = \left\{1 - \exp(-\alpha x^\beta)\right\}^\theta, \quad (5)$$

$$f_{EW}(x) = \alpha\beta\theta x^{\beta-1} \left\{1 - \exp(-\alpha x^\beta)\right\}^{\theta-1}, \quad (6)$$

respectively, where  $\beta > 0$  and  $\theta > 0$  are shape parameters,  $\alpha > 0$  is scale parameter and  $x > 0$ . The EW distribution is reduced the Weibull distribution for  $\theta = 1$  in (5).

## 2.4. Generalized Lindley distribution

Lindley distribution was suggested by Lindley [9]. The CDF and PDF of Lindley distribution are

$$F_L(t) = 1 - \frac{(\beta + \beta t + 1)\exp\{-\beta t\}}{\beta + 1}, \quad (7)$$

$$f_L(t) = \frac{\beta^2(t+1)\exp\{-\beta t\}}{1 + \beta}, \quad (8)$$

respectively, where  $\beta > 0$  and  $t > 0$ .

Generalized Lindley (GL) distribution is introduced by Nadarajah et al. [3]. The CDF and PDF of the GL distribution are given by

$$F_{GL}(x) = \left[1 - \frac{(\beta + \beta x + 1)\exp\{-\beta x\}}{\beta + 1}\right]^\alpha, \quad (9)$$

$$f_{GL}(x) = \frac{\beta^2\alpha(x+1)\exp\{-\beta x\}}{1 + \beta} \left[1 - \frac{(\beta + \beta x + 1)\exp\{-\beta x\}}{\beta + 1}\right]^{\alpha-1}, \quad (10)$$

respectively, where,  $\alpha, \beta > 0$  ve  $x > 0$ .

### 2.5. Power Lindley distribution

Power Lindley distribution was proposed by Ghitany et al. [4]. The Power Lindley was obtained by considering a transformation  $X = T^{1/\alpha}$  in (7)-(8). Thus, the CDF and PDF of Power Lindley distribution are given by

$$F_{PL}(t) = 1 - \left(1 + \frac{\beta x^\alpha}{\beta + 1}\right) \exp\{-\beta x^\alpha\}, \quad (11)$$

$$f_{PL}(t) = \frac{\alpha \beta^2 (x^\alpha + 1) x^{\alpha-1} \exp\{-\beta x^\alpha\}}{1 + \beta}, \quad (12)$$

respectively, where  $\alpha, \beta > 0$  and  $x > 0$  [4]. Ghitany et al. [4] emphasized that Power Lindley distribution (PL  $(\alpha, \beta)$ ) is a mixture of Weibull  $(\alpha, \beta)$  and generalized gamma  $(2, \alpha, \beta)$  distribution with mixing proportion  $p = \beta / (\beta + 1)$ .

### 3. Point Estimation

In this section, we present the maximum likelihood estimators (MLEs) of the parameters of the examined lifetime distributions in Section 2.

Let  $X_1, X_2, \dots, X_n$  be a random sample from the Weibull  $(\alpha, \beta)$  distribution. The log-likelihood function is given by

$$\ell(\alpha, \beta | \mathbf{x}) = \log(\alpha) - \log(\beta) + (\alpha - 1) \sum_{i=1}^n \log\left(\frac{x_i}{\beta}\right) - \sum_{i=1}^n \left(\frac{x_i}{\beta}\right)^\alpha. \quad (13)$$

The MLEs of the  $\alpha$  and  $\beta$  parameters are the values that maximize the  $\ell(\alpha, \beta | \mathbf{x})$  function in (13). The MLEs of the  $\alpha$  and  $\beta$  parameters can be obtained by simultaneous solution of the nonlinear equations created by taking the derivatives of the  $\ell(\alpha, \beta | \mathbf{x})$  function according to the  $\alpha$  and  $\beta$  parameters and equating them to zero.

$X_1, X_2, \dots, X_n$ , be a random sample from the EE  $(\alpha, \beta)$  distribution. The log-likelihood function is given by

$$\ell(\alpha, \beta | \mathbf{x}) = \log(\alpha) + \log(\beta) + (\beta - 1) \sum_{i=1}^n \log\{1 - \exp(-\alpha x_i)\} - \alpha \sum_{i=1}^n x_i, \quad (14)$$

[1].

The MLEs of the  $\alpha$  and  $\beta$  parameters are the values that maximize the  $\ell(\alpha, \beta | \mathbf{x})$  function in (14). The MLEs of the  $\alpha$  and  $\beta$  parameters can be obtained by simultaneous solution of the nonlinear equations created by taking the derivatives of the  $\ell(\alpha, \beta | \mathbf{x})$  function according to the  $\alpha$  and  $\beta$  parameters and equating them to zero.

$X_1, X_2, \dots, X_n$ , be a random sample from the EW  $(\alpha, \beta, \theta)$  distribution. The log-likelihood function is given by

$$\begin{aligned} \ell(\alpha, \beta, \theta | \mathbf{x}) = & \log(\alpha) + \log(\beta) + \log(\theta) \\ & + (\beta - 1) \sum_{i=1}^n \log x_i + (\theta - 1) \sum_{i=1}^n \log\{1 - \exp(-\alpha x_i^\beta)\}, \end{aligned} \quad (15)$$

[2].

The MLEs of the  $\alpha, \beta$  and  $\theta$  parameters are the values that maximize the  $\ell(\alpha, \beta | \mathbf{x})$  function in (15). The MLEs of the  $\alpha, \beta$  and  $\theta$  parameters can be obtained by simultaneous solution of the nonlinear equations created by

taking the derivatives of the  $\ell(\alpha, \beta | \mathbf{x})$  function according to the  $\alpha, \beta$  and  $\theta$  parameters and equating them to zero.

$X_1, X_2, \dots, X_n$ , be a random sample from the GL  $(\alpha, \beta)$  distribution. The log-likelihood function is given by

$$\begin{aligned} \ell(\alpha, \beta | \mathbf{x}) = & 2\log(\beta) + \log(\alpha) - \log(\beta + 1) + \sum_{i=1}^n \log(x_i + 1) - 2\beta \sum_{i=1}^n x_i \\ & + (\alpha - 1) \left[ \sum_{i=1}^n \log(\beta x_i + 1) - \log(\beta + 1) \right], \end{aligned} \quad (16)$$

[3].

The MLEs of the  $\alpha$  and  $\beta$  parameters are the values that maximize the  $\ell(\alpha, \beta | \mathbf{x})$  function in (16). The MLEs of the  $\alpha$  and  $\beta$  parameters can be obtained by simultaneous solution of the nonlinear equations created by taking the derivatives of the  $\ell(\alpha, \beta | \mathbf{x})$  function according to the  $\alpha$  and  $\beta$  parameters and equating them to zero.

$X_1, X_2, \dots, X_n$ , be a random sample from the PL  $(\alpha, \beta)$  distribution. The log-likelihood function is given by

$$\ell(\alpha, \beta | \mathbf{x}) = n[\log(\beta) + \log(\alpha) - \log(\beta + 1)] + \sum_{i=1}^n \log(x_i^\alpha + 1) - \beta \sum_{i=1}^n x_i^\alpha + (\alpha - 1) \sum_{i=1}^n \log(x_i) \quad (17)$$

[4].

The MLEs of the  $\alpha$  and  $\beta$  parameters are the values that maximize the  $\ell(\alpha, \beta | \mathbf{x})$  function in (17). The MLEs of the  $\alpha$  and  $\beta$  parameters can be obtained by simultaneous solution of the nonlinear equations created by taking the derivatives of the  $\ell(\alpha, \beta | \mathbf{x})$  function according to the  $\alpha$  and  $\beta$  parameters and equating them to zero.

In this study, the **optim** function in the **R** program and the BFGS algorithm, which was first studied by Fletcher [10] were used to solve the related likelihood equations.

#### 4. Model Evaluation

In this section, we present two earthquake data sets and some selection criteria to compare the fits of models to data sets. We consider some selection criteria such as Akaike information criterion (AIC), Bayesian information criterion (BIC), Anderson-Darling statistics ( $A^*$ ), Cramér-von Mises statistics ( $W^*$ ), Kolmogorov-Smirnov statistics (K-S), and p-values ( $A^*$ ,  $W^*$ , KS) for earthquake data analysis. These measures are given by

$$AIC = -2\ell + 2k, \quad (18)$$

$$BIC = -2\ell + k \log(n), \quad (19)$$

$$A^* = -n - \frac{1}{n} \sum_{i=1}^n (2i - 1) \log \left[ F(X_{(i)}) (1 - F(X_{(n-i+1)})) \right], \quad (20)$$

$$W^* = \frac{1}{12n} + \sum_{i=1}^n \left( F(X_{(i)}) - \frac{2i-1}{2n} \right)^2, \quad (21)$$

$$KS = \sup |F_n(x) - F_0(x)|, \quad (22)$$

respectively, where  $X_{(i)}$  denotes  $i^{th}$  order statistics,  $m$  denotes to the number of parameters,  $n$  is the sample size,  $\ell$  is the value of the log-likelihood function,  $F_n(x)$  denotes empirical distribution function, and  $F_0(x)$  refers to the CDF of the examined model.

##### 4.1. Data Description

In this subsection, we present two real data sets including the magnitudes of the earthquakes in Kuşadası bay. The first data set refers to the magnitudes of the earthquakes on November 23, 2020 while the second data set

includes the magnitudes of the earthquakes on November 24, 2020. Some descriptive statistics of the data sets are given in Table 1.

**Table 1.** Some descriptive statistics of the earthquake data sets

<i>Data Set</i>	<i>n</i>	<i>Min.</i>	<i>Max.</i>	<i>Mean</i>	<i>Var.</i>	<i>CS</i>	<i>CK</i>
<i>1</i>	20	1.2	2.5	1.780	0.17	0.308	-1.013
<i>2</i>	28	1.3	2.5	1.785	0.077	0.519	0.402

Min.: Minimum, Max.: Maximum, Var.: Variance,  
CS: Coefficient of Skewness, CK: Coefficient of Kurtosis

## 5. Results

In this section, the results of the earthquake data analysis are presented. Table 2 contains the maximum likelihood estimates and their standard errors (SEs) of the parameters of the distributions fitted to the data given in Section 2. Table 3 shows the comparison statistics used to compare the models fitted to the data sets.

**Table 2.** The MLEs and SEs of the parameters of the fitted models for the earthquake datasets

Data set	Model	$\hat{\alpha}$	$\hat{\beta}$	$\hat{\theta}$	$SE(\hat{\alpha})$	$SE(\hat{\beta})$	$SE(\hat{\theta})$
1	Weibull	4.8565	1.9424	-	0.8392	0.0947	-
	EE	2.9180	101.5109	-	0.5271	80.9166	-
	EW	1.2362	1.6353	14.0620	2.7924	1.8372	52.4211
	GL	77.8533	3.2482	-	61.7207	0.5364	-
	PL	3.5973	0.1856	-	0.5254	0.0715	-
2	Weibull	6.6413	1.9049	-	0.9009	0.0575	-
	EE	1100.3067	4.2306	-	1077.9688	0.6193	-
	EW	1.0281	2.1623	22.3760	1.6700	1.5381	58.1391
	GL	4.5730	825.2685	-	0.6171	794.5009	-
	PL	4.9163	0.0889	-	0.5911	0.0364	-

**Table 3.** The selection criteria for the earthquake datasets

Data set	Model	AIC	BIC	KS	A*	W*	p-value (KS)	p-value (A*)	p-value (W*)
1	Weibull	24.7687	26.7601	0.1271	0.4265	0.0614	0.9031	0.8203	0.8111
	EE	23.7226	25.7140	<b>0.1012</b>	0.3139	0.0383	<b>0.9866</b>	0.9265	0.9459
	EW	25.5679	28.5551	0.1014	0.3129	0.0384	0.9863	0.9274	0.9453
	GL	<b>23.6953</b>	<b>25.6867</b>	0.1013	<b>0.3120</b>	<b>0.0380</b>	0.9864	<b>0.9281</b>	<b>0.9472</b>
	PL	24.9289	26.9203	0.1258	0.4152	0.0581	0.9095	0.8318	0.8316
2	Weibull	14.0751	16.7395	0.1241	0.5293	0.0727	0.7813	0.7156	0.7388
	EE	10.0468	12.7112	0.1170	0.3096	0.0541	0.8383	0.9302	0.8550
	EW	11.3317	15.3283	<b>0.0952</b>	<b>0.2270</b>	<b>0.0380</b>	<b>0.9613</b>	<b>0.9812</b>	<b>0.9460</b>
	GL	<b>9.9860</b>	<b>12.6504</b>	0.1160	0.3034	0.0530	0.8457	0.9351	0.8618
	PL	12.7474	15.4118	0.1121	0.4093	0.0566	0.8730	0.8383	0.8397

Bold text indicates the best model

From the Table 3, it can be concluded that except for the KS test statistic and the its p value, the GL distribution is the best fitted model to first data set according to other selection criteria while the EE distribution has more fit than other models according to KS statistics and its p-value for the first data set. On the other hand, we observe that except for the AIC and BIC, the EW distribution is the best fitted model to second data set according to other selection criteria while the GL distribution has more fit than other models according to AIC and BIC for the second data set.

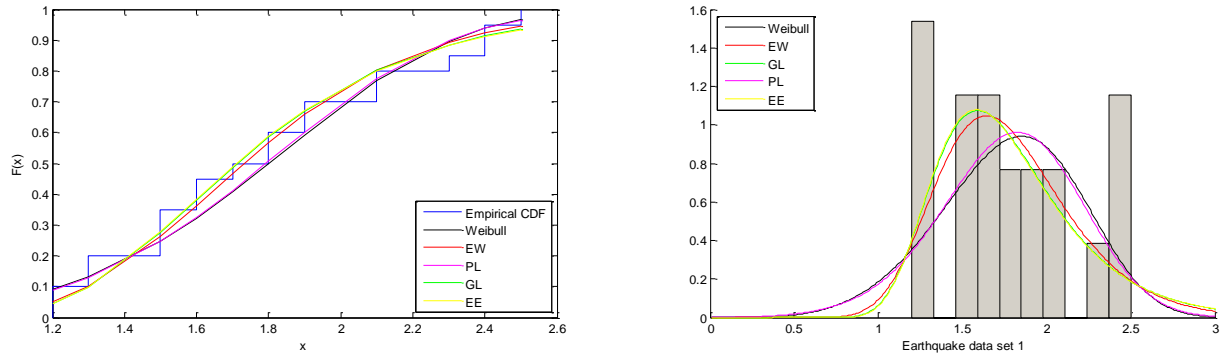


**Figure 1.** The fitted CDFs (on left) and PDFs (on right) for data set 1

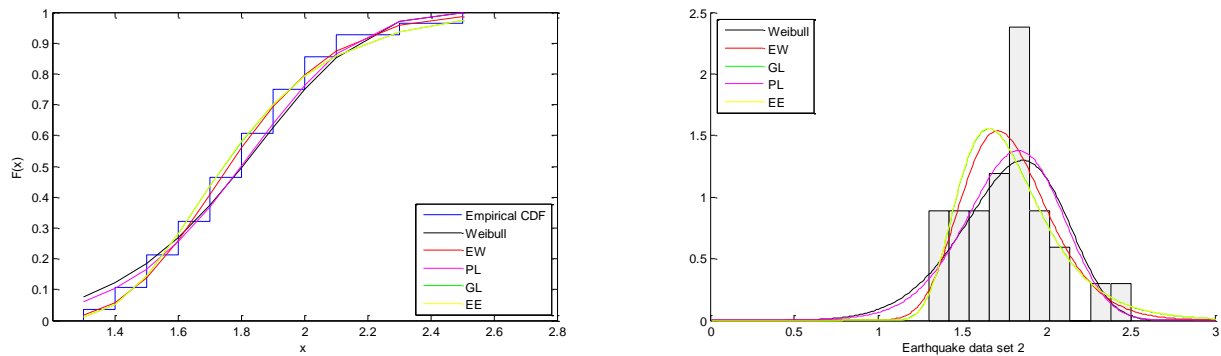


**Figure 2.** The fitted CDFs (on left) and PDFs (on right) for data set 2

**Table 4.** The estimated average magnitude of the earthquakes for datasets

Data Set	Weibull	EE	EW	GL	PL
1	1.7804	1.7828	1.7784	1.7822	1.7765
2	1.7769	1.7919	1.7855	1.7916	1.7810

Figures 1-2 illustrate the fitted CDFs and PDFs for two datasets. Table 4 provides the estimates of the average magnitude of the earthquakes for data sets. These estimates are computed by using the expected values of the distributions under MLEs in Table 2. From Table 4, it can be concluded that the estimates are very close the true mean of the samples in Table 1.

## References

- [1] Gupta, R. D., Kundu, D., (2001), Generalized exponential distribution: different method of estimations, *Journal of Statistical Computation and Simulation*, 69 (4), 315-337.
- [2] Pal, M., Masoom M.A., Jungsoo W. (2006). Exponentiated weibull distribution. *Statistica* 66 (2) 139-147.
- [3] Nadarajah, S., Bakouch, H. S., Tahmasbi, R. (2011). A generalized Lindley distribution. *Sankhya B*, 73(2), 331-359.
- [4] Ghitany, M. E., Al-Mutairi, D. K., Balakrishnan, N., Al-Enezi, L. J. (2013). Power Lindley distribution and associated inference. *Computational Statistics & Data Analysis*, 64, 20-33.
- [5] [https://jfm.sakarya.edu.tr/sites/jfm.sakarya.edu.tr/file/30\\_Ekim\\_2020\\_Kusadasi\\_Korfezi\\_depremi\\_bilgi\\_notu.pdf](https://jfm.sakarya.edu.tr/sites/jfm.sakarya.edu.tr/file/30_Ekim_2020_Kusadasi_Korfezi_depremi_bilgi_notu.pdf), Utkucu, M., Budakoğlu, E., Doğan, E. 30 EKİM 2020 KUŞADASI KÖRFEZİ DEPREMİ BİLGİ NOTU, Access date: August 22, 2022.
- [6] [http://www.koeri.boun.edu.tr/sismo/2/wp-content/uploads/2020/10/20201030\\_izmir\\_V1.pdf](http://www.koeri.boun.edu.tr/sismo/2/wp-content/uploads/2020/10/20201030_izmir_V1.pdf), Access

date: August 22, 2022.

- [7] <https://www.hurriyet.com.tr/gundem/izmirdeki-depremde-enkazdan-cikartilan-mahir-tahirler-hayatini-kaybetti-41672849>, Access date: August 22, 2022.
- [8] <https://www.hurriyet.com.tr/galeri-izmir-depremi-son-dakika-iste-busenin-enkaz-altindan-kurtarildigi-anlar-canli-yayinda-iletisime-gecilmisti-41650162>, Access date: August 22, 2022.
- [9] Lindley, D.V., 1958. Fiducial distributions and Bayes' theorem. Journal of the Royal Statistical Society, Series A 20, 102–107.
- [10] Fletcher R. (1987). Practical methods of optimization. John and Sons, Chichester.



# Investigation of a Grid-Connected System Design on a Rooftop in ÇAKU

Said NASSER AHMED<sup>1</sup> , Muhammed Bora AKIN<sup>1\*</sup> 

<sup>1</sup> Faculty of Engineering, Department of Chemical Engineering, Çankırı Karatekin University, Çankırı, Türkiye

## Abstract

The energy need, which has increased with the rapidly rising demands after Covid19, has increased even more with the developing tension between Ukraine and Russia. In addition to this cost increase, the climate crisis also makes people look for ways to produce energy from new sources. The first thing that comes to mind is undoubtedly solar energy, when it comes to renewable energy. Electrical energy is possible by using photovoltaic cells in solar energy. These systems must be carefully designed and simulated before installing them. Simple mistakes can cause the systems not to work and even some components to be damaged. In this study, a grid-connected solar energy system was designed and simulated on the roof of Çankırı Karatekin University Engineering Faculty using the PVSyst program. In the designed solar energy systems, the data obtained by changing the distance between the arrays are given as a result. The distance between the panel arrays is varied between 2.2 and 6 m. As a result, it has been revealed that the design that will give the highest energy with the least components will transfer 208.5 MWh of energy annually. (This study was made from the thesis work of the first ranked student.)

**Keywords:** Photovoltaic, PVSyst, Grid-connected, On-Grid, Rooftop PV Model

## 1. Introduction

It is very important to use computer support during the design of a system and especially to be able to simulate it. In the design of solar energy systems, many factors such as grouping of PV panels, adjustment of PV panel angles, inverter selection, battery selection, knowing the annual sunshine and other weather conditions of the region, physical conditions of the installation area, shadow formation should be considered. Therefore, using a simulation program will reduce the probability of error. Different programs such as PVcase, PVsol, Helioscope are widely used by designers, financial experts and investors for the design and simulation of solar energy systems [1].

Solar energy systems, which are developing in our country, are also widely studied academically. Various studies have been carried out for many provinces. In the literature, Uşak [2], Şanlıurfa [3], Van [4], Aydın [5], Sivas [6, 7], Karabük [8], Afyonkarahisar [9], Isparta [10], Karaman [11], Diyarbakır [12], Aksaray [13], Balıkesir [14], Kocaeli [15], Osmaniye [16], Bursa [17], Eskişehir [18], Kütahya [19], Nevşehir [20], Kayseri [21], and many more provinces' [22-28] solar energy potentials were investigated.

In this study; using the PVSyst V7.2 software program, it is aimed to simulate in which evaluations can be made on the amount of energy to be produced by the on-grid system, which will be designed to meet the energy need of a building located in the Çankırı Karatekin University Uluyazı Campus, with roof type photovoltaic systems, the system performance and the compatibility of the elements in the system with each other. The geographical location of the building was specified in the PVSyst software program and the meteorological data of the region were synthetically produced from the Meteonorm 7.2 database, which is one of the services offered in the program. Five different grid-connected designs were made on the roof of the Engineering Faculty building in Çankırı Karatekin University Uluyazı Campus. While making these designs, the distance between the PV arrays was chosen as 2.2, 3, 4, 5 and 6 m. The effects of changing the distance are given as a result.

## 2. Materials and Methods

PVSyst program was used to carry out the study. In the study, Google Earth Pro and Microsoft Excel programs were also partially utilized in the process of transferring the area of the selected engineering faculty building

\* Corresponding author. e-mail address: mbakin@karatekin.edu.tr

rooftop ( $40.62^\circ$  N,  $33.62^\circ$  E). The programs were loaded on a laboratory computer with an Intel processor and a Windows 10 operating system in the Faculty of Engineering building. Design and simulation processes were done on this computer.

The study was carried out in three stages. In the first stage, the latitude and longitude information of the selected building was found in the Google Earth Pro program. In the second stage, this information was organized in MS Excel program and transferred to PVSyst program. In the last stage, the PV system was designed in the PVSyst program. During this design, the distance between the panel arrays (2.2, 3, 4, 5, and 6 m) was chosen as a variable. The program chooses the distance between the panel arrays as 2.2 m in order to provide access to the panels in case of construction or failures. However, this value is not mandatory and it is possible to make more panel placement by reducing the distance.

Si-poly PV modules used in the designs were preferred as CS6K - 265P 1500V belonging to Canadian Solar company. The Pnom value (peak power of the photovoltaic modules) of these modules is 265 Wp. The collector width is 2.01 m, the tilt angle is  $30^\circ$  and the azimuth angle is  $0^\circ$ . Images of the designs are given in Figure 1.

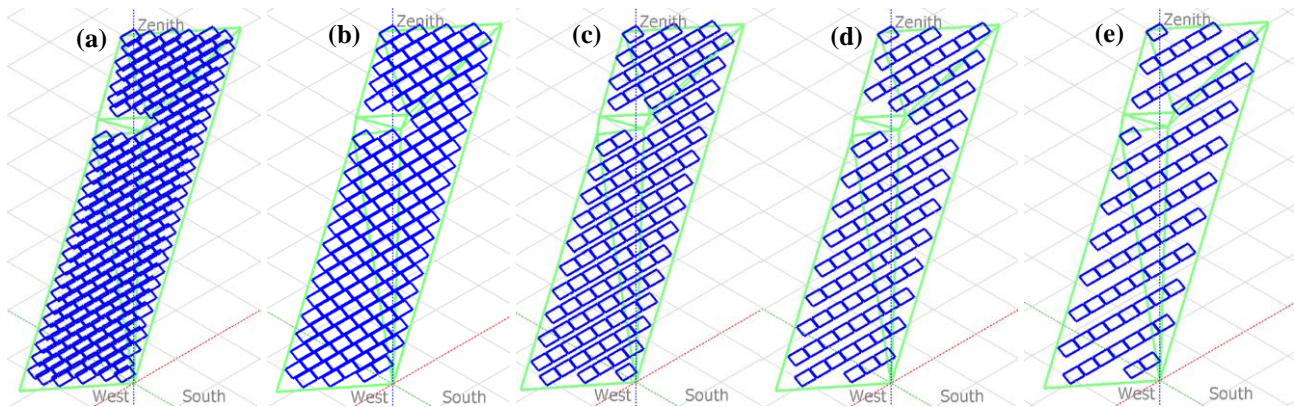


**Figure 1.** Perspective of the PV-fields: (a) 2.2 m, (b) 3 m, (c) 4 m, (d) 5 m, and (e) 6 m

### 3. Results and Discussion

The increase in the distance between the PV panel strings naturally causes the number of strings to decrease. A decrease in the number of arrays means that the number of modules, the module area, and the cell area all decrease. Table 1 summarizes these results.

**Table 1.** Summary of the results

Project	Modul area (m <sup>2</sup> )	Cell area (m <sup>2</sup> )	Total number of PV module	Module number in series	Number of strings	Number of inverter	Total power (kWp)	Total pnom (kW ac)	Pnom ratio	Transferred energy (MWh)
Engineering 2.2m	1368	1221	836	22	38	3	222	180	1.23	209.7
Engineering 3m	1002	864	612	34	18	1	162	150	1.08	208.5
Engineering 4m	753	672	460	23	20	2	122	120	1.02	170.8
Engineering 5m	596	532	364	13	28	8	96.5	80	1.21	134
Engineering 6m	504	450	308	22	14	1	81.6	75	1.09	116.5

In Figure 2, it is seen that the module area and the PV cell area decrease as the distance between the PV arrays increases. Here, the connection between areas and distance is connected to fit second order equation model, the regression coefficients are found 0.9956 and 0.9891.



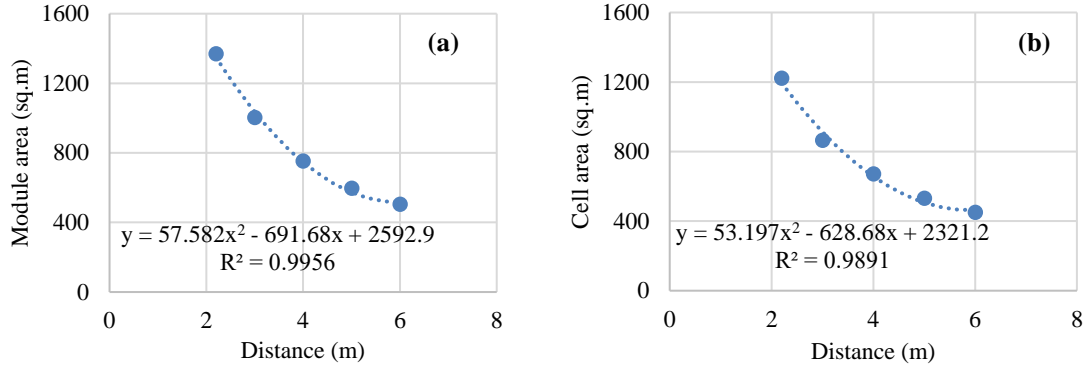


**Figure 2.** Effect of distance on module area (a) and cell area (b)

By increasing the distance between PV modules from 2.2 m to 6 m, the number of modules from 836 becomes 308. In this study, the correlation between the number of PV modules and the distance corresponds to a quadratic expression and the  $R^2$  value is 0.9955 (Figure 3).

It can be seen in Figure 3b that the number of PV modules in arrays does not have a trend. This is because the modules in the arrays are grouped together to provide a close voltage when making the inverter connections. In addition, the inverter must have as many connections as the number of obtained groups which the connection will be made. This situation complicates the selection of inverter when some groupings are made or causes selections that will increase the number of inverters. The increase in the number of inverters will cause an inevitable increase in the installation cost. In this study, it was found that the number of modules for each PV array to be installed in the roof area is around 23 (Figure 3b).

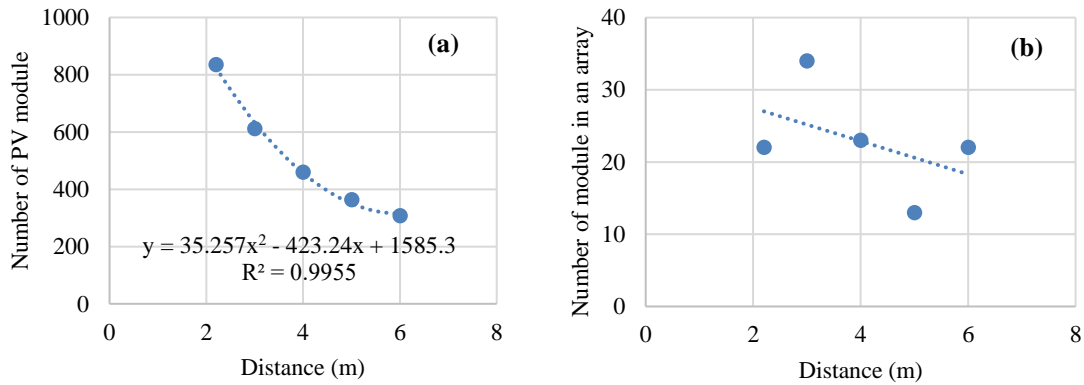


**Figure 3.** Effect of distance on module (a) and array (b) numbers.

In this study; showed in Figure 4, a situation where the number of inverters was eight as a result of grouping was encountered. Production of this design will be avoided due to increased cost.

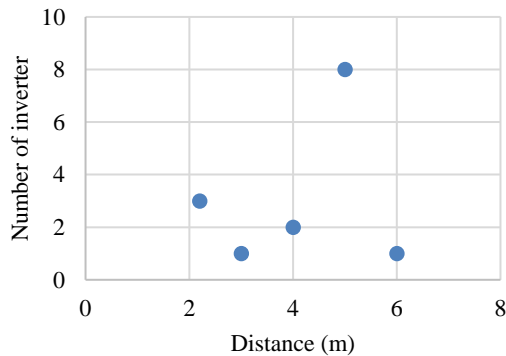


**Figure 4.** Effect of distance on number of inverter.

It is seen in Figure 5 that the total installed PV power, whether in kWp or kW ac unit, decreases with the decrease in the number of modules due to the increase in the distance between them.

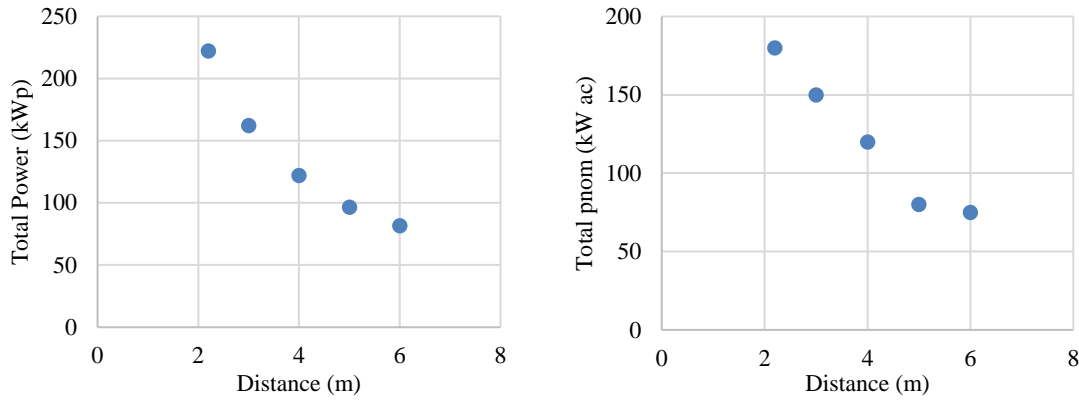


**Figure 5.** Effect of distance on total power a) kWp, and b) kW ac.

It is desired that the pnom ratio takes a value of approximately 1. PVSyst program warns the user when this value is found. In the study, which is within the specified intervals, the lowest pnom rate is in the project where the intervals are applied 4 m with 1.02. The value of 1.04 was taken for the projects where the intervals were applied as 3 m and 6 m (Figure 6a). In Figure 6b, where the transferred energy is compared, it is noteworthy that there is almost no difference in the use of 2.2 m and 3 m shade spacing.

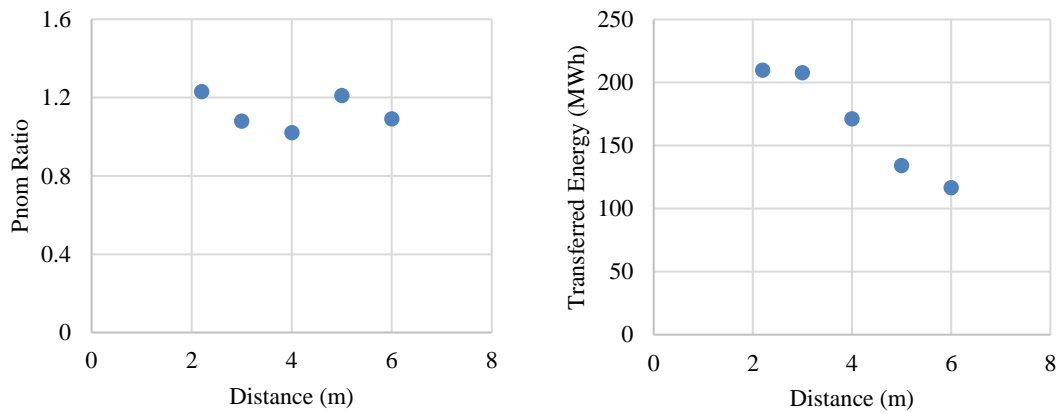


**Figure 6.** Effect of distance on pnom ratio and transferred energi to grid.

#### 4. Conclusion

Considering the transferred energy amounts of the PV systems designed on the rooftop, it is seen that approximate values are obtained for the shade spacing at 2.2 m and 3. The fact that the pnom rate is lower in the system using 3 m shade spacing is a reason for preference. It is considered that fewer inverters and PV modules are used, it is appropriate to choose a design with a shade spacing value of 3 m, where installation costs will be lower. The energy that this installation will transfer to the grid annually is calculated as 207.8 MWh by the PVSyst program. In this way, it is understood that the shade spacing of 2.2 meters is not sufficient.

#### Acknowledgement

In this study, the authors declare that there is no conflict of interest and thank to PVSyst SA for the PVSyst program, and Faculty of Engineering for the computer provided.

## References

- [1] Ozden, T., Karaveli, A.B., & Akinoglu, B.G. (2020). Comparison of the Models of Solar PV Performance Calculations for Ankara – Middle Anatolia. *European Journal of Science and Technology*, (18), 54-60.
- [2] Taktak, F. & Ili, M. (2018). Güneş Enerji Santrali (GES) Geliştirme: Uşak Örneği. *Geomatik*, 3(1), 1-21.
- [3] Özcanlı, M., Güzel, A. & Akgün, B. (2021). Şanlıurfa ili'nde kurulu GES'lerin topoğrafik özellikler (yükselti, eğim, bakı) açısından uygunluk analizi. *Türk Coğrafya Dergisi*, (78), 127-144.
- [4] Yalılı, M. (2021). Lisanslı Fotovoltaik Güneş Enerji Santrali Yatırımının Finansal Analizi: Van İli Örneği, *Bitlis Eren Üniversitesi Fen Bilimleri Dergisi*, c. 10(3), 1055-1074.
- [5] Bayrakçı H.C., Gezer T. (2019). Bir Güneş Enerjisi Santralının Maliyet Analizi: Aydın İli Örneği. *Teknik Bilimler Dergisi*, 9(2): 46-54.
- [6] Sarı V., Özyiğit F.Y. (2020). Sivas İlinin Farklı İlçelerinde Şebeke Bağlantılı Güneş Enerji Santrallerinin Tasarımı ve Analizi. *Avrupa Bilim ve Teknoloji Dergisi*, 20: 425-437.
- [7] Sarı, V. & Özyiğit, F.Y. (2020). Sivas Cumhuriyet Üniversitesi Yerleşkesinde Güneş Enerjisi Santralının Ekonomik Analizi. *Dokuz Eylül Üniversitesi Mühendislik Fakültesi Fen ve Mühendislik Dergisi*, 22(65), 517-526.
- [8] Oral, M. (2020). Solar energy potential of Turkey and evaluation of PV applications in local scale: Case of Karabük province. *International Journal of Geography and Geography Education (IGGE)*, 42: 482-503
- [9] Orhun, M., Koca, Y.B., Hocaoglu, F.O. Çınar, S.M. (2012). Farklı Yüzey Açılarındaki Işınım Şiddetlerinin Afyonkarahisar Bölgesi İçin Karşılaştırılması ve Güneş Panellerinden Elde Edilebilecek En Yüksek Elektrik Enerjisi Üretimi İçin Uygun Açıların Tespiti, *Afyon Kocatepe University Journal of Science and Engineering*, Cilt. 12, s. 1-5.
- [10] Ceylan, O., Taşdelen, K. 2018. Isparta İli için Fotovoltaik Programlarının Simülasyon Sonuçlarının Doğruluğunun İncelenmesi, *Afyon Kocatepe University Journal of Science and Engineering*, Cilt. 18, s. 895-903.
- [11] Girgin, M.H. Bir Fotovoltaik Güneş Enerjisi Santralının Fizibilitesi, Karaman Bölgesinde 5 MW'lık Güneş Enerjisi Santrali için Enerji Üretim Değerlendirmesi ve Ekonomik Analizi, Master Thesis, İstanbul Technical University, Energy Institute, İstanbul, 2011.
- [12] Haydaroglu, C. and Gümüş, B. 2016. Dicle Üniversitesi Güneş Enerjisi Santralının PVsyst ile Simülasyonu ve Performans Parametrelerinin Değerlendirilmesi, *Dicle Üniversitesi Mühendislik Fakültesi Dergisi*, Cilt. 7(3), s. 491-500.
- [13] Öztürk, H. Bir Güneş Enerji Santralının Üretim İle Simülasyon Değerlerinin Karşılaştırılması Ve Kayıp Analizi: Beştepe Enerji Örneği, Master Thesis, İstanbul Technical University, Institute of Science, Gaziantep, 2021.
- [14] Atlım, F. , Esen, B. & Demirtaş, M. (2019). Balıkesir ilinde farklı iki GES tesisinin panel yerleşimi açısından verimliliklerinin karşılaştırılması. *Balıkesir Üniversitesi Fen Bilimleri Enstitüsü Dergisi*, 21(2), 679-696.
- [15] Başoğlu M. E., Kazdaloğlu A., Bilgin M.Z., Erfidan T., Çakır B. (2014). Farklı Güneş Paneli Teknolojilerinin Kocaeli ili için Performans Değerlendirmesi, Eleco 2014, Bursa, 96-100.
- [16] Nacar, F. (2021). Güneş Enerjisi Santrallerinin Arazi Kullanımına Etkisi ve Sonuçları: Osmaniye Örneği. *Avrupa Bilim ve Teknoloji Dergisi*, Ejosat Özel Sayı 2021 (ARACONF), 98-105.
- [17] Biçen, T. Güneş Panelleri İle Elektrik Üretiminin Teknik ve Ekonomik Analizi: Bursa Örneği, Master Thesis, Bursa Uludağ University, Institute of Science, Bursa, 2018.
- [18] Yıldızay, H.D., Aras, H. and Yılmaz V. (2014). Eskişehir'de rüzgar ve güneş enerjisi potansiyelinin belirlenmesi, *Dicle Üniversitesi Mühendislik Fakültesi Mühendislik Dergisi*, c. 5, sayı. 1, ss. 49-58.
- [19] Atalay Ayran, Z. Kütahya İli Güneş Enerji Potansiyelinin Araştırılması Ve Örnek Bir Güneş Enerji Santralının Ekonomik Analizi, Master Thesis, Kütahya Dumlupınar University, Institute of Science, Kütahya, 2019.
- [20] Bilhan, A.K., Emikönel, S., (2021). Nevşehir İli Güneş Enerji Potansiyelinin Analizi ve Kurulu Güneş Enerji Santralleri. *Avrupa Bilim ve Teknoloji Dergisi*, (24), 289-294.
- [21] Oğuz, M. and Akkurt, Ş. (2017). Kayseri İlinin Yenilenebilir Enerji Potansiyeli. *Ömür Halisdemir Üniversitesi Mühendislik Bilimleri Dergisi*, 6(2), 362-374.
- [22] Çifci, A. and Altundağ, E. (2017). Burdur Bölgesi Güneş Enerjisi Potansiyelinin Elektrik Üretiminde Kullanımı. *Mesleki Bilimler Dergisi*, 6(2), 111-120.
- [23] Çırak, B. (2019) Karaman İlinde Yenilenebilir Enerji Uygulamaları. *KMÜ Mühendislik ve Doğa Bilimleri Dergisi*, 1(1), 19-49.
- [24] Bulut, N., Kuncan, M. and Horoz, S. (2018). Türkiye'de Güneş Enerjisinin Kullanım Alanları ve Siirt Güneş

- Enerji Potansiyeli. Ahtamara I. Uluslararası Multidisipliner Çalışmalar Kongresi, 1315-1319.
- [25] Alcan, Y., Demir, M. and Duman, S. (2018). Sinop İlinin Güneş Enerjisinden Elektrik Üretim Potansiyelinin Ülkemiz Ve Almanya İle Karşılaştırarak İncelenmesi. *El-Cezeri Fen ve Mühendislik Dergisi*, 5(1), 35-44.
- [26] Kaynar, N. K. (2020). Yenilenebilir Enerji Kaynaklarından Güneş Enerjisinin Amasya İlindeki Potansiyeli. *Bilge International Journal of Science and Technology Research*, 4(2), 48-54.
- [27] Geçen, R. (2019). Hatay İlinde Güneş Enerjisi Potansiyeli ve Güneş Enerjisi Potansiyeli ve Güneş Enerjisi Santrali Kurulacak Alanların Belirlenmesi. *Turkish Studies – Social Sciences*, 14(6), 3031-3054.
- [28] Taşkın, O. and Korucu, T. (2014). Kahramanmaraş İli İçin Güneş Enerjisi Potansiyeli ve Kullanım Olanakları. *KSÜ Doğa Bilim Dergisi*, 17(4), 12-16.



# A Successful Falciparum Malaria Treatment with Hemodiafiltration in an African Patient

*Alparslan KOC<sup>1,\*</sup>* 

<sup>1</sup> Erzincan Binali Yıldırım University Mengenek Gazi Training and Research Hospital Department of Anesthesiology and Reanimation, Erzincan, Turkey

## Abstract

Malaria is a serious infectious illness that has existed since ancient times. Despite its prevalence in sub - saharan africa, it remains a global public health issue. However, Plasmodium falciparum causes the most severe and fatal form of malaria, accounting for almost 80% of global mortality. Malarial acute kidney injury (AKI) caused by malaria can progress rapidly. An early initiation to renal replacement therapy is advised because AKI induced by malaria may worsen fast. This paper report a successful severe malaria therapy with hemodiafiltration in the ICU of an African student studying in Turkey. The patient, whose blurring of consciousness increased and Glasgow coma scale (GCS) decreased GCS=8, was admitted to the anesthesiology and reanimation ICU. The patient was treated for 3 days with malaria medications and continuous renal replacement therapy (CRRT). Malaria persists everywhere, especially among nonimmunized people. AKI is common in malaria patients. Patients with severe malaria should be examined for renal involvement, including electrolyte abnormalities and fluid overload. Supportive treatment is recommended for oliguric AKI. If feasible, CRRT may help these patients.

**Keywords:** Malaria, Plasmodium falciparum, AKI, Hemodiafiltration

## 1. Introduction

Malaria is a serious infectious illness that has existed since ancient times. Over three million individuals in over 100 countries are infected with this parasitic illness, which causes over 400 thousand fatalities annually. Despite its prevalence in Sub-Saharan Africa, it remains a global public health issue [1]. Plasmodium falciparum, plasmodium vivax, plasmodium ovale, plasmodium malaria, and plasmodium knowlesi are the five human parasites. However, P falciparum produces the most severe and life-threatening type of malaria and is responsible for more than 80% of malaria deaths worldwide [2]. Mortality is linked to the degree of parasitaemia. Case fatality rates are higher in patients with high parasite densities. If the parasite count is greater than 10%, exchange transfusions may be helpful, as they eliminate parasitemia faster than optimum treatment alone [3]. The diagnosis of malaria underlines the value of early diagnosis and treatment in easing patient suffering. The gold standard for diagnosing malaria is a peripheral blood smear [4]. Although the pathophysiology of malarial acute kidney injury [AKI] is unknown, many pathways have been hypothesized. Hypotheses include hemodynamic (mechanical changes, immune-mediated glomerular damage, and metabolic changes [5]. Fluid overload [pulmonary edema, heart failure), refractory electrolyte imbalances (hyperkalemia, metabolic acidosis), or symptomatic uremia may require specialist therapy such as dialysis. Malaria causes hypercatabolism in these patients, increasing their requirement for dialysis. Because AKI caused by malaria can progress rapidly, it is recommended to start renal replacement treatment as soon as possible [6]. We will present the successful severe malaria treatment that we applied with hemodiafiltration in the intensive care unit (ICU) of a university student who came to Turkey from Africa for education.

## 2. Case Report

A 22-year-old man came to Turkey from the Republic of Guinea-Bissau, one of the West African countries, for university education. The patient, who applied to the emergency department due to confusion and fever, was hospitalized by the infectious diseases clinic. In his story, he stated he returned from his country three days ago

\* Corresponding author. e-mail address: dralparslankoc@gmail.com

and that his fever started while he was in his country. After examinations, the patient was diagnosed with *P falciparum* malaria. The patient, whose blurring of consciousness increased and Glasgow coma scale [GCS] decreased GCS=8, was admitted to the anesthesiology and reanimation ICU. There was no acidosis in blood gas, but the pO<sub>2</sub> value was 62 mmHg despite high flow oxygen support. The patient whose blurred consciousness increased in the ICU follow-up was intubated and connected to a mechanical ventilator. It was determined that the patient had no urine output, and the creatinine value increased from 1.3 to 4.1 within one day. Jaundice was observed in the conjunctiva, and the measured total bilirubin value was 23.28 mg/dl, of which 12.74 mg/dl was direct bilirubin. When hepatitis markers were examined, anti-Hav IgG was positive, and HBs Ag and anti-HCV were negative. Ultrasound imaging at the bedside revealed minimal hepatomegaly, and the bladder was empty.

Transfusion of 6 units of platelet suspension was applied to the patient whose platelet count decreased to 31.000. The patient's admission laboratory values are presented in Table 1. With the recommendation of infectious diseases, Artesunate 120 mg intravenous [iv] loading dose was followed by maintenance treatment, as Artemeter 20 mg + Lumefantrine 120 mg nasogastric 2x4 tablets. Continuous renal replacement therapy (CRRT) was decided, and a jugular dialysis catheter was applied. The device was arranged as continuous venovenous hemodiafiltration (CVVHDF). A total of 1000 ml of dialysate, 1000 ml replacement fluid, and 100 ml ultrafiltration per hour were adjusted. Malaria and supportive treatments were continued with CRRT for approximately 72 hours.

**Table 1.** ICU entrance laboratory values

Hemoglobin	9.8 mg/dL	Low (13.5 - 17.5)
Platelet	31x10 <sup>3</sup>	Low (150 - 450)
Total bilirubin	23.28 mg/dL	High (0.3 - 1.2)
Direct bilirubin	12.74 mg/dL	High (0 - 0.2)
AST	102 u/L	High (0 - 50)
ALT	27 u/L	N (0 - 50)
Urea	124 mg/dL	High (17 - 43)
Creatinin	4.1 mg/dL	High (0.5 - 1.2)
Na	128 mmol/L	Low (135 - 145)
K	3.4 mmol/L	Low (3.5 - 5.1)
INR	1.21 Sn % INR	N (0.8 - 1.24)

During this period, the patient was sedated for mechanical ventilation and compliance with CRRT. In the first 24 hours of CRRT, the creatinine value increased to 7.2 mg/dl and then gradually decreased and regressed to 2.3 mg/dl after CRRT. On the second day of CRRT, the hemoglobin level decreased to 6.8 mg/dL, and two units of hemoglobin suspension were transfused. Urine output started on the third day of CRRT. After CRRT was ended, sedation was stopped, and the patient waited for awakening. The patient, who was almost entirely conscious of the situation, was weaned off the mechanical ventilator. On the fifth day of hospitalization for the patient in the ICU, GCS = 15 and creatinine=1.55 mg/dl. He was discharged to the infectious diseases clinic in good health [Table 2.].

**Table 2.** ICU discharge laboratory values

Hemoglobin	10.6 mg/dL	Low (13.5 - 17.5)
Platelet	295x10 <sup>3</sup>	N (150 - 450)
Total bilirubin	3.32 mg/dL	High(0.3 - 1.2)
Direct bilirubin	1.41mg/dL	High (0 - 0.2)
AST	49 u/L	N (0 - 50)
ALT	58 u/L	N (0 - 50)
Urea	69 mg/dL	High (17 - 43)
Creatinin	1.55 mg/dL	High (0.5 - 1.2)
Na	136 mmol/L	Low (135 - 145)
K	4.5 mmol/L	Low (3.5 - 5.1)
INR	1.18 Sn % INR	N (0.8 - 1.24)

### 3. Results and Discussion

The severe and deadly consequences associated with *P. falciparum* infection make it more dangerous than other malaria species. Hyperparasitaemia, Blackwater fever, renal failure, acute malarial hepatitis, adult respiratory distress syndrome, adrenal insufficiency syndrome, cardiac arrhythmias, and gastrointestinal symptoms, including secretory diarrhea, are all caused by this deadly parasite [7]. *P. falciparum* infects erythrocytes of any age, causing high-grade parasitemia. The parasite count can grow up to 20-fold in 48 hours without treatment because of its fast replication. In the therapeutic environment, parasitemia helps define severe *P. falciparum* malaria and tracks the effectiveness of antimalarial medication [8]. There is a clear association between an individual's asexual erythrocytic-stage parasite density at the time of presentation and the severity of clinical illness in *P. falciparum* malaria [9]. Here, the patient encountered the agent in his own country and came to our country within three days of his illness. Several researchers advise only considering exchange transfusion for individuals with severe parasitemia [10]. A reduction in the risk of severe intravascular hemolysis and its consequences, better rheology, reduced microcirculatory sludging, and increased oxygen carrying capacity with transfused erythrocytes are all reasons to use exchange transfusion treatment [11]. The patient was in a precoma state. We started CRRT as we can decide quickly and start the fastest. Malaria-associated AKI has a death rate of up to 51%, with the poorest prognosis being delayed referral, severe jaundice, oliguria, and multiorgan involvement [12]. Zheng et al. performed successful treatment in 12 patients with CRRT combined with artesunate [13]. A small RCT compared CRRT with peritoneal dialysis in Vietnamese patients with AKI, mainly due to malaria. Twelve CRRT patients had decreased mortality and overall expenditures [14].

### 4. Conclusions

In conclusion, malaria remains a global problem, particularly among nonimmunized populations. AKI is prevalent in severe malaria patients. Severe malaria patients should be continuously monitored for renal involvement, including refractory electrolyte imbalances and fluid overload. Patients with oliguric AKI should be treated with supportive therapy. CRRT may be an effective option in these patients if possible.

### References

- [1] Kazancıoğlu S., Bodur H. (2022). İmporte Sıtma Vakalarının Değerlendirilmesi: Ankara’da Bir Eğitim ve Araştırma Hastanesi Deneyimi. *Sağlık Bilimlerinde Değer*, 12[1]:1-5.
- [2] Julien J-P., Wardemann H. (2019). Antibodies against *Plasmodium falciparum* malaria at the molecular level. *Nature Reviews Immunology*, 19[12]:761-75.
- [3] Weir E.G., King K.E., Ness P.M., Eshleman S.H. (2000). Automated RBC exchange transfusion: treatment for cerebral malaria. *Transfusion*, 40[6]:702-7.
- [4] Arshad A.R. (2015). Thrombocytopenia in malaria: can platelet counts differentiate malaria from other

- infections? *J Coll Physicians Surg Pak.*, 25[1]:31-4.
- [5] Eiam-Ong S., Sitprija V. (1998). Falciparum malaria and the kidney: a model of inflammation. *Am J Kidney Dis.*, 32[3]:361-75.
  - [6] Brown D.D., Solomon S., Lerner D., Del Rio M. (2020). Malaria and acute kidney injury. *Pediatric Nephrology.*, 35[4]:603-8.
  - [7] Ali H., Ahsan T., Mahmood T., Bakht S.F., Farooq M.U., Ahmed N. (2008). Parasite density and the spectrum of clinical illness in falciparum malaria. *J Coll Physicians Surg Pak.*, 18[6]:362-8.
  - [8] Dubey M.L., Weingken C., Ganguly N.K., Mahajan R.C. (1999). Comparative evaluation of methods of malaria parasite density determination in blood samples from patients & experimental animals. *Indian J Med Res.*;109:20-7.
  - [9] McElroy P.D., Beier J.C., Oster C.N., Beadle C., Sherwood J.A., Oloo A.J., et al. (1994). Predicting outcome in malaria: correlation between rate of exposure to infected mosquitoes and level of Plasmodium falciparum parasitemia. *Am J Trop Med Hyg.*, 51[5]:523-32.
  - [10] Kute V.B., Shah P.R., Munjappa B.C., Gumber M.R., Patel H.V., Jain S.H., et al. (2012). Outcome and prognostic factors of malaria-associated acute kidney injury requiring hemodialysis: A single center experience. *Indian J Nephrol.*, 22[1]:33-8.
  - [11] Zucker J.R., Campbell C.C. (1993). Malaria. Principles of prevention and treatment. Infectious disease clinics of North America., 7[3]:547-67.
  - [12] Brown D.D., Solomon S., Lerner D., Del Rio M. (2020). Malaria and acute kidney injury. *Pediatric nephrology* [Berlin, Germany]., 35[4]:603-8.
  - [13] Yishan Z., Yongfu L., Dongyang S., Hu L. (2018). Effect evaluation of hemodiafiltration rebuilding homeostasis while fatal dysregulation of homeostasis in *severe malaria*., 18[7]:657-61.
  - [14] Phu N.H., Hien T.T., Mai N.T., Chau T.T., Chuong L.V., Loc P.P., et al. (2002). Hemofiltration and peritoneal dialysis in infection-associated acute renal failure in Vietnam. *The New England journal of medicine.*, 347[12]:895-902.





# Production and Characterization of Diatomite Reinforced MDI-Based Composites

***Zehra Gülten YALÇIN<sup>1</sup>***, ***Mustafa DAĞ<sup>1</sup>***, ***Ercan AYDOĞMUŞ<sup>2</sup>***

<sup>1</sup>Chemical Engineering, Engineering Faculty, Çankırı Karatekin University, Çankırı, Türkiye

<sup>2</sup>Chemical Engineering, Engineering Faculty, Fırat University, Elazığ, Türkiye

## Abstract

In this study, new composite materials have been improved by commercial polyol and methylene diphenyl diisocyanate (MDI). Diatomite filler in the particle size range of 149 to 74 microns is prepared for composite production as a filler after drying at 105 °C. Diatomite reinforced composites at different ratios by mass (0 %, 1 %, 2 %, 3 %, 4 %, and 5 %) are produced at room temperature under open conditions to the atmosphere. After mixing commercial polyol and diatomite filler at 1000 rpm for 5 minutes, MDI is added to the mixture and chemical reactions take place at 1500 rpm for 90 seconds. After the mixture is poured into standard molds and allowed to cure for 24 hours, necessary tests and analyzes are carried out. The chemical bond structure of the synthesized composite is determined by Fourier transform infrared (FTIR) spectroscopy. Besides, the surface morphology and pore structure of the composite are examined by scanning electron microscopy (SEM). According to the results, it is observed that as the amount of diatomite filler in the composite raises, the number of closed pores increases, and the pore diameter decreases. Besides, the rise in the amount of diatomite in the mixture provides an increase in the density of the composite. With the addition of diatomite, the thermal conductivity coefficient of the composite varies between 0.026 W/m·K and 0.039 W/m·K. Diatomite reinforcement increases both Shore D hardness and the thermal conductivity coefficient of the produced composite. Also, thermal degradation experiments of the obtained composites have been carried out in a PID-controlled system in an inert environment between 25 °C and 575 °C. The filler increases the activation energy and thus the thermal stability of the produced composite.

**Keywords:** Composite, Density, Shore D, Thermal Conductivity, Activation Energy

## 1. Introduction

When we look from the past to the present, it is understood from the literature that composite materials have a significant degree of use in human history. Thousands of years ago, the first steps were taken in the construction of houses by combining mud bricks with straw additives and using clay and ash components as mortar. Nowadays, research is carried out on composite materials due to the situations where traditional materials do not meet the needs and some properties need to be improved. Composites are defined as materials formed by combining two or more components. These components usually tend to retain their properties. With the discovery of glass fiber in the United States in the 1930s, modern composite production was started. The use of glass fiber in composites and the effect of its advantages have initiated the search for new additives and filler materials. In addition to the practical nature of the production of composite materials, the durability and long service life have led to an increasing number of areas of use. In addition to the advantages mentioned, their physical and chemical durability, lightness, fatigue strength, electrical and thermal conductivity properties, and economical cause composites to be seen as the material of the future. Due to the variety of these properties, it occupies an important place in many engineering and industrial applications.

Many R & D studies are being carried out as a candidate for the advanced material of the future to eliminate its weak properties. Various additive materials are used to improve the properties of composite materials. Diatomite, one of these additives; has a composition in the form of  $\text{SiO}_2 \cdot n\text{H}_2\text{O}$ . Diatomites are formed by the fossilization of some algae species. When the silica minerals contained in its structure are crushed, it turns into a fine, white, abrasive powder. This powder is light due to its porous structure. Due to its porosity, it has water absorption properties three times its weight. Depending on the content, the hardness of diatomite Decays between 1.5-6 according to the mohr scale. The reason why it has such a wide range can be said to be due to its

\* Corresponding author. e-mail address: zaltin@karatekin.edu.tr

fragile structure. While diatomites are resistant to chemicals, they are affected by strong bases at high temperatures and are unstable to hydrofluoric acid [1-4].

In this study, it was aimed to take advantage of the listed properties of diatomites. Again, some of the additives added to composite materials are adjusted to serve as glue. Of these additives, MDI (methylene diphenyl diisocyanate) compared to other species (phenol-formaldehyde, etc.) It is preferred because it hardens faster, has higher moisture resistance, and is used in lower doses. It is known from the literature that MDI forms covalent bonds that are strong and stable and contains isocyanate groups that can form urethane bonds by reacting with OH groups. It has also been noted that MDI shows strong resistance to hydrolysis due to its non-polar aromatic structure and cross-linking effects [5-8]. In light of all these data, this study was conducted to develop a new and durable composite.

## 2. Materials and Methods

### 2.1. Materials used in the experimental study

Commercial polyol (CP), and methylene diphenyl diisocyanate (MDI) components used in experimental studies were supplied by Kimpur Company. In addition, diatomite used as a filler was purchased from Türk Diatom Company.

### 2.2. Method used in polymer synthesis

In Figure 1, the polymer composite production scheme in experimental studies is expressed. Here, both the quantities of the ingredients and the order of use are very important. Also, the fillers should provide a homogeneous distribution to the synthesized composite.

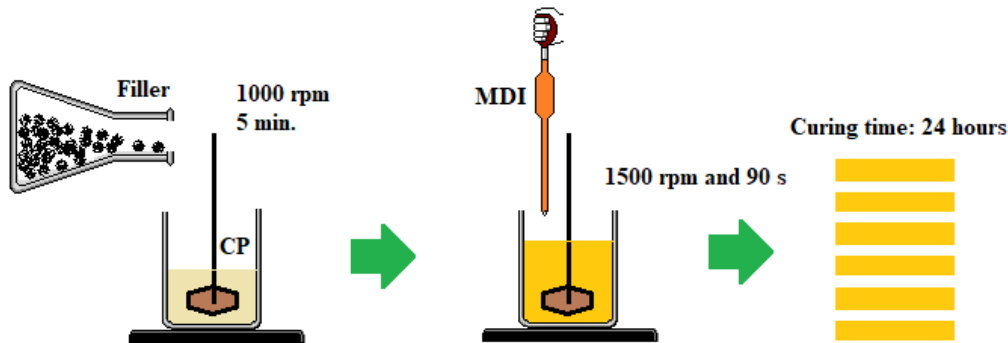


**Figure 1.** Production scheme of diatomite reinforced MDI-based composite.

The amounts of each ingredient used are expressed in Table 1. The amounts of other components are kept constant, except for the filler (diatomite) used here.

**Table 1.** Production plan of diatomite reinforced MDI-based composite

CP (g)	MDI (g)	Filler (g)
50	50	0
50	50	1
50	50	2
50	50	3
50	50	4
50	50	5

### 3. Results and Discussions

#### 3.1. Density of produced polymer composites

The variation of the density of the obtained polymer composites is shown in Figure 2 depending on the diatomite ratio by mass. It is understood from the graph that diatomite increases the density of the polymer composite.

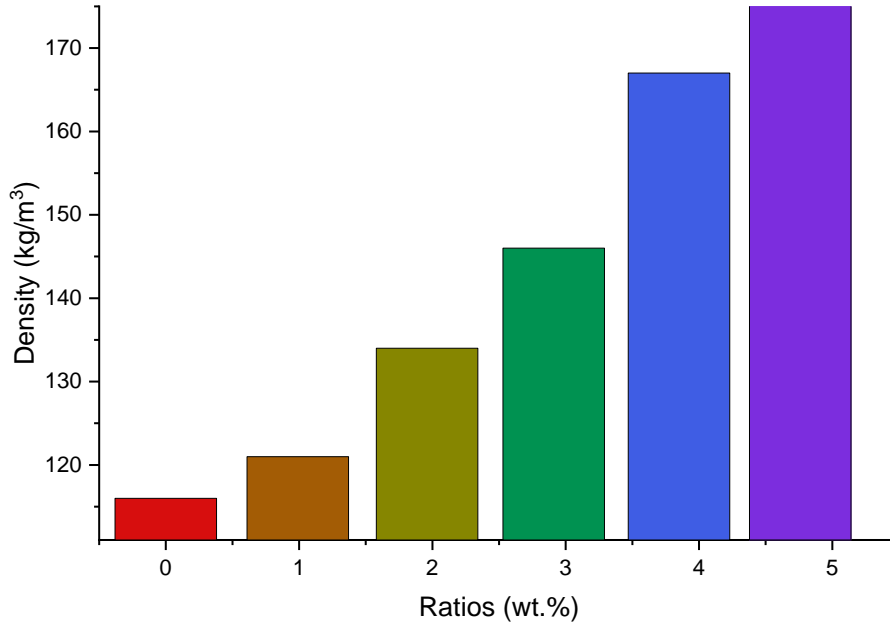


**Figure 2.** The effect of diatomite reinforcement on the density of composite.

#### 3.2. Hardness of the polymer composites

In the graphs shown in Figure 3, it is seen that the hardness of the synthesized polymer composites increased with diatomite reinforcement.

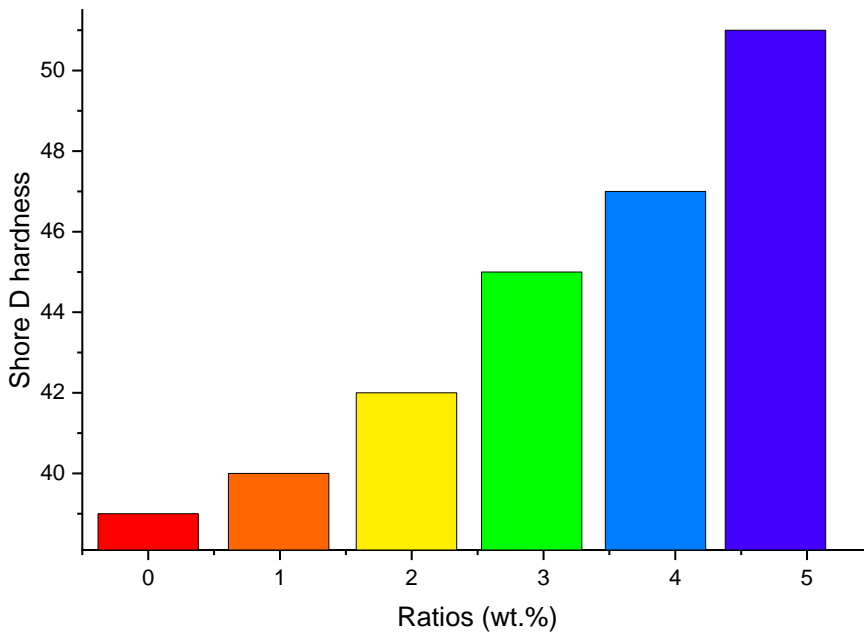


**Figure 3.** The effect of diatomite reinforcement on the hardness of the composite.

### 3.3. Thermal conductivity of the polymer composites

In Figure 4, it is seen that the thermal conductivity increases as the filler (diatomite) ratio by mass raises in the composite.

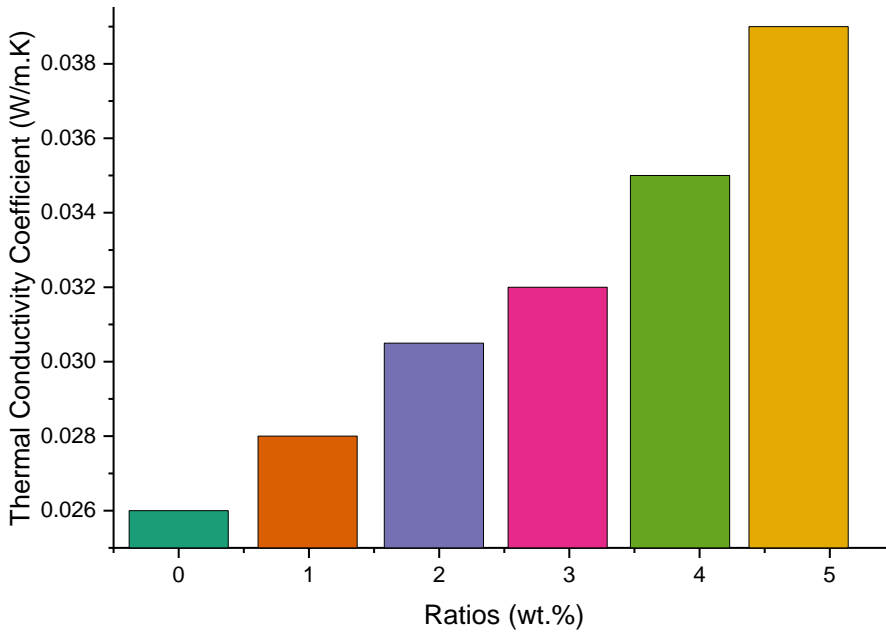


**Figure 4.** The effect of diatomite reinforcement on the thermal conductivity of the composite.

### 3.4. Activation energy of the polymer composites

Activation energy ( $E_a$ ) values are calculated according to Coats-Redfern (Table 2). In this method, the highest correlation coefficient was found in diffusion control (Crank) function. Activation energies of MDI-based composites reinforced with fillers are calculated in thermal decomposition experiments carried out at a heating rate of about 10 °C/min at 575 °C.

**Table 2.** Activation energies of the polymer composites.

Ratio (wt.%)	Activation Energy (kJ/mol)
0	71.24
0.99	75.82
1.96	83.56
2.91	87.32
3.85	92.73
4.76	96.45

### Acknowledgment

We would like to thank Fırat University Chemical Engineering Department and Çankırı Karatekin University Chemical Engineering Department for their support in laboratory studies.

### References

- [1] Kaya, A. İ. (2016). Kompozit malzemeler ve özellikleri. Putech & Composite Poliüretan ve Kompozit Sanayi Dergisi, 29, 38-45.
- [2] Bulut, Y., & Erdoğan, Ü. H. (2011). Selüloz Esaslı Doğal Liflerin Kompozit Üretiminde Takviye Materyali Olarak Kullanımı. Tekstil ve Mühendis, 18(82), 26-35.

- [3] Arat, A. Y., Kaya, H., & Çep, E. B. Grafenli ve Geri Dönüştürülmüş Karbon Fiberli Polimer Kompozit Malzemenin Üretilerek Mekanik Deney Çubuklarının Üretimi ve İncelenmesi, International Marmara Sciences Congress (Imascon Spring) 2022 Proceedings Book, Kocaeli, 2022, 323-329
- [4] Taş, B., & Çetin, M. (2012). Biyolojik orijinli tek doğal mineral: diyatomit. Tübvav Bilim Dergisi, 5(2), 28-46.
- [5] İstek, A., & Özlüsoylu, İ. Farklı Oranlarda p-MDI ile Üretilmiş Kabuk İzolasyon Levhalarının Özellikleri, 4th International Congress on Multidisciplinary Studies, KKTC, 2018, 390-400.
- [6] Yılmaz, C. (2019). Güç tutuşur su bazlı poliüretan sentezi ve polyester kumaş kaplaması olarak incelenmesi (Master's thesis, Bursa Teknik Üniversitesi).
- [7] Demiryuğuran, F. (2015). Cam elyaf, karbon elyaf ve organik madde takviyeli kompozit poliüretan köpük malzemelerin ısı bozunma ve yanma davranışlarının incelenmesi (Master's thesis, Pamukkale Üniversitesi Fen Bilimleri Enstitüsü).
- [8] Aydın, A. (2018). Antibakteriyel nefes alabilen membranların tasarımı ve üretimi (Master's thesis, Bursa Teknik Üniversitesi).



## Investigation of Mg<sup>+2</sup> Ion Behavior in Colemanite Propionic Acid Solutions

Mücahit UĞUR<sup>1,\*</sup> , M. Muhtar KOCAKERİM<sup>1</sup> , Ahmet YARTAŞI<sup>1</sup> 

<sup>1</sup>Department of Chemical Engineering, Faculty of Engineering, Çankırı Karatekin University, Çankırı, Turkey

### Abstract

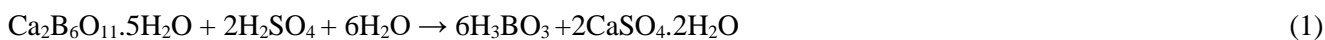
Colemanite ore, one of the most commercially important boron minerals, is used in industry to produce various boron compounds due to its rich B<sub>2</sub>O<sub>3</sub> content. Turkey's most important commercially extracted boron ores are colemanite, tincal and ulexite as the second ore. In our country, various boraxes are produced by dissolving boric acid from colemanite by the sulfuric acid process and tincalin is dissolved in hot water, and ulexite is concentrated and exported. The main problem in the production of boric acid by the sulfuric acid process is impurities. One of the impurities is Mg<sup>+2</sup> ions that pass into the solution and it is important to examine the kinetics of this ion in the solution. In this study, the dissolution of colemanite ore in propionic acid solution in an aqueous medium in a batch reactor under atmospheric pressure was investigated. As dissolution parameters; colemanite particle size (D) 100 150, 150-250, 250-400\*, 400-600 µm and solid/liquid ratio (K/S) 20 40\*-60-80 g/L. As a result of the experiments, the time-dependent variation of the Mg<sup>+2</sup> concentration in the solution was observed.

**Keywords:** Colemanite, Propionic acid, Mg<sup>+2</sup> impurity, Dissolution

### 1. Introduction

Boron and boron minerals are one of the most important mines in the world in terms of industry [1]. Boron and boron derivatives are mostly found in the form of natural compounds containing different proportions of boroxide in their structures [2]. It is known that there are about 230 free boron minerals in nature. However, colemanite (Ca<sub>2</sub>B<sub>6</sub>O<sub>11</sub>.5H<sub>2</sub>O), tincal (Na<sub>2</sub>B<sub>4</sub>O<sub>7</sub>.10H<sub>2</sub>O) and ulexite (NaCaB<sub>5</sub>O<sub>9</sub>.8H<sub>2</sub>O) are the leading ones that have commercial importance in the world [3, 4, 5]. Turkey alone has a share of 73% of the world's boron reserves and has colemanite, tincal and ulexite ore reserves, respectively [6, 7, 8]. Boron and boron derivatives are used in nearly 500 sectors from fiberglass and glass industry [9], rubber and paint industry [6], wood protection and agriculture industry, high-quality steel and heat resistant polymers [10], nuclear technology products [1] to rocket engine fuels [11] disinfectants and detergent sector [12].

Boric acid is industrially produced according to the reaction in Equation 1 with colemanite and sulfuric acid solution at 92°C. For 1 mole of colemanite ore, 6 moles of boric acid (H<sub>3</sub>BO<sub>3</sub>) are produced.



There are scientific studies in the literature on the dissolution of colemanite ore in solutions saturated with organic and inorganic acids or different acidic gases in the production of boron compounds. In the literature, leaching solutions and rate control steps of these dissolution processes are given [6]. Industrially, there are several problems in the production of boric acid from colemanite by the sulfuric acid process. Most of these problems are mainly due to the presence of calcium and magnesium-containing minerals in the colemanite ore. Ca<sup>2+</sup> and Mg<sup>2+</sup>, which go into solution in acidic environment, form impurities in boric acid and reduce product quality. For this reason, in our study, the effect of grain size and solid/liquid ratio on the dissolution of Mg<sup>+2</sup> ions passing from the colemanite ore to the solution in the presence of propionic acid was investigated.

### 2. Materials and Methods

The colemanite used in the study was obtained from boron deposits of Eti Mine Works. After the impurities on the ore were cleaned by mechanical means, they were ground with the help of a crusher-grinder, and a chemical

\* Corresponding author. e-mail address: m.ugur@karatekin.edu.tr

analysis was carried out. It is divided into 4 sizes with ASTM standard sieves 100-150, 150-250, 250-400, and 400-600  $\mu\text{m}$ . The chemicals used in the study were obtained from various companies with high purity. The chemical analysis of the ore used in the study is given in Table 1.

**Table 1.** Chemical analyses of the colemanite ore used in the studies

Component	B <sub>2</sub> O <sub>3</sub>	CaO	H <sub>2</sub> O	MgO	Humidity
%	35.22	20.25	15.76	2.72	0.73

X-Ray diffraction (XRD) to determine the phase composition of the raw colemanite ore is given in Figure 1.

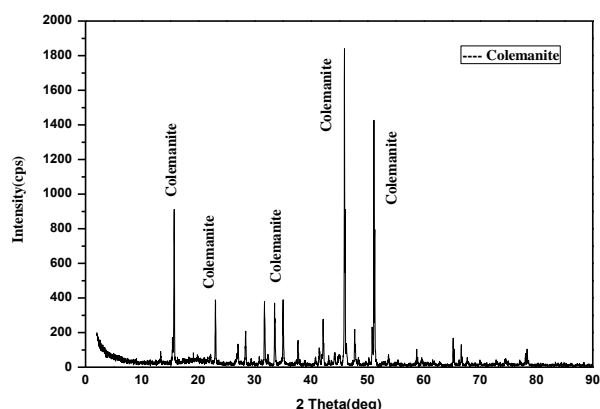


**Figure 1.** XRD analysis of colemanite

Parameter levels for dissolution were determined as a result of preliminary testing and are given in Table 1. The grain size is in two size ranges. The experimental design plan prepared accordingly is given in Appendix 1. The amount of  $\text{Mg}^{+2}$  in the solutions taken at certain intervals during the experiment was analyzed with the help of an AAS (Atomic Absorption Spectrophotometer). Table 1. Chemical analyses of the colemanite ore used in the studies.

**Table 2.** Parameters and levels selected in the investigation of the behavior of  $\text{Mg}^{+2}$  released into solution in the reaction of colemanite ore with propionic acid in an aqueous solution

	PARAMETERS	LEVELS
A	Grain size, ( $\mu\text{m}$ )	100-150, 150-250, <b>250-400*</b> , 400-600
B	Solid/liquid ratio, (g/L)	20, <b>40*</b> , 60, 80

\*Fixed parameters

The dissolution process is carried out in a batch reactor and the experimental system for the dissolution process is given in Figure 2. Experimental studies were carried out in a 500 mL jacketed glass reactor. The solution is left in the reactor with the solid/liquid ratio determined under the experimental conditions, and it is heated to the desired temperature. Then, a certain amount of colemanite was added and mixed through a mechanical mixer. During the reaction, solutions are taken at certain times and after the volume is completed to a certain amount, the amount of  $\text{Mg}^{+2}$  is determined.

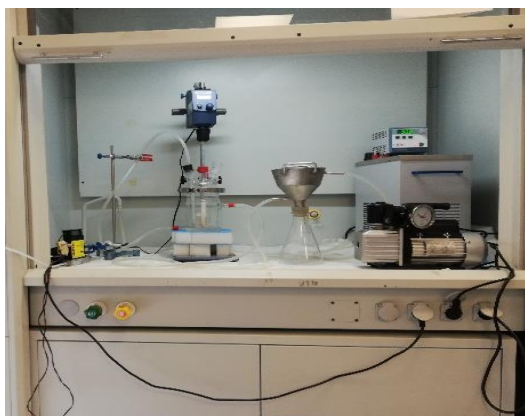
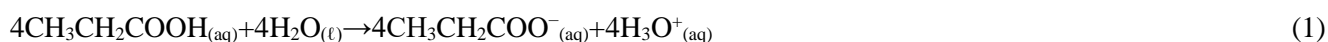


**Figure 2.** The experimental setup used in our experimental studies

### 3. Results and Discussion

#### 3.1 Reactions to solutions

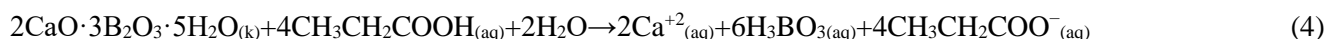
The reaction related to the dissolution of colemanite in the presence of propionic acid in aqueous solution can be written as in Equation 1-4:



The reactions that occur in the environment when colemanite is added to the propionic acid solution are as follows;



The total reaction is as follows;



#### 3.2 Effect of parameters

The behavior of solid-liquid ratio and particle size,  $\text{Mg}^{+2}$  into solution upon dissolution of colemanite ore in propionic acid solutions in a batch reactor under atmospheric pressure were investigated. Experimental results are plotted as percent dissolution of  $\text{Mg}^{+2}$  ion behavior versus time.

##### Effect of particle size

The effect of particle size on the solution penetration rate of  $\text{Mg}^{+2}$  was investigated at grain sizes of 100-150  $\mu\text{m}$ , 150-250  $\mu\text{m}$ , 250-400  $\mu\text{m}$  and 400-600  $\mu\text{m}$ . During the study, the reaction temperature was 303°K, the acid concentration was 6.75 M, the solid-liquid ratio was 40 g/L, and the stirring speed was kept constant at 400 rpm. The percentages of the dissolution fraction of  $\text{Mg}^{+2}$  that passed into the solution as a result of the experiment are given in Figure 3. As seen in the time versus percent dissolution graph in Figure 3., there is an inverse relationship between the increase in grain size and the penetration of  $\text{Mg}^{+2}$  into solution. It is seen that the dissolution rate decreases with increasing grain size.



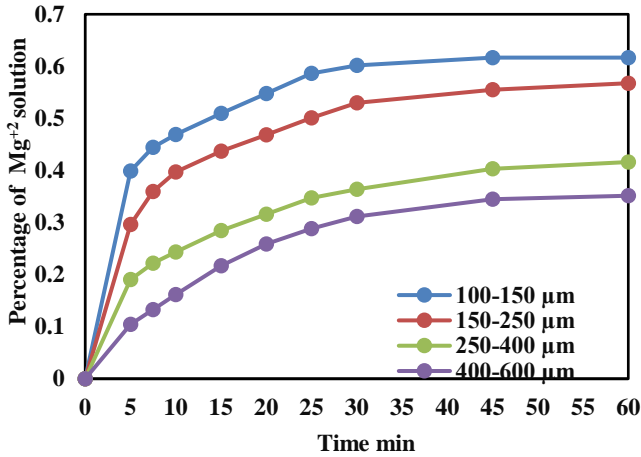


**Figure 3.** The effect of grain size on the passage of  $Mg^{+2}$  into solution in the dissolution of colemanite

### Effect of solid-liquid ratio

The effect of solid/liquid ratio on the rate of  $Mg^{+2}$  passing into solution; was investigated in solid-liquid ratios of 20 g.L-1, 40 g.L-1, 60 g.L-1 and 80 g.L-1. During the study, the reaction temperature was 303°K, the acid concentration was 6.75 M, the particle size was 250-400 µm, and the stirring speed was kept constant at 400 rpm. The percentages of the dissolution fraction of  $Mg^{+2}$ , which passed into the solution as a result of the experiment, are given in Figure 4. As seen in the time versus percent dissolution graph in Figure 4., there is an inverse relationship between the increase in the solid/liquid ratio and the passage of  $Mg^{+2}$  into solution. It is seen that the dissolution rate decreases with the increase in the solid-liquid ratio.

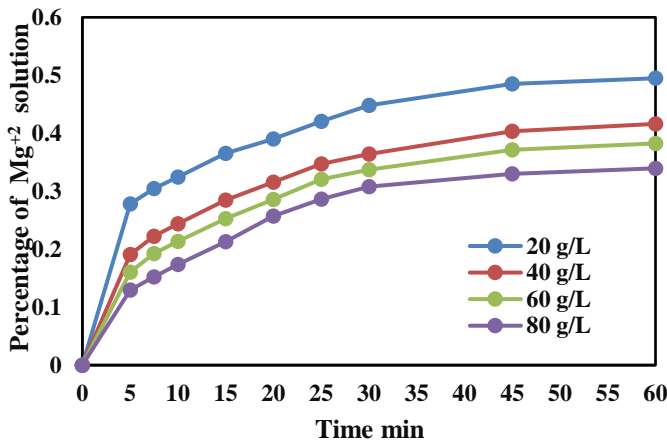


**Figure 4.** The effect of solid-liquid ratio on the transition of  $Mg^{+2}$  to solution in the dissolution of colemanite.

## 4. Results

This study aims to investigate the  $Mg^{+2}$  ion behavior of colemanite in propionic acid solution in a batch reactor at atmospheric pressure and to determine an alternative reactant for boric acid production.

- ✓ It is seen that there is an inverse relationship between the increase in solid-liquid ratio and the particle size of the colemanite ore, and the rate of  $Mg^{+2}$  ion passing into the solution.
- ✓ It was determined that propionic acid, which has weak acidic properties, can dissolve colemanite ore for boric acid production.

## Appendix

**Table 1** Experimental plan

Experiment No	Sabit Parametreler	Particle size ( $\mu\text{m}$ )	Solid/fluid ratio (g/L)
1	303 K 6.75 M 400 rpm 40 g/L	100-150	40
2		150-250	40
3		250-400	40
4		400-600	40
5	303 K 6.75 M 400 rpm 250-400 $\mu\text{m}$	250-400	20
6		250-400	60
7		250-400	80

## 5. References

- [1] Doğan, H., & Yartaşı, A. (2009). Kinetic investigation of reaction between ulexite ore and phosphoric acid. *Hydrometallurgy Volume, 96, Issue 4, Pages 294-299*.
- [2] Kopac, T., Kırca, Y. & Toprak, A. (2017). Synthesis and characterization of KOH/boron modified activated carbons from coal and their hydrogen sorption characteristics. *Int J Hydrogen Energy* 42:23606e16.
- [3] Küçük, A.V., & Kocakerim, M.M., (2019). Effects of Leaching Parameters on the Impurity Ion Concentrations at Ulexite Ore Leaching: An Experimental Design Approach. *Iran. J. Chem. Chem. Eng.* 38, No. 3, 2019.
- [4] Küçük. Ö., & Korucu. H., (2018). Optimization of Boric Acid Extraction From Colemanite With An Environmentally Friendly Process By Using The Taguchi Method. *J. Chem. Soc. Pak.*, 40, No. 03.
- [5] Sert H, Yıldırım H, & Toscalı D. (2012). An investigation on the production of sodium metaborate dihydrate from ulexite by using trona and lime. *Int J Hydrogen Energy* 37: 5833e9.
- [6] Guliyev, R., Kuşlu, S., Çalban, T. & Çolak, S., 2012. Leaching kinetics of colemanite in ammonium hydrogen sulphate solutions. *Journal of Industrial and Engineering Chemistry*, 18 (38), 1202-1207.
- [7] Elçiçek, H., & Kocakerim, M.M., (2018). Leaching kinetics of ulexite ore in aqueous medium at different CO<sub>2</sub> partial pressure. *Brazilian Journal of Chemical Engineering. Vol. 35, No. 01, pp.*
- [8] Şimşek. H., Guliyev. R., & Beşe. A., (2018). Dissolution kinetics of borogypsum in di-ammonium hydrogen phosphate solutions. *International Journal of Hydrogen Energy Volume 43, Issue 44, Pages 20262-20270*.
- [9] Arasu A.V., Sornakumar T., (2007). Design, Manufacture and Testing of Fiberglass Reinforced Parabola Trough for Parabolic Trough Solar Collectors. *Solar Energy*, 81: 1273-1279.
- [10] Kızılcı, M., & Çopur, M. (2015). Kinetic Investigation of Reaction Between Colemanite Ore and Methanol. *Journal Chemical Engineering Communications*, 202, 1528-1534.
- [11] Alkan. M., & Doğan. M., (2003). Dissolution kinetics of colemanite in oxalic acid solutions. *Chemical Engineering and Processing* 43 867–872.
- [12] M, Tunç., M, H, Çalımlı., S. Çolak., Ö. Küçük., & M. M. Kocakerim. (2008). Dissolution Kinetics of Ulexite in Phosphoric Acid Solutions. *Asian Journal of Chemistry, cilt.20, ss.3161-3170*.



# Evaluation of the Performance of Reduced Graphene Oxide Samples Synthesized using Hummers and Chemical Reduction Method using Different Purity Graphite on Cement Mortar

**Haluk KORUCU\*** 

<sup>1</sup> *Department of Chemical Engineering, Faculty of Engineering, Çankırı Karatekin University, UluYazı, Çankırı 18100, Turkey*

## Abstract

In this study, 85% Nanokar, 99% Nanokar, and 99.9% Merck's different purity of graphite are used with the hummer's method and chemical reduction method to synthesize reduced graphene oxide. It is aimed to evaluate the performance of synthesized reduced graphene oxide samples by using them in cement mortar. To determine the performance of reduced graphene oxide samples on hardened concrete, 7- and 28-day Thermal Conductivity and Heat Capacity measurements and 28-day electrical resistance and compressive strength measurements are taken. A reference experiment which was reduced graphene oxide not used in this experiment was performed to determine the recovery rates in the measurements. The recovery rates for 7- and 28-day Thermal Conductivity measurements were obtained at 34,63% and 52,63%, respectively by using a reduced graphene oxide sample coded rGO3 synthesized with 99,99% Merck graphite. The recovery rates were found to be 57.10% and 47.59% for 7- and 28-day heat capacity measurements, respectively, and were obtained by using a reduced graphene oxide sample coded rGO3 synthesized with graphite 99.99% Merck. The electrical resistance and compressive strength recovery rates were found to be 15.58% and 35.03%, respectively, and were obtained by using a reduced graphene oxide sample coded rGO1 synthesized with 85% Nanokar graphite. The experimental results showed that the performance of the reduced graphene oxide sample synthesized with low-purity domestic origin graphite, especially on thermal conductivity and heat capacity, was close to the reduced graphene oxide sample synthesized using high-purity foreign origin graphite. When this is evaluated in terms of costs and production on a large scale, getting great importance.

**Keywords:** *Thermal Conductivity, Chemical reduction method, Heat Capacity, Reduced Graphene Oxide, Cement mortar*

## 1. Introduction

Chemical additives are materials that are added to the cement mortar during mixing or immediately before mixing. Nowadays, the use of chemical and mineral additives is increasing rapidly to improve the properties of concrete[1]. It improves the properties of concrete during the hardening process and transportation. Along with the use of graphene-doped cement-based composite materials and the use of less cement, a positive effect of their mechanical properties was also observed [2]. The contribution of graphene encourages innovative architecture in structural designs with its lightweight structure. Due to the low porosity, it shows excellent permeability resistance and increases its early strength values. Due to its high thermal conductivity, it increases fire resistance [3]. As can be seen from Fig 1.1, the placement of the nano-material forming a composite with cement in the cement structure has been shown that reduced graphene oxide (rGO) can improve the mechanical properties of hardened cement mortar reported in literature research. The mechanisms proposed so far to explain this strengthening, in general, are that the reduced graphene oxide disperses well in the pores of the portland cement mortar and enlarges the nucleation site as a reinforcing agent during hydration [4].

---

\* Corresponding author e-mail address: halukkorucu@karatekin.edu.tr

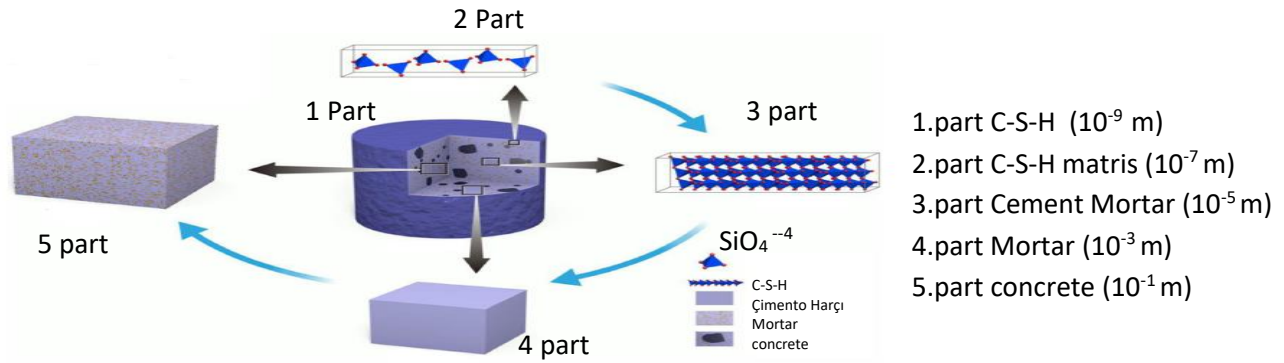


**Fig 1.1** The relationship between different material scales in cement-based composite [4]

## 2. Materials and Methods

Three different graphene oxide samples were synthesized by the hummers method using different purity of graphite samples (85% Nanokar -99% Nanokar- 99,99% Merck). Three different properties of reduced graphene oxide (rGO) were synthesized by using ascorbic acid with the chemical reduction method of synthesizing the graphene oxide samples. During the synthesis of reduced graphene oxide, 2 grams of graphene oxide samples were taken for each experiment, and sonication was performed in 600 mL of water with an ultrasonic power of 40% for 30 minutes. Then, the mixture was taken to the reactor and 6 grams of ascorbic acid was added to it, and experiments were carried out for 24 hours in a double-walled glass reactor at 80°C. Impurities were removed by pure water, acetone, and ethyl alcohol with a decantation process at the end of the reaction. After this process, the product was dried in a vacuum oven at 60°C. In the experiments of reduced graphene oxide doped concrete mortar (rGO-Concrete), 0.6 grams of rGO was taken for use and subjected to ultrasonication with an ultrasonic probe with 40% power for 30 minutes in 270 ml of pure water. Then these solutions were mixed with 600g portland cement and 1 gram of superplasticizer was added to them. The samples were cast into 50x50x50 mm molds. The samples poured into molds were removed from the molds after 1 day. Thermal conductivity and heat capacity measurements were taken from these samples on days 7-28, and electrical resistance and compressive strength measurements were taken on days 28. The effects of reduced graphene oxide on concrete mortar were analyzed according to the criteria given in Table 2.1. Example reference in concrete mortar concrete, reduced graphene oxide, and reduced graphene oxide samples synthesized using 3 different purity graphite is unused and determined in criteria aimed to determine recovery rates. To determine the properties of rGO-CONCRETE mortar, molds were filled into at least 3 pieces for each experiment. In Fig 2.1, the images taken during the experiment are given.

**Table 2.1** Quality criteria of the reduced graphene oxide-Concrete mortar experiments

Quality Criteria	Symbol	Explanation	Information	The goal for rGO-Concrete
1	T7	Thermal conductivity (W/(m.K))	7 Days	Larger is better
2	T28	Thermal conductivity(W/(m.K))	28 Days	Larger is better
3	CP7	Specific heat capacity (Mj/m <sup>3</sup> .K)	7 Days	Larger is better
4	CP28	Specific heat capacity (Mj/m <sup>3</sup> .K)	28 Days	Larger is better
5	E.R	Electrical resistivity (kΩ.m)	28 Days	Smaller is better
6	CS	Compressive strength (N/mm <sup>2</sup> )	28 Days	Larger is better

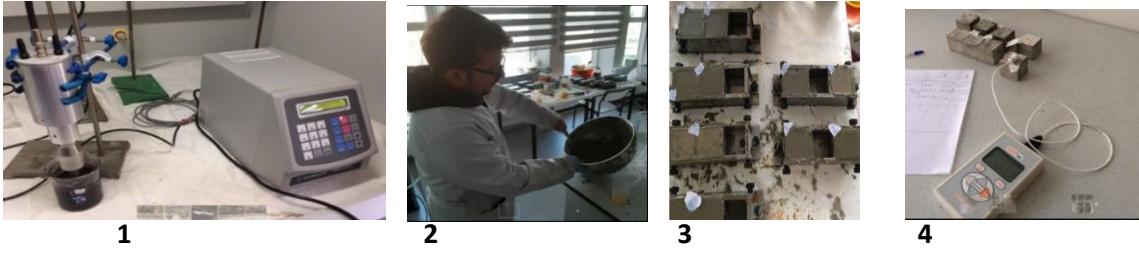


**Fig 2.1** Images of cement mortar experiments ( 1-Ultrasonication process, 2-Pouring cement mortar into molds 3-Samples removed from molds 4-Making measurements with Kd2 pro)

### 3. Results and Discussion

Using 85% Nanocar, 99% Nanocar and 99% Merck, branded graphite of different purity, graphene oxide of 3 different properties was synthesized by the hummers method and encoded as GO1-GO2-GO3, respectively. The synthesized graphene oxide in 3 different properties was reduced using ascorbic acid by chemical reduction method and synthesized 3 different types of reduced graphene oxide which was encoded as rGO1-rGO2-rGO3. In Figures 3.1, 3.2, and 3.3, FTIR analyses of graphite-graphene oxide and reduced graphene oxide samples are given.

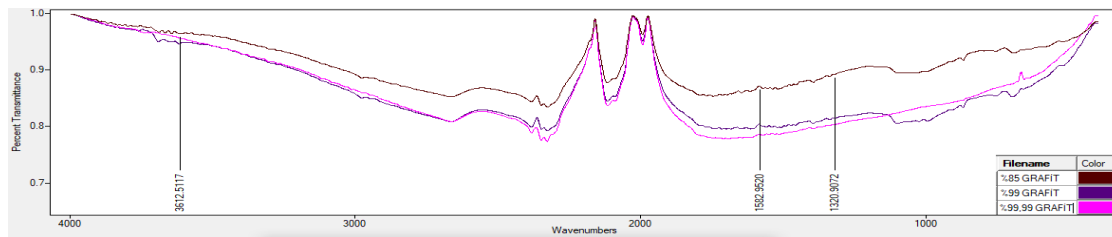


**Fig 3.1.** FTIR images of graphite samples of different purity(85% -99%Nanocar, 99.99% Merck)

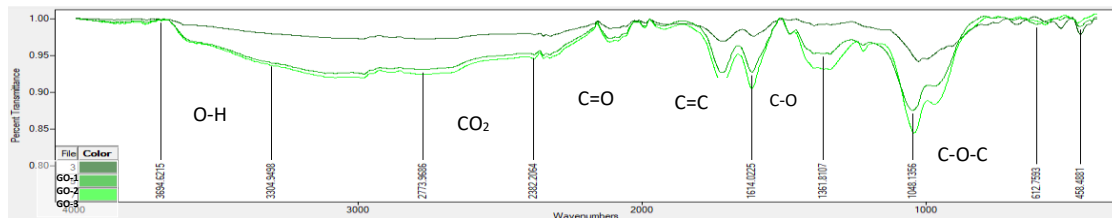


**Fig 3.2.** FTIR images of graphene oxide samples(GO1-GO2-GO3) synthesized by Hummers method using different purity graphite

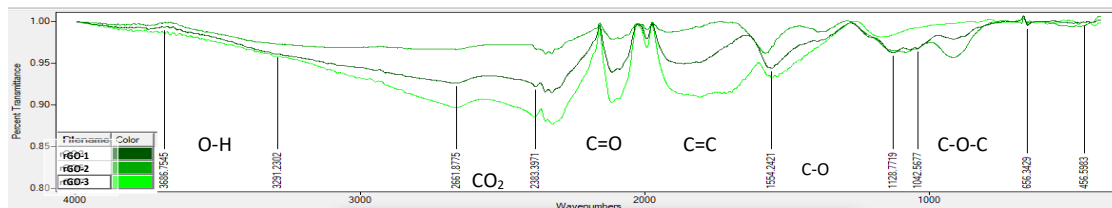


**Fig 3.3.** Reduced graphene oxide samples (rGO1-rGO2-rGO3) synthesized using graphene oxide samples of different properties (GO1-GO2-GO3)

In Figure 3.2, the results of the FTIR analysis have shown that the presence of oxygen-containing functional groups indicates that the synthesis of graphene oxide from graphite is successful [5]. In Figure 3.3 graphene oxide and O-H groups and the peaks of the oxygen-containing functional groups (-OH, C-O, and C-O-C) the disappearance of the structure of graphene oxide, and reduced graphene oxide indicate that the synthesis was successful[6-7]. Figures 3.2 and 3.3 indicate that the synthesized graphene oxide and reduced graphene oxide samples were successful. The successfully synthesized reduced graphene oxide samples (rGO1-rGO2-rGO3)

were distributed by ultrasonication process and the measurements given in Table 2.1 were performed using cement mortar. The measurement results and recovery rates are given in Table 3.1. When the improvement rates in the results of the rGO-Concrete experiments were evaluated; If the improvement rates in terms of thermal conductivity turned out to be very close to each other, the experiment with the code rGO3-Concrete gave the best value (52,63%). In terms of heat capacity, although the recovery rates are very close to each other, the best value (57.10%) was given by the experiment with the code rGO3-Concrete. The experiment with the rGO1-Concrete code gave the best result (15.58% and 35.03%) in terms of electrical resistance and compressive strength.

**Table 3.1** Recovery ratios reference-concrete between Reduced graphene oxide-concrete

Answers	Ref <sup>a</sup> Concrete	rGO1- Concrete	rGO2- Concrete	rGO3- Concrete	Recovery Rate rGO1- Concrete (%)	Recovery Rate rGO2- Concrete (%)	Recovery Rate rGO3- Concrete (%)
T7 (W/(m <sup>2</sup> .K))	0,391	0,547	0,538	0,526	<b>39,89<sup>b</sup></b>	37,59	34,53
T28 (W/(m <sup>2</sup> .K))	0,323	0,453	0,435	0,493	<b>40,25</b>	34,67	<b>52,63</b>
Cp7(Mj/(m <sup>3</sup> .K))	1,352	2,128	2,032	2,124	57,40	50,30	<b>57,10</b>
Cp28(Mj/(m <sup>3</sup> .K))	1,202	1,737	1,701	1,774	44,51	41,51	<b>47,59</b>
ED (kΩ.m)	0,6675	0,5635	0,7435	0,701	<b>15,58</b>	-11,39	5,01
B.D.(MPa)	16,922	22,85	18,750	20,072	<b>35,03</b>	10,80	18,61

*Calculation of the % recovery rate of the experiment performed under optimal conditions*

<sup>a</sup> The reference experiment is experiment No. 1, which has the lowest levels of the parameter in its design

<sup>b</sup>  $((0,547-0,391) / 0,391) * 100 = 39,89$  (plus value means improvement)

When analyzing the results of quality characteristics in concrete experience, GO1, rGO1 and GO2, rGO2 coded domestic-brand low-purity graphite and reduced graphene oxide samples synthesized with graphene oxide and reduced graphene oxide synthesized using high-purity graphite overseas brand of the samples according to your sample, showed higher performance in applications, it is observed that the concrete and mortar. This paves the way for graphene oxide and reduced graphene oxide to be widely used in concrete mortar applications when considering terms of costs and performance

## Acknowledgment

This research was carried out with the support of the Scientific Research Project (MF210621B08) funded by Çankırı Karatekin University. Author thank to Çankırı Karatekin University, Scientific Research Project Management Unit (ÇAKÜ-BAP).

## References

- [1] Korucu H., Investigation of the Physical and Chemical Properties of Carbon-based Material Additive Cement Mortar: An Experimental Design-Based Multi-Response Optimization Application. Phd Thesis. Çankırı Karatekin University. Institute Of Science. 2019
- [2] Korucu, H., Şimşek B., and Yartaşı A. 2018. Statistical approach to carbon based materials reinforced cementitious composites: Mechanical, thermal, electrical and sulfuric acid. *Composites Part B*, 171: 347-360
- [3] Wang M., Wang R., Yao H., Farhan S., Zheng S., Du C. 2016, Study on the three dimensional mechanism of graphene oxide nanosheets modified cement., *Construction and Building Materials* 126, 730-739
- [4] Yang H., Cui H., Tang W., Li Z., Han N. and Xing F., 2017. A critical review on research progress of graphene/cement based composites. *Composites : Part A* 102, 273-296
- [5] Korucu, H., Şimşek B., and Yartaşı A. 2018. 'A TOPSIS-based Taguchi design to investigate optimum mixture proportions of graphene oxide powder synthesized by hummers method', *Arabian Journal for Science and Engineering*, 43: 6033-55.

- [6] Korucu, H, Şimşek, B., Kocakerim M.M., and Karakaş İ.H.. 2019. 'Effective reduction of graphene oxide using sulfur dioxide-containing chemical compounds', *International Journal of Environmental Science and Technology*: 1-14.
- [7] Korucu H. 2022. 'Evaluation of the performance on reduced graphene oxide synthesized using ascorbic acid and sodium borohydride: Experimental designs-based multi-response optimization application. *Journal of Molecular Structure*.1268,133715.





# The Effect of Thickness on the Morphological and Optical Properties of ZnSe Thin Films

***Irmak KARADUMAN ER<sup>1,\*</sup>***, ***Aytunç ATEŞ<sup>2</sup>***, ***Selim ACAR<sup>3</sup>***

<sup>\*1</sup> Çankırı Karatekin University, Department of Medical Services and Techniques, Eldivan Medical Services Vocational School, Çankırı, Turkey

<sup>2</sup> Ankara Yıldırım Beyazıt University, Department of Metallurgy and Materials Engineering, Faculty of Engineering and Natural Sciences, Ankara, Turkey

<sup>3</sup> Gazi University, Department of Physics, Faculty of Science, Ankara, Turkey

## Abstract

With the expansion of electronics and digital industries and their penetration into all areas of our lives, the production and development of high-precision, reliable, integrated, low-noise and low-power electrical components has become a very important consideration. However, when the relationships between the structure, properties and processing of materials are fully understood and assimilated, we can make the raw materials that nature gives us more available, and as scientists develop them, we can transform them into superior technologies. Today, the rapid change that occurs with the acceleration of research and studies in thin film materials creates new opportunities for the development of new processes, materials, and technologies. Therefore, many experiments and model systems have been developed to improve the previously known properties of basic physical and chemical properties related to thin film performance and structure in various applications and to increase progress in this field. A prerequisite for the development of new thin-film systems is the combined results of experimental and theoretical investigations and shaping their structure and performance. In this sense, the characteristics of thin-film materials and their control and optimization are of great importance. One of the most important features affecting these features is the producing method. There are chemical solution-based methods such as sol-gel method, chemical bathing technique, hydrothermal method, SILAR method and spraying method. In this study, Cadmium Selenide (ZnSe) thin films were grown on glass substrate using succession ionic layer adsorption and reaction (SILAR) method. Morphological and optical properties of ZnSe thin films grown at different thicknesses (40 and 50 cycle) are given comparatively.

**Keywords:** SILAR method, thin films, Zinc Selenide

## 1. Introduction

The science of thin films plays a significant role in the development of solid materials especially for energy-efficient display devices such as diodes, transistors, display screens, photodetectors, photovoltaics, and solar cells. Thin films show distinctive behavior comparing with their bulk structure. A thin film is recognized as thin unless the properties of its surface are unlike its bulk behavior. The thin films have a higher volume surface ratio, such the thin film characteristics are determined by the surface and near-surface properties. The thickness of thin films is in a range of a few nanometers to 1 micrometer, the design of the substrate on which the films are grown, as well as the deposition research methods of deposition used in the production of thin films. Thin-film processing is generally done by depositing the required material over the appropriate substrate in the atomic deposition (atom by atom), which may lead to either a single crystalline, polycrystalline or amorphous form based on the deposition conditions. The thickness of the thin film, amount of doping, or constitute element can be changed as requested for the used substrate and deposition method. These advantages of thin films have benefits for developing advanced products and commercialization [1].

\*Corresponding author. e-mail address: irmakkaradumaner@karatekin.edu.tr



Zinc selenide (ZnSe) is II–VI, n-type semiconductor material, which has many applications like high-efficiency thin film transistors, solar cells, photoconductors, and gas sensors [2]. In order to improve the performance of the devices, key attention has been given in recent years to study the physical properties of ZnSe thin films. A variety of methods have been used to prepare ZnSe thin films, including physical vapor deposition [3], sputtering [4], spray pyrolysis [5], SILAR [6] and chemical deposition [7]. The SILAR method, cheaper and more economical than these methods, can produce at room temperature, does not require complex materials, and is suitable for making high-quality thin films. Compared to the physical vapor deposition methods used in vacuum systems, it is quite economical and the production steps are comfortable [8,9]. It is seen that there are changes in the properties of the films produced by changing the producing parameters of the SILAR method. The aim is to produce the best films with the optimal production parameters. It is reported in the literature that there are changes in the properties of the films produced by doping with different elements, changing the hot water parameter, producing cycle, cationic solution, and pH in the growth process [10]. In this study, we produced ZnSe thin films with different cycles and investigated their morphological and optical characterization.

## 2. Materials and Methods

The SILAR method was used to grow the ZnSe thin film, and appropriate solutions were created as described; At room temperature and atmospheric pressure, ZnSe thin films were formed on glass substrates using the SILAR process. The cationic and anionic precursor solutions utilized to deposit ZnSe thin films were 0.1 M  $\text{ZnCl}_2$  solution at pH 5.5 and 0.13 M  $\text{Na}_2\text{SeSO}_3$  solution at pH 10.5. The durations for adsorption, reaction, and rinsing were chosen empirically to ensure layer wise deposition and a homogeneous thin film structure. The glass substrate was immersed in the  $\text{ZnCl}_2$  solution for 40 seconds to allow cadmium ( $\text{Zn}^{+2}$ ) and small amounts of chlorine ( $\text{Cl}^-$ ) ions to settle on the surface in order to grow the ZnSe thin film using the SILAR process. The glass substrate was then placed in deionized water for 50 seconds after being removed from the  $\text{ZnCl}_2$  solution, allowing weakly bound  $\text{Zn}^{+2}$  and  $\text{Cl}^-$  ions to dissociate from the surface. As a result, the connected  $\text{Zn}^{+2}$  ions interacted with selenium ions ( $\text{Se}^{2-}$ ). Finally, the weakly attached sodium ( $\text{Na}^+$ ) ions and non-reacting selenium ( $\text{Se}^{2-}$ ) ions are removed from the surface supplied by immersing the sample holder in deionized water for 50 seconds. This procedure was continued until the necessary thickness of uniform film was achieved. Finally, the glass substrate was submerged for 40 seconds in a  $\text{Na}_2\text{SeSO}_3$  solution and held.

## 3. Results and Discussion

Figure 1 shows the SEM analysis of ZnSe thin films with 40 cycle(a) and 50 cycle(b). Although the ZnSe thin films have a compact, flat, and homogeneous surface, there are some pinholes, cracks, and other defects. All of the films have the same granular structure, with round-shaped grains tightly packed in larger irregular-shaped particles. Aggregates dispersed on the film surface have been observed, which is common in the chemical deposition of some semiconductor films. Figure 2 shows the EDAX analysis of ZnSe thin films with 40 cycle (a), 50 cycle (b). ZnSe thin films were produced on glass substrates with the different SILAR cycles under the same ambient conditions. The change of Zn and Se on the EDAX spectrum was associated with the producing cycle. The presence of Mg, Na, Si, O and Ca elements in the spectra may have originated from the glass substrates. And also, some pinholes, cracks, or other defects were observed from the surface, therefore, the higher oxygen value can be found from the EDAX analysis.

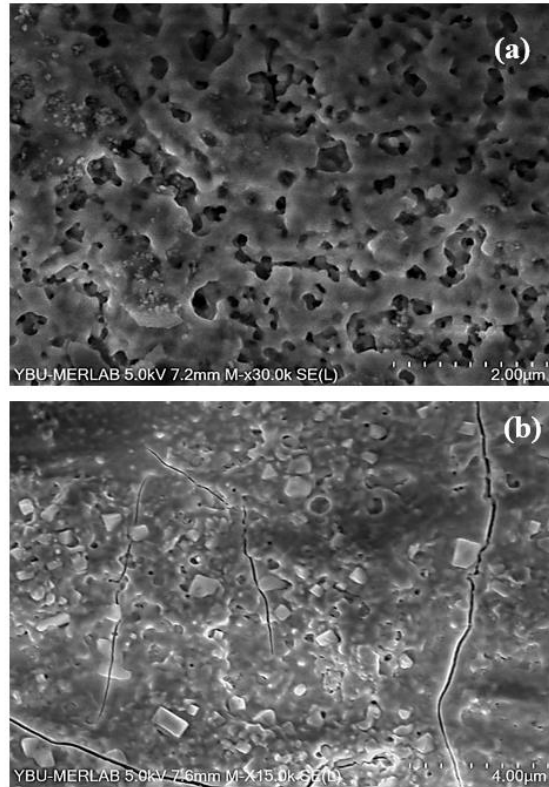


**Figure 1.** SEM analysis of 40ZnSe (a) and 50ZnSe (b) thin films

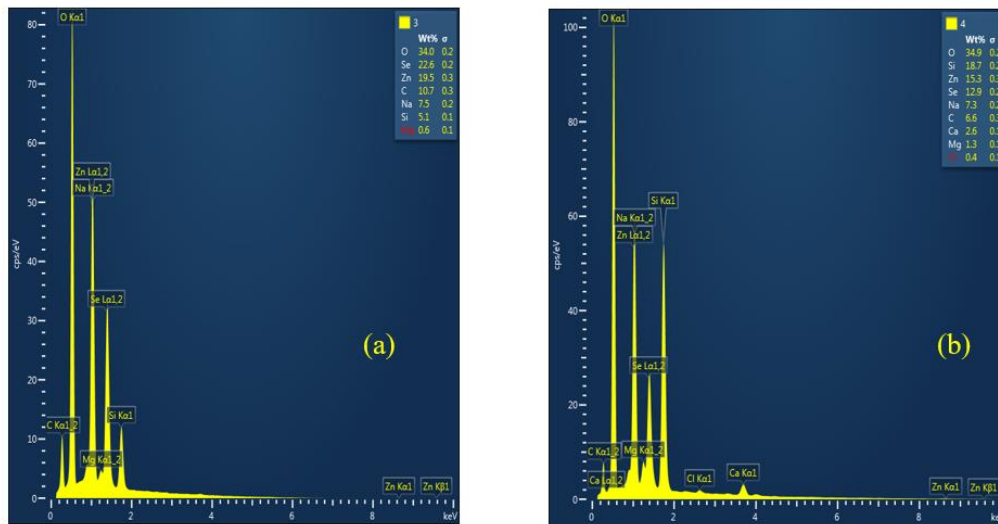


**Figure 2.** EDAX analysis of 40ZnSe (a) and 50ZnSe (b) thin films

Fig. 3 shows the absorbance spectra of the ZnSe thin films. The absorbance spectra increase with the increasing of film thickness. It is found that the absorption spectra for Zn–Se system are blue shifted due to increase in the optical band gap for these materials. An opposite behavior was observed for transmittance spectra, as shown in Figure 4. Figure 5 shows the plot of  $(\alpha h\nu)^2$  against  $h\nu$ . The optical band gap was determined by using the below Tauc plot [11];

$$\alpha = \frac{A(h\nu - E_g)^n}{h\nu}$$

where A is a constant and n is an index for allowed direct and non-direct transitions are 1/2 and 2, respectively. When the slope of the graph is taken, the value where it intersects the x point gives the optical band gap value. Extrapolating the straight portion of the plot  $(\alpha h\nu)^2$  against  $h\nu$  to energy axis, optical band gap energy values of 2.42 eV and 2.33 eV were estimated for 40ZnSe and 50ZnSe, respectively. The values were decreased with increasing film thickness because of the bulk material does not have discrete energy states. But as the particle becomes smaller, the energy levels become discrete. According to the particle in a box concept, the energy gap between different energy states is inversely proportional to the square of the length of the box, for a quantum dot, the length of the box is actually its size. So with a decrease in size, the energy gap increases. This is the primary reason behind dependence of bandgap energy of nanocrystalline thin films [3].

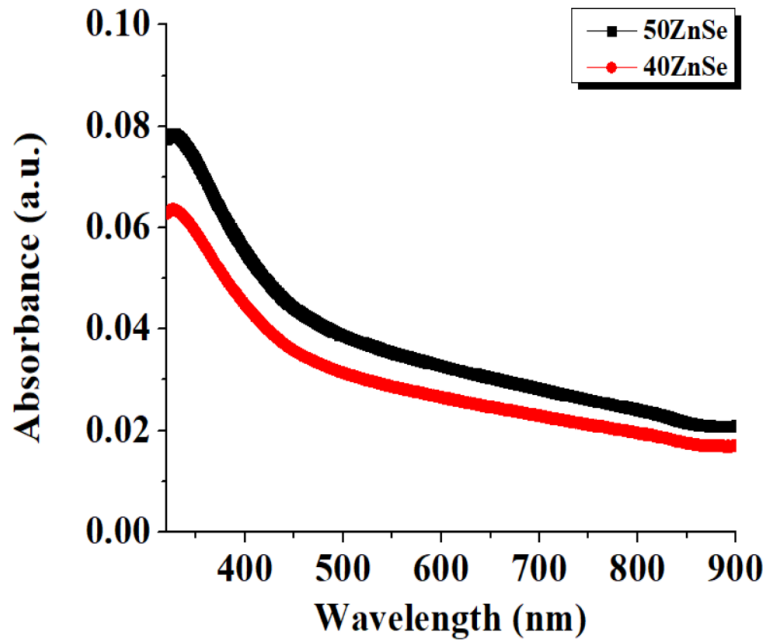


**Figure 3.** Absorbance measurements of 40ZnSe and 50ZnSe thin films

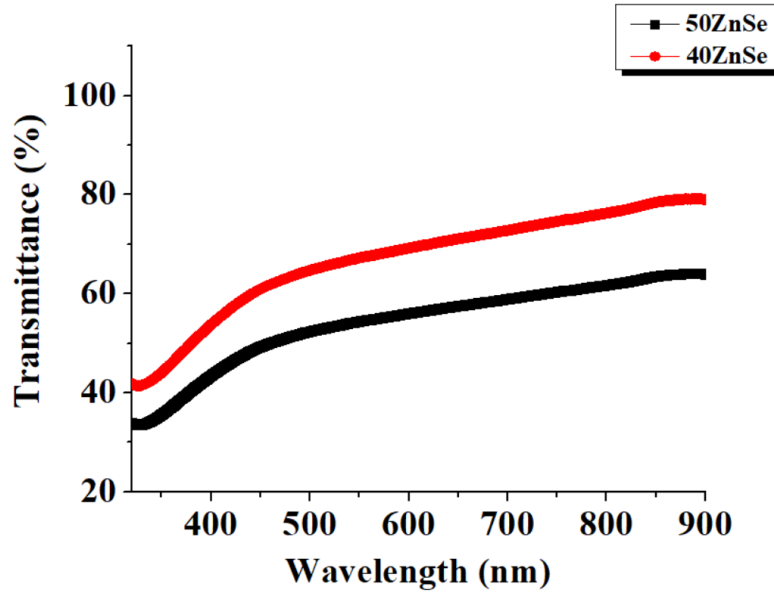


**Figure 4.** Transmittance measurements of 40ZnSe and 50ZnSe thin films

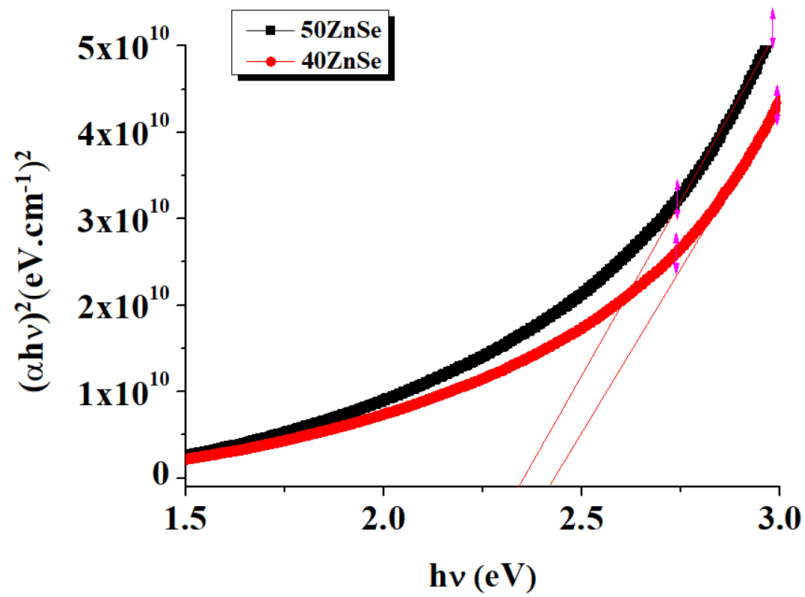


**Figure 5.** The plot of  $(\alpha h\nu)^2$  against  $h\nu$  for 40ZnSe and 50ZnSe

Figure 6 shows the Raman spectra of ZnSe thin films. We interpret the series of up to 4 peaks (at  $\approx 250, 500, 850 \text{ cm}^{-1}$ ) as being due to the so-called longitudinal optical LO-phonon replicas in ZnSe, well known in polar semiconductors. As the 1LO band is the most intensive in the Raman spectrum excited by the 457.9 nm line, the energy of this line should be close to the optical band gap. The peaks at  $251 \text{ cm}^{-1}$  which shifted from the ZnSe peaks at ( $253 \text{ cm}^{-1}$ ). Another peak observed at  $550 \text{ cm}^{-1}$  was closer to the peak for ZnS ( $546 \text{ cm}^{-1}$ ).

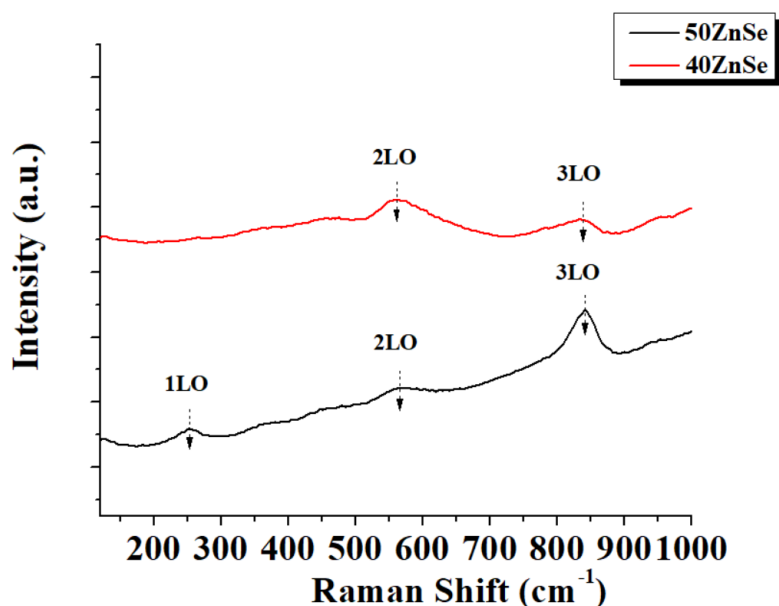


**Figure 6.** Raman spectra of 40ZnSe and 50ZnSe thin films

#### 4. Conclusion

SEM research shows that ZnSe thin films have a compact, flat, and homogenous surface, yet there are some pinholes, cracks, and other flaws. Round-shaped grains are closely packed in larger irregular-shaped particles in all of the films. Aggregates scattered on the film surface have been found, which is frequent in the chemical deposition of some semiconductor films. According to the EDAX analysis, the atomic ratios of Cd and Se changed as the cycle changed. Mg, Na, Si, and Ca elements were found in the spectra, which could have come from the glass substrates. Because of the increase in the optical band gap for these materials, the absorption spectra for the Zn–Se system are blue shifted. From Raman analysis, the series of up to 4 peaks (at  $\approx 250$ , 500, 850  $\text{cm}^{-1}$ ) as being due to the so-called longitudinal optical LO-phonon replicas in ZnSe, well known in polar semiconductors.

#### References

- [1] Abebe G.H., Hone, F.G., (2019). “The influence of malonic acid on the structural, morphological and optical properties of CdSe thin films prepared by chemical bath deposition method”, *F Inorganic Chemistry Communications*, 103, 107–112
- [2] Amalraj A.S. & Senguttuvan, G., (2014). “Effect of multiple dipping of SILAR deposited ZnO thin films by physico-chemical process”, *Journal of Materials Science: Materials in Electronics*, 25, 2035–2040
- [3] Chaudhari, K.B., Gosavi, N.M., Deshpande, N.G., Gosavi, S.R., (2016). “Chemical synthesis and characterization of CdSe thin films deposited by SILAR technique for optoelectronic applications”, *Journal of Science: Advanced Materials and Devices*, 1, 476–481
- [4] Devadasona, S. & Muhamad, M.R., (2007). “Structural and optical properties of vapor deposited multi-layer CdSe thin films”, *Physica B: Condensed Matter*, 393, 125–132
- [5] Karaduman Er, I., (2021). “Effect of Synthesis Parameters on the Structural, Optical and Electrical Properties of Successive Ionic Layer Adsorption and Reaction (SILAR)-Deposited CuO Thin Films”, *Russ J Appl Chem* 94, 1334–1343
- [6] Karaduman Er, I., Yıldırım, M.A., Örkçü, H.H., Ateş, A., and Acar, S., (2021). “Structural, morphological and gas sensing properties of  $\text{Zn}_{1-x}\text{Sn}_x\text{O}$  thin films by SILAR method”, *Appl. Phys. A*, 127, 230, 1–14
- [7] Pathan, H.M., Sankapal, B.R., Desai, J.D., Lokhande C.D., (2002). “Preparation and characterization of nanocrystalline CdSe thin films deposited by SILAR method”, *Materials Chemistry and Physics*, 78, 11–14

- [8] Rosly, H.N., Rahman, K.S., Harif, M.N., Doroody, C., Isah, M., Misran, H., Amin, N., (2020). “Annealing temperature assisted microstructural and optoelectrical properties of CdSe thin film grown by RF magnetron sputtering”, *Superlattices and Microstructures*, 106716
- [9] Sharma, K., Saini, G.S.S., Tripathi, S.K., Siwatch, P., (2018). “A comparative study of transport properties of copper doped cadmium selenide thin films at two dopant concentrations”, *J. Mater. Sci. Mater. Electron*, 29, 9596–9604
- [10] Yadav, A.A., Barote, M.A., Masumdar, E.U., (2010). “Studies on cadmium selenide (CdSe) thin films deposited by spray pyrolysis”, 121, 53-57
- [11] Zgair, I.A., Omran Alkhayatt, A.H., Muhmood, A.A., and Hussain, S. K., (2019). “Investigation of structure, optical and photoluminescence characteristics of Li doped CuO nanostructure thin films synthesized by SILAR method”, *Optik*, 191, 48–54

# A Comparison Study on Five Estimation Methods for Power Shanker Distribution

**Caner TANIS<sup>1,\*</sup>** 

<sup>1</sup> Science Faculty, Department of Statistics, Çankırı Karatekin University, Çankırı, Turkey

## Abstract

Power Shanker distribution is suggested by Shanker and Shukla [1]. Shanker and Shukla [1] discussed some distributional properties of the Power Shanker distribution. However, there is no comparison study regarding the another estimators of the parameter of the Power Shanker distribution in the literature. Therefore, we provide a new expansion for point estimation of the Power Shanker distribution in this study. This study presents five different methods of estimation, such as maximum likelihood, least-squares, weighted least-squares, Anderson-Darling, and Crámer–von-Mises methods to estimate the parameters of the Power Shanker distribution. It is compared the performances of these estimators via a extensive Monte Carlo simulation study. In the simulation study, 5000 repetitions have taken at different sample sizes and parameter settings. We compute average bias and mean square error (MSE) of the parameters of the Power Shanker distribution. It is seen that the average bias and MSE decrease when the sample sizes increase as expected according to the simulation results. Thus, it can be concluded that the estimators provide the procedures of the estimation.

**Keywords:** Shanker distribution, Power Shanker distribution, Point Estimation, Monte Carlo simulation

## 1. Introduction

Recently, it is seen that many researchers have dealt with parameter estimation for various lifetime distributions. The maximum likelihood method is popularly used to estimate the unknown parameters of the distributions. However, in the last decade, many estimators have been studied by many authors as an alternative to the maximum likelihood method. Some of these papers can be listed as follows: Karakaya and Tanış [2], Karakaya and Tanış [3], Tanış and Karakaya [4], Tanış and Karakaya [5], Tanış [6], Tanış [7].

The main aim of this study is to compare the estimation methods for the Power Shanker distribution.

Shanker distribution is proposed by Shanker [8]. The cumulative distribution function (CDF) and probability density function (PDF) of the Power Shanker distribution are

$$F_s(x; \theta) = 1 - \left[ 1 + \frac{\theta x}{\theta^2 + 1} \right] \exp\{-\theta x\} \quad (1)$$

and

$$f_s(x; \theta) = \frac{\theta^2}{\theta^2 + 1} (\theta + x) \exp\{-\theta x\}, \quad (2)$$

where  $\theta > 0$  and  $x > 0$  [8].

Power Shanker distribution is suggested by Shanker and Shukla [1] by using the transformation  $X = Y^{1/\alpha}$  in (1)-(2). Then CDF and PDF of the Power Shanker distribution are given by

$$F_{PS}(x; \alpha, \theta) = 1 - \left[ 1 + \frac{\theta x^\alpha}{\theta^2 + 1} \right] \exp\{-\theta x^\alpha\} \quad (3)$$

\*Corresponding author. e-mail address: canertanis@karatekin.edu.tr

and

$$f_{PS}(x; \alpha, \theta) = \frac{\alpha \theta^2}{\theta^2 + 1} x^{\alpha-1} (\theta + x^\alpha) \exp\{-\theta x^\alpha\}, \quad (4)$$

respectively, where  $\theta > 0$  is a scale parameter,  $\alpha > 0$  is a shape parameter and  $x > 0$  [1]. We briefly denote Power Shanker distribution as  $PS(\alpha, \theta)$  in this paper. Shanker and Shukla [1] mentioned that the  $PS(\alpha, \theta)$  distribution is a mixture of *Weibull* $(\alpha, \theta)$  and generalized gamma  $(2, \alpha, \theta)$  distributions. For more details about the  $PS(\alpha, \theta)$  distributions please see [1].

## 2. Point Estimation

In this section, we present five different estimators of the parameters of the  $PS(\alpha, \theta)$  distribution such as maximum likelihood estimator (MLE), least squares estimator (LSE), weighted least squares estimator (WLSE), Anderson-Darling estimator (ADE), and Cramér-von Mises estimator (CvME).

Let  $X_1, X_2, \dots, X_n$  be a random sample from the  $PS(\alpha, \theta)$  distribution and  $X_{(1)} < X_{(2)} < \dots < X_{(n)}$  denote the corresponding order statistics. In addition,  $x_{(i)}$  denotes the observed value of  $X_{(i)}$ . The log-likelihood function of the  $PS(\alpha, \theta)$  distribution is

$$\ell(\gamma) = n \left[ 2 \log \theta + \log \alpha - \log(\theta^2 + 1) \right] + (\alpha - 1) \sum_{i=1}^n \log(x_i) + \sum_{i=1}^n \log(\theta + x_i^\alpha) - \theta \sum_{i=1}^n \log x_i^\alpha. \quad (3)$$

where  $\gamma = (\alpha, \theta)$  is a parameter vector. Then, maximum likelihood estimator (MLE) of  $\gamma$  is given as follows:

$$\hat{\gamma}_{MLE} = \arg \max_{\gamma} \{\ell(\gamma)\}. \quad (4)$$

Let us define the following four functions which are used to obtain the different type of estimates:

$$\begin{aligned} Q_{LS}(\gamma) &= \sum_{i=1}^n \left[ \left( 1 - \left( 1 + \frac{\theta x_{(i)}^\alpha}{\theta^2 + 1} \right) \exp\{-\theta x_{(i)}^\alpha\} \right) - \frac{i}{n+1} \right]^2, \\ Q_{WLS}(\gamma) &= \sum_{i=1}^n \frac{(n+2)(n+1)^2}{i(n-i+1)} \left[ \left( 1 - \left( 1 + \frac{\theta x_{(i)}^\alpha}{\theta^2 + 1} \right) \exp\{-\theta x_{(i)}^\alpha\} \right) - \frac{i}{n+1} \right]^2, \\ Q_{CvM}(\gamma) &= \frac{1}{12n} + \sum_{i=1}^n \left[ \left( 1 - \left( 1 + \frac{\theta x_{(i)}^\alpha}{\theta^2 + 1} \right) \exp\{-\theta x_{(i)}^\alpha\} \right) - \frac{2i-1}{2n} \right]^2 \end{aligned}$$

and

$$\begin{aligned} Q_{AD}(\gamma) &= -n - \frac{1}{n} \sum_{i=1}^n \left( (2i-1) \log \left[ \left( 1 - \left( 1 + \frac{\theta x_{(i)}^\alpha}{\theta^2 + 1} \right) \exp\{-\theta x_{(i)}^\alpha\} \right) \right] \right) \\ &\quad + \frac{1}{n} \sum_{i=1}^n \left( \log \left[ \left( 1 + \frac{\theta x_{(i)}^\alpha}{\theta^2 + 1} \right) \exp\{-\theta x_{(i)}^\alpha\} \right] \right). \end{aligned}$$

the LSEs, WLSEs, CvMEs, and ADEs of the parameters  $\gamma = (\alpha, \theta)$  are given, respectively, by



$$\hat{\gamma}_{LSE} = \arg \min_{\gamma} \{Q_{LS}(\gamma)\}, \quad (5)$$

$$\hat{\gamma}_{WLSE} = \arg \min_{\gamma} \{Q_{WLS}(\gamma)\}, \quad (6)$$

$$\hat{\gamma}_{CvME} = \arg \min_{\gamma} \{Q_{CvM}(\gamma)\}, \quad (7)$$

$$\hat{\gamma}_{ADE} = \arg \min_{\gamma} \{Q_{AD}(\gamma)\}. \quad (8)$$

The estimators given in (4)-(9) can be obtained by **optim ()** function in R with Broyden–Fletcher–Goldfarb–Shanno (BFGS) algorithm. The BFGS algorithm is firstly studied by Fletcher [9].

### 3. Simulation Study

In this section, we provide a comprehensive Monte Carlo simulation study to evaluate the performances of five estimators according to biases and MSEs. In the simulation study is performed based on 5000 repetitions. We consider the sample size 25, 50, 100, 250, 500 and four parameter settings as follows:

Case 1:  $(\alpha = 0.5, \theta = 0.7)$ , Case 2:  $(\alpha = 1.2, \theta = 0.9)$ ,

Case 3:  $(\alpha = 2, \theta = 2)$ , Case 4:  $(\alpha = 4, \theta = 3.5)$ .

**Table 1.** Average biases of MLEs, LSEs, WLSEs, ADEs, and CvMEs of  $\alpha$  and  $\theta$  parameters

Parameters	n	$\hat{\alpha}$					$\hat{\theta}$				
		MLE	LSE	WLSE	ADE	CvME	MLE	LSE	WLSE	ADE	CvME
$\alpha = 0.5, \theta = 0.7$	50	0,0882	0,0531	0,0670	0,0649	0,0682	0,0459	0,0528	0,0503	0,0522	0,0438
	100	0,0834	0,0558	0,0695	0,0647	0,0632	0,0465	0,0493	0,0472	0,0500	0,0448
	250	0,0801	0,0561	0,0703	0,0633	0,0591	0,0472	0,0474	0,0456	0,0493	0,0456
	500	0,0789	0,0568	0,0708	0,0632	0,0583	0,0471	0,0460	0,0445	0,0484	0,0450
$\alpha = 1.2, \theta = 0.9$	50	0,0253	-0,0079	0,0006	0,0041	0,0270	0,0041	0,0112	0,0093	0,0089	0,0053
	100	0,0130	-0,0040	0,0023	0,0022	0,0132	0,0011	0,0048	0,0034	0,0036	0,0018
	250	0,0051	-0,0018	0,0013	0,0006	0,0050	-0,0006	0,0007	0,0001	0,0004	-0,0005
	500	0,0028	-0,0007	0,0013	0,0007	0,0027	$-1.9 \times 10^{-5}$	0,0009	0,0004	0,0005	0,0002
$\alpha = 2, \theta = 2$	50	0,0603	0,0004	0,0152	0,0210	0,0644	0,0473	0,0187	0,0248	0,0286	0,0597
	100	0,0302	0,0002	0,0111	0,0105	0,0317	0,0233	0,0101	0,0147	0,0145	0,0295
	250	0,0076	-0,0044	0,0013	$-1.8 \times 10^{-5}$	0,0080	0,0087	0,0025	0,0054	0,0049	0,0101
	500	0,0052	-0,0009	0,0022	0,0011	0,0053	0,0061	0,0030	0,0046	0,0041	0,0067
$\alpha = 4, \theta = 3.5$	50	0,1096	-0,0118	0,0218	0,0308	0,1127	0,1579	0,0530	0,0760	0,0819	0,2067
	100	0,0522	-0,0128	0,0105	0,0103	0,0484	0,0691	0,0088	0,0284	0,0282	0,0804
	250	0,0265	0,0013	0,0125	0,0102	0,0257	0,0284	0,0061	0,0154	0,0134	0,0340
	500	0,0156	0,0041	0,0097	0,0077	0,0162	0,0176	0,0072	0,0119	0,0099	0,0211

**Table 2.** Average MSEs of MLEs, LSEs, WLSEs, ADEs, and CvMEs of  $\alpha$  and  $\theta$  parameters

Parameters	n	$\hat{\alpha}$					$\hat{\theta}$				
		MLE	LSE	WLSE	ADE	CvME	MLE	LSE	WLSE	ADE	CvME
$\alpha = 0.5, \theta = 0.7$	50	0,0111	0,0071	0,0081	0,0078	0,0092	0,0116	0,0126	0,0122	0,0121	0,0121
	100	0,0085	0,0052	0,0066	0,0060	0,0062	0,0068	0,0073	0,0070	0,0071	0,0069
	250	0,0071	0,0040	0,0056	0,0047	0,0043	0,0041	0,0042	0,0040	0,0043	0,0041
	500	0,0065	0,0037	0,0053	0,0044	0,0038	0,0032	0,0031	0,0030	0,0033	0,0031
$\alpha = 1.2, \theta = 0.9$	50	0,0167	0,0236	0,0196	0,0180	0,0259	0,0102	0,0106	0,0103	0,0102	0,0110
	100	0,0080	0,0113	0,0093	0,0089	0,0119	0,0050	0,0051	0,0050	0,0050	0,0052
	250	0,0030	0,0045	0,0035	0,0035	0,0045	0,0019	0,0020	0,0019	0,0019	0,0020
	500	0,0015	0,0022	0,0017	0,0017	0,0022	0,0010	0,0010	0,0010	0,0010	0,0010
$\alpha = 2, \theta = 2$	50	0,0599	0,0825	0,0697	0,0636	0,0933	0,0579	0,0691	0,0615	0,0587	0,0819
	100	0,0281	0,0407	0,0334	0,0316	0,0433	0,0258	0,0318	0,0279	0,0269	0,0347
	250	0,0102	0,0152	0,0122	0,0120	0,0155	0,0098	0,0119	0,0105	0,0104	0,0123
	500	0,0051	0,0078	0,0062	0,0061	0,0079	0,0048	0,0060	0,0052	0,0052	0,0061
$\alpha = 4, \theta = 3.5$	50	0,2428	0,3261	0,2769	0,2546	0,3641	0,3876	0,5552	0,4594	0,3999	0,7113
	100	0,1136	0,1584	0,1310	0,1253	0,1665	0,1526	0,2157	0,1777	0,1662	0,2420
	250	0,0418	0,0586	0,0479	0,0472	0,0602	0,0567	0,0831	0,0670	0,0655	0,0871
	500	0,0205	0,0303	0,0241	0,0238	0,0308	0,0275	0,0418	0,0327	0,0323	0,0429

From Tables 1-2, We observe as the sample size increases, the MSEs and biases of all estimators decrease and approach zero. It is clearly seen that the MSEs and biases of the estimators are very close to each other.

#### 4. Conclusion

In this study, we compare the estimation methods for the  $PS(\alpha, \theta)$  distribution. Firstly, five estimators (MLE, LSE, WLSE, CvME, ADE) of the parameters of the  $PS(\alpha, \theta)$  distribution is obtained in point estimation section. Then, a Monte Carlo simulation study is carried out to observe the performances of these estimators according to MSE criterion. As a result of the simulation study, The f MLE is the best estimators according to MSE in Case 2,3 and 4. However, The MSE of LSE of the  $\alpha$  parameter is the smallest in Case 1. We recommend the maximum likelihood method and least square method to estimate the parameters of the  $PS(\alpha, \theta)$  distribution according to simulation results.

#### References

- [1] Shanker, R., Shukla, K. K. (2017). Power Shanker distribution and its Application. *Türkiye Klinikleri Biyoistatistik*, 9(3), 175-187.
- [2] Karakaya, K., Tanış, C. (2020). Different methods of estimation for the one parameter Akash distribution. *Cumhuriyet Science Journal*, 41(4), 944-950.
- [3] Karakaya, K., Tanış, C. (2020). Estimating the Parameters of Xgamma Weibull Distribution. *Adıyaman University Journal of Science*, 10(2), 557-571.
- [4] Tanış, C., Karakaya, K. (2021). A Comparison of Estimation Methods for one Parameter Inverse Gompertz Distribution. *Journal of Science and Arts*, 21(3), 659-668.
- [5] Tanış, C., Karakaya, K. (2021) A Comparison of Estimation Methods for Gompertz Flexible Weibull Distribution. *Erzincan University Journal of Science and Technology*, 14(3), 887-897.
- [6] Tanış, C. (2021a). On transmuted power function distribution: characterization, risk measures, and estimation. *Journal of New Theory*, (34), 72-81.
- [7] Tanış, C. (2021b) Transmuted Lower Record Type Power Function Distribution. *Journal of Science and Arts* 21(4) , 951-960.
- [8] Shanker, R. (2015). Shanker distribution and its applications. *International journal of statistics and Applications*, 5(6), 338-348.
- [9] Fletcher, R., *Practical methods of optimization*, John and Sons, Chichester, 1987.



## Ram Pump Application for Agricultural Irrigation in Çankırı

Hüseyin GÖKÇE<sup>1\*</sup> , Sakine KIRATLI<sup>1</sup> , Mehmet Ali BİBERCİ<sup>1</sup>

<sup>1</sup>Engineering Faculty, Mechanical Engineering, Çankırı Karatekin University, Çankırı, Turkey

### Abstract

It is of great importance that water, which is the key to life, is transported from its source to another place and/or transferred to higher levels than it is. Many studies have been done and are still in progress to solve this problem. Conventional thinking is that these transfers will be made by various types of water pumps driven by electricity or an internal combustion engine. These pump systems operate at high efficiency but they get their energy from electricity or fossil fuels. Although the ability to transfer water with the help of the power of running water or the vacuum effect dates back to the VI centuries BC, it is still used especially in agricultural irrigation. In this study, water ram pump application for irrigation of approximately 40000 m<sup>2</sup> of agricultural land in Çankırı city center Karaköprü location is presented. Two electric motor centrifugal pumps with 1000 l/s flow rate are used in the current irrigation system. The aim is to minimize the electricity consumption used in irrigation. The water will flow into a canal 9 meters high and 30 meters away from the source, and the agricultural lands associated with this channel will be irrigated. The amount of water required for irrigation is 2000 liters per hour. As a result of the theoretical calculations, it has been seen that carrying all the water needed with a ram pump will bring additional costs due to insufficient slope, but a ram pump can be used instead of an electric motor. In addition, alternative methods that can be used other than water pumps are also presented in the study.

**Keywords:** Irrigation, Pumps, Ram pump, Çankırı

### 1. Introduction

The main element of life and the most basic need is water. Clean waters that can meet the needs of living things are very limited, especially when compared to salty waters. The total amount of water on earth is about 1.4 million km<sup>3</sup> and 97.5% of this water is salt water in the seas and oceans. Only 0.5% of the remaining amount is usable, while more than 90% of the freshwater is at the poles and underground [1].

Fresh water can be found on the earth; collected in a reservoir or flowing in the streams. Transporting the water from these sources to living spaces is one of the problems that need to be solved today, as it was in the past. Today, these problems are overcome with advanced technological equipment. It has become quite easy to transport water with many different pump systems to be selected depending on the type of water, its distance to the source, and the required amount of water [2].

There are many different pump systems that allow water to be transported from or to higher levels from the source (such as centrifugal, reciprocating, immersion, peristaltic, gear pumps). In order for these pump systems to operate, they must be driven from the outside by an external motor. These motors can be electric or internal combustion and run on electricity or energy from fossil fuels [3].

It is of great importance that water, which is the key to life, is transported from its source to another place and/or moved to higher levels than it is. The source of the first studies on the transport of water goes back to ancient times. It is known that the "shaduf" system, which works with human power, was used in Mesopotamia and Egypt around 3000 BC. This system is still used especially in the primitive tribes of Africa. When it comes to the VI centuries BC, it is seen that the mechanical systems (water wheel) consisting of a series of shafts and wheels moved by animal power began to be used. Archimedes, who lived between 287-212 BC, developed the "Archimedes Screw", which is named after him [4, 5].

Apart from the aforementioned systems that get their power from humans, animals, or engines, there are systems that get their power from the flow of water and the height difference of the waterbed. The first studies on this subject were made by er-Rezzâz el-Cezerî (Cezerî). The Muslim scholar, inventor and engineer Cezerî, who lived in the Turkish-Islamic geography between 1136-1206, included his work that works with the piston

\* Corresponding author. e-mail address: huseyingokce@karatekin.edu.tr

principle (lift and force) by making use of the flow of water in his book [6]. By the middle of the 18th century, French Montgolfier, known as one of the inventors of hot air, invented the water ram pump in a paper mill to raise the water to a higher position. This pump system was developed and commercialized in the following years. In parallel with the development of electric motors and power line systems, the demand for water ram pumps has decreased. Towards the end of the 20th century, the interest in water ram and similar pump systems has revived due to the need for sustainable technology in developing countries and energy saving in developed countries [7, 8].

In this study, necessary theoretical calculations and designs are presented for the irrigation of approximately 40000 m<sup>2</sup> of agricultural land in the central Karaköprü locality of Çankırı province, for the transportation of the water flowing through the city centre and flowing from Tatlıçay to the related lands with the water ram pump. Two electric motor centrifugal pumps with 1000 l/s flow rate are used in the existing irrigation system. The aim is to minimize the electricity consumption used in irrigation. The water will flow into a canal at a height of 9 meters and 30 meters from the source, and the agricultural lands connected to this canal will be irrigated. The amount of water required for irrigation is 2000 liters per hour.

## 2. Materials and Methods

### 2.1. Water Ram Pump

The fluid flowing in a pipe with constant flow loses its continuous flow regime and gains variable flow characteristics when its flow is stopped or slowed. This causes the kinetic energy of the fluid to change. For example, in pipes with a valve at the outlet, if the valve is suddenly closed, a dynamic load will occur in addition to the normal static load inside the pipe and this dynamic load is called water hammer. When the valve is closed, the kinetic energy of the fluid trapped in the pipe turns into potential energy. Since the flow will stop when the valve is closed, its kinetic energy becomes zero. However, this energy is not lost in accordance with the principle of conservation of energy and turns into turbulent energy in the form of extreme pressure waves, causing water. Compression of the pipe and expansion of the pipe wall is called “water shock” [9, 10].

With the closure of the valve, we stop the movement of the water flowing continuously (constant flow) in the pipe in a short time, that is, we apply a braking acceleration ( $b$ ) (Equation 2) to the mass of the water ( $m$ ) (Equation 1). In this case, the inertia resistance ( $P_{dA}$ ) that will occur due to the speed change is expressed by Equation 3.

$$m = Q/g \quad (1)$$

$$b = \frac{dv}{dt} \quad (2)$$

$$P_{dA} = m \times b = m \times \frac{dv}{dt} \quad (3)$$

If the valve is closed abruptly ( $dt = 0$ ), the value of  $P_{dA}$  becomes infinity (Equation 3). However, in practice, it is not possible to close the valve suddenly; a certain time is required for closing. The shorter the closing time ( $dt$ ), the greater will be the magnitude of the force generated. This increase in force (water hammer) can be exploited by a device that will be placed at the end of the pipe close to the valve. The water ram pump is a hydro-mechanical mechanism based on the evaluation of this energy. The working principle of the water ram pump is shown in Figure 1.

The water flowing from the water source (1) flows into the forebay (3) via the supply pipe (2). The  $D_0$  diameter loading pipe (4) coming out of the forebay conveys the water in the pool to the entrance part of the water ram body (5) below with a height difference of  $h$  and a flow rate of  $Q_0$  ( $Q_m + Q_r$ ). The water reaches the valve (6), which is open under the influence of its own weight in the normal position, and some water ( $Q_m$ ) comes out of

this valve at the first moment and flows out of the body. Under the influence of the speed and pressure of the water coming from the loading pipe (4) to the water ram body (5), valve number 6 closes rapidly. The shock wave, which occurs as a result of the water impact caused by the sudden pause of the water flow, quickly moves backward. The excessive pressure caused by this shock wave opens valve 7; water quickly enters the reservoir (V) of the water ram from here, compressing the air there, and at the same time rises a little in the outlet (rise) pipe (8) of diameter  $D_i$ . The air trapped in the reservoir of the water hammer reacts in the opposite direction to the water with the increase in its pressure, allowing valve number 7 to close and the water to rise in the riser pipe (8) and reach the water tank (9) above. Initially, the pressure waves that occur with the sudden closing of valve number 6 move towards the loading pipe, and at the same time, with the opening of valve number 7, the water enters the V reservoir. As soon as valve 7 is closed, the water pressure in valve 6 drops below the normal pressure and this valve opens from its own weight and some water flows out of the water ram body again. As long as the process continues, some of the water in the forebay ( $Q_m$ ) continues to flow out of valve 6 intermittently, and some ( $Q_r$ ) continues to flow into the reservoir (such as the channel, tank) above. This is a cycle and when the cycle is completed, the process continues unless there is any external intervention to the system. The time between the two openings of valve 6 is 1 cycle. It is repeated 40-200 times per minute, depending on the size, capacity, construction, and establishment characteristics of the water ram pump.

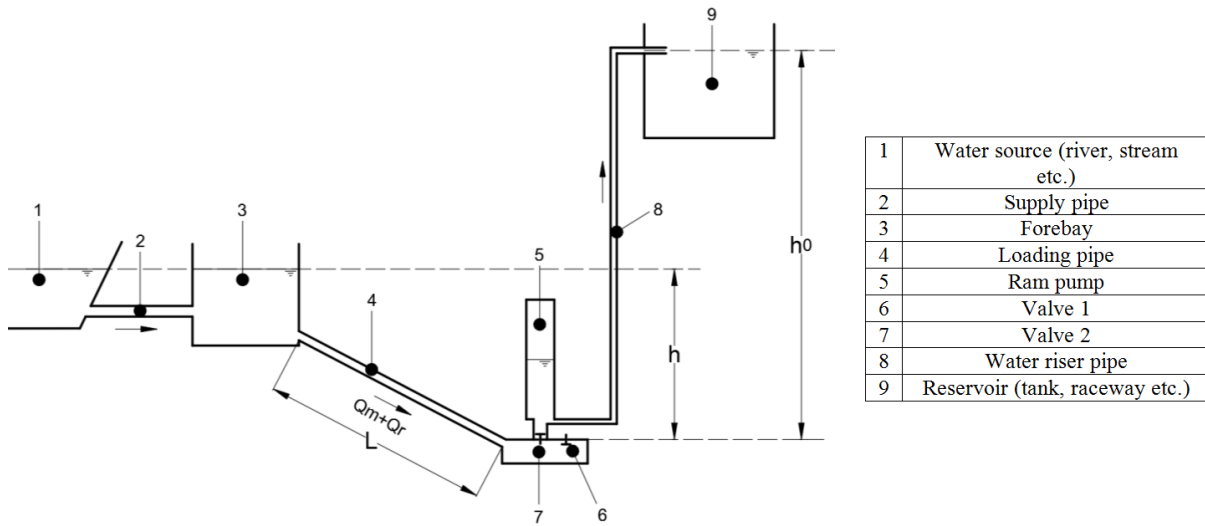


**Figure 1.** Working principle of water ram pump

The efficiency in water ram pumps is found by the equations Aubusson (Equation 4) (the most widely known) and Rankine (Equation 5). In these equations;  $r_A$ : Aubusson water ram pump efficiency,  $r_R$ : Rankine water ram pump efficiency,  $Q_0 = Q_m + Q_r$ : Amount of water coming into the water hammer (l/sec),  $Q_m$ : Amount of water flowing from the body of the water hammer (l/sec),  $Q_r$ : Raised by the water hammer water amount (l/sec),  $h$ : incoming water drop height (m),  $h_0$ : water ram (raising) height (m).

$$r_A = \frac{Q_r}{(Q_m + Q_r)} \times \frac{h_0}{h} \quad (4)$$

$$r_R = \frac{Q_r}{Q_m} \times \left( \frac{h_0}{h} - 1 \right) \quad (5)$$

In these equations, the efficiency of the water ram pump essentially changes depending on the  $h_0/h$  ratio, along with the amount of water coming into the water ram pump ( $Q_0 = Q_m + Q_r$ ) and the diameter of the loading pipe ( $D_0$ ). It is possible to raise the water to a height of 20-25 times the drop height ( $h$ ) with the water ram.

However, its efficiency is as low as 20%. However, if the  $h_0/h$  ratio is around 5-10, its efficiency can increase up to 80%.

## 2.2. Application

Theoretical calculations for the water ram pumps and the necessary pipeline design were made in order to irrigate the agricultural land covering an area of approximately 4 hectares (40000 m<sup>2</sup>) in the Çankırı city center Karaköprü locality. Two electric motor centrifugal pumps with 1000 l/s flow rate are used in the existing irrigation system. The amount of water required for irrigation is 2000 liters per hour ( $\approx 33.34$  l/min). Water ram pumps will be used in order to completely eliminate or partially reduce electricity consumption. The water source is Tatlıçay, which flows within the city centre and from the border of the related agricultural lands. The water will be pumped into an irrigation canal 9 meters high and 30 meters from the source. In the current system, water is pumped into this canal by centrifugal pumps, and agricultural lands are irrigated using the water in this canal. Figure 2 represents the application area.

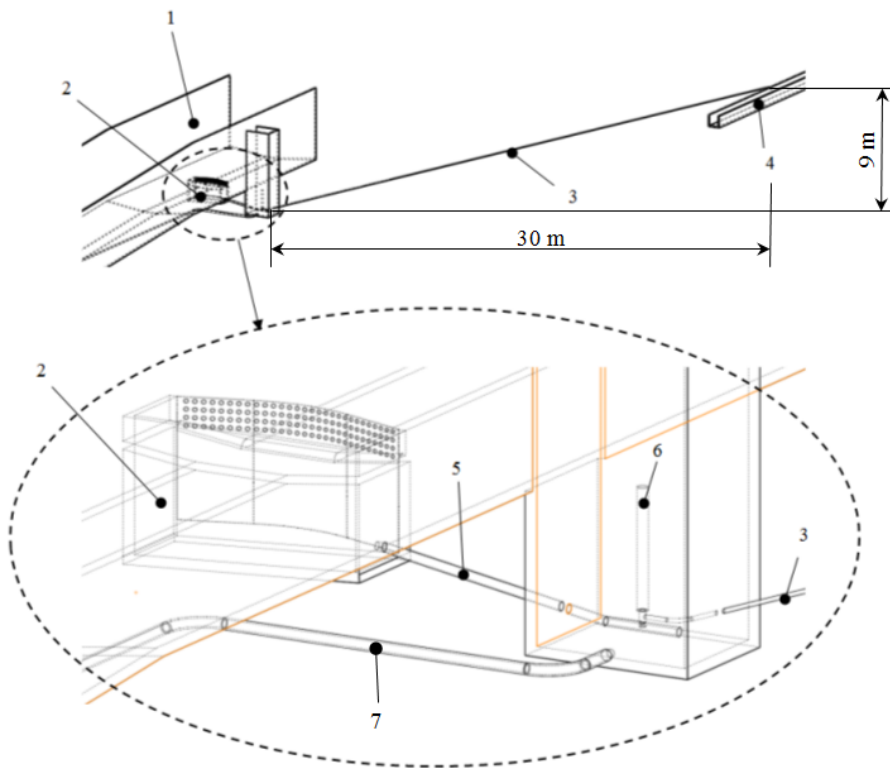


**Figure 2.** Application (1: Water source (river, stream etc.), 2: Forebay, 3: Water riser pipe, 4: Reservoir (tank, raceway etc.), 5: Loading pipe, 6: Ram pump, 7: Bleed pipe)

The water flowing in the water source (1) will be collected in an open-top reservoir (2) of 1×2×3 m dimensions above the source. The reservoir will be made of concrete material, but the reservoir entrance and top will be made of perforated sheet metal. In this way, foreign objects that may hinder the operation of the water ram pump in the water will be prevented from entering the reservoir. The purpose of collecting water in a reservoir is to create a higher pressure effect (increase the water drop height) of the water entering the water ram pump and to partially purify the water from foreign materials. Water will be transmitted from the reservoir floor to the water hammer by a galvanized pipe (5), 3 m long and 1" ( $\approx 25.4$  mm) nominal diameter. The water ram pump is positioned 0.5 m below the reservoir floor and outside the existing water bed in order to be able to intervene easily in case of any malfunction, to prevent damage to the pump in case of flood, and to benefit from the water pressure effectively. With the operation of the water ram pump, the water that will come out of the pump will be discharged to the water source through a PVC pipeline (7). The water coming to the water ram pump will be

transported to the water channel (4) at a height of 9 meters and at a distance of 30 meters, by a galvanized pipeline (3) with a nominal diameter of 1/2".

In the light of these data, a water ram pump that will operate under 2.5 m drop height (reservoir depth (2 m) + height difference between reservoir floor and water ram pump (0,5 m)) and which will be increased to 9 m height, will be designed with a flow rate of 1 l/min the water it can pump per hour is about 200 litter. Considering the annual average flow of the water source and the pipe selections, the flow that feeds the water ram pump is 200 l/min. In this case, the amount of water that the water ram pump can remove from the water channel in 24 hours:

$$200 \times 24 = 4800 \text{ litter}$$

is calculated as. This too,

$$4800 / 24 \times 60 \cong 40 \text{ l/min}$$

corresponds to.

Aubusson efficiency of the water ram pump in the light of calculations:

$$r_A = \frac{40}{200} \times \frac{9}{2,5} \cong 0,50 \text{ (%50)}$$

is calculated as.

### 3. Results and Discussion

The amount of water required for irrigation of the agricultural lands subject to the application is 33.34 l/min. As a result of the theoretical calculations, it has been calculated that the water ram pump, which will operate for 24 hours, will pump water with a maximum flow of 27.78 l/min, and its efficiency will be 50%. According to these results, it is seen that it is not possible to pump all the needed water with a water ram pump. However, it is anticipated that the number and/or capacities of existing electric pumps can be reduced and thus energy consumption will decrease. In addition, it is predicted that the water ram pump, which is thought to work for 24 hours, will make a loud noise during the valve opening and closing process and will cause noise pollution. It is inevitable that the pump will be a negative choice since it is thought to work in the residential area.

The variable flow rate of the water source depending on the seasons and precipitation, as well as the possible noise problem, have negative effects on the use of the water ram pump. However, there are alternative pump systems that can be used other than the ram pump. Water can be transported by using a piston pump based on the lift and force (suction-discharge) principle developed by Cezeri by utilizing the flow of water. In addition, with various systems that provide water absorption by creating a pressure difference in a closed system, the electrical energy used in the existing system can be saved.

### References

- [1] Aküzüm, T., Çakmak, B. & Gökalp, Z. (2010). Türkiye’de su kaynakları yönetiminin değerlendirilmesi. *Tarım Bilimleri Araştırma Dergisi*, 1, 67-74.
- [2] Üzen, N. & Çetin, Ö. (2012). Geçmişten günümüze su ve sulama yönetimi. *Batman Üniversitesi Yaşam Bilimleri Dergisi*, 1(2), 281-290.
- [3] Ertöz, A. Ö. Pompalarda enerji verimliliği. *VI. Ulusal Tesisat Mühendisliği Kongresi ve Sergisi*.
- [4] Görcelioğlu, E. (1975). Su koçu ve ülkemiz koşullarında önemi. *İstanbul Üniversitesi Orman Fakültesi Dergisi*, B,XXV,169-182.
- [5] Veren, E. (2014). Bozkır yöresinde çingiraklı kuyu (seren) kültürü. *Uluslararası Sempozyum: Geçmişten Günümüze Bozkır*.
- [6] Çırak, B. & Yörük, A. (2016). Mekatronik biliminin öncüsü İsmail El - Cezeri. *Siirt Üniversitesi Sosyal*

*Bilimler Enstitüsü Dergisi*, 4, 175-194.

- [7] Young, B.W. (1995). Design of hydraulic ram pump systems. *Proceedings of the Institution of Mechanical Engineers, Part A: Journal of Power and Energy*, 209 (4), 313-322.
- [8] Özbay, E. Gençoğlu M.T., (2011). Küçük hidroelektrik santrallerde yük-frekans kontrolü. *Firat University Journal of Engineering*, 23 (2), 119-128.
- [9] Sheikh, S., Handa, C.C. & Ninawe, A.P. (2013). Design methodology for hydraulic ram pump (Hydram), *International Journal of Mechanical Engineering and Robotics Research*, 2(4), 170-175.
- [10] Guo, X. Li, J., Yang, K., Fu, H., Wang, T., Guo, Y., Xia, Q. & Huang W. (2018). Optimal design and performance analysis of hydraulic ram pump system. *Proceedings of the Institution of Mechanical Engineers, Part A: Journal of Power and Energy*, 232(7), 841-855.





# Classification of Network Attacks with LSTM Architecture Method

**Fuat TÜRK<sup>1,\*</sup>** 

<sup>1</sup>Çankırı Karatekin University, Faculty of Engineering, Dept. of Computer Engineering, Çankırı, Turkey

## Abstract

Detection of unknown attacks in network traffic is an extremely important issue due to the increasing dependency of systems on the internet today. Until recently, traditional machine learning models were generally preferred for network security detection. Nowadays, it is not being preferred as much as before. Even though machine learning models can acquire a wide variety of features, they require the manual design of network traffic, obtaining a low-rate accuracy. On the other hand, an attack detection system is a very critical situation for protecting information from malicious treatment. Attack detection systems are a system mechanism that can classify data as normal or attacked. The LSTM model is proposed for systems that can operate with higher accuracy as an alternative to classical machine learning models. The proposed LSTM model can automatically learn the basic features of the hierarchy and does not require manual design principles. This model has been tested with the publicly available NSL-KDD dataset acquiring 80% accuracy. Experimental results show that the model can be used as an alternative to other methods.

**Keywords:** Network Attacks, LSTM architecture, NSL-KDD data set, Network Attack classification

## 1. Introduction

Today, network security has become a more important issue due to the increasing use of network-based devices. With the development of internet technology, internet services offered to people have also diversified. Therefore, the probability of facing various security threats is more likely to increase [1]. In addition, intrusion detection into network systems is becoming more and more difficult [2]. In particular, how to detect unexpected malicious network traffic is an important issue. [2-3].

Network traffic can be divided into two basic categories, normal traffic, and malicious traffic. From this point of view, attack detection can be considered a classification problem. By effectively detecting and blocking malicious traffic, and improving the performance of classifiers, system accuracy can be greatly improved. Machine learning (ML) methods are widely used in intrusion detection to identify malicious traffic. However, these methods require basic learning and feature selection. On the other hand, they have difficulties in attribute selection. Also, they cannot effectively solve the huge intrusion data classification problem that leads to low recognition accuracy and a high false alarm rate. Nowadays, deep learning-based intrusion detection methods have started to replace ML methods. [4-5].

Shrivastava and Devangan performed a highly accurate study on the NDSL-KDD dataset using the Artificial Neural Network (ANN) and Bayesian Net with Gain Ratio (GR) feature selection method [6]. Abhirop et al. tried three different ML algorithms. In this study, Support Vector Machine (SVM), Naive Bayes (NB) and Neural Network (NN) methods were used to detect the attack system. The researchers opted for the open-source protocol to collect group features to generate the training data. ML techniques were based on five features, and experimental results show that SVM gives a low accuracy rate compared to the last two classifiers. [7]. In the study of Serinelli et al., a passive defense system aimed at monitoring and protecting computer networks is introduced. It has also been tried to provide guidance on the selection and execution of methodology for training Machines and Deep Learning models. Their goal is to minimize the Attack Undetected percentage, False Alarm Rate percentage, and overall test time [8]. Staudemeyer and Omlin have tested the performance of the Long Short-Term Memory (LSTM) network in classifying intrusion traffic. The study results indicate that LSTM can learn all network attacks hidden in the training data. [9].

\* Corresponding author. e-mail address: fuatturk@karatekin.edu.tr

## 2. Materials and Methods

### 2.1. NSL-KDD dataset

NSL-KDD is a dataset designed by Tavalae et al. [10]. This dataset is open to access for everyone. It contains a total of 37 attack types, where 27 attacks are used by the test dataset and 23 attacks are used by the training dataset for experiments. It includes 41 features and 5 network attacks in total. There are 5 types of network attacks one of which is normal and the other 4 are Research Attacks (Probe), Denial of Service attacks (DoS), User-to-Root (U2R), and Remote-to-Local (R2L) [11,12]. The removal of excess records of NSL-KDD helps the classifier produce unbiased results, and it is its most important advantage over other datasets.

### 2.2. LSTM Architecture

LSTM networks were designed by Hochreiter and Schmidhuber to predict special cases that Recurrent Neural Networks (RNN) cannot solve. A structure is available in LSTM networks to calculate hidden states. The memory cells in the LSTM are the structures that hold the previous state and the input information. These cells are the mechanisms that decide which data to keep or which data to delete. Then they merge the previous state with the current memory. With such an approach, long-term dependencies are eliminated and data sets are maintained. The LSTM structure is given in Figure 1. The gate given as input controls when the new information should enter the memory, the forget-memory gate controls the forgetting of the existing information and the recall of new data. The final stage decides when the information in the cell will be used at the exit [13].

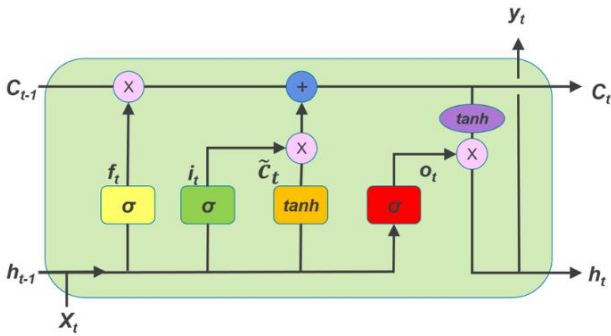


**Figure 1.** LSTM architecture [14]

The basic structure of the proposed LSTM architecture is shown in Figure 2. The output is arranged in 5 types with the softmax function. Unit means the size of the inner cells in LSTM. Here, the unit value is set to 50.

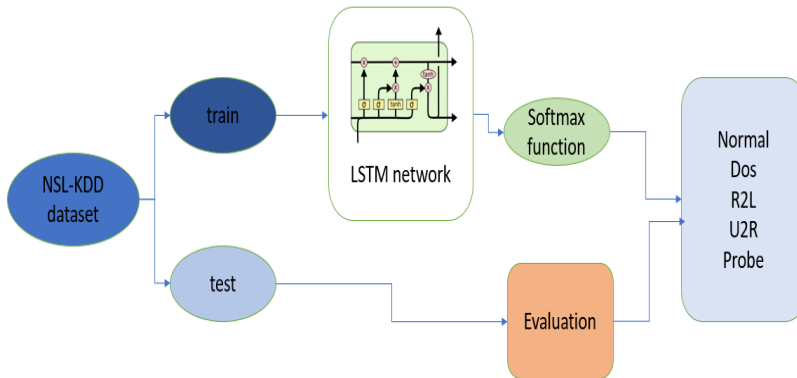


**Figure 2.** Proposed LSTM architecture and workflow diagram

### 3. Results and Discussion

#### 3.1. Performance metrics with LSTM architecture.

The performance metrics obtained as a result of training the NSL-KDD data set with the LSTM network are shown in Table 1.

**Table 1.** LSTM architecture performance metrics

	Precision	Recall	F1-Score
<b>Dos</b>	0.83	0.96	0.89
<b>Probe</b>	0.77	0.87	0.82
<b>R2L</b>	0.15	0.71	0.24
<b>U2R</b>	0.28	0.79	0.42
<b>Normal</b>	0.97	0.71	0.82
<b>Accuracy(avg)</b>	0.80		

The confusion matrix is shown in Figure 3. It is seen that the success of the R2L and U2R attack types is low and is confused with the normal type. When we look at other types, we can say that success is higher. In Figure 4 the ROC curve analysis for the LSTM classifier is shown. When the ROC analysis is carefully examined, it can be said that R2L is a comparatively low area, and the calculated areas for the other types are close to each other. However, we can talk about classification success because all types have a curve above the mid-level area.

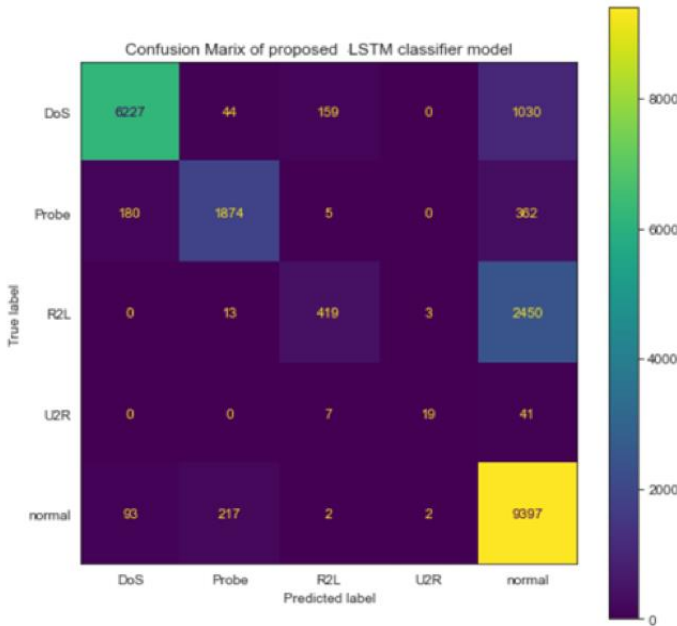


**Figure 3.** LSTM architecture confusion matrix values

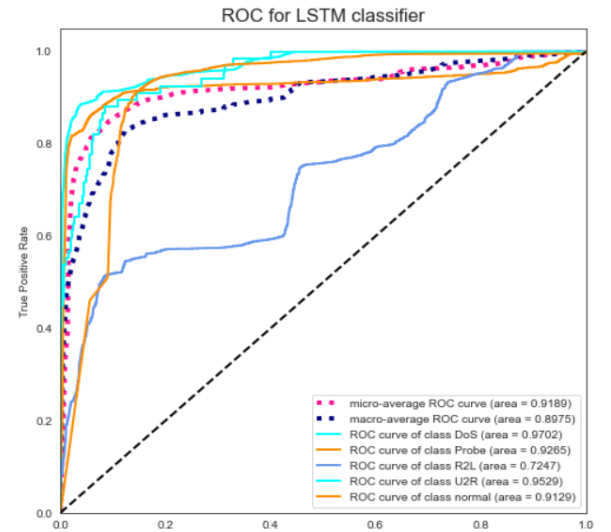


**Figure 4.** ROC analysis graph for LSTM architecture

#### 3.2. Evaluation results

As a result of the data obtained from the existing graphics and tables, it can be recommended to use LSTM networks as an alternative to machine learning and classical Convolutional Neural Networks in the detection of network attacks. Here, studies can be carried out to increase the detection rates of R2L and U2R classes with low accuracy values. At this stage, the selection of hyperparameters, and updates on the network structure design may be recommended. Apart from this, the NSL-KDD data set can be merged with other data sets or the samples can be increased in the number of classes with low success. As a result of these processes, I think that networks trained with high accuracy can be a good application option for attack detection and classification, especially in all server-based systems.

## References

- [1] Su, T., Sun, H., Zhu, J., Wang, S., Li, Y. (2018). BAT: Deep Learning Methods on Network Intrusion Detection Using NSL-KDD Dataset, 8, 29575 – 29585.
- [2] Zarpelão, BB., Sanches, M.R., Kawakani C.T., Carliso D. A. (2017). *A survey of intrusion detection in Internet of Things*. Doi: 10.1016/j.jnca.2017.02.009
- [3] Mukherjee, B., Heberlein, L.T., Levitt, K.N. (1994). Network intrusion detection, 8(3), 26-41.
- [4] Kuang, F., Xu, W., Zhang, S. (2014). A novel hybrid KPCA and SVM with GA model for intrusion detection. *Applied Soft Computing*, 18, 178–184. Doi: 10.1016/j.asoc.2014.01.028.
- [5] Garg, S., Batra, S. (2018). A novel ensembled technique for anomaly detection. *International Journal of Communication Systems*, 30, 3248. Doi:10.1002/DAC.3248.
- [6] Kumar, S.A., Kumar, D.A. (2014). An Ensemble Model for Classification of Attacks with Feature Selection based on KDD99 and NSL-KDD Data Set. *IJCA* 99, 8–13.
- [7] Abhiroop, T. Sarath, B., Manoj, B.S. (2022). A Machine Learning Approach for Detecting DoS Attacks in SDN Switches, National Conference on Communications.
- [8] Serinelli, BM., Collen A., Nijdam, NA. (2020). Training Guidance with KDD Cup 1999 and NSL-KDD Data Sets of ANIDINR: Anomaly-Based Network Intrusion Detection System. *Procedia Computer Science*, 175, 560–565, Doi: 0.1016/J.PROCS.2020.07.080
- [9] Staudemeyer, RC., Omlin, CW. (2013). Evaluating performance of long short-term memory recurrent neural networks on intrusion detection data. *ACM International Conference Proceeding Series* 218–224.
- [10] Tavallae, M., Bagheri, E., Lu, W., Ghorbani, AA. (2009). A detailed analysis of the KDD CUP 99 data set. *IEEE Symposium on Computational Intelligence for Security and Defense Applications, CISDA*, Doi:10.1109/CISDA.2009.5356528
- [11] Ritu B., Ritu, N. (2019). A Review On Kdd Cup99 And Nsl Nsl-Kdd Dataset, *International Journal of Advanced Research in Computer Science*, 10, 2.
- [12] Shaheen, S.M. (2022). A Comparative Analysis of Intelligent Techniques for Detecting Anomalous Internet Traffic, King Fahd University of Petroleum and Minerals, Saudi Arabia.
- [13] Hochreiter S, Schmidhuber, J., (1997). Long Short-Term Memory., *Neural Computation*, 9,1735–1780. Doi :10.1162/NECO.1997.9.8.1735
- [14] Uzun Kısa Dönemli Bellek (Long / Short Term Memory) (LSTM). Available at: <https://medium.com/@batincangurbuz/uzun-k%C4%B1sa-d%C3%B6nemli-bellek-long-short-term-memory-lstm-c526980c28b1>, Retrieved Augst 10, 2022.



# Hormonal and Biochemical Study of the Effect of Vitamin D on Polycystic Ovaries in Women

Jamal Sami Taha ALJUMAILI<sup>1,\*</sup> , Hakan ÇOLAK<sup>2</sup>  Ahmed Sulimaan JUMAAH<sup>3</sup> 

<sup>1,2,3</sup> Chemistry Department, Çankırı Karatekin University, Türkiye

## Abstract

Polycystic ovary syndrome (PCOS) is a shared reason for ovarian dysfunction in women with anovulation. The main symptoms are branded by chronic anovulation, hyperandrogenism, and/or the presence of ovarian cysts on ultrasound examination. Low levels of vitamin d3 exacerbate PCOS symptoms, including insulin resistance, ovulation, menstrual irregularities, infertility, hyperandrogenism, and obesity, and increase the risk of cardiovascular disease. In this study, we will try to find a relationship between PCOS and vitamin D deficiency in affected women. The study included (120) samples distributed into two groups, the patient's group consisted of (80) samples and the control group consisted of (40) samples. Some chemical and hormonal tests were done such as Vit D3, TT, PRL, FSH, LH, TG, CHO, HDL, LDL, VLDL. We found low levels of Vitamin D, Follicle-Stimulating hormone, Cholesterol level, High-density Lipoprotein (HDL) level, and Low-density Lipoprotein (LDL) level. Also, we found high levels of Testosterone level, Prolactin level, Luteinizing hormone level, Triglyceride level, and Very Low-density Lipoprotein (VLDL) level.

**Keywords:** Polycystic ovary syndrome, Vitamin D, Testosterone hormone, Prolactin hormone, LH

## 1. Introduction

Polycystic ovary syndrome (PCOS) is the most commonplace endocrine complaint amongst ladies of generative age. It is a multifactorial sickness branded by way of the living of hyperandrogenism with ovulatory dysfunction [1]. PCOS influences about 5-10% of ladies of childbearing age [2]. It is the maximum not unusual motive of infertility because of anovulation. Metabolic disorders are commonplace in co-taking place ladies, having insulin resistance, weight problems, type 2 diabetes mellitus, dyslipidemia, metabolic syndrome, high blood pressure, cardiovascular disease, and while menstrual disease is considered [3].

a hormonal imbalance reasons too many follicles (small fluid-stuffed sacs in which eggs develop) on the ovaries. These numerous follicles appear to be cysts, that's where the term "polycystic" originates from [4]. In polycystic ovaries, the ovaries are large than ordinary. That PCOS is a disorder related to the whole frame, not just the ovaries, proof that a problematic or dysfunction in unique area reasons dysfunction in other regions due to the fact the body is a unified entire [5].

The affiliation of PCOS and endometriosis changed into first pronounced in 1949, and the complex overlap among endometrial cancer and PCOS [6]. Women with PCOS percentage several threat factors associated with the improvement of endometrial cancer along with peculiar uterine bleeding [7]. A hormonal imbalance reasons too many follicles (small fluid-stuffed sacs in which eggs develop) on the ovaries. These numerous follicles appear to be cysts, that's where the term "polycystic" originates from [4].

Vitamin D can also play a first-rate role in the development of PCOS. There has been a focal point on diet D supplementation as an accessory in PCOS [8]. Several studies have said low nutrition D degrees in ladies with PCOS, with regular vitamin D ranges amid 11 and 31 ng/ml, with values as low as 20 ng/ml (67-85) [9].

Giving vitamin D to ladies with PCOS has a helpful influence on markers of systemic irritation and oxidative harm. Certain studies have designated that nutrition D lack is a hassle in sufferers with PCOS, despite the fact that consequences of randomized trials assessing the result of nutrition D supplementation on metabolic outlines amongst women with PCOS are contradictory [10]. Vitamin D deficiency is also related to expanded tiers of overall testosterone and dehydroepiandrosterone sulfate (DHEAS) in PCOS patients [11].

\* Corresponding author. e-mail address: jamalsami@yahoo.com

## 2. Materials and Methods

Specialized hormonal materials and reagents applied, Specialized biochemical materials and reagents are illustrated in Table 1.

**Table 1.** The subject name and the manufacturing company

Subject Name	The manufacture company
Testosterone test kit	Korea / boditech
Prolactin test kit	Korea / boditech
FSH test kit	Korea / boditech
LH test kit	Korea / boditech
Vitamin D	Korea / boditech
Cholesterol	Spain / Linear
Triglyceride	Spain / Linear
HDL	Germany / Human

## 3. Results and Discussion

### 3.1 Vitamin D

Vitamin D level in subjects showed least level in patients pcos followed by then the higher level in control, it is illustrated in Table 2.

**Table 2.** Vitamin D level difference among the studied group

Variable		Mean	SE	SD
VITAMIN D	Control	38.55	0.72	4.57
	PCOS	22.25	1.18	10.62
	P-value		1.06 <sup>NS</sup>	

NS: None statistically significant variance (p>0.05).

### 3.2 Testosterone

Testosterone hormone levels in subjects showed higher levels in patients PCOS followed by then the least level in control, it is illustrated in Table 3.

**Table 3.** Testosterone hormone level difference among the studied group

Variable		Mean	SE	SD
Testosterone (ng/mL)	Control	0.7	0.02	0.14
	pcos	1.34	0.065	0.58
	p-value		8.18 <sup>NS</sup>	

NS: None statistical significant variance (p>0.05).

### 3.3 Prolactin

Prolactin hormone level in subjects showed higher level in patients PCOS followed by then the least level in control, it is illustrated in Table 4.

**Table 4.** Prolactin hormone level difference among the studied group

Variable		Mean	SE	SD
Prolactin (ng/mL)		17.4	0.7	4.47
	pcos	31.13	1.52	13.6
	p-value		9.79 <sup>NS</sup>	

NS: None statistical significant variance ( $p>0.05$ ).

### 3.4 Luteinizing Hormone

Luteinizing hormone level in subjects showed higher level in patients PCOS followed by then the least level in control, it is illustrated in Table 5.

**Table 5.** Luteinizing Hormone level differences among the studied group

Variable		Mean	SE	SD
Luteinizing hormone (mIU/ml)	Control	10.07	0.52	3.3
	pcos	14.87	0.61	5.53
	p value		1.61 <sup>NS</sup>	

NS: None statistical significant variance ( $p>0.05$ ).

### 3.5 Follicle-Stimulating Hormone

Follicle-Stimulating hormone levels in subjects showed the least level in patients PCOS followed by then the higher level in control, it is illustrated in Table 6.

**Table 6.** Follicle-Stimulating Hormone level difference among the studied group

Variable		Mean	SE	SD
Follicle-Stimulating Hormone(mIU/ml)	Control	6.28	0.32	2.06
	pcos	4.56	0.23	2.13
	p value		0.00005 <sup>**</sup>	

<sup>\*\*</sup>: High statistical significant variance ( $p\leq 0.05$ ).

### 3.6 Cholesterol

Cholesterol levels in subjects showed the least level in patients PCOS followed by then the higher level in control, it is illustrated in Table 7.

**Table 7.** Cholesterol level difference among the studied group

Variable		Mean	SE	SD
CHO (mg/dl)	Control	170.075	2.44	15.46
	pcos	133.225	2.72	24.34
	p value		2.04 <sup>NS</sup>	
NS: None statistical significant variance (p>0.05).				

### Acknowledgement

In this study, the financial support was provided by the Author. All experimental works were conducted in Diyala Hospital Laboratory. The author would like to thanks to all supporters due to their precious contributions.

I would like to express my thanks to my advisor, Prof. Dr. Hakan ÇOLAK, for his support, guidance, and understanding. And the second supervisor, Dr. Ahmed sulaiman JUMAAH for his guidance and assistance. and Dr. Huseen for his support and always being available to help. Also, I'd want to express my heartfelt gratitude to my father and mother for their unwavering support throughout my academic career.

### References

- [1] Johansson, J. (2013). *Polycystic ovary syndrome-Effect of acupuncture on insulin resistance and neuroendocrine function*. <https://gupea.ub.gu.se/handle/2077/31711>
- [2] Banaszewska, B., Spaczyński, R. Z., Pelesz, M., & Pawelczyk, L. (2003). Incidence of elevated LH/FSH ratio in polycystic ovary syndrome women with normo-and hyperinsulinemia. *Insulin*, 15, 17.
- [3] Barbosa, G., de Sá, L. B. P. C., Rocha, D. R. T. W., & Arbex, A. K. (2016). Polycystic Ovary Syndrome (PCOS) and Fertility. In *Open Journal of Endocrine and Metabolic Diseases* (Vol. 06, Issue 01, pp. 58–65). <https://doi.org/10.4236/ojemd.2016.61008>.
- [4] Hoeger, K. M., Legro, R. S., & Welt, C. K. (2014). A patient's guide: polycystic ovary syndrome (PCOS). *The Journal of Clinical Endocrinology & Metabolism*, 99(1), 35A-36A.
- [5] Dunne, N., & Slater, W. (2006). *The Natural Diet Solution for PCOS and Infertility: How to Manage Polycystic Ovary Syndrome Naturally* (p. 528). <http://books.google.com/books?id=2bpWLux--uwC&pgis=1>.
- [6] Zuo, T., Zhu, M., & Xu, W. (2016). *Roles of Oxidative Stress in Polycystic Ovary Syndrome and Cancers*.
- [7] Legro, R. S., Arslanian, S. A., Ehrmann, D. A., Hoeger, K. M., Murad, M. H., Pasquali, R., & Welt, C. K. (2013). *Diagnosis and Treatment of Polycystic Ovary Syndrome: An Endocrine Society Clinical Practice Guideline*.
- [8] He, C., Lin, Z., Robb, S. W., & Ezeamama, A. E. (2015). Serum vitamin D levels and polycystic ovary syndrome: a systematic review and meta-analysis. *Nutrients*, 7(6), 4555–4577.
- [9] Thomson, R. L., Spedding, S., & Buckley, J. D. (2012). Vitamin D in the aetiology and management of polycystic ovary syndrome. *Clinical Endocrinology*, 77(3), 343–350.
- [10] Ostadmohammadi, V., Jamilian, M., Bahmani, F., & Asemi, Z. (2019). *Vitamin D and probiotic co-supplementation affects mental health, hormonal, inflammatory and oxidative stress parameters in women with polycystic ovary syndrome*.
- [11] Williams, A., Babu, J. R., Wadsworth, D. D., Burnett, D., & Geetha, T. (2020). The effects of vitamin D on metabolic profiles in women with polycystic ovary syndrome: A systematic review. *Hormone and Metabolic Research*, 52(07), 485–491.





# Optimization Approach to the Design of Dual Band Slotted Circular Microstrip Antenna

***Mahmud Esad YİĞİT<sup>1,2\*</sup>*** , ***Tayfun GÜNEL<sup>3</sup>*** 

<sup>1</sup>Department of Electrical and Electronics Engineering, Çankırı Karatekin University, Çankırı, Türkiye

<sup>2</sup>Graduate School, Department of Electronics & Communication Engineering, Istanbul Technical University, Istanbul, Türkiye

<sup>3</sup>Department of Electronics & Communication Engineering, Istanbul Technical University, Istanbul, Türkiye

## Abstract

In this paper, a circular microstrip antenna with circular slots has been designed via optimization approach. Aim of the optimization is to design an antenna operating on dual WLAN bands with desired gains. Circular slots have been added to antenna patch in order to obtain desired resonance frequencies and gain. Optimization tool of ANSYS High Frequency Structural Simulator (HFSS) has been used for design process. Genetic Algorithm has been chosen as optimizer in HFSS optimization tool. HFSS optimization and simulation results have been given.

**Keywords:** Circular Microstrip Antenna, Dual Band Antenna, Optimization, Slotted Antenna, WLAN

## 1. Introduction

In recent years, there has been an increasing interest in wireless communication. This interest has led to numerous studies on microstrip patch antennas and their applications [1-3]. Microstrip patch antennas have many advantages in terms of size, usability, easy installation, low cost, integration and durability. Microstrip patch antennas can also be modified by various techniques in order to obtain the desired results and improve performance of the antenna. Changing the feeding method, combining antennas, creating antenna arrays, adding slots etc. can be applied to microstrip antennas. Most of these techniques are relatively easy to implement on microstrip antennas. Microstrip patch antennas can be designed in a variety of ways. Different antenna shapes show different radiation characteristics. The most commonly used shapes are rectangular, triangular and circular antennas. In this study, a circular microstrip patch antenna has been designed. The circular antenna gives similar characteristics to the rectangular antenna, but the patch size of it is smaller than that of rectangular antenna.

In this paper circular slots have been added to the antenna patch in order to improve antenna performance. There is no general formulation for every type and number of slots. Designers use trial and error method with their experience in order to achieve desired antenna performance. Parametric analysis in simulation programs can give some perspective about the structure but there is no guarantee to obtain desired performance. The increase in slot numbers increases required time for design of the antenna.

In order to overcome these difficulties learning techniques such as Artificial Neural Networks (ANN) [4-8], Support Vector Regression (SVR) [9-13] and optimization algorithms [14-18] have widely been used. In the present study, we aimed to design a circular microstrip antenna operating in WLAN frequency bands (2.4 GHz and 5 GHz) with satisfactory gains. In order to adjust resonance frequencies and improve the gain circular slots have been added to the antenna patch. Optimization tool of ANSYS High Frequency Structural Simulator (HFSS) [19] has been used to find the radii and center positions of circular slots that give the desired resonance frequencies and gains. In order to analyze antenna, Finite Element Method (FEM) is employed in HFSS.

---

\* Corresponding author. e-mailing address: eyigit@karatekin.edu.tr

## 2. Circular Microstrip Antenna

A circular microstrip antenna is presented in Fig. 1. Design of circular antenna is easier than rectangular antenna because only the radius of antenna patch is needed to find. For a resonance frequency of  $f_r$  and substrate with a relative permittivity of  $\epsilon_r$  and thickness of  $h$ , radius of the antenna patch ( $a$ ) can be calculated by [1];

$$a = \frac{F}{\sqrt{1 + \frac{2h}{\pi\epsilon_r F} \left[ \ln\left(\frac{\pi F}{2h}\right) + 1.7726 \right]}} \quad (1)$$

where

$$F = \frac{8.791 \times 10^9}{f_r \sqrt{\epsilon_r}} \quad (2)$$

where  $f_r$  in Hz and  $h$  in cm.

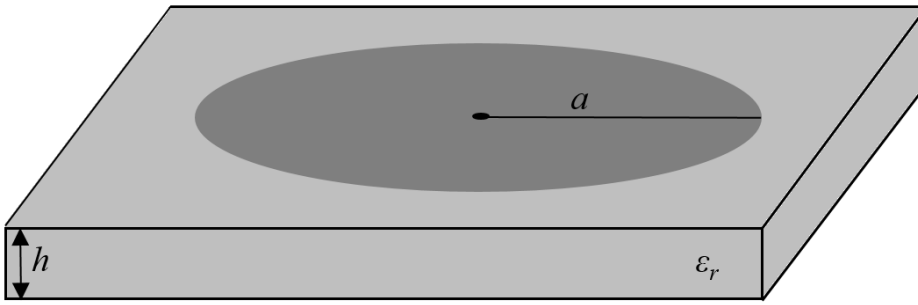


**Figure 1.** Schematic of the circular microstrip antenna.

In this study, Rogers RT/duroid 5880 antenna substrate with a relative permittivity of 2.2 and a thickness of 1.6 mm has been used. Antenna patch radius  $a$  is calculated via (1-2) as 23.62 mm for a resonance frequency of 2.4 GHz. HFSS simulation has been carried out with this radius value and resonance frequency is obtained as 2.38 GHz.

In order to obtain resonance frequencies and improve the antenna gain, circular slots has been formed on the circular antenna patch. Rogers RT/duroid 5880 substrate with a relative permittivity of 2.2 and a thickness of 1.6 mm is used. Antenna patch radius  $a$  is calculated to be 23.62 mm, antenna substrate length and width are both obtained as 53.75 mm. The feed point is found as  $x_f=6.5$  mm and  $y_f=0$  mm via parametric analysis. General schematic and HFSS drawing of the proposed slotted circular antenna are shown in Fig. 2a and 2b respectively.

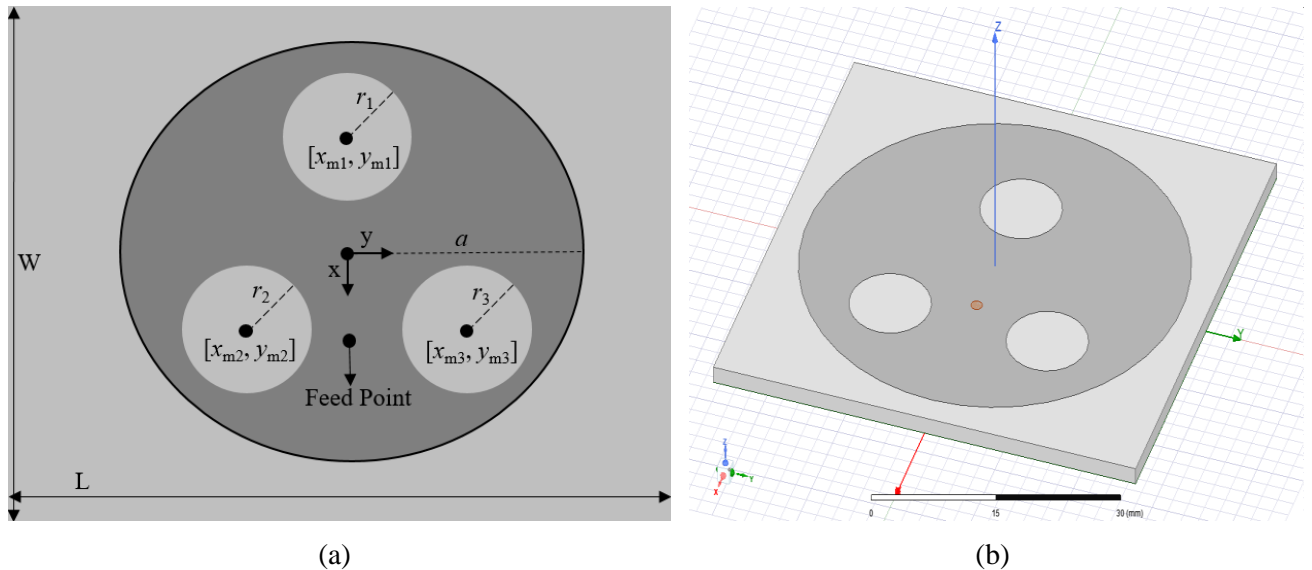


**Figure 2.** a) The proposed slotted circular microstrip antenna, b) HFSS drawing of the antenna.

### 3. Results and Discussion

HFSS optimization tool is useful due to having different kind of optimization methods such as gradient based and search based algorithms. Designers can specify optimization parameters, design parameters and select goals by setting up various calculations. Optimization tool in HFSS uses HFSS's own numerical electromagnetic analysis method for computing the value of cost function defined in optimization algorithm.

Genetic Algorithm (GA) [14, 20-24] has been selected as optimizer to estimate slot radii and centers of the antenna for desired resonance frequencies and gains. Optimization parameters for GA optimizer are given in Table 1. Slot radii  $r_1$ ,  $r_2$  and  $r_3$  and the slot center positions  $[x_{m1}, y_{m1}]$ ,  $[x_{m2}, y_{m2}]$  and  $[x_{m3}, y_{m3}]$  are selected as the variables of optimization. Intervals of optimization variables are given in Table 2.

**Table 1.** Optimization parameters for genetic algorithm optimizer of HFSS

Parameter	Value
Number of Individuals	30
Crossover Type	Simulated Binary
Mutation Type	Polynomial
Selection Type	Roulette
Maximum Number of Iterations	1000
Mutation Probability	0.01
Crossover Probability	0.98
Cost Function Norm Type	L1
Weights	1

**Table 2.** Intervals of optimization variables

Variable	Interval
$r_1$	$1 \text{ mm} \leq r_1 \leq 5 \text{ mm}$
$r_2$	$1 \text{ mm} \leq r_2 \leq 5 \text{ mm}$
$r_3$	$1 \text{ mm} \leq r_3 \leq 5 \text{ mm}$
$x_{m1}$	$-20 \text{ mm} \leq x_{m1} \leq -5 \text{ mm}$
$y_{m1}$	$-5 \text{ mm} \leq y_{m1} \leq 5 \text{ mm}$
$x_{m2}$	$0 \text{ mm} \leq x_{m2} \leq 20 \text{ mm}$
$y_{m2}$	$5 \text{ mm} \leq y_{m2} \leq 20 \text{ mm}$
$x_{m3}$	$0 \text{ mm} \leq x_{m3} \leq 20 \text{ mm}$
$y_{m3}$	$-20 \text{ mm} \leq y_{m3} \leq -5 \text{ mm}$

Desired resonant frequencies are selected as  $f_{r1}=2.4$  GHz and  $f_{r2}=5.1$  GHz. Desired gains at resonance frequencies are selected as  $g=3$  dB. Minimum cost value is reached at the 539<sup>th</sup> iteration. HFSS optimization via GA optimizer has been taken 4 hours and 12 minutes with a computer that has 2.4 GHz CPU and 8 GB RAM. Radii of slots are found as  $r_1=3.73$  mm,  $r_2=1.89$  mm and  $r_3=4.84$  mm. Center positions of slots are obtained as  $[x_{m1}, y_{m1}]=[-5.44 \text{ mm}, 0]$ ,  $[x_{m2}, y_{m2}]=[19.33, 10.60 \text{ mm}]$  and  $[x_{m3}, y_{m3}]=[19.33, -10.60 \text{ mm}]$ .

By using slot radii and center position values which are obtained by HFSS optimization, HFSS simulation has been carried out. HFSS drawing of the optimized antenna is given in Fig. 3.  $|S_{11}|$  plot is given in Fig. 4. The resonance frequencies are obtained as 2.42 GHz and 5.09 GHz. The 10-dB bandwidth for 2.42 GHz is 60 MHz and for 5.09 GHz it is obtained as 150 MHz.

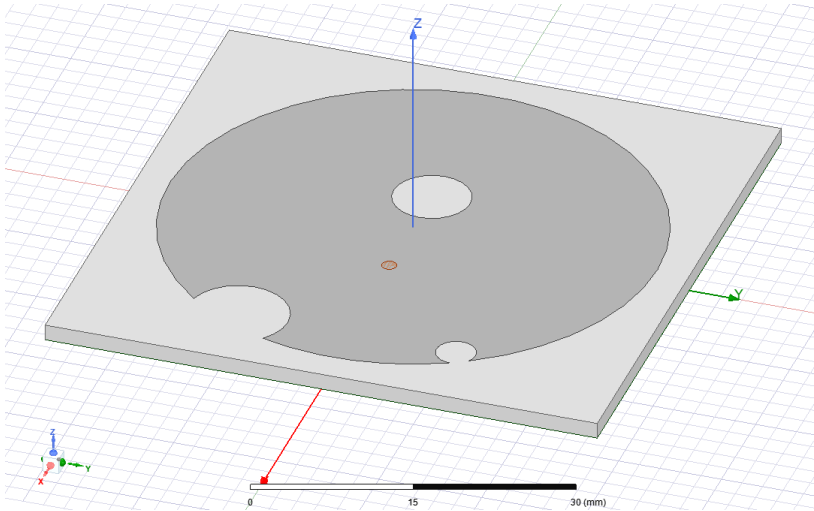


**Figure 3.** HFSS drawing of the optimized slotted circular microstrip antenna.

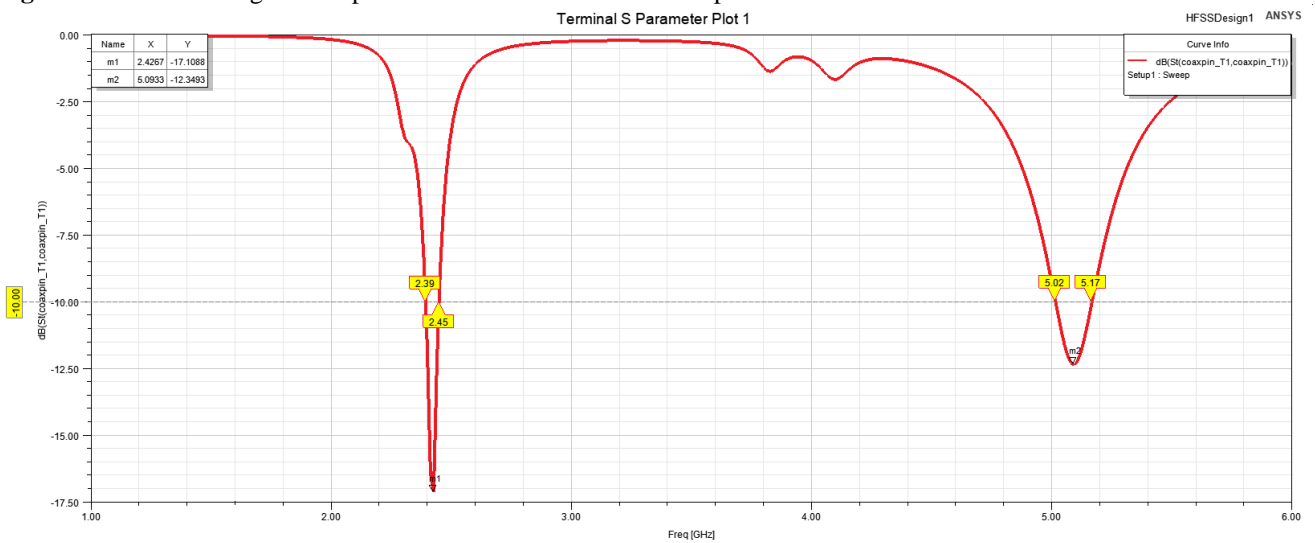


**Figure 4.**  $|S_{11}|$  plot of slotted circular microstrip antenna.

Gain plots for 2.42 GHz and 5.09 GHz are presented in Fig. 5a and 5b, respectively. The antenna gain for 2.42 GHz is 3.9 dB and for 5.09 GHz it is obtained as 3.7 dB.

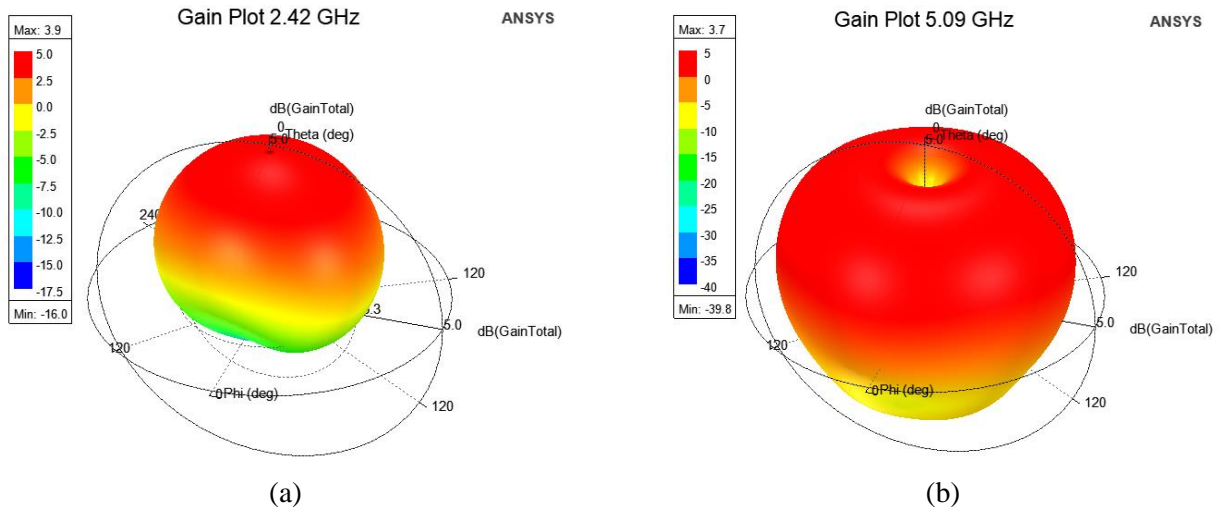


**Figure 5.** Gain plot of slotted circular microstrip antenna for a) 2.42 GHz, b) 5.09 GHz.

The radiation diagrams of slotted circular microstrip antenna for 2.42 GHz and 5.09 GHz are illustrated in Fig. 6a and 6b, respectively.

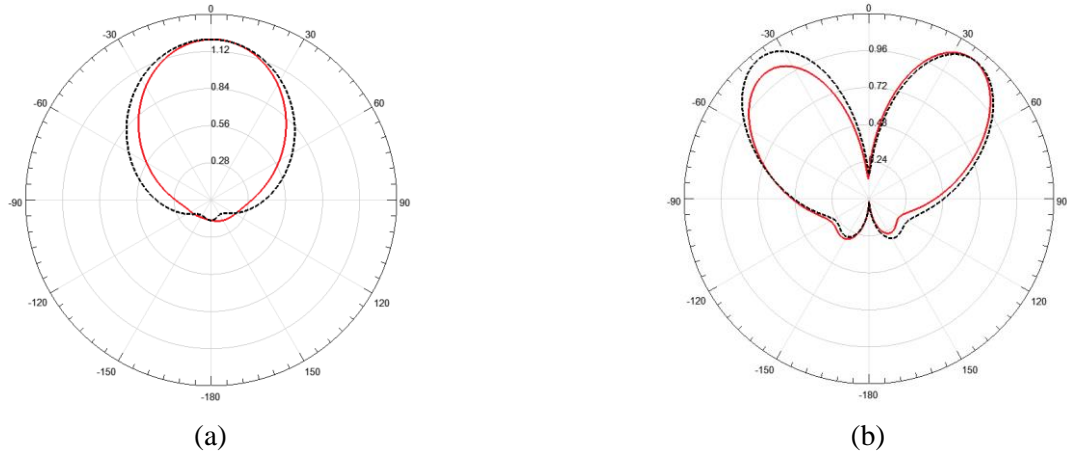


**Figure 6.** Radiation diagrams of slotted circular microstrip antenna for a) 2.42 GHz, b) 5.09 GHz (- xz-plane, -- yz-plane). Surface current distributions of the antenna for 2.42 GHz and 5.09 GHz are shown in Fig. 7a and 7b, respectively.

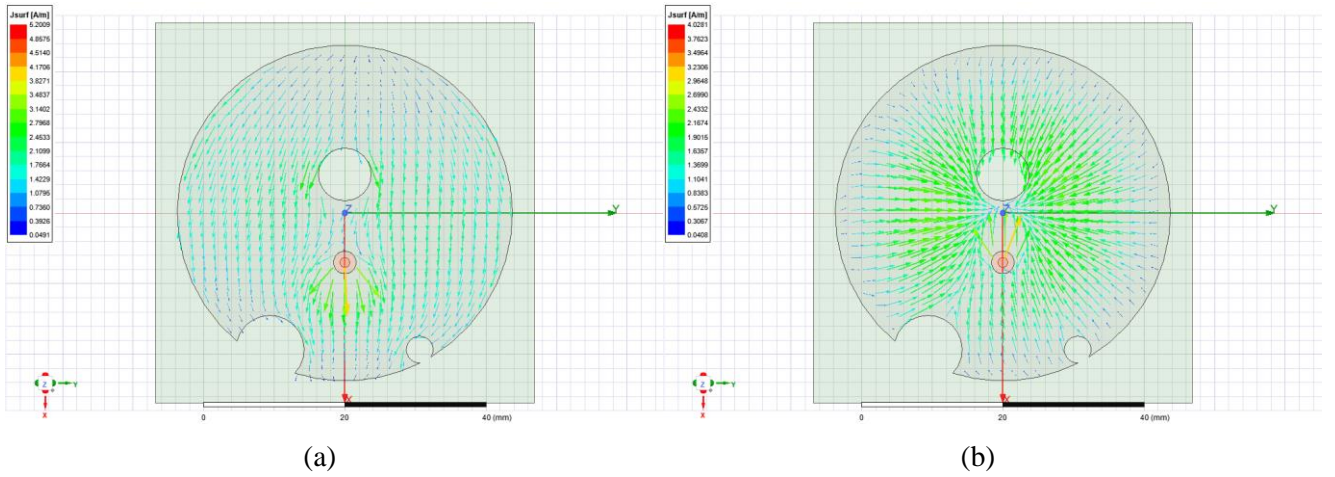


**Figure 7.** Surface current distributions of slotted circular microstrip antenna for a) 2.42 GHz, b) 5.09 GHz.

In this work, a circular microstrip antenna with triple slots has been designed to operate in dual resonance frequencies of WLAN. HFSS optimization tool has been employed to find slot radii and slot center positions that give the desired resonant frequencies and desired gains. Genetic Algorithm has been selected as optimizer in HFSS optimization tool. HFSS simulation has been carried out by using the obtained slot radii and slot center positions from HFSS optimization. HFSS simulations shows that desired resonance frequencies and gains are obtained via HFSS optimization.

## References

- [1] Balanis, C. A. (2005). *Antenna Theory Analysis and Design*, 3rd ed. NJ, USA:John Wiley & Sons, Inc.
- [2] Günel, T. (2004). Continuous hybrid approach to the modified resonant frequency calculation for circular microstrip antennas with and without air gaps. *Microwave and Optical Technology Letters*, 40(5), 423-427.
- [3] Günel, T. (2011). Modified resonant frequency calculation for E-shaped and H-shaped microstrip patch antennas. *Microwave and Optical Technology Letters*, 53(10), 2348-2351.
- [4] Haykin, S. (2009). *Neural Networks and Learning Machines*, 3rd ed. NJ, USA:Pearson Prentice Hall, 268-312.
- [5] Khan, T., & De, A. (2015) . Modeling of microstrip antennas using neural networks techniques: a review. *Int J RF and Microwave Comp Aid Eng*, 25, 747-757.
- [6] Wang, Z., Fang, S., Wang, Q., & Liu, H. (2012). An ANN-based synthesis model for the single-feed circularly-polarized square microstrip antenna with truncated corners. *IEEE Trans. on Antennas Propag.*,

60, 5989–5992.

- [7] Aneesh, M. J., Ansari, A., Kamakshi, A. S., & Sayeed, S. S. (2014). Investigations for performance improvement of X shaped RMSA using artificial neural network by predicting slot size. *Progress In Electromagnetics Research C*, 47, 55–63.
- [8] Aşık, U., Günel, T., & Erer, I. (2004). A wavelet-based radial basis function neural network approach to the inverse scattering of conducting cylinders. *Microwave and Optical Technology Letters*, 41(6), 506-510.
- [9] Cortes, C., & Vapnik, V. (1995). Support vector network. *Machine Learn.*, 20, 273-297.
- [10] Angiulli, G., Cacciola, M., & Versaci, M. (2007). Microwave devices and antennas modelling by support vector regression machines, *IEEE Transactions on Magnetics*, 43(4), 1589-1592.
- [11] Roy, C., Khan, T., & Kanaujia, B. (2016). Performance parameters prediction of slotted microstrip antennas with modified ground plane using support vector machine. *International Journal of Microwave and Wireless Technologies*, 9(5), 1169-1177.
- [12] Yiğit, M. E., Günel, T., & Günel, G. Ö., SVR Approach to the Design of Dual-Band Rectangular Microstrip Antenna with a Pair of Slots for WLAN Applications, 11th International Conference on Electrical and Electronics Engineering (ELECO), Bursa, Turkey, 2019, 659-663.
- [13] Yiğit, M. E., Günel, G. Ö., & Günel, T., SVR Based Design of Triple Band Rectangular Microstrip Antenna for WLAN and 5G Applications, 4th Int.Symp. on Advanced Electrical and Communication Technologies (ISAECT), Khobar, Suudi Arabia, 2021, pp. 1-5.
- [14] Haupt, R. L. (1995). An introduction to genetic algorithms for electromagnetics. *IEEE Antennas and Propagation Magazine*, 37(2), 7-15.
- [15] Robinson, J., & Rahmat-Samii, Y. (2004). Particle swarm optimization in electromagnetics. *IEEE Transactions on Antennas and Propagation*, 52(2), 397-407.
- [16] Günel, T., & Erer, I. (2002). Application of fuzzy genetic algorithm to the problem of synthesizing circular microstrip antenna elements with thick substrates. *AEÜ International Journal of Electron. Commun.*, 56(3), 215-217.
- [17] Aydemir, E., Günel, T., & Üstüner, F. (2006). Genetic approach to the minimization of the coupling between aircraft antennas. *AEÜ International Journal of Electron. Commun.*, 60(4), 299-305.
- [18] Günel, T., Yiğit, M. E., & Günel, G. Ö., Genetic-Based Approach to the Synthesis of Rectangular Microstrip Antenna Elements with Reduced Mutual Coupling, International Symposium on Advanced Electrical and Communication Technologies (ISAECT), Rabat-Kenitra, Morocco, 2018, 1-5.
- [19] ANSYS, ANSYS HFSS | 3D High Frequency Simulation Software. Available at: <https://www.ansys.com/products/electronics/ansys-hfss>. Retrieved July 27, 2022.
- [20] Goldberg, D. E. (1989). *Genetic Algorithms in Search, Optimization and Machine Learning Reading*, Boston, MA, USA: Addison-Wesley.
- [21] Haupt, R. L. (1994). Thinned arrays using genetic algorithms. *IEEE Transactions on Antennas and Propagation*, 42(7), 993-999.
- [22] Weile, D. S., & Michielssen, E. (1997). Genetic algorithm optimization applied to electromagnetics: a review. *IEEE Transactions on Antennas and Propagation*, 45(3), 343-353.
- [23] Johnson, J. M., & Rahmat-Samii, V. (1997). Genetic algorithms in engineering electromagnetics. *IEEE Antennas and Propagation Magazine*, (39)4, 7-21.
- [24] Haupt, R. L., & Werner, D. H. (2007). *Genetic Algorithm in Electromagnetics*. Hoboken, N.J., USA: Wiley-Interscience.



# Circularly Polarized Patch Antenna Using Metamaterial for 5G Applications

***Mustafa KOÇER***<sup>1\*</sup> , ***Tayfun GÜNEL***<sup>2</sup> 

<sup>1</sup>Graduate School, Department of Electronics & Communication Engineering, Istanbul Technical University, Istanbul, Türkiye

<sup>2</sup> Department of Electronics & Communication Engineering, Istanbul Technical University, Istanbul, Türkiye

## Abstract

In this paper, a new circularly polarized microstrip patch antenna operating at 3.5 GHz in the n78 frequency band of the 5G frequency spectrum below 6 GHz has been presented. AMC (Artificial Magnetic Conductor), a subclass of metamaterials, has been used to increase the performance of the antenna. AMC structure designed as a 4x4 array has been placed on the microstrip antenna without using air gap. HFSS (High Frequency Structural Simulator) has been used for simulation process. According to the obtained results, the designed AMC structure increases the performance of the antenna and reduces the size of the antenna. In addition, the effects of substrate and metamaterial thickness on the antenna performance have been examined. The results are also compared with the results given in literature.

**Keywords:** 5G, Patch Antenna, Metamaterial, Artificial Magnetic Conductor, HFSS

## 1. Introduction

With developing communication technology, the amount of data increases in parallel. Therefore, high-frequency communication systems are now a necessity [1, 2]. Circularly polarized antennas have gained more importance in 5G communication systems [3]. However, it is not easy to design high gain microstrip antennas with circular polarization in the desired frequency range. In recent years, metamaterials have widely been used to increase the bandwidth and the gain of circularly polarized microstrip antenna [4, 5]. In [5] the antenna's performance is satisfactory but its dimension is large in terms of wavelength. In literature, in order to increase the performance of the antenna designed with FR-4 material, the design of the AMC structure is placed over a certain distance from the antenna. The antenna presented in [6] works in the frequency range of 3.31-3.9 GHz while it has circular polarization in the frequency range of 3.31-3.73 GHz and the gain of the antenna is 5.62 dBic. However, the dimension of the antenna is large as 44mm x 44mm x 14.8mm. FR-4 material is used in [7] and the gain of the microstrip antenna is obtained as 6.6 dBic. It is aimed to increase the bandwidth of the antenna with periodic metallic plates placed in a square shape next to the coaxial fed microstrip antenna [8].

In order to obtain circular polarization some techniques can be used [9, 10]. In this work, arc truncated corners and slot are used. Microstrip antennas with various thicknesses and a 4x4 array AMC structure have been designed at 3.5 GHz. HFSS software is used for the analysis and design processes. The microstrip antenna has been designed on the FR-4 substrate material with a dielectric constant of 4.4 and a tangent loss of 0.025. The thicknesses of microstrip antennas (heights of the substrate) are selected as 1.2 mm, 1.6 mm and 2 mm respectively. The thickness of the material used in the AMC structure is chosen the same as the thickness of the microstrip antenna underneath.

## 2. AMC and Microstrip Patch Antenna Design

In this study AMC structure whose reflection phases bandwidth is between +90 and -90 degrees [11] is used. Figure 1 shows the AMC structure.

\* Corresponding author. e-mail address: kocer21@itu.edu.tr



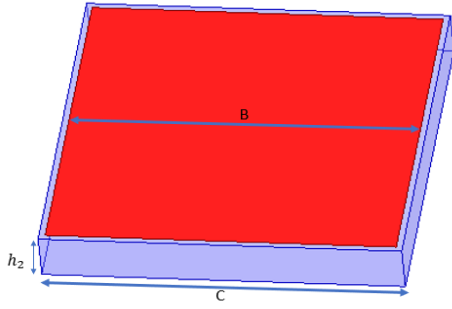


**Figure 1.** AMC structure.

AMC structure is designed with FR-4 material in 3 different thicknesses by using Floquet Port in HFSS software. The dimensions and operating frequency ranges of the square-shaped AMC structure are given in Table 1.

**Table 1.** AMC structure dimensions and working frequencies

$h_2$ (mm)	Operating frequency (GHz) range	B(mm)	C(mm)
1.2	3.29-3.57	17.5	18
1.6	3.34-3.74	15.5	16
2	3.32-3.82	14	14.5

Arc truncated corners and slots are used to design the microstrip antenna with circular polarization. Rectangular slot is in the center of the square-shaped microstrip antenna. It is rotated to the right at an angle of  $45^\circ$  to conform to the left-handed circular polarization (LHCP). The AMC structure is designed as a  $4 \times 4$  array. It is integrated on the microstrip antenna (Figure 2).

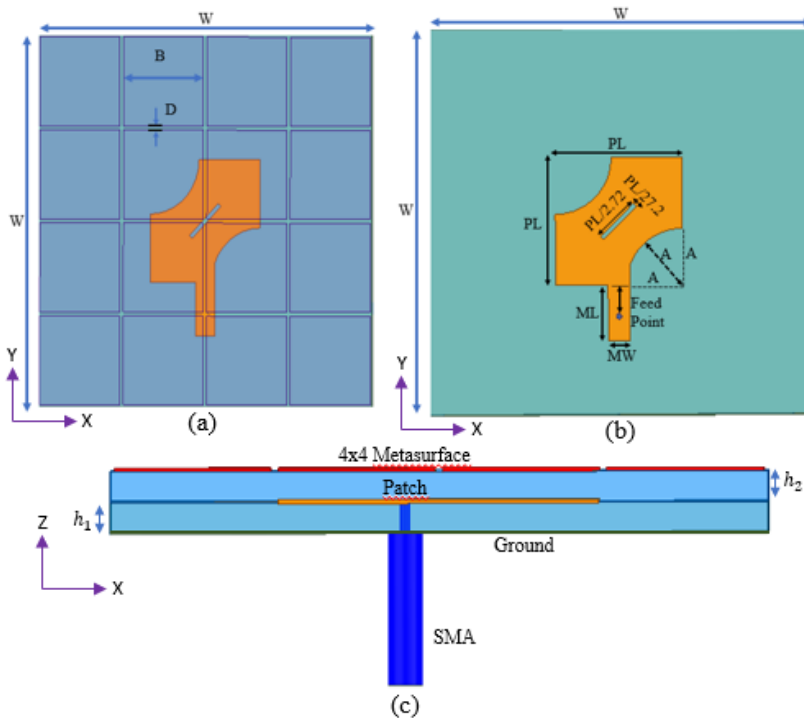


**Figure 2.** Geometry of the proposed antenna. (a) Top view of antenna with metamaterial. (b) Top view of antenna without metamaterial. (c) Side view.

The dimensions of the antennas designed in 3 different thicknesses are given in Table 2. When the B values given in Table 1 have been used, a decrease in size is obtained. By using the B values given in Table 2 instead of the B



values given in Table 1, a size reductions of 39.5%, 43.75% and 47.56% have been obtained respectively. While the thickness of the antennas increases the antenna size reduces.

**Table 2.** AMC based patch antenna dimensions

Antenna Parameters	$h_1 = h_2 = 1.2\text{mm}$	$h_1 = h_2 = 1.6\text{mm}$	$h_1 = h_2 = 2\text{mm}$
PL	15.2	15.8	16.5
A	7.3	7	6.6
ML	15	13.85	13
MW	2.2	2.7	3
Feed Point	4.4	3.9	4.25
B	13.5	11.5	10
D	0.5	0.5	0.5
W	56	48	42
Total Dimensiones	56x56x2.4	48x48x3.2	42x42x4

### 3. Results and Discussion

$|S_{11}|$  parameter of the antenna is shown in Figure 3. According to the simulation results, the bandwidth for  $h_1 = h_2 = 1.2\text{ mm}$  is 1.23 GHz, for  $h_1 = h_2 = 1.6\text{ mm}$  the bandwidth is 1.57 GHz and for  $h_1 = h_2 = 2\text{ mm}$  the bandwidth is 1.77 GHz.

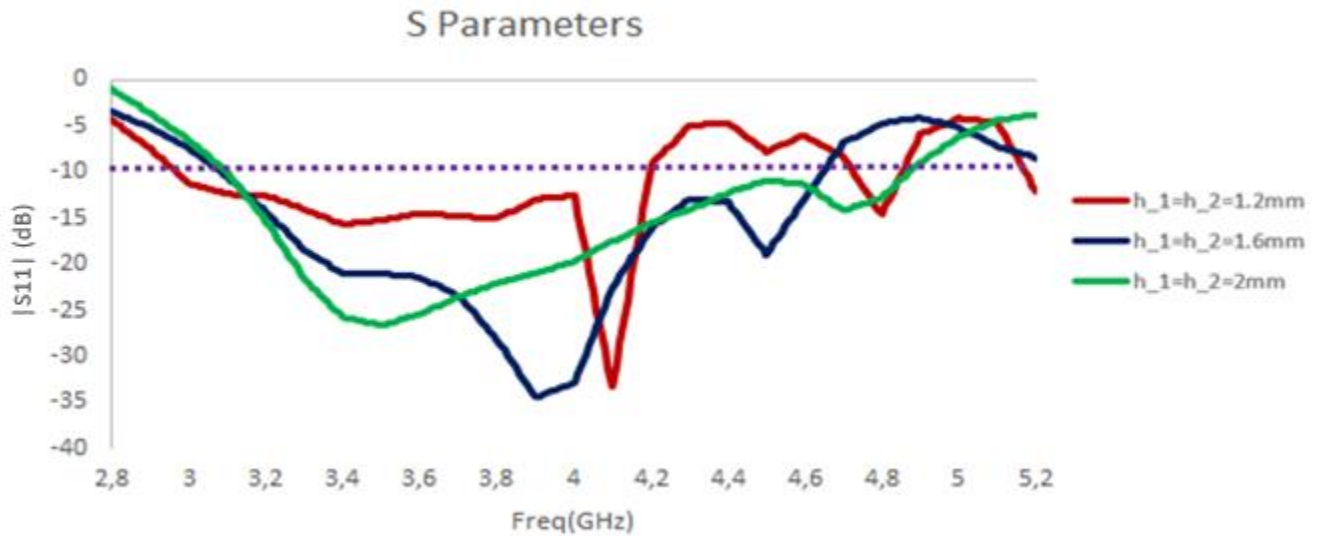


**Figure 3.**  $|S_{11}|$  parameter of the antenna.

The gains and efficiencies of the antennas are shown in Figure 4. The peak maximum gain and peak maximum efficiency of the antennas have been computed to be 7.1 dBic and 89.38%, 6.66 dBic and 89.7%, 6.25 dBic and 89.9%, respectively.

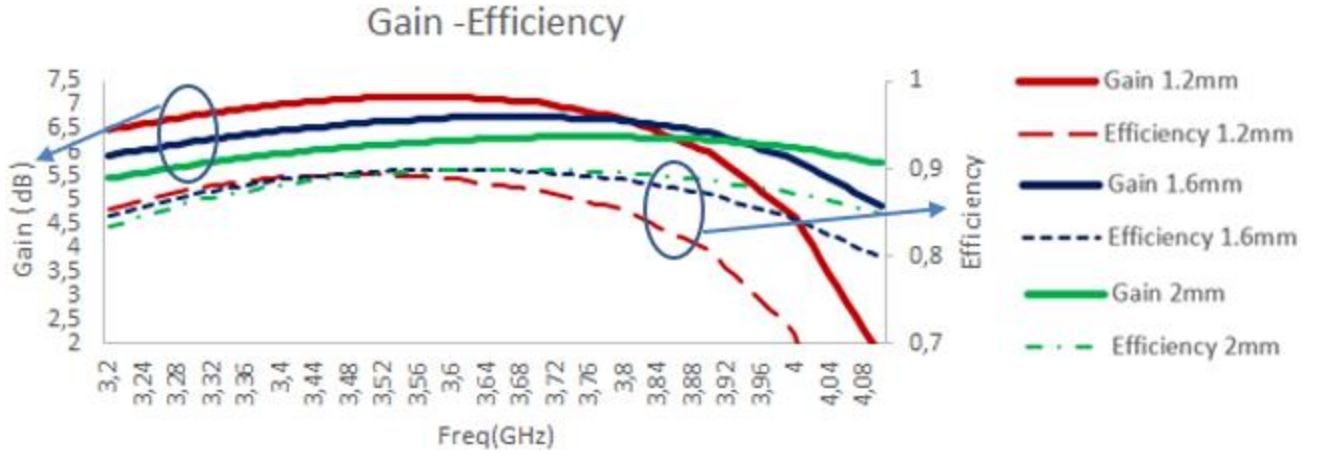


**Figure 4.** Gain and Efficiency of the antenna.

In Figure 5, axial ratios of the antennas are shown. The AR bandwidths of the antennas have been obtained as 0.57 GHz, 0.75 GHz and 0.87 GHz, respectively.

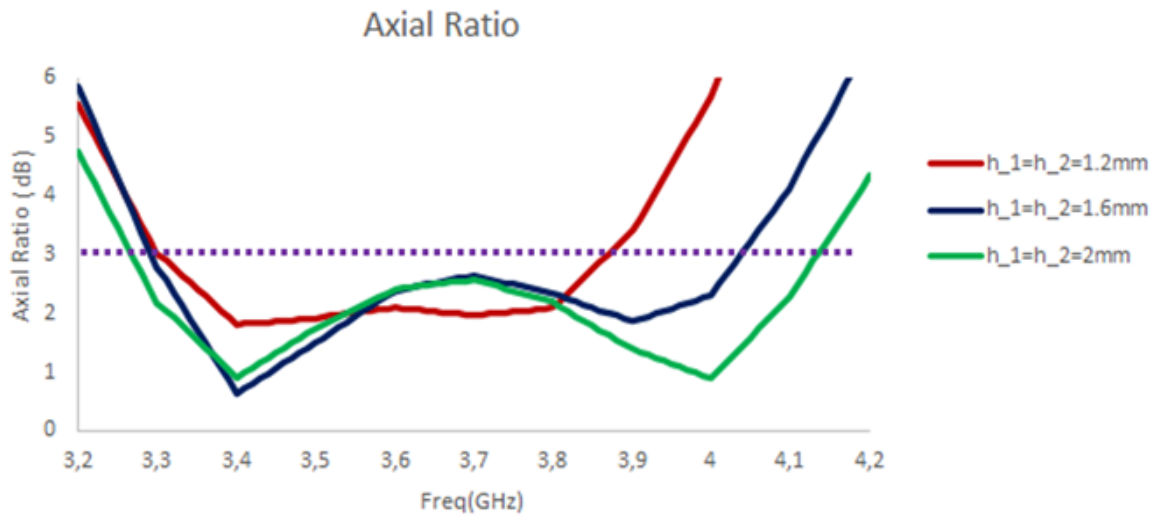


**Figure 5.** Axial ratio of the antenna.

Radiation patterns of the antennas are shown in Figure 6. In Table 3 results of the proposed antenna for  $h_1=h_2=2$  mm are compared with the results of the antennas given in literature.

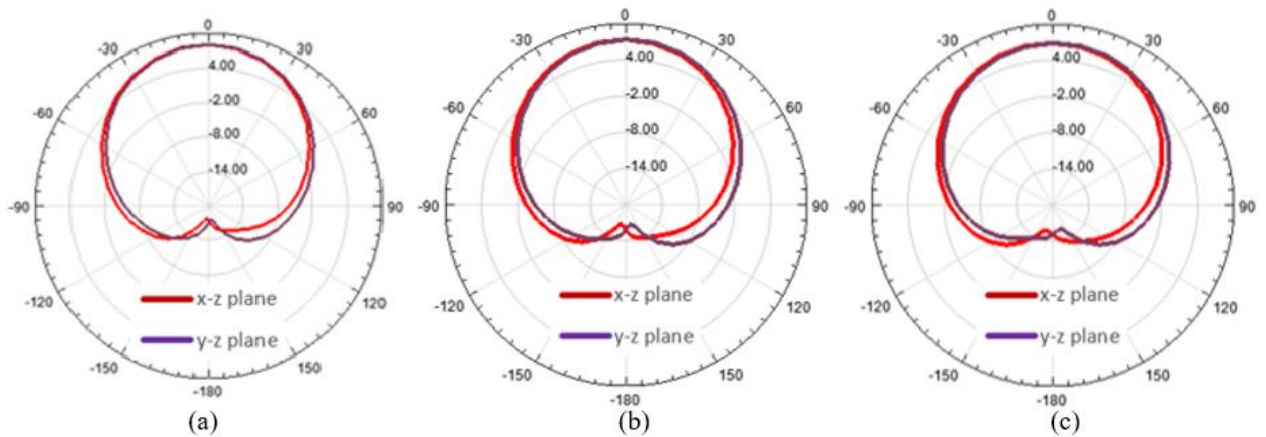


**Figure 6.** Radiation patterns of the antennas at 3.5 GHz (a)  $h_1 = h_2 = 1.2$  mm (b)  $h_1 = h_2 = 1.6$  mm (c)  $h_1 = h_2 = 2$  mm.

**Table 3.** Comparison with other antennas in literature.

Results	[5]	[6]	[7]	[8]	Proposed ( $h_1=h_2=2$ mm)
Bandwidth(GHz)/ (%)	(4.7-7.48)/ (45.6)	(3.31-3.9) / (16.36)	(5.02-7.3)/ (37)	(5.1-6.2)/ (19.7)	(3.1-4.87)/ (50.6)
AR BW(GHz)/ (%)	(4.9-6.2)/ (23.4)	(3.31-3.73)/ (11.93)	(5.24-5.56)/ (5.9)	(5.12-6.32)/ (21)	(3.27-4.14)/ (24.86)
Polarization	LHCP	LHCP	LHCP	RHCP	LHCP
Efficiency	>90%	82.8%	Not Reported	Not Reported	89.9%
Gain	7.6 dBic	5.62 dBic	6.6 dBic	6.9 dBic	6.25 dBic
Total Size(mm)/ ( $\lambda$ )	32 x 32 x 3/ (0.58 x 0.58 x 0.056)	(44 x 44 x 14.8)/ (0.51 x 0.51 x 0.16)	Not Reported/ (0.616 x 0.616 x 0.065)	Not Reported / (0.6 x 0.6 x 0.06)	(42 x 42 x 4)/ (0.49 x 0.49 x 0.047)
Size Reduction	Not Reported	38.7%	Not Reported	Not Reported	47.56%

While the thickness of the proposed antenna increases, the bandwidth, size reduction and efficiency values increase. The gain and overall size decrease while the thickness of the antennas increases. The bandwidth of the proposed antenna is 50.6%. Although FR-4 material is used, its efficiency is 89.87%. The size reduction value is obtained as 47.56%. The dimension of the proposed antenna given in wavelength is the smallest among others in Table 3. The proposed antenna can be efficiently used in n78 frequency band for 5G applications.

## References

- [1] Al-Bawri, Samir Salem, et al., Multilayer base station antenna at 3.5 GHz for future 5G indoor systems, First International Conference of Intelligent Computing and Engineering (ICOICE), Hadhramout, 2019, p. 1-4.
- [2] Sufian, Md Abu, et al. (2021). Isolation enhancement of a metasurface-based MIMO antenna using slots and shorting pins. *IEEE Access*, 9, 73533-73543.
- [3] Wang, Jianquan. LV, Zhaobiao. LI, Xinzhong. (2014). Analysis of MIMO diversity improvement using circular polarized antenna. *International Journal of Antennas and Propagation*.
- [4] Hussain, N., Jeong, M. J., Abbas, A., & Kim, N. (2020). Metasurface-based single-layer wideband circularly polarized MIMO antenna for 5G millimeter-wave systems. *IEEE Access*, 8, 130293-130304.
- [5] Ta, S. X., & Park, I. (2015). Low-profile broadband circularly polarized patch antenna using metasurface. *IEEE transactions on antennas and propagation*, 63(12), 5929-5934.
- [6] Ameen, M., & Chaudhary, R. (2020). Metamaterial circularly polarized antennas: Integrating an epsilon negative transmission line and single split ring-type resonator. *IEEE Antennas and Propagation Magazine*, 63(4), 60-77.
- [7] Verma, A., Singh, A. K., Srivastava, N., Patil, S., & Kanaujia, B. K. (2021). Performance enhancement of circularly polarized patch antenna using slotted circular EBG-based metasurface. *Frequenz*, 75(1-2), 35-47.
- [8] Tran, H. H., Hussain, N., & Le, T. T. (2019). Single-layer low-profile wideband circularly polarized patch antenna surrounded by periodic metallic plates. *International Journal of RF and Microwave Computer-Aided Engineering*, 29(12), e21969.
- [9] Chowdhury, M. H., Hossain, Q. D., Hossain, M. A., & Cheung, R. C. C. (2019). Single feed circularly polarized crescent-cut and extended corner square microstrip antennas for wireless biotelemetry. *Int. J. Electr. Comput. Eng*, 9(3), 1902-1909.
- [10] Balanis, C. A. (2005). *Antenna theory: analysis and design*. 3rd ed. John Wiley & sons, 859-864.
- [11] Alibakhshi-Kenari, M., Naser-Moghadasi, M., Sadeghzadeh, R. A., Virdee, B. S., & Limiti, E. (2016). Periodic array of complementary artificial magnetic conductor metamaterials-based multiband antennas for broadband wireless transceivers. *IET Microwaves, Antennas & Propagation*, 10(15), 1682-1691.



## The Study Relation of Endothelin-1 and Malondialdehyde with Chronic Kidney Disease

**Zainab AHMED**<sup>1\*</sup> , **Şevki ADEM**<sup>1</sup> , **Abdullah RAOOF**<sup>2</sup> , **Volkan EYUPOĞLU**<sup>1</sup> 

<sup>1</sup>Graduate School of Natural and Applied Sciences, Chemsty Department, Çankırı Karatekin University, Çankırı, Turkey

<sup>2</sup>Medicine Faculty, Kirkuk University

### Abstract

Chronic kidney disease is a worldwide public health problem with an increasing incidence and prevalence. A cross-control study was carried out for estimation of endothelin-1 and MDA and some parameters in patients with chronic renal disease. The number of patients under the study were 40 patients with chronic renal disease (under hemodialysis) their ages were between 20-75 years old. The study included 40 healthy control group who apparently haven't any disease, with the same demographic properties. The study showed that the highest mean level of endothelin-1 and MDA were found in patients with chronic renal disease as respectively (102.6±15.1 pg/ml) and (12.03±3.94 nmol/ml). The lowest mean of the two markers were in the control group as respectively (39.03±5.94 pg/ml) and (7.56±2.25nmol/ml). The current study showed that the mean age of patients enrolled in the study was 51.7 years, the highest mean of endothelin-1 in HD patients was recorded within the age group >50 year with hypertension (P<0.05). The study showed that the highest means level of B. urea, S. creatinine and Cystatin were found in patients with chronic renal disease (156.3±22.4 , 7.22±2.91 mg/dl and 12.88±2.16 mg/dl) respectively, and the lowest means of the tests above were noted in the control group with highly significant relation (P. value <0.01). The study showed positive correlation of ET-1 and MDA with B. urea, S. creatinine and cystatin c. The study showed significant positive correlation of MDA with ET-1 in CKD patients (r: 0.57, P<0.01).

**Keywords:** Endothelin-1, Malondialdehyde, Chronic kidney disease

### 1. Introduction

Chronic kidney disease is a very important worldwide public health problem with an increasing incidence and prevalence, that cause poor outcomes, and high cost. Outcomes of chronic kidney disease include not only kidney failure but also complications of decreased kidney function and cardiovascular disease [1].

In recent years, a pivotal role for the Endothelin system (ETs) has been documented in normal renal function, and also in renal disease. Endothelin-1 (ET-1) acts as an autocrine and paracrine manner in renal vessels and nephron segments, it is modulating renal hemodynamics by tubular water and minerals reabsorption [4]. ET-1 has been implicated in pathological conditions such as renal fibrosis, glomerular sclerosis which leads to the progressive decline in renal function, development of hypertension and cardiovascular hypertrophy.

On the otherwise renal disease is associated with a graded elevation in oxidative stress (OS) markers even in early CKD [2]. Oxidative stress can enhance renal injury progression and contribute to increased cardiovascular risk. Some studies have documented that peritoneal dialysis is associated with decreased levels of OS and inflammatory markers more than hemodialysis [3]. Malondialdehyde (MDA) is the marker of OS produced by peroxidation of unsaturated fats, it is associated in atherosclerosis progression in patients with chronic kidney disease (CKD) not yet on dialysis compared to patients on peritoneal dialysis is less known, particularly concerning cardiometabolic syndrome [5].

\* Correspondence author. e-mail address: zeyneperi99@gmail.com

## 2. Material and Methods

### 2.1 Study Design

The study is performed in Kirkuk city from 27th of October 2020 to 30th of November 2020. For the study, the relationship between Endothelin-1 and Malondialdehyde with the chronic kidney disease we depended on the samples taken from CKD patients on hemodialysis and other samples were taken from healthy people as the control group. The number of patients under study reached 40 patients with chronic kidney disease (under dialysis). The study included also 40 healthy control group who haven't any disease, with the same demographic properties (healthy individuals). Five ml of the blood sample was taken by vein puncture without using tourniquet from each subject registered in this study. Blood samples were placed into sterile test tubes, after blood clotting, centrifuged at 3000 rpm for 15 minutes then clot removed and remain re-centrifuged at 3000 rpm for 10 minute and the obtained serum were aspirated using a mechanical micropipette and transferred into clean test tubes which labelled and stored in a deep freeze at -20 °C for biochemical measurement of blood urea, serum creatinine, serum (MDA), as well as estimation of human Endothelin-1 by ELISA technique.

### 2.2 Estimation of Human Endothelin-1 by ELISA

For estimation of human Endothelin-1 by ELISA kit Sandwich-ELISA method is used. The Microelisa strip plate provided in the kit has been pre-coated with an antibody specific to ET-1. Each of the standards and samples were added to the appropriate Microelisa strip plate wells and combined to the specific antibody. Then a Horseradish Peroxidase (HRP)-conjugated antibody specific for ET-1 is added to each well and incubated. Then TMB, substrate solution was added to each well. The wells which contain ET-1 and HRP conjugated ET-1 antibody will appear blue and when added the stop solution it will turn to yellow. The optical density (OD) is measured by the spectrophotometer at a wavelength of 450 nm. The concentration of ET-1 is proportional to the OD value. We can calculate the concentration of ET-1 in the prepared samples by comparing the OD of the samples to the standard curve.

### 2.3 Determination of Serum Malondialdehyde

The level of malondialdehyde was determined by the reaction of MDA with thiobarbituric acid –TBA, forming an MDA-TBA2 according to the modified method described by Schmedes and Holmer.

#### Manual procedure

In the Table 2.1 below the details of the manual procedure for the determination of serum malondyaldehyde is showed.

**Table 2.1** Manual procedure for the determination of serum malondyaldehyde

Pipette into well identified test tubes:	Test	Standard
Serum	150 µl	-
Distilled water	-	150 µl
TCA(17.5%)	1 ml	1 ml
Mix well		
TBA (0.6%)	1 ml	1 ml
The tubes were mixed well by vortex, incubated in boiling water bath for 15 minutes, and then allowed to cool.		
TCA(70%)	1 ml	1 ml
The mixture was let to stand at room temperature for 20 minutes, The tubes were centrifuged at 2000 rpm for 15 minutes, and the supernatant was taken for measurement of the absorbance at 532nm.		

### 3. Results and Discussion

#### 3.1. General Characteristics of the Studied Groups

**Table 3.1.** General characteristics of the studied groups

Parameters	CKD patient (n:40)	Control group (n:40)	P. value
Age (Mean±SD)	51.7±3.9	50.3±3.8	NS
BMI	27.5±3.8	27.2±4.2	NS
Sex	25 male/ 15 female	24 male/ 16 female	NS
Residence (urban)	55%	56%	NS

#### 3.2 Relation of Endothelin-1 with CKD

The study showed that the highest mean level of endothelin-1 was found in patients with chronic renal disease (102.6±15.1 pg/ml) and the lowest mean was in the control group (39.03±5.94 pg/ml), ( $P < 0.01$ ), Table 3.2.

**Table 3.2.** Endothelin-1 levels

Studied groups	N	Endothelin-1 level (pg/ml)		
		Mean	SD	SE Mean
CKD	40	102.6	15.1	8.5
Control group	40	39.03	5.94	1.1
<b>P. value: 0.001</b>				

#### 3.3 Level of Malondialdehyde (MDA) in Patients with CKD and The Control Group.

The study showed that the highest mean level of MDA was found in patients with chronic renal disease (12.03±3.94 nmol/ml) and the lowest mean was recorded in the control group (7.56±2.25nmol/ml), ( $P < 0.01$ ), Table 3.3.

**Table 3.3.** MDA levels

Studied groups	N	MDA level (nmol/ml)		
		Mean	SD	SE Mean
CKD	40	12.03	3.94	1.1
Control group	40	7.56	2.25	0.80

#### 3.4 Relation of ET-1 with Age of CKD Patients

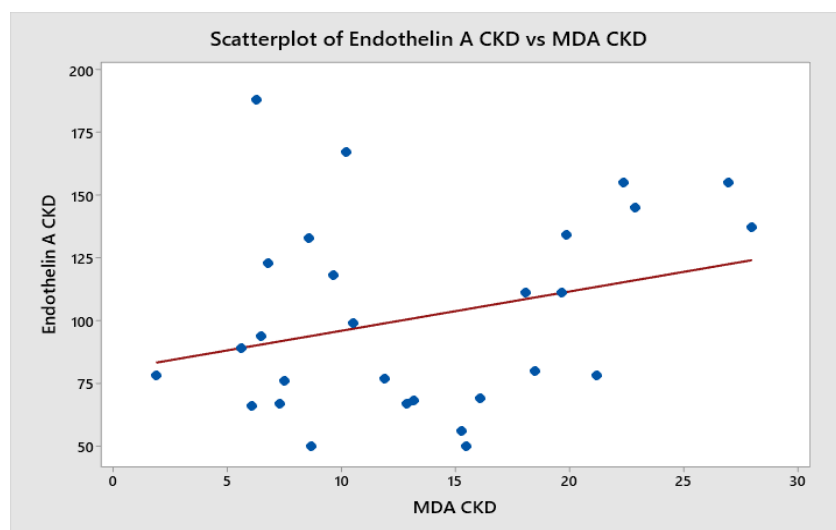
The current study showed that the mean age of patients enrolled in the study was 51.7 years, the highest mean of endothelin-1 in HD patients was recorded within the age group >50 year ( $P < 0.05$ ), Table 3.4.

**Table 3.4.** Endothelin-1 levels

Age groups (years)	Endothelin 1 level (pg/ml) (Mean±SD.)	
	No.	Chronic renal disease (n:30)
<30	8	88.5±22.5
30-50	18	109.1±31.5
>50	14	115.4±29.4
P. value: 0.014		

### 3.5 Correlation of MDA with ET-1 of CKD patients

The study showed significant positive correlation of MDA with ET-1 in CKD patients ( $r: 0.57$ ,  $P<0.01$ ) (Fig.1).

**Figure 1.** Correlation of MDA with ET-1 of CKD patients

### References

- [1] Brophy, P.D., Charlton, J.R., Carmody, J.B., Reidy, K.J., Harshman, L., Segar, J., Askenazi, D., Shoham, D. and Bagby, S.P., 2018. Chronic kidney disease: A life course health development perspective. In *Handbook of Life Course Health Development* (pp. 375-401). Springer, Cham.
- [2] De Vecchi, A.F., Bamonti, F., Novembrino, C., Ippolito, S., Guerra, L., Lonati, S., Salini, S., Aman, C.S., Scurati-Manzoni, E. and Cighetti, G., 2009. Free and total plasma malondialdehyde in chronic renal insufficiency and in dialysis patients. *Nephrology Dialysis Transplantation*, 24(8), pp.2524-2529.
- [3] Khoubnasabjafari, M., Ansarin, K. and Jouyban, A., 2016. Critical review of malondialdehyde analysis in biological samples. *Current Pharmaceutical Analysis*, 12(1), pp.4-17.
- [4] Komers, R. and Plotkin, H., 2016. Dual inhibition of renin-angiotensin-aldosterone system and endothelin-1 in treatment of chronic kidney disease. *American Journal of Physiology-Regulatory, Integrative and Comparative Physiology*, 310(10), pp.R877-R884.
- [5] Papac-Milicevic, N., Busch, C.L. and Binder, C.J., 2016. Malondialdehyde epitopes as targets of immunity and the implications for atherosclerosis. In *Advances in immunology* (Vol. 131, pp. 1-59). Academic Press.
- [6] Ahmed Z., The Study Relation of Endothelin-1 and Malondialdehyde with Chronic Kidney Disease, Master thesis, Çankırı Karatekin University, science institution, 2021.





## Examining the Levels of Anxiety and Depression Among Nurses Working at Al-Diwaniyah Teaching Hospital During COVID-19 Pandemic

Fatimah Salam QASIM ALHABEEB <sup>1</sup> , Songül KAMIŞLI <sup>2\*</sup> , Ali Kareem AL-JUBOORI <sup>3</sup>

<sup>1</sup>Al-Diwaniyah Teaching Hospital, Diwaniya, Iraq

<sup>2</sup>Health Science Institute, Health Science Faculty, Gerontology Department, Çankırı Karatekin University, Çankırı, Türkiye

<sup>3</sup>Kerbela University, College of Nursing, Karbala, Iraq

### Abstract

This study investigated the anxiety and depression of nurses working at Al-Diwaniyah Hospital during the COVID-19 pandemic. The study also looked into the effect of demographic characteristics (age, gender, and marital status) on their anxiety and depression levels. This descriptive study was conducted at Al-Diwaniyah Teaching Hospital in Iraq during the COVID-19 pandemic between December 27, 2020, and February 26, 2021. The sample consisted of 150 nurses. Participation was voluntary. Data were collected face-to-face using a personal information form and the Hospital Anxiety and Depression Scale (HADS). More than half the participants were women (65.3%). More than a quarter of the participants were younger than 26 (34%). More than half the participants were married (58.7%). Less than half the participants had bachelor's or higher degrees (45.3%). Most participants were non-smokers (71.3%). More than half the participants had been working for less than five years (54.7%) and had no chronic disease (69.3%). One-third of the participants had mild anxiety (33.3%), while fifteen participants had severe anxiety (10%). Half the participants had normal depression (50%), while ten participants had severe depression (6.7%). Married participants had a significantly higher mean depression score than single participants. Participants with more than five years of work experience had a significantly higher mean depression score than those with less than five years of work experience. Age, education, income status, gender, place of residence, and smoking habits did not affect participants' HADS scores. Authorities should provide nurses with psychosocial services to support their mental health in times of crisis, such as pandemics.

**Keywords:** COVID-19, Anxiety, Depression, Nursing

## 1. Introduction

Healthcare professionals experienced high levels of stress and anxiety during the COVID-19 pandemic because they had no direct medical information and no full training in personal protective equipment and infection control procedures [1]. The study was conducted a global multicenter trial during the COVID-19 pandemic [2]. They reported that four in five healthcare professionals (n=906) suffered moderate to severe depression. The COVID-19 pandemic significantly impacts the mental health of healthcare professionals. They have worked tirelessly and without pause for months to combat the COVID-19 pandemic. Healthcare professionals were away from their families for months. They lost their colleagues to the pandemic. They worked for months wearing protective equipment [3]. Since the onset of the pandemic, there has been a growing demand for nurses in areas with high COVID-19 hospitalization rates. COVID-19 cases are predicted to exceed hospital capacity, and personal protective equipment may be in short supply. Nurses are more likely to experience PTSD and burnout in high-stress and high-risk working conditions [4]. The study was found that COVID-19 patients were more likely to suffer from despair, anxiety, and insomnia when cared for by healthcare staff in China [5]. They also determined that nurses had more serious mental health problems than other healthcare professionals. This study investigated the effect of sociodemographic characteristics on the anxiety and depression of nurses during the COVID-19.

## 2. Materials and Methods

This was a descriptive cross-sectional study. Data were collected in Al-Diwaniya teaching hospital, Iraq, between December 27, 2020, and February 26, 2021. The study population consisted of 300 nurses. The sample consisted of 150 nurses recruited using purposive sampling. Data were collected using a personal information form and the Hospital Anxiety and Depression Scale (HADS). There are the research questions: What HADS scores do

\* Corresponding author. e-mail address: songulkamisli@karatekin.edu.tr



participants have?; Is there a difference between participants' anxiety and depression levels? and do participants' demographic characteristics affect their HADS scores? The study was approved by the ethics committee of the Ministry of Higher Education and Scientific Research – the University of Kerbala - College of Nursing. All nurses were informed about the research purpose and procedure. Informed consent was obtained from those who agreed to participate. Data were nonnormally distributed. Therefore, nonparametric tests were used to analyze the data. The Mann-Whitney U test was used to determine the effect of sociodemographic characteristics (gender, marital status, monthly income, place of residence, smoking status, and having a chronic disease) on HADS scores. The Kruskal-Wallis H test was used to determine the effect of age, education, and work experience on HADS scores.

### 3. Results and Discussion

More than half the participants were women (65.3%). More than a quarter of the participants were younger than 26 (34%). More than half the participants were married (58.7%). Almost half the participants had bachelor's or higher degrees (45.3%). Most participants were non-smokers (71.3%). More than half the participants had less than six years of work experience (54.7%). Most participants had no chronic disease (69.3%) (Table 1)

**Table 1.** Demographic Characteristics and HADS scores (n = 150)

Demographic Characteristics	n	%
<b>Age (years)</b>		
≤25	51	34
26 – 30	40	26.7
31 – 35	23	15.3
36 – 40	15	10
41≥	21	14
<b>Gender</b>		
Woman	98	65.3
Man	52	34.7
<b>Marital status</b>		
Single	62	41.3
Married	88	58.7
<b>Education (degree)</b>		
Secondary school of nursing	36	24
Institute of nursing	46	30.7
Bachelor's or higher	68	45.3
<b>Monthly income</b>		
Enough	89	59.3
Not enough	61	40.7
<b>Residence</b>		
Rural	44	29.3
Urban	106	70.7
<b>Smoking</b>		
Yes	43	28.7
No	107	71.3
<b>Work experience</b>		
≤ 5	82	54.7
6 – 10	29	19.3
11- 15	15	10
16≥	24	16
<b>Chronic disease</b>		
Yes	46	30.7
No	104	69.3

**Table 1.** Demographic Characteristics and HADS scores (n = 150) (Continued)

Demographic Characteristics	n	%
<b>HADS Anxiety Scores</b>		
Normal (0-7)	42	28
Mild (8-10)	50	33.3
Moderate (11-14)	43	28.7
Severe (15-21)	15	10.0
<b>HADS Depression Scores</b>		
Normal (0-7)	75	50
Mild (8-10)	37	24.7
Moderate (11-14)	28	18.7
Severe (15-21)	10	6.7
Total	150	100

One-third of the participants experienced mild anxiety (33.3%). Three in ten participants experienced moderate anxiety (28.7%). Fifteen participants experienced severe anxiety (10%). Half the participants did not experience depression (50%). A quarter of the participants experienced mild depression (24.7%). One in five participants experienced moderate depression (18.7%). Ten participants experienced severe depression (6.7%).

Married participants had a significantly higher mean HADS-D score than single participants ( $p < 0.05$ ). Participants with more than five years of work experience had a significantly higher mean HADS-D score than those with less than five years of work experience. However, the other variables did not significantly affect participants' HADS scores (Table 2)

**Table 2:** The relationship between HADS scores and age, education, work experience and marital status (n = 150)

Grouping Variables	HADS-Anxiety					HADS-Depression			
Age (years)	N	Mean Rank	SD	Chi-Square**	P**	Mean Rank	SD	Chi-Square**	p**
≤25	51	80.44	16.0	4.246 df=4	0.37	67.53		5.846 df=4	0.21
26-30	40	69.51	13.9			77.64			
31-35	23	70.87	14.1			71.04			
36-40	15	64.83	12.9			78.27			
41≥	21	87.60	17.52			93.69			
Education (degree)									
Secondary school of nursing	36	74.08	24.6	0.127 df=2	0.93	64.72	21.5	4.222 df=2	0.121
Institute of nursing	46	71.59	23.8			66.87	22.29		
College and post.	61	71.08	23.6			80.16	26.72		
Work experience (year)									
≤5	82	74.12	14.8	2.608 df=3	0.45	67.59	16.8	8.826 df=3	<b>0.03</b>
6-10	29	76.90	19.2			86.17	21.5		
11-15	15	63.73	15.9			69.67	17.4		
16≥	24	85.90	21.4			93.27	23.3		
Marital Status									
Single	58	78.78	39.3	U*=2478; p=0.46		64.94	32.4	U=2055; <b>p=0.01</b>	
Married	92	73.43	46			82.16	41.0		

\*Mann Whitney U Test; \*\* Kruskal Wallis H Test

Half of our participants had no depression (50%), while ten had severe depression (6.7%). These results are consistent with the literature [5-7]. Nadeem et al. also found that the prevalence of normal and severe depression among nursing staff in Pakistan was 50% and 7.1%, respectively [8]. This study was conducted in Iraq during

the COVID-19 pandemic. However, due to cultural factors, Iraqi nurses are not significantly affected by anxiety and depression. However, there are individual differences between nurses based on demographic data.

Married participants had a significantly higher mean depression score than single participants. Çelik and Dağlı also found that nurses married with children had higher depression than singles [9]. On the other hand, Sheikhbardsiri et al. reported that single nurses experienced more anxiety and depression than their married counterparts [10]. Married Iraqi people experience more depression probably because they have more burdens than single people.

Participants with more than five years of work experience had a significantly higher mean depression score than those with less than five years of work experience. Some study was reported that a significant association between depression and work experience and monthly working hours among nurses during the pandemic [11, 12]. Hospitals should provide married nurses with counseling programs to alleviate their depression. Such programs can help married nurses feel better and provide effective patient care. Authorities should develop social bulletins and programs for all healthcare professionals, especially nurses with less than five years of experience, to help reduce their depression levels. Mental health nurses can treat COVID-19-related mental health concerns using cutting-edge technologies, such as telemedicine. Registered community nurses or advanced practice nurses can provide psychotherapy or psychosocial support to our colleagues for mental health.

## References

- [1] Tan, B.Y.Q., Chew, N.W.S., Lee, G.K.H. et al. (2020). Psychological Impact of the COVID-19 Pandemic on Health Care Workers in Singapore. *Ann Intern Med.* 173(4), 317–320. <https://doi.org/10.7326/M20-1083>
- [2] Chew, N., Lee, G., Tan, B. et al. (2020). A multinational, multicentre study on the psychological outcomes and associated physical symptoms amongst healthcare workers during COVID-19 outbreak. *Brain, behavior, and immunity*, 88, 559–565. <https://doi.org/10.1016/j.bbi.2020.04.049>
- [3] Muhhammed, A., Dias, C., Muley, D., Shahin, M. (2020). Exploring the impacts of COVID-19 on travel behavior and mode preferences, *Transportation Research Interdisciplinary Perspectives*, 8, 100255.
- [4] Sood, S. (2020). Psychological effects of the Coronavirus disease-2019 pandemic. *Research & Humanities in Medical Education*, 7, 23– 26.
- [5] Lai, J. Ma, S. Wang, Y. Cai et. al. (2020). Factors associated with mental health outcomes among health care workers exposed to coronavirus disease. *JAMA network open.* 3(3):e203976. doi: 10.1001/jamanetworkopen.2020.3976.
- [6] Ali, S. Shah, J. Talib, Z. (2021). COVID-19 and mental well-being of nurses in a tertiary facility in Kenya, *Plos ONE*, 16(7), <https://doi.org/10.1371/journal.pone.0254074>
- [7] Alnazly, E. Khraisat, M., Al-Bashaireh, M., Bryant, L. (2021). Anxiety, depression, stress, fear and social support during COVID-19 pandemic among Jordanian healthcare workers. *PLoS ONE* 16(3), e0247679. <https://doi.org/10.1371/journal.pone.0247679>
- [8] Nadeem, F. Sadiq, A. Raziq, A. Iqbal Q. et al. (2021). Depression, Anxiety, and Stress Among Nurses During the COVID-19 Wave III: Results of a Cross-Sectional Assessment, *J Multidiscip Healthc.* 14: 3093–3101.
- [9] Çelik, F. and Dağlı , R. (2021). Comparison of the Mental Status of COVID-19 Intensive Care Unit and General Intensive Care Unit Staff, *Duzce Medical Journal* , 23 (2) , 197-204 doi: 10.18678/dtfd.915010
- [10] Sheikhbardsiri H, Doustmohammadi MM, Afshar PJ, et al. (2021). Anxiety, stress and depression levels among nurses of educational hospitals in Iran: Time of performing nursing care for suspected and confirmed COVID-19 patients. *J Edu Health Promot* 10:447
- [11] Zakeri, M. Rahiminezhad, E.Salehi, F. Ganjeh, H. and Dehghan, M. (2021). Burnout, Anxiety, Stress, and Depression Among Iranian Nurses: Before and During the First Wave of the COVID-19 Pandemic. *Front. Psychol.* doi.org/10.3389/fpsyg.2021.789737
- [12] An, Y., Yang, Y., Wang, A. et al. (2020). Prevalence of depression and its impact on quality of life among frontline nurses in emergency departments during the COVID-19 outbreak. *Journal of Affective Disorders.* doi:10.1016/j.jad.2020.06.047.



## What is Osteomyelitis of the Jaw Bones? Its History and Classification.

**Özgün YILDIRIM<sup>1,\*</sup>** 

<sup>1</sup>Cankiri Karatekin University, Faculty of Dentistry, Department of Oral and Maxillofacial Surgery, Cankiri, Turkey

### Abstract

Osteomyelitis is defined as an infection of the bone. The treatment is difficult and the success rate is very low. Many patients use too many antibiotics and undergo multiple surgeries. Accurate identification of osteomyelitis is very important in the treatment phase. Revealing the microbiological origin with various tests and choosing the appropriate antibiotic directly affect the success of the treatment. Therefore, in this article, what osteomyelitis is, its history, causative factors and classification will be emphasized.

**Keywords:** Classification, Dentistry, Osteomyelitis

### I. General Information

Osteomyelitis; It is a progressive disease that occurs as a result of a microorganism causing damage to the bone tissue through infectious and inflammatory processes. Only a part of the bone may be involved, and all of the medullary canal, periosteum, cortex and surrounding soft tissues may be included in this picture. The success of treatment in bone and joint infections is low compared to the successes in the treatment of infections in other parts of the body due to some anatomical and pathophysiological features. Most of the patients are patients who have been operated many times, have been treated with different antibiotics for a long time, but the infection still continues. This chronic state of osteomyelitis is a condition that limits the patient both physically and can leave psychiatric sequelae [1].

It is most common between the ages of 1-20. This disease is 2.5 times more common in boys than girls. Local causes of bone tissue (trauma) and low systemic defense of the patient (immunodeficiency syndromes, diabetes, malnutrition, chronic diseases, etc.) play a role in the formation of infection [2].

As can be understood from the roots of the word, “osteon” means the smallest unit that makes up the bone, “myelo” means bone marrow and “itis” means inflammation. Osteomyelitis can occur in a variety of ways, such as by dissemination by bacteremia from a focus of infection elsewhere in the body, by infection of adjacent soft tissue or joints, or by direct contamination of the microorganism after a penetrating trauma or surgery [1].

Infection may be limited to only one area of the bone; It can spread to the bone marrow, cortex, periosteum, and even to the surrounding soft tissues, and if not treated, it can drain into the skin as fistulized [2].

It is known that approximately 20% of patients with chronic osteomyelitis died until the beginning of the 19th century, and significant disabilities remained in survivors [2].

Bone and joint infections, an infection that is relatively common despite the increase in antibiotic types and efficacy, and the improvement of operating room conditions with surgical techniques. It is one of the diseases [1] It is known that the effective treatment of chronic osteomyelitis is still very difficult, and early diagnosis and appropriate surgical and antimicrobial therapy are required for successful treatment [2]

With the term osteomyelitis, it is mostly acute or chronic, depending on the onset of infection and the duration of symptoms; Hematogenous or exogenous, depending on the mode of transmission of the causative agent; Depending on the immune system's response, the terms pyogenic or granulomatous are used [1]

\* Corresponding author. e-mail address: ozgunyldrm89@gmail.com

The definitive diagnosis of osteomyelitis is made by bone biopsy. The material should be obtained percutaneously with a biopsy needle or during surgical debridement. The sample taken must be examined both microbiologically and pathologically [2]

Basically, a successful treatment of osteomyelitis; After diagnosis by bone biopsy, radical removal of dead tissue and long-term effective antibiotic therapy [2]

## II. History

Osteomyelitis is an insidious and stubborn disease that has existed since the beginning of human history. 4000-year-old chronic osteomyelitis (COM) lesions have been found in Egyptian mummies. The earliest records of osteomyelitis in history are found in Hindu inscriptions around 2500 BC. B.C. In 500-400 BC, Hippocrates revealed the obvious relationship between bone infection and trauma; defined the surgical intervention that enables the removal of the infected sequestrant formed in the body and the acceleration of this process. He also established the connection between non-healing sinus discharge and dead bone tissue. M.S. In the 1st century, Celcus made the first attempt to understand the pathology of disease. Celcus describes the four main signs of inflammation; defined as redness, swelling, warmth and pain. He tried to explain the bone pathology with decay, ulceration, blackness, fistulas and gangrene. In 1830, Brodie published his series of nine cases of chronic bone abscess and described the type of osteomyelitis that occurs with low virulence microorganisms [1].

Use of sulfonamides in osteomyelitis Michtell in 1938; The use of penicillin was reported by Trueta in 1941. In this way, the mortality rate decreased from 20% to 3.5% with the introduction of chemotherapeutics in this previously life-threatening disease. Although mortality was almost eliminated with the discovery of various antibiotics, advances in surgical techniques and a better understanding of the pathogenesis of osteomyelitis; osteomyelitis may still be unresponsive to treatment from time to time. In 1962, Willenegger introduced a continuous irrigation and drainage system for the treatment of osteomyelitis. Upon understanding that implants increase the risk of orthopedic infection; In 1969, antibiotic bone cement was started to be used by Bucholz during the revision of infected total hip prostheses. In 1972, Klemm developed gentamicin-impregnated cemented beads and chains in Darmsadt, Germany [1].

Despite this increase in recovery rates, osteomyelitis still remains a problem for orthopedists, pediatricians and infectious diseases specialists. Considering that there are cases of osteomyelitis that flared up again 40 years after the treatment, it will be understood how difficult it is to talk about the cure of this disease [2].

In summary, acute osteomyelitis can be successfully treated in developed countries. Along with the improvement in quality of life, hygiene and nutrition, the incidence of acute hematogenous osteomyelitis has decreased. However, the disease still maintains its severity in developing countries. Although there are certain basic rules in the treatment of chronic osteomyelitis, complications and difficulties can be encountered everywhere [2].

## III. Osteomyelitis in Oral and Maxillofacial Surgery

As in some other diseases, osteomyelitis has become a very rare disease with the intensive use of antibiotics and attention to general body health and oral health. Today, it is seen in infants in underdeveloped countries or in those with impaired body resistance due to diabetes mellitus, chronic kidney failure, drug addiction and alcoholism [3].

The disease is seen at all ages and mostly in men. Although it is more common in the maxilla during infancy, the mandible is more affected in later ages. This ratio is approximately 6:1 [3].

Microorganisms causing pyogenic osteomyelitis are mostly *Staphylococcus aureus*; but it also occurs with *Staphylococcus albus*, streptococci, pneumococci, typhoid bacillus. There are also specific osteomyelitis caused by *Actinomyces Israeli*, Koch bacillus, *Treponema pallidum* and fungi [3]. *Hemophilus influenzae* can be effective in children aged 1-4 years, and group B streptococcus and *Escherichia coli* can be effective in children of other ages. Fungal infection and associated osteomyelitis may develop in people receiving long-term

intravenous therapy. *Staphylococcus epidermidis* may be responsible for osteomyelitis due to prostheses used in the body [4]. Microorganisms causing osteomyelitis are listed in Table 1 according to their frequency percentages. Accordingly, *Staphylococcus aureus* is the most common causative agent [5].

**Table 1. Causes of osteomyelitis**

Subject	Percentage (%)
<i>S. aureus</i>	60
<i>Enterobacteriaceae</i> <i>Proteus species(Spp)</i> <i>Escherichia coli(E. coli)</i> <i>Klebsiella spp.</i> <i>Enterobacter spp.</i> <i>Salmonella spp</i>	20-30
<i>Streptococcus spp</i>	10
<i>Pseudomonas spp</i>	5
Others	5

Chronic infected teeth with caries, infection in neighboring anatomical structures and its spread, septic thrombosis spreading from metastatic septic focus, advanced chronic periodontitis and factors that reduce body resistance (nutrition disorder, radiation therapy, neoplasia, drug treatments, blood diseases, diabetes, tuberculosis, osteopetrosis) such as bone diseases) are among the causes of osteomyelitis [3]. The most important reasons for the onset of osteomyelitis are trauma and odontogenic infections. Bone infection occurs when the bone is affected by any of the factors listed above and is invaded by bacteria. In osteomyelitis that develops due to osteoradionecrosis, however, the bone is primarily damaged due to radiation and bacteria are involved secondarily [4]. Table 2 shows the relationship between the type of causative microorganism and the underlying diseases in osteomyelitis [5].

**Table 2. Type of Microorganism and Underlying Diseases in Osteomyelitis**

Factor	Cause of osteomyelitis Predominant	Cause of osteomyelitis Others
Sickle cell anemia	<i>Salmonella spp.</i>	<i>S. aureus</i> <i>H. influenza</i> <i>S. pneumoniae</i>
Heroin habit	<i>S. aureus</i>	<i>Pseudomonas spp.</i> <i>Gram negative basil</i>
Hemodialysis	<i>S. aureus</i>	<i>S. epidermidis</i> <i>Mycobacterium tuberculosis</i> ( <i>M. tuberculosis</i> )
Pulmonary tb	<i>M. tuberculosis</i>	
Brucellosis	<i>Brucella spp</i>	

Osteomyelitis of the jaws is of hematogenous and non-hematogenous origin. Nonhematogenous infection occurs as bacteria enter through an open wound or spread of infection from adjacent anatomical regions. Hematogenous infections are more common in children and the elderly. It can originate from an angina, peritonsillar abscess, furunkel, or any primary infection. The location of the entry cannot always be determined exactly. Microorganisms can enter the bone from the primary infection site via blood. Hematogenous osteomyelitis may also develop during an infectious disease. Approximately 85% of osteomyelitis of the long bones in children younger than 16 years of age is of hematogenous origin. Types of osteomyelitis of the jaw that occur with hematogenous infection are very rare [3].

The diagnosis of osteomyelitis is made by isolating the causative agent and imaging the bone, as well as anamnesis and physical examination findings. Early diagnosis and treatment of osteomyelitis is extremely

important for the course of the disease. Therefore, in the presence of findings such as bone pain, soft tissue swelling, and limitation of extremity movements, patients should be investigated in detail for osteomyelitis [1] While sinus drainage culture was used previously, studies have shown that bone biopsy culture is superior in terms of both specificity and sensitivity. Bone biopsy culture should not be neglected in order to produce gram-positive cocci other than *S.aureus*, especially gram-negative bacteria and enterococci [1]

Proving the presence of the causative pathogen histologically or by culture makes the definitive diagnosis of osteomyelitis, but it is difficult to isolate the causative microorganism. For this reason, it is an accepted approach to diagnose and start treatment based on clinical and radiological findings. The diagnosis of osteomyelitis can be made in the presence of two of the following criteria. These:

- a) Aspirating pus from the bone,
- b) Reproduction in bone or blood culture,
- c) Clinical findings such as pain, swelling, temperature increase, joint movement limitation,
- d) Radiological findings [1]

The main conditions in which the causative agent may be anaerobic in osteomyelitis are as follows:

- a) Osteomyelitis caused by abdominal sepsis
- b) Osteomyelitis caused by decubitus ulcer
- c) Skull and facial bone osteomyelitis
- d) Osteomyelitis caused by chronic foot ulcers
- e) Presence of foul-smelling exudate
- f) Presence of bacteria in smear, no growth in culture<sup>5</sup>

Table 3 shows the differences in predisposing factors, involved bones and causative microorganisms in osteomyelitis that develops according to the mechanism of formation. The factors of osteomyelitis differ according to age [5]

**Table 3. Factor, Predisposing Factor and Affected Bones in Osteomyelitis According to Formation Mechanism**

	<b>Hematogenous osteomyelitis</b>	<b>Osteomyelitis due to close infection focus</b>	<b>Osteomyelitis due to vascular insufficiency</b>
<b>Factor</b>	<i>S. aureus</i> <i>H. influenza</i> Gram negative bacilli ( <i>E.coli</i> , <i>klebsiella</i> , <i>salmonella</i> , <i>proteus</i> , <i>pseudomonas</i> )	(usually mixed) <i>S. aureus</i> Gram negative bacilli Anaerobic bacteria	(Can be mixed) <i>S. aureus</i> <i>S.epidermitis</i> Enterococci Streptococci Gram negative bacilli Anaerobic bacteria
<b>Predisposing factors</b>	<i>bacteremia</i> Trauma	Operation Open fracture reduction Soft tissue infection (Decubitus ulcer)	Diabetes mellitus Peripheral vascular diseases
<b>Retained bones</b>	long bones (in child), Vertebra (adult)	Femur, tibia, skull, mandible	foot bones

#### IV. Classification

Osteomyelitis classification; It varies according to the duration of the disease, the age of the patient, the presence of the underlying predisposing factor, the host factors, the causative microorganism, the mechanism of infection, and the host's response to the infection [1].

The classification made by Schelhorn P and Zenk W in 1989 according to the clinical picture;

I. Acute osteomyelitis

Secondary chronic osteomyelitis

III. Primary chronic osteomyelitis

IV. Special forms

- Osteomyelitis sicca

- It is in the form of chronic sclerosing osteomyelitis (Garre) [6].

The classification made by Topazian RG in 1994 according to clinical picture, radiological findings and etiology;

I. Suppurative osteomyelitis

1) Acute suppurative osteomyelitis

2) Chronic suppurative osteomyelitis

- Primary chronic suppurative osteomyelitis

- Secondary chronic suppurative osteomyelitis

3) Infantile osteomyelitis

II. Nonsuppurative osteomyelitis

1) Chronic sclerosing osteomyelitis

- Focal sclerosing osteomyelitis

- Diffuse sclerosing osteomyelitis

2) Garre's sclerosing osteomyelitis

3) Actinomycotic osteomyelitis

4) Radiation osteomyelitis and necrosis [6].

Classification made by Bernier S, Clermont S, Maranda G, Turcotte JY in 1995 according to clinical picture and radiological findings;

I. Suppurative osteomyelitis

1) Acute suppurative osteomyelitis

2) Chronic suppurative osteomyelitis

II. Nonsuppurative osteomyelitis

1) Chronic focal sclerosing osteomyelitis

2) Chronic diffuse sclerosing osteomyelitis

3) Garre's chronic sclerosing osteomyelitis (proliferative osteomyelitis)

III. It is in the form of osteoradionecrosis [6].

Wassmund M's classification according to clinical picture and radiological findings in 1935;

I. Exudative osteitis

II. Resorptive osteitis

III. Productive osteitis

IV. Acute necrotizing osteitis (osteomyelitis)

V. Chronic osteomyelitis

1) Chronic course of acute osteomyelitis

2) Occult osteomyelitis

3) Chronic necrotizing osteomyelitis with hypertrophy

4) Chronic exudative osteomyelitis

5) It is in the form of productive osteomyelitis [6].

Osteomyelitis in the jaw bones;

1) Acute suppurative osteomyelitis

2) Chronic suppurative osteomyelitis

3) Focal chronic sclerosing osteomyelitis (Condensing osteitis)

4) Diffuse chronic sclerosing osteomyelitis

5) Chronic osteomyelitis with proliferative periostitis (Garre's osteomyelitis)

6) Childhood osteomyelitis



- 7) Osteomyelitis due to osteoradionecrosis
- 8) Actinomycosis osteomyelitis
- 9) Tuberculous osteomyelitis
- 10) Syphilis osteomyelitis
- 11) Coccidioidmycosis osteomyelitis
- 12) Herpes zoster osteomyelitis
- 13) Neoplastic osteomyelitis
- 14) It can be classified as idiopathic osteomyelitis [3,4].

## V. Conclusion

Osteomyelitis is still an important disease. Although rare, it may occur. should be well known by dentists.

## References

- [1] Hamidanoğlu M. Osteomyelitli Hastalarda Oksidan ve Antioksidan Kapasitelerinin Değerlendirilmesi. Uzmanlık Tezi. Harran Üniversitesi Tıp Fakültesi Enfeksiyon Hastalıkları ve Klinik Mikrobiyoloji Anabilim Dalı, 2011.
- [2] Gökalp MA. Uzun Kemiklerde Kronik Osteomyelitin Oluklaştırma ve Kas Flebi Yerleştirme Yöntemiyle Tedavisi ve Erken Dönem Klinik Sonuçlarımız. Uzmanlık Tezi. Yüzüncü Yıl Üniversitesi Tıp Fakültesi Ortopedi ve Travmatoloji Anabilim Dalı, 2010.
- [3] Türker M, Yücetaş Ş. Ağız, Diş, Çene Hastalıkları ve Cerrahisi. 3.Baskı. Ankara, 2004.
- [4] Yücetaş Ş. Ağız ve Çevre Dokusu Hastalıkları. 5.baskı. Ankara, 2005.
- [5] Değirmenci E. Ratlarda Deneyisel, İmplant İlişkili, Metisilin Dirençli Stafilokokkus Aureus Osteomyelit Modelinde Tigesiklin ve Teikoplanin Antibiyotiklerinin Etkinliklerinin Karşılaştırılması. Düzce Üniversitesi Tıp Fakültesi Ortopedi ve Travmatoloji Anabilim Dalı, 2008.
- [6] Marc M, Baltensperger, Gerold K. H. Eyrich, Osteomyelitis of the Jaws, Bölüm 2, 2009.



# Menopausal Hormones Disturbance in Young and Elder Breast Cancer Patients in Iraq

**Ahmed Abdulameer Hussien HUSSEIN**<sup>1,\*</sup> , **Ayşe Şahin YAĞLIOĞLU**<sup>2</sup> , **Maha Elttayef JASIM**<sup>3</sup> 

<sup>1</sup>Çankırı Karatekin University, Faculty of Science and Arts, Department of Chemistry, Çankırı, Turkey

<sup>2</sup>Amasya University, Faculty of Science and Arts, Department of Chemistry, Amasya, Turkey

<sup>3</sup>Northern Technical University, Institute of medical Al-dour, Department of Biochemistry, Tikrit, Iraq

## Abstract

Breast cancer (BC) is a disease that breast cells grow out of control. Therefore, the early detection of breast cancer disease was the main aim of this study. In this study, several significant chemical tests have been done according to the aim of study. The study included 130 women at the age range between 26 - 66 years old. These women were divided in two groups known as patient group and control group. The control group included 65 healthy women (group A), while group B included 65 patients suffering from breast cancer disease. Anthropometric tests were performed as a function of some parameters such as; age, BMI, and weight. In addition, preformed some other significant chemical tests were also performed such as; FSH, E2, Testosterone, Progesterone, Blood Urea, and S. Creatinine. In our results, there was a statistical significance for the FSH, Testosterone, Progesterone, ALP, Hb tests. The results of statistical analysis refer to significant differences and can be used as chemical markers to early diagnoses for women that suffering from the breast cancer disease. While there were no significant differences for some other tests such as; Got, Gpt, Blood urea, and creatinine.

**Keywords:** Breast cancer, Women, Anthropometric

## 1. Introduction

Breast cancer disease consider one of the foremost common kinds of cancer that female suffered from, and also the second leading reason for death, caused by cancer [1]. Breast carcinoma could be a sickness that specifically affects girls, however, it should additionally have an effect on men, albeit at a far lower rate [2]. Advances in screening and treatment have considerably improved survival rates since 1989, awareness of symptoms. In addition, those wishing to screen for ways to reduce the risk of disease have suggested that carcinoma may have a similar effect on men. Doctors have recently created nice progress within the areas of early detection and treatment of carcinoma, reducing the number of deaths caused by the sickness. Previously, screening for carcinoma meant an entire extirpation. Today, these operations are performed solely in rare cases, as there's a large variety of treatments out there [3]. Menopause in women refers to many indicators, as it represents the time during which a woman's body naturally moves to menopause, so menopause signals the end of a woman's ability to pregnant and give birth. Menopause is also called the menopausal transition [4]. Hormonal causes caused by various disorders of the endocrine system, over time, damage the functioning of the ovary. As a result, the ovarian function is partial and produces only the estrogen hormone, or it does not work at all and does not produce ovarian hormones [5]. The FSH hormone is responsible in women for the development of follicles in the ovaries (an important stage for the development of fertilized mature eggs) and important for the development of healthy sperm cells in men. The abbreviation (LH) refers to the Luteinizing Hormone, this hormone considered significantly for women even for men, it is known as gonadotropin, and for women, it affects the ovaries [6]. This test looks for an antigen called CA-125 found in the serum of some cancer cells. This sign is mainly positive in people with ovarian cancer, but it may also be positive in women who do not have any malignant tumors at all. It can also be obtained in this test a false positive result in women before menopause, more than is possible in women after menopause. Therefore, a cancerous tumor should never be diagnosed based on the result of this test alone [7]. The current study's primary objective is to assess hormone levels, liver function tests, kidney function tests, and hematological parameters (WBC, PCV, and HB) in young and old women (pre- and postmenopausal) with breast cancer in Salah-Aldin City.

\* Corresponding author. e-mail address: ahmedtaqni@gmail.com

## 2. Materials and Methods

### 2.1. Sample Collection

A total of (130) clinical samples of whole blood were collected from patients admitted at Salah Al-Din General Hospital and the Oncology Center of Salah Al-Din during the period from 1/8/2020 to 15/11/2020. Whole Blood were taking from patients and divided into two parts. The first part collected into EDTA tubes for testing complete blood tests which included white blood cells (WBC), packed cell volume (PCV) and Haemoglobin (HB). The second part collected into gel-tubes and separated by Centrifuge to obtain the serum which is required for doing tests like hormones and other bio-chemical tests which included in this work. This thesis analyzed 130 individuals ranging in age from 26 to 66 years. The control group consisted of 65 individuals (Group A), while Group B consisted of 65 patients with breast cancer diseases.

### 2.3. Apparatus and Biochemical kits

All the apparatus and material that used in this study listed in Table 1.

**Table 1.** Materials and Kits that used

Equipment and Apparatus	Company	Country
Semi auto spectrophotometer	Mindray	China
Chemiluminescence immunoassay CL_900i	Mindray	China
Centrifuge PLC Series	Gemmy Industrial Corp.	Taiwan
Hematology auto-analyzer	Mindray	china
Freezer	Hicool	China
Micropipettes (different size)	Eppendorf	Germany
Refrigerator	Concord	Lebanon
Water bath	HUMAN	Germany
Water Distillator	GFL	Germany
Conical Flasks 1L, 500ml, 250ml	Germany	Germany
Disposable Syringes	China	China
Serum Separator Gel Tubes (Clot Activator with Gel)	South Korea	South Korea
Plain Tubes	AFCO	Jordan
Tips (Different size)	AFCO	Jordan

## 3. Results and Discussion

### 3.1. Breast Cancer Analysis

Breast cancer is a condition in which the cells of the breast develop uncontrollably. A breast is composed of three major structural components: lobules, ducts, and connective tissue. Breast cancer comes in a variety of forms. Breast cancer has the potential to spread beyond the breast through blood and lymph vessels. The type of breast cancer is determined from which cells in the breast become cancerous [8]. This thesis analyzed 130 individuals ranging in age from 26 to 66 years. The control group consisted of 65 individuals (Group A), while Group B consisted of 65 patients with breast cancer diseases.

### 3.2. Age with Breast Cancer

The results of have been showed that a significantly in young according to the mean age of the Control group and patients ( $22.5 \pm 2.59$ ;  $34.6 \pm 5.02$  year) respectively, In same time, results have been showed there were a significant differences in elder age between control group and patients group, as shown in Table 2., which was ( $46.4 \pm 5.48$ ;  $59.8 \pm 10.7$  year) respectively.

**Table 2.** Age in Patients and Control groups

Variable	Groups	Mean $\pm$ SD	Sig.
(Youth)	(Control)	22.5 $\pm$ 2.59	0.011
	(Patient)	34.6 $\pm$ 5.02	0.032
(Adult)	(Control)	46.4 $\pm$ 5.48	0.040
	(Patient)	59.8 $\pm$ 10.7	0.011

### 3.2. Anthropometric Measurements with Cancer

Anthropometric scales are a set of quantitative measurements of muscle, bone, and adipose tissue that are used to determine the body's composition. There are some components of anthropometry. These components include height, weight, body mass index (BMI), circumferences of the body (waist, hip, and limbs), and skinfold thickness [9]. The studies including the two element, height and weight. In same studies as demonstrated in Table 3., the mean of height (CM) in young was has a significant difference between patients group (165.6  $\pm$  19.6) as compare to the control groups (167.8  $\pm$  2.94), while there was statistic a significant difference between patients (166.6  $\pm$  3.63) and controls (170.9  $\pm$  6.37) group in Elderly. Also the mean of Weight (Kg) was has a significant difference between patients (71.2  $\pm$  8.78) and controls (71.4  $\pm$  3.35) group in Young and in elderly was significant difference between patients (80.3  $\pm$  13.3) and controls (73.3  $\pm$  5.53) group, as shown in Table 4.

**Table 3.** Height in Patients and Control group

Variable	Groups	Mean $\pm$ SD	Sig.
(Youth)	(Control)	167.8 $\pm$ 2.94	0.001
	(Patient)	165.6 $\pm$ 19.6	0.001
(Elderly)	(Control)	170.9 $\pm$ 6.37	0.001
	(Patient)	166.6 $\pm$ 3.63	0.001

**Table 4.** Weight in Patients and Control group

Variable	Groups	Mean $\pm$ SD	Sig.
(Youth)	(Control)	71.4 $\pm$ 3.35	0.001
	(Patient)	71.2 $\pm$ 8.78	0.002
(Adult)	(Control)	73.3 $\pm$ 5.53	0.001
	(Patient)	80.3 $\pm$ 13.3	0.003

### 3.2. Follicle-Stimulating Hormone (FSH), Estradiol (E2), Testosterone and Progesterone

The results have been displayed in Table 5. that the mean of FSH (mIU/mL) in young has a significant difference between patients group (59.6  $\pm$  29.3) as compare to the control groups (16.3  $\pm$  11.4). There are importantly in patients with breast cancer (BC) while there wasn't a significant difference between patients and controls group in elderly. Also the mean of E2 (pg/mL) displayed a non-significant difference between patients and controls group in elderly and young, the results was (Yp, 95.7  $\pm$  66.4, Yc, 116.7  $\pm$  45.3; Ap, 72.7  $\pm$  7.48, Ac, 68.2  $\pm$  18.9) as displayed in Table 6. Also the mean of testosterone (ng/ml) in patients and controls group was (Yp, 0.55  $\pm$  0.27, Yc, 0.70  $\pm$  0.20; Ap, 0.57  $\pm$  0.20, Ac, 0.57  $\pm$  0.23), which showed a significant difference in elderly and Young with breast cancers, as shown in the Table 7. Also, as displayed in Table 8, the mean of Progesterone (ng/mL) in young was has a significant difference between patients group (2.05  $\pm$  2.03) as compare to the control groups (0.92  $\pm$  0.33). There are importantly in patients with breast cancer (BC) while there wasn't a significant difference between patients and controls group in elderly.

**Table 5.** FSH in patients and control group

Variable	Groups	Mean $\pm$ SD	Sig.
(Youth)	(Control)	16.3 $\pm$ 11.4	0.001
	(Patient)	59.6 $\pm$ 29.3	0.001
(Adult)	(Control)	56.6 $\pm$ 29.4	0.001
	(Patient)	66.6 $\pm$ 47.3	0.001

**Table 6.** E2 in patients and control group

Variable	Groups	Mean $\pm$ SD	Sig.
(Youth)	(Control)	116.7 $\pm$ 45.3	0.062
	(Patient)	95.7 $\pm$ 66.4	0.062
(Adult)	(Control)	68.2 $\pm$ 18.9	0.050
	(Patient)	72.7 $\pm$ 7.48	0.050

**Table 7.** Testosterone in Patients and Control group

Variable	Groups	Mean $\pm$ SD	Sig.
(Youth)	(Control)	0.70 $\pm$ 0.20	0.02
	(Patient)	0.55 $\pm$ 0.27	0.017
(Adult)	(Control)	0.57 $\pm$ 0.23	0.01
	(Patient)	0.57 $\pm$ 0.20	0.01

**Table 8.** Progesterone in patients and control group

Variable	Groups	Mean $\pm$ SD	Sig.
(Youth)	(Control)	0.92 $\pm$ 0.33	0.001
	(Patient)	2.05 $\pm$ 2.03	0.001
(Adult)	(Control)	0.80 $\pm$ 0.21	0.001
	(Patient)	1.17 $\pm$ 0.54	0.001

### 3.3. Blood Urea and S. Creatinine

Also the mean of Blood Urea (mg/dl) have been showed a non-significant difference between patients and controls group in elderly and young, the results was (Yp, 30.4  $\pm$  6.22, Yc, 29.3  $\pm$  3.93; Ap, 36.2  $\pm$  10.6, Ac, 34.1  $\pm$  5.10) as shown in Table 9. Also the mean of S. Creatinine (mg/dl) in patients and controls group was (Yp, 0.64  $\pm$  0.11, Yc, 0.62  $\pm$  0.08; Ap, 0.76  $\pm$  0.17, Ac, 0.72  $\pm$  0.14), which showed a non-significant difference in elderly and Young with breast cancers, as shown in the Table 10.

**Table 9.** Blood Urea in Patients and Control group

Variable	Groups	Mean $\pm$ SD	Sig.
(Youth)	(Control)	29.3 $\pm$ 3.93	0.08
	(Patient)	30.4 $\pm$ 6.22	0.08
(Adult)	(Control)	34.1 $\pm$ 5.10	0.08
	(Patient)	36.2 $\pm$ 10.6	0.08

**Table 10.** S. Creatinine in Patients and Control group

Variable	Groups	Mean $\pm$ SD	Sig.
(Youth)	(Control)	0.62 $\pm$ 0.08	0.071
	(Patient)	0.64 $\pm$ 0.11	0.071
(Adult)	(Control)	0.72 $\pm$ 0.14	0.071
	(Patient)	0.76 $\pm$ 0.17	0.071

### 3.4. Glutamic-Oxaloacetate Transaminase (GOT), Glutamic-Pyruvic Transaminase (GPT) and Alkaline-Phosphatase(ALP)

The results have been showed in Table 11 the mean of S. GOT (U/l) in young was has a non-significant difference between patients group (18.9  $\pm$  5.53) as compare to the control groups (18.2  $\pm$  2.28). There are importantly in patients with breast cancer (BC) while there wasn't a significant difference between patients (18.1  $\pm$  5.93) and controls (21.1  $\pm$  5.73) group in elderly. On the other hand, the mean of S. GPT (U/l) was has a non-significant difference between patients and controls group in young. While was little a significant

difference in elderly and the results was (Yp,  $16.3 \pm 6.17$ , Yc,  $15.5 \pm 2.11$ ; Ap,  $17.2 \pm 5.46$ , Ac,  $19.8 \pm 5.03$ ) as shown in Table 12. Also, the results showed the mean of ALP (U/l) in patients and controls group at Young and Elderly was (Yp,  $169.5 \pm 58.6$ , Yc,  $132.2 \pm 19.4$ ; Ap,  $187.9 \pm 65.4$ , Ac,  $150.8 \pm 39.5$ ) respectively, which demonstrated a statistically significant distinction between the patients and controls in the Young and Elderly breast cancer groups, as can be shown in Table 13 respectively.

**Table 11.** GOT in patients and control group

Variable	Groups	Mean $\pm$ SD	Sig.
(Youth)	(Control)	$18.2 \pm 2.28$	0.059
	(Patient)	$18.9 \pm 5.53$	0.059
(Adult)	(Control)	$21.1 \pm 5.73$	0.059
	(Patient)	$18.1 \pm 5.93$	0.059

**Table 12.** GPT in Patients and Control group

Variable	Groups	Mean $\pm$ SD	Sig.
(Youth)	(Control)	$15.5 \pm 2.11$	0.081
	(patient)	$16.3 \pm 6.17$	0.081
(Adult)	(Control)	$19.8 \pm 5.03$	0.081
	(Patient)	$17.2 \pm 5.46$	0.081

**Table 13.** ALP in Patients and Control group

Variable	Groups	Mean $\pm$ SD	Sig.
(Youth)	(Control)	$132.2 \pm 19.4$	0.001
	(Patient)	$169.5 \pm 58.6$	0.001
(Adult)	(Control)	$150.8 \pm 39.5$	0.001
	(Patient)	$187.9 \pm 65.4$	0.001

### 3.5. White Blood Cells (WBC), Paked Cell Volume (PCV) and Hemoglobin (HB) with Breast Cancer

The results showed in Table 14 the mean of WBC ( $10^9/l$ ) in Young was has a non-significant difference between patients group ( $5.87 \pm 1.41$ ) as compare to the control groups ( $6.30 \pm 1.0$ ), while also, there wasn't a significant difference between patients and controls group in Elderly. Also, the mean of PCV (%) in Young and Elderly patients exhibited a significant difference from that of the control group., the results was (Yp,  $32.9 \pm 4.7$ , Yc,  $40.4 \pm 0.61$ ; Ap,  $35.4 \pm 2.98$ , Ac,  $40.8 \pm 0.86$ ) as shown in Table 14. Also the mean of Hb (g/dl) in patients and controls group was (Yp,  $10.3 \pm 4.25$ , Yc,  $12.5 \pm 0.40$ ; Ap,  $9.2 \pm 0.95$ , Ac,  $12.8 \pm 0.49$ ), which showed a significant difference but it is little statistically significant in Elderly and Young with breast cancers, as shown in the Table 16.

**Table 14.** WBC in patients and control group

Variable	Groups	Mean $\pm$ SD	Sig.
(Youth)	(Control)	$6.30 \pm 1.0$	0.053
	(Patient)	$5.87 \pm 1.41$	0.053
((Adult)	(Control)	$9.65 \pm 1.17$	0.057
	(Patient)	$5.90 \pm 1.72$	0.054

**Table 15.** PCV in patients and control group

Variable	Groups	Mean $\pm$ SD	Sig.
(Youth)	(Control)	$40.4 \pm 0.61$	0.001
	(Patient)	$32.9 \pm 4.7$	0.001
(Adult)	(Control)	$40.8 \pm 0.86$	0.031
	(Patient)	$35.4 \pm 2.98$	0.031

**Table 16.** Hb in patients and control group

Variable	Groups	Mean $\pm$ SD	Sig.
(Youth)	(Control)	12.5 $\pm$ 0.40	0.001
	(Patient)	10.3 $\pm$ 4.25	0.001
(Adult)	(Control)	12.8 $\pm$ 0.49	0.001
	(Patient)	9.2 $\pm$ 0.95	0.001

### 3.6. Discussion

In the Young and Elderly populations, there was a significant difference in the mean of Age and Higher between patients and controls. Tallness, regardless of when it was reached, was correlated with an elevated risk of breast cancer detection at both young (50 years) and older ages, with an adult height of 68 cm or higher raising risks by about 50% to 80% relative to statures shorter than 62 cm [10], and this research coincides with ours, as weight was a major difference between patients and controls. Weight loss can serve as a biomarker for the diagnosis of breast cancer. After the age of 18, women who gained almost 20 pounds had a 15% greater risk of breast cancer compared to women who gained little or no weight [11], which is compatible with our results. Increased body mass indices based on early adulthood weights were also associated with a decrease in danger [10]; this study corroborates our results.

Although the mean of FSH expression differed significantly between patients and controls in the Young and Elderly, the mean of E2 expression did not vary significantly between patients and controls in breast cancer patients in the Young and Elderly and was unrelated to disease occurrence. The E2 levels of women with breast cancer were impaired [12], and this study contradicts my observations, since the majority of patients were post-surgery and taking tamoxifen, an anti-estrogen that results in a decrease in the amount of estrogen. This explains why E2 was a consistent value in my study. The mean Testosterone and Progesterone levels are slightly different across young and elderly breast cancer patients and control groups. FSH and testosterone levels were shown to be significantly higher in patients with breast cancer diagnosis in another study [13], correlating with our results. In the Young and in Elderly populations, the mean blood urea and S. Creatinine concentrations did not differ substantially between patients and controls. There were no clinically significant differences in blood urea nitrogen or creatinine levels between the two groups [14], which corroborates our results.

The mean of Got expression was slightly different between the Young and the Elderly, but not between breast cancer patients and non-breast cancer patients. Aspartate aminotransferase (AST or SGOT), alanine aminotransferase (ALT or SGPT), and alanine aminotransferase (ALP) amounts were found to be inside the normal reference range [15], correlating with our results. ALP expression was slightly different between the youth and the old, and was consistent with the activity of breast cancer disease.

There was a major gap in the mean of PCV and Hb expression between patients and controls in the Young and Elderly, but not in WBC. Due to the WBC in certain patients, their immune level drops immediately after the first dose and lasts for a period of seven days. Additionally, the majority of patients were receiving immune injections called Filgrastim, also known as Neupogen, when their immunity level decreased, which explained the usual WBC findings in my study. The research discovered that when cancer patients were linked to standard control groups, there was a substantial decrease in HB, PCV, RBC, and WBC levels and a significant increase ( $P < 0.05$ ) in HB, PCV, RBC, and WBC levels [16].

### Acknowledgment

I would like to thank all the people who helped me make this work possible. To My supervisor Prof. Dr. Ayşe ŞAHİN YAĞLIOĞLU and second supervisor Dr. Maha Lateef Jasem for their guidance and assistance. To Dr. Ali abbas and Dr. Saif Abedalaziz BANIDAHIR for his support and always being available to help. To the oncology department at Tikrit General Hospital for the time and effort they spent to provide me with datas

### References

- [1] Kelsey, J. L., Gammon, M. D. and John, E. M. 1993. Reproductive factors and breast cancer. *Epidemiologic reviews*, 15(1), 36.

- [2] Ramakrishna, N., Temin, S., Chandarlapaty, S., Crews, J.R., Davidson, N.E., Esteva, F.J., Giordano, S.H., Kirshner, J.J., Krop, I.E., Levinson, J. and Modi, S., 2018. Recommendations on disease management for patients with advanced human epidermal growth factor receptor 2-positive breast cancer and brain metastases: ASCO clinical practice guideline update. *J Clin Oncol*, 36(27), 2804-2807.
- [3] Hartmann, L. C., Schaid, D. J., Woods, J. E., Crotty, T. P., Myers, J. L., Arnold, P. G. and Frost, M. H. 1999. Efficacy of bilateral prophylactic mastectomy in women with a family history of breast cancer. *New England Journal of Medicine*, 340(2), 77-84.
- [4] Li, J., Yang, L., Qin, W., Zhang, G., Yuan, J. and Wang, F. 2013. Adaptive induction of growth differentiation factor 15 attenuates endothelial cell apoptosis in response to high glucose stimulus. *PloS one*, 8(6), e65549.
- [5] Kapoor, D. and Jones, T. H. 2005. Smoking and hormones in health and endocrine disorders. *European journal of endocrinology*, 152(4), 491-499.
- [6] Martin, V. T., Pavlovic, J., Fanning, K. M., Buse, D. C., Reed, M. L. and Lipton, R. B. 2016. Perimenopause and menopause are associated with high frequency headache in women with migraine: results of the American migraine prevalence and prevention study. *Headache: The Journal of Head and Face Pain*, 56(2), 292-305.
- [7] Nustad, K., Lebedin, Y., Lloyd, K. O., Shigemasa, K., De Bruijn, H. W. A., Jansson, B. and O'Brien, T. J. 2002. Epitopes on CA 125 from cervical mucus and ascites fluid and characterization of six new antibodies. *Tumor Biology*, 23(5), 303-314.
- [8] Harbeck, N., Penault-Llorca, F., Cortes, J., Gnant, M., Houssami, N., Poortmans, P., Ruddy, K., Tsang, J. and Cardoso, F. 2019. Breast cancer. *Nature reviews. Disease primers*, 5(1), 66.
- [9] Casadei, K. and Kiel, J. 2020. Anthropometric Measurement. *StatPearls Publishing*, 2 :3-12.
- [10] Brinton, L. A. and Swanson, C. A. 1992. Height and weight at various ages and risk of breast cancer. *Annals of epidemiology*, 2(5), 597-609.
- [11] Elmlinger, M. W., Kühnel, W. and Ranke, M. B. 2002. Reference ranges for serum concentrations of lutropin (LH), follitropin (FSH), estradiol (E2), prolactin, progesterone, sex hormone-binding globulin (SHBG), dehydroepiandrosterone sulfate (DHEAS), cortisol and ferritin in neonates, children and young adults. *Clinical Chemistry and Laboratory Medicine (CCLM)*, 40(11), 1151-1160.
- [12] Bighin, C., Lunardi, G., Del Mastro, L., Marroni, P., Taveggia, P., Levaggi, A. and Pronzato, P. 2010. Estronesulphate, FSH, and testosterone levels in two male breast cancer patients treated with aromatase inhibitors. *The oncologist*, 15(12), 1270.
- [13] Winand, F. J., Boegemann, M., Gallitz, I., Hertle, L., Semjonow, A., Eveslage, M. and Steinbicker, A. U. Kyvernitis, I., Albert, U. S., Kalder, M., Winarno, A. S., Hars, O. and Hadji, P. 2015. Effect of anastrozole on hormone levels in postmenopausal women with early breast cancer. *Climacteric*, 18(1), 63-68.
- [14] Malya, F. U., Kadioglu, H., Hasbahceci, M., Dolay, K., Guzel, M. and Ersoy, Y. E. 2018. The correlation between breast cancer and urinary iodine excretion levels. *Journal of International Medical Research*, 46(2), 687-692..
- [15] Swapna, V. S., Sudhakar, V. and Javerappa, D. 2018. Study of liver function tests in breast carcinoma patients before and after chemotherapy. *International Journal of Biotechnology and Biochemistry*, 14(3), 177-184.
- [16] Alsaadi, J. H. H. and Younus, B. M. 2009. Study of Some Biochemical and Blood Parameters as Screening Markers for Breast Cancer Patients before Adjuvant Therapy in ThiQar Government-Southern Iraq.





## Study of the Changes That Occur in Some Biochemical Variables after Cholecystectomy for Patients in Al-Anbar Governorate / Iraq

***Omar Khalid Mustafa AL-BAYATI***<sup>1,\*</sup> , ***Hakan ÇOLAK***<sup>2</sup> , ***Khalid Farouq AL-RAWI***<sup>3</sup> 

<sup>1</sup>Çankırı Karatekin University, Faculty of Science, Department of Chemistry, Çankırı, Turkey

<sup>2</sup>Çankırı Karatekin University, Faculty of Sciences, Department of Chemistry, Çankırı, Turkey

<sup>3</sup> University of Al-Anbar, Faculty of Science, Department of Chemistry, Al-Anbar, Iraq

### Abstract

The study included (90) Iraqi persons with age ranged from (20 - 70), that divided for two groups, group (1) control group consist of 30 healthy persons (males and females) and group (2) consist of 60 patient had a cholecystectomy, samples were obtained from Al-Ramadi teaching hospital and Haditha general hospital during the duration of October 2020 to March 2021, and measuring concentrations of TSB, ALT, AST, ALP, cholesterol, TG, LDL, HDL, VLDL, LDL, S. amylase, S. lipase, and CCK. Regarding the age of all participant the Mean  $\pm$  SE of patient group was  $(45.47 \pm 1.57)$  that is lower than the control group  $(50.53 \pm 1.73)$  with p- value 0.05 indicate a difference of statistical significant between the two group. The TSB mean level of patient group was  $0.81 \pm 0.02$  that is statically different from mean level in control group  $(0.74 \pm 0.01)$ , with p-value 0.04. TG and VLDL result showed a statistical difference between patient and control group, p-value was 0.01 for both markers. Measuring CCK for both group indicate a statistical significant difference in between as p- value 0.008.

**Keywords:** Cholecystectomy, Liver function test, Lipid profile, Amylase, Lipase

### 1. Introduction

Gallstones are stone like structure made from the hardened deposition of the bile and formed mainly within the gallbladder but can be found also in common bile duct, the stones have various size, shape and composition. The disease is about a chronic frequency hepatobiliary disease, gallstone formation is cause mainly due to chemical imbalance in constituents of bile, impaired metabolism of bile acids, bilirubin and cholesterol leading to precipitation of one or more of the components [1], It is consisting of calcium bilirubinate, cholesterol monohydrate crystals, proteins and mucin gels. It can be classified their according to a chemical composition of their as (1) cholesterol stone ( $> 75\%$  is cholesterol), (2) Pigment or black, and (3) Mixed stones that contains  $< 75\%$  cholesterol with calcium and bilirubin salts in various concentration. About 75% of stones in western country is cholesterol gallstones, black pigment stones about 20%, and brown pigment stones just 5% [2]. Cholecystitis is an inflammation of the gallbladder because of presence of gallstone that develops over hours, the development of condition slowly will refer to chronic cholecystitis, and the symptoms include right upper quadrant pain with tenderness that probably associated with fever, vomiting and chills nausea [3]. The stone move near cystic duct opening and cause stagnation of flow bile, lead to the classic biliary colicky ache. If the blockage cystic duct continues for several hours, lead to the gallbladder wall inflammation (Cholecystitis). If gallstone moves further and cause occlusion, leading to abdominal pain and jaundice. Progressive fibrosis and loss of motor function of the gallbladder is result from the chronic gallstones disease [4]. Bile stasis will trigger the release of liver enzymes, as the gallstones blocks fluid passage to the gallbladder irritated and swollen in gallbladder will develop that will transmit to nearby liver cell. Irritation of liver cell can progress to cell damage which will be seen as elevation in liver enzymes. Ultrasound is the main diagnostic tool to diagnosis gall stone disease after physical examination. The treatment of gallstones is mainly surgical, cholecystectomy. The prevalence of gallstones in increase with age, in women higher than in men, in the developed countries 20% of adult will have [5]. GD is common gastrointestinal disease, one of the most economic load medical conditions at the world [6]. In the US over 14.2 million males and 6.3 million females with age's range of 20 – 74 suffering from. However, maximum case of gallstones is without symptoms, however 10% of them within five years will develop symptoms, and about 20% will have symptoms in period 20 years of diagnosing gallstones. Cholecystectomy is the surgery treatment, which is best choice of acute cholecystitis patient, which

\* Corresponding author. e-mail address: omarkhalidhadithi@gmail.com

can either laparoscopic procedure or open surgery. The assessment of biliary injuries before surgery is necessary that include biochemical testing of liver enzymes. Studies has been find that the liver function test LFT sensitivity in detecting obstructions in biliary flow that reach 90% [7]. Hepatocyte function can be estimated by the ratio of GOT to GPT. Common bile duct (CBD) stones are associated with an increase in serum transaminases, and ALP rises when the biliary system is blocked. However, increased LFTs are commonly seen shortly after surgery, and it is transient that back to normal values without any intervention. Routine preoperative LFT testing has been shown to be a factor in determining whether a cholecystectomy can be performed laparoscopically or must be performed openly. Aim of the study: The main study aims that exploring in whether or not there are changes occur on constructions and activity of some enzymes and lipids levels after the cholecystectomy for the patients in AL-Anbar governorate.

## 2. Materials and Methods

### 2.1. Study Design Settings and Data Collection Time

The study included (90) Iraqi persons with age ranged from (20 – 70 years), that divided for two groups as following: The control group 30, 60 patients having who underwent cholecystectomy surgery. Samples were obtained from Al-Ramadi teaching hospital and Haditha general hospital during the duration of October 2020 to March 2021.

### 2.3. Apparatus and Biochemical kits

The Instruments that used in this study are shown in Table 1.

**Table 1.** Materials and Kits that used

Instrument		Company
1	Bio pipette (1-10) mL	Lab. net USA
2	Centrifuge	Kukosan Japan
3	Tips (blue, yellow)	AFCO, Jordan
4	Eppendorf tube (1.5mL)	Jet bio fil USA
5	Deep freezer	FROILABO France
6	Disposable syringes (5mL)	Medical jet (Syria)
7	Genex	Florida, USA
8	Spectrophotometer	APEL, Japan
9	FUJIFILM	Japan
10	Disposable test tubes (10mL)	Meheco, (China)
11	ELISA	BIOTEK, USA
12	Bio pipette (2-100) mL	Lab. net USA

The Kits and chemicals that used in study are shown in Table 2.

**Table 1.** Kits and chemicals

Kit		Company
1	Alkaline phosphatase kit	Beckman coulter USA
2	S GOT kit	Beckman coulter USA
3	S GPT kit	Beckman coulter USA
4	S Amylase kit	Beckman coulter USA
5	S Lipase kit	FUJIFILM Japan
6	HUMAN ELISA kit CCK	Sunlong Biotech Co. Ltd
7	HDL Cholesterol kit	Biolabo, France
8	Total Cholesterol kit	Biolabo, France
9	Triglyceride kit	Biolabo, France
10	TSB kit	Biolabo, France

### 3. Results and Discussion

#### 3.1. Description of data

The study is case-control study that enrolled 60 patients who were having gallstone disease and underwent cholecystectomy and 30 other healthy persons. The age of patient was divided into 3 groups as the following, 20 - 30 years old (9 - 10.0%), 31 - 40 years old, (16 - 17.8%) and 41 - 70 years old, (65 - 72.2%), in which can notice that most patient age are above 40 years old with mean (65 - 72.2%). 75.6% of the participant are females and 24.4% are males. The BMI of patient was calculated and the result was divided in 4 groups, (4 - 4.4%) have normal BMI, (0 - 44.4%) have overweight, (42 - 46.7%) have obesity, and (4-4.4%) have morbid obesity, as presented in Table 3.

**Table 3.** Variables study groups, subgroup, frequency and percentage

		Frequency	Percent
Group	Patient	60	66.7%
	Control	30	33.3%
Age group	20 – 30 Years Old	9	10.0%
	31 - 40 Years Old	16	17.8%
	41 - 70 Years Old	65	72.2%
Gender	Female	68	75.6%
	Male	22	24.4%
BMI groups	Normal	4	4.4 %
	Over Weight	40	44.4 %
	Obese	42	46.7 %
	Morbid Obesity	4	4.4 %
	Total	90	100.0%

#### 3.2. Compare between patient and control according to biochemical tests

The liver function of each participant was estimated using the measure of the following biomarkers: Total serum bilirubin (TSB), Aspartate transaminase (GOT), Alanine transaminase (GPT), Alkaline phosphatase (ALP), Cholesterol (CHOL), Triglyceride (TG), High density lipoprotein (HDL), Low density lipoprotein (LDL), Very low density lipoprotein (VLDL), Serum amylase, Lipase, and Cholecystokinin (CCK) for each group. In order to evaluated the changes in these biomarkers between the two studied groups, the mean  $\pm$  SE of each biomarker of both group was calculated using independent t-test, as well as p-value and confidence interval, as presented in Table 4. Regarding the age of all participant the Mean  $\pm$  SE of patient group was  $45.47 \pm 1.57$  that is lower than the control group  $50.53 \pm 1.73$  with p- value 0.05 indicate a difference of statistical significant between the two group. The TSB mean level of patient group was  $0.81 \pm 0.02$  that is statically different from mean level in control group  $0.74 \pm 0.01$ , with p-value 0.04. GOT, GPT, ALP, amylase and lipase mean level was not statistically significant differences between the group, as mean was  $27.82 \pm 0.88$ ,  $26.08 \pm 1.54$ ,  $173.07 \pm 13.44$ ,  $44.62 \pm 1.93$ , and  $37.38 \pm 1.08$  in patient group, respectively. The mean in control group was  $25.97 \pm 1.08$ ,  $23.53 \pm 1.96$ ,  $156.27 \pm 6.64$ ,  $42.47 \pm 4.06$ , and  $34.13 \pm 2.19$ , respectively. TG and VLDL result showed a statistical difference between patient and control group, p-value was 0.01 for both markers, mean level of TG  $140.62 \pm 5.33$ , and VLDL  $28.12 \pm 1.06$  in patient group which statistically lowered from control group as mean level of TG  $174.07 \pm 15.04$ , and VLDL  $34.84 \pm 3.01$  in control group. HDL and LDL show non statistical significant difference between the two groups. Measuring CCK for both group indicate a statistical significant difference as p- value 0.008, the mean level of CCK in higher in patient group  $59.68 \pm 3.01$  than in control  $46.46 \pm 3.21$ . Both group has insignificant statistical differences in BMI. See Table 4.

**Table 4.** Mean level of studied biomarkers in both groups

Factors	Group	Mean $\pm$ S.E.	P -value	95% confidence interval	
				Lower	Lower
Age year	patient	45.47 $\pm$ 1.57	0.050*	-10.12	-0.007
	Control	50.53 $\pm$ 1.73			
TSB	Patient	0.81 $\pm$ 0.02	0.040*	0.003	0.14
	Control	0.74 $\pm$ 0.01			
GOT	Patient	27.82 $\pm$ 0.88	0.20	-1.05	4.75
	Control	25.97 $\pm$ 1.08			
GPT	Patient	26.08 $\pm$ 1.54	0.32	-2.60	7.70
	Control	23.53 $\pm$ 1.96			
ALP	Patient	173.07 $\pm$ 13.44	0.39	-22.21	55.81
	Control	156.27 $\pm$ 6.64			
CHOL	Patient	155.93 $\pm$ 2.41	0.80	-10.12	7.85
	Control	157.07 $\pm$ 4.20			
TG	Patient	140.62 $\pm$ 5.33	0.01*	-59.28	-7.61
	Control	174.07 $\pm$ 15.04			
HDL	Patient	46.95 $\pm$ 0.55	0.43	-1.38	3.22
	Control	46.03 $\pm$ 1.20			
LDL	Patient	81.23 $\pm$ 2.39	0.39	-4.94	12.54
	Control	77.43 $\pm$ 3.98			
VLDL	Patient	28.12 $\pm$ 1.06	0.01*	-11.89	-1.54
	Control	34.84 $\pm$ 3.01			
amylase	Patient	44.62 $\pm$ 1.93	0.58	-5.72	10.02
	Control	42.47 $\pm$ 4.06			
Lipase	Patient	37.38 $\pm$ 1.08	0.13	-1.07	7.57
	Control	34.13 $\pm$ 2.19			
CCK	Patient	59.68 $\pm$ 3.01	0.008*	3.61	22.82
	Control	46.46 $\pm$ 3.21			
BMI	Patient	29.77 $\pm$ 0.37	0.22	-2.22	0.521
	Control	30.63 $\pm$ 0.61			
P-value is significant if $\leq 0.05$					

### 3.3. Compare between patient and control group according to gender

The study enrolled 68 females and 22 males, the participant were divided according to their gender into male group and female group that further divided into patient (46 females, 14 male) and control group (22 females, 8 males). Mean age of female participant in patient group  $46.20 \pm 1.80$  is lower than in control group  $51.23 \pm 2.17$ , that statically insignificant differences, p-value 0.09. Mean TSB of female patient group ( $0.79 \pm 0.012$ ) is statically higher than in female mean TSB in control group ( $0.74 \pm 0.01$ ), p-value 0.02. Mean GPT level is lower in patient female group  $23.91 \pm 1.45$  than in female control group  $24.68 \pm 2.58$ , p-value 0.78 indicate no-statistical significant differences. CCK mean level in female patient group higher  $59.87 \pm 3.52$  than in control group  $49.02 \pm 3.97$ , that is statically insignificant as p-value 0.06. Regarding other liver enzymes, result showed that mean of GOT  $28.37 \pm 0.99$ , ALP  $163.89 \pm 7.61$ , CHOL  $155.80 \pm 2.82$ , TG  $146.80 \pm 6.04$ , HDL  $47.09 \pm 0.65$ , LDL  $79.86 \pm 2.74$ , VLDL  $29.36 \pm 1.20$ , amylase  $43.28 \pm 2.15$ , lipase  $37.20 \pm 1.19$  and BMI  $30.1 \pm 0.36$  in female patient group are statistically insignificant different from control female group as mean was  $26.59 \pm 1.18$ ,  $152.18 \pm 7.92$ ,  $158.45 \pm 5.00$ ,  $173.59 \pm 19.56$ ,  $46.32 \pm 1.52$ ,  $77.25 \pm 4.87$ ,  $34.76 \pm 3.92$ ,  $39.77 \pm 4.53$ ,  $32.82 \pm 2.79$  and  $30.88 \pm 0.94$ , see Table 5.

**Table 5.** Compare between female patient and control group

Gender		Group	Mean ± S.E.	P -value	95% confidence interval	
					Lower	Upper
Female	Age years	Patient	46.20 ± 1.80	0.09	-11.03	0.97
		Control	51.23 ± 2.17			
	TSB	Patient	0.79 ± 0.012	0.02*	0.006	0.08
		Control	0.74 ± 0.01			
	GOT	Patient	28.37 ± 0.99	0.28	-1.52	5.08
		Control	26.59 ± 1.18			
	GPT	Patient	23.91 ± 1.45	0.78	-1.52	5.08
		Control	24.68 ±2.58			
	ALP	Patient	163.89 ± 7.61	0.34	-12.89	36.31
		Control	152.18 ± 7.92			
	CHOL	Patient	155.80 ±2.82	0.62	-13.34	8.04
		Control	158.45 ± 5.00			
	TG	Patient	146.80 ± 6.04	0.09	-58.78	5.21
		Control	173.59 ± 19.56			
	HDL	Patient	47.09 ± 0.65	0.58	-2.04	3.58
		Control	46.32 ± 1.52			
	LDL	Patient	79.86 ± 2.74	0.61	-7.76	12.97
		Control	77.25 ± 4.87			
	VLDL	Patient	29.36 ±1.20	0.09	-11.80	1.01
		Control	34.76 ± 3.92			
	amylase	Patient	43.28 ± 2.15	0.42	-5.29	12.3
		Control	39.77 ± 4.53			
	lipase	Patient	37.20 ± 1.19	0.09	-.77	9.53
		Control	32.82 ±2.79			
	CCK	Patient	59.87 ± 3.52	0.06	-0.73	-22.4
		Control	49.02 ± 3.97			
	BMI	Patient	30.1 ± 0.36	0.34	-2.30	0.8
		Control	30.88 ± 0.82			
* P-value is significant if ≤ 0.05						

Regarding male gender, GPT mean level was statistically significant higher in patient group (33.21  $\pm$  4.17) than control group (20.38  $\pm$  1.70), with p-value 0.03. TG and VLDL mean level was 120.29  $\pm$  9.79, 24.05  $\pm$  1.95 respectively, statically different from mean level in control group 175.38  $\pm$  18.91, 35.07  $\pm$  3.78, respectively. The CCK mean level was 59.06  $\pm$  5.90 in patient group that is statistically higher than the mean of control group 39.42  $\pm$  4.54. Other markers were not statically significant different between the two groups.

**Table 6.** Compare between male patient and control group

Gender		group	Mean $\pm$ SE	p-value	95% confidence interval	
					Lower	upper
male	Age year	patient	43.07 $\pm$ 3.30	0.26	-15.62	4.51
		control	48.63 $\pm$ 2.63			
	TSB	patient	0.91 $\pm$ 0.09	0.2	-0.10	0.44
		control	0.73 $\pm$ 0.01			
	GOT	patient	26.00 $\pm$ 1.87	0.57	-4.69	8.19
		control	24.25 $\pm$ 2.42			
	GPT	patient	33.21 $\pm$ 4.17	0.03*	-0.89	24.7
		control	20.38 $\pm$ 1.70			
	ALP	patient	203.21 $\pm$ 52.57	0.62	-112.08	183.51
		control	167.50 $\pm$ 11.98			
	CHOL	patient	156.36 $\pm$ 4.73	0.72	-15.02	21.23
		control	153.25 $\pm$ 8.03			
	TG	patient	120.29 $\pm$ 9.79	0.009*	-95.12	-15.05
		control	175.38 $\pm$ 18.91			

**Table 6.** Compare between male patient and control group (Continued)

HDL	patient	46.50 ± 1.07	0.53	-2.87	5.37
	control	45.25 ± 1.84			
LDL	patient	85.7 ± 4.86	0.36	-9.72	26.47
	control	77.92 ± 7.17			
VLDL	patient	24.05 ± 1.95	0.009*	-19.02	-3.01
	control	35.07 ± 3.78			
amylase	patient	49.00 ± 4.25	0.92	-18.84	17.09
	control	49.88 ± 8.72			
Lipase	patient	38.0 ± 2.57	0.95	-8.11	8.6
	Control	37.75 ± 2.76			
CCK	Patient	59.06 ± 5.90	0.03*	-1.72	37.54
	Control	39.42 ± 4.54			
BMI	Patient	28.64 ± 1.28	0.37	-4.37	1.7
	Control	29.9 ± 1.00			
* P-value is significant if ≤ 0.05					

### 3.4. Correlation between CCK and other markers

Table 7, illustrates the link that can be found between CCK and the many other tested markers. The result showed non-statistical significant correlation between CCK and other markers. CCK and age spearman correlation was -0.11 indicate a very weak negative non-significant correlation, p-value 0.28. The correlation coefficient of CCK and TSB was 0.03 indicate a very weak positive non-significant correlation, p-value 0.75. The correlation coefficient of CCK and GOT was 0.06 indicate a very weak positive non-significant correlation, p-value 0.54, r of CCK and GPT was -0.005 indicate a very weak negative non-significant correlation, p-value 0.96, of CCK and ALP was 0.10 indicate a very weak positive non-significant correlation, p-value 0.33 of CCK and lipid profile marker CHOL was 0.06, CCK and TG was -0.11, HDL was 0.13, LDL was 0.07, and VLDL was -0.11, with p-value of 0.54, 0.27, 0.19, 0.45, and 0.27, all indicate a non-significant very weak correlation. Both serum amylase and lipase show insignificant very weak correlation with CCK as r was 0.05 and 0.1 with p-value of 0.59 and 0.3.

**Table 7.** The Linear regression correlation between CCK and measured markers in all enrolled participant

	CCK	
	R	p-value
Age	-0.11	0.28
TSB	0.03	0.75
GOT	0.06	0.54
GPT	-0.005	0.96
ALP	0.10	0.33
CHOL	0.06	0.54
TG	-0.11	0.27
HDL	0.13	0.19
LDL	0.07	0.45
VLDL	-0.11	0.27
Amylase	0.05	0.59
Lipase	0.1	0.31

## 4. Discussion

The current study includes 90 participants, 60 of them are patient who underwent cholecystectomy surgery. The liver enzyme, lipid profile, S. amylase, S. lipase and cholecystokinin patient and control. Gallstone disease will induce liver damage due to the chronic obstruction of extra-hepatic bile duct and stagnation of bile or a frequent episodes of cholangitis that can develop to biliary cirrhosis. Prolong biliary blockage will cause change in other enzyme as lipid profile, S. amylase, S. lipase and cholecystokinin. Cholecystectomy surgery is most common treatment for gallstones disease, which is nowadays is laparoscopic cholecystectomy procedure.

However, Cholecystectomy surgery carry some risk to patient by injury to biliary tree, biochemical testing of liver enzymes has been used to assess biliary duct injury. In Table 3.1, the description of included data is presented. The study includes 68 women and 22 men, the compared ratio between females and males was 3:1 with various ages ranging from 20 - 70 divided into 3 group, mean of patient age was  $45.47 \pm 1.57$  while mean age of control was  $50.53 \pm 1.73$ , most of the enrolled participant have high BMI (81.1%). In O Hamad and R Al-Luwaizi, study that is prospective case control study included 74 cholecystitis patients to assess the effect of surgery on enzymes of the liver and serum bilirubin between two groups who have different procedures [8]. Mean of age of patient was 45.1 years with range of 22 - 76 years that is approach current study result, female: male ratio was 6:1 that is higher than current study. The agreement between both study can be explained as the following, many studies has been agreed that gallstone disease tend to be cluster in middle age female that support current study result [9]. The result of mean of each measured biochemical markers is presented in Table 4. According to Maleknia and Ebrahimi, study that is a cross sectional study that involve 128 patients (109 females, 19 male) with mean age of  $65.1 \pm 14.6$  years, and mean calculated BMI was  $19.43 \pm 2.19$  kg/m<sup>2</sup> (mean of BMI in patient of current study was  $29.77 \pm 0.37$ ) who will have laparoscopic cholecystectomy to evaluate the pre and post-op result of TSB and liver enzymes [10]. The demographic data of patient did not approach current study result. The result of the study found that no statistical significant difference found between pre and post-op result of ALP, that agreed with current study regarding ALP, no change in ALP level post op from the healthy control group but the level of ALP in patient group was above the normal limit which can explain by ALP levels are consistent with the biliary tract injury, the number of sample was may have a role in inability to detect a significant difference. The study found that TSB is higher in post-op patient which agreed with current study as TSB is higher in post-op patient than control, that can be explained by TSB is increase post-op but return to normal few days after surgery. The GPT and GOT values were significantly different in between pre and post-op with agreed with current study which found no change in GPT or GOT level in post-op patient and no difference between patient and control, studies has been found that liver enzymes tent to return to their normal level few days after the operation.

The result of Khare and Sahani, study no significant change in TSB liver post-op. Measurement of lipid profile is important which give a clue to the cause of stone formation, hyperlipidemia is a triggering factor for stone formation, as stone composed of cholesterol [11]. A prospective study carried on by Menezes and Katamreddy, the aimed to evaluate the lipid profile in cholecystectomy patient, the result showed that significant differences in the lipid profiles in post cholecystectomy patient in which the level of total cholesterol, low density lipoprotein (LDL) cholesterol, very low density lipoprotein (VLDL) cholesterol and triglycerides is decreased, increase in the high density lipoprotein (HDL) cholesterol [12]. In the current study, CHOL, LDL and HDL show no significant change from the control group that disagree with [12]. Study, however, the level CHOL, LDL and HDL the range value of the both groups were normal. The level of TG and VLDL show a significant decrease in post cholecystectomy patient group than control group. A case control study done by Gill and Gupta, that aim to evaluate cholecystectomy on lipid profile in patients suffer from gallstones [13]. study involves 50 patients had gallstones and 30 healthy that approach current study sample size, with BMI 27.45 and 25.66 kg/m<sup>2</sup>, respectively.

Result show a significant decrease in CHOL and TG with significant increase in HDL levels after surgery, and non-significant change in VLDL that inconstant with current study, while LDL levels were not statistically changed that is constant with current result. Serum amylase is increased in gallstone disease due to induction of pancreatitis by stone blockage to biliary tree and not done routinely. The test is used to differentiate acute biliary pancreatitis, the current shows no significant change in S. amylase level in both patient and control. According to [14] study S. amylase is higher value in the biliary pancreatitis patient with positive predictive value of 78.8%. Lipase is another enzyme which used to diagnosis pancreatitis which tent to elevated extrahepatic gallstone disease, the current study found no significant change in post-op S. lipase in compare to control which is lie in the normal range value. No study has been found that evaluating S. lipase in post-op patient. Cholecystokinin is important regulator for gallbladder contraction post meal, any disturbance in CCK secretion or function will promote gallstones formation. According to [15] study which is a case control study enrolled 67 participant divided into 3 groups, healthy control (15), symptomatic gallstones (27) and cholecystectomy patient (25), result showed that Fasting CCK levels have no statistical significant difference between the three groups, but in post cholecystectomy patients, meal-stimulated plasma show a significant elevation in compared to controls. Those result are constant with current study result, as CCK level is statistically higher in post cholecystectomy patients in compare to control as p-value is 0.008. In Table 5, the

participant was divided according to their gender into female and male group that include patient and control, all the measured biomarkers were compared between patient and control groups in each gender separately from the other gender.

Result show no statistical significant changes in females between patient and control group regarding LFT which explained by returning of enzymes level to normal value soon after operation, GOT and GPT were in the normal range between patient and control, but ALP level was above the normal range in both groups. Lipid profile level show no statistical significant changes in females between patient and control group and all the result of both groups fall in the normal range. The same result for S. amylase, s. lipase and CCK show no statistical significant changes in females between patient and control group and all the result of both groups fall in the normal range. Regarding male group (Table 6) that show the same insignificant changes between patient and control group, except in the result of GPT which is significantly higher in patient group but both of them lie in the normal range, TG and VLDL are significantly lower in patient in compare to control group, and CCK is significantly higher in patient group in compare to control. No study has been found that compare result of LFT, lipid profile, S. amylase, S. lipase and cholecystokinin in post cholecystectomy patient to compare with current study result. In Table 7. the correlation between CCK and other measured markers is presented, result show no significant correlation between CCK and any other measured markers. No study has been found to compare current study result with, as no study evaluate the correlation between CCK and LFT, lipid profile, S. amylase and S. lipase in cholecystectomy patient.

## Acknowledgment

I would like to thank my thesis advisor, Assoc. Prof. Dr. Hakan ÇOLAK, for his patience, guidance and understanding.

## References

- [1] Njeze G. E. 2013. Gallstones. Nigerian journal of surgery: official publication of the Nigerian Surgical Research Society, 19(2), 49–55.
- [2] Portincasa, P., Molina-Molina, E., Garruti, G. and Wang, D. Q. 2019. Critical Care Aspects of Gallstone Disease. Journal of critical care medicine (Universitatea de Medicina si Farmacie din Targu-Mures), 5(1), 6–18.
- [3] Yeo, D. M. and Jung, S. E. 2018. Differentiation of acute cholecystitis from chronic cholecystitis: Determination of useful multidetector computed tomography findings. Medicine, 97(33).
- [4] Lammert, F., Gurusamy, K., Ko, C.W., Miquel, J.F., Méndez-Sánchez, N., Portincasa, P., Van Erpecum, K.J., Van Laarhoven, C.J. and Wang, D.Q.H. 2016. Gallstones. Nature reviews Disease primers, 2(1), 1-17.
- [5] Portincasa, P., Moschetta, A., & Palasciano, G. 2006. Cholesterol gallstone disease. Lancet (London, England), 368(9531), 230–239.
- [6] Bagaudinov, K.G., Saidov, S.S., Garilevich, B.A., Zubkov, A.D., Abdulaev, R.A. and Ovakimian, G.S. 2007. Improvement of extracorporeal shockwave cholelithotripsy in the comprehensive treatment of cholelithiasis. Klinicheskaia meditsina, 85(10), 56-59.
- [7] Ahmad N. Z. 2011. Routine testing of liver function before and after elective laparoscopic cholecystectomy: is it necessary? JSLS: Journal of the Society of Laparoendoscopic Surgeons, 15(1), 65–69.
- [8] O Hamad, S. and R Al-Luwaizi, K. 2013. Changes of liver enzymes and serum bilirubin after laparoscopic cholecystectomy. Annals of the College of Medicine, Mosul, 39(2), 113-117.
- [9] Sachdeva, S., Khan, Z., Ansari, M. A., Khalique, N. and Anees, A. 2011. Lifestyle and gallstone disease: scope for primary prevention. Indian journal of community medicine: official publication of Indian Association of Preventive & Social Medicine, 36(4), 263–267.
- [10] Maleknia, S. A. and Ebrahimi, N. 2020. Evaluation of Liver Function Tests and Serum Bilirubin Levels After Laparoscopic Cholecystectomy. Medical archives (Sarajevo, Bosnia and Herzegovina), 74(1), 24–27.
- [11] Khare, N. and Sahani, I. S 2018. Evaluation of Serum Bilirubin Level Alterations in Patients Undergoing Cholecystectomy: An Observational Study.
- [12] Menezes, J. V. F. and Katamreddy, R. R. 2019. The effect of cholecystectomy on the lipid profile of patients with gallstone disease: a prospective study. International Surgery Journal, 6(11), 4112-4116.



- [13] Gill, G. S. and Gupta, K. 2017. Pre-and Post-operative comparative analysis of serum lipid profile in patients with cholelithiasis. *International Journal of Applied and Basic Medical Research*, 7(3), 186.
- [14] Güngör, B., Çağlayan, K., Polat, C., Şeren, D., Erzurumlu, K. and Malazgirt, Z. 2011. The predictivity of serum biochemical markers in acute biliary pancreatitis. *International Scholarly Research Notices*, 3, 2-8.
- [15] McDonnell, C. O., Bailey, I., Stumpf, T., Walsh, T. N. and Johnson, C. D. 2002. The effect of cholecystectomy on plasma cholecystokinin. *The American journal of gastroenterology*, 97(9), 2189-2192.



## Study of Relationship Between Levels of Hepcidine Hormone and GDF15 for Patients with Prostatic Cancer and Their Clinical Importance

***Omer Zedan Khalaf KHALAF***<sup>1,\*</sup> , ***Ayşe Şahin YAĞLIOĞLU***<sup>2</sup> , ***Maysaa Jalal MAJEED***<sup>3</sup> 

<sup>1</sup>Çankırı Karatekin University, Faculty of Science and Arts, Department of Chemistry, Çankırı, Turkey

<sup>2</sup>Amasya University, Faculty of Science and Arts, Department of Chemistry, Amasya, Turkey

<sup>3</sup> University of Baghdad, Faculty of Medicine, Department of Biochemistry, Baghdad, Iraq

### Abstract

Prostate cancer (PCa) is a considered of malignancy worldwide, particularly among the elderly. In Europe, about 417.000 men were diagnosed with PCa for the first time in 2012. Since PCa is so diverse, there is a growing The development of novel biomarkers capable of predicting prognosis, cancer incidence, therapy effectiveness, & patient outcomes is critical. Additionally, biomarkers are required in advanced PCa that has progressed to CRPC following first therapy, it is possible to anticipate tumor growth and aggressiveness in connection to a range of potentially life-extending drugs. Hepcidin and Growth Differentiation Factor 15 have been shown to be present in significant concentrations in a variety of cancers (GDF-15). The levels of serum hepcidin and GDF-15 have been proven to be prognostic markers in cancer patients in the past. To determine the significance of hepcidin, Growth Differentiation Factor 15, Prostate-Specific Antigen, & several other associated Harmons in the prediction or early detection of prostate cancer, the investigators conducted a research. As a result, this research will be regarded as significant in the area of Iraqi patients.. There were substantial disparities in our research. ( $P \leq 0.05$ ) with Hepcidin Hormone (H. H.), C-Reactive Protein (C-RP), Growth Differentiation Factor 15 (GDF-15), & Follicle-Stimulating Hormone (FSH), Because of the high importance (correlation) shown by our study (H.H, C-RP, GDF15, & PSA) between the Patient Group and Control Group, it can be used these variables to precise prediction of prostate diseases. There are relationships of strength between Hepcidin Hormone variables and some biochemical variables such as Age, C - Reactive Protein (C-RP), Prostate-Specific Antigen (PSA), & Growth Differentiation Factor 15 (GDF-15).

**Keywords:** Prostate Cancer, Hepcidine, GDF15, PSA

### 1. Introduction

Cancer affects more than just a single cell or a community of homogeneous tumor cells. As a result, research into the mechanisms that modulate the tumour cells, particularly the relationship with tumor and stromal cells, as well as the immune response, is essential. Humans are adamant that cancer are being healed as soon as practicable; indeed, this isn't always the case. Humans, on the other hand, hold this belief. This prevalent ideas that have negative implications for certain types of cancer, such as prostate cancer [1]. Prostate cancer is the most common form of cancer among men in many countries. A man's lifetime risk of developing prostate cancer is about 30%, with a 10% to 11% chance of dying from it. Prostate cancer starts out small and then develops into an invasive, migratory, & metastatic disease. A localized prostate cancer is usually androgen-dependent and can be treated with surgery or other treatments such as radiation therapy [2]. A tubuloalveolar gland of the reproductive area makes up the male prostate gland. The genitourinary system of a male's body is situated inside the pelvic cavity. It is situated down part of the bladder and in front of the rectum. It is considered both muscular and glandular. The prostate gland in a young male weighs about 20 grams and has a volume similar to that of a golf ball (4×2×3cm). Because of benign conditions like prostate cancer (BPH) or cancerous conditions like adenocarcinoma, men are more likely to develop prostate cancer, the prostate volume rises with increasing the ménage. It is composed of 70 percent of overall glandular tissue and 30 percent of overall fibromuscular stroma [3, 4].

\* Corresponding author. e-mail address: maysaajmajeed@comed.uobaghdad.edu.iq

## 2. Materials and Methods

### 2.1. Premable of study

This study included two groups, first group included 60 person as control Group (Group A), while Second Group 70 person (patients group or Group B), in our study the total of cases 130 people, their ages between 26 - 66 year for analysis.

### 2.3. Apparatus and Biochemical kits

All the apparatus and material that used in this study listed in Table 1.

**Table 1.** Materials and Kits that used in study

Equipment and Apparatus	Company	Country
BioTek Elisa ELx800	BioTek	U S A
Roche Cobas c 311 Automated Chemistry Analyzer	Roche	Germany
Centrifuge PLC Series	Gemmy Industrial Corp.	Taiwan
Refrigerator	Bosch	Germany
Prostate Specific Antigen	mbH	Germany
Growth Differentiation Factor 15	MyBioSource	USA
Hepcidin	-	Germany
FSH	Monobid	USA
C reactive protein kit	Roche	Germany

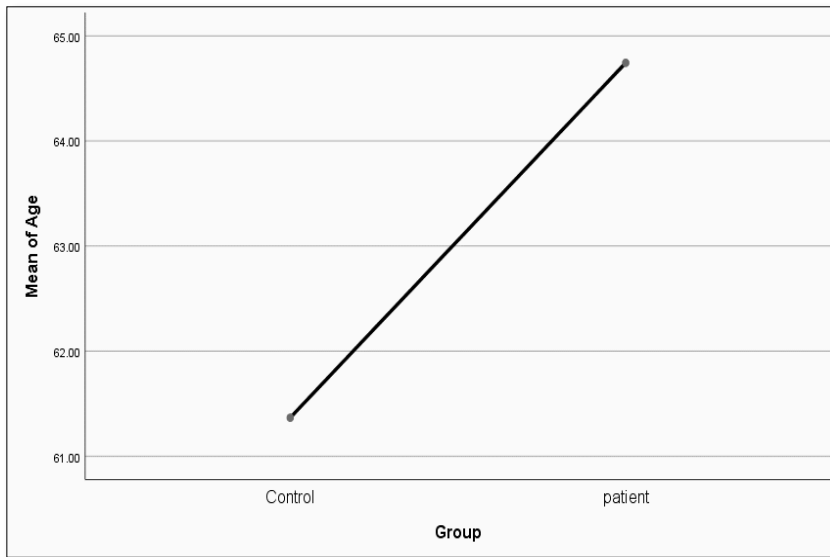
## 3. Results and Discussion

### 3.1. Prostate cancer Analysis

As can be seen in Table 1 and Figure 1., there were no statistically significant variations in mean age between Group A (Controls) and Group B (Patients), with Group A having a mean age of 61.3 9.26 years and Group B having a mean age of 64.7 10.8 years. While there are correlation between Hepcidin Hormone and age ( $r = 0.257^{**}$ , P-Value 0.003).

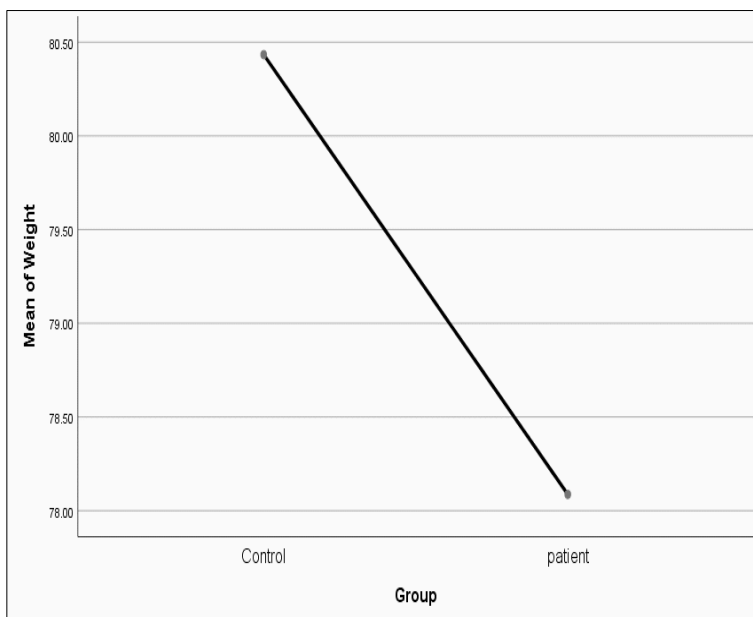
**Table 2.** Age in Patients and Control

Variable	Groups A Mean $\pm$ SD	Group B Mean $\pm$ SD	Sig.
Age	64.7 $\pm$ 10.8	38.3 $\pm$ 7.62	0.031
Weight	80.5 $\pm$ 12.9	78.9 $\pm$ 12.5	0.287
C.R.P	12.9 $\pm$ 30.6	92.5 $\pm$ 79.3	0.001
FSH	2.89 $\pm$ 3.37	4.88 $\pm$ 5.45	0.016
PSA	2.19 $\pm$ 0.57	36.4 $\pm$ 13.3	0.001
H.H	2.44 $\pm$ 1.91	5.47 $\pm$ 3.24	0.001
GDF15	33.3 $\pm$ 19.2	53.8 $\pm$ 50.8	0.004



**Figure 1.** The relation between Control group and patient group with Mean of age

As a result shown in Table 2 the mean of weight (kg) was has a no significant difference between control group (group A,  $80.5 \pm 12.9$ ) as compare to the patients group (B group,  $78.9 \pm 12.5$ ) (Figure 2). There are link between rheumatoid arthritis (RA) weights [5], this study agreed with our study. While don't there are correlation between Hecpidin Hormone and weight ( $r = 0.082$ , P-Value 0.354) (Figure 2). The association between BMI and risk of prostate cancer differed by stage and grade at diagnosis [6]. There are not was adiposity related positively to prostate cancer incidence [7].

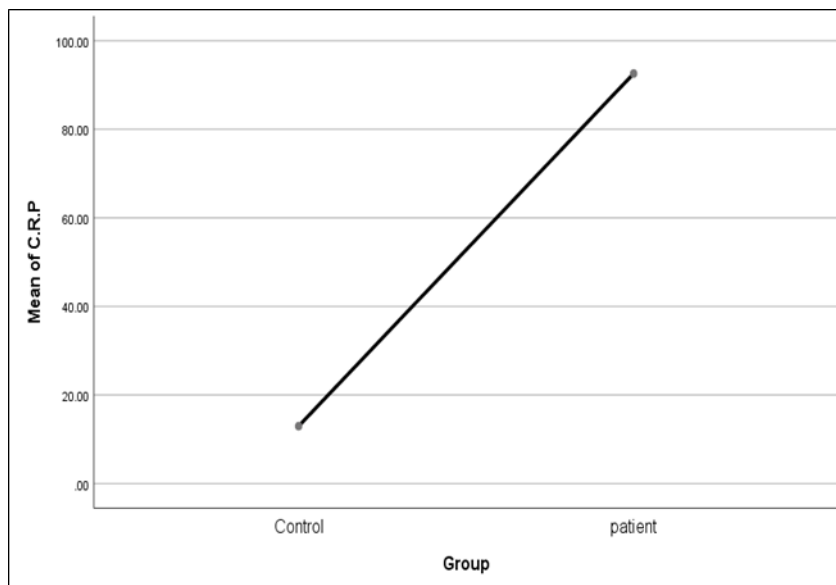


**Figure 2.** The relation between Control group and patient group with Mean of weight (Kg)

As indicated in Table 2 and Figure 3., there is a substantial difference in the mean C-reactive protein concentration (mg/dl) between the control group (group A) ( $12.9 \pm 30.6$ ) and the patient group (group B) ( $92.5 \pm 79.3$ ). As well as the mean of BMI (kg/m<sup>2</sup>) in group A was ( $28.32 \pm 3.60$ ), addition, the Correlation between Hecpidin Hormone and C-RP was strong ( $r=0.376^{**}$ , P-Value=0.001) showing in Table 3. In a study Steven Lehrer and other friends in 2005, there was also a significant correlation of CRP level with prostate-specific antigen (PSA) in those with cancer, & this agreement with our study. The level of C-reactive protein in another study is elevated in prostate cancer patients [8], and this agree with our study.

**Table 3.** Correlation between Hepcidin Hormone and Some Variables in all Case of Prostate cancer

Variables	Hepcidin Hormone	
	<i>R</i>	<i>P</i> -Value
Hepcidin Hormone - Age (years)	0.257**	0.003
Hepcidin Hormone - Weight (kg)	0.082	0.354
Hepcidin Hormone –C-RP (mg/dl)	0.376**	0.001
Hepcidin Hormone – FSH ( MU/ML)	0.163	0.063
Hepcidin Hormone – PSA (mg/dl)	0.454**	0.001
Hepcidin Hormone – Gdf15 (mg/dl)	0.220*	0.012
no risk: $P > 0.05$ ; ** highly significant at ( $P < 0.01$ ); * Statistically significant at ( $P < 0.05$ ); N.S. : non-significant.		

**Figure 3.** The relation between Control group and patient group with Mean of CRP

### 3.2. Hormons Results

#### 3.2.1. FSH

As shown in Table 2, the mean of FSH concentration was has a significant difference between the control group (group A,  $2.89 \pm 3.37$ ) as compared to the patients' group (B groups,  $4.88 \pm 5.45$ ) at  $P > 0.05$ , also the correlations with Hepcidin Hormone was no significant difference positively ( $r = 0.163$ ,  $P = 0.063$ ) as shown in Table 3. Immunohistochemistry revealed the found of FSH in PC3 and Du145 cells, as well as in human adenocarcinoma of the prostate [9]. In the study of Mariani et al., It has become clear recently recent interest focusing on gonadotropin, follicle-stimulating hormone (FSH). FSH is generated in and FSH receptors are expressed in the prostate, according to research conducted over the past decade [10]. Additionally, researchers discovered that prostate cancer alters FSH production: FSH levels are increased and receptor synthesis is enhanced in the malignant prostate. These findings corroborate previous research.

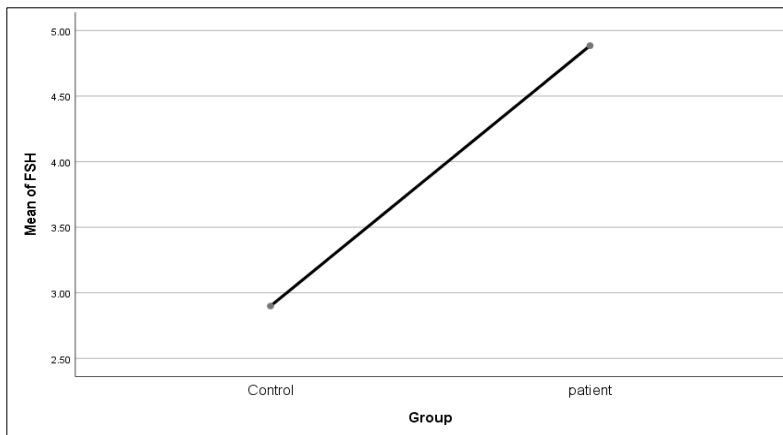


**Figure 4.** The relation between Control group and patient group with Mean of FSH

As shown in Table 2., The mean of PSA (mg/dl) in the Control group (Group A) there was ( $2.19 \pm 0.57$ ), a significant difference with patient's group (Group B), also, the correlation between Hepcidin Hormone and PSA was positive as shown in Table 3. These results agreed with a previous study [11], Serum PSA levels ranged from 4.0 to 9.9  $\mu$ g per liter, which means an elevation of PSA in men with prostate cancer. Prostate-specific antigen (PSA) may be elevated in men with prostate disease [12]. See Figure 5.

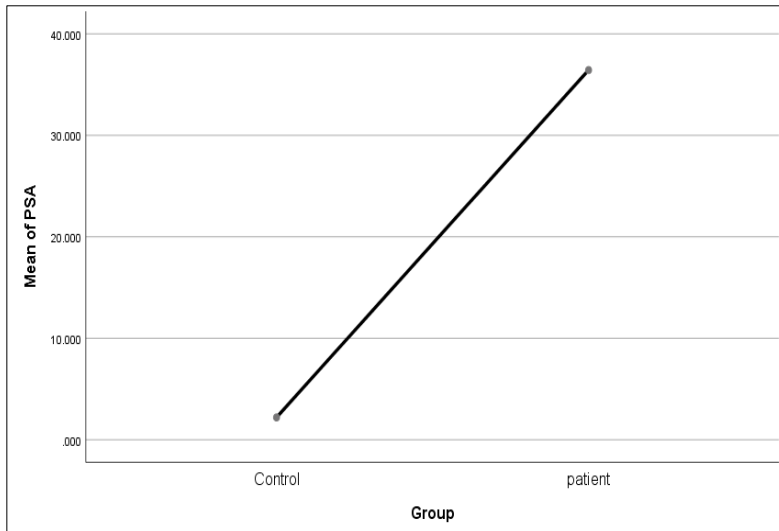


**Figure 5.** The relation between Control group and patient group with Mean of PSA

### 3.2.3. Hepcidin Hormone

Hepcidin hormone is a circulating peptide hormone produced by the human liver. It is a critical regulator of systemic iron absorption and recycling [13]. The data of this study showed that there were significant differences in level of Hepcidin Hormone (mg/dL) in Control group (group A) with patient (Group B) ( $2.44 \pm 1.91$ ;  $5.47 \pm 3.24$ ) respectively, as shown in Table 2 and Figure 6. Hepcidin hormone in patients with Prostate cancer increasing than in controls ( $p < 0.01$ ) [13]. High concentration of urea and creatinine in RA [14], there was a trend to higher serum hepcidin [15], this result shows agreed with our study.

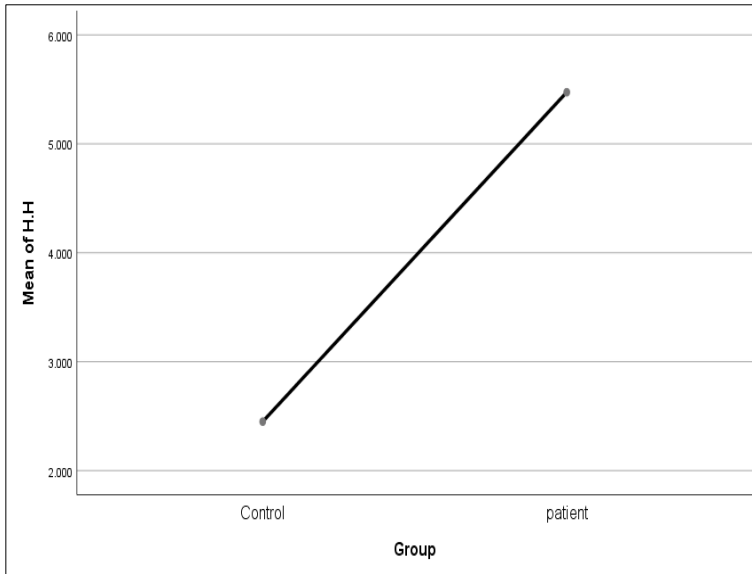


**Figure 6.** The relation between Control group and patient group with Mean of HH

### 3.2.4 GDF-15

The mean of GDF15 (mg/dl) in control group (Group A) was ( $5.25 \pm 0.91$ ), while patient group (Group B) Non a significant difference between group A with B, groups. Also, the correlation between Hepcidin Hormone and Gdf15 was therebare correlated ( $r=0.220^*$ ,  $P=0.012$ ) as showed in Table 3. (Figure 7). There was a correlation between prostate-specific antigen (PSA) and serum levels of hepcidin and GDF15. There was a correlation between serum GDF15 levels and serum hepcidin levels [15]. This result shows agree compared this study with our study.

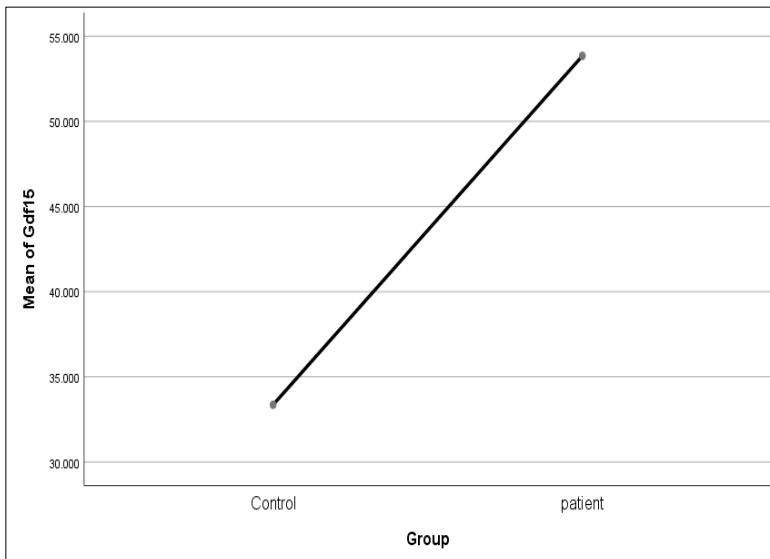


**Figure 7.** The relation between Control group and patient group with Mean of GDF15

### Acknowledgment

I would like to thank my thesis advisor, Prof. Dr. Ayşe Şahin YAĞLIOĞLU, for his patience, guidance and understanding.

## References

- [1] Jemal, A., Thomas, A., Murray, T. and Thun, M. 2002. Cancer statistics, 2002. *Ca-A Cancer Journal for Clinicians*, 52(1), 23-47.
- [2] Davison, B. J., Goldenberg, S. L., Gleave, M. E., & Degner, L. F. (2003). Provision of individualized information to men and their partners to facilitate treatment decision making in prostate cancer. *Oncology nursing forum*, 30(1), 107–114.
- [3] Ward, A. D., Crukley, C., McKenzie, C. A., Montreuil, J., Gibson, E., Romagnoli, C. and Fenster, A. 2012. Prostate: registration of digital histopathologic images to in vivo MR images acquired by using endorectal receive coil. *Radiology*, 263(3), 856-864.
- [4] Balk, S. P., Ko, Y. J. and Bubley, G. J. 2003. Biology of prostate-specific antigen. *Journal of clinical oncology*, 21(2), 383-391.
- [5] Pødenphant, J., Gotfredsen, A., Engelhart, M., Andersen, V., Heitmann, B. L. and Kondrup, J. 1996. Comparison of body composition by dual energy X-ray absorptiometry to other estimates of body composition during weight loss in obese patients with rheumatoid arthritis. *Scandinavian journal of clinical and laboratory investigation*, 56(7), 615-625.
- [6] Rodriguez, C., Freedland, S. J., Deka, A., Jacobs, E. J., McCullough, M. L., Patel, A. V. and Calle, E. E. 2007. Body mass index, weight change, and risk of prostate cancer in the Cancer Prevention Study II Nutrition Cohort. *Cancer Epidemiology and Prevention Biomarkers*, 16(1), 63-69.
- [7] Wright, M. E., Chang, S. C., Schatzkin, A., Albanes, D., Kipnis, V., Mouw, T. and Leitzmann, M. F. 2007. Prospective study of adiposity and weight change in relation to prostate cancer incidence and mortality. *Cancer: Interdisciplinary International Journal of the American Cancer Society*, 109(4), 675-684.
- [8] Stark, J. R., Li, H., Kraft, P., Kurth, T., Giovannucci, E. L., Stampfer, M. J. and Mucci, L. A. 2009. Circulating prediagnostic interleukin-6 and C-reactive protein and prostate cancer incidence and mortality. *International journal of cancer*, 124(11), 2683-2689.
- [9] Ben-Josef, E., YANG, S. Y., Ji, T. H., BIDART, J. M., Garde, S. V., Chopra, D. P. and Tang, D. G. 1999. Hormone-refractory prostate cancer cells express functional follicle-stimulating hormone receptor (FSHR). *The Journal of urology*, 161(3), 970-976.
- [10] Mariani, S., Salvatori, L., Basciani, S., Arizzi, M., Franco, G., Petrangeli, E. and Gnassi, L. 2006. Expression and cellular localization of follicle-stimulating hormone receptor in normal human prostate, benign prostatic hyperplasia and prostate cancer. *The Journal of urology*, 175(6), 2072-2077.
- [11] Catalona, W. J., Smith, D. S., Ratliff, T. L., Dodds, K. M., Coplen, D. E., Yuan, J. J., Petros, J. A. and Andriole, G. L. 1991. Measurement of prostate-specific antigen in serum as a screening test for prostate cancer. *The New England journal of medicine*, 324(17), 1156–1161.
- [12] Catalona, W. J., Southwick, P. C., Slawin, K. M., Partin, A. W., Brawer, M. K., Flanigan, R. C. and Lange, P. H. 2000. Comparison of percent free PSA, PSA density, and age-specific PSA cutoffs for prostate cancer detection and staging. *Urology*, 56(2), 255-260.
- [13] Tesfay, L., Clausen, K. A., Kim, J. W., Hegde, P., Wang, X., Miller, L. D., Deng, Z., Blanchette, N., Arvedson, T., Miranti, C. K., Babitt, J. L., Lin, H. Y., Peehl, D. M., Torti, F. M. and Torti, S. V. 2015. Hepcidin regulation in prostate and its disruption in prostate cancer. *Cancer research*, 75(11), 2254–2263.
- [14] Patrick, M., Heptinstall, S. and Doherty, M. 1989. Feverfew in rheumatoid arthritis: a double blind, placebo controlled study. *Annals of the rheumatic diseases*, 48(7), 547-549.
- [15] Winand, F. J., Boegemann, M., Gallitz, I., Hertle, L., Semjonow, A., Eveslage, M. and Steinbicker, A. U. 2014. GDF15 and Hepcidin as prognostic factors in patients with prostate Cancer. *Journal of Molecular Biomarkers and Diagnosis*, 5(6), 1.





## The insecticidal and AChE inhibitory activities of *Diplotaxis tenuifolia* essential oils and their determination of chemical contents

Ali Rıza TÜFEKÇİ\* 

Faculty of Science, Department of Chemistry, Cankiri Karatekin University, Cankiri, Türkiye

### Abstract

In the scope of this study, Flowers and leaves of *Diplotaxis tenuifolia* plant collected from Çankırı province were separated from each other. Essential oils (EOs) were obtained from these parts separately by using the method of steam distillation with neo-clavenger apparatus. Firstly, we have investigated contact toxicity effects of EOs. Contact activity test of essential oils were conducted on *Sitophilus granarius* and *Rhyzopertha dominica* species. In contact activity studies with *S. granarius* and *R. dominica*, larvae of 3., 4. and 5. stages were used. Finally, the effects of essential oils, which are thought to be associated with insecticidal activities, on acetylcholine esterase enzyme were evaluated. The major constituent of the essential oils extracted leaf (DTL-EO) were identified as 1-Isothiocyanato-4-(methylthio) butane (% 27.21), Isophytol (%44.15) and Squalene (% 8.41) by comparison of mass spectra. The major constituent of the essential oils extracted flower (DTF-EO) were identified as 1-Isothiocyanato-4-(methylthio) butane (%84.03), 2-thianonane (% 4.81) and 2-pentadecanone, 6,10,14-trimethyl (% 2.08) by comparison of mass spectra. Experimental results showed that DTL and DTF oils activate the acetylcholine esterase enzyme by % 70-85. These results indicated that essential oil of *D. tenuifolia* have significant potential which merits to be studied further in possible applications as contact insecticide in the control of *S. granarius* and *R. dominica*. The major constituent (91%) of the oil was identified as 5-methylthiopentananitrile by comparison of its mass spectra.

**Keywords:** *Diplotaxis tenuifolia*, Essential Oil, Insecticidal activity, Enzyme activity, Chemical analysis

### 1. Introduction

Plants constitute the first rank of basic food sources all over the world. Naturally, being in this first place means that it has been attacked from outside many times. Like all living things, plants interact with many diseases and pests. These harmful organisms are harmful to plants by feeding directly from plants, laying eggs, forming hosts and causing different disease factors [1]. It is known that plants have various defense mechanisms to protect themselves from pests. As a result of the biochemical defense mechanism in the plant, it synthesizes some chemicals and these secondary metabolites have an important role in the plant-harmful relations. These metabolites, which have behavioral and physiological effects on pests, are divided into groups such as terpenoids, flavonoids, amines, glycosides, alkaloids, phenols and saponins [2]. It is also referred to with titles such as herbal insecticides (insecticide drugs), natural insecticides and pheromones. Before the discovery of organic insecticides containing chlorine and phosphorus groups (1930-1940), plant-based insecticides were used in the control of crop pests in agricultural areas. Over the years, synthetic insecticides have become more common to use because they are more effective and have a longer duration of action than herbal insecticides. As technology develops, synthetic insecticides can be obtained more cheaply in developed countries, which has increased the interest in them. However, as a result of the unconscious use of synthetic insecticides over time, toxic effects such as drug resistance in pests, negative effects on human and animal health, residue problem and environmental pollution have been revealed by scientific studies. For centuries, human beings have used different methods to protect their crops from insects and other pests, both in the field and in the post-harvest warehouse. In our country, most of the time, warehouse products are carried out in the form of chemical control from pests. Among these struggles, the use of plant extracts and essential oils against pests has an important place. It has been demonstrated that volatile,

\* Corresponding author. e-mail address: areb@karatekin.edu.tr

repellant, antifeedant, growth and reproduction inhibitory effects against pests, most of which are obtained from plants, are toxic [3].

The vast majority of insecticides kill insects by acting on the central nervous system. The main cause of death is the special sensitivity of the nervous system. Even insecticides, whose primary targets are often other targets, exert their final effects on the nervous system. When interacting with the insecticide, the body has a strong counter-mechanism with metabolic breakdown and excretion mechanisms that reduce the insecticide's effect [4]. The most important feature of nerve cells is that they receive and respond to the signals coming from the internal and external environment of a living thing, and transmit the warnings to very long distances. Neurons do this with their thin cytoplasmic extensions [5]. *Sitophilus granarius* and *Rhyzopertha dominica* are pests causing damage in stored cereal crops. It has been reported that losses from insects in grains and legumes can reach up to 40% in countries where modern storage techniques are not available for these two storage pests [6].

The mechanism of action of insecticides on insects is becoming more elucidated by the day. The importance of the enzyme system in insects has emerged. Inhibition or activation of acetylcholinesterase (AChE) by natural insecticides can affect the movement and balance of the organism or organisms exposed to it. AChE is typically synthesized in nerve, muscle, and some blood-related cells. The enzyme is localized extracellularly in excitable tissues, both nerve and muscle. The enzyme acetylcholinesterase hydrolyzes acetylcholine to choline and acetic acid. The formed choline is transported back to the nerve centers to form new ACh molecules [7]. Acetylcholine is a neurotransmitter found at the intersections of nerves and muscles, in lymph nodes in the visceral motor systems, and in various parts of the central nervous system. Studies show that acetylcholine affects the speed of individual neurons. AChE inhibitors are used in the treatment of Alzheimer's disease, glaucoma, smooth muscle weakness and various autonomic nervous system disorders [8].

*Diplotaxis tenuifolia* (L.) DC is a perennial species represented by 5 species in the flora of Turkey, found in waste land and nitrate-rich soils. It is widely grown in fallow areas, roadsides and plowed soils in Central Anatolia, Marmara and Black Sea regions. It continues to bloom during the period between april-november and can grow in all kinds of habitats as a drought-resistant species by staying green. It shows very good antifungal properties due to the nitrile, thiocyanate and isothiocyanate compounds it contains. Due to these properties, it may be possible to prevent fungal diseases such as rust disease that occurs in cultivated plants with suitable extracts or extracts to be prepared from the plant. For this reason, it can become an important plant in organic agriculture. It is stated in very few sources that the base leaves are used as a salad among the people as well as medicinally among the people [9]. *D. tenuifolia* is rich in vitamin C, carotenoids, flavonoids, glucosinolates and phenolics [10,11,12]. Phenolic compounds in their structure are naturally antioxidants and due to their radical scavenging abilities, they play an important role in reducing the risk of chronic diseases [13]. Glycosinolates are mostly found in the leaves of the *Diplotaxis* plant and are important compounds in terms of flavor, as they are broken down into isothiocyanates by the myrosinase enzyme when exposed to mechanical damage such as chopping, chewing, shredding, as well as heat treatment [14,15]. It has been scientifically proven that both glucosinolates and isothiocyanates have beneficial effects in protecting against many cancers and heart diseases, as well as nutritionally beneficial to the normal cell [16]. *D. tenuifolia* has volatile organic compounds with high volatile properties in the structure of aldehydes, ketones and alcohol, as well as sulfur and nitrogen-containing components, especially sulfide, in the rich sulphur and nitrogen-containing plant [17,18].

In this study, both insecticidal and acetylcholinesterase enzyme activities of essential oil obtained from flower and leaf parts of diplotaxis plant were determined. There are no reports of insecticidal and enzyme activity studies on the existing study plant in the literature. Therefore, insecticidal activity studies against these harmful species and acetylcholinesterase enzyme activities are reported for the first time.

## 2. Materials and Methods

### 2.1. Plant materials

*Diplotaxis tenuifolia* plant was collected from the inner parts of Çankırı Karatekin University Uluyazı campus in July-August and during the flowering period. The plant collected during this period was identified by Assoc. Prof. Melda DÖLARSLAN and included in the university herbarium.

### 2.2. Preparation of essential oil

One kilogram of flower (DTF) and leaf (DTL) parts of the plant were crushed and combined with a blender. The plant materials were processed for approximately 3 h in a Neo-Clevenger hydro distillation apparatus. The aqueous fraction collected in the water chamber of the Neo-Clevenger device was removed and placed in a separate separatory funnel. Liquid-liquid extraction was performed by adding chloroform to the separatory funnel. The portion passing into the organic solvent was separated and dried by adding anhydrous sodium sulfate. Finally, filtration was performed using blue band filterpaper. The essential oils (for flower code: DTF-EO and for leaf code: DTL-EO) were stored in amber glass bottles at 4°C.

### 2.3. GC-MS Analysis

Essential oils analysis of DTF and DTL extracts were carried by GC-MS performed on an Thermo Scientific Trace 1310 GC/MS system, equipped with a DB-5MS capillary column (30 m x 0.25 mm ID and 0.25 µm) according to Alkan et al 2021 [20]. Ultra-pure helium was used as a carrier gas at a flow rate of 1 ml/min, a split mode (60:1) 1 µL injections were used. Electron impact (EI) ion source were used at 70 eV. The injection site temperature was set at 280°C. The column oven temperature was programmed as follows: the initial column oven temperature was 60°C, hold for 3 min, ramp to 200°C at a rate of 10°C/min and held for 0 min and, ramp to 240°C at a rate of 5°C/min and hold for 5 min. The total run time was 30 min. The mass spectrometer conditions were as follows: transfer line and ion source temperature were 280°C. The percentages of the essential oil components were calculated using peak areas without any correction factors. Compounds in samples were identified comparing with those in the NIST and WILEY search database. Mass spectra were recorded in the m/z 50–550 mass range [19,21].

### 2.4. Acetylcholinesterase enzyme activity

The activities of essential oils against acetylcholinesterase enzyme were measured by making minor changes in the spectrophotometric method applied by Ellman et al [20]. AChE from electric eel was used, while acetylthiocholine iodide was employed as substrates of the reaction. Galantamine was used as a positive reference compound. Results are given as % inhibition and activation.

### 2.5. Insecticidal activity

The essential oil of *D. tenuifolia* were dissolved in acetone at a concentration of 10%. From the solution in this concentration, *Sitophilus granarius* and *Rhyzopertha dominica* insects were applied with a micro applicator considering the adulthood (1 µl/insect 3rd larval stage, 2 µl/insect 4th larval stage and 3 µl/insect). Acetone (1 µl/insect) was used as a blank control. As in the 2012 study of Karakoç and Gökçe, solutions of essential oils in the prepared concentration were applied to the dorsal surface of the thorax of insects with a micro applicator. After treatment, insects were transferred to 9 cm petri dishes containing 10 g of wheat. Insects were incubated in a climate chamber at 25±2 °C. Mortality was recorded after 24 hours. Each procedure was repeated three times and the whole experiment was repeated three different times. Twenty larvae were used for each replication [6, 22].

### 3. Results and Discussion

The results of GC-MS analysis are given in Table 1. In addition, the GC-MS chromatograms of both EOs are presented in Figure 1 and Figure 2. The major constituent of the essential oils extracted leaf (DTL-EO) were identified as 1-Isothiocyanato-4-(methylthio) butane (% 27.21), Isophytol (%44.15) and Squalene (% 8.41) respectively. For flower (DTF-EO) were 1-Isothiocyanato-4-(methylthio) butane (%84.03), 2-thianonane (% 4.81) and 2-pentadecanone, 6,10,14-trimethyl (% 2.08) respectively.

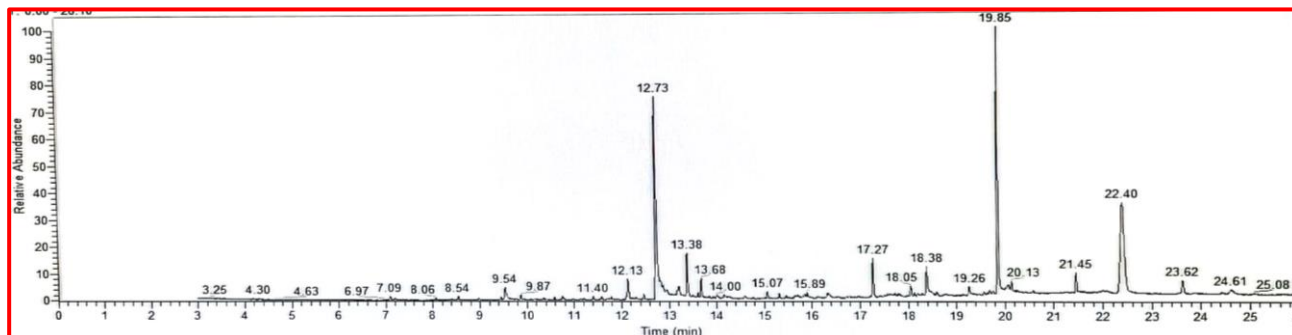


**Figure 1.** GC-MS chromatogram of essential oil obtained from the leaf of *D. tenuifolia* (DTL-EO)

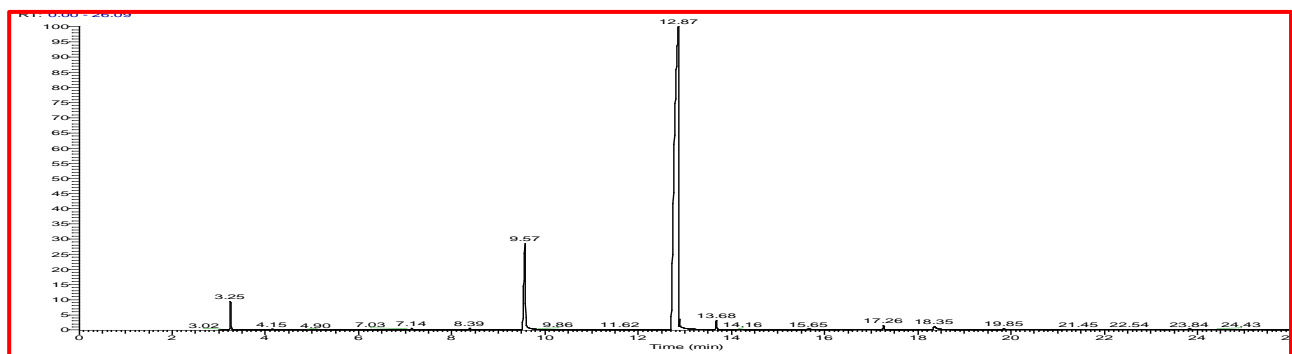


**Figure 2.** GC-MS chromatogram of essential oil obtained from the leaf of *D. tenuifolia* (DTF-EO)

**Table 1.** GC-MS results of essential oils for *D. tenuifolia* (DTF-EO and DTL-EO)

No	RT (min)	Compounds name	% Area	
			DTF-EO	DTL-EO
1	4.54	o-Xylene	0.18	-
2	7.03	Eucalyptol	0.17	-
3	7.09	Propylbenzene	-	0.12
4	7.14	2-Cyclohexen-1-one, 3,5,5-trimethyl	0.91	tr
5	8.06	Dimethyl sulfide	0.31	0.33
6	8.38	Isophorone	1.12	tr
3	8.55	2-Thianonane	4.81	0.13
4	9.54	Pentanenitrile, 5-(methylthio)	rr	3.42
5	12.14	(+)-3-Carene, 10-(acetylmethyl)	tr	3.87
6	12.78	1-Isothiocyanato-4-(methylthio) butane	84.03	27.21
7	13.20	Thiophene, 2-buthyl-5-propyl	tr	0.78
8	13.39	Alpha-ionone	tr	2.41
9	17.26	2-Pentadecanone, 6,10,14-trimethyl	2.08	3.57
10	18.39	Hexadecanoic acid	1.87	1.12
11	19.85	Isophytol	0.12	44.15
12	21.45	Docosane	0.87	0.89
13	22.40	Squalene	0.74	8.41
14	23.63	Nonacosane	0.12	0.25

**Table 2.** Contact toxicities of essential oils from *D. tenuifolia* on *S. granarius* ve *R. dominica*

	% Mortality	
	<i>R. dominica</i>	<i>S. granarius</i>
Control	6,6	0
DTL-EO	100	100
DTF-EO	100	100

Table 2 shows the results of contact toxicity activity. Contact toxicity activity study of essential oils obtained from leaves and flowers of *D. tenuifolia* plant on *S. granarius* and *R. dominica* storage pests was conducted. Accordingly, the highest activity at % 10 concentration was observed in essential oils obtained from the plant. According to the results obtained from both essential oils, %100 mortality rate was obtained. This activity is thought to originate from the main components of the essential oil obtained from the plant. These results showed that the essential oil of *D. tenuifolia* plant may have an important potential as contact insecticides in the control of *S. granarius* and *R. dominica*.

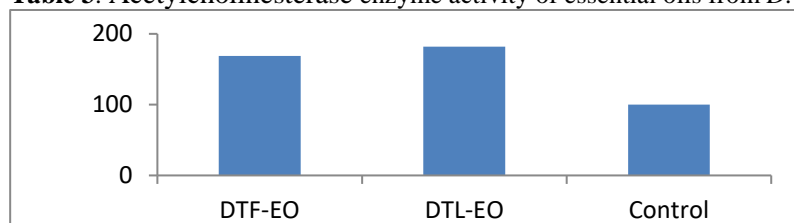
**Table 3.** Acetylcholinesterase enzyme activity of essential oils from *D. tenuifolia*

Table 3 shows the results of acetylcholinesterase enzyme activity. When the results are examined, it has been revealed that the essential oils obtained from two different parts have a very high activating feature against the acetylcholine esterase enzyme. Especially % 80-85 of DTL-EO coded essential oil activated this enzyme.

The scientific importance of wild arugula species has not been demonstrated much. *D. tenuifolia* is one of these species. While pharmacopoetic chemistry strives to meet the needs of all humanity, this plant species, which is considered to be inactive, has always been ignored. Because they contain such unique chemicals, they have different biological properties. This study represents the first report on the potential of essential oils from *D. tenuifolia* grown in Turkey on in vitro pesticide and acetylcholine esterase enzyme activity. It is these compounds that give the plant the heavy odor. Although the essential oil content varies quantitatively in the plant part, the main main components are 1-Isothiocyanato-4-(methylthio) butane, squalene and isophytol compounds. The compound 1-Isothiocyanato-4-(methylthio)butane is a compound containing nitrogen and sulfur. The analogue of this compound, erucin, has been reported to have a very high antimicrobial effect [23]. Our results showed that the concentration of essential oils dissolved with ten percent acetone against *S. granarius* and *R. dominica* insects completely killed both insect species. In order to explain the reason for this, a parallel study was conducted and the acetylcholine esterase enzyme activity of essential oils was examined. As a result, nearly 90% activation was observed on the existing enzyme. The reason for this is that the substances in the essential oil will increase the acetylcholine esterase enzyme and decrease the acetylcholine in the cell, and as a result, deformations in the nerve conduction will occur, and sudden brain and muscle death will occur. According to this proposed mechanism, the essential oil analysis result supporting the current conclusion was reached. Because of its high sulfur and nitrogen content, it has been used as an insecticide on harmful insect species for a long time. In fact, there is an increasing interest in natural origin components in this derivative.

## Acknowledgment

In this study, the financial support was provided by University of Çankırı Karatekin.

## References

- [1] Karakaş, M. (2018). Önemli Bazı Bitkisel İnsektisitler. *Turkish Journal of Scientific Reviews*, 11 (2): 32-37.
- [2] Shanker, C. & Solanki, K.R. (2000). Botanical insecticides: A historical perspective. *Asian agrihistory* 4(2), 21-30.
- [3] Topuz, E., & Madanlar, N. (2006). Bitkisel kökenli eterik yağlar ve zararlılara karşı kullanım olanakları. *Batı Akdeniz Tarımsal Araştırma Enstitüsü*, 23: 54-66.
- [4] Aydın, Ç., & Mammadov, R. (2017). İnsektisit aktivite gösteren bitkisel sekonder metabolitler ve etki mekanizması. *Marmara Pharmaceutical Journal*, 21(2017), 30-37.
- [5] O'Brien R.D., Insecticides -Action and Metabolism. Academic Press Inc. London. 1974, pp 332
- [6] Karakoç, Ö., Tüfekçi, A.R., Gül, F., Koldas, S., & Alkan, M. (2020). Essential oil composition and insecticidal activity of *Satureja boissieri* against *Sitophilus granarius* (Coleoptera:Curculionidae) and *Spodoptera littoralis* (Lepidoptera: Noctuidae). *Plant Protection Bulletin*, 60(2), 111-117.
- [7] Purves, D., Augustine, G.J., Fitzpatrick, D., Hall, W.C., LaMantia, A.S., McNamara, J.O., & White, L.E. (2008). Neuroscience. The 4th Edition. Sinauer Associates, Sunderland, MA, USA.
- [8] Taylor, P., Camp, S., & Radić, Z. (2009). Encyclopedia of Neuroscience (Squire, L.R., Editor-in-Chief). Academic Press, Elsevier Inc. pp. 5-7.
- [9] Erik, S. (2012). Çok yönlü ruderal bir tür: *Diplotaxis tenuifolia* (L) DC. *Ankara Üniversitesi Çevre Bilimleri Dergisi*, 4(1), 27-35.
- [10] Cavaiuolo, M., & A. Ferrante, A. (2014). Nitrates and glucosinolates as strong determinants of the nutritional quality in rocket leafy salads. *Nutrients*, 6(4), 1519-1538.
- [11] Hall, M.K.D., Jobling, J.J., & Rogers, G.S. (2012). Some perspectives on rocket as a vegetable crop: A review. *Veg. Crop Res. Bull.*, 76, 21-41.
- [12] Villatoro-Pulido, M., Priego-Capote, F., Álvarez-Sánchez, B., Saha, S., Philo, M., Obregón-Cano, S., De Haro-Bailón, S., Font, R., & Del Río-Celestino, M. (2013). An approach to the phytochemical profiling of rocket [*Eruca sativa* (Mill.) Thell]. *J. Sci. Food Agric*, 93(15), 3809-3819.
- [13] Mata, C.A.T., Proenca, C., Ferreira, A.R., Serralheiro, M.L.M., Nogueira, J.M.F., & Araújo, M.E.M. (2007). Antioxidant and antiacetylcholinesterase activities of five plants used as Portuguese food spices. *Food Chem*, 103(3), 778-786.
- [14] Bennett, R.N., Mellon, F.A., Botting, N.P., Eagles, J., Rosa, E.A.S., & Williamson, G. (2002). Identification of the major glucosinolate (4-mercaptobutyl glucosinolate) in leaves of *Eruca sativa* L. (salad rocket). *Phytochemistry*, 61(1), 25-30.
- [15] Bennett, R.N., Rosa, E.A.S., Mellon, F.A., & Kroon, P.A. (2006). Ontogenic profiling of glucosinolates, flavonoids, and other secondary metabolites in *Eruca sativa* (salad rocket), *Diplotaxis eruroides* (wall rocket), *Diplotaxis tenuifolia* (wild rocket), and *Bunias orientalis* (Turkish rocket). *J. Agric. Food Chem.*, 54(11), 4005-4015.
- [16] Traka, M., & Mithen, R. (2009). Glucosinolates, isothiocyanates and human health. *Phytochem. Rev.*, 8(1), 269-282.
- [17] Blazević, I., & Mastelić, J. (2008). Free and bound volatiles of rocket (*Eruca sativa* Mill.). *Flavour Frag. J.*, 23(4), 278-285.
- [18] Miyazawa, M., Maehara, T., & Kurose, K. (2002). Composition of the essential oil from leaves of *Eruca sativa*. *Flavour Frag. J.*, 17(3), 187-190.
- [19] Alkan, M., Güzel, M., Akşit, H., Bağdat, R.B., Alkan, F.R. & Evlice, E. (2021). Chemical components and insecticidal effects of essential oils from three lavender cultivars against adult *Sitophilus granarius* (L., 1758) (Coleoptera: Curculionidae). *Türk Entomol. Derg.*, 45(4), 405-416.
- [20] Ellman, G.L., Courtney, K.D., Andres, V., & Featherston, R.M. (1961). A new and rapid colorimetric determination of acetylcholinesterase activity. *Biochemical pharmacology*, 7, 88-95.
- [21] Aksit, H., Bayar, Y., Simsek, S., & Ulutas, Y. (2022). Chemical composition and antifungal activities of the essential oils of thymus species (*Thymus pectinatus*, *Thymus convolutus*, *Thymus vulgaris*) against plant pathogens. *Journal of Essential Oil Bearing Plants*, 25(1), 200-207
- [22] Karakoç Ö.C., & Gökçe A. (2012). Bitki ekstraktlarının *Spodoptera littoralis* (Lepidoptera: Noctuidae)'e olan kontak toksisiteleeri. *Türkiye Entomoloji Dergisi*, 36(3), 423-431.
- [23] Khoobchandani, M., Ojeswi, B.K., Ganesh, N., Srivastava, M.M., Gabbanini, S., Matera, R., Iori, R., & Valgimigli, L. (2010). Antimicrobial properties and analytical profile of traditional *Eruca sativa* seed oil. comparison with various aerial & root plant extracts. *Food Chem*. 120, 217-224.



## The Inhibition Effects Investigation of Metal Complexes with Coumarin Schiff Base on G6PD Activity

Zeyad Adil HAMEED<sup>1,\*</sup> , Ümmühan Özdemir ÖZMEN<sup>2</sup> , Şevki ADEM<sup>1</sup> , Volkan EYÜPOĞLU<sup>1</sup> 

<sup>1</sup>Department of Chemistry, Çankırı Karatekin University, Çankırı, Türkiye

<sup>2</sup>Department of Chemistry, Gazi University, Ankara, Türkiye

### Abstract

The G6PD enzyme is the primary focus of this investigation. Cancer cells cannot survive or spread without G6PD. A G6PD deficit of less than one percent has no influence on the onset or progression of cancer. Inhibition of G6PD, which regulates cell growth and division, has a negative impact on cell development. Glucometabolism definition of cancer In order to synthesize NADPH and DNA, cancer cells rely on G6PD. NADPH and DNA synthesis are both inhibited when SIRT2 is turned on. G6PD is activated by Ras, Src, and PI3K/AKT in cancer cells. Glioma, lung, and ovarian cancers are all known to have G6PD (ROS). G6PD has an impact on treatment outcomes. In bladder cancer, BCG expression is linked with a bad prognosis. G6PD may be used to predict glioma treatment sensitivity and risk. In this study, we investigated the effect of some Schiff bases and their complexes on G6PD activity *in vitro* by spectrophotometric methods. In addition, potential attachment patterns were estimated using the Molegro Virtual Docker software. Lead complexes have been shown to inhibit it. The IC<sub>50</sub> value of Pd(5MCTS)<sub>2</sub> as a G6PD inhibitor was 13.59 µM. And the docking analysis gave a score of -159.521 on the MolDock scale.

**Keywords:** Coumarin, Schiff base, Metal complexes, G6PD, Inhibition

### 1. Introduction

Cancer metabolism is characterized by increased glucose intake and poor lactate breakdown despite the presence of normal oxygen tension. There are a number of recent studies that have shown that the pentose phosphate pathway (PPP) plays an important part in the "Warburg effect" because of its function in recognizing both intracellular and extracellular signals. In light of this, the pathway's diverse roles and the dual-step nature of its response sequence are highlighted. In fact, the initial PPP oxidative phase is preferentially augmented under redox stress in order to increase NADPH equivalents for antioxidant responses. RNA and DNA are synthesized by bio-reductive syntheses, which result in high NADPH levels, when significant quantities of d-ribose-5-phosphate (R5P) are combined with high levels of bio-reductive syntheses and other coenzymes such as NADH, FADH<sub>2</sub>, and NADPH [2]. Warburg discovered glucose-6P dehydrogenase in 1931, and since then, PPP has been viewed as an intracellular pathway with a rate-limiting phase mediated by this enzyme (G6PD). PPP role in cancer metabolism was the primary focus of most studies on this enzyme, which indicated that G6PD activity is necessary for the survival and proliferation of cancer cells cultured *in vitro*. A G6PD deficit of less than one percent does not seem to have a significant impact on cancer incidence or progression in live persons, despite the fact that many cancers are more likely to be fatal in people with a G6PD deficiency. The sluggish pace of cytosolic PPP in delivering the enormous quantities of NADPH and R5P needed by actively proliferating cells should be bypassed by developing an alternative mechanism based on these epidemiological data. This enzyme, known as H6PD, is located in the endoplasmic reticulum of practically all eukaryotic cells and is capable of oxidizing a significant number of both phosphorylated hexoses and free hexoses (thus the alternative name of glucose dehydrogenase). New study shows that H6PD activity is elevated in many cancer types, adding to their proliferative and migrating potential, despite the fact that its function in glucose breakdown has been overlooked [3].

\* Corresponding author. E-mail address: zeyad95adil@gmail.com



## 2. Materials and Methods

Solutions used in activity measurement: 1 M Tris-HCl (pH= 8.0): 0.6057 g (5 mmol) of Tris was dissolved in 90 mL of distilled water. The pH was adjusted to 8.0 with HCl solution. Then the total volume was made up to 50 mL with water. 6 mM 6PGA: 9.1 mg (0.3 mmol) of 6PGA was taken and dissolved in some water. The volume was made up to 5 mL with water. 2mM NADP<sup>+</sup> Solution: 7.6 mg of NADP<sup>+</sup> (0.1 mmol) was taken and dissolved in some water. The volume was made up to 5 mL with water. Inhibitor stock solutions: Stock solutions were prepared by dissolving the compounds in DMSO at 1mg/mL.

Molecular docking studies: The 3D structures of the compounds whose inhibition effects were determined were downloaded from the PubMed (<https://pubchem.ncbi.nlm.nih.gov>) web page in sdf format. The crystal structure of the human 6PGD enzyme was downloaded from the Protein Data Bank web page in pdb format [1].

Docking protocol for Molegro Virtual Docker: The protein has been imported into the program. Water molecules on the crystal structure of the protein and heteroatoms other than the ligand were removed. Molecules were transferred to the program (Molegro 2019). The binding site of NADPH was determined for docking. X:16.05, Y:-90.18, Z:-90.79 coordination center and an area of 19 Å were chosen for docking as the docking area. The program was set to make 10 docking attempts for each ligand. The highest MolDock Scores were considered.

## 3. Results and Discussion

The inhibitory effect of three different compounds against the G6PD enzyme was investigated. Results obtained in vitro and in silico are presented in Table 1.

**Table 1.** The effects of compounds on G6PD enzyme activity

Compounds	G6PD IC <sub>50</sub> μM	MolDock Score	Rerank Score	HBond
Pd(3MeOCTS) <sub>2</sub>	8.453012	-172.867	-74.5334	-1,8399
Pd(3TbCTS) <sub>2</sub>	17.32868	-127.828	-106.631	0
Pd(5mCTS) <sub>2</sub>	13.59112	-126.251	-104.616	-2.0394

Pd(5MCTS)<sub>2</sub> compound exhibited inhibitory effects against G6PD enzyme with 13,59 μM IC<sub>50</sub> value. % activity – [Pd(5MCTS)<sub>2</sub>] graph was presented in Figure 1 and 2D interactions maps was given in Figure 2. According to the docking results, it was determined as -159.521 MolDock scores.

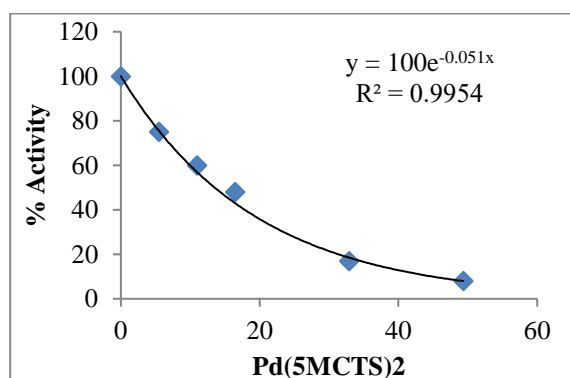


**Figure 1.** Pd(5MCTS)<sub>2</sub> compound % activity – [Pd(5MCTS)<sub>2</sub>] graph G6PD enzyme activity

When the 2D interaction map with the enzyme is examined, Lys366 and Arg370 amino acids made hydrogen bond interactions with Pd(5MCTS)<sub>2</sub>. In Figure 2, we notice the presence of hydrogen bonds, which are represented by the blue lines, and separating interactions, which are represented by the red lines.



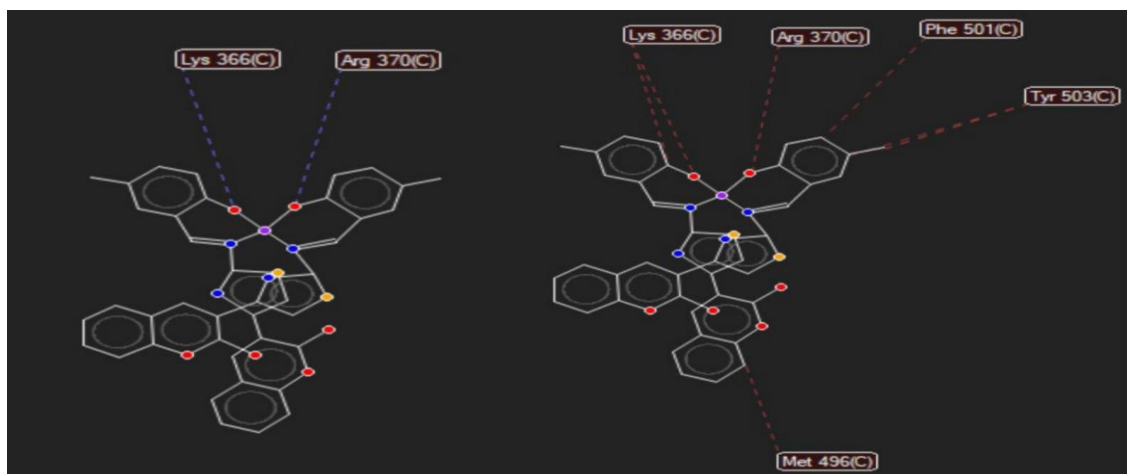


**Figure 2.** The interactions of Pd(5MCTS)<sub>2</sub> with the active region of G6PD

Pd(3MeOCTS)<sub>2</sub> compound exhibited inhibitory effects against G6PD enzyme with 8,45  $\mu$ M IC<sub>50</sub> value. % activity – [Pd(3MeOCTS)<sub>2</sub>] graph was presented in Figure 3 and 2D interactions maps was given in Figure 4. According to the docking results, it was determined as -159.521 MolDock scores.

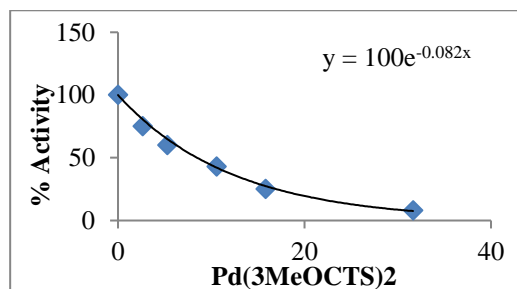


**Figure 3.** Pd(3MeOCTS)<sub>2</sub> compound % activities – [Pd(3MeOCTS)<sub>2</sub>] graph G6PD enzyme activity

When the 2D interaction map with the enzyme is examined, Tyr503 amino acids made hydrogen bond interactions with Pd(3MeOCTS)<sub>2</sub>. In Figure 4, we notice the presence of hydrogen bonds, which are represented by the blue lines, and separating interactions, which are represented by the red lines.



**Figure 4.** The interactions of Pd(3MeOCTS)<sub>2</sub> with the active region of G6PD

$\text{Pd}(\text{3TbCTS})_2$  compound exhibited inhibitory effects against G6PD enzyme with 17,32  $\mu\text{M}$   $\text{IC}_{50}$  value. % activity –  $[\text{Pd}(\text{3TbCTS})_2]$  graph was presented in Figure 5 and 2D interactions maps was given in Figure 6. According to the docking results, it was determined as -159.521 MolDock scores.

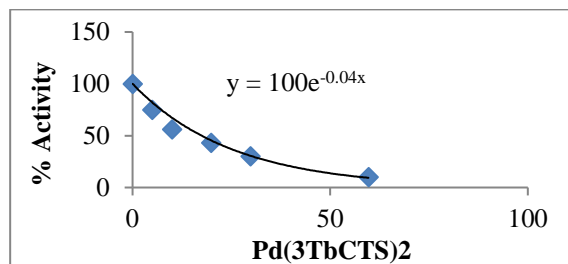


**Figure 5.**  $\text{Pd}(\text{3TbCTS})_2$  compound % activities –  $[\text{Pd}(\text{3TbCTS})_2]$  graph G6PD enzyme activity

When the 2D interaction map with the enzyme is examined, Tyr 503 and Asn 363 amino acids made hydrogen bond interactions with  $\text{Pd}(\text{3TbCTS})_2$ . In Figure 6, we notice the presence of hydrogen bonds, which are represented by the blue lines, and separating interactions, which are represented by the red lines.

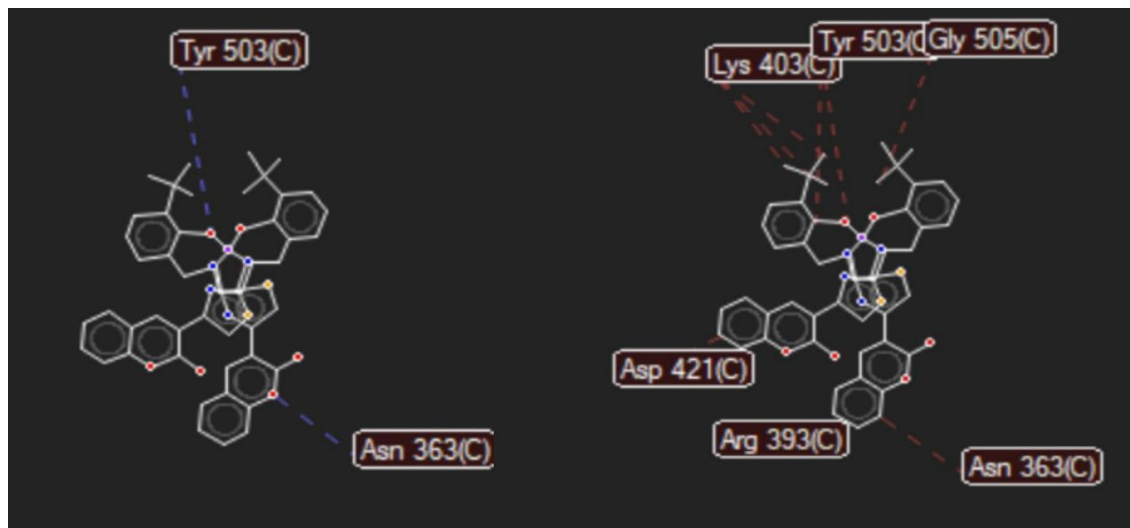


**Figure 6.** The interactions of  $\text{Pd}(\text{3TbCTS})_2$  with the active region of G6PD

#### 4. Conclusion

The relationship between the G6PD enzyme and cancer is in order to control the development and death of cells, G6PD plays an important role in signaling. Tumors and malignancies are associated with faulty activation of G6PD in rapidly expanding cancer cells. If G6PD is a therapeutic target, it opens up the possibility that current anticancer drugs can be combined with it to combat cancer resistance. Methods using G6PD inhibitors in the form of chemical or molecular inhibitors have commonly been developed. G6PD inhibitors are developed on the basis of metabolic modification. To avoid fast transformation, tumor cell proliferation, metastatic spread, as well as heterogeneity, redox homeostasis and protein-protein interactions are critical. We can explore the role of G6PD in cancer.

#### References

- [1] Au, S. W., Gover, S., Lam, V. M., and Adams, M. J. 2000. Human glucose-6-phosphate dehydrogenase: the crystal structure reveals a structural NADP<sup>+</sup> molecule and provides insights into enzyme deficiency. *Structure.*, 8: 293-303.
- [2] Senesi, S., Csala, M., Marcolongo, P., Fulceri, R., Mandl, J., Banhegyi, G. and Benedetti, A. 2010. Hexose-6-phosphate dehydrogenase in the endoplasmic reticulum., 391:1–8.
- [3] Tsachaki, M., Mladenovic, N., Štambergová, H., Birk, J. and Odermatt, A. 2018. Hexose-6-phosphate

dehydrogenase controls cancer cell proliferation and migration through pleiotropic effects on the unfolded-protein response, calcium homeostasis, and redox balance. *The FASEB Journal.*, 32: 2690-2705.



# Production and Characterization of Nano-Sized Calcium Carbonate-Zinc Oxide Composites

***Maher JAWAD KADHIM KADHIM*<sup>1</sup> , *Muhammed Bora AKIN*<sup>2\*</sup> **

<sup>1</sup> Ministry of Oil - South Refineries Company, Dhi Qar, Iraq

<sup>2</sup> Faculty of Engineering, Department of Chemical Engineering, Çankırı Karatekin University, Çankırı, Türkiye

## Abstract

Zinc oxide has attracted significant attention due to its similar properties with titanium oxide. Zinc oxide is non-toxic, chemically stable, environmentally friendly, easy to manufacture, and less expensive than TiO<sub>2</sub> [1-3]. Since it has a wide band gap of about 3.2 eV (3.37 eV for wurzite), it has been proven by various studies to be an excellent photocatalyst for the degradation and energy storage of organic pollutants [4-6]. Creating a composite photocatalyst is also a successful approach. Composite photocatalysts such as ZnO/SnO<sub>2</sub>, NiO/TiO<sub>2</sub>, ZnO/In<sub>2</sub>O<sub>3</sub>, and p-ZnO/TiO<sub>2</sub> have been extensively investigated [7-9]. The results show that the activity of the composite photocatalyst is higher than that found alone [10-15]. In this study, the synthesis and characterization of CaCO<sub>3</sub>/ZnO composite is carried out. (This study was made from the thesis work of the first ranked student.)

**Keywords:** Composite, CaCO<sub>3</sub>, Calcium carbonate, ZnO, Zinc oxide

## 1. Introduction

Calcium carbonate (CaCO<sub>3</sub>) is a kind of chemical compound popularly known as limestone. CaCO<sub>3</sub> is abundant in nature. Conversely, the crystal form of zinc oxide (ZnO), zincite mineral is rare in nature. Zinc oxide used many areas such as in the rubber industry, concrete manufacture, medical applications. Beyond all areas of use, its photocatalytic properties and being cheaper than TiO<sub>2</sub>, which is an effective photocatalyst, allowed its use as a catalyst to be investigated. The most important principle for the formation of photocatalysis is the voids in the crystal structure. These voids will be more abundant in a crystal with imperfections than in a perfect crystal. These gaps can be provided with the additives used during crystallization. The excessive amount of this substance, also known as impurity, causes the emergence of composite materials with new properties. Many composite photocatalysts such as ZnO/SnO<sub>2</sub>, NiO/TiO<sub>2</sub>, ZnO/In<sub>2</sub>O<sub>3</sub> and p-ZnO/TiO<sub>2</sub> have been synthesized and characterized. [7-9]

In this study, nano sized CaCO<sub>3</sub>-ZnO composites were synthesized by hydrothermal process. The size and morphological properties of the synthesized composites were characterized by SEM, XRD and BET analyses.

## 2. Materials and Methods

The reactants used in the experiments to synthesize composite were chosen as calcium chloride dihydrate (ACS reagent >99%), sodium carbonate (ACS reagent >99.5%), zinc nitrate hexahydrate (ACS reagent >99%) and sodium hydroxide (ACS reagent >98%). Solutions were prepared using reactants using Type II water produced from Merck Millipore. Reactant concentrations were kept [CaCl<sub>2</sub>]=[Na<sub>2</sub>CO<sub>3</sub>]=0.1 M and [Zn(NO<sub>3</sub>)<sub>2</sub>]=[NaOH]=0.03 M in each experiment. The additive concentration was changed between 0 and 150 mg/L. Initial pH value was tuned 10. The reactions were carried out in a 1 L jacketed glass-lid reactor and the temperature was kept constant at 25°C using cooled - circulated water bath. A magnetic stirrer (Heidolph MR Hei Tech) was used in the experiments and the mixing speed was set as 300 rpm. The precipitate, which is filtered and dried after washing was dried in a vacuum oven at 80 °C about 12 hours. XRD, SEM and BET analyzes of the obtained powder were made. X-ray diffraction Bruker D8 Discover instrument was used in the investigation of the powder materials. The composite structure was investigated by comparing the scan results with the International Center for Diffraction Data (ICDD) database. 2Theta values ranged from 15° to 90° in

\* Corresponding author. e-mail address: mbakin@karatekin.edu.tr

XRD analysis scans. SEM microphotographs taken with a Carl Zeiss Sigma 300 VP field emission scanning electron microscope were used to investigate the size and morphology of the synthesized composites. Brunauer–Emmett–Teller (BET) specific surface analyzes were performed using the Quantachrome Nova Touch LX4 instrument for determination the specific surface area of the synthesized materials. BET specific surface area measurements were made by multi-point nitrogen adsorption isotherm at 77K after degasing the composites with helium flow for 10 hours at 80 °C.

### 3. Results and Discussion

The peak values obtained in XRD analyzes were investigated, and as a result of this investigation, it was determined that calcite/zincite composite were formed. All of the materials synthesized with no additives, in the presence of 5, 50, and 150 mg/L additives are calcite/zincite composite (Figure 1).

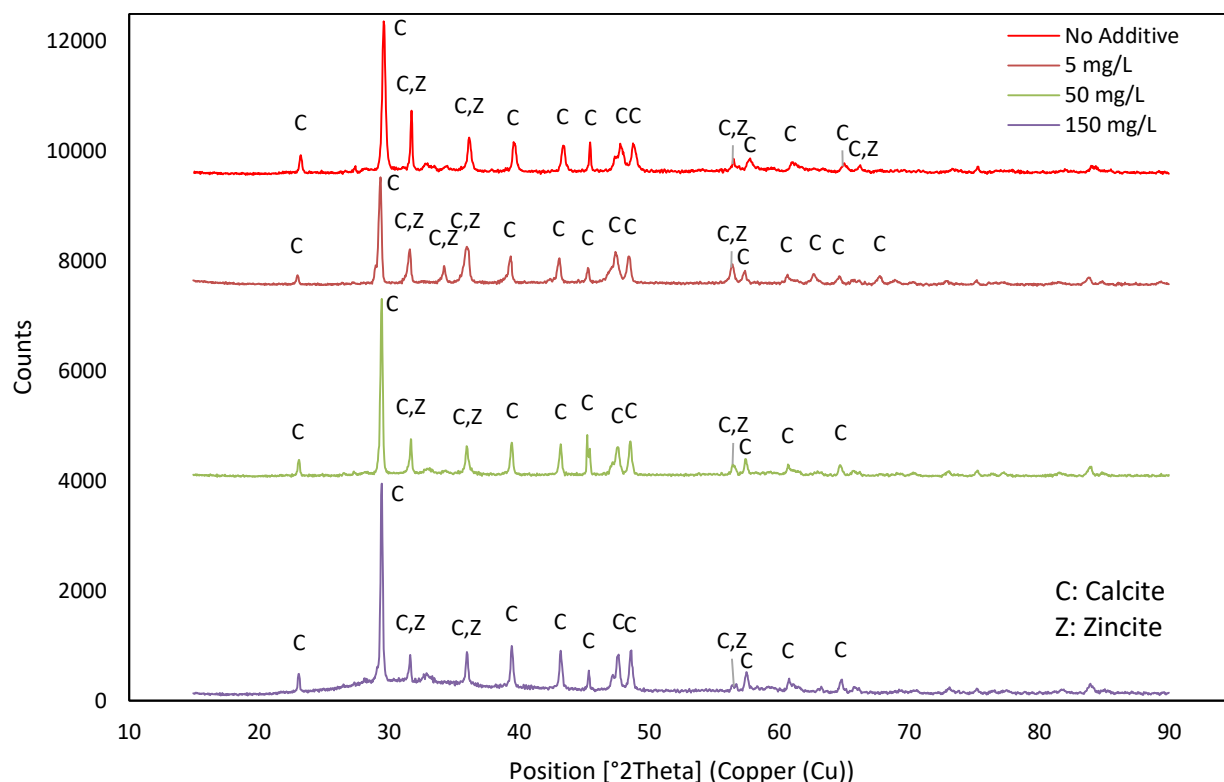


**Figure 1.** XRD analyses of the composites: (a) No additive, (b) 5 mg/L, (c) 50 mg/L, (d) 150 mg/L.

As a result of the comparison made from the ICDD database for synthesized materials, it is seen that peaks of the calcite match JCPDS 98-007-9222 and the zincite peaks match JCPDS 98-002-8922.

In SEM microphotograph analyses, it was seen that calcite/zincite composite material was synthesized in all experiments. In all SEM photographs, it was observed that the calcite crystals surrounded by the nano-zincite crystals (Figure 2), so that the calcite crystals remained embedded and agglomeration occurred in many areas. In the SEM images of the material obtained as a result of the experiment without additives, it was seen that the average composite particle size was approximately 14  $\mu\text{m}$  (Figure 2a). It was observed that the diameters of the composite spheres decreased with the increase in the amount of additive. It is seen that the composite particles are spherical and approximately 12  $\mu\text{m}$  in diameter (Figure 2b, 2c). In the photograph taken at higher magnification, it is seen that the zinkite crystals are generally in the form of rods. (Figure 2d).



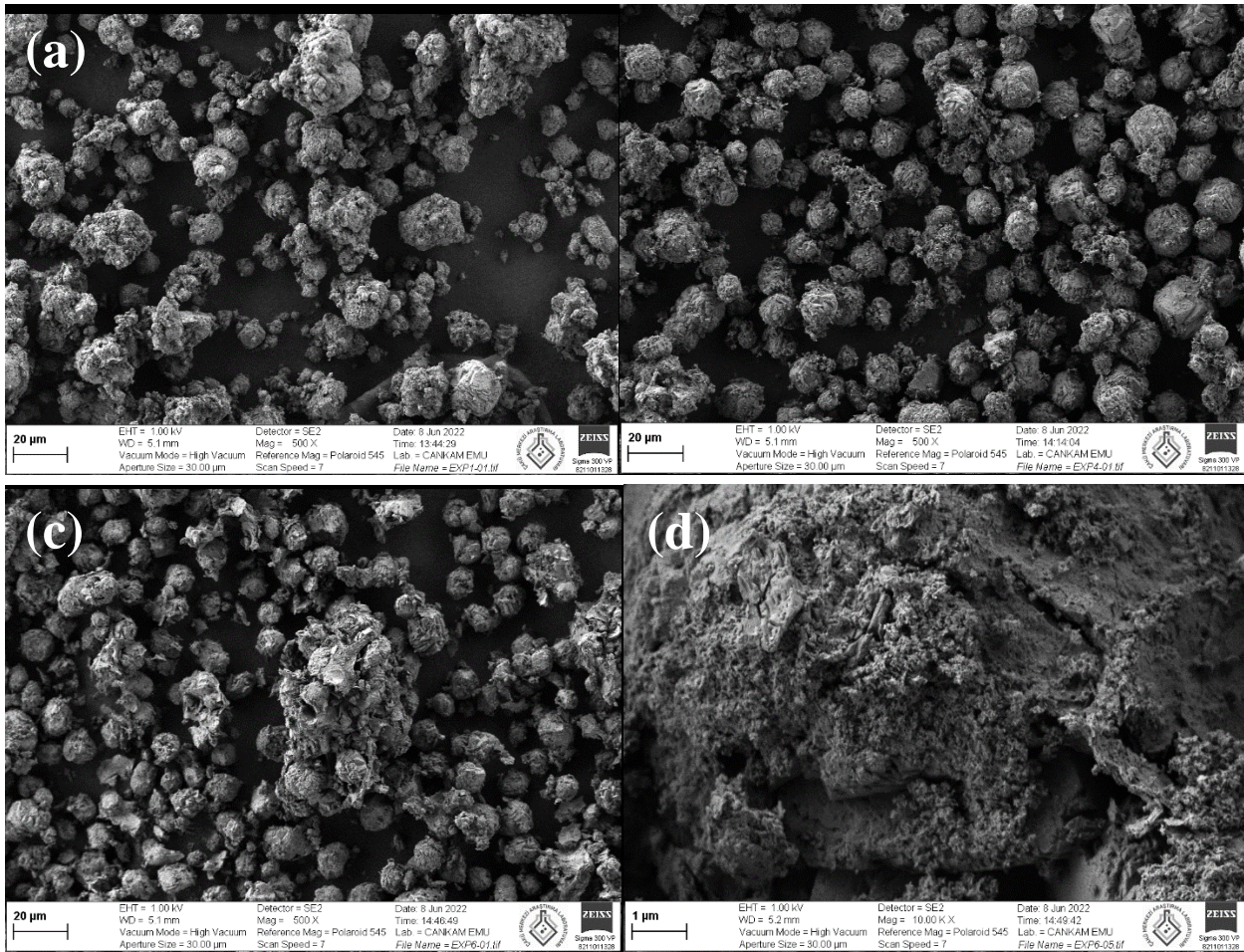


**Figure 2.** SEM micrographs showing the morphology of composite in different additive amount: (a) No additive; (b) 5 mg/L; (c) 50 mg/L; (d) 50 mg/L (higher magnification).

The BET specific surface area value increase with the increase in the amount of additive due to the increase nano-sized ZnO crystals synthesized in the presence of additives (Figure 3). Although the zincite crystals produced on the composite material are produced in nano size, it is thought that the agglomeration behavior on the material affects the BET surface area value. Thus, it can be explained that the increase in the BET surface area stopped after the presence of 5 mg/L additive. In the experiments, the highest BET surface area was obtained as 14.91 m<sup>2</sup>/g.

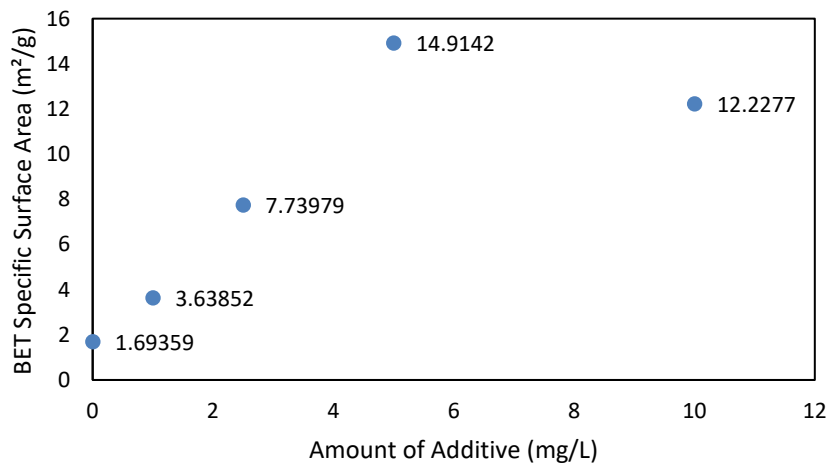


**Figure 3.** Plot of BET specific surface area with amount of additive

#### 4. Conclusion

In this study,  $\text{CaCO}_3$ -ZnO nano-composites were synthesized using hydrothermal method. In the presence of additive, calcium chloride ( $\text{CaCl}_2$ ) and sodium carbonate ( $\text{Na}_2\text{CO}_3$ ) solutions supported  $\text{CaCO}_3$  formation, composite synthesis was successful using zinc nitrate hexahydrate ( $\text{Zn}(\text{NO}_3)_2 \cdot 6\text{H}_2\text{O}$ ) and sodium hydroxide ( $\text{NaOH}$ ) in the simultaneous formation of nano-ZnO, and the synthesized composites were characterized by SEM, XRD and BET analyses. Experiments were carried out at  $25^\circ\text{C}$ , at a stirring speed of 300 rpm. In experiments, reactant solutions were equimolar and kept  $[\text{CaCl}_2]=[\text{Na}_2\text{CO}_3]=0.1 \text{ M}$  and  $[\text{Zn}(\text{NO}_3)_2]=[\text{NaOH}]=0.03 \text{ M}$ . Analysis of all materials synthesized under these conditions showed that  $\text{CaCO}_3$ -ZnO composites were successfully obtained. Increase in crystal size is observed with the increase in the concentration of additive. It was observed that nano-sized ZnO crystals accumulated on micron-sized  $\text{CaCO}_3$  crystals. It was also determined that the BET specific surface area decreased with the increase in amount of additive.

#### Acknowledgement

In this study, the authors declare that there is no conflict of interest and would like to thank Çankırı Karatekin University, Department of Chemical Engineering for their support of the laboratory studies.

#### References

- [1] Pauporté, T., & Rathouský, J. (2007). Electrodeposited Mesoporous ZnO Thin Films as Efficient Photocatalysts for the Degradation of Dye Pollutants. *The Journal of Physical Chemistry C*, 111(21), 7639–7644.
- [2] Qiu, X., Li, L., Zheng, J., Liu, J., Sun, X., & Li, G. (2008). Origin of the Enhanced Photocatalytic Activities of Semiconductors: A Case Study of ZnO Doped with  $\text{Mg}^{2+}$ . *The Journal of Physical Chemistry C*, 112(32), 12242–12248.
- [3] Yu, J., & Yu, X. (2008). Hydrothermal Synthesis and Photocatalytic Activity of Zinc Oxide Hollow Spheres. *Environmental Science & Technology*, 42(13), 4902–4907.
- [4] Mezni, A., Mlayah, A., Serin, V., & Smiri, L. S. (2014). Synthesis of hybrid Au-ZnO nanoparticles using a one pot polyol process. *Materials Chemistry and Physics*, 147(3), 496–503.
- [5] Ong, C. B., Ng, L. Y., & Mohammad, A. W. (2018). A review of ZnO nanoparticles as solar photocatalysts: Synthesis, mechanisms and applications. *Renewable and Sustainable Energy Reviews*, 81(July 2016), 536–551.
- [6] Zhang, Y., Ram, M. K., Stefanakos, E. K., & Goswami, D. Y. (2012). Synthesis, characterization, and applications of ZnO nanowires. *Journal of Nanomaterials*, 2012. <https://doi.org/10.1155/2012/624520>
- [7] Shifu, C., Lei, C., Shen, G., & Gengyu, C. (2006). The preparation of coupled  $\text{SnO}_2/\text{TiO}_2$  photocatalyst by ball milling. *Materials Chemistry and Physics*, 98, 116–120.
- [8] Shifu, C., Sujuan, Z., Wei, L., & Wei, Z. (2008). Preparation and activity evaluation of p–n junction photocatalyst  $\text{NiO}/\text{TiO}_2$ . *Journal of Hazardous Materials*, 155(1), 320–326.
- [9] Wang, Z., Huang, B., Dai, Y., Qin, X., Zhang, X., Wang, P., Liu, H., & Yu, J. (2009). Highly Photocatalytic ZnO/ $\text{In}_2\text{O}_3$  Heteronanostructures Synthesized by a Coprecipitation Method. *The Journal of Physical Chemistry C*, 113(11), 4612–4617.
- [10] Cun, W., Jincai, Z., Xinming, W., Bixian, M., Guoying, S., Ping'an, P., & Jiamo, F. (2002). Preparation, characterization and photocatalytic activity of nano-sized ZnO/ $\text{SnO}_2$  coupled photocatalysts. *Applied Catalysis B: Environmental*, 39(3), 269–279.
- [11] Hong, R. Y., Zhang, S. Z., Di, G. Q., Li, H. Z., Zheng, Y., Ding, J., & Wei, D. G. (2008). Preparation, characterization and application of  $\text{Fe}_3\text{O}_4/\text{ZnO}$  core/shell magnetic nanoparticles. *Materials Research Bulletin*, 43(8), 2457–2468.

- [12] Qiu, X., Li, L., Fu, X., & Li, G. (2008). Size-induced variations in lattice dimension, photoluminescence, and photocatalytic activity of ZnO nanorods. *Journal of Nanoscience and Nanotechnology*, 8(3), 1301–1306.
- [13] Tang, H., Chang, J. C., Shan, Y., & Lee, S.-T. (2008). Surfactant-Assisted Alignment of ZnO Nanocrystals to Superstructures. *The Journal of Physical Chemistry B*, 112(13), 4016–4021.
- [14] Wen, Z., Wang, G., Lu, W., Wang, Q., Zhang, Q., & Li, J. (2007). Enhanced Photocatalytic Properties of Mesoporous SnO<sub>2</sub> Induced by Low Concentration ZnO Doping. *Crystal Growth & Design*, 7(9), 1722–1725.
- [15] Zheng, Y., Chen, C., Zhan, Y., Lin, X., Zheng, Q., Wei, K., & Zhu, J. (2008). Photocatalytic Activity of Ag/ZnO Heterostructure Nanocatalyst: Correlation between Structure and Property. *The Journal of Physical Chemistry C*, 112(29), 10773–10777.





## Using Transdermal Patches on Controlled Drug Release

*Emel AKYOL*<sup>1,\*</sup> 

<sup>1</sup> Department of Chemical Engineering, Yildiz Technical University, Istanbul, Türkiye

### Abstract

The aim of the given study is the formation as well as the development of patches of Donepezil HCl, which is used in the treatment of Alzheimer's disease (AD). AD is a progressive brain disease and the leading cause of dementia in the elderly. Conventional treatments for the management of AD have all been given orally, thus Donepezil is commonly used as an oral tablet, although a transdermal patch may offer advantages as an alternate therapy. Transdermal medication administration for Alzheimer's disease has been shown to enhance patient compliance through reduced dosage frequency, improve bioavailability, reduce undesirable side effects, and make it easier to attain optimal levels. Furthermore, it promotes patient compliance in older patients since the patient does not have to remember to take their prescription or bring tablets for further administration later in the day. The transdermal approach provides various advantages over the oral route, including the ability to maintain sustained therapeutic plasma. In the present work, matrix-type transdermal patches of Donepezil HCl were prepared using the solvent casting method. Formulations were synthesized using Hydroxyethyl-cellulose (HEC), Poly (acrylic acid sodium salt) and Poly (acrylic acid) as polymers -individually- with varying degrees of hydrophilicity with Gelatin as a jelly to provide flexibility and Glycerol as a plasticizer additive, and to improve drug release by increasing permeability.

**Keywords:** Transdermal patch, donepezil HCl, solvent casting method, plasticizer.

### 1. Introduction

Every pharmaceutical researcher and company aspire to create a safe and effective medication delivery mechanism [1-2]. Traditional oral medication administration methods have some drawbacks, including pass metabolism, plasma level fluctuations, drug disintegration in the gastrointestinal tract owing to enzymes, pH, and so on. The introduction of innovative (novel) drug delivery technologies solves these problems. Transdermal drug delivery techniques are one of them. Drug administration via the transdermal method can have both local and systemic therapeutic effects. Because medications are given through the skin at a predefined and regulated rate, this approach is meant to increase therapeutic efficacy and safety. Selfadministered transdermal medication administration allows the medicine to flow through undamaged skin for a specified amount of time, achieving a local or systemic impact. Many drugs have been developed that can be injected directly into the bloodstream through the skin. The transdermal drug delivery system (TDDS) allows for medication release to be sustained while also reducing the intensity of action, reducing the adverse effects associated with oral treatment [3]. Patches are the most widely used transdermal technology on the market. Drugs can be given in dissolved lipid-based form via transdermal patches, allowing them to achieve the desired effectiveness. A transdermal patch is a medical patch that adheres to the skin and used to deliver a certain amount of medicine into the bloodstream via the skin. It (the Skin patch) employs a unique membrane to regulate how quickly the liquid medicine stored in the patch's reservoir passes through the skin and into the circulatory system. The fundamental goal of a transdermal medication distribution system is to transfer pharmaceuticals into the systemic circulation via the skin at a predefined rate with little fluctuation between and within patients [1,4]. Transdermal drug delivery systems (TDDSs) are ways for applying preparations across the skin without causing discomfort. The drug initially enters the stratum corneum (SC), then moves into the inner epidermis and dermis, leaving no drug deposit at the dermal level. As soon as the medicine reaches the dermal layer, it seems to be ready for systemic absorption via skin microcirculation [5]. The essential components of any transdermal administration system are the drug(s) dispersed or distributed in a reservoir or inert polymer matrix; an exterior backing sheet of paper, foil or plastic; and a pressure-sensitive adhesive that adheres the patch to the skin. A release liner that covers the adhesive must be pulled off before placing the patch on the skin. Transdermal delivery provides for not only regulated and

\* Corresponding author: E-mail address: eakyol@yildiz.edu.tr

uniform medications delivery, but also continuous input of drugs with short biological half-lives and avoids pulsed entry into the blood circulation, which can lead to unwanted side effects (Jawale et al., 2017a). [6].

## 2. Materials and Methods

### 2.1. Experimental materials

All the chemicals used in this research were of standard pharmaceutical grade. The list of chemicals used in the experiments is given in the table below.

**Table 1.** List of chemicals and their brands

Components	Brand
Donepezil Hydrochloride	Abdi İbrahim İlaç
Hydroxyethyl-cellulose (HEC)	Sigma
Poly (acrylic acid sodium salt)	Sigma
Poly (acrylic acid)	Sigma
Glycerol	Sigma
Gelatin	Carlo Erba

### 2.2. Preparation and formulation of matrix transdermal patches

In the present study, matrix-type transdermal patches of Donepezil Hydrochloride were produced by using the solvent casting method (molding technique). Formulation of transdermal patches using the solvent casting method are given in Table 2.

**Table 2.** Formulations

Ingredients	Formulation 1 (F1)	Formulation 2 (F2)	Formulation 3 (F3)
Donepezil Hydrochloride	0.2 g	0.2 g	0.2 g
Hydroxyethyl-cellulose (HEC)	1 g	-	-
Poly (acrylic acid sodium salt)	-	1 g	-
Poly (acrylic acid)	-	-	1 g
Glycerol	0.3 g	0.3 g	0.3 g
Gelatin	2 g	2 g	2 g
Distilled water	6.5 g	6.5 g	6.5 g

## 3. Results and Discussion

### 3.1. Drug Release Evaluation

In-vitro drug release studies were performed by using a Franz diffusion cell with a receptor chamber capacity of 30 ml. First of all, circular-shaped sections were cut from the HEC polymer-based patch with specific dimensions that fit the cover of the cell. The cellulose acetate membrane was used as a diffusion controlling membrane for the determination of drug release from the prepared transdermal matrix type patches. The cellulose acetate membrane having a pore size of 0.45 $\mu$  was mounted between the donor and receptor chamber of the diffusion cell. The receptor chamber of the diffusion cell was filled with buffer pH 7.4 up to the lid part. Here the membrane will be acted as the skin while prepared pH 7.4 solution will act as the blood and the whole cell present the body. The prepared transdermal film was placed on the cellulose acetate membrane that is located in the part between the cover and the receptor chamber. The upper part of the cover, the end of the sampling tube, and the heater circulators of the diffusion cell are covered with parafilm so that no evaporation or foreign body escapes into the cell. The whole assembly was placed in a hot shaking ultrasonic bath, to remain the solution in the receptor chamber constantly and continuously in motion for uniform distribution and the temperature was maintained at 37 °C, as the normal body temperature of a human. Sampling was carried out by withdrawing samples of 5 ml (1 ml from the cell and completed with 4 ml of pH 7.4 solution) for each at different time intervals throughout 24 h

(1, 2, 3, 4, 6, 8, 20 and 24 h). Each sample withdrawn from the cell, the receptor phase was replaced with an equal amount of fresh dissolution buffer solution (pH 7.4 solution). The absorbance of the solution of samples was measured and analyzed after suitable dilution using a UV-visible spectrophotometer at a wavelength of 270 nm for determining drug content. The cumulative percent drug permeated at various time intervals were calculated and plotted against time. The drug release was plotted on the graph as Time (min) on X-axis and Absorbance on Y-axis.

The study's goal was to create a Donepezil HCl transdermal treatment device employing a polymeric matrix film. The transdermal patch of Hydroxyethyl-cellulose (HEC) polymer was effectively formulated via the solvent casting method. As illustrated in Figure 1, the produced film was found to be uniform, flexible, smooth, and transparent. Physical inspection of the formulations revealed that the films were homogeneous and somewhat transparent, indicating that the medication was not totally solubilized but rather suspended/dispersed in the matrix. This allows one to manage the total release of the medicine by selecting the right polymers and polymer blends. The polymer-created diffusion pathways aid in achieving the ultimate goal of consistent and sustained pharmaceutical delivery from the patches.



**Figure 1.** Formulation of various transdermal patches after drying

In-vitro release studies use UV-vis spectroscopy to investigate the presence and amount of donepezil hydrochloride medication released from the patch, as well as the release efficiency of drug active components. Furthermore, it is a useful technique for predicting how medicine would act in vivo. Drug release studies are also necessary to predict the repeatability and reproducibility of drug release rate and duration. Figure 2 illustrates the drug release profiles and percentages. It has been shown that the release rate rises with time, reaching a peak of 65.5% after 24 hours. However, as seen in Figure 2, the medication was released rapidly from the patch at first. This fast drug release (burst effect) from the manufactured transdermal patch might be attributed to the surface drug's quick breakdown. The burst release can be effective in a variety of situations.

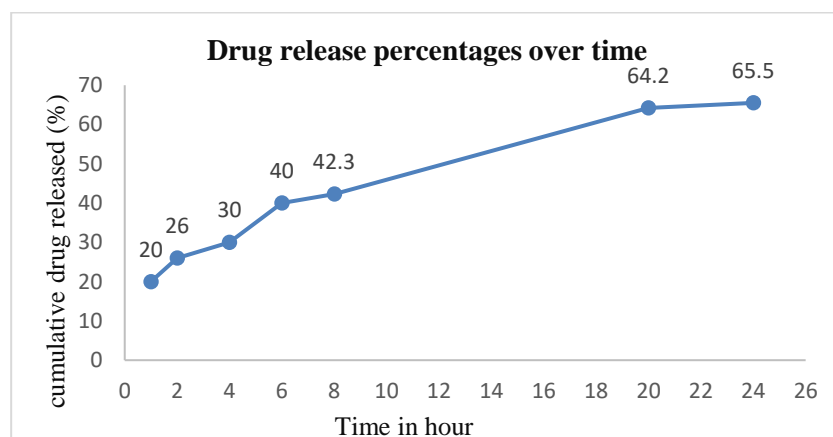


**Figure 2.** Drug release study of Donepezil HCl transdermal patch

Because studies have demonstrated that the medication active component of Donepezil HCl is effective for transdermal delivery, transdermal patches of Donepezil HCl were created and produced in this study. Transdermal patches improve patient compliance over traditional dose forms. Transdermal medication provides a continuous infusion of medicine over an extended length of time. Transdermal drug input can have an equal curative effect with a lower daily prescription dosage than is necessary, e.g. the drug is delivered orally. Hence, it is reasonable to conclude that Donepezil HCl can be formulated into transdermal matrix type patches to maintain its release characteristics, and the polymeric composition of (HEC) was found to be the best choice for manufacturing Donepezil HCl transdermal patches among the formulations studied because it was similar to standard transdermal patch properties. According to an in-vitro release study, a transdermal patch of HEC can release 65.5 % of the medication in the first 24 hours. To be employed in transdermal patches, films with positive findings needed to be validated by in vivo research.

### Acknowledgment

In this study, the financial support was provided by Research Fund of the Yildiz Technical University, Project No. FBA-2021-4491. All experimental works were conducted in Yildiz Technical University Research Laboratory. The author would like to thanks to all supporters due to their precious contributions.

### References

- [1] Al Hanbali, O. A., Khan, H. M. S., Sarfraz, M., Arafat, M., Ijaz, S., & Hameed, A. (2019). Transdermal patches: Design and current approaches to painless drug delivery. *In Acta Pharmaceutica*, 69(2), 197–215.
- [2] Senol, S. & Akyol, E., (2018). Synthesis and characterization of hydrogels based on poly(2- hydroxyethyl methacrylate) for drug delivery under UV irradiation, *J. Mater. Sci.*, 53, 14953-14963.
- [3] Agrahari, S., Sharma, A., Kumar, S., Sharma, A., & Sagar, M. K. (2019). Formulation and Development of Transdermal Patches of Piroxicam. *Asian Journal of Pharmaceutical Research and Development*, 7(3), 119–128.
- [4] Kharia, A., Gilhotra, R., & Singhai, A. K. (2019). Overview of Transdermal Medicated Patches with its research updates in preceding years. *Journal of Drug Delivery & Therapeutics*, 9, 1094–1102.
- [5] Keservani, R.K., Bandopadhyay, S., Bandyopadhyay, N., & Sharma, A.K. (2020). *Design and fabrication of transdermal/skin drug-delivery system. In Drug Delivery Systems*; Elsevier: Amsterdam, The Netherlands,. 131–178.
- [6] Jawale, N., Bhangale, C., Chaudhari, M., & Deshmukh, T. A. (2017a). Physical Approach To Transdermal Drug Delivery: A Review. *Journal of Drug Delivery and Therapeutics*, 7(3), 28-35.



## Synthesis, Characterization and Antioxidant Activity of N1-(5-Chloro-2-Oxoindoline-3-Ylidene) Thiocarbohydrazone Schiff Bases

**Jamal LAWAG**<sup>1,\*</sup> , **Temel BAKIR**<sup>2</sup> , **Halit MUĞLU**<sup>2</sup>

<sup>1</sup>Faculty of Chemistry, Department of Biochemistry, Çankiri Karatekin University, Çankiri, Türkiye.

<sup>2</sup> Faculty of Chemistry, Kastamonu University, Kastamonu, Türkiye

### Abstract

In this study seven new Schiff bases were prepared from monothiocarbohydrazones and 5-chloro isatin. The monothiocarbohydrazones were synthesized in the presence of ethanol under reflux with the reaction thiocarbohydrazide and substituted aldehydes. The reaction of synthesized benzothiocarbohydrazone, 4-hydroxy benzothiocarbohydrazone, 3-ethoxy-4-hydroxyl benzothiocarbohydrazone, 3,5-dimethoxy-4-hydroxyl benzothiocarbohydrazone and 4-N, N, dimethyl benzothiocarbohydrazone with 5-chloro isatin in acidic medium under reflux with N1- (5-Chloro-2-oxoindolin-3-ylidene) Schiff bases were obtained. The chemical structures of the products were confirmed by <sup>1</sup>H-NMR, <sup>13</sup>C-NMR, IR and elemental analysis. Physicochemical properties such as melting point, color and solubility were determined. In vitro antioxidant activity of all compounds was determined by 1,1-Diphenyl-2-Picryl Hydrazil (DPPH) free radical scavenging method. Antioxidant activities of molecules and standard used Gallic Acid> 3,5-dimethoxy-4-hydroxyl benzothiocarbohydrazone> 3-ethoxy-4-hydroxyl benzothiocarbohydrazone> 4-hydroxy benzothiocarbohydrazone> Benzothiocarbohydrazone> N1- (5-Chloro-2-oxoindolin-3-ylidene) ) 4-N, N, dimethyl benzothiocarbohydrazone> N1- (5-Chloro-2-oxoindolin-3-ylidene) 3, ethoxy-4-hydroxyl benzothiocarbohydrazone> 4-N, N, dimethyl benzothiocarbohydrazone> N1- (5-Chloro-) 2-oxoindolin-3-ylidene) 3,5-dimethoxy-4-hydroxyl benzothiocarbohydrazone> N1- (5-Chloro-2-oxoindolin-3-ylidene) 4, hydroxy benzothiocarbohydrazone> N1- (5-Chloro-2-oxoindoline-3-ylidene) benzothiocarbohydrazone.

**Keywords:** N1- (5-Chloro-2-Oxoindolin-3-Ylidene) Thiocarbohydrazone, Antioxidant Activity, DPPH method, NMR spectroscopy.

### 1. Introduction

Schiff bases were first reported by Nobel laureate German chemist Hugo Schiff in 1864. Hugo Schiff synthesized Schiff bases at the end of his research on imines and aldehydes. The general formula of Schiff bases is R<sub>1</sub>R<sub>2</sub>C = NR<sub>3</sub>. Wherein R is an organic side chain and comprises a carbon-nitrogen double bond to which the nitrogen atom is attached to an aryl or alkyl group and not to hydrogen. According to this definition, some researchers limit the Schiff base to azomethines to which carbon is attached to a hydrogen atom and thus to the general formula RCH = NR [1]. In the Schiff bases, the - C = N - imine bond gives these compounds a broad spectrum of biological activities. Electrophilic carbon and nucleophilic nitrogen in the imine bond inhibit enzymes or DNA replication in certain diseases by providing excellent binding with different nucleophiles and electrophiles. Schiff bases have been reported to form complexes with all D-block metals and lanthanides and also serve as versatile ligands for coordinating some metal ions. Among these, sulfonamide Schiff bases and their metal complexes occupy a special place in medical chemistry [2-3]. In addition to the antibacterial and antifungal properties of molecules such as sulfa guanidine, sulfa thiazole and sulfamethoxazole, it has been reported that certain sulfonamide Schiff bases and their metal complexes are inhibitors of carbonic anhydrase enzyme [4]. Schiff bases are useful chelators due to their potential diversity and structural diversity, such as nitrogen [5,6]. A Schiff base is usually formed by condensation of an aldehyde or ketone with a primary amine, in which the C = O group is replaced by the C = N-R group. Wherein R may be alkyl or aryl group. Schiff bases containing aryl substituents are significantly more stable and more easily synthesized, while those

\* Corresponding author. E-mail address: elawaj@yahoo.com

containing alkyl substituents are relatively unstable. Schiff bases of aliphatic aldehydes are relatively unstable and can easily polymerize [7].

Schiff bases, which are biologically active molecules, have been shown to have various pharmacological activities [8,9].

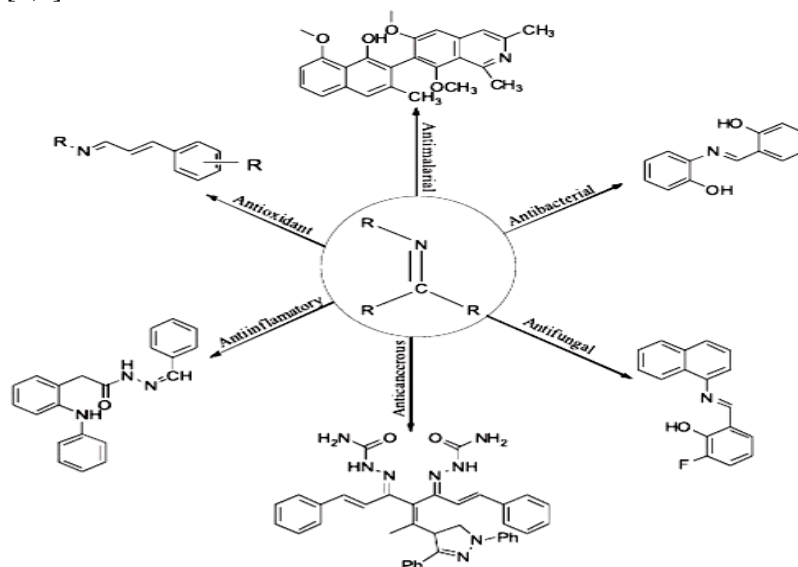


**Figure1.1.** Pharmacologically Active Schiff bases

**Antioxidant Activity-** Aging is a phenomenon that people have to face. The production of reactive oxygen species (ROS) increases with the passage of time and causes many physiological disorders in the human body, such as cardiovascular diseases. Schiff bases and metal complexes may play an important role in ROS production and exhibit antioxidant properties. For example, the antioxidant activities of Schiff bases and tin metal complexes derived from methoxylatedcinnamyl aldehydes from natural phenyl propene have recently been investigated [10].

## 2. Materials and Methods

### 2.1. Devices and Chemicals Used

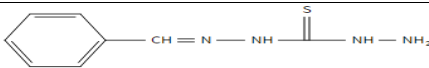
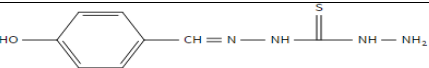
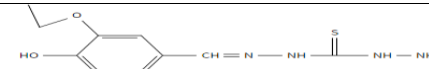
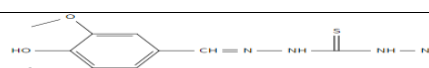
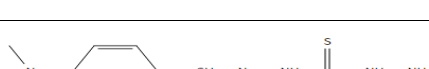
5-chloro isatin, Thiocarbohydrazone and aldehydes are provided from Sigma-Aldrich Co. Ltd. LLC. company. Deionized purity water was used in each step. C, H and O elemental analyzes and FTIR analyzes were performed in Kastamonu University Central Research Laboratory. <sup>1</sup>H-NMR and <sup>13</sup>C-NMR analyzes were performed in Bolu Abant University Central Research Laboratory. All solvents were used in analytical purity. Absorbances were measured by SHIMADZU UVmini-1240 UV-Visible spectrophotometer (Schimadzu Corp., Kyoto, Japan manufactures) using a pair of equivalent quartz cuvettes of 1 cm thickness at 517 nm.

Compounds synthesized in the study were examined in two stages. In the first step, the synthesis of the semifinished products was performed and the synthesized compounds are given in Table 2.1. In the second step, the final products were synthesized and the synthesized compounds are given in Table 2.2. The chemical materials used in this study are as follows:

- 1) Thiocarbohydrazone
- 2) Benzaldehyde
- 3) 4, hydroxy benzaldehyde
- 4) 3,5 dimethoxy-4-hydroxyl –benzaldehyde
- 5) 3,ethoxy-4-hydroxyl –benzaldehyde
- 6) N1- 5-Chloro-2-oxoindolin-3-ylidene
- 7) 4-N,N, dimethyl benzaldehyde

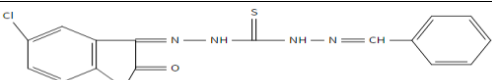
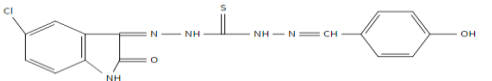
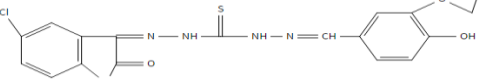
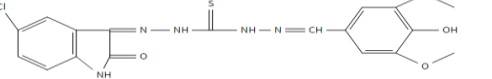
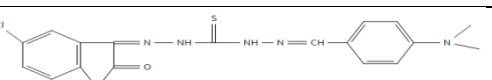
### 3. Results and Discussion

**Table 1.1** List of Synthesized Compounds (Semi Product)

Compound Number	Compound Name(Semi Product)	Molecular Structure
1*	Benzothiocarbohydrazone	
2*	4-hydroxyBenzothiocarbohydrazone	
3	3-ethoxy-4-hydroxyl Benzothiocarbohydrazone	
4	3,5-dimethoxy-4-hydroxyl Benzothiocarbohydrazone	
5*	4-N,N-dimethylBenzothiocarbohydrazone	

\* These compounds have been synthesized previously and are available in the literature.

**Table 1.2.** List of Synthesized Compounds (Final Product)

Compound Number	Compound Name(Final Product)	Molecular Structure
1	N1-(5-Chloro-2-oxoindolin-3-ylidene) Benzothiocarbohydrazone	
2	N1-(5-Chloro-2-oxoindolin-3-ylidene) 4-hydroxyBenzothiocarbohydrazone	
3	N1-(5-Chloro-2-oxoindolin-3-ylidene) 3-ethoxy-4-hydroxyl Benzothiocarbohydrazone	
4	N1-(5-Chloro-2-oxoindolin-3-ylidene) 3,5-dimethoxy-4-hydroxyl Benzothiocarbohydrazone	
5	N1-(5-Chloro-2-oxoindolin-3-ylidene) 4-N,N-dimethylBenzothiocarbohydrazone	

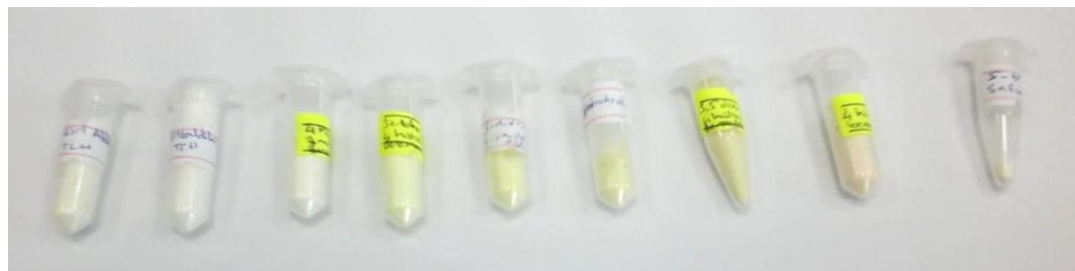


**Figure 1.1.** Synthesized Semi Products





**Figure 1.2.** Synthesized Final Products

Some physicochemical parameters of the synthesized products are given in Table 3.1 for semi-products and Table 3.2 for final products. In addition to the structural determinations, the calculated and experimental elemental analyzes ((N), (C) and (H)%) of the compounds were performed and given in Table 3.3.

**Table 3.1.** Physicochemical Parameters of Synthesized Compounds (Semi-Product)

Compound (Semi Product)	Molecular Weight	Melt Point (°C)	Colour	Resolution	Efficiency (%)
1	194,27	184	White	DMSO (+)	74,73
2	210,27	214	Light cream color	DMSO (+)	74,84
3	254,32	206	Light yellow	DMSO (+)	76,73
4	270,32	226	Light yellow-cream color	DMSO (+)	79,61
5	237,34	198	% 70 yellow- % 30 green	DMSO (+)	-

**Table 3.2** Physicochemical Parameters of Synthesized Compounds (Final Product)

Compound (Final Product)	Molecular Weight	Melt Point (°C)	Colour	Resolution	Efficiency (%)
1	357,85	234	% 80 Light brown- % 20 Yellow	DMSO (+)	56,70
2	373,85	254	Light orange	DMSO (+)	82,96
3	417,90	248	Matte yellow	DMSO (+)	76,44
4	433,90	267	% 30 Brown-% 10 orange-% 60yellow	DMSO (+)	90,54
5	400,92	238	Dark brown	DMSO (+)	50,29



**Table 3.3** Calculated and experimental elemental analysis of synthesized compounds ((N),(C) ve (H)%)

Compound	Calculated			Experimental		
	%N	%C	%H	(N) %	(C) %	(H) %
Final Products 1	19,561	53,653	3,380	18,998	52,769	3,219
Final Products 2	18,724	51,357	3,235	18,312	50,829	3,193
Final Products 3	16,750	51,687	3,859	16,374	50,730	3,813
Final Products 4	16,132	49,781	3,716	15,897	48,153	3,676
Final Products 5	20,951	53,876	4,274	20,615	51,973	4,236
* Semi-products 1	28,825	49,415	5,188	-	-	-
* Semi-products 2	26,632	45,655	4,793	-	-	-
Semi-products 3	22,019	47,184	5,548	21,387	46,417	5,447
Semi-products 4	20,716	44,391	5,220	20,375	42,926	5,131
* Semi-products 5	29,49355	50,560	6,370	-	-	-

\*These compounds have been synthesized previously and are available in the literature.

#### 4. Conclusion

Isatin and its derivatives, which are known to exhibit many biological activities in the pharmaceutical field, constitute an important class of hetero-compounds. In this study, Schiff base compounds with azomethine group ( $-C=N-$ ) bound to different aldehydes synthesized as intermediates and final product compounds formed with 5-chloro isatin were investigated in terms of antioxidant activities. It has been found that the antioxidant activities of the semi products are obtained not only from the substitutes present on the aromatic ring, but also from the H donor groups bound to the azomethine group and therefore show higher activity than the end products containing isatin. Although all synthesized molecules exhibit lower activity than gallic acid, which is a natural antioxidant, intermediates with methoxy and ethoxy groups can be considered as an alternative industrial product after toxicological and biological studies.

#### Acknowledgment

In this study, the financial support was provided by The Scientific and Technological Research Council of Turkey (TUBITAK), Project No. 112T806. All experimental works were conducted in Kastamonu University Research Laboratory. The author would like to thanks to all supporters due to their precious contributions.

#### 5. References.

- [1] IUPAC, Compendium of Chemical Terminology, 2nd ed. (the "Gold Book") (1997). Online corrected version: (2006-) "Schiff base".
- [2] Eman T., S.(2016). Preparation and Characterization of new Schiff base Derived from Pyridine and its metal complexes. *Int. J. Curr. Res. Chem. Pharm. Sci.* 3(4):118-123.
- [3] Abu-Khadra, A. S., Farag, R. S., & Abdel-Hady, A. E. D. M. (2016). Synthesis, characterization and antimicrobial activity of Schiff base (E)-N-(4-(2-hydroxybenzylideneamino) phenylsulfonyl) acetamide metal complexes. *American Journal of Analytical Chemistry*, 7(3).
- [4] Da Silva CM, Da Silva DL, Modolo LV, Rosemeire B Alves, Maria A de Resende, et al. (2011) Schiff bases: A short review of their antimicrobial activities. *J of adv res* 2(1): 1-8.
- [5] Hodnett, E. M., & Dunn, W. J. (1970). Structure-antitumor activity correlation of some Schiff bases. *Journal of Medicinal Chemistry*, 13(4), 768-770.
- [6] Hodnett, E. M., & Mooney, P. D. (1970). Antitumor activities of some Schiff bases. *Journal of medicinal chemistry*, 13(4), 786-786.
- [7] Urbach, F. L. (1981). The properties of binuclear copper centers in model and natural compounds (Vol. 13, p. 73). Dekker: New York.

- [8] Nucci, M., & Marr, K. A. (2005). Emerging fungal diseases. *Clinical Infectious Diseases*, 41(4), 521-526.
- [9] Njobeh, P. B., Dutton, M. F., Koch, S. H., Chuturgoon, A., Stoev, S., & Seifert, K. (2009). Contamination with storage fungi of human food from Cameroon. *International Journal of Food Microbiology*, 135(3), 193-198.
- [10] Sharma, U. K., Sood, S., Sharma, N., Rahi, P., Kumar, R., Sinha, A. K., & Gulati, A. (2013). Synthesis and SAR investigation of natural phenylpropene-derived methoxylated cinnamaldehydes and their novel Schiff bases as potent antimicrobial and antioxidant agents. *Medicinal Chemistry Research*, 22(11), 5129-5140.



## Flexible Alternating Current Transmission System

Okan GÜMÜŞ<sup>1,\*</sup> , Hakan GÜMÜŞ<sup>2</sup> , Gözde GÜMÜŞ<sup>3</sup> 

<sup>1</sup> Engineering Faculty, Electrical and Electronic Department, Çankırı Karatekin University, Ankara, Turkey

### Abstract

With the developing technology, most of the loads used in industrial applications consist of inductive loads. Due to their nature, inductive loads use inductive reactive energy. The reactive energy used degrades the system's quality and efficiency, as well as causing power factor issues. Flexible alternating current transmission systems (FACTS) are vital for increasing the power system's performance and quality. The FACTS system makes it faster and easier to regulate a power system. The most popular FACTS device used to enhance power quality is the Distribution Static Synchronous Compensator (D-STATCOM). According to apply FACTS applications, we are talking about FACTS devices their applications. After the comparing of the FACTS devices, discuss the differences and apply the simulation model using MATLAB/SIMULINK. After the preparing simulation, results will be discussed and researching about future applications.

**Keywords:** DC, AC, FACT, MW, VA, VAR.

### 1. Introduction

All of the world's electrical power supply systems are linked, including intra-utility connections, cross-grid connections from outside their own areas, inter-regional connections from multinational firms, and finally worldwide connections. Transmission line interconnections guarantee that power is delivered to loads reliably and at a low cost. FACTS Technology has provided the transmission planner with a new opportunity to control power and increase existing capacity as well as transmission line upgrades the current through the line may be managed at a reasonable cost, allowing existing lines with huge conductors to be expanded significantly, while the use of FACTS controllers maintains the power flow steady. FACTS controllers regulate factors that influence transmission system functioning, such as at frequencies below the normal frequency, series impedance, shunt impedance, current, voltage, phase angle, and oscillation damping are all important. In an AC power flow, electricity generation and load must always be balanced. Since the electrical system is self-regulating, if one of the generators supplies less power than the load, the voltage, and frequency drop, hence the transmission losses, and the load continues to decrease to equalize the power produced. But self-regulation has a small margin. If the voltage drops due to reactive power, the load will increase and the frequency will continue to decrease, resulting in the system crashing. "The consumed reactive power should be regulated to eliminate all of these issues. Reactive power control has become more important especially in transmission and distribution systems due to difficulties in the construction of new transmission lines. Therefore, in order to control the reactive power, the reactive power drawn by the industrial and lighting loads should be fed from the point where these loads are located or from the closest place to them." [1] In other words, compensation is the process of balancing the inductive reactive power they have created on the network and bringing the phase current back to the required position due to the magnetization effect of inductive loads in the electrical system, due to the shifting of the phase current of the devices that convert the electrical energy back to electrical energy or different energy.

### 2. Problem Definition

In alternative energy systems, criteria such as the current and voltage having a pure sine wave shape, the constant frequency at the nominal value (50Hz or 60Hz), and the voltage on the load being at the nominal value or within acceptable limits are the desired quality conditions. Energy quality is proportional to the fulfillment of these criteria under all conditions. Power quality problems include disturbances that will disrupt the operation of

\* Corresponding author. e-mail address: okangumus9@gmail.com

sensitive industrial loads and cause production losses. Although there are different classifications for power quality problems, the IEEE 1159:2019 standard collects power quality problems under 7 headings.

- Transients
- Short-Term Voltage Changes
- Long Term Changes
- Voltage Imbalance
- Power Frequency Changes
- Waveform Distortion
- Voltage Fluctuations

**Table 1.** Energy quality problems according to IEEE 1159:2019 Energy quality problems according to IEEE 1159:2019 according to IEEE 1159:2019 standard [1]

Category			Typical Spectral	Duration	Amplitude
Transient Events	percussive	ns	5 ns increase	<50ns	
		μs	1 μs increase	50ns-1ms	
		ms	0.1 ms increase	>1 ms	
	oscillating	Low	< 5 kHz	0.3-50 ms	0-4 pu
		Medium	5-500 kHz	20 μs	0-8 pu
		High	0.5-5 MHz	5 μs	0-4 pu
Short temprary Changes	Sudden Changes	Collapse		0.5 – 30	0.1-0.9 pu
		Rise		0.5 - 30	1.1-1.8 pu
	Temporary Changes	Interruption		0.5 - 3 s	< 0.1 pu
		Collapse		30 - 3 s	0.1-0.9 pu
		Rise		30 - 3 s	1.1-1.4 pu
		Voltage Imbalance		30 - 3 s	2-15 %
	Long Temporary Changes	Interruption		>3 s - 1min	< 0.1pu
		Collapse		>3 s - 1min	0.1-0.9pu
		Rise		>3 s - 1min	1.1-1.2pu
		Voltage Imbalance		>3 s - 1min	2-15 %
Long Temporary Changes		Collapse		> 1min	0.0 pu
		Voltage Drop		> 1min	0.8-0.9 pu
		Voltage Rising		> 1min	1.1-1.2 pu
		Over Current		> 1min	
Voltage Imbalance Current Imbalance				Stable	0.5-5 %
				Stable	1.0-3.0 %
Waveform Distortion		DC Ofset		Stable	0-0.1 %
		Harmonic	0-9 kHz	Stable	0-20 %
		Hidden Harmonics	0-9 kHz	Stable	0-2 %
		notches		Stable	

### Short Term Voltage Changes

Changes in the source voltage for periods longer than half a period and not exceeding one minute are defined as short-term. These changes are classified as sudden, instantaneous and temporary voltage sag, voltage spike and momentary voltage interruption as seen in Figure 1.1. Voltage sag refers to voltages lower than 90% of line voltage nominal value, while voltage spike refers to high values exceeding 110% of nominal value. [2]

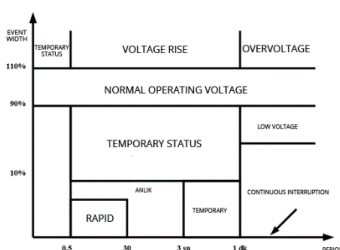


**Figure 1.** IEEE Std. Strain relief standard according to 1159-2019 [1]

### Voltage Imbalance

It is defined as the situation where the three-phase voltage magnitudes of the source are not equal. The main reason is single-phase loads. The greatest deviation derived from the average of the three phase voltages is also determined. Undervoltage imbalances are caused by single-phase loads in three-phase systems. Furthermore, when three-phase loads are left on a single phase, a massive voltage imbalance arises, causing considerably more serious issues.

### Waveform Distortion

It is defined as the variation of the power frequency in steady state from an ideal sine wave. Direct current component, harmonics, interharmonics, notches, and noise are all types of distortions. Harmonics are defined as deviations from the pure sinusoidal condition of a voltage or current waveform in a power system. Interharmonics are entire multiples of the power frequency (for example, 100 Hz, 150 Hz) as well as fractional multiples (125 Hz, 175 Hz). The waveform containing harmonics is also periodic. All harmonic components except the 50 Hz component, which is the basic component, cause increased power losses, voltage drops and reduced efficiency of the electrical system. The DC component in the system can saturate the power transformers. In addition, current commutating rectifier circuits in DC and AC motor drivers, uninterruptible power supplies (UPS) cause notches in power systems. Increasing the duration and depth of voltage notches may damage other loads fed from the same voltage source.[4]

### Voltage Fluctuations

They are defined as rapid and systematic changes in the source voltage with amplitudes between 90% and 110% of the rated voltage. These are also known as voltage flicker. They are caused by rapid and large changes in the amplitude of the current caused by low power factor loads. On the contrary, in the power system; frequency and voltage are expected to be constant, no harmonics, current and voltage to be in the same phase. For this, the control of reactive power is very important in increasing the system's electrical quality. Changes in the source voltage at the fundamental frequency for periods exceeding one minute, such as overvoltage, undervoltage, and prolonged interruption. For periods exceeding one minute, the effective value (rms) of the rated voltage is defined as an overvoltage increase of more than 110%, undervoltage when it falls below 90%, and long-term interruption when it is zero. Switching on and off of a large load with a low power factor causes overvoltage or undervoltage. Reactive energy limitations according to installed power for consumers directly connected to the transmission line in accordance with the "Electricity Transmission Systems Supply Safety and Quality Regulation" by the Turkish Energy Market Regulatory Authority (EPDK) It is shown in Table 2. In transmission and distribution systems, reactive power compensation is utilized for voltage management and load adjustment.

**Table 2.** Reactive energy limitations put into effect by EPDK [3]

Installed Power of the Business	Energy Demand/Month		
	Active Energy (%)	Reactive Energy (%)	
		inductive	capacitive
<50kVA	100	$\leq 33$	$\leq 20$
>50kVA	100	$\leq 20$	$\leq 15$

Load compensation is used to decrease current harmonics caused by high non-linear loads, correct the system's power factor, and balance the active power extracted from the network. Voltage regulation's goal is to decrease voltage variations at the regulated point. To increase power quality and adjust voltage, proper reactive power compensation is required. FACTS and Special Power devices are excellent choices for controlling reactive power quickly.[4]

### Reactive Power Compensation

If a circuit contains an inductor, capacitor, or both, some of the energy introduced during a period is stored and then returned to the source. This period will continue as long as the source is present in the circuit. In an AC circuit with just a capacitor, the energy received from the source is stored in the electric field between the plates

of the capacitor during a half-period time period. In the second half-period, the stored energy is restored to the source.[5] Two circuit components that work together are the inductor and the capacitor. The phase difference between these two circuit elements is 180 degrees when they are linked in series. This situation causes unnecessary loading of transmission lines and increases losses. This power, which is withdrawn from the network and given back to the network without being used, is known as reactive power and is represented by the letter Q.

$$Q = V.I.\sin\Phi \quad (1)$$

is expressed as. In the above equation, the  $\sin\Phi$  factor is called the reactive power factor.[7] Reactive power does not show energy loss, but shows the peak value of the instantaneous power received and delivered by the inductor or capacitor. Since reactive power will cause voltage decrease and losses by loading the transmission line and transmission devices unnecessarily, it is desirable to minimize the reactive power drawn from the network. In AC circuits, active power is drawn by resistors, reactive power by inductors and capacitors. In an AC circuit with resistance and reactance, there will be active and reactive power, which combined produce the perceived power. (S). Apparent power phasor for an inductive load;

$$S = P + jQL \quad (2)$$

Apparent power phasor for a capacitive load;

$$S = P - jQC \quad (3)$$

is defined as apparent power S;

$$S = \sqrt{P^2 + Q^2} \quad (4)$$

The scalar quantities of active power P, reactive power Q, and apparent power S created by the two powers may be represented geometrically as the horizontal side, vertical side [6], and hypotenuse of a right triangle, respectively, as illustrated in Figure 1.2. This triangle is referred to as the power triangle. The power triangle is the Z impedance triangle scaled by the factor I, as seen in Figure 2.

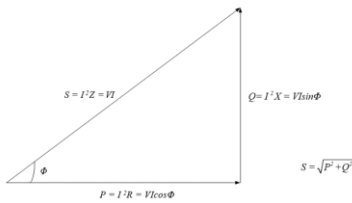


**Figure 2.** Power Triangle [8]

### 3. Results and Discussion

In this chapter we are talking to methods and their applications to FACTS system. We need to understand the topics and the application type of FACTS. Applied FACTS system has many ways. That will be a simple circuit breaker or complex UPFC devices. FACTS systems have many types and Table 3.

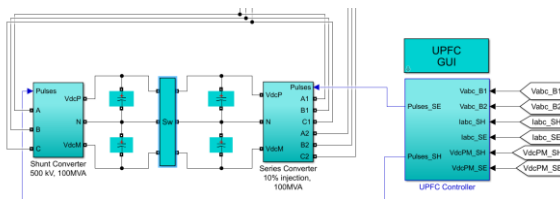
According to table we have many types of FACTS devices. In this study planning to do something similar to UPFC systems. Our FACTS system has a distinctive feature. According to this UPFC device. Determine the parameters in simulation. In that condition, device topology is need to be explain.

**Table 3.** FACTS device types [9]

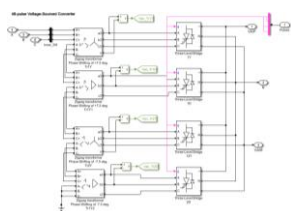
FACTS Name	Connection Type	Control Parameters
Voltage Source Switching Inverter FACTS Devices		
STATCOM	Parallel	Voltage control, VAr compensation, Transient and dynamic stability, Voltage stability, Damping oscillations
SSSC	Serial	Current control, Transient and dynamic stability, Voltage stability, Oscillation damping, Fault current limitation
UPFC	Combined Structured Series-Parallel	Active and reactive power control, Voltage control, VAr compensation, Transient and dynamic stability, Voltage stability, Oscillation damping, Fault current limitation
IPFC	Combined Structure Series-Series	Voltage control, Reactive power control, Transient and dynamic stability, Voltage stability, Damping oscillations

#### 4. Developed or Applied Approach

Due to the nature of FACTS devices, different methods have been developed day by day. As discussing at the simulation, The UPFC, which is situated between the 500 kV buses B1 and B2 at the left end of the 75 km line L2, is used to regulate the voltage at bus B1 and the active and reactive energy flowing via bus B2. It consists of two 100-MVA, three-level, 48-pulse GTO-based converters, one linked in series between buses B1 and B2, the other in shunt at bus B1. Through a DC bus, the shunt and series converters can trade power. The series converter may connect line L2 in series with a maximum of 10% of the nominal line-to-ground voltage (28.87 kV). When the shunt and series converters are coupled together through the DC bus, this is known as the Unified Power Flow Controller (UPFC) mode. Two more modes are accessible when the disconnect switches between the DC buses of the shunt and series converter are opened. The shunt converter functions as a STATCOM when the two converters are used in UPFC mode. It permits active power transmission to the series converter through the DC bus while also regulating the absorbed or produced reactive power, which regulates the bus B1 voltage. By changing the DC bus voltage, the reactive power fluctuation may be produced. A quasi-sinusoidal 48-step voltage waveform is produced by the four three-level shunt converters operating at a constant conduction angle ( $\text{Sigma}=180-7.5 = 172.5$  degrees). The 47th and 49th harmonics are the first important harmonics.

**Figure 3.** UPFC device

As you see in figure 3. you can clearly see the UPFC device working principle if want to explain detailly each part:

**Figure 4.** Shunt Converter

Shunt and series converter control the circuit configuration of two connected converters allows for many UPFC control modes, series voltage injection, and separately adjustable reactive power exchange. The alternatives to the method used for power flow control are reactive shunt compensation and free control of series voltage

injection. Shunt and series converter control the circuit configuration of two connected converters allows for many UPFC control modes, series voltage injection, and separately adjustable reactive power exchange. The shunt inverter runs on a closed-loop current control architecture that allows for independent control of the actual and reactive power components. In order for series insertion to simulate reactive impedance as viewed from the line, the main purpose of series compensation is to adjust the magnitude of the injected voltage in proportion to the line current.

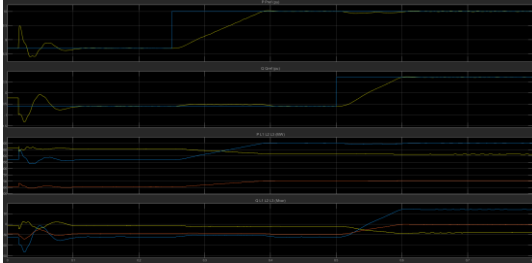


**Figure 5.** Simulation output-1

In the figure 5 you can clearly see the P and Q graphs in whole circuit. This figure is help us to compare reference and real time values.

## 5. Conculsions

FACTS in general: in the energy transmission system, it is a collection of power electronics-based controllers and systems designed to provide quicker and more effective control, boost the transmission system's power carrying capability, and mitigate abnormal operating circumstances. Its application to transmission systems is referred to as flexible alternating current transmission systems (FACTS), power electronics-based circuit architectures act. The word flexible here refers to the ability of these controllers to comfortably control the variables of the power transmission system, such as current or voltage. Thanks to FACTS structures (devices, controllers or controllers): Power flows in the network can be controlled, and the power carrying capacity of the lines can be increased. [10] In addition, solutions can be found for problems such as sub synchronous resonance, voltage instability, power oscillations and transient stability in the network. Rapid events that may occur in the network can be intervened in a very short time. FACTS controllers are structures based on power electronics and their operation is generally based on the on and off of semiconductor switches.

## References

- [1] «IEEE Recommended Practice for Monitoring Electric Power Quality».
- [2] C. S., «Wide Area Voltage Protection,» *IET Gener. Transm. Distrib*, 2010, p. 1164–1179.
- [3] Available: <https://www.epdk.gov.tr>. [Acces: 17 April 2022].
- [4] E. A. V. S. Furbo, «Thermal destrafication in small standart solar tanks due to mixing during tapping,» *Proceeding of ISES Solar Wolar Congress*, Jerusalem,Israel, 1999.
- [5] Marzo, Understanding Buck Power Stages in Switchmode Power Supplies, T. Instruments, 1999 .
- [6] J G. C. Restrepo, «A noninverting buck-boost dc-dc switching converter with high efficiency and wide bandwidth,» %1 içinde *IEEE Transactions on Power Electronics*, vol. 26, September 2011, p. 2490 2503.
- [7] C. W. F.Y. Chen Yaow-Ming, « Multi-input DC/DC converter based on the multiwinding transformer for renewable energy applications.,» *IEEE Trans Ind Appl* , 2002, p. 38:1096–104.
- [8] Solero, «Design of multiple-input a dc dc power converter for hybrid vehicles,» *IEEE Trans. Power Electron.*, Oct. 2005., pp. vol. 20, no. 5,1007–1016.
- [9] Available: <https://www.ti.com/tool/PMP8740> . [Acces: 04 20222].
- [10] P. [1Georgilakis ve N. Hatziargyriou, «Unified power flow controllers in smart power systems: models, methods, and future research,» *IET Smart Grid*, pp. 2-10, 2019.
- [11] G. W. Stagg and A. Abiad, “Computer Methods in Power System Analysis”, McGraw-Hill, New York, First Edition.





## Separation of rhodium from simulated rhodium plating solutions with imidazolium derivative ionic liquids

***Aboubakar Ibrahim MOHAMED*<sup>1\*</sup>** , ***Meryem Nilufer YARAŞIR***<sup>2</sup> , ***Volkan EYUPOGLU***<sup>1</sup> ,  
***Asuman UNAL***<sup>3</sup> , ***Şevki ADEM***<sup>1</sup> , ***Ahmet YARTASI***<sup>4</sup> 

<sup>1</sup> Department of Chemistry, Faculty of Science, Çankırı Karatekin University, Uluşazı, Çankırı 18100, Turkey

<sup>2</sup> Department of Chemistry, Faculty of Science, Sakarya University, Sakarya, Turkey

<sup>3</sup> ÇANKAM, Çankırı Karatekin University, Uluşazı, Çankırı, Turkey

<sup>4</sup> Department of Chemical Engineering, Faculty of Engineering, Çankırı Karatekin University, Uluşazı, Çankırı, Turkey

### Abstract

Separation of rhodium Rh(III) ions from an acidic solution containing HCl by solvent extraction method was optimized by using 1-octyl-3-methyl imidazolium bromide (MOIMBr) and 1-decyl-3-methyl imidazolium bromide (MDIMBr) salts as extractants. In addition, parameters such as HCl concentration, ionic liquid concentration, extraction time and phase ratio, which affect the recovery of Rh(III), were optimized experimentally. At the end of the experimental process, the parameters of the extraction steps of Rh(III) were tested under optimum conditions and the selectivity of the process was tested in the presence of metal ions (Pt, Au, Cu, Ni, Fe) that can be found together with rhodium in the ore or industry, and the selectivity was found to be quite high.

**Keywords:** Rhodium, ionic liquid, Phase ratio, Extraction method, Imidazolium bromide

### 1. Introduction

Recently, there has been an increasing demand for platinum group metals (Ruthenium, Rhodium, Platinum, Palladium, Osmium and Iridium). Because of their excellent physical and chemical properties, they are widely used in electronic devices, chemical and oil refining industries, catalysis, glass industries and pharmaceutical industries, etc. Rhodium is one of the most expensive platinum metals and indispensable for automotive catalytic converters [1]. Although several sophisticated techniques are used for the determination of traces and ultra-traces, the rhodium amounts, the spectrometric technique still has the advantage of simplicity and low operating costs, but suffers from matrix effects. For this reason, the removal of Rh (III) from the synthetically prepared acidic solutions with chlorine from the aqueous solution medium to the organic phase (extraction) using the solvent extraction technique and the selective recovery of the Rh (III) taken into the organic phase into the aqueous solution medium by the stripping process has been achieved. For this purpose, an OS-based recovery process was developed by using asymmetric imidazolium salts (MDIMBr MOIMBr) synthesized within the scope of the study we concluded [2]. A solvent extraction process has been developed in which we can perform the selective extraction of Rh (III) by optimizing the aqueous phase and organic phase conditions that will affect the recovery.

Positive and highly efficient results were obtained in the studies of rhodium extraction and separation of asymmetric imidazolium bromide salts by solvent extraction technique. In this study, a new dimension has been added to the use of imidazolium bromide-based ionic liquids for extraction purposes.

### 2. Materials and Methods

Synthesized asymmetric imidazolium bromide salts were optimized by liquid liquid solvent extraction method for Rh (III) extraction from HCl solution medium. The chemicals used are chloroform, diethylether, toluene, dimethyl formamide (DMF), Hexane, N-methyl imidazole, n-octyl bromide, n-decylbromide, HCl, NaOH, KOH, Na<sub>2</sub>CO<sub>3</sub>, Na<sub>2</sub>SO<sub>3</sub>, NaCl, Fe, Ni, Cu, Pt, Au, Rh AAS standard solutions Sigma-Aldrich (USA) and Merck. Inch. (Germany) and used directly without any preliminary purification.

\* Corresponding author. e-mail address: aboubakeribrahim18@gmail.com

## 2.1 Synthesis of asymmetric imidazolium bromide salts

1-alkyl-3-methyl imidazolium bromide salts/ionic liquids were synthesized in accordance with the literature by a one-step method. 0.1 mole (8.2 grams) of N-methyl imidazole was placed in a 100 mL conical tube and dissolved in approximately 20 mL of toluene. 0.1 mol (1 equivalent) of alkyl bromide was added to it. Stirring was continued at room temperature. Within 1 hour, salt formation was observed as turbidity first. Then the turbidity darkened and after 2-3 hours the mixing was complete. The reaction mixture was allowed to settle and the salt formed was allowed to settle to the bottom. Excess solvent was removed by decanting. The remaining reaction mixture was washed 3 times with mixing with hexane (10 mL). After each washing, hexane was decanted and removed from the environment. After the last washing, the reaction mixture, which was mixed with diethyl ether and washed and the solvent was decanted, was applied vacuum to remove the solvent from the salt-attached part. The purity of the obtained salt was checked by TLC (thin layer chromatography). Cleaning was continued until a single spot was observed for each item. The reaction scheme is given in Figure 1.

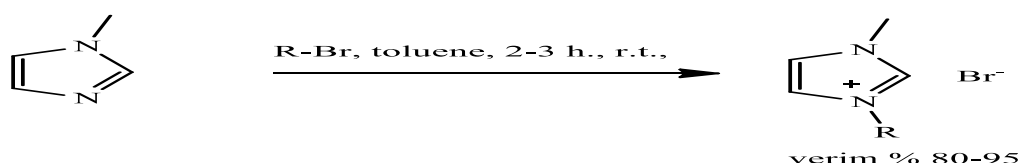


**Figure 1.** Synthesis of methyl imidazole derivative asymmetric ionic liquids (imidazolium salts).

## 2.2. Solvent extraction procedure

In the solvent extraction (SE) process, organic phase (ionic liquid phase), feed phase HCl medium (Rh(III)) and stripping phase basic solutions were used. Solvent extraction process was carried out at room temperature and in a test cell similar to Figure 2. With the prepared feed solution The organic phase containing ionic liquids was filled into the cell and mixed with the help of a magnetic stirrer, and after a certain period of time for the phases to be agitated with each other, it was waited for phase separation. Then, the sample taken from the aqueous phase was diluted and analyzed by ICP-MS and thus the Rh(III) phase in the aqueous phase was analyzed. Quantitative analysis of) was carried out. The reverse of this procedure for extraction was carried out on the basis of removing rhodium from the rhodium-saturated organic phase into the aqueous phase by means of stripping reagents for stripping. It was diluted with HNO<sub>3</sub> solution.

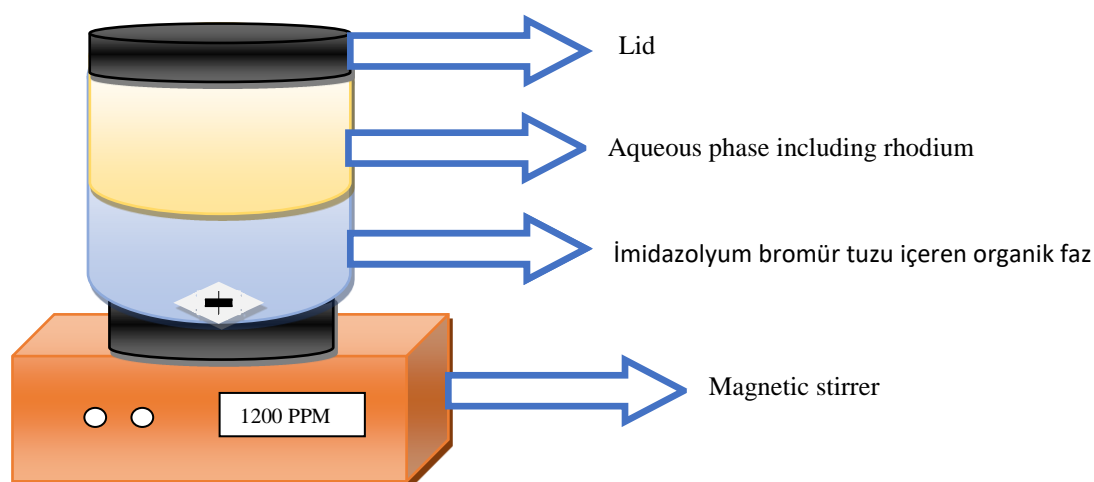


**Figure 2.** Representative figure of the extraction setup.

### 3. Results and Discussion

#### 3.1. Synthesis and Molecular Characterization of Asymmetric Imidazolium Salts

In the study, the synthesis of asymmetric imidazolium bromide salts was carried out. Their molecular characterizations were performed using ATR-FTIR spectroscopy.

MOIMBr, the ATR-FTIR spectrum of the compound are given in Figure 3. ATR-FTIR peaks seen in the figure were observed as  $1161\text{ cm}^{-1}$ ,  $1663\text{ cm}^{-1}$ ,  $2925\text{ cm}^{-1}$  and  $3450\text{ cm}^{-1}$  and were determined by marking the functional groups corresponding to the peaks on the spectrum.

If it is MDIMBr, the ATR-FTIR spectrum of the compound is given in Figure 4. The ATR-FTIR peaks seen in the figure were observed as  $1162\text{ cm}^{-1}$ ,  $1660\text{ cm}^{-1}$ ,  $2923\text{ cm}^{-1}$  and  $3347\text{ cm}^{-1}$  and the functional groups corresponding to the peaks on the spectrum were determined by marking them.

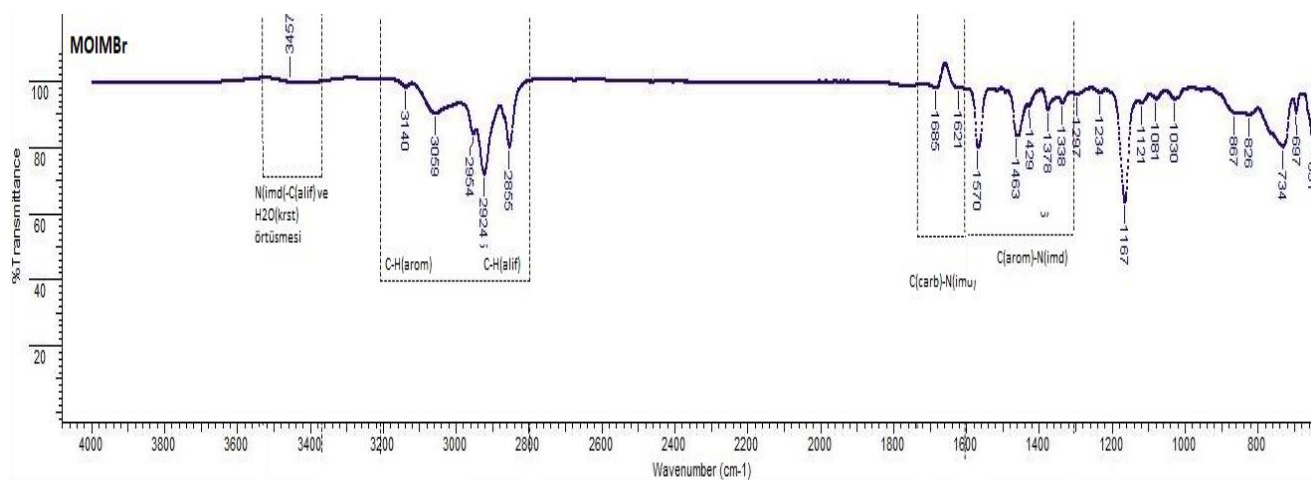


**Figure 3.** ATR-FTIR spectrum of MOIMBr

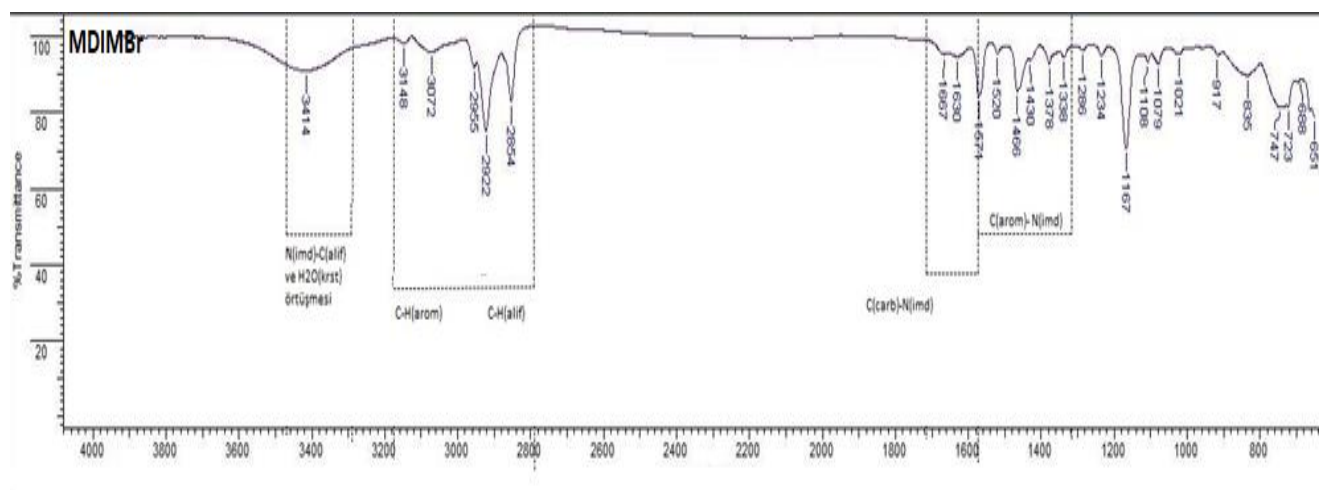


**Figure 4.** ATR-FTIR spectrum of MDIMBr

#### 3.2. Rh(III) Separation Studies by Solvent Extraction

##### 3.2.1. Determination of optimum Rh(III) recovery conditions

In current study, the effective aqueous phase and organic phase conditions (Time, HCl concentration, NaCl concentration, phase ratio and imidazolium salts concentrations) were investigated experimentally. So, the

optimum recovery conditions have been determined as below;

HCl concentration = 0.01 mol/L

NaCl concentration = 0.3 mol/L

Time: 5 min.

Phase Ratio (Vorg/Vaq): 4/2

Imidazolium Salt Concentration: 0.1 mol/L

### 3.2.2. Rh(III) recovery and separation in optimum conditions

#### 3.2.2.1. Effect of different metal ions on Rh (III) extraction under optimum conditions

Another experimental parameter to determine the effectiveness of the optimized process is to perform Rh(III) extraction in the presence of different ions under optimum extraction conditions. For this purpose, Rh(III) extraction from initial solutions prepared with Cu, Au, Pt, Ni, Fe metals, where rhodium is generally found together in nature and for industrial purposes, was investigated and the results are given in Figure 5. In parallel, the separation factors, which are a measure of the separability of Rh(III) from other metals, are given in Table 1. Accordingly, it was determined that rhodium was extracted with high yield and especially high separation factors against Ni, Cu, Fe and Au in the presence of other metal ions, and its separation factor was relatively lower against Pt.

**Table 1.** Effect of foreign ion on Rh(III) extraction under optimum conditions

Distribution Coefficients D ( $C_{org}/C_{aq}$ )		
	MDIMBr-Rh(III)	MOIMBr-Rh(III)
Rh	6,56	5,89
Pt	0,66	0,54
Cu	0,29	0,21
Fe	0,40	0,23
Au	0,26	0,17
Ni	0,02	0,02
Separation Factors SF ( $\beta$ )		
SF	MDIMBr-Rh(III)	MOIMBr-Rh(III)
$\beta_{Rh/Pt}$	10,01	10,84
$\beta_{Rh/Cu}$	22,55	27,46
$\beta_{Rh/Fe}$	16,26	25,49
$\beta_{Rh/Au}$	24,81	35,58
$\beta_{Rh/Ni}$	324,80	291,38

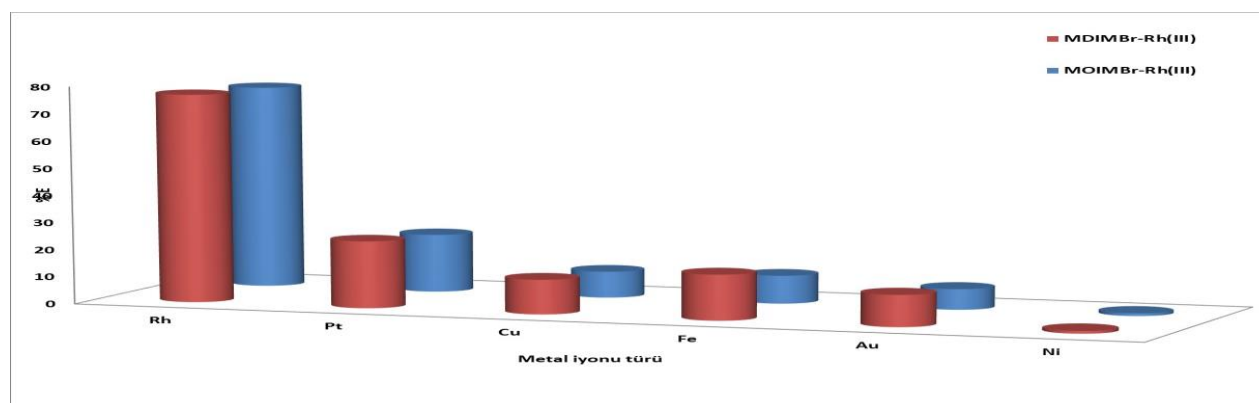


**Figure 5.** Effect of different metal ions on Rh(III) extraction under optimum conditions

## 4. Conclusion

In this study, Rh(III) recovery with newly synthesized asymmetrical imidazolium bromide salts has been achieved by the traditional solvent-solvent extraction method. In the recovery conditions, we have reached max separation factors values against nickel ions with the longer alkyl chain including imidazolium bromide salts.

## 5. Acknowledgement

All experimental studies were performed in Cankiri Karatekin University chemistry department laboratories and its instrumental facilities. The study also supported by Cankiri Karatekin University Scientific Research Project Commission ennumbered as FF060515B25.

## References

- [1] Diamantatos, A. (1981). *A Solvent-Extraction Scheme for the Determination of Platinum, Palladium, Rhodium, Iridium and Gold in Platiniferous Materials*. *Analytica Chimica Acta*, 131(Nov), 53-62.
- [2] Zhu, L., Liu, Y., Chen, J., & Liu, W. (2011). Extraction of scandium(III) using ionic liquids functionalized solvent impregnated resins. *Journal of Applied Polymer Science*, 120(6), 3284-3290. Doi: 10.1002/app.33501



# Self-Assembling Peptides in Oral and Maxillofacial Surgery

***Hacer EBERLİKÖSE***<sup>I\*</sup> 

<sup>I</sup>Faculty of Dentistry, Department of Oral and Maxillofacial Surgery, Ankara Medipol University, Ankara, Turkey

## Abstract

Long-term studies have shown that there is an important connection between ‘biomaterials’ and biological materials [1]. Recently, studies have been carried out on different materials that mimic the production mechanisms in nature [2]. As a result of research, self-assembled artificial systems (e.g Peptides, nucleic acids) have been developed. The self-assembly mechanism is a bottom-up system, producing stable biological constructions. Among the self-assembly molecules, peptides are the most easily modified and functionalized structures. Application areas of self-assembly peptides include drug release and tissue engineering [2]. Especially tissue engineering is a very important and complex issue in Oral and Maxillofacial surgery [3]. In the literature review, it has been determined that self-assembly peptides are used especially in the field of hard tissue regeneration together with stem cells [4]. In this context, it has also started to be used as dental implant coatings. Self-assembly peptides with antimicrobial properties have been investigated in cases such as osteomyelitis. Another usage area of peptides in Oral and Maxillofacial Surgery is nerve injuries [5]. Peptides are being investigated not only in oral and maxillofacial surgery but also in other areas of dentistry. Considering all these studies, peptides are thought to be promising and clinically useful in dentistry.

**Keywords:** Self-Assembling Peptides, Tissue Engineering, Dental implant, Maxillofacial defects, bone graft

## 1. Introduction

Long-term studies have shown that there is an important connection between ‘biomaterials’ and biological materials [1]. Recently, studies have been carried out on different materials that mimic the production mechanisms in nature [2]. As a result of research, self-assembled artificial systems (e.g Peptides, nucleic acids) have been developed. The self-assembly mechanism is a bottom-up system, producing stable biological constructions. Among the self-assembly molecules, peptides are the most easily modified and functionalized structures. The first peptide molecule was identified incidentally in 1989 by Zang incidentally [1]. These novel molecules have one hydrophobic and one hydrophilic side. External stimuli such as temperature, pH, light and electrical force can alter the function of self-assembled peptide nanostructures [2]. The researches found out that the peptide can form spontaneously well-organized nanofiber structures and assemble into a scaffold [1]. Peptides can be modified using different sequences, and it is possible to add functionality to their construction by adding enzymes and fluorescent structures [2].

## 2. Materials and Methods

The PubMed (MEDLINE) database was used for a literature search of articles self assembling peptides and oral and maxillofacial surgery until 2022. The following search terms were used in different combinations via the conjunctions ‘and’ and ‘or’ self-assembling peptides, oral and maxillofacial surgery, dental implants and facial nerve injuries. I vitro and in vivo researches about topics in oral and maxillofacial surgery where selected. and reports which contains cutaneous paleness due to local anaesthesia were selected. Researches about other issues in dentistry, like remineralization, were excluded. Eighteen publication finally met the inclusion criteria. One study was listed twice in the literature search. The research contents are briefly summarized below.

\* Corresponding author. e-mail address: [Hacer.Eberlikose@ankaramedipol.edu.tr](mailto:Hacer.Eberlikose@ankaramedipol.edu.tr)

### **Self-assembling peptides in implant dentistry**

Dental implant treatments cover a large part of dentistry. For a successful implant treatment the osseointegration process between bone and the implant surface must be completed. In the process of osseointegration, adhesion, proliferation and differentiation of cells are important [6]. During the implant socket preparation procedure surgical trauma causes bleeding and hemostasis in the bone [7]. Moreover, this surgical trauma activates the growth and differentiation factors released from the bone debris. These cells and structures get in relation with the implant surface in nano and micro levels [7]. By changing the implant surfaces, faster bone healing and osseointegration is aimed. Because of this implant surfaces are still a major topic to investigate. These researches aimed to accelerate and optimize the osseointegration process. Ryu et al revealed that dental implant surfaces which are modified with a self-assembling peptide by chemical grafting are successful in vitro examinations [7].

In the study of Kohgo et al., implants were placed in bone areas regenerated with self-assembling peptides and the results obtained were found to be successful [8]. Sargeant et al stated that self-assembling peptides fill the metal foams and the peptides have the potential to induce new bone formation from the host tissue in an in vivo model [6]. Despite all these researches, no studies with long follow-up were found in the literature.

### **Self-assembling peptides in bone regeneration**

In 2011 Kohgo et al used self-assembling peptides (Pura Matrix) as grafting material in dogs around dental implants. The result of the peptide sequence used in this study creates a scaffold similar to the nanofiber and porous structure of the natural ECM [9]. Pura matrix is used as a scaffold with combinations of Platelet rich Plasma and stem cells. Promising results have been obtained at the end of the study [10]. In the literature review, it was determined that peptides were mixed and used with many different materials such as PRP, BMP 2 and stem cells [10,11]. Hayashi et al analyzed the self-assembling peptide nanofibers in combination with pluripotent stem cells in a rat critical size defect and declare successful results [12].

### **Using self-assembled peptides for nerve injuries**

During surgical procedures, like wisdom tooth surgeries, injuries to peripheral nerves can occur. Branches of the mandibular division of the trigeminal nerve, inferior alveolar nerve, lingual nerve and mental nerve may be affected as a result of operations performed in oral and maxillofacial surgery. After nerve injuries, a gap occurs between the distal and proximal parts of the nerve. In the clinic, these two nerve endings are routinely brought closer together to provide regeneration. For nerve regeneration self-assembling peptides mimickes the extracellular matrix (ECM) topography [12]. Although there are many in vitro studies on the effect of self-assembling peptides on nerve regeneration, there are only few in vivo studies. Panseri et al used flexible tubular electrospun with self assembled peptides for the nerve regeneration in rats [13].

### **The antimicrobial effects of self-assembled peptides**

Effective antimicrobial self assembling peptides are often broad-spectrum antimicrobials and carry the risk of being toxic for eukaryotic cell [14,15]. In the literature antimicrobial self-assembled peptides are used more for topical rather than systematic applications [14,15]. Nowadays, with the help of antimicrobial peptides, the surface properties of many materials are changed and they become more resistant to bacteria [15]. Ye et al used the GL13k antimicrobial peptide for dental implants coatings. This peptide sequence exhibited high antimicrobial activity against bacteria causing implant infections in vitro [16]. Thanks to these properties of self-assembling peptides, the need for antibiotics can be reduced.

## **3. Conclusion**

Preliminary studies show that; Self-assembled peptides are particularly successful in bone regeneration. Self-assembled peptides have the potential to impart osteogenic properties to the material. In addition to being a

synthetic material that successfully mimics the natural structure, peptides also stand out with their ease of use and production. To summarize the subject, self-assembling peptides are a very promising nanomaterial for oral and maxillofacial surgery.

## References

- [1] Hauser, C. A., & Zhang, S. (2010). Designer self-assembling peptide nanofiber biological materials. *Chemical Society Reviews*, 39(8), 2780-2790.
- [2] Aydın, Ş. & Kesmen, Z. (2020). Kendiliğinden Montajlı Peptidler ve Kullanım Alanları. *International Journal of Life Sciences and Biotechnology*, 3(3). p. 361-385.
- [3] Bhatnagar, R. S., Qian, J. J., Wedrychowska, A., Sadeghi, M., Wu, Y. M., & Smith, N. (1999). Design of biomimetic habitats for tissue engineering with P-15, a synthetic peptide analogue of collagen. *Tissue Engineering*, 5(1), 53-65.
- [4] Galler, K. M., Cavender, A., Yuwono, V., Dong, H., Shi, S., Schmalz, G., ... & D'Souza, R. N. (2008). Self-assembling peptide amphiphile nanofibers as a scaffold for dental stem cells. *Tissue Engineering Part A*, 14(12), 2051-2058.
- [5] Sivoilella, S., Brunello, G., Ferrarese, N., Puppa, A. D., D'Avella, D., Bressan, E., & Zavan, B. (2014). Nanostructured guidance for peripheral nerve injuries: a review with a perspective in the oral and maxillofacial area. *International journal of molecular sciences*, 15(2), 3088-3117.
- [6] Sargeant, T. D., Guler, M. O., Oppenheimer, S. M., Mata, A., Satcher, R. L., Dunand, D. C., & Stupp, S. I. (2008). Hybrid bone implants: self-assembly of peptide amphiphile nanofibers within porous titanium. *Biomaterials*, 29(2), 161-171.
- [7] Ryu, J. J., Park, K., Kim, H. S., Jeong, C. M., & Huh, J. B. (2013). Effects of anodized titanium with Arg-Gly-Asp (RGD) peptide immobilized via chemical grafting or physical adsorption on bone cell adhesion and differentiation. *International Journal of Oral & Maxillofacial Implants*, 28(4).
- [8] Kohgo, T., Yamada, Y., Ito, K., Yajima, A., Yoshimi, R., Okabe, K., ... & Ueda, M. (2011). Bone regeneration with self-assembling peptide nanofiber scaffolds in tissue engineering for osseointegration of dental implants. *International Journal of Periodontics & Restorative Dentistry*, 31(4).
- [9] Yoshimi, R., Yamada, Y., Ito, K., Nakamura, S., Abe, A., Nagasaka, T., ... & Ueda, M. (2009). Self-assembling peptide nanofiber scaffolds, platelet-rich plasma, and mesenchymal stem cells for injectable bone regeneration with tissue engineering. *Journal of Craniofacial Surgery*, 20(5), 1523-1530.
- [10] Chan, B., Wong, R. W. K., & Rabie, B. (2011). In vivo production of mineralised tissue pieces for clinical use: a qualitative pilot study using human dental pulp cell. *International Journal of Oral and Maxillofacial Surgery*, 40(6), 612-620.
- [11] Hayashi, K., Ochiai-Shino, H., Shiga, T., Onodera, S., Saito, A., Shibahara, T., & Azuma, T. (2016). Transplantation of human-induced pluripotent stem cells carried by self-assembling peptide nanofiber hydrogel improves bone regeneration in rat calvarial bone defects. *Bdj Open*, 2(1), 1-7.
- [12] Sivoilella, S., Brunello, G., Ferrarese, N., Puppa, A. D., D'Avella, D., Bressan, E., & Zavan, B. (2014). Nanostructured guidance for peripheral nerve injuries: a review with a perspective in the oral and maxillofacial area. *International journal of molecular sciences*, 15(2), 3088-3117.
- [13] Panseri, S., Cunha, C., Lowery, J., Del Carro, U., Taraballi, F., Amadio, S., ... & Gelain, F. (2008). Electrospun micro-and nanofiber tubes for functional nervous regeneration in sciatic nerve transections. *BMC biotechnology*, 8(1), 1-12.
- [14] Bozzini, S., Petrini, P., Tanzi, M. C., Arciola, C. R., Tosatti, S., & Visai, L. (2011). Poly (ethylene glycol) and hydroxy functionalized alkane phosphate self-assembled monolayers reduce bacterial adhesion and support osteoblast proliferation. *The International journal of artificial organs*, 34(9), 898-907.
- [15] Lombardi, L., Falanga, A., Del Genio, V., & Galdiero, S. (2019). A new hope: self-assembling peptides with antimicrobial activity. *Pharmaceutics*, 11(4), 166.
- [16] Ye, Z., Sang, T., Li, K., Fischer, N. G., Mutreja, I., Echeverría, C., ... & Aparicio, C. (2022). Hybrid nanocoatings of self-assembled organic-inorganic amphiphiles for prevention of implant infections. *Acta biomaterialia*, 140, 338-349.





## Selective transport of cadmium from acidic leach solutions by emulsion liquid membrane using TIOA as the carrier

**Aboubakar IBRAHIM<sup>1</sup>** , **Asuman UNAL<sup>2,\*</sup>** , **Volkan EYUPOGLU<sup>2</sup>** , **Recep Ali KUMBASAR<sup>3</sup>**

<sup>1</sup>Department of Chemical Engineering, Faculty of Engineering, Cankiri Karatekin University, Cankiri, 18200, Turkey

<sup>2</sup>Department of Chemistry, Faculty of Science, Cankiri Karatekin University, Cankiri, 18200, Turkey

<sup>3</sup>Department of Chemistry, Faculty of Science, Sakarya University, Adapazari, 54100, Turkey

### Abstract

In the present study, the selective separation of cadmium from the hydrochloric acid media was investigated experimentally by emulsion liquid membranes (ELMs) using tri-iso-octylamine (TIOA) as extractant and applied to the leach solution prepared from the zinc plant purification cake (CINKUR Co., Kayseri, Turkey). The effective parameters on both membrane and aqueous phase properties, such as the nature of acid and concentration of the acidic leach solution, concentration of stripping solution, extractant and surfactant concentrations, mixing speed, phase ratio, and cadmium concentration of the acidic leach solution on the extraction of cadmium was optimized using a solution of synthetic cadmium in HCl. The selectivity and the efficiency of the improved ELM process were examined for the leach solution under optimum conditions. The results showed that 95% of cadmium was extracted by the ELM from the acidic leach solutions, containing Cd<sup>2+</sup>, Zn<sup>2+</sup>, Co<sup>2+</sup> and Ni<sup>2+</sup> ions, within 10 min with a higher selectivity coefficient.

**Keywords:** Emulsion liquid membrane, Tri-iso-octylamine, Copper cake, Acidic leach solution, Cadmium extraction.

### 1. Introduction

Cadmium occurs naturally as a minor constituent of base metal ores and coal deposits. Therefore, cadmium is often obtained commercially as a by-product in base metal recycling and refining. For instance, 95% of cadmium comes as a by-product from zinc-based hydrometallurgical processes. Because of its economic value, the recovery of the cadmium metal has attached great interest of many scientists [1–5].

Extensive work has been done on the development of methods for the separation and recovery of cadmium ions [6–10]. Precipitation and filtration of metal hydroxide are commonly used when higher concentrations are processed [11]. Contrary to its simplicity, most wastewaters have an acidic nature and require sensitive pH adjustment to keep the solution in alkaline conditions. The disposal of the produced sludge and the higher consumption of chemical and auxiliary chemicals are also considered another problem in this process. In addition, ion-exchange treatments with ionic resins [12], clays [13], or zeolites [14] can be used as an alternative method for metal removal and recycling. The disadvantage of this method is that it requires the use of more reagents for regeneration, which causes serious secondary pollution. Meantime, adsorption of cadmium on the surface of materials such as carbon [15] or alumina [16] can be completed with good results, but these methods are expensive when pure sorbents are employed. Another alternative is to apply a biofiltration process using microalgae [17] or bacteria [18]. However, these processes require a constant source of nutrients and strict control of temperature, humidity, air pressure, etc. to keep algae or bacteria alive for a continuous and efficient removal and recycling process [19]. Solvent extraction methods become an important alternative in recent years for the recovery and separation of metal from aqueous solutions [20–24].

Emulsion liquid membranes (ELM), one of the solvent extraction methods, is a well-known technique for the separation and purification of metal ions from aqueous solutions due to their low capital investment, space

\* Corresponding author. e-mail address: [asumanunal@karatekin.edu.tr](mailto:asumanunal@karatekin.edu.tr)

requirements and energy consumption [25–30]. In such techniques, the nature of the selected carrier plays a crucial role in the selectivity and efficiency of the extraction process [31]. There are many studies in the literature on the recovery of heavy metals from water and wastewater using ELM processes [32–36].

The main advantages of ELM processes can be described as follows; (a) high interfacial area for mass transfer due to the small size of the aqueous phase droplets; (b) high diffusion rate of the metal ions through the membrane; (c) simultaneous performance of extraction (at the outer interface) and stripping (at the inner phase) in the same process, and (d) capability of treating a variety of ions and compounds for industrial applications with a greater speed and with a high degree of effectiveness.

In the present work, the recovery of cadmium ions in HCl media was experimentally performed using ELM to improve a sensitive and efficient process for cadmium extraction. Afterward, the optimum conditions obtained for synthetic solution were applied to pretreated acidic leach solutions containing  $\text{Cd}^{2+}$ ,  $\text{Zn}^{2+}$ ,  $\text{Co}^{2+}$  and  $\text{Ni}^{2+}$ .

## 2. Materials and Methods

### 2.1. Reagents

The liquid membrane phase consists of a surfactant, an extractant and a diluent. Two types of surfactants were used in this study. The first surfactant is a non-ionic polyamine, which is commercially known as ECA 4360J, supplied by Exxon-Mobil. The other non-ionic surfactant is sorbitan monooleate, a product of Fluka, commercially known as Span 80. As an extractant, tri-iso-octylamine (TIOA) was purchased from Sigma-Aldrich Company. Commercial kerosene (TUPRAS Oil Company, Turkey) was used as diluents as it is a complex mixture of aliphatic origin containing also about 15% w/w aromatic compound.  $\text{CdCl}_2$ , HCl,  $\text{H}_2\text{SO}_4$ ,  $\text{HNO}_3$ ,  $\text{NH}_3$ ,  $(\text{NH}_4)_2\text{CO}_3$ ,  $\text{CH}_3\text{COONH}_4$ ,  $\text{NH}_4\text{Cl}$  were in analytic grades and were purchased from (Merck, Germany) and used directly from the manufacturer.

### 2.2. Preparation of feed solutions and membranes

The leach solutions produced from zinc plants purification cake (CINKUR Co., Turkey) containing an average of 20%  $\text{Zn}^{2+}$ , 10%  $\text{Cu}^{2+}$ , 1%  $\text{Pb}^{2+}$ , 0.1%  $\text{Fe}^{3+}$ , 2.2%  $\text{Co}^{2+}$ , 3.1%  $\text{Ni}^{2+}$ , 3.0%  $\text{Cd}^{2+}$  and 1%  $\text{Al}^{3+}$  on mass basis was leached by adding of 2 M HCl solution at 85°C for 240 minutes. This solution was used for real sample application of the optimized transport conditions for  $\text{Cd}^{2+}$  transport through ELM processes. After the preparation of  $\text{Zn}^{2+}$ ,  $\text{Cu}^{2+}$ ,  $\text{Pb}^{2+}$ ,  $\text{Fe}^{3+}$ ,  $\text{Co}^{2+}$ ,  $\text{Ni}^{2+}$ ,  $\text{Cd}^{2+}$  and  $\text{Al}^{3+}$  solutions, the metal ions, except Cd, Ni and Co, in the acidic leach solution were precipitated by adding various reagents and adjusting the pH of the solution. Then, these stock leach solutions, containing 1650 mg/L  $\text{Cd}^{2+}$ , 130 mg/L  $\text{Zn}^{2+}$ , 1305 mg/L  $\text{Co}^{2+}$  and 1725 mg/L  $\text{Ni}^{2+}$ , were diluted three times by adding hydrochloric acid and water to use as feed solution in real sample application experiments.

To prepare the membranes, a 30 mL portion of TIOA and Span 80 in kerosene are emulsified in a 250 mL beaker with a variable speed mixer at a stripping speed of 1800 rpm. Then, 18 mL of 6 M ammonia solution was added dropwise to the stirred membrane solution until the ratio of the desired volume of membrane solution to stripping solution. The solution is stirred continuously for 20 minutes to obtain a stable ELM.

### 2.3. Method

48 mL of prepared ELM and 250 mL of feed solution were mixed in a 600 mL beaker. The contents were stirred for 10 minutes at 250 rpm with a variable speed mixer equipped with a turbine-type impeller. Important parameters such as acid concentrations in the acidic feed solution, mixing speed, type and concentration of stripping solution, extractant concentration, surfactant concentration and phase ratio are effective in the permeability and separation of cadmium from the acidic leach solution containing, cobalt, nickel and zinc, acid and cadmium, were investigated. At the end of each extraction-stripping cycle, the emulsion phase was recovered

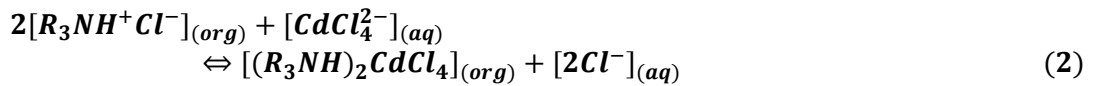
and subsequently separated its constituents as organic phase and ammonia solutions using a high voltage splitter with niobium electrodes.

In further, the qualitative and quantitative analyses of the removal ions were carried out by taking samples from the feed solution periodically. For this, atomic absorption spectrophotometry (Shimadzu AA-6701F model, Tokyo, Japan) was used for trace level metal analysis of  $\text{Cd}^{2+}$ ,  $\text{Co}^{2+}$ ,  $\text{Ni}^{2+}$  and  $\text{Zn}^{2+}$  determinations. All the extraction experiments were carried out batchwise at the ambient temperature of  $25 \pm 1^\circ\text{C}$ . All aqueous solutions were prepared using Milli-Q ultra-pure water.

#### 2.4. The extraction mechanism of cadmium from the leach solution

Tri-iso-octylamine is an ammonia-derivative organic compound, so its solubility is much lower than ammonia due to its long chain alkyl groups. Typically, it can react on the central basic nitrogen atom, such as various inorganic amine salts, which can undergo ion-exchange reactions with many anions. In the presence of  $\text{HCl}$  in the feed solution, the extraction, and stripping reactions of  $\text{Cd}^{2+}$  via ELM can be illustrated as follows [37,38].

Initially, TIOA (shown as  $\text{R}_3\text{N}$ ) in the membrane phase reacts with  $\text{HCl}$  in the feed solution and  $\text{CdCl}_4^{2-}$  is replaced with  $\text{Cl}^-$  in the membrane solution according to Equations 1 and 2.



Then,  $\text{NH}_3$  in the stripping solution reacts with  $[(\text{R}_3\text{NH})_2\text{CdCl}_4]$  to strip  $\text{Cd}^{2+}$  ions into the stripping solution.

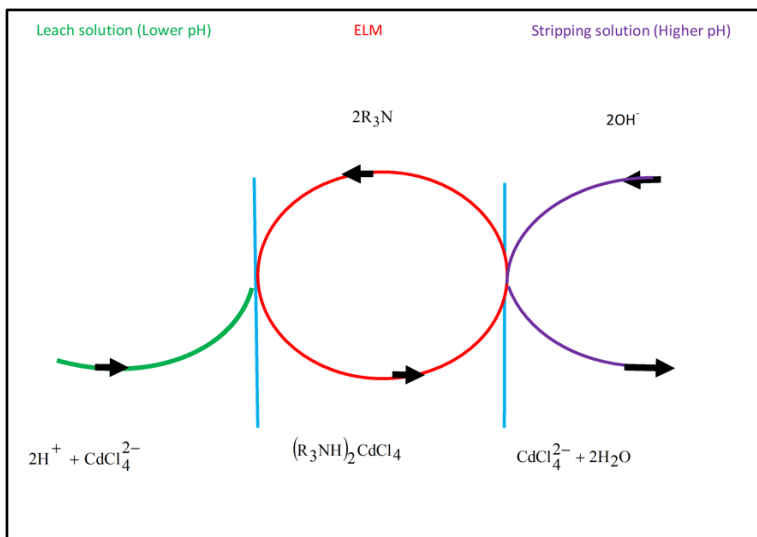
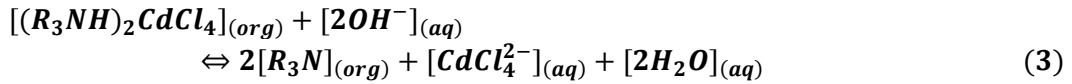


**Figure 1.** Extraction of  $\text{Cd}^{2+}$  ions by ELM using TIOA as extracted from acidic leach solutions of zinc plant copper cake

### 3. Results and Discussions

### 3.1. Effect of acid concentration in feed solution on the extraction of cadmium

The extraction of  $\text{Cd}^{2+}$  ions was studied in the feed solutions containing HCl concentration in the range of 0.01 M – 2.0 M. The results show that the percentage of extraction of  $\text{CdCl}_4^{2-}$  ions increase with increasing HCl concentration up to 0.5 M. Further increase resulted in a decrease  $\text{CdCl}_4^{2-}$  extraction as shown in Figure 2.

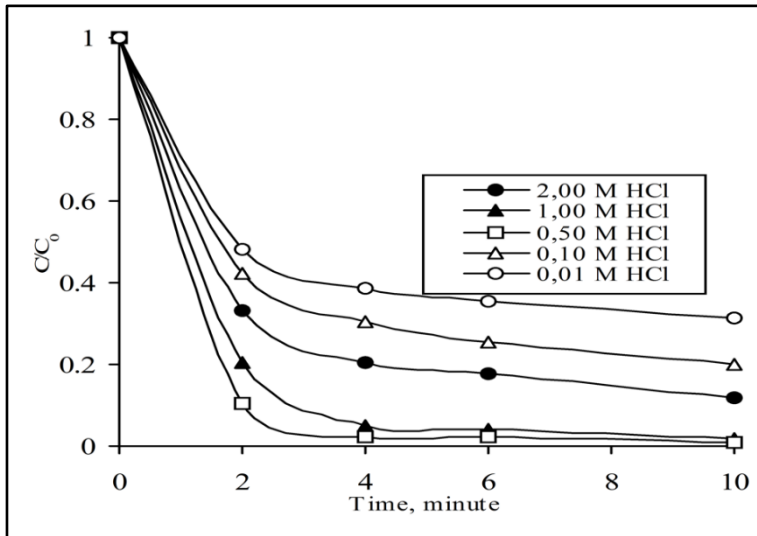


**Figure 2.** Effect of acid concentration of feed solution on the extraction rate of  $\text{Cd}^{2+}$  (Span 80; 6% TIOA; 6% kerosene; 88% stripping solution; 18 mL of 6 M  $\text{NH}_3$  solution; acid concentration of the feed solution in 0.1-2.0 M HCl; 100 mg/L  $\text{Cd}^{2+}$  concentration of feed solution; mixing speed 250 rpm; phase ratio 3/5; treatment ratio; 250/48)

The extraction of  $\text{CdCl}_4^{2-}$  and  $\text{CdCl}_3^-$  anions increase with increasing proton and  $\text{Cl}^-$  concentration up to a limit, and above this proton concentration limit, neutral cadmium species are formed. After reaching the maximum value of cadmium extraction, the percentage of the extraction of cadmium decreases with increasing acid concentration due to the reduction of anionic cadmium species in the aqueous solution. This phenomenon can be explained according to Equation 4.



$\text{H}_2\text{CdCl}_4$  species will form in the acidic aqueous leach solution with increasing proton concentration, and this cadmium species may not ionize completely at higher acid and  $\text{Cl}^-$  concentrations. Therefore, an organometallic complex cannot be formed between  $\text{R}_3\text{NH}^+$  cation and  $\text{H}_2\text{CdCl}_4$ . Hence, the extraction of anionic cadmium decreases with  $\text{R}_3\text{NH}^+$  will decrease, and thereby the percentage of extraction of cadmium decrease with increasing acid and  $\text{Cl}^-$  concentration. In this study, 0.5 M HCl was determined as the most suitable acid concentration, which provides 98.9% cadmium extraction efficiency.

### 3.2. Effect of stripping solution type and concentration

The stripping agent type is well known as the most influential parameter for an effective ELM design [39,40]. In this study, we examined the four different types of stripping solutions ( $\text{NH}_3$ ,  $\text{Na}_2\text{CO}_3$ ,  $\text{NH}_4\text{Cl}$  and  $\text{CH}_3\text{COONH}_4$ ) in the same molar concentrations (6 M) to form stable and effective ELM. The results of the effect of the stripping solutions on the  $\text{Cd}^{2+}$  extraction was given in Figure 3.

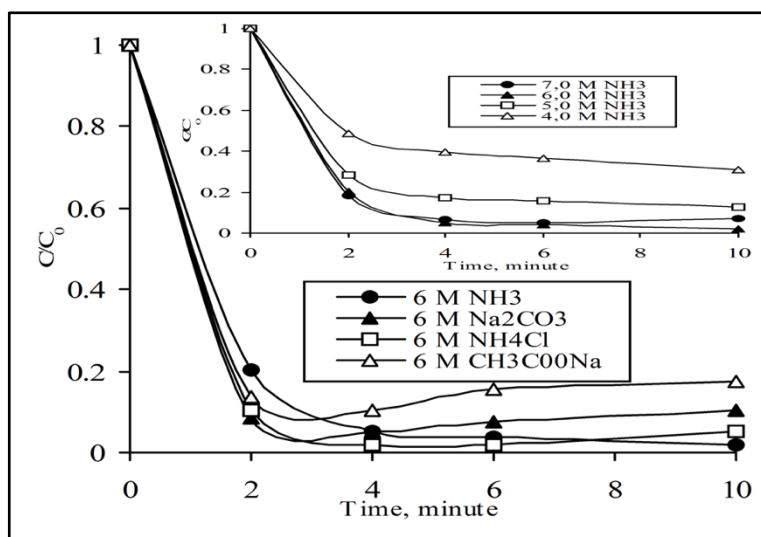


**Figure 3.** Effect of the nature of stripping solution on the  $\text{Cd}^{2+}$  extraction (Span 80; 6% TIOA; 6% kerosene; 88% stripping solution; 18 mL of 6 M  $\text{NH}_3$  solution; acid concentration of the feed solution in 0.1-2.0 M HCl; 100 mg/L  $\text{Cd}^{2+}$  concentration of feed solution; mixing speed 250 rpm; phase ratio 3/5; treatment ratio; 250/48)

As seen in Figure 3, the presence of ammonia solution increased the percentage of  $\text{CdCl}_4^{2-}$  extraction, reaching a maximum at 6.0 M, whereas it decreased slightly at higher ammonia concentrations. Possibly, a higher concentration of ammonia solution causes deterioration of emulsion stability and adversely affects the transport efficiency of anionic cadmium species. Consequently, the most effective ammonia solution concentration in the stripping phase was determined as 6.0 M for the selective extraction of  $\text{CdCl}_4^{2-}$ .

### 3.3. Effect of surfactant type and concentration

The results of surfactant type and concentration on  $\text{Cd}^{2+}$  transport were studied using two different surfactants at different concentrations for ELM, and the results were presented in Figure 4.

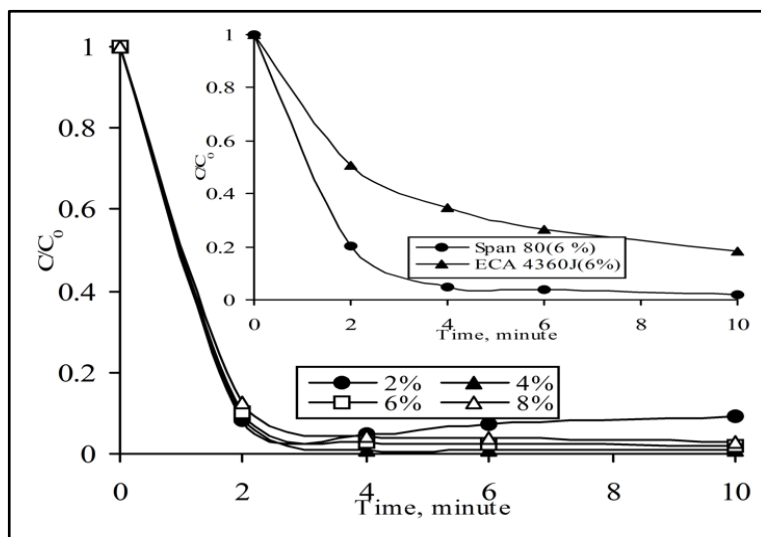


**Figure 4.** Effect of surfactant type and concentration on the  $\text{Cd}^{2+}$  extraction (Span 80; 6% TIOA; 6% kerosene; 88% stripping solution; 18 mL of 6 M  $\text{NH}_3$  solution; acid concentration of the feed solution in 0.1-2.0 M HCl; 100 mg/L  $\text{Cd}^{2+}$  concentration of feed solution; mixing speed 250 rpm; phase ratio 3/5; treatment ratio; 250/48)

It is observed that Span 80 has a higher extraction ability than ECA 4360J with 98.0% of  $\text{CdCl}_4^{2-}$  extraction, which overlaps the results reported in the literature [41]. According to these reports, the membrane combined

with Span 80 exhibits less resistance to mass transfer than other surfactants but suffers from osmotic swelling and poor chemical stability due to hydrolysis and macroemulsion formation [41]. Wasan *et. al.* also reported that ECA 4360J can form very stable emulsions compared to Span 80 [42], but Strzelbicki and Schlosser reported higher interfacial mass transfer resistance and interactions with organic [43]. Therefore, Span 80 was chosen as the most appropriate surfactant for further studies.

Looking at Figure 4, it is clear that the surfactant concentration also plays an important role in the extraction of  $\text{CdCl}_4^{2-}$ . Here, it is seen that the extraction percentage increases with decreasing Span 80 concentration. However, the final volume of emulsion decreased after extraction in the presence of a 2% surfactant concentration. This indicates a strong relationship between emulsion stability and surfactant concentration. In another word, the increasing concentration of surfactant from 2.0% to 4.0% increased both stability of the emulsion liquid membrane and the extraction percentage of  $\text{CdCl}_4^{2-}$  from 90.8% to 99.0%. On the other hand, above the 4.0% concentration of Span 80, the extraction rate decreased. Thus, 4.0% Span 80 was chosen as the best surfactant concentration.

### 3.4. Real sample application of $\text{Cd}^{2+}$ transport

The optimum conditions for the  $\text{Cd}^{2+}$  extraction process via ELM was given in Table 1.

**Table 1.** Optimum conditions for the  $\text{Cd}^{2+}$  extraction via ELM

Parameter	Value
Surfactant (Span 80)	4 %
Extractant (TIOA)	2 %
Diluent (Kerosene)	94 %
Type and concentration of stripping solution	18 mL of 6 M $\text{NH}_3$
Acid type and concentration of the feed solution	0.5 M HCl
Cadmium concentration in the feed solution	500 mg/L
Mixing speed	350 rpm
Phase ratio	3/5
Treatment ratio	250/48

The effect of the other ions on the cadmium extraction from the acidic leach solution containing 500 mg/L  $\text{Cd}^{2+}$ , 395 mg/L  $\text{Co}^{2+}$ , 525 mg/L  $\text{Ni}^{2+}$  and 35 mg/L  $\text{Zn}^{2+}$  was shown in Figure 7.

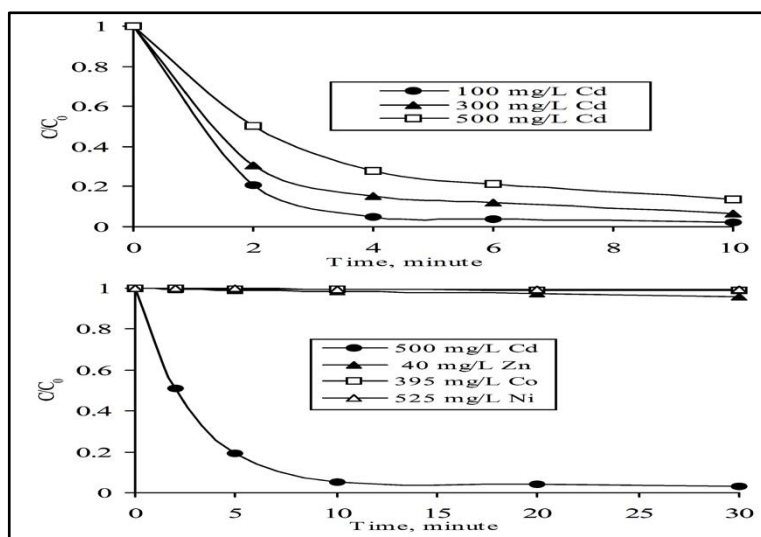


**Figure 7.** Effect of cadmium concentration in feed solution on the extraction rate of  $\text{Cd}^{2+}$  and real sample application under optimum conditions

It was observed that the cadmium concentration in the feed solution was reduced at the end of the thirty minutes from 500 mg/L to 15 mg/L with an extraction efficiency of 97 % and the emulsion stability was also maintained throughout the study. As the 500 mg/L cadmium concentration in the feed solution decreases over time, the cobalt, nickel and zinc ion concentrations in the first ten minutes remain relatively steady. However, after these minutes, zinc (especially at intervals of 20-30 minutes) was extracted into the stripping solution at a higher rate than nickel and cobalt ions. The extraction percentages of  $\text{Cd}^{2+}$ ,  $\text{Ni}^{2+}$ ,  $\text{Co}^{2+}$  and  $\text{Zn}^{2+}$  at 10 minutes were 95%, 0.3%, 0.6% and 1.4%, respectively.

#### 4. Conclusions

This study described the development of a new ELM-based process with TIOA as the extractant for the extraction of cadmium ions from an HCl medium. Cadmium extraction was obtained from the acidic leach solution prepared synthetically containing 500 mg/L  $\text{Cd}^{2+}$  with a yield of approximately 86.2%. The effect of the nature and concentration of the acid, stripping solution and surfactant used in the ELM process on cadmium extraction were comprehensively investigated and optimum conditions were determined. Liquid membrane selectivity and real sample applicability of  $\text{Cd}^{2+}$  over other ions in the acidic leach solutions were examined under optimal conditions. The results show that the validity of the ELM process can be used for the selective extraction and concentration of cadmium from hydrochloric acid leach solutions with environmental sustainability.

#### Acknowledgments

The author would like to express his sincere gratitude to the State Planning Organization of Turkey (DPT) and Sakarya University BAPK Coordinator Mehmet Yilmaz for their support of this study.

#### References

- [1] J. Fang, B. Tang, M. Li, Z. Xu, Recovery of cadmium from a zinc hydrometallurgical leachate using reactive emulsion liquid membrane technology, *Journal of Chemical Technology and Biotechnology*. 79 (2004). <https://doi.org/10.1002/jctb.946>.
- [2] G. Cote, D. Bauer, Liquid-liquid extraction of germanium with oxine derivatives, *Hydrometallurgy*. 5 (1980). [https://doi.org/10.1016/0304-386X\(80\)90035-3](https://doi.org/10.1016/0304-386X(80)90035-3).

- [3] T.C. Huang, T. hua Tsai, Extraction of Nickel(II) from Sulfate Solutions by Bis(2-ethylhexyl)phosphoric Acid Dissolved in Kerosene, *Ind Eng Chem Res.* 28 (1989). <https://doi.org/10.1021/ie00094a022>.
- [4] J.A. Golding, C.D. Barclay, Equilibrium characteristics for the extraction of cobalt and nickel into di(2-ethylhexyl) phosphoric acid, *Can J Chem Eng.* 66 (1988). <https://doi.org/10.1002/cjce.5450660612>.
- [5] R.A. Kumbasar, O. Tutkun, Selective separation of gallium from acidic leach solutions by emulsion liquid membranes, *Sep Sci Technol.* 41 (2006). <https://doi.org/10.1080/01496390600786150>.
- [6] A. Afkhami, T. Madrakian, H. Siampour, Flame atomic absorption spectrometric determination of trace quantities of cadmium in water samples after cloud point extraction in Triton X-114 without added chelating agents, *J Hazard Mater.* 138 (2006). <https://doi.org/10.1016/j.jhazmat.2006.03.073>.
- [7] M. Soylak, M. Tuzen, Diaion SP-850 resin as a new solid phase extractor for preconcentration-separation of trace metal ions in environmental samples, *J Hazard Mater.* 137 (2006). <https://doi.org/10.1016/j.jhazmat.2006.04.027>.
- [8] L. Gotfryd, M. Cox, The selective recovery of cadmium(II) from sulfate solutions by a counter-current extraction-stripping process using a mixture of diisopropylsalicylic acid and Cyanex® 471X, *Hydrometallurgy.* 81 (2006). <https://doi.org/10.1016/j.hydromet.2006.01.001>.
- [9] A.L. Ahmad, A. Kusumastuti, M.M.H. Shah Buddin, C.J.C. Derek, B.S. Ooi, Emulsion liquid membrane based on a new flow pattern in a counter rotating Taylor-Couette column for cadmium extraction, *Sep Purif Technol.* 127 (2014). <https://doi.org/10.1016/j.seppur.2014.02.029>.
- [10] R.A. Kumbasar, Selective Extraction of Cadmium from Multicomponent Acidic Leach Solutions by Emulsion Liquid Membrane using Amberlite LA-2 as Extractant, *Separation Science and Technology (Philadelphia).* 48 (2013). <https://doi.org/10.1080/01496395.2012.760600>.
- [11] H.A. Aziz, N. Othman, M.S. Yusuff, D.R.H. Basri, F.A.H. Ashaari, M.N. Adlan, F. Othman, M. Johari, M. Perwira, Removal of copper from water using limestone filtration technique determination of mechanism of removal, *Environ Int.* 26 (2001). [https://doi.org/10.1016/S0160-4120\(01\)00018-6](https://doi.org/10.1016/S0160-4120(01)00018-6).
- [12] S. Yalçın, R. Apak, J. Hizal, H. Afşar, Recovery of copper (II) and chromium (III, VI) from electroplating-industry wastewater by ion exchange, *Sep Sci Technol.* 36 (2001). <https://doi.org/10.1081/SS-100105912>.
- [13] K.R. Reddy, S. Chinthamreddy, Sequentially Enhanced Electrokinetic Remediation of Heavy Metals in Low Buffering Clayey Soils, *Journal of Geotechnical and Geoenvironmental Engineering.* 129 (2003). [https://doi.org/10.1061/\(asce\)1090-0241\(2003\)129:3\(263\)](https://doi.org/10.1061/(asce)1090-0241(2003)129:3(263)).
- [14] P. Li, F. Handan Tezel, Adsorption separation of N<sub>2</sub>, O<sub>2</sub>, CO<sub>2</sub> and CH<sub>4</sub> gases by  $\beta$ -zeolite, *Microporous and Mesoporous Materials.* 98 (2007). <https://doi.org/10.1016/j.micromeso.2006.08.016>.
- [15] K. Kadirvelu, C. Faur-Brasquet, P. le Cloirec, Removal of Cu(II), Pb(II), and Ni(II) by adsorption onto activated carbon cloths, *Langmuir.* 16 (2000). <https://doi.org/10.1021/la0004810>.
- [16] M.L. Cervera, M.C. Arnal, M. de La Guardia, Removal of heavy metals by using adsorption on alumina or chitosan, *Anal Bioanal Chem.* 375 (2003). <https://doi.org/10.1007/s00216-003-1796-2>.
- [17] A.M.Y. Chong, Y.S. Wong, N.F.Y. Tam, Performance of different microalgal species in removing nickel and zinc from industrial wastewater, *Chemosphere.* 41 (2000). [https://doi.org/10.1016/S0045-6535\(99\)00418-X](https://doi.org/10.1016/S0045-6535(99)00418-X).
- [18] M. Vainshtein, P. Kuschik, J. Mattusch, A. Vatsourina, A. Wiessner, Model experiments on the microbial removal of chromium from contaminated groundwater, *Water Res.* 37 (2003). [https://doi.org/10.1016/S0043-1354\(02\)00455-4](https://doi.org/10.1016/S0043-1354(02)00455-4).
- [19] N.K. Srivastava, C.B. Majumder, Novel biofiltration methods for the treatment of heavy metals from industrial wastewater, *J Hazard Mater.* 151 (2008). <https://doi.org/10.1016/j.jhazmat.2007.09.101>.
- [20] L. Wang, R. Paimin, R.W. Cattrall, W. Shen, S.D. Kolev, The extraction of cadmium(II) and copper(II) from hydrochloric acid solutions using an Aliquat 336/PVC membrane, *J Memb Sci.* 176 (2000). [https://doi.org/10.1016/S0376-7388\(00\)00436-1](https://doi.org/10.1016/S0376-7388(00)00436-1).
- [21] A. Hachemaoui, K. Belhamel, H.J. Bart, Emulsion liquid membrane extraction of Ni(II) and Co(II) from acidic chloride solutions using bis-(2-ethylhexyl) phosphoric acid as extractant, *J Coord Chem.* 63 (2010). <https://doi.org/10.1080/00958972.2010.500375>.



- [22] S. Venkatesan, K.M. Meera Sheriffa Begum, Emulsion liquid membrane pertraction of benzimidazole using a room temperature ionic liquid (RTIL) carrier, *Chemical Engineering Journal*. 148 (2009). <https://doi.org/10.1016/j.cej.2008.08.026>.
- [23] D. Mondal, D. Saha, A. Bhowal, S. Datta, Mass transfer characteristics in extraction by emulsion liquid membrane system - Immobilized emulsion phase, *Indian Journal of Chemical Technology*. 15 (2008).
- [24] S. Chakraborty, S. Datta, P. Bhattacharya, Studies on extraction of chromium(VI) from acidic solution by emulsion liquid membrane, *Indian Journal of Chemical Technology*. 12 (2005).
- [25] L.G. Wu, J.N. Shen, C.H. Du, T. Wang, Y. Teng, B. van der Bruggen, Development of AgCl/poly(MMA-co-AM) hybrid pervaporation membranes containing AgCl nanoparticles through synthesis of ionic liquid microemulsions, *Sep Purif Technol*. 114 (2013). <https://doi.org/10.1016/j.seppur.2013.04.010>.
- [26] B.S. Chanukya, N.K. Rastogi, Extraction of alcohol from wine and color extracts using liquid emulsion membrane, *Sep Purif Technol*. 105 (2013). <https://doi.org/10.1016/j.seppur.2012.12.001>.
- [27] M.A. Hasan, Y.T. Selim, K.M. Mohamed, Removal of chromium from aqueous waste solution using liquid emulsion membrane, *J Hazard Mater*. 168 (2009). <https://doi.org/10.1016/j.jhazmat.2009.03.030>.
- [28] M. Chakraborty, C. Bhattacharya, S. Datta, Mass transfer analysis of the extraction of nickel(II) by emulsion liquid membrane, *Indian Journal of Chemical Technology*. 10 (2003).
- [29] P.S. Kulkarni, K.K. Tiwari, V. v. Mahajani, Studies in extraction of nickel by liquid emulsion membrane process, *Indian Journal of Chemical Technology*. 6 (1999).
- [30] S. v. Kumar, G.L. Tulasi, M. Ravindram, M. Chanda, J.R. Mudakavi, A.K. Mukherjee, Treatment of electroplating effluent through emulsion-free liquid membrane, *Indian Journal of Chemical Technology*. 2 (1995).
- [31] S. Jafari, M.R. Yaftian, M. Parinejad, Facilitated transport of cadmium as anionic iodo-complexes through bulk liquid membrane containing hexadecyltrimethylammonium bromide, *Sep Purif Technol*. 70 (2009). <https://doi.org/10.1016/j.seppur.2009.09.003>.
- [32] F. Valenzuela, C. Fonseca, C. Basualto, O. Correa, C. Tapia, J. Sapag, Removal of copper ions from a waste mine water by a liquid emulsion membrane method, *Miner Eng*. 18 (2005). <https://doi.org/10.1016/j.mineng.2004.05.011>.
- [33] S. Bourenane, M.E.H. Samar, A. Abbaci, Extraction of cobalt and lead from waste water using a liquid surfactant membrane emulsion, *Acta Chim Slov*. 50 (2003).
- [34] H.R. Mortaheb, H. Kosuge, B. Mokhtarani, M.H. Amini, H.R. Banihashemi, Study on removal of cadmium from wastewater by emulsion liquid membrane, *J Hazard Mater*. 165 (2009). <https://doi.org/10.1016/j.jhazmat.2008.10.039>.
- [35] A.L. Ahmad, A. Kusumastuti, C.J.C. Derek, B.S. Ooi, Emulsion liquid membranes for cadmium removal: Studies of extraction efficiency, *Membrane Water Treatment*. 4 (2012). <https://doi.org/10.12989/mwt.2013.4.1.011>.
- [36] A. Balasubramanian, S. Venkatesan, Removal of phenolic compounds from aqueous solutions by emulsion liquid membrane containing Ionic Liquid [BMIM] + [PF 6] - in Tributyl phosphate, *Desalination*. 289 (2012). <https://doi.org/10.1016/j.desal.2011.12.027>.
- [37] Q. Li, Q. Liu, K. Li, S. Tong, Separation study of cadmium through an emulsion liquid membrane, *Talanta*. 44 (1997). [https://doi.org/10.1016/S0039-9140\(96\)02098-X](https://doi.org/10.1016/S0039-9140(96)02098-X).
- [38] D. He, S. Gu, M. Ma, Simultaneous removal and recovery of cadmium (II) and CN- from simulated electroplating rinse wastewater by a strip dispersion hybrid liquid membrane (SDHLM) containing double carrier, *J Memb Sci*. 305 (2007). <https://doi.org/10.1016/j.memsci.2007.07.001>.
- [39] N. Othman, H. Mat, M. Goto, Separation of silver from photographic wastes by emulsion liquid membrane system, *J Memb Sci*. 282 (2006). <https://doi.org/10.1016/j.memsci.2006.05.020>.
- [40] N. Othman, N.F.M. Noah, K.W. Poh, O.Z. Yi, High Performance of Chromium Recovery from Aqueous Waste Solution Using Mixture of Palm-oil in Emulsion Liquid Membrane, in: *Procedia Eng*, 2016. <https://doi.org/10.1016/j.proeng.2016.06.611>.

- [41] J. Saji, T. Prasada Rao, C.S.P. Iyer, M.L.P. Reddy, Extraction of iron(III) from acidic chloride solutions by Cyanex 923, *Hydrometallurgy*. 49 (1998). [https://doi.org/10.1016/s0304-386x\(98\)00030-9](https://doi.org/10.1016/s0304-386x(98)00030-9).
- [42] D.T. Wasan, Z.M. Gu, N.N. Li, Separation of metal ions by ligand-accelerated transfer through liquid surfactant membranes, *Faraday Discuss Chem Soc.* 77 (1984). <https://doi.org/10.1039/DC9847700067>.
- [43] J. Strzelbicki, S. Schlosser, Influence of surface-active substances on pertraction of cobalt(II) cations through bulk and emulsion liquid membranes, *Hydrometallurgy*. 23 (1989). [https://doi.org/10.1016/0304-386X\(89\)90018-2](https://doi.org/10.1016/0304-386X(89)90018-2).



# Planning Optimal Forest Road Network Using Unmanned Aerial Vehicle (Eldivan Sample)

**Turgay ÇÖLKÜŞÜ<sup>1,\*</sup> , Ender BUĞDAY<sup>2</sup> **

<sup>1</sup>Graduate School of Natural and Applied Science, Çankırı Karatekin University, Çankırı, Turkey

<sup>2</sup>Faculty of Forestry, Çankırı Karatekin University, Çankırı, Turkey

## Abstract

This study, using Unmanned Aerial Vehicle (UAV) for the existing forest road network on forest roads, which undertakes the basic infrastructure in the execution of various forestry activities, is used to determine and plan the forest road locations required for the optimal forest road network, such as drones, etc. This study was conducted to demonstrate the usability of featured technologies. In this study, a practical approach is presented in the use of databases that can be processed with the help of Geographic Information Systems (GIS) software to make evaluations about national forest road networks with the data obtained. Within the scope of the study, the current orthomosaic data was obtained by making flights from various heights with the drone (UAV) device of the forest assets within the borders of Çankırı Karatekin University Faculty of Forestry Eldivan Research and Application Forest (367 ha). With the advantageous analysis environment provided by better quality and sensitive data, a multi-database containing the data of the entire study area has been created. After the current state of the forest road network has been determined, the existing forest road network has been defined in the digital environment and the necessary locations to reach the optimal road network have been determined by the GIS software. By using the orthomosaic and high-resolution Digital Elevation (DEM) data produced within the scope of the study, the locations needed in accordance with the relevant communiqué of the General Directorate of Forestry (GDF) were included in the planning and alternative routes were revealed for the project design studies. By using the UAV device, practical and effective data can be obtained in a short time in practice and a suitable decision-making environment can be provided for decision makers. All the data produced as a result of this study are represented in a database that can be used by scientists and other interested participants.

**Keywords:** *Unmanned aerial vehicle, forest road, planning, alternative route*

## 1. Introduction

In our country, the main infrastructure facility that serves to carry out forestry studies and various forestry plans is forest roads. It has an important place in the continuation of forestry activities throughout the year and without interruption [1]. In Turkey, road planning and construction works started in 1937 [1], but acceleration was seen in the early 1960s [2]. Forest road network planning studies in the world show a constant change until today with the rapidly developing and widespread technology [3]. In the period until today, there have been transformations with the effect of science and technology in terms of forest road network evaluation. In the past, studies carried out with traditional planning included various errors and deficiencies as they were not more detailed and clearer. This disadvantageous situation is on its way to an advantageous situation due to the use of computer software of Remote sensing (UA) techniques and Geographic Information Systems (GIS) approaches, and the increasing number of experts day by day. In planning and evaluation works that require time and expense, significant distances have been covered in terms of both time and costs, and an advantageous situation has been achieved.

Since detailed and sensitive evaluations are possible with the presence of clearer and higher quality information, the information obtained within the framework of the "Precision Forestry" approach can be beneficial in achieving the desired goal or objectives [4,5,6]. Along with the advantages of GIS software, it is possible to put forward more applicable strategies at every stage of the evaluation process. Obtaining quality information with modern and technological devices, processing this information with various software and contributing to the decision-making process; It means that it is an important support for planners, implementers or decision makers [7].

\* Corresponding author. e-mail address: tugaycolkus@hotmai.com

Planning, construction, maintenance and repair of forest roads in Turkey are carried out in accordance with the communiqué numbered 292 published by the General Directorate of Forestry (GDF) in 2008 [8]. According to this communiqué, forest roads are divided into main and secondary forest roads. Secondary forest roads are also classified in subgroups as A type and B type. Although B-type secondary forest roads are the most widely used forest roads among all forest roads, it can be said that the most important features of this type of forest roads are that they have very low geometric features and that they are obtained at a very low cost compared to other forest road types with higher standards [9]. The most important step after planning and revealing the alternative routes is to determine the route with the least inconsistency between the land characteristics and the plan among the alternative routes [10]. Here, in the evaluation of the optimum forest road network, it is essential to determine the existing forest road network and to make evaluations including this road network.

After examining the forest roads built and completed with the existing forest road network plan in terms of technique and forest transport, it is essential to try to reach the highest possible opening rate [11]. In our country, in the evaluation of forest roads, the current tulle is generally taken into consideration. The importance and innovative aspect of this study is the production of the Digital Terrain Model (SAM) using Unmanned Aerial Vehicle (UAV) and the evaluation of the optimal forest road network using this high-resolution data. In addition, this study also showed what kind of advantages the use of UAVs can provide in the evaluation of optimal forest road network.

One of the main objectives of the relevant department is the construction, maintenance and repair of roads that will enable the continuation of various forestry activities for the next years, while meeting the increasing need for wood raw materials by protecting the forest areas effectively and efficiently [1]. In this context, the final point of this study is to determine the optimal forest road network for each sub-unit and to contribute to our national forestry by making programs and plans for this. It is possible to provide a homogeneous application unity by spreading the planning and orientation works to be done from the center to sub-units in a hierarchical order. In order to realize this ideal, the approach produced in this study is an exemplary model in determining the optimal forest road networks in order to provide the desired conditions in terms of efficiency and where work and operations can be carried out from a single point. Through this model, all desired forest areas can be tested in terms of optimal forest road network criteria and a strong forestry management approach can be served by eliminating the weaknesses as a result of the detection of deficiencies.

The aim of this study is to plan the optimal forest road network and to plan the optimal forest road network by using Unmanned Aerial Vehicles (UAV) [12] on the forest roads, which serve as the basic infrastructure in the fulfillment of forestry activities, and drone etc. The aim is to demonstrate the applicability of specific technologies in such studies. The other purpose of this study is to provide a practical approach in the evaluation of forest road networks with the data to be obtained.

## 2. Materials and Methods

The study area was carried out within the boundaries of the Central Anatolia Region, Çankırı Forest Directorate, Eldivan Forest Subdistrict. It is located between 40°30'30"- 40°29'01" north latitudes and 33°25'49" - 33°27'09" east longitudes (Figure 1). The study was carried out on the existing forest road network located in Çankırı Karatekin University, Faculty of Forestry, Eldivan Research and Application Forest (RAF) covering an area of approximately 367 ha. A drone device was used to detect the existing forest road network in the study area. UAV-based high resolution orthomosaic data obtained by drone was processed using ArcGIS 10.3 TM [13] software and prepared to be used in the study area for optimum forest road network evaluation.

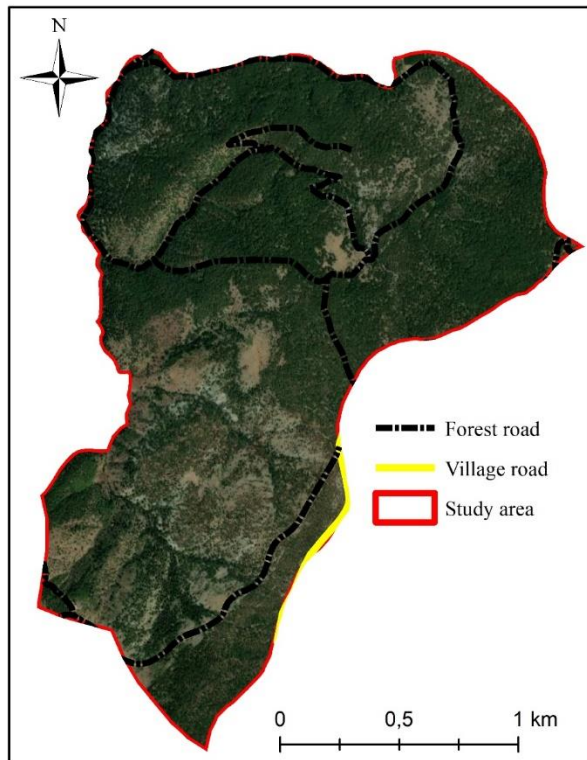


**Figure 1.** Location of the study area

Flights were carried out with drones from various heights on the road route. The flight path was determined by using professional photogrammetry and Pix4d software, which is widely preferred in the drone-mapping field, working in integration with the IOS loaded tablet. High resolution digital terrain model (SAM) data were obtained by using the raw data obtained from the flights using Pix4d software. The SAM data of this area were combined in a computer environment. As a last step, the existing road network of the study area was examined and the locations suitable for reaching the optimal road network were determined in order to maximize the commissioning rate in line with the objectives and targets, and the locations were expressed on the produced maps. The GNSS-RTK measuring device, which has an advanced and sensitive system, was used to obtain the precise coordinate data and heights of the ground control points for the ground verification after the flights made in the field, and for the coordinate validation of the measurement on the flight line. For the drone ground measurement validation, marking was made with spray paint and measurements were made with the GNSS-RTK device at random points in the study area.

### 3. Results and Discussion

Elevation, slope and aspect maps of the study area were obtained with ArcGIS 10.3 TM software. The lowest elevation of the study area is 1303 m, the highest elevation is 1685 m and the average height is 1520 m. The lowest slope of the study area is 0 degrees, the highest slope is 39.68 degrees, and the average slope is 15.13 degrees. When the slope of the study area is expressed as a percentage, these values are 0%, 82.96% and 27.03%, respectively. The dominant aspect of the study area is southwest (Figure 2).

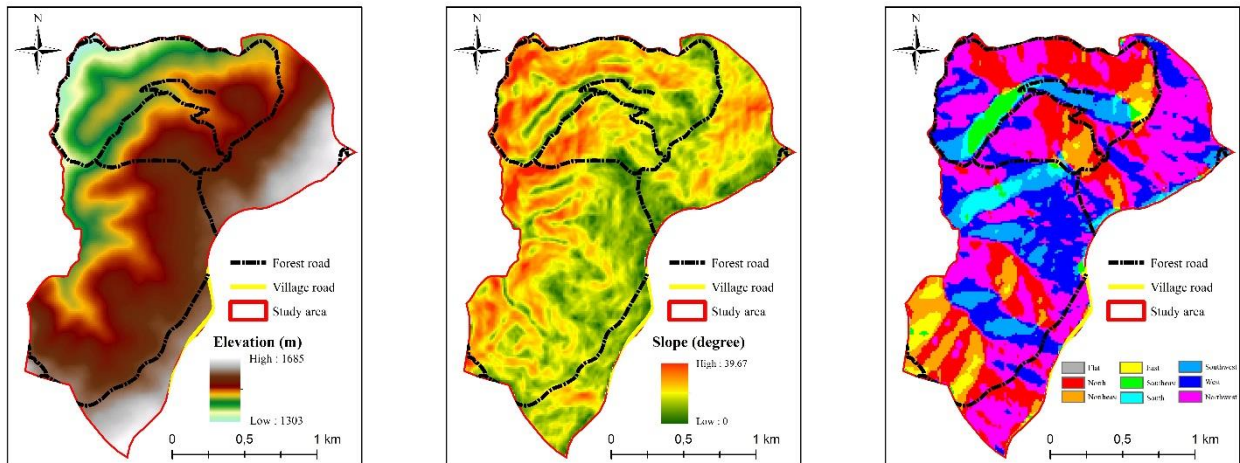


**Figure 2.** Study area Digital Elevation Model, slope and aspect maps

The total existing forest road length of the study area is 10531.9 meters (Figure 3). These forest roads are type B secondary forest roads. As stated in the "Forest Roads Planning, Construction and Maintenance" communiqué no. 292 of the General Directorate of Forestry (GDF), the geometric features of B-type secondary forest roads are designed as 4 m road width, 0.5 m shoulder widths on both sides, and a total width of 5 m.

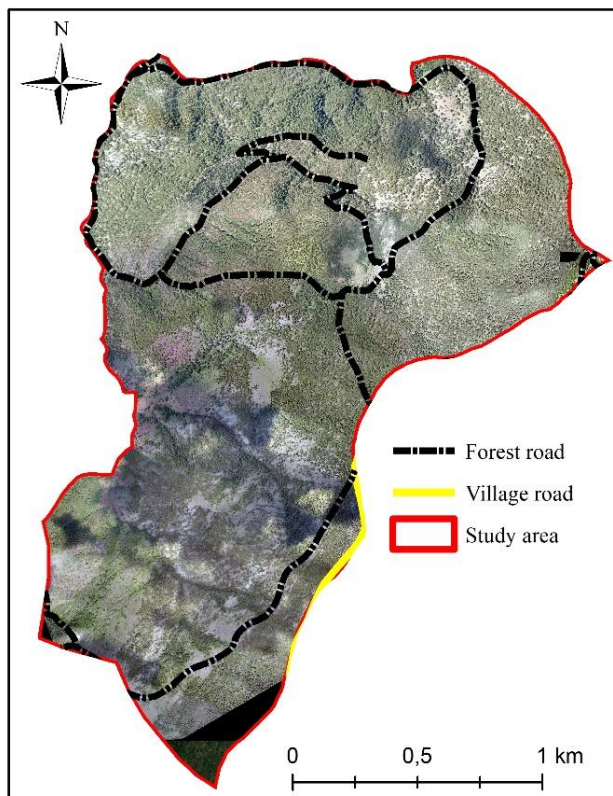


**Figure 3.** Existing forest road and village road locations in the study area

Road density and road spacing criteria are used in the optimal evaluation of forest roads. Accordingly, the road density formed by the existing 10531.9 m road in the study area is 28.9 m/ha. This value is appropriate as the GDF is above the usual target of 25 m/ha. However, in the future, it is foreseen that eliminating the need for roads in the middle-south part of the study area, which has no access, can provide significant advantages both in the transportation of forestry services and in firefighting. For this reason, the locations of alternative routes that can be created in case of any road need in the coming years are given in Figure 4, considering the slope criterion.



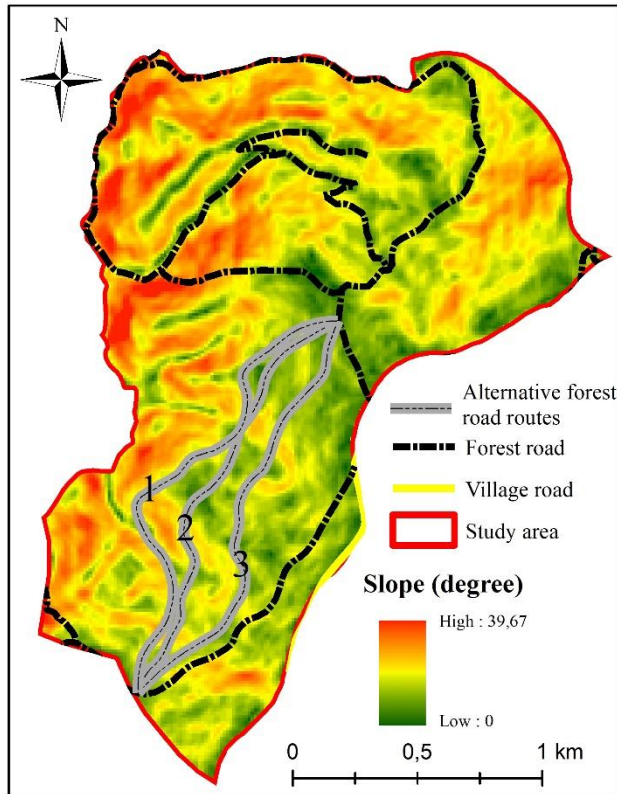


**Figure 4.** Alternative forest road routes

Three of the alternative routes obtained in this study are presented in Figure 4. Accordingly, alternative route number 1 is 2041.01 m long, route number 2 is 1815.90 m and alternative route number 3 is 1819.21 m long. By adding the alternative route number 1 to the existing forest road network plan, the road density is 34.26 m/ha, by adding the alternative route number 2 to the existing forest road network plan, the road density is 33.64 m/ha, and by adding the alternative route number 3 to the existing forest road network plan, the road density is 33.65 m/ha. It is calculated that it will be 33.65 m/ha. With this road density value, it is predicted that a suitable forest road network can be obtained for a healthier and more effective management of forestry works. The other criterion examined for the roads in the study area is the road spacing criterion. This criterion includes the distances of two different coded forest roads to each other. Regarding the road spacing values, the application in Turkey is as follows; It can be said that the road spacing is determined as 1000 m on the slopes with less than 250 m<sup>3</sup>/ha value in the forest, and 500 m on the slopes with more than 250 m<sup>3</sup>/ha value (Erdaş, 1997). According to this, it has been calculated that the road spacing on the roads in the north of the study area varies between 450 m and 850 m on average, but the road spacing value in the mid-south part of the study area has increased and reached approximately 1500 m. It has been determined that the road spacing value has decreased from 1500 m to 550 m and 700 m when the route number 1 is considered from the alternative routes. Any of the alternative routes mentioned in the study can be applied in order to carry out various maintenance works that can be done in the future in a more effective and healthy way.

#### 4. Conclusion

When considered in the context of today's technology possibilities, not only quality information is produced, but also new perspectives can be gained in terms of efficiency with the use of modern devices and the direct transfer of current modeling approaches to the application. Since productivity is one of the most important parameters that directly contribute to the economic management of business and operations, a platform can be created for an economically efficient and ideal environment. Since this study creates a decision support system directly related to the application and practitioners, the database production and the results obtained from the project can be used by researchers and practitioners of the General Directorate of Forestry.

It has been determined in the comparison made after the data obtained from the drone device that there is a 736, 7 m long road located in the study area but not included in the current digital database. This road was added to the database and current forest road density calculations were carried out. The road density formed by the existing 10531.9 m road in the study area is 28.9 m/ha. As a result of this study, three alternative forest road routes were determined. With the implementation of any of these routes, it has been calculated that the forest road density will be around 33-34 m/ha. It is thought that any of these routes, which are important in meeting the road need of the middle-south part of the study area, which has no access in the coming years, will provide significant advantages in both forestry services and firefighting. By using the UAV device, practical and effective data can be obtained in a short time in practice and a suitable decision-making environment can be provided for decision makers. For this reason, it is thought that the use of such studies in areas of different sizes and characteristics in the future period is important in terms of both practice and literature.

## Acknowledgment

This study, titled "Planning Optimal Forest Road Network Using Unmanned Aerial Vehicle (Eldivan Sample)" by Turgay ÇÖKÜŞÜ, who was carried out in the Department of Forest Engineering, Graduate School of Natural and Applied Sciences at Çankırı Karatekin University, is derived from Master's Thesis.

## References

- [1] Erdaş, O., (1986). Odun hammaddesi üretimi, bölmeden çıkarma ve taşıma safhalarında sistem seçimi. *KTÜ Orman Fakültesi Dergisi*, 9(1-2): 91-113.
- [2] Seçkin, Ö. B. (1978). Orman yollarında drenaj. *İstanbul Üniversitesi Orman Fakültesi Dergisi*, 28(1), 149-165.
- [3] Akay, A. E., & Sessions, J. (2005). Applying the decision support system, TRACER, to forest road design. *Western Journal of Applied Forestry*, 20(3), 184-191.
- [4] Kellndorfer, J.M., Dobson, M.C., Vona, J.D., Clutter, M., (2003). Toward precision forestry: Plot-level parameter retrieval for slash pine plantations with JPL AIRSAR. *IEEE Transactions on Geoscience and Remote Sensing*, 41(7):1571-1582
- [5] Gülci, N., Akay, A.E., Erdaş, O., Gülci, S., (2015). Forest operations planning by using RTK-GPS based digital elevation model. *Journal of the Faculty of Forestry Istanbul University*, 65(2):59-68.
- [6] Buğday, E. (2016). Ormancılıkta üretimin planlaması ve hassas ormancılık anlayışı. *Anadolu Orman Araştırmaları Dergisi*, 2(1-2), 54-57.
- [7] Kangas, A., Gobakken, T., Puliti, S., Hauglin, M., Næsset, E., (2018). Value of airborne laser scanning and digital aerial photogrammetry data in forest decision making. *Silva Fennica*, 52(1).19p. <https://doi.org/10.14214/sf.9923>.
- [8] Anonim. (2008). 292 sayılı tebliğ: "Orman Yolları Planlaması, Yapımı ve Bakımı". Orman Genel Müdürlüğü, Ankara
- [9] Erdaş, O. (1997). *Orman Yolları-Cilt I*. KTU Orman Fakültesi Yayınları, 187, 25.
- [10] Demir, M., Hasdemir, M., (2005). Functional planning criterion of forest road network systems according to recent forestry development and suggestion in Turkey. *American Journal Environmental Science*, 1(1):22-28.
- [11] Acar, H. H. (2011). Orman yol planlaması ve yol zemini üzerine bir araştırma. *Pamukkale Üniversitesi Mühendislik Bilimleri Dergisi*, 7(1), 125-130.
- [12] Buğday, E. (2018). Capabilities of using UAVs in Forest Road Construction Activities. *European Journal of Forest Engineering*, 4(2), 56-62.
- [13] ESRI, (2018). *Spatial Analyst Toolbox*. <http://desktop.arcgis.com/en/arcmap/10.3/tools/spatial-analyst-toolbox/how-cut-fill-works.htm>.





# The Potential Use of Salivary Cytokines in Diagnosis of Periodontal Diseases

**Başak KARASU<sup>1,\*</sup>** 

<sup>1</sup> Faculty of Dentistry, Department of Periodontology, Cankiri Karatekin University, Cankiri, Türkiye

## Abstract

The aim of this review is to highlight the potential of saliva as a diagnostic tool for periodontal diseases. Periodontitis is a major public health problem due to its high prevalence and it significantly decreases the quality of life. It has been shown that a massive number of cytokines play a crucial part in the pathogenesis of periodontitis, which causes the destruction of soft tissue and the resorption of bone. The release of inflammatory mediators and cytokines into the periodontal tissues, caused by periodontal bacteria, leads to periodontal tissue breakdown. To avoid consequences that could have a negative impact on a patient's quality of life, early diagnosis of diseases is essential. Salivary biomarkers have the potential to detect periodontal disease and determine the disease stage. Salivary diagnostics provide higher level of care and lessen the need for unnecessarily intrusive treatments by serving as an easily accessible and non-invasive primary test for diseases.

**Keywords:** Saliva, Diagnostics, Periodontal disease, Cytokines

## 1. Introduction

Periodontitis is a chronic multifactorial inflammatory disease associated with dental plaque biofilms and characterized by progressive destruction of the tooth-supporting apparatus [1]. Periodontitis is a major public health problem due to its high prevalence and it significantly decreases the quality of life [2]. Clinical indicators like bleeding on probing, probing pocket depths, and clinical attachment loss are used in the traditional diagnosis of periodontal diseases. Clinical attachment loss evaluation utilizing the periodontal probe requires a 2 to 3 mm threshold change before a site with considerable breakdown may be identified, while being simple to use, affordable, and relatively non-invasive. This is the most common method for determining whether a patient is experiencing periodontal tissue loss, which results in irreversible dental loss [3].

To avoid consequences that could have a negative impact on a patient's quality of life, early diagnosis of diseases is essential [4]. New technology has been developed by dental research to assist dentists in identifying individuals who are going through pathological processes. Numerous studies have been conducted in the area of inflammatory research to examine the development of diagnostic techniques whose benefits include early identification, a non-invasive approach, high sensitivity, and specificity. As a result, this scenario motivates researchers to develop a technique that may detect periodontal problems early, bringing in a time of individualized clinical care and personalized medicine. In this regard, it becomes apparent that salivary-based diagnosis, which is currently receiving a lot more attention, is used [3].

Saliva, an exocrine secretion of the salivary glands that contains 99 percent water, electrolytes, proteins, and enzymes, aids in chewing, swallowing, and digestion of food in addition to providing sensory perception of the food[5]. Saliva contains hormones, antibodies, growth factors, enzymes, microbes, and their products[6]. Through passive diffusion, active transport, or extracellular ultrafiltration, these components enter saliva from blood. Therefore, it is often possible to consider saliva to be a reflection of how the body functions physiologically [7,8]. There are some benefits to using saliva as a diagnostic tool instead of blood. Saliva is a desirable diagnostic fluid for the detection and monitoring of various biomarkers in infants, children, adults, and reluctant patients since it is non-invasive, simple to use, affordable, low risk of cross-contamination, generally stress-free, and safer to administer than serum sampling [9,10]. Even when several samples are required, the collection procedure is manageable because saliva is easily accessible. Its collection is noninvasive, which increases patient acceptance of the treatment and provides a stress-free appointment. Saliva is also easier to handle because it does not clot [11].

\* Corresponding author. e-mail address: basakkarasu@karatekin.edu.tr

Systemic alterations have been seen to have an impact on salivary composition, making it possible to identify disease-related biomarkers. Saliva has been studied as a potential diagnostic tool due to how simple and non-invasive it is to acquire, and the number of biomarkers it contains, such as genetic information and proteins [6,9]. Two conditions must be met before saliva-based diagnostics can achieve the objective mentioned above: (1) finding biomarker(s) for various diseases among the complex components of saliva; and (2) improving the sensitivity and specificity of the biomarker(s) through continued technological advancement [9].

### **Collection of Saliva**

Expectorated whole saliva, a mixture mostly made up of the secretions from the major salivary glands with slight contributions from the minor salivary glands and gingival crevicular fluid (GCF), is the fluid that is typically collected for salivary diagnostic purposes. Resting or unstimulated saliva is collected by passive drooling into a graduated tube or preweighed vial so that the flow rate per unit time may be calculated. Saliva can be collected on cotton swabs, cotton rolls, gauze, or strips of filter paper when volume measurement is not necessary, and then it can be eluted, centrifuged, or aspirated straight from the mouth's floor using plastic pipettes [12].

Saliva is stimulated by a masticatory or gustatory stimulation, expectorated, and handled similarly to the unstimulated fluid when significant amounts of saliva are needed for analytical purposes. The typical masticatory stimulus is softened paraffin wax or a cleaned rubber band, while the typical gustatory stimulus is 2 percent citric acid administered straight to the tongue [12].

Oral swabs or the passive drool technique can be used to collect saliva. In healthy people, the unstimulated salivary flow rate ranges from 0.1-2 mL/min, depending on age and gender [13].

### **Salivary markers of periodontal soft tissue inflammation**

The salivary biomarkers may have diagnostic value for detecting periodontal disease and evaluating the response to periodontal therapy. Various salivary biomarkers have been investigated for the diagnosis and prognosis of periodontal diseases. These include salivary ions, enzymes, immunoglobulins, epithelium keratins, hormones, and inflammatory mediators [14].

The primary role of cytokines, which are highly significant peptide mediators, is cell signaling and communication. Cytokines serve a variety of purposes, including regulating immunological reactions, inflammatory reactions, cell proliferation, and cell differentiation. The term "cytokines" refers to small soluble proteins (5-20 kDa) that bind to certain receptors on particular cells, start some internal cellular changes, and affect numerous chemical and genetic processes. Numerous other cells' behavior is influenced by cytokines, which are produced by particular cells.[15] The release of inflammatory mediators and cytokines into the periodontal tissues, caused by periodontal bacteria, leads to periodontal tissue breakdown.[16]. Inflammation can be caused by a variety of conditions, including oxidative stress, overweight/obesity, poor oral hygiene, and nutritional deficiencies[5,17]. These possible indicators have been identified in periodontics using saliva and GCF.

It has been shown that a massive number of cytokines play a crucial part in the pathogenesis of periodontitis, which causes the destruction of soft tissue and the resorption of bone [18]. The inflammatory process of periodontitis is accompanied by the presence of elevated levels of cytokines like interleukin (IL)-1, IL-6, IL-10, IL-12, interferon (IFN), induced protein (IP)-10, IL-1 receptor antagonist (RA), IL-4, and tumor necrosis factor- $\alpha$  (TNF- $\alpha$ ). Additionally, there is increased expression of regulatory cytokines, including IL-4, IL-1RA, IL-10, and IP-10 as well as proinflammatory cytokines like IL-1, IL-6, IL-12, and TNF- $\alpha$  [19].

Williamson et al. reported the presence of 27 cytokine biomarkers, including IL-1, IL-1 receptor agonist, IL-2, IL-4, IL-5, IL-6, IL-7, IL-8, IL-9, IL-10, IL-12, IL-13, IL-17, eotaxin, basic fibroblast growth hormone, growth-colony stimulating factor, granulocyte-macrophage colony-stimul A commercially available cytokine multiplex test kit that combines the use of fluorescence flow cytometry and enzyme-linked immunoassay (ELISA) technologies were used to measure these cytokines. Only three cytokines, IL-6, IFN- $\gamma$ , and macrophage inflammatory protein (MIP)-1, identified in saliva samples obtained by passive drooling, showed a significant connection ( $p < 0.05$ ) with plasma levels out of the 27 cytokines studied, according to these investigators[20].

Proinflammatory cytokines are generated by cells of the junctional epithelium, connective tissue fibroblasts, macrophages, and polymorphonuclear leukocytes. These cytokines include prostaglandin E2 (PGE2), IL-1 $\beta$ , IL-6, and TNF- $\alpha$ . Osteoclasts and polymorphonuclear leukocytes both generate the enzyme matrix metalloproteinase (MMP)-8, MMP-9, and MMP-13, which all contribute to the breakdown of alveolar bone and connective tissue collagen. PGE2 has been demonstrated in studies to have significant vasodilatory effects and to enhance capillary permeability, both of which lead to the clinical symptoms of redness and edema. Additionally, it induces fibroblasts and osteoclasts to produce more MMPs [21]

MMP-8: The most common MMP in GCF and diseased periodontal tissue. Recently, a quick point-of-care microfluidic device was used to show that the amount of MMP-8 in saliva from patients with periodontal disease was significantly raised [22]. Periodontitis progression has been positively correlated with the level of MMP-8, an enzyme responsible for tissue destruction, in GCF[22,23].

As IL-1 levels demonstrated a high correlation with the several clinical indicators examined, they would be linked to the onset, severity, and progression of periodontal disease. They may also be a good indicator of how a patient will respond to treatment for periodontal disease. Being detectable in human oral fluids makes it a powerful candidate biomarker for periodontal diseases, predicting a person's risk of developing such a disease[24].

TNF- $\alpha$  may be able to help us identify patients who are more likely to develop periodontitis, such as diabetes patients or smokers. TNF- $\alpha$  would also be helpful as a measurable salivary inflammatory mediator whose levels could be related to the severity of the disease and demonstrate its progression, as this possibility is a potent tool to give patients the best care based on their disease stage[24].

Salivary IL-1 and many oral pathogens showed a connection with periodontitis when elastase, lactate dehydrogenase, IL-1, IL-6, and TNF- $\alpha$  concentrations and the presence of five pathogens were compared in patients with advanced periodontal disease and healthy controls [25]. Additionally, the validation study demonstrated a significant connection between moderate to severe periodontitis and salivary MMP-8, IL-1, and *Porphyromonas gingivalis*[26].

IL-4 and salivary soluble toll-like receptor-2 have recently been found to be positively correlated with the progression of periodontal disease[27].

IL-6, a cytokine involved in the death of periodontal tissue, can be genotypically analyzed in a patient's salivary DNA at an authorized laboratory. Recent research has confirmed that among Caucasians, hereditary IL-6 gene variants represent a substantial risk factor for chronic periodontitis [28].

Salivary biomarkers can be utilized to assess the host reaction to bacterial invasion, according to research on gingivitis that used a multiplex protein array for specific biomarkers linked to host defense, inflammation, tissue damage, and angiogenesis. Salivary IL-6 and IL-8 levels have been found to be the most accurate indicators of high and low responders[29]. Increasing salivary IL-6 levels were also shown to correspond with the severity of dysplasia in a study on dysplastic oral leukoplakia in connection to tobacco use and periodontitis [30].

These findings indicate that salivary biomarkers have the potential to detect periodontal disease and determine the disease stage.

## 2. Materials and Methods

We used PubMed, Scopus, Embase, Web of Science, and Google Scholar databases for keywords: saliva, periodontal disease, periodontitis, biomarkers, and inflammatory cytokines and retrieved only human clinical research papers and reviews that were written in English. Observational studies were excluded from analyses, as well as those that did not meet these criteria after reading the abstract.

## 3. Results and Discussion

Saliva is rich in protein and nucleic acid molecules, indicators of physiological status. Salivary biomarkers have the potential to detect periodontal disease and determine disease stage. Compared to blood sample, saliva offers a viable diagnostic alternative for identifying inflammatory, metabolic, and cardiovascular risk factors, especially in pediatric and geriatric populations where blood sampling may be challenging. Salivary diagnostics provide an

easy, affordable, safe, and noninvasive alternative for disease identification, and they have a significant potential to change the next generation of diagnostics.

Although there are still obstacles to overcome, the use of saliva-based oral fluid diagnostics appears to have the potential for future application to identify periodontal disorders and forecast the effectiveness of periodontal therapy.




## References

- [1] Papapanou, P. N., Sanz, M., Buduneli, N., Dietrich, T., Feres, M., Fine, D. H., . . . Graziani, F. (2018). Periodontitis: Consensus report of workgroup 2 of the 2017 World Workshop on the Classification of Periodontal and Peri-Implant Diseases and Conditions. *Journal of periodontology*, 89, S173-S182.
- [2] Sanz, M., Herrera, D., Kebschull, M., Chapple, I., Jepsen, S., Berglundh, T., . . . Merete Aass, A. (2020). Treatment of stage I–III periodontitis—The EFP S3 level clinical practice guideline. *Journal of clinical periodontology*, 47, 4-60.
- [3] Giannobile, W. V., Beikler, T., Kinney, J. S., Ramseier, C. A., Morelli, T., & Wong, D. T. (2009). Saliva as a diagnostic tool for periodontal disease: current state and future directions. *Periodontology 2000*, 50, 52.
- [4] Holschneider, C. H., & Berek, J. S. (2000). *Ovarian cancer: epidemiology, biology, and prognostic factors*. Paper presented at the Seminars in surgical oncology.
- [5] de Almeida, P. D. V., Gregio, A., Machado, M., De Lima, A., & Azevedo, L. R. (2008). Saliva composition and functions: a comprehensive review. *J contemp dent pract*, 9(3), 72-80.
- [6] Pfaffe, T., Cooper-White, J., Beyerlein, P., Kostner, K., & Punyadeera, C. (2011). Diagnostic potential of saliva: current state and future applications. *Clinical chemistry*, 57(5), 675-687.
- [7] Gröschl, M. (2009). The physiological role of hormones in saliva. *Bioessays*, 31(8), 843-852.
- [8] Lima, D. P., Diniz, D. G., Moimaz, S. A. S., Sumida, D. H., & Okamoto, A. C. (2010). Saliva: reflection of the body. *International Journal of Infectious Diseases*, 14(3), e184-e188.
- [9] Lee, Y.-H., & Wong, D. T. (2009). Saliva: an emerging biofluid for early detection of diseases. *American journal of dentistry*, 22(4), 241.
- [10] Chiappin, S., Antonelli, G., Gatti, R., & Elio, F. (2007). Saliva specimen: a new laboratory tool for diagnostic and basic investigation. *Clinica chimica acta*, 383(1-2), 30-40.
- [11] Major, C., Read, S., Coates, R., Francis, A., McLaughlin, B., Millson, M., . . . MacFadden, D. (1991). Comparison of saliva and blood for human immunodeficiency virus prevalence testing. *Journal of infectious diseases*, 163(4), 699-702.
- [12] Mandel, I. D. (1990). The diagnostic uses of saliva. *Journal of oral pathology & medicine*, 19(3), 119-125.
- [13] FenolI-Palomares, C., Muñoz-Montagud, J., Sanchiz, V., Herreros, B., Hernández, V., Mínguez, M., & Benages, A. (2004). Unstimulated salivary flow rate, pH and buffer capacity of saliva in healthy volunteers. *Revista espanola de enfermedades digestivas*, 96(11), 773-783.
- [14] Kaufman, E., & Lamster, I. B. (2000). Analysis of saliva for periodontal diagnosis: a review. *Journal of clinical periodontology*, 27(7), 453-465.
- [15] Di Benedetto, A., Gigante, I., Colucci, S., & Grano, M. (2013). Periodontal disease: linking the primary inflammation to bone loss. *Clinical and Developmental Immunology*, 2013.
- [16] Kumaresan, D., Balasundaram, A., Naik, V. K., & Appukuttan, D. P. (2016). Gingival crevicular fluid periostin levels in chronic periodontitis patients following nonsurgical periodontal treatment with low-level laser therapy. *European journal of dentistry*, 10(04), 546-550.
- [17] Yoon, A. J., Cheng, B., Philipone, E., Turner, R., & Lamster, I. B. (2012). Inflammatory biomarkers in saliva: assessing the strength of association of diabetes mellitus and periodontal status with the oral inflammatory burden. *Journal of clinical periodontology*, 39(5), 434-440.
- [18] Nyman, S., Lindhe, J., & Lindhe, J. (2003). Clinical periodontology and implant dentistry. *Clinical Periodontology and Implant Dentistry*, Lindhe J, Karring T and Lang NP eds, Copenhagen: Blackwell Munksgaard, 403-413.
- [19] Cairo, F., Nieri, M., Gori, A. M., Tonelli, P., Branchi, R., Castellani, S., . . . Pini-Prato, G. P. (2010). Markers of systemic inflammation in periodontal patients: chronic versus aggressive periodontitis. An explorative cross-sectional study. *Eur J Oral Implantol*, 3(2), 147-153.

- [20] Williamson, S., Munro, C., Pickler, R., Grap, M. J., & Elswick, R. (2012). Comparison of biomarkers in blood and saliva in healthy adults. *Nursing research and practice*, 2012.
- [21] Airila-Månsson, S., Söder, B., Kari, K., & Meurman, J. H. (2006). Influence of Combinations of Bacteria on the Levels of Prostaglandin E2, Interleukin-1 $\beta$ , and Granulocyte Elastase in Gingival Crevicular Fluid and on the Severity of Periodontal Disease. *Journal of periodontology*, 77(6), 1025-1031.
- [22] Herr, A. E., Hatch, A. V., Throckmorton, D. J., Tran, H. M., Brennan, J. S., Giannobile, W. V., & Singh, A. K. (2007). Microfluidic immunoassays as rapid saliva-based clinical diagnostics. *Proceedings of the National Academy of Sciences*, 104(13), 5268-5273.
- [23] Kinane, D., Darby, I., Said, S., Luoto, H., Sorsa, T., Tikanoja, S., & Mäntylä, P. (2003). Changes in gingival crevicular fluid matrix metalloproteinase-8 levels during periodontal treatment and maintenance. *Journal of periodontal research*, 38(4), 400-404.
- [24] Gomes, F. I. F., Aragão, M. G. B., Barbosa, F. C. B., Bezerra, M. M., Pinto, V. d. P. T., & Chaves, H. V. (2016). Inflammatory cytokines interleukin-1 $\beta$  and tumour necrosis factor- $\alpha$ -novel biomarkers for the detection of periodontal diseases: a literature review. *Journal of oral & maxillofacial research*, 7(2).
- [25] Gursoy, U. K., Könönen, E., Uitto, V. J., Pussinen, P. J., Hyvärinen, K., Suominen-Taipale, L., & Knuuttila, M. (2009). Salivary interleukin-1 $\beta$  concentration and the presence of multiple pathogens in periodontitis. *Journal of clinical periodontology*, 36(11), 922-927.
- [26] Salminen, A., Gursoy, U. K., Paju, S., Hyvärinen, K., Mäntylä, P., Buhlin, K., . . . Sinisalo, J. (2014). Salivary biomarkers of bacterial burden, inflammatory response, and tissue destruction in periodontitis. *Journal of clinical periodontology*, 41(5), 442-450.
- [27] Prakasam, S., & Srinivasan, M. (2014). Evaluation of salivary biomarker profiles following non-surgical management of chronic periodontitis. *Oral diseases*, 20(2), 171-177.
- [28] Song, G. G., Choi, S. J., Ji, J. D., & Lee, Y. H. (2013). Association between tumor necrosis factor- $\alpha$  promoter- 308 A/G,- 238 A/G, interleukin-6- 174 G/C and- 572 G/C polymorphisms and periodontal disease: a meta-analysis. *Molecular biology reports*, 40(8), 5191-5203.
- [29] Lee, A., Ghaname, C. B., Braun, T. M., Sugai, J. V., Teles, R. P., Loesche, W. J., . . . Kinney, J. S. (2012). Bacterial and salivary biomarkers predict the gingival inflammatory profile. *Journal of periodontology*, 83(1), 79-89.
- [30] Sharma, M., Bairy, I., Pai, K., Satyamoorthy, K., Prasad, S., Berkovitz, B., & Radhakrishnan, R. (2011). Salivary IL-6 levels in oral leukoplakia with dysplasia and its clinical relevance to tobacco habits and periodontitis. *Clinical oral investigations*, 15(5), 705-714.



# The Relation of Serum Uric Acid with a Risk Markers of Cardiovascular Disease Patients

Haydar Jassim Shawkat AL-KHALIDI<sup>1,\*</sup> , Şevki ADEM<sup>1</sup> , Dunya Adnan Mohammed Salih ALAABED<sup>2</sup> 

<sup>1</sup>Institute of science, Faculty of Natural and Applied Sciences, Biochemistry, Çankırı Karatekin University, Çankırı, Türkiye

<sup>2</sup>Ministry of Health, Medical City, Welfare Teaching Hospital, Baghdad, Iraq.

## Abstract

Uric acid is the last product of purine metabolism. There has been a recent rise in the prevalence of cardiovascular disorders which have been associated to elevated levels of serum uric acid (SUA). This study evaluated a group of people with cardiovascular disease to see whether there was any correlation between serum uric acid and a range of biochemical markers. Thrombosis, ischemic heart disease (IHD), and cardiovascular disease (CVD) patients were all included in the research, which had a total enrollment of 150. Patients with IHD and CVD who had higher uric acid, glucose, cholesterol, triglycerides, urea, and creatinine levels as well as lower HDL. Thromboembolism patients had elevated levels of uric acid, glucose, cholesterol, triglyceride, urea, and creatinine, and lower levels of HDL. logistic regression analysis showed a significant link between elevated uric acid levels (hyperuricemia) and an increased risk of ischemic heart disease (IHD). We concluded that hyperuricemia has a significant influence in the development of cardiovascular vascular illnesses such as ischemic heart disease and thromboembolism.

**Keywords:** Uric acid, Cardiovascular disease, Ischemic heart disease, Thromboembolism, D-dimer, Troponin

## 1. Introduction

Uric acid (UA) is the last product of purine metabolism. The body's UA production and excretion are in equilibrium under normal circumstances. Hyperuricemia results from a disturbance in this delicate equilibrium. A UA level of 7 mg/dL or higher in males and 6 mg/dL or higher in females is considered to be hyperuricemia [1]. the UA level threshold increased risk much lower than clinical diagnostic criteria for overall mortality (4.7 mg/dL) and cardiovascular mortality (5 mg/dL), respectively [2]. Hyperuricemia has superseded hypertension, hyperglycemia, and hyperlipidemia as the "fourth greatest" risk factor for cardiovascular disease, according to a new research [1,3-5].

Metabolic syndrome may be caused by hyperuricemia, according to certain theories [6,7]. Myocardial infarction, coronary artery disease, heart failure, and thromboembolism may all be predicted by uric acid levels in healthy individuals, as well as troponin and D-Dimer [8,9]. In the present study, we aimed to illuminate the risk ratio and the relation of serum uric acid with risk marker of cardiovascular disease like troponin and D-Dimer.

## 2. Materials and Methods

### 2.1. Subjects

Our study conducted on 150 patients divided in to 3 groups which diagnosed by physicians, first group suffering from IHD Troponin-I positive >0.3 (ng/mL), the second group was within thrombosis D-Dimer positive >500 (mg/dL) and third group was within CVD under control. The mean of age for all patients was 40-70 years old.

Study samples were collected from patients attending to Respiratory care unit and cardiac care unit at Baghdad teaching hospital/ Medical city from January 2022 to July 2022. All participants were informed about the study procedure through a written consent form before participation. The study complied with the Declaration of Helsinki, and the research protocol was approved by Medical City Research Ethics Committee (Decision date: 01.06.2022, Decision no: 2022/21853).

\* Corresponding author. e-mail address: haydarjassim5@gmail.com

A body mass index BMI (Kg/m<sup>2</sup>) and blood pressure category (mm Hg) was defined according to American Heart Association (AHA) [10].

Blood samples were obtained from the subjects by venipuncture and centrifuged immediately, and serum samples were analyzed directly without storage. In the central laboratory of Baghdad Teaching Hospital, a serum concentration of total serum uric acid, cholesterol, triglyceride high density lipoprotein (HDL), urea and creatinin was measured by enzymatic methods, whereas plasma glucose was measured by the hexokinase method by an autoanalyzer. Troponin-I and D-Dimer levels were assayed by the chemiluminescent immunoassay technique by an autoanalyzer.

## 2.2 Statistical Analysis

Chi-square (X<sup>2</sup>) tests were used to compare percentages in the present study's data. A test to compare two numerical variables was used. Measurement of the linear connection between two variables was done using Pearson correlation test. A significance threshold of 0.05 was used in the test. Logistic regression analysis and its 95% confidence intervals was used to measure odd ratio. SPSS v.23 programs used to analyze current data

## 3. Results and Discussion

### 3.1. Results

The mean ages of the studied groups were within fifth to sixth decades, and this difference was statistically non-significant (P= 0.2). Also, the results of this table documented that most cases of Ischemic patients and cardiovascular under control were among male groups with 42(84.0%), 32(64.0%) respectively, while most cases of Thrombolysis in patients with Covid-Positive were recorded among female groups 32(64.0%), and these differences were statistically highly significant (P< 0.001) as shown in table 1.

**Table 1.** Demographical picture of studied groups (N=150)

Parameters	Test	Ischemic group (N=50)	Thrombolysis group (N=50)	Cardiovascular under Control (N=50)	Sig.
Age (Years)	M± SD	60.46±10.67	56.56±14.05	57.68±10.74	P-value=0.2 (N.S)
(30-44)	N (%)	2 (4.0%)	10 (20.0%)	5 (10.0%)	Chi-square=7.6 P-value=0.2 (N.S)
(45-59)	N (%)	25 (50.0%)	18 (36.0%)	24 (48.0%)	
(60-74)	N (%)	17 (34.0%)	18 (36.0%)	17 (34.0%)	
(75-89)	N (%)	6 (12.0%)	4 (8.0%)	4 (8.0%)	
Gender N (%)	Male	42 (84.0%)	18 (36.0%)	32 (64.0%)	Chi-square=24.5 P-value <0.001 (H.S)
	Female	8 (16.0%)	32 (64.0%)	18 (36.0%)	
BMI (Kg/m <sup>2</sup> )	Normal weight	3 (6.0%)	2 (4.0%)	4 (8.0%)	Chi-square=3.6 P-value= 0.4 (N.S)
	Overweight	23 (46.0%)	16 (32.0%)	16 (32.0%)	
	Obese	24 (48.0%)	32 (64.0%)	30 (60.0%)	
Blood pressure	Normal	10 (20.0%)	16 (32.0%)	11 (22.0%)	Chi-square=3.7 P-value= 0.4 (N.S)
	Hypotension	7 (14.0%)	9 (18.0%)	6 (12.0%)	
	Hypertension	33 (66.0%)	25 (50.0%)	33 (66.0%)	

Table 2 demonstrated that there was increased in serum glucose levels in the three groups (<110 mg/dL) Ischemic group, Thromboembolism group and Cardiovascular under control with means and standard deviation (S.Ds)

value ( $209.04 \pm 133.20$ ,  $140.20 \pm 73.22$ ,  $197.22 \pm 89.38$ ) respectively, with this highly significant differences ( $P=0.001$ ). In regard to cholesterol (mg/dL) and triglyceride (mg/dL) levels, there was an increase in their levels among the three groups above the normal value of both indicated by the increase in their mean and (S.Ds) value

**Table 2.** Means of biochemical parameters among the studied groups (N=150).

Parameter	Studied group	Mean+SD	*P value
Glucose	Ischemic group (N=50)	$209.04 \pm 133.20$	0.002 (H.S)
	Thrombolisim group (N=50)	$140.20 \pm 73.22$	
	Cardiovascular under Control (N=50)	$197.22 \pm 89.38$	
Cholesterol	Ischemic group (N=50)	$199.74 \pm 49.56$	0.009 (H.S)
	Thrombolisim group (N=50)	$162.24 \pm 55.21$	
	Cardiovascular under Control (N=50)	$184.82 \pm 74.73$	
Triglycerdie	Ischemic group (N=50)	$183.74 \pm 101.60$	0.04 (S)
	Thrombolisim group (N=50)	$176.40 \pm 97.67$	
	Cardiovascular under Control (N=50)	$243.78 \pm 206.04$	
HDL	Ischemic group (N=50)	$46.64 \pm 15.86$ , $43.84 \pm 10.93$	0.01 (S)
	Thrombolisim group (N=50)	$38.68 \pm 14.07$	
	Cardiovascular under Control (N=50)	$43.84 \pm 10.93$	
Tn-I	Ischemic group (N=50)	$7.62 \pm 7.09$ ,	<0.001 (H.S)
	Thrombolisim group (N=50)	$0.034 \pm 0.03$	
	Cardiovascular under Control (N=50)	$0.026 \pm 0.03$	
D-Dimer	Ischemic group (N=50)	$318.10 \pm 78.95$	>0.001 (H.S)
	Thrombolisim group (N=50)	$2089.76 \pm 1560.34$	
	Cardiovascular under Control (N=50)	$307.82 \pm 85.88$	
Uric acid	Ischemic group (N=50)	$6.42 \pm 2.06$	0.1 (N.S)
	Thrombolisim group (N=50)	$5.71 \pm 1.98$	
	Cardiovascular under Control (N=50)	$5.66 \pm 2.11$	
Urea	Ischemic group (N=50)	$51.24 \pm 25.06$	0.3 (N.S)
	Thrombolisim group (N=50)	$49.56 \pm 20.91$	
	Cardiovascular under Control (N=50)	$43.80 \pm 18.95$	
Creatinine	Ischemic group (N=50)	$1.17 \pm 0.9$ , $1.14 \pm 0.54$ , $1.13 \pm 0.59$	0.2 (N.S)
	Thrombolisim group (N=50)	$1.14 \pm 0.54$	
	Cardiovascular under Control (N=50)	$1.13 \pm 0.59$	

( $199.74 \pm 49.56$ ,  $162.24 \pm 55.21$ ,  $184.82 \pm 74.73$ ) , ( $183.74 \pm 101.60$ ,  $176.40 \pm 97.67$ ,  $243.78 \pm 206.04$ ) respectively, and these differences ranged from highly significant to significant ( $P=0.009$ ,  $P=0.04$ ) respectively. On the other hand, the levels of HDL were normal (40-60) mg/dL among the Ischemic and Cardiovascular under control groups with means and (S.Ds) values ( $46.64 \pm 15.86$ ,  $43.84 \pm 10.93$ ) respectively versus lower levels of of HDL ( $> 40$  mg/dL) with mean and (S.Ds) ( $38.68 \pm 14.07$ ) among thromboembolism group, with a statistically significant difference ( $P=0.01$ ). The results of the current study also showed that the levels of Tn-I were increased among the Ischemic groups ( $< 0.3$  ng/mL) compared to normal levels up to 0.3 ng/mL among the thromboembolism and cardiovascular under control groups with mean and (S.Ds) values ( $7.62 \pm 7.09$ ,  $0.034 \pm 0.03$ ,  $0.026 \pm 0.03$ ) respectively, with highly significant differences ( $P=0.001$ ). It was found that the levels of D-dimer were highly elevated ( $< 400$  mg/dL) among patients attacked with Thromboembolism and Covid-19 with means and (S.Ds) values of ( $2089.76 \pm 1560.34$ ), while the levels among the Ischemic and cardiovascular under control group were within the normal range (up to 500 mg/dL), with a highly significant difference ( $P=0.01$ ). The results of this table also revealed that the levels of uric acid were within normal among the three groups ( $> 7.2$  mg/dL) with different range of means and (S.Ds), with non-significant differences ( $P=0.1$ ). In regard to renal function tests including urea, there was an increase in urea levels among ischemic and Thromboembolism group with means and (SDs) values ( $51.24 \pm 25.06$ ,  $49.56 \pm 20.91$ ) versus the cardiovascular under control group ( $43.80 \pm 18.95$ ), with non-significant difference ( $P=0.3$ ). While the levels of the creatinine were found to be normal



among the three groups with different means and (SDs) values ( $1.17 \pm 0.9$ ,  $1.14 \pm 0.54$ ,  $1.13 \pm 0.59$ ) respectively, with non-significant differences ( $P=0.2$ ).

Results in Table 3 showed that 21(42.0%) cases out of 50 cases of Ischemic group suffered from hyperuricemia versus 29(58.0%) had normal uric acid, and lower cases of hyperuricemia were found among cardiovascular under control group 11(22.0%) out of 50, while the rest cases 39(78.0%) under the same group were having normal uric acids, and only 15(30.0%) cases out of 50 of Thromboembolism group had hyperuricemia versus 35(70.0%) were having normal uric acid, with non-significant differences (Chi-square= 4.7,  $P= 0.09$ ).

**Table 3.** Comparison of serum uric acid according to cutoff point among studied groups (N=150).

Categorical uric acid levels (mg/dL)	N (%)	Study Groups (N=150)			Total
		Ischemic group (N=50)	Thrombolisim group (N=50)	Cardiovascular under Control (N=50)	
2.5-7.2 Normal	N (%)	29 (58.0%)	35 (70.0%)	39 (78.0%)	103 (68.7%)
>7.2 Hyper	N (%)	21 (42.0%)	15 (30.0%)	11 (22.0%)	47 (31.3%)
Total	N (%)	50 (100.0%)	50 (100.0%)	50 (100.0%)	150 (100.0%)
Chi-sequare	4.7				
P-value	0.09 (N.S)				

In logistic regression analysis, the assessment of ischemic risk was based on three models, in crude analysis we assessed the effect of hyperuricemia as predictor of ischemia in unadjusted analysis hyperuricemia considerable as a risk factor in model 1 and 2 with 1.165% and 1.16% respectively, in model 3 after removing most of the confounder there was significant association with 1.36.6% increased risk of ischemic with hyperuricemia which indicate that hyperuricemia is dependent predictor of ischemia, as illustrated in Table 4. In all models including crude analysis, there was no significant association between hyperuricemia and increased risk of thrombotic events, as illustrated in Table 4.

**Table 4.** Logistic regression analysis and its 95% confidence intervals for both ischemic and thromboembolic groups according to uric acid levels.

	OR	95%CI	p-value
Ischemic group risk assessment			
Crude analysis	1.197	0.983 – 1.457	0.074
Model 1	1.165	0.951 – 1.428	0.141
Model 2	1.16	0.916 – 1.468	0.219
Model 3	1.366	1.013 – 1.841	0.041
Thromboembolic group risk assessment			
Crude analysis	1.013	0.835 – 1.229	0.898
Model 1	1.023	0.835 – 1.253	0.829
Model 2	0.908	0.712 – 1.159	0.440
Model 3	0.846	0.636 – 1.129	0.256
Model 1: age and gender			
Model 2: Model 1 + BMI, urea, and creatinine			
Model 3: Model 2 + HDL, TG, cholesterol, glucose, D-Dimer (were excluded in the second group)			
OR: odd ratio, CI: confidence interval			

### 3.2. Discussion

The average age of the patients evaluated of our study was found to be between the fifth and sixth decades. There were more instances of thromboembolism in patients with Covid-Positive in women than men, which further

supports the notion that males are more likely to suffer from ischemic heart disease and have their cardiovascular systems under control.

AHA reports that the incidence of cardiovascular disease (CVD) among men and women in the United States is approximately 40% between the ages of 40 and 59, and approximately 75% between the ages of 60 and 79 [12]. Most cardiovascular disease (CVD) fatalities occur between the ages of 60 and 79, according to the AHA's 2019 Heart Disease and Stroke Statistical Update, which is conduct with our study [11,12].

In the three groups we analyzed, thromboembolism, ischemic heart disease, and cardiovascular disease under control, we found an increase in glucose, cholesterol, triglycerides, troponin, and urea, while HDL levels were normal in the aforementioned categories and dropped in the thromboembolism cases.

In thromboembolism, D-dimer levels were shown to be elevated, but they were unaltered in CVD and ischemic heart disease. However, creatinine levels were found to be within the normal range in all three groups investigated.

T2DM patients have a greater risk of cardiovascular disease (CVD) and a still remarkable cardiovascular mortality, despite advancements in many risk factors targeting T2DM patients [13]. People with diabetes have a two to three times greater risk of developing cardiovascular disease and mortality than those without the condition. People with diabetes over the age of 40 have a shortened life expectancy of 6–7 years, and this decrease is compounded in individuals with chronic cardiovascular disease, which is identical to our study finding [14].

Dyslipidemia is now well recognized as a risk factor for heart disease (CVD). Lowering LDL-C levels with statins reduces one's chance of developing a life-threatening cardiovascular illness [15]. In epidemiological studies, elevated triglyceride levels have been related to a greater risk of cardiovascular disease (CV) [16]. According to scientific investigations, persons with high triglyceride levels are less likely to develop cardiovascular disease (CVD) [17].

Biochemical indicators such as glucose, cholesterol, triglyceride, D-Dimer and Troponin are important biomarkers for the identification of cardiovascular diseases, according to our study.

Fibrin breakdown product that has been cross-linked Solvent degradation generates D-dimer, which is a soluble by-product. D-dimer levels are associated with thrombosis-related illnesses [18]. D-dimer is often used to diagnose and monitor thrombosis, pulmonary embolism, and blood clots [19]. People with coronary artery disease have been shown to have an elevated risk of cardiovascular disease and an even worse prognosis if their D-dimer levels are high [20].

Using cardiac troponin is the gold standard for diagnosing acute coronary syndrome or acute myocardial infarction [21]. As more cardiac troponin testing is available and used, more people are showing elevated cardiac troponin levels that may be clinically relevant [22]. Greater troponin levels in the early and mid-stages after a heart attack are now shown in retrospective clinical trial populations to be related with a higher risk of recurrent cardiovascular events [23].

The findings showed a rise in uric acid in most instances of cardiovascular disease (CVD) under management, IHD and thromboembolism, as well as associated risk factors, as serum uric acid levels were significantly connected.

After hypertension, high blood sugar, and high cholesterol, it is currently the "fourth highest" risk factor for cardiovascular disease. There are around 170 million Chinese and 32,5 million Americans who are affected by hyperuricemia, according to these estimates, which is conduct with our study [1,3].

According to our results from an analysis using logistic regression, excessive levels of uric acid (hyperuricemia) are linked to a higher risk of ischemic heart disease (IHD).

Several long-term investigations have shown an association between increased levels of uric acid in the blood and various cardiovascular diseases, strokes included[24]. According to current studies, a high SUA level may worsen cardiovascular disease, such as heart attacks and strokes [25,26] According to a recent study [27,28], hyperuricemia has been linked to an increase in intracellular oxidative stress, inflammation, vascular constriction, and an endothelial dysfunction that leads to atherosclerosis and cardiovascular disease [9].

For future studies, we recommend increase the sample size of the study patients to obtain more precise results. Include other types of cardiovascular types and complication within the study a several health issues like excessive blood pressure and coronary artery disease as well as congenital and heart failure are addressed.

## Acknowledgment

The author would like to dedicate this research to the soul of the martyr Bassam AL-KHALIDI.

## References

- [1] Hao, Y., Li, H., Cao, Y., Chen, Y., Lei, M., Zhang, T. and Qian, Z. 2019. Uricase and horseradish peroxidase hybrid CaHPO<sub>4</sub> nanoflower integrated with transcutaneous patches for treatment of hyperuricemia. *Journal of Biomedical Nanotechnology*, 15(5): 951-965.342.
- [2] Viridis, A., Masi, S., Casiglia, E., Tikhonoff, V., Cicero, A. F. G. and Ungar, A. 2020. Identification of the Uric Acid Thresholds Predicting an Increased Total and Cardiovascular Mortality Over 20 Years. *Hypertension*, 75 (2): 302–308.
- [3] Singh, G., Lingala, B. and Mithal, A. 2019. Gout and hyperuricaemia in the USA: prevalence and trends. *Rheumatol. (Oxford)*, 58 (12): 2177–2180.
- [4] Kuwabara, M., Niwa, K., Hisatome, I., Nakagawa, T., Roncal-Jimenez, C. A. andres-Hernando, A. and Johnson, R. J. 2017. Asymptomatic hyperuricemia without comorbidities predicts cardiometabolic diseases: five-year Japanese cohort study. *Hypertension*, 69(6): 1036-1044.
- [5] Maruhashi, T., Hisatome, I., Kihara, Y. and Higashi, Y. 2018. Hyperuricemia and endothelial function: from molecular background to clinical perspectives. *Atherosclerosis*, 278: 226-231.
- [6] Fujimoto, T. and Parton, R. G. 2011. Not just fat: the structure and function of the lipid droplet. *Cold Spring Harbor perspectives in biology*, 3(3): a004838.
- [7] Rana, J. S., Liu, J. Y., Moffet, H. H., Boklage, S. H., Khan, I. and Karter, A. J. 2018. Risk of incident atherosclerotic cardiovascular DiseaseEvents by achieved Atherogenic lipid levels Among62, 428 statin-treated individuals with diabetes mellitus. *The American Journal of Cardiology*, 122(5): 762-767.
- [8] Go, A. S., Mozaffarian, D., Roger, V. L., Benjamin, E. J., Berry, J. D., Borden, W. B. and Turner, M. B. 2013. Heart disease and stroke statistics—2013 update: a report from the American Heart Association. *Circulation*, 127(1): e6-e245.
- [9] Zhao, G., Huang, L., Song, M. and Song, Y. 2013. Baseline serum uric acid level as a predictor of cardiovascular disease related mortality and all-cause mortality: a meta-analysis of prospective studies. *Atherosclerosis*, 231(1): 61-68.
- [10] American Heart Association. 2014. Heart Attack and Stroke Symptoms.
- [11] Yazdanyar, A. and Newman, A. B. 2009. The burden of cardiovascular disease in the elderly: morbidity, mortality, and costs. *Clinics in geriatric medicine*, 25(4): 563-577.
- [12] Benjamin, E. J., Muntner, P., Alonso, A., Bittencourt, M. S., Callaway, C. W., Carson, A. P. and American Heart Association Council on Epidemiology and Prevention Statistics Committee and Stroke Statistics Subcommittee. 2019. Heart disease and stroke statistics—2019 update: a report from the American Heart Association. *Circulation*, 139(10): e56-e528.
- [13] Rawshani, A., Rawshani, A., Franzén, S., Eliasson, B., Svensson, A. M., Miftaraj, M. and Gudbjörnsdottir, S. 2017. Mortality and cardiovascular disease in type 1 and type 2 diabetes. *New England journal of medicine*, 376(15): 1407-1418.
- [14] Menotti, A., Lanti, M., Kromhout, D., Kafatos, A., Nedeljkovic, S. and Nissinen, A. 2005. Short and long term association of a single serum cholesterol measurement in middle-aged men in prediction of fatal coronary and other cardiovascular events: a cross-cultural comparison through Europe. *European journal of epidemiology*, 20(7): 597-604.
- [15] Rana, J. S., Liu, J. Y., Moffet, H. H., Boklage, S. H., Khan, I. and Karter, A. J. 2018. Risk of incident atherosclerotic cardiovascular DiseaseEvents by achieved Atherogenic lipid levels Among62, 428 statin-treated individuals with diabetes mellitus. *The American Journal of Cardiology*, 122(5): 762-767.
- [16] Boullart, A. C. I., De Graaf, J. and Stalenhoef, A. F. 2012. Serum triglycerides and risk of cardiovascular disease. *Biochimica et Biophysica Acta (BBA)-Molecular and Cell Biology of Lipids*, 1821(5): 867-875.
- [17] Miller, M., Stone, N. J., Ballantyne, C., Bittner, V., Criqui, M. H., Ginsberg, H. N. and Pennathur, S. 2011. Triglycerides and cardiovascular disease: a scientific statement from the American Heart Association. *Circulation*, 123(20): 2292-2333.
- [18] DeFilippis, A. P., Young, R., Carrubba, C. J., McEvoy, J. W., Budoff, M. J., Blumenthal, R. S. and Blaha, M. J. 2015. An analysis of calibration and discrimination among multiple cardiovascular risk scores in a modern

- multiethnic cohort. *Annals of internal medicine.*, 162(4): 266-275.
- [19] Lu, W., Resnick, H. E., Jablonski, K. A., Jones, K. L., Jain, A. K., Howard, W. J. and Howard, B. V. 2003. Non-HDL cholesterol as a predictor of cardiovascular disease in type 2 diabetes: *the strong heart study*. *Diabetes care.*, 26(1): 16-23.
- [20] Laakso, M. 1999. Hyperglycemia and cardiovascular disease in type 2 diabetes. *Diabetes.*, 48(5): 937-942.
- [21] Park, K. C., Gaze, D. C., Collinson, P. O. and Marber, M. S. 2017. Cardiac troponins: from myocardial infarction to chronic disease. *Cardiovascular research.*, 113(14): 1708-1718.
- [22] Anand, A. and Mills, N. L. 2019. A look back: diagnosing myocardial infarction in the era of high-sensitivity troponin after the High-STEACS trial. *Cardiovascular Research.*, 115(14): e158-e160.
- [23] Bonaca, M. P., O'Malley, R. G., Jarolim, P., Scirica, B. M., Murphy, S. A., Conrad, M. J. and Sabatine, M. S. 2016. Serial cardiac troponin measured using a high-sensitivity assay in stable patients with ischemic heart disease. *Journal of the American College of Cardiology.*, 68(3): 322-323.
- [24] Jayachandran, M. and Qu, S. 2021. Harnessing hyperuricemia to atherosclerosis and understanding its mechanistic dependence. *Medicinal Research Reviews.*, 41(1): 616-629.
- [25] Gaubert, M., Bardin, T., Cohen-Solal, A., Diévar, F., Fauvel, J. P., Guieu, R. and Paganelli, F. 2020. Hyperuricemia and hypertension, coronary artery disease, kidney disease: from concept to practice. *International Journal of Molecular Sciences.*, 21(11): 4066.
- [26] Borghi, C., Rosei, E. A., Bardin, T., Dawson, J., Dominiczak, A., Kielstein, J. T. and Mancia, G. 2015. Serum uric acid and the risk of cardiovascular and renal disease. *Journal of hypertension.*, 33(9): 1729-1741.
- [27] Kanbay, M., Segal, M., Afsar, B., Kang, D. H., Rodriguez-Iturbe, B. and Johnson, R. J. 2013. The role of uric acid in the pathogenesis of human cardiovascular disease. *Heart.*, 99(11): 759-766.
- [28] Jayachandran, M. and Qu, S. 2021. Harnessing hyperuricemia to atherosclerosis and understanding its mechanistic dependence. *Medicinal Research Reviews.*, 41(1): 616-629.



## Electrocoating of polyaniline and polypyrrole from deep eutectic solution

***Aboubakar IBRAHIM<sup>1</sup>*** , ***Asuman UNAL<sup>2,\*</sup>*** , ***Volkan EYUPOGLU<sup>2</sup>*** 

<sup>1</sup>Department of Chemical Engineering, Faculty of Engineering, Cankiri Karatekin University, Cankiri, 18200, Turkey

<sup>2</sup>Department of Chemistry, Faculty of Science, Cankiri Karatekin University, Cankiri, 18200, Turkey

### Abstract

The high conductivity, chemical stability and simple synthesis of polyaniline and polypyrrole have given these polymers a wide range of applications in energy storage devices, chemical sensors and biosensors. Polyaniline and polypyrrole, which are conducting polymers, have been produced by electrochemical and chemical methods in aqueous and non-aqueous media. However, the synthesis of these polymers in an aqueous medium may result in the loss of electroactive sites of the final polymer films. On the other hand, using a non-aqueous medium during electrochemical synthesis can improve not only electrochemical properties but also the physical properties of the final polymer films. Therefore, this study focused on the synthesis of polyaniline and polypyrrole from deep eutectic solvents under optimal conditions, and the findings show that the use of a non-aqueous medium provides more homogeneous and better electroactive polymer film production than aqueous media.

**Keywords:** Conducting polymers, Polyaniline, Polypyrrole, Deep eutectic solvents

### 1. Introduction

Polyaniline and polypyrrole are the most promising materials among conducting polymers due to their high conductivity, excellent reversibility between conducting and insulating states, ease of preparation, great environmental stability and thermal stabilities [1–4]. Polyaniline is synthesized from the aniline monomer while polypyrrole is synthesized from the pyrrole monomer [5]. The electroactivity of polyaniline is much greater than that of polypyrrole, due to the flexible -NH- group that contributes to  $\pi$ -bond formation, which stabilizes the protonation and deprotonation of polyaniline [6–8]. In addition, polyaniline can exist in three different forms depending on its oxidation state: leucoemeraldine, emeraldine and pernigraniline. The conductivity and appearance (color) of polyaniline films vary according to their states, emeraldine is the most conductive form when doped with a salt or protonated with acid [6,9]. However, both conducting polymers have great potential applications in rechargeable batteries, electrode surface modifications, electrochromic devices, display devices, corrosion protection, sensors and supercapacitors [10–12].

Both polyaniline and polypyrrole can be synthesized in an aqueous or non-aqueous environment by chemical and electrochemical methods [13–16]. Although a large amount of polymers can be easily synthesized by chemical synthesis, electrochemical synthesis gives a chance to control polymer properties such as polymer thickness, conductivity and morphology during synthesis under optimum conditions [17–19]. For these reasons, electrochemical methods can be considered the most attractive method for producing polymer films. It is important to emphasize that the synthesis of polyaniline requires an acidic environment ( $\text{pH} < 4$ ), whereas polypyrrole can be produced in neutral environments [9]. In electrochemical synthesis, polymer films with high conductivity and strong adhesion can be obtained by choosing suitable conditions. Meantime, the doping process significantly affects not only the conductivity of the polymer films but also their morphology. In the other words, the studies reported in the literature show that the nature of the electrolyte, environment, acid and counter anion used during the electrochemical synthesis of polyaniline and polypyrrole greatly affects their electrochemical and physical properties. For instance, the use of large counter ions such as sulfuric acid and nitric acid results in

\* Corresponding author. e-mail address: [asumanunal@karatekin.edu.tr](mailto:asumanunal@karatekin.edu.tr)

the formation of more swollen films, while the use of small counter ions results in the production of more compact films [20]. Similarly, the use of organic solvents and ionic liquids enables the production of high-quality electroactive polymer films on the electrode surface. Deep eutectic solvents also have properties similar to ionic liquids, promising for the electrochemical synthesis of conducting polymers that may have higher conductivity and better physical properties [21,22].

Deep eutectic solvents (DESs) are a mixture of cationic compounds such as ammonium salts (choline chloride, ChCl) and neutral organic hydrogen bond donors (e.g., acids, amides, amines and carboxylic acid). DESs exhibit properties similar to ionic liquids, but have their own advantages, such as being inexpensive and being simple to prepare in an unlimited range of components. DESs are prepared from a eutectic mixture of [Bronsted-Lowry] acids and bases with a large number of non-symmetric ionic species. During hydrogen bonding, there is a delocalization between the anion and hydrogen bond donor (HBD). This delocalization lowers the melting point of the mixture compared to the individual components [23,24].

The present work has described the electrosynthesis of polyaniline and polypyrrole from a deep eutectic solvent (Ethaline) to obtain a better understanding of the polymerization dynamic capacity of polyaniline and polypyrrole growth. For this aim, electrochemical quartz crystal microbalance (EQCM), which is a combination of cyclic voltammetry and quartz crystal microbalance, was used to monitor the mass and charge change as well as the growth rate of the polyaniline and polypyrrole films on the electrode surface.

## 2. Materials and Methods

### 2.1. Reagents

Aniline (99%) and pyrrole (98%) were purchased from Sigma-Aldrich and used without further purification. NaF and NaCl purchased from Analar were used in ion-exchange experiments. Sulfuric acid (99.9%) used in the synthesis of polyaniline was purchased from Fisher Chemicals. For the preparation of Ethaline, choline chloride (ChCl) and ethylene glycol ( $C_2H_6O_2$ ) were supplied from Sigma Aldrich. Figure 1 shows the molecular structure of choline chloride and ethylene glycol.

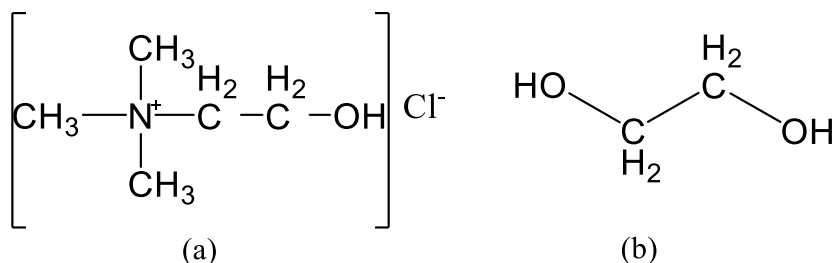


**Figure 1.** Molecular structure of (a) choline chloride; (b)ethylene glycol

### 2.2. Preparation of monomer solutions

Aniline monomer solutions were prepared from a solution containing 1.0 M aniline and 0.5 M  $H_2SO_4$ , while pyrrole monomer solution was prepared from 0.7 M pyrrole using the deep eutectic solution, namely Ethaline. All monomer solutions, particularly aniline solutions, were kept in a dark and cold room to prevent monomer oxidation by light and air.

### 2.3. Synthesis of Ethaline

Initially, Ethaline was prepared by mixing choline chloride (ChCl) and ethylene glycol in 1:2 (ETH200) at  $60^\circ C$  until it turned into a colorless liquid (Ethaline) as seen in Figure 2.

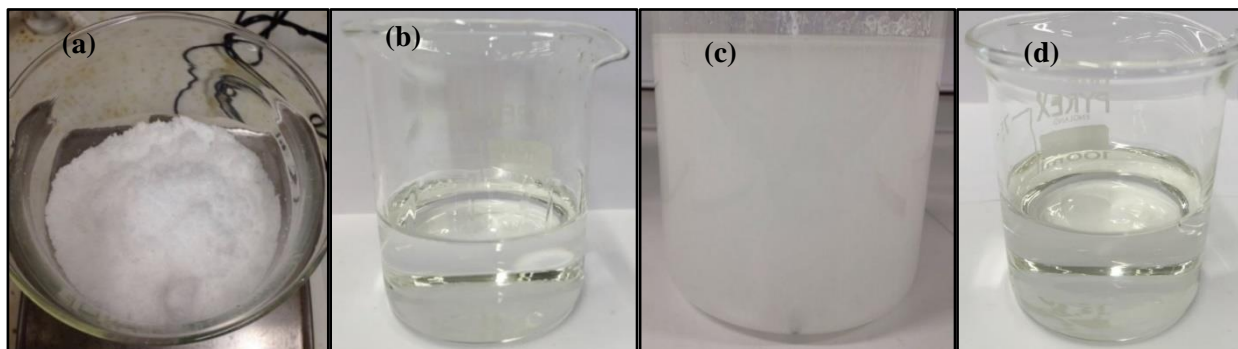


**Figure 2.** Images of (a) choline chloride; (b) ethylene glycol; (c) Mixture; and (d) ETH200

The property of Ethaline depends on the composition of the mixture. The pyrrole monomer solution prepared from ETH200 remained liquid form at room temperature although the aniline monomer solution crystallized as shown in Figure 2. For this reason, aniline monomer solution was prepared at 60°C under identical conditions at 1:4 molar ratios of choline chloride and ethylene glycol, called ETH400. Figure 2b show a homogenous aniline monomer solution prepared with ETH400. Both ETH200 and ETH400 were kept at 50°C in an oven to prevent water absorption.

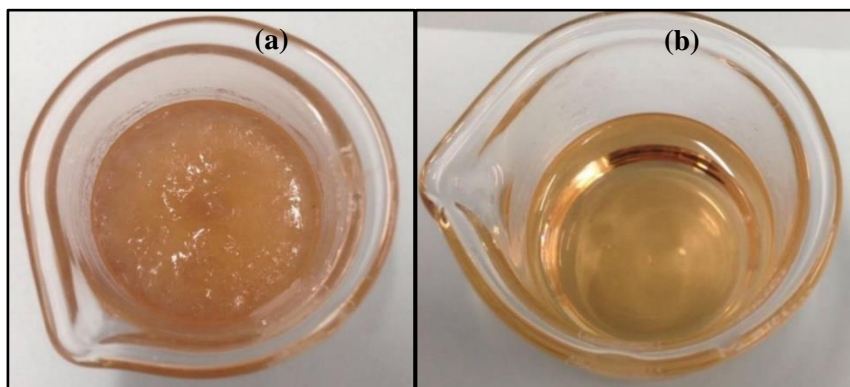


**Figure 3.** Image of aniline monomer solution (a) in ETH200 and (b) in ETH400

## 2.4. Instrumentalization

All electrochemical experiments were carried out by the electrochemical quartz crystal microbalance technique (Autolab PGSTAT12 potentiostat controlled with GPES2 software) in a conventional three-electrode system. During these studies, a platinum flag and an Ag wire electrode were employed as a counter electrode and a reference electrode, respectively. 0.23 cm<sup>2</sup> polished quartz crystals (Crystal Manufacturing (ICM) Co. Ltd. Oklahoma City, USA) were used as working electrodes. All EQCM measurements were performed in the vicinity of the fundamental mode ( $f_0 = 10$  MHz) by a Hewlett Packard HP8751A network analyzer, connected by a 50  $\Omega$  coaxial cable.

## 3. Results and Discussions

### 3.1. Electrochemical synthesis of polyaniline and polypyrrole

While the electrochemical deposition process of polyaniline is routinely applied in an acidic environment (pH<4), some exceptional studies in the literature show that it can be deposited in a neutral and alkaline environment. However, the multiple results in the literature is that the electroactivity of polyaniline increases with the acidity of the environment. A recent study reported that the surface coverage of polyaniline synthesized from an aqueous medium was 78.4 nmol cm<sup>-2</sup> [25] when synthesized under optimum conditions. This indicates that this polyaniline film has a high electroactivity. Meantime, this electroactivity can be further enhanced with the use of deep eutectic solvents. Figure 4 shows the electrochemical and gravimetric data of the polyaniline

growth from 1 M aniline monomer and 0.5 M H<sub>2</sub>SO<sub>4</sub> in ETH400 using the EQCM technique.

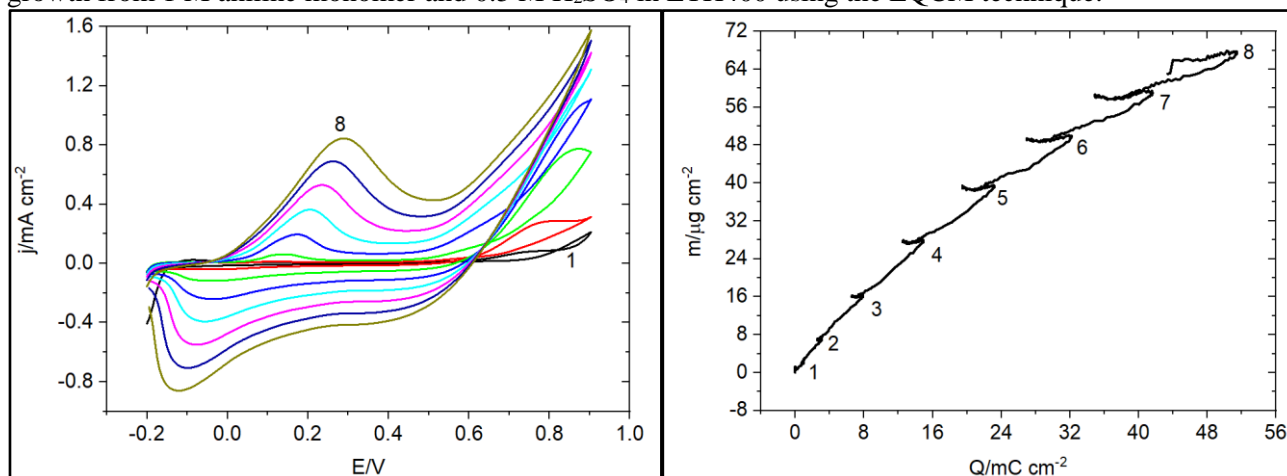


**Figure 4.** Electrochemical and gravimetric data of polyaniline growth from ETH400 at 5 mV s<sup>-1</sup> with 10 cycles between -0.2 V and 1.0 V

As seen in Figure 4, the electroactive sites of polyaniline increase with number of cycles. Redox peaks appeared at about 0.1 V and -0.05 V, then shifted to the more positive potential while irreversible peak current density increased steadily. At the same time, the mass and charge values of polyaniline on the quartz crystal electrode gradually increased with number of cycling. At the end of electrodeposition, 16.56 ng polymer film was observed. The surface coverage of the polyaniline film was 333.4 nmol cm<sup>-2</sup>, which is much better than the polyaniline deposition reported in the literature [25]. Also, the resultant film showed a uniform and compact surface, proving the high-quality polyaniline film from Ethaline. An image of the obtained polyaniline film is shown in Figure 6a.

The other conducting polymer film, polypyrrole, was deposited on a quartz crystal electrode from 0.7 moles of pyrrole in ETH200 at 5 mV s<sup>-1</sup> with 78 cycles. Figure 5 presented the electrochemical and gravimetric data of polypyrrole growth acquired by the EQCM technique.

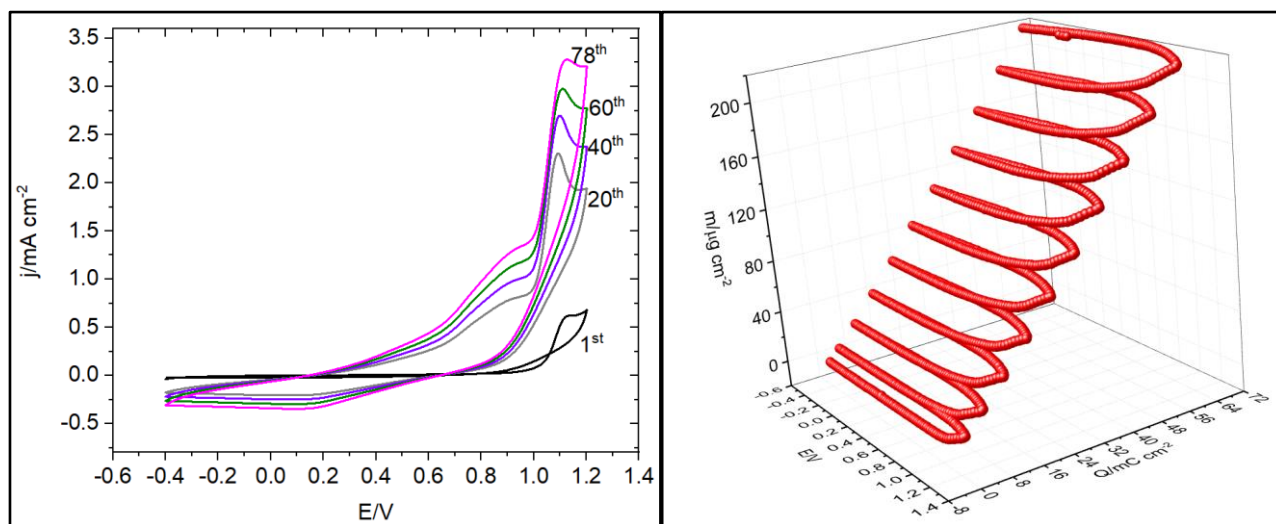


**Figure 5.** Electrochemical and gravimetric data of the polypyrrole growth from ETH200 at 5 mV s<sup>-1</sup> with 78 cycles between -0.4 V and 1.2 V

The current density gradually increases with the number of cycling and the oxidation peak appears at 0.22 V, while the reduction peak is observed at 0.14 V. The mass and charge loading show a proportional increase with the number of cycling, which is the indication of the formation of highly electroactive and stable polypyrrole film on the quartz crystal electrode surface. At the end of electrodeposition, the mass of the polypyrrole film



was found as 46 ng on the electrode surface. Figure 6b show an image of the obtained polypyrrole film.

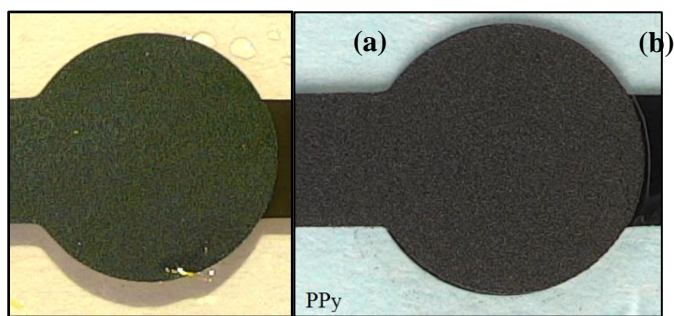


**Figure 6.** Images of polyaniline (a) and polypyrrole (b) film synthesized from Ethaline

### 3.2. Characterization of polyaniline and polypyrrole film electroactivity

The electroactivity of polyaniline and polypyrrole films was investigated in monomer-free ETH200 solvents. First, the electroactivity of polyaniline film was investigated in ETH200 containing 0.5 M  $\text{H}_2\text{SO}_4$ , as shown in Figure 7a. The polyaniline film gives oxidation at 0.48 V and a reduction peak at 0.37 V remarkably different positions compared with polyaniline synthesized in an aqueous medium [25]. Also, the current density values of these peaks are higher as well while remaining the same over ten scans. This proves that the polyaniline film synthesized from a deep eutectic solvent exhibits electroactive and stable behavior. In other words, the electrochemical properties were considerably improved with the use of Ethaline.

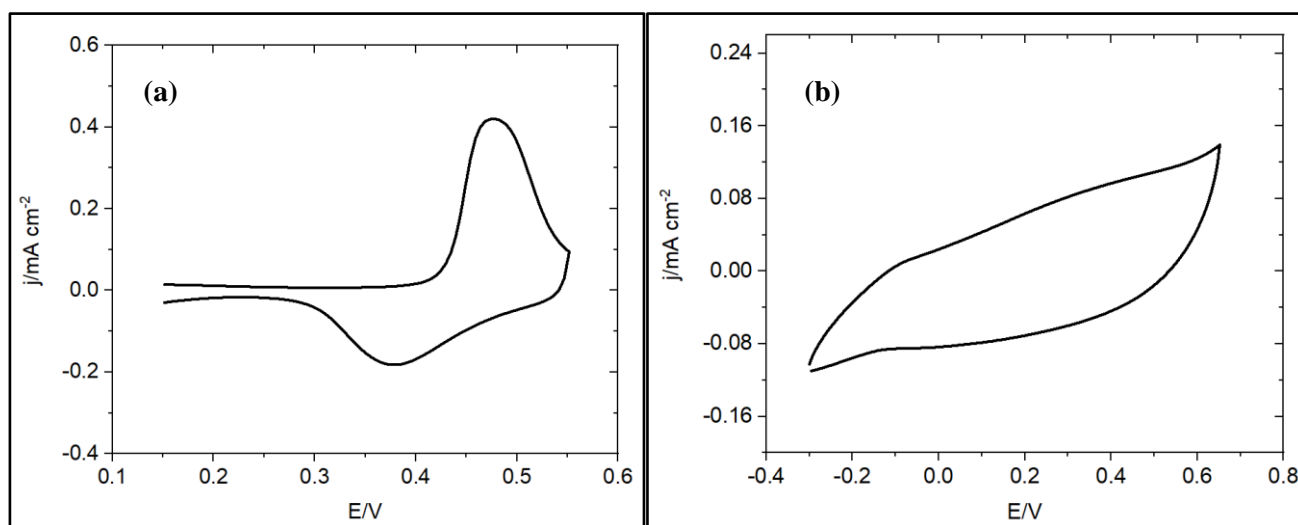


**Figure 7.** Characterization of (a) polyaniline film and (b) polypyrrole film in monomer-free ETH200

Figure 7b presents the electrochemical characterization of the polypyrrole film synthesized from ETH200. There is a broad oxidation and reduction peak, and their current densities slowly increased. On the other hand, their current density values almost remained over 10 scans, which is a sign of a stable behavior of polypyrrole film.

### 3.3. Surface characterization of polyaniline and polypyrrole films

Surface characteristics of polyaniline and polypyrrole films were investigated by scanning electron microscopy (SEM) technique. The SEM images were presented in Figure 8, showing markedly distinctive properties of each other. The polyaniline has a starfish appearance while the polypyrrole has a more uniform surface.

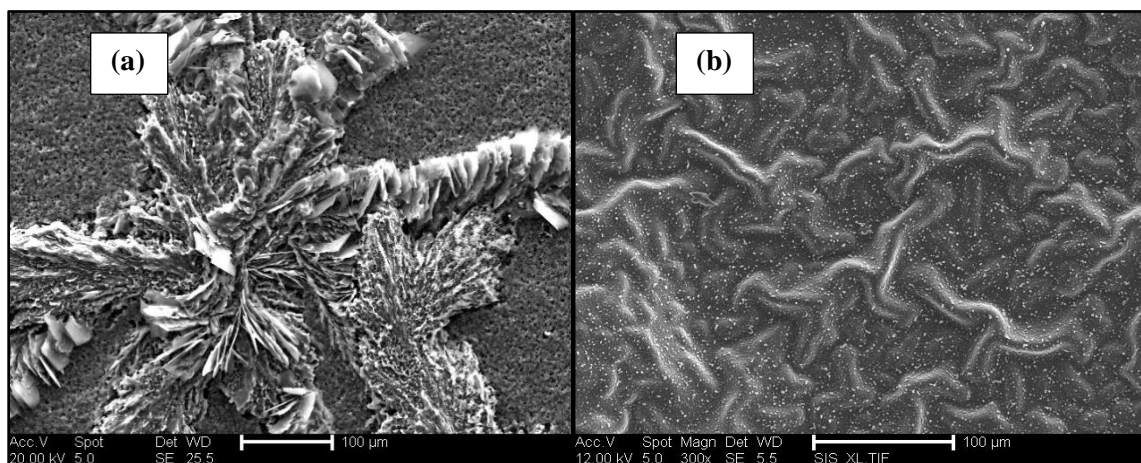


**Figure 8.** Surface images of polyaniline and polypyrrole generated from Ethaline

#### 4. Conclusion

In this work, the electrochemical deposition of polyaniline and polypyrrole film from Ethaline was extensively investigated under optimum conditions using the electrochemical quartz crystal microbalance technique. Initially, electrochemical deposition of polyaniline was implemented in ETH200, but crystallization of aniline monomer solutions at room temperature made the deposition difficult to proceed. To overcome this, electrochemical deposition of polyaniline was applied in ETH400 solvent. In doing so, the problem was solved and polymerization of aniline from ETH400 was carried out at  $5 \text{ mV s}^{-1}$  over 10 cycles. Eventually, a thin, smooth, compact green polyaniline film was formed on the quartz crystal. Electrochemical characterization of this film was investigated in monomer-free ETH200 containing  $0.5 \text{ M H}_2\text{SO}_4$ . The findings show that the use of Ethaline provides a distinctive polyaniline film with new redox peaks located at different positions compared to polyaniline synthesized in an aqueous medium. Similarly, polypyrrole was synthesized from pyrrole monomer in ETH200 under optimum conditions. A thin black film was observed on the quartz crystal. Afterward, the electrochemical characterization of the polypyrrole film was examined in ETH200 and gave broad redox peaks with high electroactivity. The current densities of both polymer films remained almost the same, which is an indication of stable behavior during cycling. Lastly, the surface characteristics of the obtained polyaniline and polypyrrole film were investigated using the SEM technique. The findings show that polyaniline is very different from the synthesized aqueous medium [7,25]. These indicate that it is possible to synthesize high-quality polyaniline and polypyrrole with different electrochemical characteristics possible with the use of deep eutectic solvents for various applications in the future.

#### Acknowledgments

I express my deep gratitude to the Ministry of National Education in Turkey for providing financial support throughout my study. I would also like to thank the University of Leicester for their support during this period.

#### References

- [1] G. Ciric-Marjanovic, Recent advances in polyaniline research: Polymerization mechanisms, structural aspects, properties and applications, *Synth Met.* (2013). <https://doi.org/10.1016/j.synthmet.2013.06.004>.
- [2] S.M. Park, H.J. Lee, Recent advances in electrochemical studies of  $\pi$ -conjugated polymers, *Bull Korean Chem Soc.* (2005). <https://doi.org/10.5012/bkcs.2005.26.5.697>.
- [3] A.F. Diaz, J.I. Castillo, A polymer electrode with variable conductivity: Polypyrrole, *Journal of the Chemical Society - Series Chemical Communications.* (1980). <https://doi.org/10.1039/C39800000397>.

- [4] A.F. Diaz, J.I. Castillo, J.A. Logan, W.Y. Lee, Electrochemistry of conducting polypyrrole films, *Journal of Electroanalytical Chemistry*. (1981). [https://doi.org/10.1016/S0022-0728\(81\)80008-3](https://doi.org/10.1016/S0022-0728(81)80008-3).
- [5] G. Inzelt, Conducting polymers: past, present, future, *Journal of Electrochemical Science and Engineering*. (2017). <https://doi.org/10.5599/jese.448>.
- [6] N. Gospodinova, L. Terlemezyan, Conducting polymers prepared by oxidative polymerization: Polyaniline, *Progress in Polymer Science (Oxford)*. (1998). [https://doi.org/10.1016/S0079-6700\(98\)00008-2](https://doi.org/10.1016/S0079-6700(98)00008-2).
- [7] A. Unal, A. Robert Hillman, K.S. Ryder, S. Cihangir, Electrogravimetric analysis of poly(aniline-co-o-toluidine) copolymer films in the presence of fluoride ions, *Journal of Electroanalytical Chemistry*. 895 (2021). <https://doi.org/10.1016/j.jelechem.2021.115519>.
- [8] A.R. Hillman, K.S. Ryder, H.K. Ismail, A. Unal, A. Voorhaar, Fundamental aspects of electrochemically controlled wetting of nanoscale composite materials, *Faraday Discuss.* (2017). <https://doi.org/10.1039/c7fd00060j>.
- [9] A.A. Syed, M.K. Dinesan, Review: Polyaniline-A novel polymeric material, *Talanta*. (1991). [https://doi.org/10.1016/0039-9140\(91\)80261-W](https://doi.org/10.1016/0039-9140(91)80261-W).
- [10] M. Gerard, A. Chaubey, B.D. Malhotra, Application of conducting polymers to biosensors, *Biosens Bioelectron*. 17 (2002). [https://doi.org/10.1016/S0956-5663\(01\)00312-8](https://doi.org/10.1016/S0956-5663(01)00312-8).
- [11] P.C. de León, S.A. Campbell, J.R. Smith, F.C. Walsh, Conducting polymer coatings in electrochemical technology Part 2 – Application areas, *Transactions of the IMF*. (2008). <https://doi.org/10.1179/174591908X264392>.
- [12] T.K. Das, S. Prusty, Review on Conducting Polymers and Their Applications, *Polymer - Plastics Technology and Engineering*. (2012). <https://doi.org/10.1080/03602559.2012.710697>.
- [13] S. Dey Sadhu, P.L. Meena, J. Kumar, J. Gupta, S. Choudhary, A. Gupta, Preparation and characterization of polyaniline- and polythiophene-based copolymer and its nanocomposite suitable for electro-optical devices, *Polym Compos*. (2020). <https://doi.org/10.1002/pc.25738>.
- [14] Y. Wei, W.W. Focke, G.E. Wnek, A. Ray, A.G. MacDiarmid, Synthesis and electrochemistry of alkyl ring-substituted polyanilines, *Journal of Physical Chemistry*. (1989). <https://doi.org/10.1021/j100338a095>.
- [15] A.F. Diaz, J.A. Logan, Electroactive polyaniline films, *Journal of Electroanalytical Chemistry*. (1980). [https://doi.org/10.1016/S0022-0728\(80\)80081-7](https://doi.org/10.1016/S0022-0728(80)80081-7).
- [16] L.X. Wang, X.G. Li, Y.L. Yang, Preparation, properties and applications of polypyrroles, *React Funct Polym*. (2001). [https://doi.org/10.1016/S1381-5148\(00\)00079-1](https://doi.org/10.1016/S1381-5148(00)00079-1).
- [17] C. Weidlich, K.M. Mangold, Electrochemically switchable polypyrrole coated membranes, in: *Electrochim Acta*, 2011. <https://doi.org/10.1016/j.electacta.2010.11.065>.
- [18] J.-E. Park, S.-G. Park, A. Koukitu, O. Hatozaki, N. Oyama, Electrochemical Behavior of the Polyaniline-Organosulfur Composite Film Containing Ag Nanoparticles, *J Electrochem Soc*. 150 (2003). <https://doi.org/10.1149/1.1580134>.
- [19] V. Karpakam, K. Kamaraj, S. Sathiyarayanan, G. Venkatachari, S. Ramu, Electrosynthesis of polyaniline-molybdate coating on steel and its corrosion protection performance, *Electrochim Acta*. (2011). <https://doi.org/10.1016/j.electacta.2010.11.099>.
- [20] V. v. Abalyaeva, O.N. Efimov, Regularities of electrochemical behavior of polyaniline doped by electroactive anions, *Russian Journal of Electrochemistry*. (2011). <https://doi.org/10.1134/s1023193511110036>.
- [21] T. Welton, Room-Temperature Ionic Liquids . Solvents for Synthesis and Catalysis Room-Temperature Ionic Liquids . Solvents for Synthesis and Catalysis, *Chem Rev*. (1999). <https://doi.org/10.1021/cr980032t>.
- [22] J.D. Mota-Morales, M.C. Gutiérrez, M.L. Ferrer, R. Jiménez, P. Santiago, I.C. Sanchez, M. Terrones, F. del Monte, G. Luna-Bárcenas, Synthesis of macroporous poly(acrylic acid)-carbon nanotube composites by frontal polymerization in deep-eutectic solvents, *J Mater Chem A Mater*. (2013). <https://doi.org/10.1039/c3ta01020a>.
- [23] H. Mąka, T. Spychar, K. Kowalczyk, Imidazolium and deep eutectic ionic liquids as epoxy resin crosslinkers and graphite nanoplatelets dispersants, *J Appl Polym Sci*. (2014). <https://doi.org/10.1002/app.40401>.
- [24] Q. Zhang, K. de Oliveira Vigier, S. Royer, F. Jérôme, Deep eutectic solvents: Syntheses, properties and applications, *Chem Soc Rev*. (2012). <https://doi.org/10.1039/c2cs35178a>.
- [25] A. Unal, A.R. Hillman, K.S. Ryder, S. Cihangir, Highly Efficient Defluoridation of Water through Reusable poly(aniline-co-o-aminophenol) Copolymer Modified Electrode Using Electrochemical Quartz Crystal Microbalance, *J Electrochem Soc*. 168 (2021). <https://doi.org/10.1149/1945-7111/abd926>.



## Morphology and functions of cup cells in the epithelium of small intestine

***Mustafa YILDIZ***<sup>1,\*</sup> 

<sup>1</sup> Can Faculty of Applied Sciences, Department of Occupational Health and Safety, Canakkale Onsekiz Mart University, Canakkale, Türkiye

### Abstract

The aim of this study was to investigate the morphological and functional properties of cup cells. The cup cells are located in the epithelium of the small intestine. They have a specific morphology and are mostly observed in the ileum. They are also most abundant in rabbits and guinea pigs. The brush border of the cup cells is shorter than the absorptive cells, and their cytoplasm has less electron density. In addition, there is a cup-like depression at the lumen margin of the brush border of the cup cells. It has been found that cup cells showed vimentin-positive immunoreactivity in the rabbit ileum. Besides, it has been observed that the mitochondria of cup cells are smaller and the alkaline phosphatase activity at the brush border is weaker than the absorptive cells. The functions of cup cells are unclear. But it has been shown that bacteria were attached to the area above the cup cells. Therefore, it is thought that they have functions associated with the immune response to bacteria. Also, cup cells bind distinctive lectins, lack secretory granules, and do not transport antigens such as M cells. As a result; in this study, the morphological features, distribution, and functions of cup cells were explained. Thus, detailed information about cup cells was presented to researchers working on the subject.

**Keywords:** Cup cell, small intestine, light microscopy, electron microscopy

### 1. Introduction

The small intestine is the longest section of the digestive tract, starting after the stomach and ending with the large intestine. It consists of three parts: duodenum, jejunum and ileum [1, 2]. The small intestine is an organ in which foods are digested the most in the digestive system. Foods are broken down to the smallest molecules in the small intestine. Chemical digestion of all nutrients is completed in the small intestine. The digested foods are absorbed in the small intestine. In addition, unabsorbed nutrients are transferred to the large intestine [3].

The small intestinal epithelium acts as a barrier between the internal environment of the organism and the intestinal lumen [4]. It plays a role in the body's defense against harmful bacteria that enter through the mouth and are abundant in the intestinal lumen [5]. The small intestinal epithelium consists of different cell types with specific morphological and functional features [6], originating from pluripotent stem cells found in the crypt epithelium [7, 8]. These cells, which are found in different densities in the small intestinal epithelium; are known as enterocytes, goblet cells, enteroendocrine cells, Paneth cells, membranous cells (M cells), tuft cells and cup cells [5, 9].

In this study, it was aimed to provide a resource for researchers who will work on this subject by referring to the morphological and functional properties of cup cells.

### 2. Materials and Methods

In the present study, a literature search was carried out using the keywords 'Cup cell' and 'Small intestine' on Pubmed, Google, and Google Scholar. As a result of the investigation, national and international publications spanning the years 1974 to 2019 were obtained. This review study was prepared by including appropriate sources about the subject.

\* Corresponding author. e-mail address: mustafayildiz@comu.edu.tr

### 3. Results and Discussion

#### 3.1. Light microscopic properties of cup cells

The cup cells are randomly located between the enterocytes in the villus epithelium and have a thin goblet-like morphology. Cup cells are approximately 8-12  $\mu\text{m}$  in diameter and their nuclei are oval, similar to absorptive cells [10].

In mammals, cup cells are mostly observed in the ileum [5]. They are very rare in the jejunum and have only been detected in the jejunum of guinea pigs. These cells are most abundant in the ileums of rabbits and guinea pigs. The rate of cup cells in the ileums of guinea pigs and rabbits is approximately 3 to 6 percent [10]. They were rarely determined in the ileum of monkeys [4]. However, they were not found in the ileum of rats [10]. In addition, villus epithelial cells similar to cup cells in experimental animals have been observed in the human small intestine [11]. On the other hand; it has been determined that cup cells were localized in the villus adjacent to Peyer's patches in rabbit ileum. It also has been noted that there were one or two intraepithelial lymphocytes on the lateral surfaces of the cup cells [5, 12].

In histochemical examinations, it has been observed that the microvilli brush border of the cup cells in the ileum epithelium of rabbits stained with toluidine blue was shorter and their cytoplasm was lighter than the neighboring absorptive cells [4, 5, 10]. Similarly, the alkaline phosphatase activity on the brush border of the cup cells was found to be weaker than that of the absorptive cells [4, 5]. In immunohistochemical examinations, it has been determined that the cup cells in the villus epithelium of the rabbit ileum showed vimentin-positive immunoreactivity (Figure 1A) [5, 12, 13].

#### 3.2. Electron microscopic properties of the cup cells

The brush border of the cup cells is shorter than the adjacent absorptive cells and the lumen margin of the brush border has a cup-like depression [4, 10, 13, 14]. Also, the cytoplasm of cup cells has less electron density than adjacent enterocytes (Figure 1B) [4, 10, 13]. Small vesicles have been observed in the apical cytoplasm of the cup cells [13]. It has been thought that these vesicles may partially be pinocytotic vesicles. Besides, membrane-bound granules resembling endocrine cell granules have not been found in the apical or basal cytoplasm of cup cells [10]. But it has been noted that there were lysosome-like compartments in the cytoplasm of cup cells [10, 14]. Also, it has been observed that cup cells had less smooth endoplasmic reticulum than adjacent absorptive cells [10]. It has been determined that the mitochondria of cup cells were sparsely distributed in the apical cytoplasm [4, 10]. Cup cell mitochondria are smaller than the mitochondria of absorptive cells. Also, they have large intra-cristal gaps and dense inner mitochondrial matrices indicating a strong metabolic activity. Besides, the nucleus of the cup cells is qualitatively similar to the nuclei of absorptive cells [10].

Cup cells are in touch with the basement membrane like absorptive cells [4]. The cup cell and the absorptive cell have been combined by tight junctions and desmosomes. The networks of lateral intermediate filament in both cells are connected to desmosomes [5]. The glycocalyx of the cup cells is more extensive than neighboring absorptive cells [14]. In addition, the terminal web of cup cells is dense but poorly defined [10].

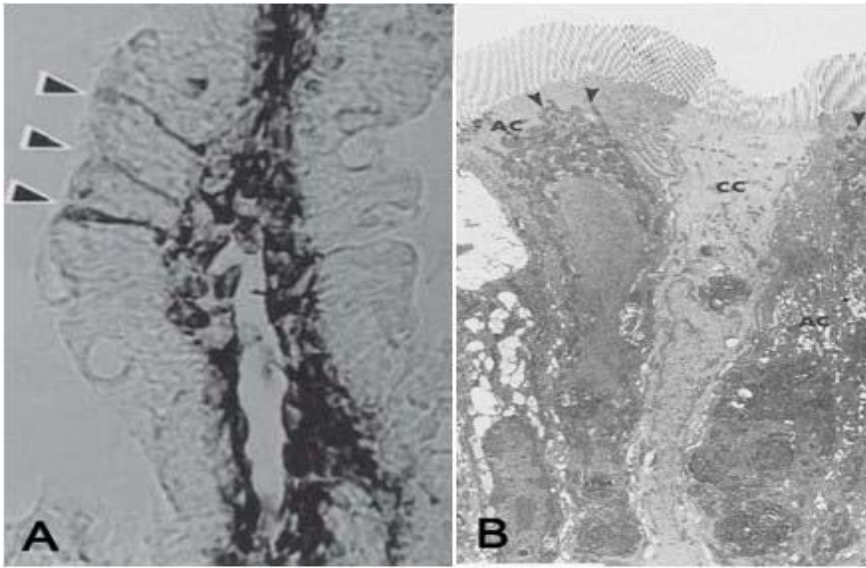


**Figure 1.** **A.** Light micrograph of vimentin-positive cup cells in villus epithelium of small intestine (arrowheads) It was modified from Fujimura and Iida [5]. **B.** Electron micrograph of a cup cell (CC) between two absorptive cells (AC). In absorptive cells, dense cytoplasmic organelles are seen (arrowheads) It was modified from Madara [10].

### 3.3. Functions of cup cells

The functions of cup cells are unclear but it is thought that they have functions associated with the immune response against bacteria in the lumen of small intestine. In a study, it has been determined that cup cells acted as a colonization area for an unidentified bacterium species in the ileum of guinea pigs. Also, it has been found that the cup cells demonstrated bacterial association at a rate of 28%. By examining the thin sections, it has been detected that the bacteria were attached to the area above the cup cells [14]. Similarly, it has been stated that cup cells may be intestinal immune system cells, since they are localized in the villi epithelium adjacent to Peyer's patches and have a close relationship with intraepithelial lymphocytes [12]. In addition, cup cells bind distinctive lectins [15] and do not transport antigens like M cells [13]. On the other hand, cup cells lack secretory granules and do not transfer intact protein into the intracellular space. Besides, cup cells pinocytose and poorly absorb lipid-bile salt solutions [10].

As a conclusion, the morphological structure of the cup cells in the small intestinal epithelium was explained at the levels of light and electron microscopy. In addition, the functions of the cup cells were summarized. Thus, it was intended to contribute to the literature about cup cells and to shed light on researchers working in this field.

### References

- [1] Hazirolu, R. M., Cakir, A., Yildiz, B., Yildiz, B., Oto, C., Orhan, I. O., & Ekim, O. (2019). *Temel veteriner anatomi*. 1st Ed. Eskişehir: Anadolu Üniversitesi Basımevi, 63-64.
- [2] Gokhan, K., Karadere, S., Uzuner, K., Uyar, R., & Aydın, Y. (2019). *İnsan beden yapısı ve fizyolojisi*. 1st Ed. Eskişehir: Anadolu Üniversitesi Basımevi, 142-144.
- [3] Milli Eğitim Bakanlığı (2012). Mesleki Eğitim ve Öğretim Sisteminin Güçlendirilmesi Projesi-MEGEP, *Ortak alanlar: Sindirim sistemi*. 1st Ed. Ankara: MEB Yayınları, 20-26.
- [4] Madara, J. L. (2011). *Functional morphology of epithelium of the small intestine*. In *Comprehensive Physiology*. 1st Ed. New York: Wiley, 83-120.
- [5] Fujimura, Y., & Iida, M. (2001). A new marker for cup cells in the rabbit small intestine: expression of vimentin intermediate filament protein. *Medical Electron Microscopy*, 34(4), 223-229.
- [6] Cheng, H., & Leblond, C. P. (1974). Origin, differentiation and renewal of the four main epithelial cell types in the mouse small intestine. *The American Journal of Anatomy*, 141(4), 461-562.
- [7] Garcia-Carbonell, R., Yao, S. J., Das, S., & Guma, M. (2019). Dysregulation of intestinal epithelial cell RIPK pathways promotes chronic inflammation in the IBD gut. *Frontiers in Immunology*, 10, 1094.

- [8] Marshmann, E., Booth, C., & Potten, C. S. (2002). The intestinal epithelial stem cell. *Bioessays*, 24(1), 91-98.
- [9] Heath, J. P., Kömüves, L. G., & Nichols, B. L. (1996). Lenten cell: ultrastructure, absorptive properties, and enzyme expression of a novel type of cell in the newborn and suckling pig intestinal epithelium. *The Anatomical Record*, 244(1), 95-104.
- [10] Madara, J. L. (1982). Cup cells: structure and distribution of a unique class of epithelial cells in guinea pig, rabbit, and monkey small intestine. *Gastroenterology*, 83(5), 981-994.
- [11] Finzi, G. M., Cornaggia, M., Capella, C., Fiocca, R., Bosi, E., Solcia, E., & Samloff, I. M. (1993). Cathepsin E in follicle associated epithelium of intestine and tonsil: localization to M cells and possible role in antigen processing. *Histochemistry*, 99(3), 201-211.
- [12] Beyaz, F., Ergun, E., Ergun, L., & Bayraktaroglu, A. G. (2010). Ankara tavşanı ileum epiteline vimentin pozitif hücrelerin yapısal özellikleri. *Ankara Üniversitesi Veteriner Fakültesi Dergisi*, 57(4), 229-234.
- [13] Ramirez, C., & Gebert, A. (2003). Vimentin-positive cells in the epithelium of rabbit ileal villi represent cup cells but not M-cells. *Journal of Histochemistry and Cytochemistry*, 51(11), 1533-1544.
- [14] Madara, J. L., & Carlson, S. L. (1985). Cup cells: further structural characterization of the brush border and the suggestion that they may serve as an attachment site for an unidentified bacillus in guinea pig ileum. *Gastroenterology*, 89(6), 1374-1386.
- [15] Kerneis, S., Bogdanova, A., Kraehenbuhl, J. P., & Pringault, E. (1997). Conversion by Peyer's patch lymphocytes of human enterocytes into M cells that transport bacteria. *Science*, 277(5328), 949-952.





## In Vitro Effects of Clindamycin Antibiotic on Glucose-6-Phosphate Dehydrogenase Enzyme Purified from Sheep Spleen Tissue

**Ciğdem COBAN<sup>1,\*</sup>**, **Mehmet ÇİFTÇİ<sup>2</sup>**

<sup>1</sup>*Solhan Healty Services Vocational School/Medical Services and Techniques, Bingöl Üniversitesi, Türkiye*

<sup>2</sup>*Faculty of Veterinary, Basic Sciences, Bingöl Üniversitesi, Türkiye*

### Abstract

In our study, the in vitro effects of clindamycin antibiotic on glucose-6-phosphate dehydrogenase enzyme (G6PD; E.C. 1.1.1.49) purified from sheep spleen tissue were investigated. Firstly, G6PD enzyme was partially purified from sheep spleen tissue by ammonium sulfate precipitation. The enzyme sample obtained as a result of ammonium sulfate precipitation was purified by 2', 5' ADP-Sepharose 4B gel affinity chromatography and the purity of the enzyme was controlled by sodium dodecylsulfate polyacrylamide gel electrophoresis (SDS-PAGE). Then, the effects of clindamycin antibiotic on enzyme activity were investigated. The IC<sub>50</sub> value was calculated as 28.75 mM by plotting the % Activity-[I] graph for the clindamycin antibiotic, which showed an inhibitory effect on the enzyme activity. In addition, in order to determine the Ki constant and inhibition type, preliminary experiments were carried out to determine the most suitable five different substrate concentrations and Lineweaver-Burk graphs were drawn by making measurements for each substrate concentration with the three most appropriate inhibitor concentrations. With the help of graphic, the Ki constant of the clindamycin antibiotic was determined as 41.64±11.89 mM and the inhibition type was determined competitively.

**Keywords:** Glucose 6-phosphate dehydrogenase, clindamycin, inhibition

### 1. Introduction

Glucose-6-phosphate dehydrogenase enzyme (G6PD; E.C. 1.1.1.49) in the presence of nicotinamide adenine dinucleotide (NAD<sup>+</sup>) catalyzes the first reaction of the pentose phosphate pathway, producing nicotinamide adenine dinucleotide phosphate (NADPH), as well as synthesizing ribose phosphates one of the enzymes at the key point of metabolism [1]. Ribose phosphates are components of vital biomolecules such as NAD<sup>+</sup> and deoxyribonucleic acid (DNA) adenosine triphosphate (ATP), flavin adenine dinucleotide (FAD), ribonucleic acid (RNA), acetyl coenzyme A (CoA) [2, 3]. NADPH released during the reaction catalyzed by G6PD functions as the substrate of the Glutathione reductase (GR) enzyme, which is responsible for the synthesis of the glutathione (GSH) molecule, which acts primarily as an antioxidant in cell metabolism. In addition to serving as an antioxidant, the GSH molecule is also involved in DNA and protein synthesis, amino acid transport, detoxification of some antineoplastic drugs and some metabolic end products. As can be understood from here, the G6PD enzyme, which is involved in the production of the GSH molecule, which is the intracellular defense system, acts indirectly in protecting cells against the harmful effects of oxidized molecules [4,5]. In addition, NADPH acts as a coenzyme in the reduction of another antioxidant, thioredoxin (Trx) [6]. The thioredoxin system has an important role in DNA synthesis, prevention of oxidative stress and peroxide damage, apoptosis, cellular growth and stimulation of transcription factor activity [7, 8, 9, 10]. Due to this mentioned importance, in this study, it was aimed to investigate the effects of clindamycin antibiotic on G6PD enzyme activity purified from sheep spleen tissue.

Clindamycin, a narrow-spectrum antibiotic, is effective against most gram-positive species and gram-negative anaerobic species of some pathogenic bacteria and inhibits these pathogens by binding to the 50S ribosomal subunits. It is an alternative drug to penicillin used in the treatment of bacterial infections caused by a number of

\* Corresponding author. e-mail address: ccoban@bingol.edu.tr



gram-positive odors, including bone or joint infections, strep throat, pneumonia, middle ear infections, pelvic inflammatory disease, and endocarditis [11].

It is known that many antibiotics and drugs are used in human and animal treatment in studies [12]. The target of many of these drugs is specifically regulatory enzymes in metabolism. Drug inhibitors are used in the treatment of diseases by binding to enzymes reversibly or irreversibly. Therefore, enzymes constitute an active research area in pharmacology [13]. It is known that the G6PD enzyme is purified and characterized from many living tissues in the literature searches, and inhibition studies of many drug molecules on enzyme activity are carried out [14, 15, 16]. However, the effects of clindamycin antibiotic on G6PD enzyme purified from sheep spleen tissue have not been investigated.

## **2. Material and Method**

### **2.1. Material**

The clindamycin antibiotic used in our study was commercially available, TEMED, EDTA protein standards, ammonium sulfate, Tris, 2', 5' ADP-Sepharose 4B affinity gel G6P, NADP<sup>+</sup>, electrophoresis chemicals, and other chemicals from Sigma-Aldrich Com. (St. Louis, MO) and Merck (Darmstadt, Germany).

### **2.2. Preparation of Homogeneous**

The sheep spleen tissue used in this study was obtained from the Combined Meat and Milk Institution of Bingöl according to the cold chain rules. To prepare G6PD enzyme homogenate, spleen tissue was brought to room temperature and 10 grams of tissue were cut into small pieces and suspended in 30 mL of 1 M Tris-HCl (pH= 8.0) buffer. The tissue, which was thoroughly shredded in the homogenator, was centrifuged for 1 hour at 10,000xg, and the precipitate was discarded and homogenate was formed [10,14, 17].

### **2.3. Ammonium Sulphate Precipitation and Dialysis**

For the prepared homogenate, ammonium sulfate precipitation was performed at 40%-60% saturation concentrations according to the salting-out method. The precipitate in this range was dissolved in 1 M Tris-HCl buffer (pH= 8.0) and the enzyme solution was transferred to dialysis bags and dialyzed against 50 mM K-acetate/ 50 mM K-phosphate (pH= 7.0) buffer for 2 hours [10,14, 17].

### **2.4. of 2',5'-ADP Sepharose-4B Affinity Column and Purification of Sheep spleen G6PD Enzyme**

Partially purified enzyme sample after ammonium sulfate precipitation was purified by 2', 5' ADP Sepharose-4B affinity chromatography. First of all, an affinity column was prepared. For a bed volume of 10 mL, 2 g of dry 2', 5'-ADP sepharose 4B gel was weighed and washed several times in 400 mL of distilled water to remove solids. At the same time, the gel was swollen with the washed water. After deaerating the gel with vacuum using a water trumpet, it was suspended with equilibration buffer (0.1M KH<sub>2</sub>PO<sub>4</sub> + 0.1M K-acetate pH= 6.0). The suspended gel was packed into a cooled column consisting of a 1x10 cm closed system. After the gel precipitated, it was washed with wash and equilibration buffer with the help of a peristaltic pump. The equilibration of the column was understood from the approximate equalization of the absorbance and pH of the eluate and buffer at 280 nm. Thus, the affinity column was prepared. 11 mL of G6PD enzyme solution was loaded onto the prepared column. Affinity column 25 mL 0.1M KH<sub>2</sub>PO<sub>4</sub> +0.1M K-acetate (pH= 6.0 ), 25 mL,0.1M KH<sub>2</sub>PO<sub>4</sub> +0.1M K-acetate (pH= 7.85) and 25 mL, respectively It was washed with solutions of 0.1M KH<sub>2</sub>PO<sub>4</sub> + 0.1M KCl (pH= 7.85). The washing process was followed in the spectrophotometer and the absorbance values were determined to be approximately equal to the blank. After washing the column, the G6PD enzyme was eluted from the affinity column with elution buffer (80 mM KH<sub>2</sub>PO<sub>4</sub> + 80 mM KCl + 0.5 mM NADP<sup>+</sup> + 10 mM EDTA pH= 7.85) [10, 14, 17, 18, 19, 20].

## 2.5. Measurement of Glucose 6-Phosphate Dehydrogenase Enzyme Activity

G6PD enzyme activity was measured spectrophotometrically according to the Beutler method. This method is based on the principle that NADPH, which is formed as a result of the reduction of coenzyme NADP<sup>+</sup> with GSH in the reaction catalyzed by the G6PD enzyme, gives maximum absorbance at 340 nm [21].

## 2.6. Protein Determination

Quantitative protein amount, enzyme homogenate, ammonium sulfate precipitate and pure enzyme sample were determined spectrophotometrically at 595 nm according to the Bradford method. The standard chart was created using bovine serum albumin protein [18].

## 2.7. Enzyme Purity Control with SDS-PAGE

Enzyme purity control 3-8% batch sodium dodecyl sulfate polyacrylamide gel electrophoresis (SDS-PAGE) was carried out according to the method of Laemmli [21].

## 2.8. Kinetic Studies

Inhibition effects of clindamycin antibiotic on G6PD enzyme activity were investigated in kinetic studies. The % Inhibition-[I] graph was drawn to calculate the IC<sub>50</sub> value by measuring the antibiotic, which showed an inhibitory effect as a result of the activity measurements, at different inhibitor concentrations. In addition, preliminary experiments were carried out to determine the K<sub>i</sub> constant and inhibition type, and the most suitable five different substrate concentrations were determined. K<sub>i</sub> constant and inhibition type were determined from the graph obtained [10,17].

## 3. Results and Discussion

Using ammonium sulfate precipitation and 2', 5', ADP-Sepharose-4B affinity chromatography, G6PD enzyme, which has 15.24 EU/mg protein specific activity, was purified 1120.5 times with 40% yield and the results are shown in Table 1.

**Table 1.** Sheep spleen tissue G6PD enzyme purification steps

Purification step	Total Volume (mL)	Activity (EU/mL)	Protein (mg/mL)	Total Protein (mg)	Total Activity	Specific Activity (EU/mg protein)	% Yield	Purification Number of floors
Homogenate	25	0,932	97,47	2437	23,300	0,0096	100	1
Ammonium sulfate precipitation (40-70%)	11	1,484	108,81	1197	16,324	0,0136	70,06	1,416
Affinity Chromatography	7,5	1,265	0,083	0,63	9,4875	15,24	40,71	1120,5

SDS-PAGE was performed to determine the enzyme purity. The single band obtained on the gel is shown in Figure 1.

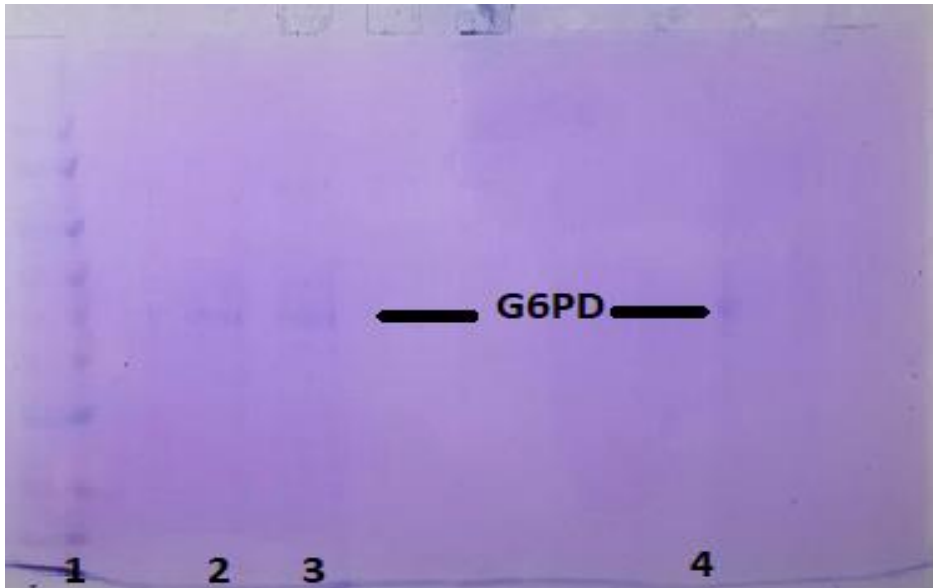


**Figure 1.** Well 1: standard proteins (14kDa - 175 kDa), wells 2, 3 and 4: Pure G6PD enzyme eluted from the affinity column.

In kinetic studies, clindamycin antibiotic was used at 1.75, 3.5, 7.04, 17.5, 35, 52.5 and 70 mM concentrations on G6PD enzyme activity purified from sheep spleen tissue. The IC<sub>50</sub> value was calculated as 28.75 mM by plotting the % Activity-[I] graphs of this antibiotic with an inhibitory effect (Figure 2). In addition, Linevawer-Burk plot was drawn for G6PD at 3 different inhibitory clindamycin and 5 different substrate concentrations, and the K<sub>i</sub> constant for clindamycin was 41.64±11.89 and the inhibition type was determined competitively (Figure 3).

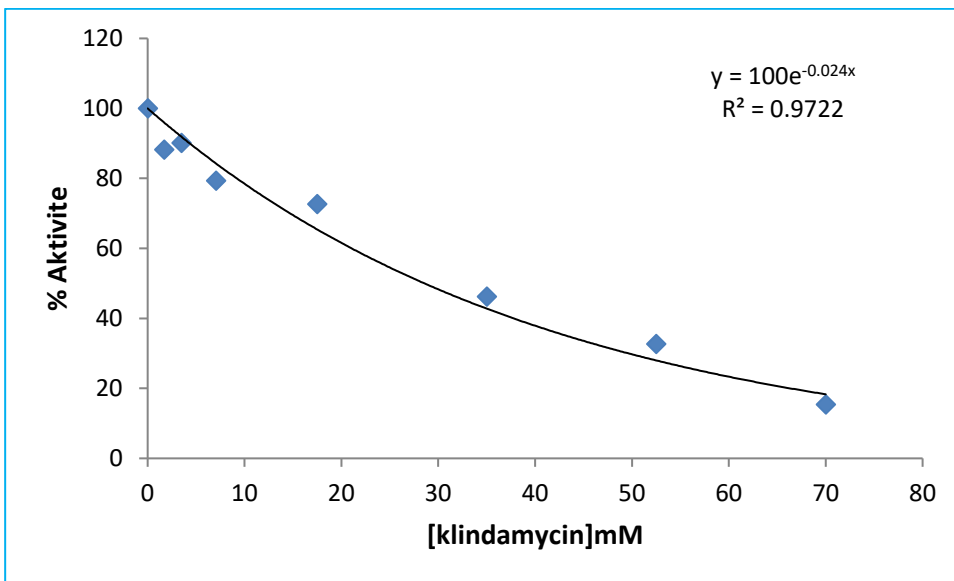


**Figure 2.** [Clindamycin]-% Activity graph on sheep spleen G6PD enzyme.

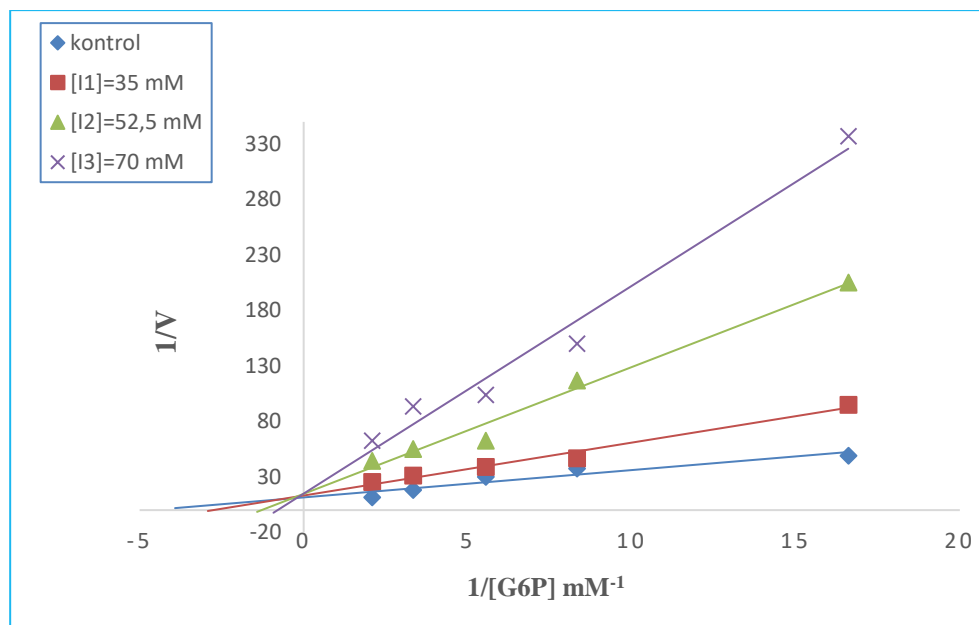


**Figure 3.** Lineweaver-Burk plot plotted for sheep spleen G6PD enzyme at 5 different substrates and 3 different clindamycin concentrations.

G6PD, the first enzyme of the pentose phosphate pathway, is responsible for the production of NADPH, which acts as a coenzyme in the antioxidant system, together with the 6-phosphogluconate dehydrogenase enzyme, as seen in the following reaction.



In the researches, it has been determined that antioxidant systems degenerate due to reasons such as drugs, nutrition and oxidative stress. The increase in malondialdehyde (MDA), an indicator of lipid peroxidation, showed that these cells were senescent [23]. This situation is related to the decrease of GSH-related enzymes such as G6PD, GR (Mieyal et al., 1991). In addition, abnormal activation of G6PD is associated with cancer. Fast-growing cancer cells increase the production of NADPH they need by constantly stimulating G6PD [24]. The liver tissue, which is the most important organ of the antioxidant system, and its enzymes have been extensively studied for GSH molecule studies in the literature. In experiments on animals, it has been determined that GSH biosynthesis is reduced by various xenobiotics such as butionine, sulfoximine, acetaminophen and bromobenzene. In hepatocytes exposed to these, GSH is depleted and liver damage occurs. It has been stated that glutathione sources should be increased in order to correct this situation [25].

Since the G6PD enzyme is directly or indirectly associated with many diseases, the research and development of G6PD inhibitors is important [26]. In our study, G6PD enzyme was purified from sheep spleen tissue by ammonium sulfate precipitation and 2',5' ADP-Sepharose-4B affinity chromatography. Affinity chromatography is a chromatography method based on specific interactions, which is common in enzyme purifications, used in the purification of protein, DNA, RNA and other macromolecules in a short time and with high purity [27]. In the second stage of the study, the effects of the antibiotic clindamycin, which is widely used in the treatment of humans and animals, on the enzyme were investigated. As a result of kinetic studies, IC<sub>50</sub> values for clindamycin were calculated as 28.75 mM, K<sub>i</sub> constant was calculated as 41.64 ± 11.89 mM, and inhibition type was also determined competitively.

In the literature review on G6PD, it was determined that the G6PD enzyme was purified from sheep erythrocyte tissue and the effects of penicillin G potassium, gentamicin sulfate and amikacin antibiotics on enzyme activity were investigated. In this study, it was observed that gentamicin sulfate inhibited the G6PD enzyme with IC<sub>50</sub> values of 10.01 mM, penicillin G potassium 12.83 mM and amikacin 41.88 mM [28]. In addition, in the study investigating the inhibitory effects of lincomycin, amoxicillin, ampicillin, ivermectin, gentamicin, streptomycin sulfate, novamizole ketogenic, cefuroxime sodium, cefazolin sodium and tylosin on the G6PD enzyme activity purified from sheep spleen tissue, ivermectin was the most effective on the enzyme with an IC<sub>50</sub> value of 0.62 mM. It was determined that lincomycin had the lowest inhibitory effect on the enzyme with an IC<sub>50</sub> value of 231 mM [14]. In another study, the effect of the hormone melatonin on the G6PD enzyme activity purified from human erythrocytes was investigated. As a result, it has been observed that this hormone increases enzyme activity (Bayindir et al., 2018). In a study in which the G6PD enzyme was purified from rat erythrocytes, clindamycin antibiotic was used on enzyme activity and it was observed that clindamycin inhibited the G6PD enzyme competitively with an IC<sub>50</sub> value of 34.65 mM and a K<sub>i</sub> constant of 39.8mM [29]. Our study is in agreement with this study. In addition, clindamycin antibiotic was studied on the GR enzyme activity purified from sheep spleen tissue and it was observed that it did not show any activation or inhibition on the enzyme [30]. In another study, G6PD enzyme was purified from rat heart and lung tissues and the effects of some drugs on its activities were investigated. These drugs; gentamicin, ceftazidime, digoxin, cefuroxime, methylprednisol, teicoplanin furosemide, dopamine, furosemide, Adrenaline, lidocaine, metoprolol tartrate, verapamil HCl, levofloxacin, cefazolin and cotin. Of these drugs, cefazolin, ceftazidime, cefuroxime furosemide, gentamicin, levofloxacin, methylprednisol, and teicoplanin inhibited the G6PD enzyme in rat lung tissue [31].

## Acknowledgment

As a result, it would be beneficial to adjust the dose considering the values obtained in the therapeutic use of clindamycin antibiotic, which has a competitive inhibition effect for the sheep spleen G6PD enzyme.

## 4. References

- [1] Adem, Sevki, and Mehmet Ciftci. 2012a. "Purification of Rat Kidney Glucose 6 Phosphate Dehydrogenase, 6- Phosphogluconate Dehydrogenase, and Glutathione Reductase Enzymes Using 2', 5'-ADP Sepharose 4B Affinity in a Single Chromatography Step." *Protein Expression and Purification* 81(1): 1–4.
- [2] Ciftci M, Kufrevioglu OI, Gundogdu M, Ozmen I, 2000. Effects of some antibiotics on enzyme activity of glucose-6-phosphate dehydrogenase from human erythrocytes. *Pharmacological Research*. 41(1):109-113.
- [3] Sevki A, Ciftci M, 2012. Purification of rat kidney glucose 6 phosphate dehydrogenase, 6-phosphogluconate dehydrogenase, and glutathione reductase enzymes using 2', 5'-ADP sepharose 4B affinity in a single chromatography step. *Protein Expression and Purification*, 81(1):1-4
- [4] Lu, Jun, and Arne Holmgren. 2014. "Free Radical Biology and Medicine The Thioredoxin Antioxidant System." *Free Radical Biology and Medicine* 66: 75–87. <http://dx.doi.org/10.1016/j.freeradbiomed.2013.07.036>.
- [5] Akkemik, E et al. 2011. "In Vitro Effects of Some Drugs on Human Erythrocyte Glutathione Reductase." 41(2): 235–41.
- [6] Kose, Leyla Polat et al. 2015. "The Effects of Some Avermectins on Bovine Carbonic Anhydrase Enzyme." *Journal of enzyme inhibition and medicinal chemistry* 6366(February 2017): 1–6. <http://www.ncbi.nlm.nih.gov/pubmed/26207514>.
- [7] Carlberg I, Mannervik B, 1981. Purification and characterization of glutathione reductase from calf liver. An improved procedure for affinity chromatography on 2', 5'-ADP-Sepharose 4B. *Analytical Biochemistry*, (116):531-536.
- [8] Ciftci M, Kufrevioglu OI, Gundogdu M, Ozmen I, 2000. Effects of some antibiotics on enzyme activity of glucose-6-phosphate dehydrogenase from human erythrocytes. *Pharmacological Research*. 41(1):109-113.
- [9] Altikat, S, M Ciftci, and ME Buyukokuroglu. 2002. "In Vitro Effects of Some Anesthetic Drugs on Enzymatic Activity of Human Red Blood Cell Glucose 6-Phosphate Dehydrogenase." *Pol. J. Pharmacol* 54(1): 67–71. <http://www.ncbi.nlm.nih.gov/pubmed/12020046>.
- [10] Keha EE, Küfrevioğlu Öİ. *Biyokimya, Aktif Yayınevi*, 6. Baskı, İstanbul, 2010.
- [11] Kayaalp SO (2002) Rasyonel tedavi yönünden tıbbi farmakoloji.10. Baskı. Kitabın muhtelif bölümleri

- [12] Dilek, Esra Bayram, İ Ömer, and Ş Beydemir. 2013. "Mpacts of Some Antibiotics on Human Serum Paraaxonase 1 Activity." 28(February 2012): 758–64.
- [13] Kose, Leyla Polat et al. 2015. "The Effects of Some Avermectins on Bovine Carbonic Anhydrase Enzyme." *Journal of enzyme inhibition and medicinal chemistry* 6366(February 2017): 1–6. <http://www.ncbi.nlm.nih.gov/pubmed/26207514>.
- [14] Çoban Ç, Çiftci M, 2022. Bazı İlaçların Koyun Dalak Dokusundan Saflaştırılan Glukoz-6-Fosfat Dehidrogenaz Enzimi Üzerine *İn Vitro* Etkileri. *Türk doğa ve fen dergisi*, 11: 1, 29 – 35
- [15] Ciftci M, Kufrevioglu OI, Gundogdu M, Ozmen I, 2000. Effects of some antibiotics on enzyme activity of glucose-6-phosphate dehydrogenase from human erythrocytes. *Pharmacological Research*. 41(1):109-113.
- [16] Sevki A, Ciftci M, 2012. Purification of rat kidney glucose 6 phosphate dehydrogenase, 6-phosphogluconate dehydrogenase, and glutathione reductase enzymes using 2', 5'-ADP sepharose 4B affinity in a single chromatography step. *Protein Expression and Purification*, 81(1):1-4.
- [17] Smith LL (1987) Cholesterol autoxidation. *Chem. Phys. Lipids* 44: 87-125
- [18] Bradford MM (1976) A rapid and sensitive method for the quantitation of microgram quantities of protein utilizing the principle of protein dye binding. *Anal. Biochem.* 72(1 2): 248–254
- [19] Demir H, Erat M, Şakiroğlu H, 2006. In vitro effects of some antibiotics on glutathione reductase obtained from chicken liver. *Turkish Journal of Veterinary and Animal Sciences*, (30):513-519.
- [20] Temel, Y., and M.Ş. Taysi. 2019. "The Effect of Mercury Chloride and Boric Acid on Rat Erythrocyte Enzymes." *Biological Trace Element Research* 191(1).
- [21] Beutler E, 1971. *Red Cell Metabolism Manual of Biochemical Methods*; Academic Press: London,
- [22] Laemmli DK (1970) Cleavage of structural proteins during in assembly of the heat of bacteriophage T4. *Nature*, London, s. 227-680
- [23] Stocks J, Offerman EL, Modell CB, Dormandy TL (1972) The Susceptibility to Autoxidation of Human Red Cell Lipids in Health and Disease. *Brit J Haematol* 23: 713-24
- [24] Patra, Krushna C, and Nissim Hay. 2014. "The Pentose Phosphate Pathway and Cancer." *Trends in Biochemical Sciences* 39(8): 347–54. <http://dx.doi.org/10.1016/j.tibs.2014.06.005>.
- [25] Atamer Y, Koçyiğit Y, Atamer A, Mete N, Canoruç N (2000) Significance of Lipid Peroxides, glutathione and antiperoxidative enzymes in ethanol and acetaminophen toxicity in the rat 11(1): 54-60
- [26] Luo, Zhongyuan et al. 2021. "Discovery and Characterization of a Novel Glucose-6-Phosphate Dehydrogenase (G6PD) Inhibitor via High-Throughput Screening." *Bioorganic & Medicinal Chemistry Letters* 40(February): 127905. <https://doi.org/10.1016/j.bmcl.2021.127905>.
- [27] Ciftci, M, D Bilici, and O I Kufrevioglu. 2001. "Effects of Metamizol and Magnesium Sulfate on Enzyme Activities of Glucose-6-Phosphate Dehydrogenase from Human Erythrocytes in Vitro and from Rat Erythrocytes in Vivo." *Pharmacol Res* 44(1): 7–11. [http://www.ncbi.nlm.nih.gov/entrez/query.fcgi?cmd=Retrieve&db=PubMed&dopt=Citation&list\\_uids=11428904](http://www.ncbi.nlm.nih.gov/entrez/query.fcgi?cmd=Retrieve&db=PubMed&dopt=Citation&list_uids=11428904).
- [28] Beydemir, Sükrü, Mehmet Ciftçi, and O Irfan Küfrevioğlu. 2002. "Purification and Characterization of Glucose 6-Phosphate Dehydrogenase from Sheep Erythrocytes and Inhibitory Effects of Some Antibiotics on Enzyme Activity." *Journal of enzyme inhibition and medicinal chemistry* 17(4): 271–77. <http://www.ncbi.nlm.nih.gov/pubmed/12530481>.
- [29] Temel, Y., A. Ayna, I. Hamdi Shafeeq, ve M. Ciftci. 2020. "In Vitro Effects of Some Antibiotics on Glucose-6-Phosphate Dehydrogenase from Rat (Rattus Norvegicus) Erythrocyte." *Drug and Chemical Toxicology* 43(2).
- [30] Çoban Ç, 2022. Glutasyon Redüktaz Enziminin Koyun Dalak Dokusundan Saflaştırılması, Karakterizasyonu ve Bazı Antibiyotiklerin Enzim Aktivitesi Üzerine Etkilerinin Araştırılması Doktora Tezi, Bingöl Üniversitesi, Fen bilimleri Enstitüsü, Kimya Anabilim Dalı, s. 88
- [31] Adem Ş. (2011) Sıçan kalp ve akciğer dokularından glukoz–6-fosfat dehidrogenaz, 6- fosfogluconat dehidrogenaz, glutasyon redüktaz enzimlerinin saflaştırılması, karakterizasyonu, kotinin ve bazı ilaçların enzimlerin aktiviteleri üzerine etkilerinin incelenmesi. Doktora Tezi, Fen Bilimleri Enstitüsü, Erzurum



## Pathological Fracture of the Mandible due to Actinomycosis Osteomyelitis: Case Report

**Zuhal ÖZATES<sup>1,\*</sup>** 

<sup>1</sup> Faculty of Dentistry , Department of Maxillofacial Radiology, Çankırı Karatekin University, Çankırı, Türkiye

### Abstract

Actinomycosis is a specific and chronic infection caused by gram-positive anaerobic bacteria. While the cervicofacial form has the highest prevalence, it can also be seen in thorax, abdominal and genital region. In this case we reported a pathological fracture caused by actinomyces osteomyelitis. 68 years-old male patients referred to our clinic with pain on left mandibular angulus. Patient is with a diagnose of a fracture due to actinomycosis infection after the clinical, radiologic and microbiologic examinations. Patient is treated with a diagnose of a fracture due to actinomycosis infection after the clinical, radiologic and microbiologic examinations. After the treatment, patient recovered and new bone formation at the fracture line were observed.

**Keywords:** Actinomycosis, Osteomyelitis, Fracture, Mandible

### 1. Introduction

Actinomycosis of the jaws is a relatively rare infection. The most common cause of cervicofacial actinomycosis infection is *Actinomyces israelii*. However, *Actinomyces naeslundii*, *Actinomyces viscosus* and *Actinomyces odontolyticus* species are also defined in the oral flora [1]. *Actinomyces* produces chronic, slowly developing infections, particularly when normal mucosal barriers are disrupted by trauma, surgery, or a preceding infection [2]. Because *Actinomyces* strains resemble both bacteria and fungi, they were generally considered to be transitional between two groups of microorganisms. However, many of the essential characteristics of *Actinomyces* indicate that they are in fact anaerobic bacteria. In addition, *Actinomyces* does not contain sterols in its cell walls and is sensitive to antibacterial chemotherapeutic agents [3]. Bacteria that enter the tissue as a result of actinomycosis infection and trauma multiply rapidly in the anaerobic environment due to the disruption of mucosal continuity. Once the infection appears, it is very difficult to completely eradicate it [3].

In general, infected tissues contain areas of severe necrosis and fibrosis. Only soft tissue involvement can occur or they can cause actinomycosis osteomyelitis involving soft tissue and bone. There are few publications in the literature on osteomyelitis caused by actinomycoses. Periostitis occurs when the infection reaches the periosteum from the soft tissue. In slowly progressing infections, the periosteum reacts to form new bone. If the infection progresses rapidly, destruction areas extending into the bone can be observed [4]. Pathological fractures can be observed in these destroyed bone areas due to chronic osteomyelitis [5].

### Case Report

A 68-year-old male patient complained of pain in his left lower jaw, He applied to Hacettepe University Faculty of Dentistry Department of Maxillofacial Radiology.

In the patient's history, mandibular teeth 36 and 37 were extracted another center. He stated that the region did not heal and that he felt numbness in the left lower lip area with increasing pain over time. The patient received medical treatment for prostate enlargement three years ago, had bypass surgery six years ago, and uses anticoagulants and beta-blockers.

\* Corresponding author. e-mail address: zuhalozates@karatekin.edu.tr

In the clinical examination, exposed bone, submandibular lymphadenopathy, purulent discharge and painful expansion on palpation in the left corpus region of the mandible were observed in the extraction region (Figure 1-2).

In the Cone Beam Computerized Tomography (CBCT) examination, radiolucent lesions in the form of moth bite, sequestered bone and pathological fracture were observed in around the extraction site (Figure 3-4). Diagnosed as osteomyelitis caused by actinomycosis has been done. The patient was referred to the surgery clinic for treatment and surgical treatment was applied after long-term antibiotic treatment (Figure 5).

## 2. Results and Discussion

Actinomycosis is a rare infection that has the potential to spread through weakened host immunity and spread to deep tissues [6]. Although they are frequently observed in the cervicofacial region after traumatic surgical procedures, they can cause osteomyelitis infection in any part of the body [7]. In the case we present, the patient's history is similar to the literature, as there are systemic diseases and drug use.

In the literature; It was determined that the vascularization of the relevant region decreased after radiotherapy, and it was stated that it was a predisposing factor in the development of actinomycosis infection [8].

Actinomycosis infections are most common in the perimandibular region of the jaws. Bone involvement is very rare in infections seen in this region [9]. Success has been observed in % 90 of actinomycosis cases after appropriate treatment [8]. In our case In the control examination performed 10 months after the treatment, the patient's complaints were resolved and secondary bone formation was observed at the fracture line in the control CBCT evaluation. The diagnosis of actinomycosis is made with the help of microbiological examinations in addition to the clinical and radiological examination findings. Although anaerobic cultures allow bacteria to be isolated, polymerase chain reaction (PZT) plays an important role in the detection of bacteria today [10]. Actinomycosis infections related to this infection and pathological fractures related to this infection are rarely seen in the cervicofacial region [11]. In the case we presented; diagnosis of pathological fracture due to actinomycosis evaluated.



**Figure 1.** Extra oral swelling



**Figure 2.** Intra oral image exposed bone, purulent discharge.



**Figure 3.** CBCT MPR image; radiolucent lesions in the form of moth bite, sequestered bone and pathological fracture



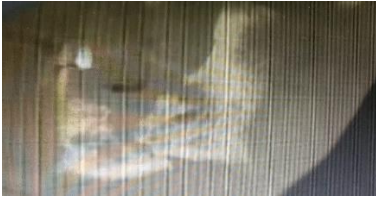


**Figure 4.** CBCT Sagittal image; radiolucent lesions in the form of moth bite, sequestered bone and pathological fracture



**Figure 5.** CBCT image postop

## References

- [1] Herman WW, Whitaker SB, Williams MF, Sanguenza OP. Acute actinomycosis presenting as an ulcerated palatal mass . *J Oral Maxillofac Surg* 1998;56:1098-101
- [2] Murray RP, Kobayashi GS, Pfaller MA, Rosental KS. *Medical Microbiology*, 2nd ed. St. Louis, MO: Mosby, 1994.
- [3] Schuster GS. *Oral Microbiology and Infectious Disease*, 3rd ed. Philadelphia, PA: Decker, 1990.
- [4] Chung Ji Liu, Kuo Ming Chang, Chia Teh Ou. Actinomycosis in a patient treated for maxillary osteoradionecrosis. *J Oral Maxillofac Surg* 1998;56:251-3.
- [5] Kaya GŞ, Yalçın E, Aras MH, Gürsan N. Kronik osteomyelitin postoperatif komplikasyonu ve tedavisi. *J Dent Fac Atatürk* 2011;21:39-42.
- [6] Russo TA: *Agents of actinomycosis* , in Mandell GL, Bennett JE, Dolin R (eds): *Principles and Practice of infectious Disease* 4th ed . New York, NY, Churchill Livingstone, 1995. p. 2280-2288.
- [7] Chung Ji Liu, Kuo Ming Chang, Chia Teh Ou. Actinomycosis in a patient treated for maxillary osteoradionecrosis. *J Oral Maxillofac Surg* 1998;56:251-3.
- [8] Weese WC, Smith IM. A study of 57 cases actinomycosis over 36-year period: *A diagnostic “failure” with good prognosis after treatment.* *Arch Intern Med* 1975;135:1562-5.
- [9] Smith MH, Harms PW, Newton DW, Lebar B, Edwards SP, Aronoff DM. Mandibular Actinomyces osteomyelitis complicating florid cemento-osseous dysplasia: case report. *BMC Oral Health* 2011;21: 21.
- [10] Hansen T, Wagner W, Kirkpatrick CJ, Kunkel M. Infected osteoradionecrosis of the mandible: follow-up study suggests deterioration in outcome for patients with Actinomyces-positive bone biopsies. *Int J Oral Maxillofac Surg* 2006;35: 1001-4.
- [11] Sharkawy AA. Cervicofacial actinomycosis and mandibular osteomyelitis. *J Infect Dis Clin North Am* 2007;25: 543-6.



## The Importance of Sedimentation Pools in Sediment Mobility: Example of Kızılırmak Basin (Çankırı) – Tımarlı Locality

Ayşe YAZICI<sup>1,\*</sup> , Ender SARIFAKIOĞLU<sup>2</sup> 

<sup>1</sup>Cankiri Provincial Directorate of National Education, Department of Construction and Real Estate, Cankiri, Türkiye

<sup>2</sup>Faculty of Engineering, Department of Civil Engineering, Cankiri Karatekin University, Cankiri, Türkiye

### Abstract

Due to the terrain characteristics of our country, heavy amounts of sediment are transported due to erosion, landslides and the shearing (carving) effect of water in stream beds. The amount of solid materials transported in a year in Turkey is more than the transported in a year from the entire European Continent. The sediment transported by the stream accumulates in the reservoir areas of the water deposit and bank structures. In this study, sedimentation pools built in Çankırı basin to hold the suspended sediment transported from the reservoir area to the transmission channel fed by the Tımarlı regulator water source built on the Kızılırmak river were examined. The sedimentation problem has been observed in the regulator reservoir area due to the heavy sediment transport in the transition areas of the Kızılırmak river. In order to prevent the problems that may be caused by the suspended sediment transported into the transmission channels, by increasing the depth and width of the sedimentation pools, the flow rate is reduced and the sediment is accumulated. In order to trap the sediment with the desired minimum particle diameter in the sediment pool, the sedimentation pool design must be made appropriately. The length of the sedimentation pool was determined with the help of the HEC-RAS software and the Sümer (1977) equation for trapping efficiency, taking into account the flow rate and cross-section in the field area where the sedimentation pool will be built. Several approaches have been proposed for more realistic estimation of sedimentation pool efficiency. The relation of Sümer is one of them. As a result, it was concluded that the calculated length for the sediment with the minimum grain diameter (0.50 mm) to be deposited in the designed sediment pool is compatible with its size in the field (40 m.).

**Keywords:** Cankiri, Kızılırmak Basin, Tımarlı, Sedimentation Pool, Sediment

## 1. Introduction

Water is the most important natural substance that ensures the continuity and life of all living things from the existence of our world to the present. Only 3% are in the category of clean water resources. According to the water resources potential data specified in the DSI website; a total of 57 billion m<sup>3</sup> of water is used in Turkey, 44 billion m<sup>3</sup> (77%) for agricultural purposes and 13 billion m<sup>3</sup> (23%) as drinking water. With the geography and rapidly developing population of our country and the increase in nutritional needs, the protection and management of water resources has a critical importance in order to obtain more products per unit area in agriculture.

### 1.1. General Information about Sediment

Sediment is the name given to any substance that is suspended in flowing waters and will precipitate if the water velocity drops [1]. While some of the sediment is formed by the grains that break off as a result of the erosion of the stream bed, the others are formed by the grains that break off as a result of natural disasters such as floods, erosion and landslides in the river basins depending on the climate and terrain characteristics. Sedimentation is defined as the settlement of sediment transported by water with the effect of gravity [2]. The amount of solid materials transported in a year in Turkey is more than the transported in a year from the entire European Continent [3]. Since there will be volume losses as a result of sediment accumulation in the reservoir areas of water storage, bank structures and water transmission channels, it adversely affects the economic life of the water structures built with great costs and increases the operating-maintenance costs.

\* Corresponding author. e-mail address: ayzc1818@gmail.com

## 2. Materials and Methods

It was studied in the field whether transition structures such as bridges, culverts, water storage and bank structures, and the structures built to prevent sediment from accumulating in water transmission and distribution channels fulfill the working principles.

### 2.1. Geological structure of the study area

The biggest and most important river within the provincial border of Çankırı is Kızılırmak. In the Kızılırmak basin, depending on the geology of the basin [4], a large amount of sediment is carried along with the water by the traction movement at the bottom and the ground, with the water flowing very fast and intensely in summer-winter months. The study area is located between the Karaömer Village of the Kızılırmak district of Çankırı and the Obruk Dam lake area in the İskilip District of Çorum. The location of the study area is shown on the highway map in Figure 1.

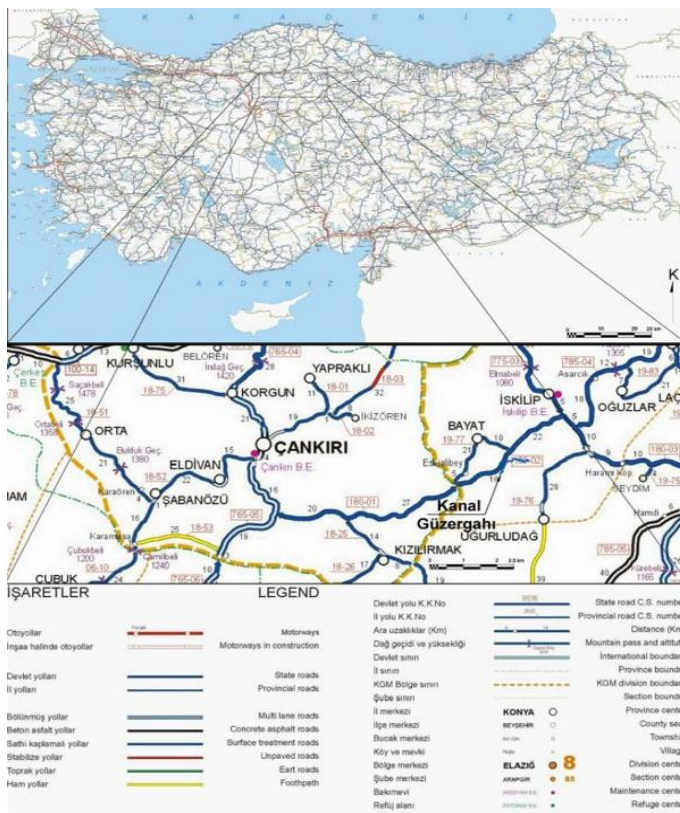


Figure 1. Location map of study area [5].

### 2.2. Information about the study area

Tımarlı Irrigation Part 2 Construction Work forms one part of a 40-year-old project that irrigates the Kızılırmak valley. In this context, Tımarlı regulator with lid (movable) regulator type was used as a water source within the borders of Çankırı province, and the regulator feeds the Left 1 and Right 1 main channels. As a result of the study carried out in the field area, it was observed that the regulator reservoir was completely filled with sediment and the sediment accumulation reached almost to the surface (Figure 2). The Left 1 main channel is 29675 meters long, and it was observed that the siphons and culverts built along the channel were filled with sediment and rendered the facility unusable (Figure 3). As the sediment is carried to the regulator reservoir and filled, the sediment does not hold the feature of the reservoir, so the sediment enters the main channel together with the water. For this reason, at the critical points determined on the transmission channel line, wide and deepened sedimentation pools suitable for the channel cross-section are built, the channel bottom height is generally lowered to a level lower than the thalweg level, and the flow velocity and turbulence effect are reduced.



**Figure 2.** Surface view of sediment accumulation of the reservoir in front of the regulator in the study area [5].



**Figure 3.** The situation of the area where the water passage should be made in the study area as a result of sediment accumulation [5].

On the other hand, in the Left 1 main channel fed by the Tımarlı regulator, there is a large sedimentation pool with a total sediment reservoir volume of  $800 \text{ m}^3$  with a length of 40 meters up to 0+43 km in the upstream part of the channel and a width of 10 meters inside (Figure 4).



**Figure 4.** The first sedimentation pool in the study area [5].

There are 4 small sedimentation pools in the upstream of the culverts and siphons built on the Left 1 main channel. The total sediment reservoir volume capacity of these pools is  $1200 \text{ m}^3$ . It has been observed that there is no sediment accumulation in the main and backup channels in the study area, and the small amount of sediment material observed is the material poured into the sedimentation pool from the sides of the channel, not by the current. It is shown in Figure 5 by examining how long the sedimentation pools built in the field extend the life of the facility and the transportation of clear water refined from sediment along the channel.





**Figure 5.** Image of sediment-free water transported in the main channel in the study area [5].

### 2.3. Cleaning the Sedimentation Pool

By adding washing (discharge) channels to the river side at the end of the area where the sedimentation pool is built, it is ensured that the sedimentation pools are self-cleaning. If the self-cleaning feature is not included in the sedimentation pool project, the cleaning process of the pool is done with the help of excavator vehicles.

## 3. Findings

### 3.1. Calculation of the first sedimentation pool in the study area

With the HEC-RAS analysis software, it is tried to determine the water profile, water velocity and depth corresponding to the project flow rate ( $7.70 \text{ m}^3/\text{s}$ ) in the sedimentation pool during the calculation phase. The HEC-RAS model was created based on the plan and cross-section images determined as a result of the preliminary design, and the resulting water surface profile is shown in Figure 6.

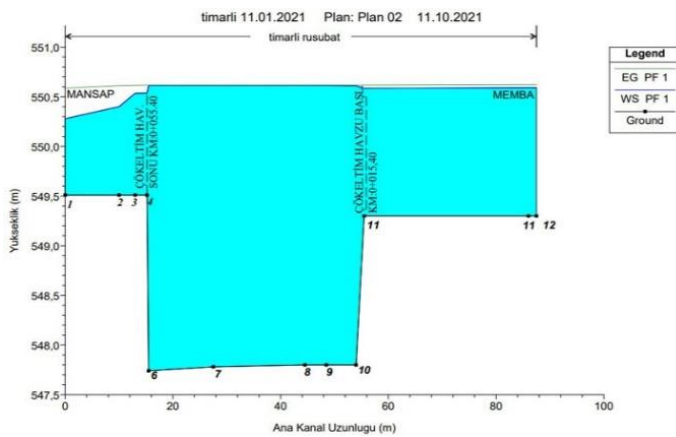


**Figure 6.** Water surface profile obtained from the HEC-RAS software [5].

In order to model along the channel in the HEC-RAS software with a preliminary estimation, the points where 12 cross-sections change are defined in the HEC-RAS software, so that the model is created exactly creating an 86 m long model in the program and representing the sedimentation pool and the inlet and outlet sections together. The cross-sectional images obtained for the project flow rate ( $7.70 \text{ m}^3/\text{s}$ ) are given in Table 1.

**Table 1.** Results of the analysis [5].

Reach	River Sta	Profile	Q Total (m <sup>3</sup> /s)	Min Ch El (m)	W.S. Elev (m)	Crit W.S. (m)	E.G. Elev (m)	E.G. Slope (m/m)	Vel Chnl (m/s)	Flow Area (m <sup>2</sup> )	Top Width (m)	Froude # Chl
timarli	86	PF 1	7.70	549.30	550.59		550.62	0.000168	0.79	9.75	7.56	0.22
timarli	85	PF 1	7.70	549.30	550.59		550.62	0.000168	0.79	9.75	7.56	0.22
timarli	55.5	PF 1	7.70	549.30	550.59		550.62	0.000170	0.79	9.71	7.56	0.22
timarli	54	PF 1	7.70	547.80	550.61		550.62	0.000015	0.34	22.45	7.99	0.07
timarli	48.5	PF 1	7.70	547.80	550.61		550.62	0.000009	0.27	28.10	9.99	0.05
timarli	44.5	PF 1	7.70	547.82	550.61		550.62	0.000009	0.28	27.90	9.99	0.05
timarli	27.5	PF 1	7.70	547.78	550.61		550.62	0.000009	0.27	28.29	9.99	0.05
timarli	15.5	PF 1	7.70	547.74	550.61		550.62	0.000008	0.27	28.70	9.99	0.05
timarli	15.2	PF 1	7.70	549.51	550.54		550.62	0.000572	1.25	6.16	6.00	0.39
timarli	13	PF 1	7.70	549.51	550.54		550.62	0.000574	1.25	6.15	6.00	0.40
timarli	10	PF 1	7.70	549.51	550.40	550.28	550.61	0.001995	2.04	3.78	5.49	0.78
timarli	0	PF 1	7.70	549.51	550.28	550.28	550.59	0.003379	2.46	3.14	5.15	1.00

HEC-RAS Plan 02 River: timarli Reach: timarli Profile: PF 1

### Determination of grain settlement criterion and control of pool length

For sizing the sedimentation pool, the required data obtained from the HEC-RAS software is taken from Table 2. and the settlement distance of the grain diameter desired to be deposited is checked.

**Table 2.** Required data for sizing the sedimentation pool [5].

Data	Explanation	Value	Unite
Q	Design Flow	7700	lt/sn
B	Sedimentation Pool Width	10	m
y	Water Depth at End of the Sedimentation Pool	2.87	m
S	Sedimentation Pool Ground Slope	0.01	m/m
P	Wetted Perimeter	15.74	m
D <sub>50</sub>	Grain Diameter to be Precipitated	0.5	mm
γ	Density of Standing Water	1.1	tons/m <sup>3</sup>
κ	Coefficient of Karman	0.42	-
r	Sediment Settling Rate Across the Pool	95	%

As a result of the preliminary estimation, Sümer (1977) method, which is one of the trapping efficiency and frequently used methods by DSI in practical calculations, was used in order to control whether the minimum grain diameter determined in the sedimentation pool sized in the HEC-RAS software is long enough for precipitation. The equation (1) was proposed by Sümer (1977) to calculate the length of the pool, corresponding to r, which represents the sediment precipitation rate throughout the pool.

$$L = -\frac{6(\frac{u_s}{u_*})y}{\kappa \lambda} \ln(1 - r) \quad (1)$$

The water velocity  $u_s$  at the end of the sedimentation pool obtained from the HEC-RAS software is 0.27 m/s. The drag speed ( $u_*$ ) value is calculated as 0.42 m/s.

The equation (2) is proposed to calculate the parameter value, which is a function of the dimensionless velocity  $\lambda$ .

$$\lambda = 8.87 \beta^{1.17} = 8.87 \cdot 0.28^{1.17} = 2.00 \quad (2)$$

Here, the following equation is used to calculate the settling velocity [6].  $\beta$  value of the suspended particles in terms of the sedimentation velocity parameter. The equation (3) is used to calculate the  $\beta$  value.

$$\beta = \frac{w_f}{\kappa \cdot u_*} = \frac{0.05}{0.42 \cdot 0.42} = 0.28 \quad (3)$$

In this equation,  $w_f$  (m/s) represents the sedimentation rate of the sediment in still water.  $D_{50}$  value of the grain diameter desired to be deposited is selected as 0.5 mm and the sedimentation pool is requested to be sized according to this determined the smallest grain diameter. In order to determine the sedimentation rate in stagnant

water for  $D_{50}$  diameter grains, the sedimentation rate according to the determined grain diameter and water density is read from Figure 7. Here, the density value ( $\gamma$ ) of the water is more turbid due to the sediments in the Kızılırmak water in the thesis study area, and it is expected to be denser than the normal pure water. Therefore, this value is determined as  $1.1 \text{ tons/m}^3$ , staying on the safe side. From Figure 7. the settling velocity is determined as  $w_f=0.05 \text{ m/s}$ .

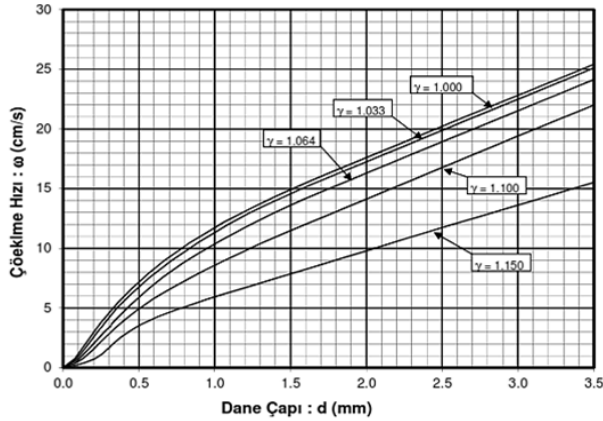


**Figure 7.** Sedimentation rate according to grain diameter [5].

By substituting all known values in Equation (1) and ignoring the turbulence effect of the water, the length of the initial sedimentation pool on the main channel is calculated as;

$$L = -\frac{6\left(\frac{u_s}{u_*}\right)y}{K\lambda} \ln(1-r) = -\frac{6 \cdot \left(\frac{0.27}{0.42}\right) \cdot 2.87}{0.42 \cdot 2.00} * \ln(1-0.95) = 39.48 \text{ m}$$

Considering the high velocity of the water taken from the water intake mouth to the transmission channel and considering the turbulence effect, the minimum particle diameter desired to be deposited is determined as  $L = 40 \text{ m}$ . by increasing the length of the sedimentation pool a little more than the calculated length, while remaining on the safe side.

#### 4. Conclusion and Recommendations

It has been observed that in the 40 m. long large sedimentation pool built at the beginning of the Left 1 main channel, the sediment accumulates by precipitating at the bottom of the pool and that the sediment, that is, the sediment carried along the sedimentation pools and the channel, is collected at the determined points, facilitating operation and maintenance.

According to the sedimentation pool length modeled in the HEC-RAS software and the minimum grain diameter desired to be deposited, the 40 m. long initial sedimentation pool size is suitable as a result of the calculation made by Sümer (1977) method [5].

It has been determined that the dimensions of the 40 m long first sedimentation pool in the study area built by DSI are exactly the same size.

Floating bodies cannot be trapped in the sedimentation pool. For this reason, gratings from profiles should be made on the upstream sides of structures such as siphons.

#### Acknowledgement

This study derived from Ayşe YAZICI's master thesis. We would like to thank Murat BİNGÖL, the 52nd Branch Manager of Çankırı, affiliated to the 5th Regional Directorate of State Hydraulic Works, and Murat ÇAVDAR, Assistant Manager, for their contributions to our work.

## References

- [1] Cöntürk H., Towards the planning of erosion and sediment survey, Chamber of Civil Engineers Turkish Civil Engineering IV. Technical Congress, Ankara, 1968, 1-9.
- [2] Onüçyıldız, M., Bostancı, İ., & Yazar, A. (2014). Determination of capacity loss of Altınapa reservoir caused by sedimentation using geographical information systems. *Selcuk University Journal of Social and Technical Researches*, 7, 12-26.
- [3] Berkün, M. (2005). *Water Resource Engineering*. İstanbul: Birsen Publisher, 30.
- [4] Sarıfakıoğlu, E., Sevin, M., Esirtgen, E., Bilgiç, T., Duran, S., Parlak, O., Karabalık, N. N., Alemdar, S., Dilek, Y., & Uysal. İ. (2011). Geology of ophiolitic rocks surrounding the Çankırı-Çorum basin: Petrogenesis, tectonics and ore contents. General Directorate of Mineral Research and Exploration Report num. 11449, Ankara (unpublished).
- [5] Yazıcı, A., Evaluation sediment dynamism in sedimentation tanks: Example of Cankiri basin – Timarli location, MSc Thesis, Cankiri Karatekin University, Faculty of Engineering, 2022.
- [6] Arslan, F. V., Settling basins, sediment removal efficiency and applications in Turkey, Master of Science Thesis, Ankara Gazi University, Faculty of Engineering, 2013.



## Investigation in Terms of Soil Characteristics of Inandik (Cankiri, Türkiye) Sinkholes due to Gypsum Karstification

**Mehmet Salih YILDIZ<sup>1\*</sup>**, **Ender SARIFAKIOĞLU<sup>2</sup>**

<sup>1</sup> Vocational School of Social Sciences, Cankiri Karatekin University, Cankiri, Türkiye

<sup>2</sup> Faculty of Engineering, Department of Civil Engineering, Cankiri Karatekin University, Cankiri, Türkiye

### Abstract

Sinkholes are karstic landforms that are formed as a result of the collapse of the ceilings of underground cavities, which are formed as a result of the interaction of groundwater with soluble rocks. The sudden occurrence of collapse makes these formations dangerous. Many buildings can be damaged due to sinkhole formations, and they can become unusable on lands that are a source of livelihood for the local people.

In this study, we investigated the sinkhole formations around Inandik village of Çankırı. When these sinkhole formations are considered in terms of the geology of the area, it is understood that they occurred as a gypsum karst. Since gypsum dissolves faster in water than carbonate rocks, it poses a greater risk. The structural damages in the region were observed with the field investigations. In addition, discontinuous gypsum units were observed in field studies and classified as extremely wide and void structures according to ISRM. When the boreholes drilled in the study area were examined, it was understood that there were molten gypsum layers underground. Point loading test was carried out with the samples taken by opening research pits in the gypsum units and it was observed that the rock had very low resistance. As a result, it was determined that the sinkholes formed around Inandik village were caused by the deformation and dissolution of the gypsum units.

**Keywords:** Sinkhole, Gypsum karst, Soil characteristic, Cankiri

### 1. Introduction

Karstifications developed on evaporitic rocks (gypsum, rock salt) on the earth cover relatively less area than karstifications developed on carbonate rocks (limestone, marble, dolomite). This is also the case in Turkey (Figure 1). However, the evaporitic rocks in contact with water dissolve faster than carbonate rocks [3 and references therein]. This means that both karstification and deformation are faster in evaporitic rocks.

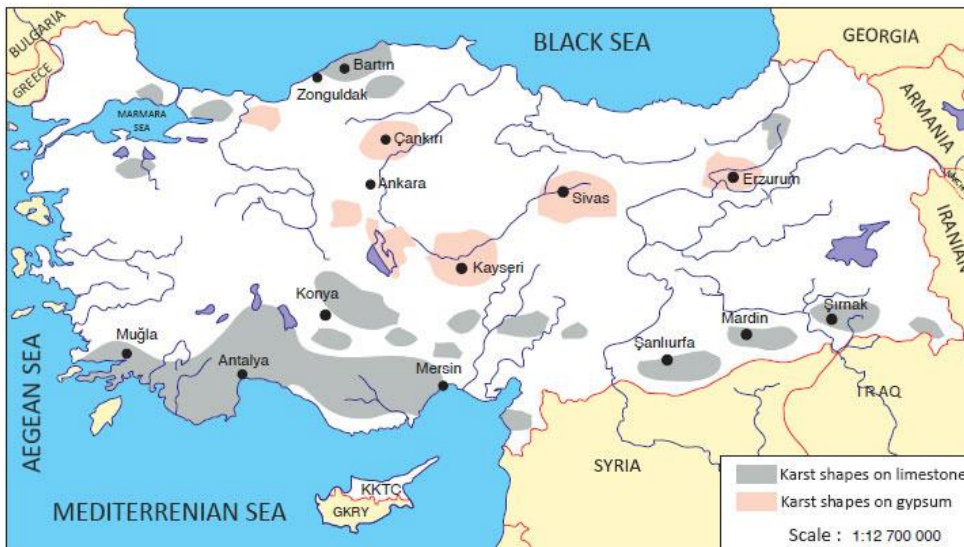


**Figure 1.** Karst regions of Turkey [9].

\* Corresponding author: e-mail address: mehmetalihyildiz@karatekin.edu.tr

The study area is the village of İnandık, located at the 40<sup>th</sup> km of the Ankara road, in the south of the province of Çankırı, where karstic shapes on gypsum are commonly seen. The İnandık village is 803 meters above the sea level. The administrative area of the village is 26.53 km<sup>2</sup>. In the İnandık village, the sinkhole formations occur due to the gypsum karstification. The map containing the location information of the study area is shown in the figure below (Figure 2).

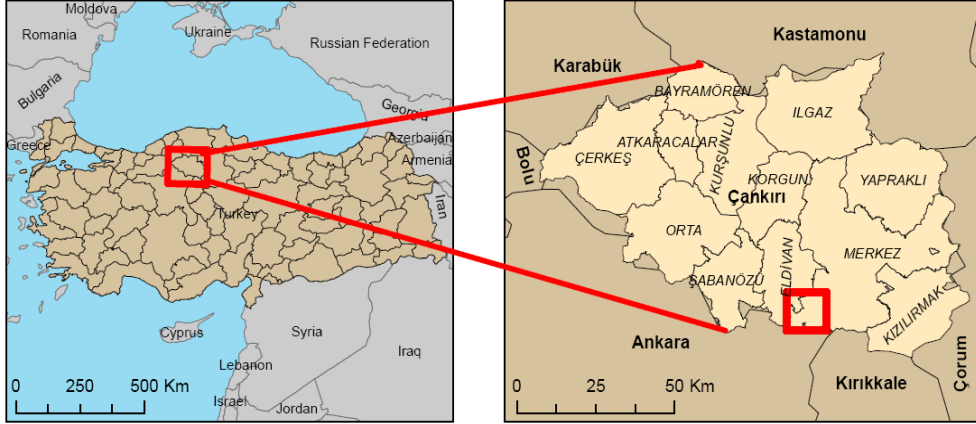


**Figure 2.** Location of the study area [11].

Sinkhole formations, one of the macro forms in karstic lands, are the product of rapid dissolution. "Sinkhole" literally means pit, hollow, depression. Sinkholes are generally defined as karstic landforms that occur as a result of the collapse of underground cavities, which are formed as a result of the interaction of underground waters with soluble rocks, over time, unable to carry the load on them. Another definition of sinkhole is that it is the name given to deep pits similar to chimneys or wells that are formed as a result of the collapse of underground rivers or active cave ceilings in stratified limestone [8]. The depths of sinkholes can vary from a few meters to several hundred meters. Sinkholes, which take a regular circular shape especially on flat lands, may form oval on sloping lands. While it is seen that there is water at the bottom of some sinkholes, some of them appear dry [4 and references therein].

Studies on sinkhole formations in Turkey until today generally belong to the Konya region. Again, the studies on gypsum formations are mostly concentrated around Sivas. In recent years, the investigations in the sinkholes around the İnandık village (Çankırı) draw attention [4-6]. In this study, research pits were opened to obtain information about the soil characteristics of the region by examining the sinkhole formations in İnandık village and its surroundings. The aim of the study is to investigate the causes and consequences of the sinkholes formed within gypsum levels close to the village settlement area and the gradual settlements that cause structural damage.

## **2. Materials and Methods**

### **2.1. On-site observation of sinkholes**

The sinkholes were observed in terms of both their size and type of soil they occurred in the place, and it was investigated whether there were other ground deformations in the vicinity. In addition, the sinkholes in the region were classified according to Walltham and Fokes (2005) and their characteristics such as the year of formation, altitude, diameter, depth and rock type were determined [10].

### **2.2. Detection of structural damage on buildings located in the residential area**

The fact that the sinkholes were formed close to the settlement and the gradual settlement of the ground in the settlement caused structural damage to the buildings there [4,6,11]. The structural damages were determined as a result of the examinations made in the region.

### 2.3. Boreholes

In the study area, three boreholes were drilled by the Çankırı Provincial Directorate of Disaster and Emergency (AFAD) [6]. By examining the drilling logs obtained from these boreholes, information about the soil properties of the study area was obtained.

### 2.4. Sampling from research pits and point load test

Since the study area consists of gypsum-bearing units and the gypsum is extremely fragile and soluble, two research pits were opened in the region to collect samples with minimum damage. The strength values were obtained by applying the point load test on the samples obtained. The point load index is used to classify the rocks according to their strengths [11].

### 2.5. Measurement of discontinuities observed in gypsum-bearing units

As a result of on-site investigations in the study area, some discontinuities were observed in gypsum units. The discontinuities measured with the help of a tape measure have occurred as a result of the surface waters dissolving and deforming the gypsum layers. The dimensions of the measured discontinuities were classified according to ISRM (2007) [5].

### 2.6. Geological Properties

Lithological, tectonic and volcanic characteristics of the ground, as well as the groundwater and flow direction, have a great impact on the formation of sinkholes. Here, the effect of lithology is relatively greater. The limestone, gypsum, dolomite and rock salt, which are soluble rocks, are the lithological elements where the karstification is most common.

The region in which the study area is located contains gypsum series belonging to the Bozkır formation [1]. Determining that the dominant rock type in the region is gypsum will be useful in determining the causes of environmental problems in the formation of sinkholes and gradual ground settlements etc. There are also occasional landslides caused by the dissolutions in the gypsum series in the Bozkır formation [7].

## 3. Results and Discussion

### 3.1. Evaluation of sinkhole observations in the study area

Until today, total of 8 sinkholes have occurred in the study area. The years in which these sinkholes were formed were examined before and after 1953 [4 and references therein]. The oldest sinkhole has occurred before 1953 and the most recent sinkhole occurred in 2012 (Figure 3). The height of the sinkholes from sea level varies between 832 - 927 m. The diameters of the sinkholes vary between 1 - 44 m, and their depths vary between 1 - 22.5 m. Three types of sinkholes were observed in the study area. These are; collapse sinkhole, dropout sinkhole, and buried sinkhole [4–11].



**Figure 3.** The oldest and biggest sinkhole in study area.



The sinkhole formations in the study area, the year of formation, altitude information, diameter, depth and type of sinkhole are given in Table 1.

**Table 1.** Characteristics of the sinkholes in the study area [4].

Sinkhole No	Year of formation	Altitude (m)	Diameter(m)	Depth(m)	Sinkhole Type
1	Before 1953	877	-	-	Buried Sinkhole
2	Before 1953	882	44	22.5	Collapse Sinkhole
3	Before 1953	881	5	-	Buried Sinkhole
4	Before 1953	886	12	-	Buried Sinkhole
5	Before 1953	916	7	-	Buried Sinkhole
6	1953-1971	927	13.5	-	Buried Sinkhole
7	1990-2008	832	1	1	Dropout Sinkhole
8	2012	898	13	10	Dropout Sinkhole

### 3.2. Evaluation of structural damages

Within the scope of field studies, the damages of the buildings in the settlement were examined on site [4,6,11]. According to the information received from both the local people and the official institutions of the province, the most recent sinkhole formation occurred in 2012 [4,6,11]. Especially after the formation of the last sinkhole, the damage observed in the structures and the anxiety of the local people have increased (Figure 4).



**Figure 4.** (a) Gypsum levels and buildings from study area; (b,c,d) Images of damaged buildings from the study area [11].

A damage assessment study was carried out in the study area [4,6]. The buildings within the area were evaluated in 4 categories [4]. These 4 categories are that; heavily damaged buildings, slightly damaged buildings, undamaged buildings and represent relatively new residences [4]. However, the studies were indicating that most buildings are damaged [4,6,11].

### 3.3. Evaluation of data from boreholes

Three boreholes were drilled in and around the settlement area [6]. From three boreholes as SK-1, SK-2 and SK-3, the "molten gypsum" units in places were observed in SK-1 and SK-2. These dissolved gypsums encountered near the surface indicate that the ground is affected by surface waters [4,6]. The drilling SK-3 was made in a relatively safe area and was observed that there was no gap. The findings obtained from the studies

indicate that dissolved gypsum layers can be found in other parts of the ground and explain the reason for the gradual soil settlements [4,6,11].

### 3.4 Evaluation of the samples taken from the research pits and the results of the point load test performed

In this study, in addition to our observations on AFAD boreholes, two research pits were dug to take samples [11]. The point load strength index was calculated on the samples taken from this research pit.



**Figure 5.** (a) A view from the exploration pit opening. (b) A view from Research Pit-1. (c) A view from Research Pit-2. (d) An image of the altered gypsum sample, which disperses even in hand [11].

**Table 2.** Point load test samples and parameters [11].

SampleName	D(cm)	W(cm)	A=W*D(cm <sup>2</sup> )	De <sup>2</sup> =4A/π (cm <sup>2</sup> )	F=(De/50) <sup>0,45</sup>	P (kgf)
1	4.11	5.38	22.1	28.17	1.03	65
2	4.28	6.11	26.2	33.31	1.07	75
3	3.11	5.98	18.6	23.69	0.99	86
4	3.55	6.24	22.2	28.22	1.03	105
5	4.17	6.36	26.5	33.78	1.07	115.5
6	3.91	5.22	20.4	26.00	1.01	72.5
7	4.03	6.19	24.9	31.78	1.06	82.5
8	5.28	7.33	38.7	49.30	1.17	69.5
9	5.11	6.80	34.7	44.26	1.14	76.8
10	3.99	6.11	24.4	31.06	1.05	81.5

In the point load test, firstly, the uncorrected point load strength value ( $I_s$ ) is found by Equation (1) using the force ( $P$ ) with which the specimen is defeated, the diameter of the specimen ( $D$ ) and the axial length ( $W$ ) of the specimen. However, in order to obtain a standard point load strength value, the correction is made according to the equivalent core diameter determined as 50 mm. It is expressed as the corrected point load strength value ( $I_{s50}$ ) and found with the help of the Equation (2).

$$I_s = P / De^2 \quad (1)$$

$$I_{s50} = F * I_s \quad (2)$$

In this test performed on 10 samples, the highest and lowest two strength values were ignored and the average of the remaining 6 strength values was taken (Table 3).

**Table 3.** Point load test results [11].

Pit name	Sample name	$I_{S50}$ (kPa)
A.Ç-1	1	232.45
A.Ç-1	2	235.51
A.Ç-1	3	351.70
A.Ç-1	4	374.97
A.Ç-2	5	358.76
A.Ç-2	6	275.87
A.Ç-2	7	268.71
A.Ç-2	8	161.06
A.Ç-2	9	193.48
A.Ç-2	10	270.23
Average		272.41

Since the average  $I_{S50}$  value found is less than 1 MPa, the rock class was determined as "very low strength" when a classification was made according to Table 4.

**Table 4.** Classification of rocks according to point load strength [2].

Rock Class	Point Load Strength ( $I_{S50}$ ) (MPa)
Very Low Strength	<1
Low Strength	1-2
Medium Strength	2-4
High Strength	4-8
Very High Strength	>8

### 3.5. Evaluation of discontinuities observed in gypsum units

During the examinations made in the study area, some discontinuities were observed in gypsum units (Figure 6) [11]. While these discontinuities are sometimes in large sizes, they can sometimes be observed in small fractures. In all probability, the discontinuities observed are indicative of weathering in the rock and at the same time it is the harbinger of the decrease in the strength of rock. These discontinuities can sometimes take the form of a cavity, sometimes horizontally and sometimes vertically. The aperture values of the discontinuities are classified as defined in ISRM (2007) (Table 5).

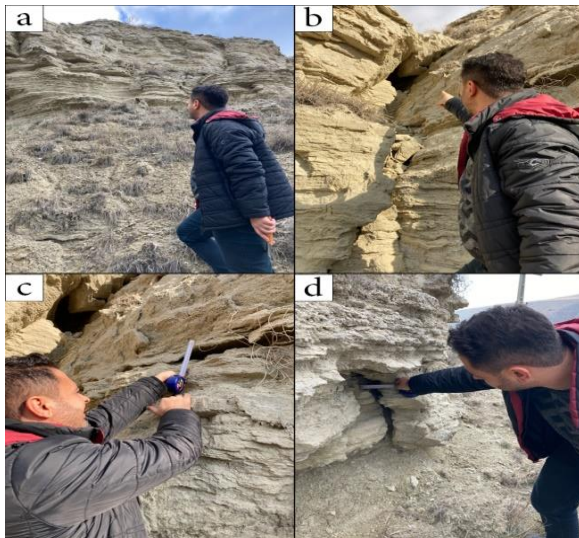


**Figure 6.** (a) A view of the gypsum units in the study area. (b) An image of cavity resulting from dissolution in the gypsum unit. (c) A view of the horizontal discontinuities occurring in the gypsum unit. (d) A view of the vertical discontinuities occurring in the gypsum unit [11].

**Table 5.** Aperture definition criteria for discontinuities [5].

Aperture (mm)	Definition	
<0,1	Very Tight	Close Structures
0,1 – 0,25	Tight	
0,25 – 0,5	Partly apertured	
0,5 – 2,5	Apertured	Apertured Structures
2,5-10	Medium Wide	
>10	Wide	
1-10	Very Wide	Open Structures
10-100	Extremely Wide	
>100	Open	

Classification of discontinuities occurring in gypsum in the region varies as "apertured structures" and "open structures" according to Table 5. Since the discontinuity in Figure 6b is considerably more than 100mm, it is possible to define it as "open". Since the horizontal discontinuity observed in Figure 6c is around 50mm and the vertical discontinuity observed in Figure 6d is around 80mm, it is possible to define it as "extremely wide" [11].

### Conclusion

In the study area, the sinkhole formations belonging to gypsum layers in the Bozkır Formation in the Inandık village (Çankırı) surroundings investigated. Previous studies have shown that the sinkholes that developed especially after 2012 caused heavy damage to the buildings in the village and therefore caused the village to be relocated [4–6]. Our study on the gypsum samples from the research pits showed that the results of the point load test were determined as "very low strength". Horizontal and vertical discontinuities are frequently observed within the gypsum levels. These are defined as "extremely wide" for discontinuities. It is inevitable that surface waters and/or groundwaters leaking from these discontinuities accelerate the formation of gypsum cavities.

### Acknowledgement

This study is derived from Mehmet Salih Yıldız's master thesis. We thank the Çankırı Provincial Directorate of Disaster and Emergency AFAD for the drilling data.

### References

- [1] Ateş, Ş., Özata, A., Gülmez, F. K., Osmañcelebioğlu, R., Mutlu, G., Özerk, O. C., Yeleser, L. ve Üstün, A. B. (2008). Geoscience data of Çankırı Province and urban areas (province-district centers). *MTA Report No: 11098 (unpublished)*, 220 p. Ankara.
- [2] Bieniawski, Z. T. (1975). The point load test in geotechnical practice. *Engineering Geology*, 9, 1-11.
- [3] Doğan, U. (2002). Subsidence Dolines Formed by Gypsum Karstification at The East of Çankırı. *G.U. Journal of Gazi Educational Faculty*, 22(1), 67-82.
- [4] Gökkaya, E. and Tunçel, E. (2019). Natural and human-induced subsidence due to gypsum dissolution: a case study from Inandık, Central Anatolia, Turkey. *Journal of Cave and Karst Studies*, 81(4), 221-232.
- [5] ISRM. (2007). The complete ISRM Suggested Methods for Rock Characterization, Testing and Monitoring: 1974-2006. *Suggested Methods Prepared by the Commission on Testing Methods, ISRM*, R. Ulusay and J.A. Hudson (eds.), Compilations Arranged by the ISRM Turkish National Group Ankara, Kozan offset; 628 p., Turkey.
- [6] Özçelik, A., Yiğit, A. E., Işık, B., Arıtürk, M. A., Özen, Ö. and Büyükurvaylı, B. (2016). Determination of karstic cavities and sinkholes by geophysical methods: Inandık Village Application, in Keskin, İ., and Göloğlu, C., eds., *Proceedings of International Symposium on Natural Hazards and Hazard Management*, 543-549.
- [7] Sarıfakıoğlu, E., Erin, B., Tırın, M., and Sezgin, İ.İ. (2021). Landslides caused by gypsum levels in Çankırı. *4. International Uni-DOKAP Symposium. Book of proceedings*, 98-113.
- [8] Şen, M. (2018). Use of unmanned aerial vehicle images for disaster management and Karapınar collapsed. Master thesis, Necmettin Erbakan University. 56 p., Konya.
- [9] URL. <https://www.cografyaci.gen.tr/turkiyede-karstik-sekiller/> Date of access: 20.07.2022.
- [10] Waltham A. C. and Fookes P. G. (2005). Engineering classification of karst ground conditions, *Speleogenesis and Evolution of Karst Aquifers*, 3, 1-20.
- [11] Yıldız, M. S. (2022). Investigation of Cankiri Inandık village sinkhole disasters in terms of soil characteristics. Master thesis. Cankiri Karatekin University. 71p., Çankırı.





## Regenerative Load Gain with Braking Systems in Elevators

***Hakan GÜMÜŞ<sup>1,\*</sup>***, ***Gözde GÜMÜŞ<sup>1</sup>***, ***Okan GÜMÜŞ<sup>1</sup>***

<sup>1</sup>*Institute of Science, Engineering Faculty, Electrical and Electronic Department, Çankırı Karatekin University, Çankırı, Türkiye*

### Abstract

The basic methods of measuring energy consumption and labeling efficiency in elevator systems are explained in ISO standards. With the guide published by the German Engineers Association in 2009, the annual energy consumption of existing and newly commissioned elevators can be calculated and compared. Thus, the elevator energy efficiency class and usage category can be determined. In addition, the ISO standard for measuring and evaluating the energy performance of elevators has been published. The VDI guide has been prepared in relation to the energy efficiency of elevators. The purpose of this guide is to evaluate and classify the energy consumption of elevators according to a standard criterion. This guide is mainly planned for the energy efficiency classification of newly installed passenger and freight elevators, and is also used for determining the energy efficiency of existing elevators, objectively examining the energy consumption values given by the manufacturers, and estimating their energy consumption. The "energy efficiency class of elevator systems", which is determined by the results obtained using the methods foreseen in the guide, is registered with a document by the notified body. Studies will be carried out within the scope of the standards specified in this master's thesis.

**Keywords:** Regenerative, ISO, Energy efficiency

### 1. Introduction

As it is known, all kinds of electronic devices, tools or machines that we use around the world work with electrical energy. Over time, as the area of use of electricity has increased, the need has arisen to reduce the cost of electricity, convert it or use it for different purposes.

The following are the achievements that we aim to achieve in accordance with these needs.

- Generating electricity through thermoelectric generators (TEG) from the friction energy generated from the mechanical braking mechanism of elevators.

- Storing the generated energy in the capacitors and allowing the engine to reuse it.

Studies have been carried out on converting the inert heat energy released in the conventional system into electrical energy with the regenerative braking system of elevators. [1] In contrast to the regenerative braking system, we aim to directly use the heat energy released in the mechanical braking mechanism of the elevator engine.

### 2. Materials and Methods

#### 2.1. Regenerative Braking Energy and Recovery

Before examining energy efficiency in elevators, it is necessary to examine the energy flow in a typical elevator drive system. Elevator motor can generate electrical energy or heat depending on some situations. These situations can be exemplified as the direction of movement of the motor or the load condition. The figure in 1 shows a typical energy flow in an elevator operating cycle. The area painted in gray represents the energy drawn from the grid during the motor phase.

---

\* Corresponding author: e-mail address: hhakangumus@gmail.com



The notched area represents the energy produced in the braking phase of the motor. Since diode rectifiers that do not allow free energy flow in both directions are used in conventional elevators, braking energy is consumed as heat in the braking resistor and there is a significant energy loss. In elevator drive systems where a fully controlled IGBT converter is used instead of a diode rectifier, it is possible to recover the regenerative braking energy to the grid.

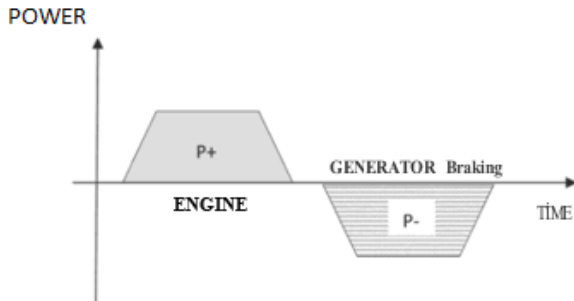


**Figure 1.** Engine and generator operating zones in the elevator operating cycle

The operating phases of the AC motor (motor, generator) are shown in the graph named 2.2 in the 4-zone coordinate plane. The regions where electrical energy is transferred to the motor as motion energy are called "motor operating zone". (Zones I and III) In these regions the power is positive. Zones 2 and 4, where the motion energy is transferred to the motor as electrical energy, are called the "generator or braking zone". This is due to the inertia of the load. In these regions, the charge is negative. In these cases, the energy released is consumed as heat energy on the brake resistor. In another possibility, it is fed back into the grid as electrical energy via the regenerative unit (AFE). Thanks to the regenerative units, II. and IV. Significant energy savings are achieved by reusing the braking energy generated in the regions. Thus, a positive contribution is made to the efficiency of the elevator. Energy work, motor operating phase (I. and III. regions) and generator operating phase (braking) (II. and III. regions) in elevator drivers are indicated in the figure named 1.2. There are two types of reverse energy work in the generator operating phase. The first is the consumption of braking energy as a heat ejection on the resistor. The second is the transmission of braking energy to the grid in the form of simple heat via the regenerative unit.

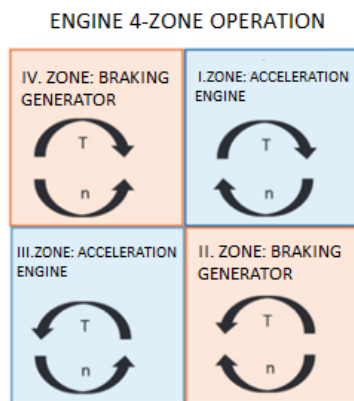
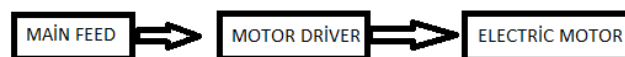


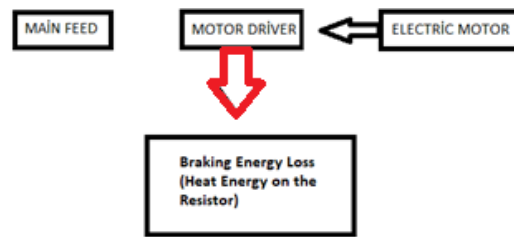
**Figure 2.** 4-Zone Operating Phases of AC Motor (T: Moment, n: Nominal Speed) [2]

## 2.2. Energy Flow in Elevator Command and Control Systems

Engine Working Phase (Zones I and III)



Generator Operating Phase (Zones II and IV) Energy Loss



Generator Operating Phase (Sections II and IV) Energy Recovery (Regenerative Solution)

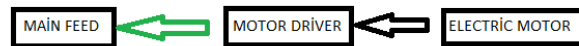
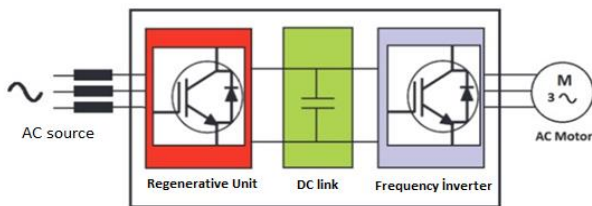


Figure 3 Energy flow in elevator drives; Engine running phase (zones I and III) and generator starting (braking) phase (zones II and IV). The reverse energy flow can be in two ways during the generator operation phase; (a) consumption of braking energy in the resistor, (b) push back to grid via regenerative unit. [3] Depending on the cabin load and the travel direction, the AC tWik unit works in two ways; engine or generator. In the motor stage, electrical energy is consumed by being drawn from the grid. In the motor braking phase, the regenerative braking energy generated feeds the DC source of the drive. In the bidirectional regenerative elevator driver design proposed in Figure 3, the regenerative unit (AFE, active-front-end) works as a rectifier in the motor phase, providing energy flow from the AC network to the motor. In the motor braking phase, it works as an inverter and provides the flow of regenerative braking energy produced in the motor from the DC source to the AC network.



**Figure 3.** Key Components of Elevator Drive System with Regenerative Unit (AFE) [4]

In Figure 3, a sketch block diagram of a proposed "ultra capacitive storage unit" supported drive design for regenerative braking energy recovery is given. In this design, the regenerative braking energy generated in the braking phase and loaded on the DC bus of the driver is stored in ultra-capacitive power storage units via a suitable DC/DC converter unit with bidirectional energy. If the energy is stored in ultra-capacitors, it can be reused in the motor phase of the elevator drive unit, making a positive contribution to the energy efficiency of the elevator. Thus, it will be more economical. Considering all these, the braking energy spent on the resistor as waste heat in traditional elevator control systems is reused in the motor phase and the energy is recycled.

### 2.3. Regenerative Brake Applications

Regenerative braking is used especially when drivers need to brake and slow down frequently. It is most beneficial to keep the high potential energy charge to a minimum at a constant rate. Motors that drive electric trains, elevators, cranes, and other loads employ regenerative braking to manage their speed. The engine cannot be stopped using regenerative braking.[5] This also applies to the change of operating mode from engine to production. The following equations contain useful braking calculations in detail. In the first of the equations below, the power transferred to the battery and supercapacitor connected in parallel as a result of useful braking is expressed as  $P_{b, in}$ . In order to calculate the expression  $P_{b, in}$ , the results of the second, third and fourth equations must be found first. The moment of inertia of the wheel group in the second equation, the aerodynamic drag resistance force in the third equation, and the rolling resistance force in the fourth equation are calculated.

$$P_{b,in} = n_{m/G} V \left[ n_t n_f \left( k f_b \left( F_{aero} + F_{rr} + \left( m_v + 4 \frac{1_w}{r_{r2}} \right) a_x \right) + 1_{driveline} \frac{N_{t2} N_{f2}}{r_{r2} a_x} \right) + I_{M/G} \frac{N_{t2} N_{f2}}{r_{r2} a_x} \right] \quad (1)$$

$$I_{w/t} = m_w r_w^2 + m_t r_t^2 \quad (2)$$

$$F_{aero} = \frac{1}{2} \rho C_D A V^2 \quad (3)$$

$$F_{rr} = [C_{rr,front} m_f + C_{rr,rear} (1 - m_f)] m_v g \cos \alpha \quad (4)$$

## 2.4. Conversion of Inert Heat Energy in Elevators

The biggest problem of our time is the rapid depletion of energy resources. As a solution to this problem, the use of renewable energy sources has been increased over time and energy saving methods are being sought in the vehicles used. One of these ways of saving is the recovery of inert energies released from the energy used. One of these inert energies, thermal energy, is currently used in thermoelectric generators recovery is possible through it. In this study, a double-shoe brake mechanism that allows elevators to slow down and stop when they arrive at the designated floor, we will consider the recovery of the released inert heat energy through TEG. As a result of our research on this problem, we found that energy conversion can be done using a regenerative braking system. In contrast to this study, we will provide the inert heat energy from the friction energy that occurs in the mechanical braking system. If we briefly refer to the regenerative braking system, then Before starting energy efficiency studies in elevators, it is necessary to study the energy flow in a typical elevator drive system. The elevator motor can either consume electrical energy (motor phase) or generate it (braking phase) depending on the direction of movement and load condition. [2] Since diode rectifiers that do not allow free energy flow in both directions are used in conventional elevators, braking energy is consumed as heat in the braking resistor and there is a significant energy loss. In elevator drive systems where a fully controlled IGBT converter is used instead of a diode rectifier, it is possible to recover the regenerative braking energy to the grid [2].

## 2.5. Mechanical Braking System

There are many systems used for braking in the elevator system. These systems have been described in detail in accordance with TS-EN 81-20 [4] and their standards have been established. In the scope of this study, the braking mechanism that we will touch on is the double-shoe engine brake, which allows the elevator to slow down and stop when it approaches the designated floor. The methods and tools to be used in this system are as follows. If we first study the brake mechanism, then there is a brake disc, which is connected by pads and drive connected to the engine. This system is activated some time in advance when the elevator needs to slow down and stop, and the pads approach the disk, which allows the engine to slow down and then stop. At this time, a heat generated by the friction force Dec the pad and the disc occurs. The copper plate Fr be made of Cu-ETP (electrolytic copper) alloy. Fr-ETP is a material with very high thermal and electrical conductivity in accordance with TS EN 13601 standards. Depending on the surface temperatures of the thermoelectric module, electricity generation is carried out in thermoelectric generators. As the temperature difference Dec the surfaces increases, the measured voltage values increase. 7.80V electrical energy is generated when the surface temperature of the thermoelectric module reaches 80°C. The power generated from the thermoelectric generator is set to 5W depending on the temperature difference [3].

## 3. Results and Discussion

In order to foresee to what extent the studies performed meet or may meet the expected results, calculations have been made with certain formulas. There are two important standards to follow when designing brakes. These;

1-  $F_{Fr} = (P + Q)$  of the braking force . 16 be (EN 81-1 Article F 3.3.3.1) and

2- The limit values of the braking acceleration are 0.2.based on g and 1 g, the average braking acceleration is

$$g_0 = 0.6 \cdot g \text{ is. [2]}$$

- Kinetic energy of the cabin, which is falling at v-speed:

$$E_K = m \frac{v^2}{2} \quad [4] \quad (1)$$

- Braking force:

$$F_{Fr} = F_N \cdot \mu \quad [4] \quad (2)$$

- The braking force in the cabin, which slides up to L distance under the influence of the braking force, is what it does:

$$E_{Fr} = F_N \cdot \mu \cdot L \quad (W) \quad [4] \quad (3)$$

$F_N$ : The normal force between the brake elements,

$\mu$ : Dec coefficient of friction between the elements and

L: This is the sliding distance of the cabin from the start of braking to the stop.

The coefficient of friction  $\mu$  is determined by experiments for the system to be used in the design. This value is usually around 0.2. Of course, it is worth noting that the rail is oily or dry that is changing. If the elevator cruising speed is v m/s, the initial speed that will require braking:

$$V_0 = 1,15 \cdot v \frac{m}{s} \quad [4] \quad (4)$$

Since kinetic energy will be absorbed by the braking work:

$$E_K = E_{Fr} \quad (5) \text{ so,}$$

$$\frac{m \cdot v_0^2}{2} = F_N \cdot \mu \cdot L \quad [4] \quad (6)$$

From these expressions, the normal force that should apply the brake element to the disk:

$$F_N = (P + Q) \cdot \frac{V^2}{2} \cdot \mu \cdot L \quad [4] \quad (7)$$

it will be obtained as follows. If the sliding distance of the cab during braking is L,

$$L = \frac{V_0^2}{2 \cdot a} \quad [4] \quad (8)$$

the braking acceleration in the expression  $a = 0.6$  it is found by taking g. As a result of these equations, we can calculate the work done by the friction force caused by braking by replacing the pads in the equations of normal force that they apply to the disc as a result of stretching the springs in a double-shoe braking system. With the work done, the thermal conductivity coefficient of the materials used in the linings can be multiplied and the heat energy can be calculated. The axial forces exerted by the lugs are selected according to the dimensions of the brake pulley in accordance with the double-lug brake assembly, the braking moment and the DIN 15435

standard attached to it.[5] Calculations are made according to the values taken according to the pulley dimensions contained in this catalog [5].

$$P_B = \frac{M_B}{d_B \cdot m_B} daN \quad [6] \quad (10)$$

Where  $d_B$  denotes the diameter of the brake pulley;  $m_B$  is also the coefficient of friction. According to the pairs of materials used, usually  $m_B = 0.3 \dots$  it is taken as 0.35. [6]

$b_0 \text{ cm}$  is the width of the shoe;

$l_0 \text{ cm}$  is length of the shoe

When the heat changes caused by the friction energy are measured and examined, it is assumed that the energy values obtained from the temperature differences that will be released as a result of braking will be as follows. The difference between the first temperature measured and the last temperature Dec;

The current that will be generated if it is:

-12 C is 38.5 A, 3.78 V and 145.53 mW [7]

If it is:

-14 C, then the current is expected to be 39 A, 3.9 V and 152.1 mW.[7]

It is foreseen that if the temperature difference increases, the current voltage and power values to be generated will also be increasing.

#### 4. Result and Discussion

The amount of heat energy varies depending on the determining parameters such as the material from which the pad is made, the braking distance, the amount of pressure exerted by the pad on the disc, and the number of friction Decays between the materials. By testing the brake system with experimental methods, it is possible to measure the heat energy released as a result of the friction caused by the brake disc. As a result, as a result of mathematical calculations and studies, it is possible to recover the heat energy generated from the double-shoe brake system. The resulting energy can be used for elevator lighting, intelligent control systems and engine power supply.

#### References

- [1] Altan D, Hamit G. Erhan O, Energy Efficiency And Efficiency In Elevators Recovery Of Regenerative Braking Energy. In: Elevator Symposium –İzmir; 2016.
- [2] Fatih C, Kadir Ç, Sliding Brakes and Design Problems in Elevators In: Uludag University, Department of Mechanical Engineering – Bursa;2018
- [3] Ramazan K, Metin K, Generation of Electricity by Thermoelectric Generator from Waste Heat of Photovoltaic Modules In: European Journal of Science and Technology No. 16, p. 310-324, İstanbul; August 2019
- [4] TS EN 81-20, Ekim 2014
- [5] Dr.C. Erdem İ., Dr İsmail G, Mechanical Brake Constructions
- [6] DIN 15435 standard
- [7] Yakup Y, Kubilay T, Experimental Study of Electricity Generation from Heating Radiators with a Thermoelectric Generator In: Bilge International Journal of Science and Technology Research



## Prevalence of Diarrhea due to *Clostridium difficile* A-B toxins in a University Hospital in Northern Cyprus

Ahmed NOURI ALSHARKSI<sup>1\*</sup>  Emrah GÜLER<sup>2</sup>, Kaya SÜER<sup>3</sup>

<sup>1</sup> Department of Biochemistry, Faculty of Medicine, Misurata University

<sup>2</sup> Department of Nutrition and Dietetics, Faculty of Health Sciences, Near East University, Nicosia, Northern Cyprus

<sup>3</sup> Department of Infectious Diseases and Clinical Microbiology, Faculty of Medicine, Near East University, Nicosia, Northern Cyprus

### Abstract

The high increase in diarrhea cases draws the attention of microbiologists to take the necessary precautions against the epidemic that occurs in some regions. It has been found each year that the mortality and morbidity rate of this infection explains about 500,000 cases in the United States. This retrospective study focuses on the investigation of the rate of *C. difficile* in a university hospital. *Clostridium difficile* toxin A / B results of patients admitted to the North Cyprus Near East University hospital between 2015-2018 were retrospectively extracted from the hospital registry system. A total of 230 patient data were used in the study. Data variables used included demographic information, department, inpatient or outpatient treatment. No significant difference was found in the age category in terms of *Clostridium difficile* toxin A / B positivity ( $p = 0.822$ ). The highest positive *C. difficile* toxin A / B ratio was found in 18.2% in the 20-44 age group, while it was 15.5% in the age group 45 and over. However, there was no statistically significant difference in the age group as the chi-square result gave  $p\text{-value} = 0.721$ . The distribution of this infection showed statistical significance between inpatients and outpatients with a  $p\text{-value}$  of 0.018. While 9.70% of positivity was detected in inpatients, it was 21.30% in outpatients. The high rate of *C. difficile* infection among outpatients is due to the unregulated guidelines in the use of antibiotics obtained from pharmaceutical stores. This study shows the inadequacy of rational use of antibiotics in practice, although the sale of antibiotics without prescription is prohibited in Northern Cyprus.

**Keywords:** Prevalence, *Clostridium difficile*, Northern Cyprus, A-B Toxins

### 1. Introduction

*Clostridium difficile* is a nosocomial pathogenic bacteria that releases proinflammatory cytotoxins namely Toxin A and B that cause the common known *C. difficile* infection (CDI). These toxins of *C. difficile* cause damage and inflammation in the colon mucosa. A clinical picture ranging from self-limiting mild diarrhea to severe pseudomembranous enterocolitis develops. Toxin A induces the production of neurokinins and cytokines which serve a pivotal role in the pathogenesis of *C. difficile* infections. Toxin B is usually targeted by the popularly approved FDA drug “Bezlotoxumab” which comprises IGHV5-51 and IGKV3-20 [1]. CDI is mostly considered a healthcare-associated nosocomial infection, but some studies outside of healthcare facilities are also noted in countries where outpatient antibiotic use is common. From studies, prevalence of toxigenic *C. difficile* varies among the Asian populations. In 2015, Cheng *et al.* [2] reported the prevalence of *C. difficile* to be 19.2% in China using PCR-based technique on stool culture, while Thailand has 9.2% [3]. In the UK, patients aged 65 and above are diagnosed for the presence of *C. difficile* associated diarrhea (CDAD) without suspecting any risk factor so as to lower its prevalence [4, 5]. Based on the current guideline, metronidazole hydrochloride has been recommended as a first line of defense for the treatment of severe CDI cases, but vancomycin was recently reported to be more effective than metronidazole [6]. Persistence rise of CDI is observed globally in developing countries due to lack of proper and early diagnostic measures. There is a scarce studies for the prevalence of *C. difficile* in Turkey and TRNC. Therefore, this study intends to investigate the prevalence of this infection in NEU hospital to start at a narrow view.

\* Corresponding author. e-mail address: ahmedalsherkas87@gmail.com

## 2. Materials and Methods

This retrospective study was conducted at Near East University Hospital, Turkish Republic of Northern Cyprus, TRNC. The study covers the period of 3 years (1<sup>st</sup> 2015-2018) with a total number of 230 samples obtained from the record unit of Near East University Hospital. Data was mainly for *C. difficile* related diarrhea. Both in-patients and out-patients were included in the study. In the experimental process, MiniVIDAS (Biomérieux) was used to test toxin A/B and as described by the manufacturer.

### 2.1. Statistical analysis

Statistical Package for the Social Sciences (SPSS) software version 20 was used to analyse variables. Continuous data such as gender and age, were analysed as percentage of total sample collected. Categorical data such as department were analysed using Chi-square test.

## 3. Results and Discussion

### 3.1. Demographic information of the patients

A total of 230 respondents from demographic and clinical tests of patient data were used for this research and it was found that male accounted for 47.00% and female with 53.00%. Patient ages result for those with less than 20 years accounted for 6.50%, between 20 to 44 years showed 43.00%, 45 to 64 years recorded 25.20% and greater than or equal to 65 years recorded also 25.20% respectively. The outcomes for the patient test result showed that those with positive were 16.10% and those with negative were 83.90% and lastly the category of admitting patients in the hospital revealed that in-patient were the least with 44.80% and out-patient have the highest with 55.20% (Table 1).

On gender basis, reveal 18(16.70%) of the male patients were positive and 90 (83.30%) tested negative. While in the female 19 (15.60%) tested positive and 103 (84.40%) tested negative. The chi-square statistic shows that the Gender categories are not statistically significantly different in terms of test outcome ( $\chi^2 = 0.051$ ,  $p = 0.822$ ). It can be inferred that gender does not have any significance association with the test result outcome. Furthermore, higher percentage was seen from the male patients compared to female patients. Subsequently from both the in-patient and out-patient result for *Clostridium difficile* A-B toxin showed that those tested negatives were higher than those tested positive. And the result from cross tabulation showed no statistically significant difference between genders versus test for *C. difficile* A-B toxin, and between age categories versus test for clostridium difficile A-B Toxin, but contrary patient admittance status was statistically significant.

On age group, the *Clostridium difficile* A-B toxin, positive *Clostridium difficile* A-B toxin and negative *Clostridium* A-B toxin showed that less than 20 years were 100.0%, 6.70% and 93.30% respectively. Age 20 to 44 showed 100.0%, 18.20% and 81.80%. Age 45 to 64 gave 100.0%, 15.50% 84.50% respectively and age greater or equal to 65 gave 100.0%, 15.50% and 84.50% respectively. Furthermore, for the ages of positive A-B toxin and negative A-B toxin showed that less than 20 years is represented with 6.70% and 93.30%. 20 to 44 years is represented with 18.20% and 81.80%. 45 to 64 years is represented with 15.50% and 84.50%. And lastly greater than or equal to 65 years represent with 15.50% and 84.50% respectively.

On hospitalization status, the result of admittance category of in-patient showed that, those tested positive *Clostridium difficile* A-B toxin were 9.70% and negative were 90.30% while for those out-patient that tested positive clostridium difficile A-B toxin gave 21.30% and for negative showed 78.70%. The Chi-square test result showed that patient admittance status was statistically significant. This means the condition of being admitted as an In-patient or as an Out-Patient have significance association with the test result outcome. The reported rise (20-28%) of CDI cases in Europe and North America are community associated infections [7]. Several interventions are needed to put in place in the case of CDAD outbreak; among few is the isolation of

affected patients to a particular section of the hospital or clinic, proper hygiene of wards and change/regulation of the given antibiotic. Among the major concern as a result of rise in the prevalence of this infection is the persistent rise in the use and misuse of many antibiotics. Previously, James et al., [8] investigated the incidence usage of antibiotics and infections that are related to health care in Northern Cyprus. The study found a statistical correlation between gender and duration of hospitalization with prevalence of health associated infections; with about 60% of inappropriate use of antibiotics. It is now necessary to investigate the prevalence of *C. difficile* toxin A-B in some parts of Northern Cyprus. This study is aimed at investigating the prevalence of *C. difficile* in Near East University Hospital.

**Table 1.** Demographic and Clinical test characteristics of the patients (n = 230).

Variables	N (%)
Gender	
Male	108(47.00%)
Female	122(53.00%)
Age	
<20 years	15(6.50%)
20-44 years	99(43.10%)
45-64 yeears	58(25.20%)
≥65 years	58(25.20%)
Test outcome	
Positive	37(16.10%)
Negative	193(83.90%)
Patient admittance category	
In-Patient	103(44.80%)
Out-Patient	127(55.20%)

Following the result of analysis, from table 1, it revealed that female patients' response was higher compared to male patients, while their ages category showed that 20 to 44 age groups recorded a higher percentage and less than 20 years accounted for the least percentage. 45 years and above seems to maintain constant prevalence of the infection. This study shows prevalence at lower age when compare to previous studies where high rate start at age greater than 65 [9]. Other previous studies also reported increase in severe *C. difficile* rate in children with bloody diarrhea [10, 11], while a study a recent study by Liao et al. [12] reported a high prevalence of 86.36% in hospitalized adults. Another recent study by Curcio et al [13] reported 15% prevalence from different regions which include developing Asia, Africa-Middle East, China and Latin America. The study is a systematic literature search from various search engines and database; and comprises both community and hospital related cases. However, in this study, patients with negative results were higher compared to those tested positive. Patients out of admission (out-patients) were higher to those patients that are on admission (in-patients). This may be due to strong and well standardized antibiotic policy adopted by the Near East University Hospital. On the other hand, Xiao et al. [14] suggest that increase in publicity awareness among both patients and clinicians should be given necessary attention so as to curb the spread of the infection.



Different units of the hospital show varying percentages of the infection with internal medicine unit recording the highest number of *Clostridium difficile* A-B toxins, but also show 75.70% of the recorded patients to be negative. Surprisingly, gastroenterology unit in our study recorded no positive result (100% negative). This is contrary to the study of Zhou et al [9] where gastroenterology department reported a prevalence of 70.4% among patients. Our study reported a prevalence of 16.10% *C. difficile* in our university hospital. This is higher than other reported studies [15]. The differences in incidence rate of *C. difficile* maybe due to technological advances and diagnostic expertise in different regions [5, 16] and also exposure to many levels of the known risk factors.

### 3.2. Distribution of toxin-positive and toxin-negative in different hospital units

Distribution of toxin-positive and toxin-negative strains in different hospital units shows internal medicine with the highest number of *C. difficile* A-B toxins, of which 27(24.30%) tested positive while 84(75.70%) tested negative. Gastroenterology unit with 30 patients is the second most dominant. But the results of gastroenterology, general surgery, oncology and orthopedics and traumatology units do not record any positive test while the only two patients found in the brain surgery unit tested all positive with no negative test result. While in total, 37(16.10%) of all the 230 patients considered in the study tested positive and 193(83.90%) tested negative (Table 2).

**Table 2.** Distribution of toxin-positive and toxin-negative strains in different hospital units

Units	No. of <i>C. difficile</i> A-B toxin (%)	No. of positive A-B toxin CD (%)	No. of negative A-B toxin CD (%)
Brain Surgery	2(0.90%)	2(100.00%)	0(0.00%)
Cardiology	7(3.00%)	2(28.60%)	5(71.40%)
Gastroenterology	30(13.00%)	0(0.00%)	30(100.00%)
General Surgery	2(0.90%)	0(0.00%)	2(100.00%)
Infectious Diseases	26(11.30%)	2(7.70%)	24(92.30%)
Internal Medicine	111(48.30%)	27(24.30%)	84(75.70%)
Intensive Care Unit	8(3.50%)	1(12.50%)	7(87.50%)
Laboratory	18(7.80%)	2(11.10%)	16(88.90%)
Pediatric	12(5.20%)	1(8.30%)	11(91.70%)
Oncology	12(5.20%)	0(0.00%)	12(100.00%)
Orthopedic and Traumatology	2(0.90%)	0(0.00%)	2(100.00%)
Total	230 (100.00%)	37(16.10%)	193(83.90%)

This study presents the prevalence of *C. difficile* in NEU Hospital and shows a rise in the rate from outpatients, which is due to the poor regulation in the use of antibiotics among outpatients. Other reasons may be transmission of the infection in the environment via contact and the diet consumed. This suggests the reverse of regulation on the use of antibiotics in TRNC as earlier done on 1st April 2016. There is also a need to take representative data from all or different hospitals within North Cyprus so as to obtain a larger population, as the results of this study are limited to that of the record unit of Near East University, TRNC.

## Acknowledgement

The author would like to thank all laboratory staff of the Near East University Hospital, TRNC.

## References

- [1] Orth, P., Xiao, L., Hernandez, L. D., Reichert, P., Sheth, P. R., Beaumont, M., ...& Racine, F. (2014). Mechanism of action and epitopes of Clostridium difficile toxin B-neutralizing antibody bezlotoxumab revealed by X-ray crystallography. *Journal of biological chemistry*, 289(26), 18008-18021.
- [2] Cheng, J. W., Xiao, M., Kudinha, T., Xu, Z. P., Sun, L. Y., Hou, X., ...& Xu, Y. C. (2015). The role of glutamate dehydrogenase (GDH) testing assay in the diagnosis of *Clostridium difficile* infections: a high sensitive screening test and an essential step in the proposed laboratory diagnosis workflow for developing countries like China. *PloS one*, 10(12), e0144604.
- [3] Putsathit, P., Maneerattanaporn, M., Piewngam, P., Kiratisin, P., & Riley, T. V. (2017). Prevalence and molecular epidemiology of Clostridium difficile infection in Thailand. *New microbes and new infections*, 15, 27-32.
- [4] Barbut, F., Delmée, M., Brazier, J. S., Petit, J. C., Poxton, I. R., Rupnik, M., & Kuipjer, E. (2003). A European survey of diagnostic methods and testing protocols for *Clostridium difficile*. *Clinical Microbiology and Infection*, 9(10), 989-996.
- [5] Planche, T., Aghaizu, A., Holliman, R., Riley, P., Poloniecki, J., Breathnach, A., & Krishna, S. (2008). Diagnosis of Clostridium difficile infection by toxin detection kits: a systematic review. *The Lancet infectious diseases*, 8(12), 777-784.
- [6] Stevens, V. W., Nelson, R. E., Schwab-Daugherty, E. M., Khader, K., Jones, M. M., Brown, K. A., ... & Goetz, M. B. (2017). Comparative effectiveness of vancomycin and metronidazole for the prevention of recurrence and death in patients with Clostridium difficile infection. *JAMA internal medicine*, 177(4), 546-553.
- [7] Kuijper, E. J., Coignard, B., Tüll, P., ESCMID Study Group for Clostridium difficile (ESGCD), & EU Member States and the European Centre for Disease Prevention and Control (ECDC). (2006). Emergence of Clostridium difficile-associated disease in North America and Europe. *Clinical microbiology and infection*, 12, 2-18.
- [8] Jame, W., Abdi, A. M., Süer, H. K., Çakir, N., & Basgut, B. (2018). Prevalence Study of Antibiotic Usage and Health Care Associated Infections in Northern Cyprus. *Journal of Pharmaceutical Research International*, 1-8.
- [9] Zhou, Y., Mao, L., Yu, J., Lin, Q., Luo, Y., Zhu, X., & Sun, Z. (2019). Epidemiology of *Clostridium difficile* infection in hospitalized adults and the first isolation of *C. difficile* PCR ribotype 027 in central China. *BMC infectious diseases*, 19(1), 232.
- [10] Karaaslan, A., Soysal, A., Yakut, N., Akkoç, G., Demir, S. O., Atıcı, S., ... & Bakır, M. (2016). Hospital acquired Clostridium difficile infection in pediatric wards: a retrospective case-control study. *Springerplus*, 5(1), 1329.
- [11] Schwartz, K. L., Darwish, I., Richardson, S. E., Mulvey, M. R., & Thampi, N. (2014). Severe clinical outcome is uncommon in *Clostridium difficile* infection in children: a retrospective cohort study. *BMC pediatrics*, 14(1), 28.
- [12] Liao, F., Li, W., Gu, W., Zhang, W., Liu, X., Fu, X., & Lu, J. (2018). A retrospective study of community-acquired Clostridium difficile infection in southwest China. *Scientific reports*, 8(1), 1-11.
- [13] Curcio, D., Cané, A., Fernández, F. A., & Correa, J. (2019). Clostridium difficile-associated diarrhea in developing countries: A systematic review and meta-analysis. *Infectious diseases and therapy*, 8(1), 87-103.
- [14] Xiao, Y., Liu, Y., & Qin, X. (2020). Comparative Study of Clostridium difficile Clinical Detection Methods in Patients with Diarrhoea. *Canadian Journal of Infectious Diseases and Medical Microbiology*, 2020.
- [15] Prattingerová, J., Sarvikivi, E., Ollgren, J., & Lyytikäinen, O. (2019). Increased hospital-specific nosocomial rates of Clostridium difficile infection in Finnish hospitals with high prevalence of imported cases at admission, 2008–2015. *Journal of Hospital Infection*, 102(2), 169-171.

- [16] Polage, C. R., Gyorke, C. E., Kennedy, M. A., Leslie, J. L., Chin, D. L., Wang, S., & Cohen, S. H. (2015). Overdiagnosis of *Clostridium difficile* infection in the molecular test era. *JAMA Internal Medicine*, 175(11), 1792-1801.



# Finite Element Solution of Contact Problem For The Functionally Graded Orthotropic Layer Resting On A Half Plane.

***Pembe Merve KARABULUT<sup>1,\*</sup>*** , ***İsa ÇÖMEZ<sup>2</sup>*** 

<sup>1</sup>Faculty of Engineering, Civil Engineering Department, <sup>1</sup>Cankiri Karatekin University, Çankırı, Turkey

<sup>2</sup>Faculty of Engineering, Civil Engineering Department, <sup>2</sup>Karadeniz Technical University, Trabzon, Turkey

## Abstract

In this study, the receding contact problem between a functionally graded orthotropic layer and a homogeneous half space is considered using finite element method. The functionally graded orthotropic layer pressed by two rectangular rigid stamps placed symmetrically. It is assumed that the contact surfaces are frictionless, only normal tractions can be transmitted through the contact areas. The finite element solution of the problem is constituted using ANSYS software. The main objective of this paper is the study the effect of inhomogeneity parameters and orthotropic material properties on the functionally graded orthotropic layer mismatch on the contact pressure and the size of the contact regions.

**Keywords:** Finite element method, Functionally Graded Material, Receding Contact, Mechanic

## 1. Introduction

Since the contact problems have possible application to a variety of structures of practical interest such as foundation grillages, pavements in roads and runways, railway ballasts and other structures consisting of layered media, there is large body of literature concerned with contact problems.

Chen et al. studied frictional contact problem of a rigid punch on an arbitrarily oriented gradient half-plane. [2] Receding contact problem for two-layer functionally graded media pressed by a rigid punch is investigated Çömez et al. [3]. Frictional receding contact problem for a graded bilayer system intended by a rigid punch and sliding frictional contact analysis of a monoclinic coating/isotropic substrate system investigated Yılmaz et al. [4]. Continuous and discontinuous contact problem of a functionally graded orthotropic layer lying on an isotropic layer bonded to a rigid substrate is solved Karabulut [6].

In the present study, we aimed to show effect of inhomogeneity parameters and orthotropic material properties on the functionally graded orthotropic layer mismatch on the contact pressure and the size of the contact regions. The finite element solution of the problem is constituted using ANSYS software. Finally the results obtained from FEM are verified by comparison of the analytical results for the special isotropic case in Karabulut et al. [7].

## 2. Definition of the Problem

In this paper receding contact problem between functionally graded orthotropic layer and homogeneous half space is considered. The layer pressed by two rectangular rigid stamps placed symmetrically. It is assumed that the contact surfaces are frictionless and only compressive traction can be transmitted through the contact surfaces. In addition, the effect of body forces is neglected.

As shown in Figure 1, the functionally graded orthotropic layer is subjected to concentrated loads by two rectangular rigid stamps placed symmetrically. The thickness of functionally graded layer is  $h$  and the stiffness of the layer changes exponentially from the bottom surfaces of the layer.

\* Corresponding author. e-mail address: pembemervekarabulut@karatekin.edu.tr

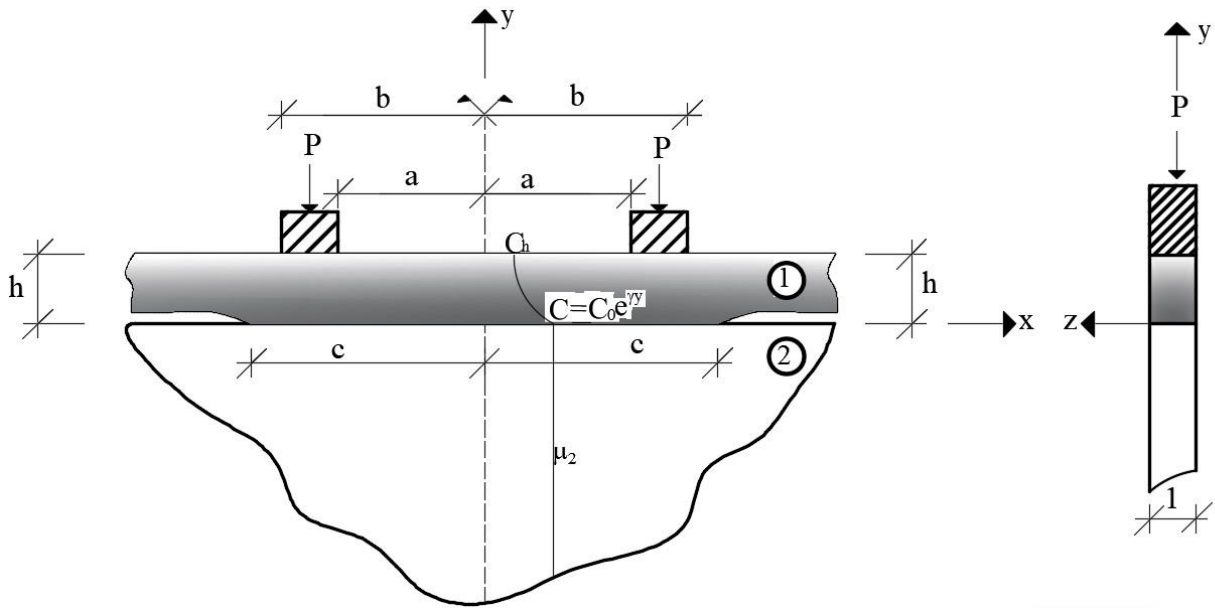


**Figure 1.** Geometry of the receding contact problem

### 3. The Finite Element Solution

The finite element method is a numerical method for solving problems of engineering and mathematical physics. In this method, problem divides into simpler parts that are called finite elements and the model transform into large system of equations. With the recent developments in computer technology, large system of equation is fulfilled.

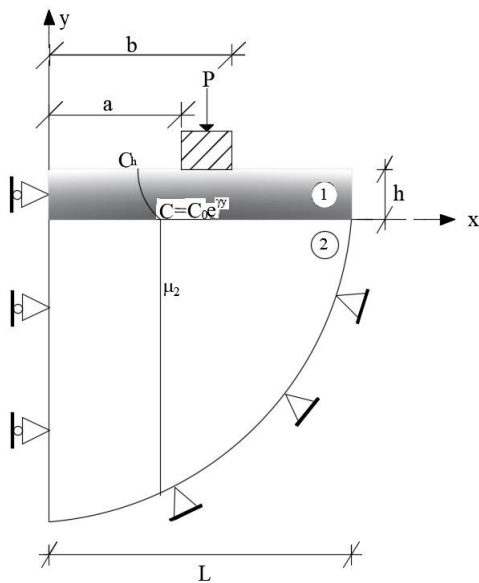


**Figure 2.** Geometry of the finite element model.

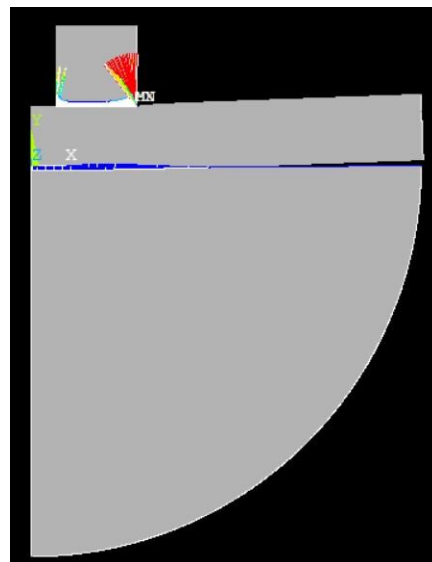


**Figure 3.** Deformed shape after the analysis.

In this paper, receding contact problem of functionally graded orthotropic layer resting on a half plane pressed by two rectangular rigid stamps is solved using the ANSYS package program. Because of the problem exhibits symmetry in geometry, material properties and geometry, only half of the problem is modeled. Geometry of the finite element model is shown in Figure 2. In the analysis, geometric properties are taken as  $L=6$  m (length of the layer in x direction) and  $h=1$  m (thickness of the layer in y direction). PLANE 183 structural element type is used finite element analysis of the problem. TARGET 169 and CONTACT 172 elements are used and SURFACE to

SURFACE contact model is created. Augmented Lagrange Method was used with SURFACE to SURFACE elements. After the analysis, contact lengths and contact pressures are obtained. In the finite element model (FEM), 1668625 nodes, 776827 elements and 2725 contact elements are used and the deformed shape after the analysis is given in Figure 3.

#### 4. Results and Discussion

**Table 1.** Orthotropic material properties (Binienda and Pindera, 1994)

Parameter Name	Material Name				
	A(Gr/Ep P75/934)	B(Tr/Ep T300/934)	C(GI/Ep)	D(Gr/Al)	E(B/Al)
E <sub>xx</sub> (GPa)	243.000	144.800	42.70	402.600	227.500
E <sub>yy</sub> (GPa)	7.200	10.300	11.70	24.100	137.900
E <sub>zz</sub> (GPa)	7.200	10.300	11.70	24.100	137.900
$\mu_{xy}$ (GPa)	3.929	5.515	8.238	16.750	55.150
$\mu_{xz}$ (GPa)	3.929	5.515	8.238	16.750	55.150
$\mu_{yz}$ (GPa)	2.406	3.447	3.778	8.340	49.240
$\nu_{xy}$	0.33	0.30	0.27	0.29	0.24
$\nu_{xz}$	0.33	0.30	0.27	0.29	0.24
$\nu_{yz}$	0.49	0.50	0.55	0.45	0.40

**Table 2.** Dimensionless contact lengths between the FG layer and homogeneous half-plane with different stiffness ratios and stiffness parameters. (Isotropic special case;  $E_{xx} = E_{yy} = E_{zz} = E$ ,  $\nu_{xy} = \nu_{yz} = \nu_{xz} = \nu = 0.25$ )

$\frac{\mu_0}{\mu_2}$		c/h			
		$\gamma = -1$	$\gamma = 0.001$	$\gamma = 1$	$\gamma = 2$
0.2	Analytical [7]	2.512500	2.511000	2.561000	2.665625
	<b>FEM</b>	<b>2.587500</b>	<b>2.587500</b>	<b>2.625000</b>	<b>2.700000</b>
	Difference(%)	2.98	3.00	2.50	1.28
0.4	Analytical [7]	2.568750	2.597200	2.684700	2.84500
	<b>FEM</b>	<b>2.660000</b>	<b>2.662500</b>	<b>2.737500</b>	<b>2.88250</b>
	Difference(%)	3.55	2.51	1.9	1.3
1	Analytical [7]	2.718750	2.809900	2.972400	3.203125
	<b>FEM</b>	<b>2.737500</b>	<b>2.850000</b>	<b>3.037500</b>	<b>3.187500</b>
	Difference(%)	0.7	1.42	2.19	0.48
2	Analytical [7]	2.912500	3.073900	3.315450	3.622656
	<b>FEM</b>	<b>2.909500</b>	<b>3.150000</b>	<b>3.300000</b>	<b>3.632500</b>
	Difference(%)	0.10	2.47	0.47	0.27
4	Analytical [7]	3.187500	3.433300	3.764550	4.168750
	<b>FEM</b>	<b>3.185000</b>	<b>3.450000</b>	<b>3.750000</b>	<b>4.125000</b>
	Difference(%)	0.08	0.486	0.386	1

In Table 2, dimensionless contact lengths between the FG layer and homogeneous half-plane with different stiffness ratios and stiffness parameters for the isotropic special case is given. As can be seen from the table, the half contact lengths between the functionally graded orthotropic layer and the half plane increase with the increasing  $\gamma$  stiffness parameter and stiffness ratio of the bottom surface of the layer to the half plane. It is also

seen that results obtained from the finite element approach are quite close from the analytical results from Karabulut et al. [7]

In Figure 4, variations of contact stress distributions under the stamp and between functionally graded orthotropic layer and a half plane for five different materials is shown. The greatest half contact length between the functionally graded orthotropic layer and the half plane is seen in the Material D with the highest modulus of elasticity in the x direction. The maximum value of the contact stresses under the stamps is observed in the Material C with the lowest stiffness values.

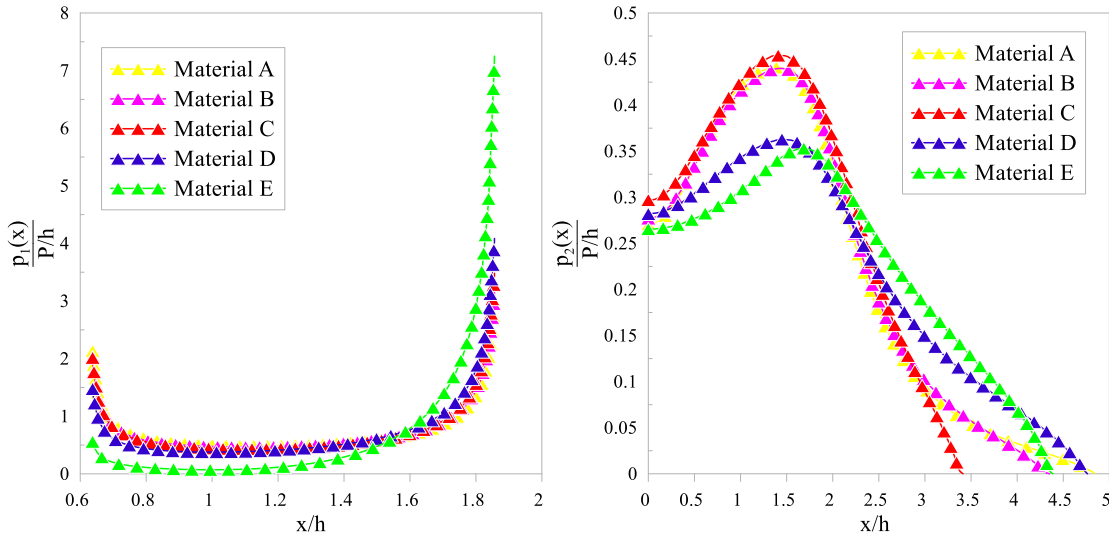


**Figure 4.** Variations of contact stress distributions under the stamp and between functionally graded orthotropic layer and half plane for five different materials ( $(b-a)/h=1.25$ ,  $(b+a)/(2h)=1.25$ ,  $\mu_2/(\mu_{xy})_A=2$ ,  $C_{top}/C_{bottom}=2$ ,  $\nu_2=0.25$ ,  $P/h=100$ ).

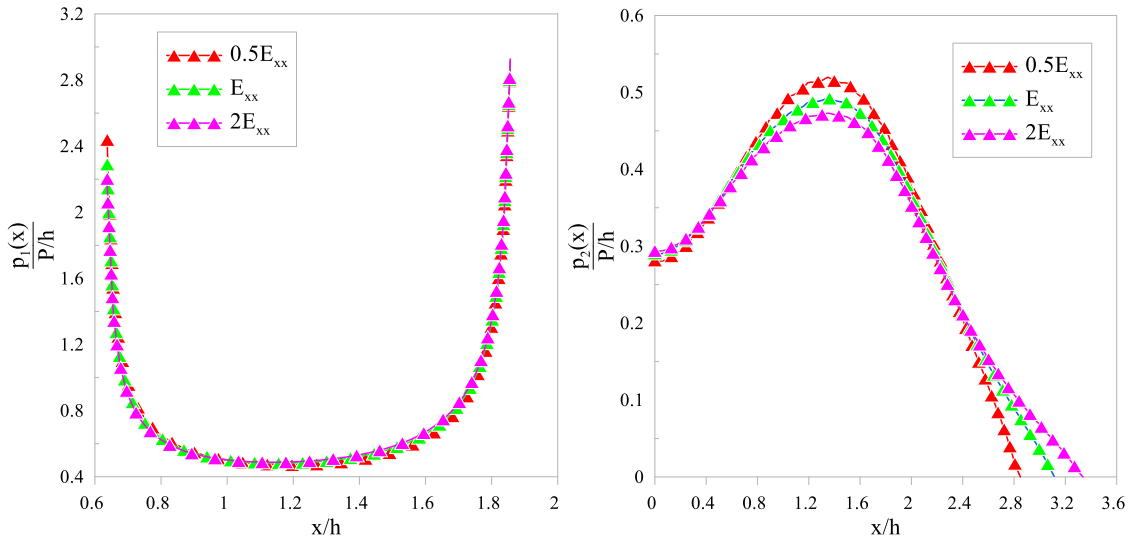


**Figure 5.** Variations of contact stress distributions under the stamp and between functionally graded orthotropic layer and half-plane by the  $E_{xx}$  ( $(b-a)/h=1.25$ ,  $(b+a)/(2h)=1.25$ ,  $\mu_2/C_{550}=2$ ,  $C_{top}/C_{bottom}=2$ ,  $\nu_2=0.25$ ,  $P/h=100$ , Material C).

Figures 5, 6 and 7 show the variation of the contact stresses under the stamps and between the functionally graded orthotropic layer and homogeneous half plane according to modulus of elasticity  $E_{xx}$ ,  $E_{yy}$  and  $E_{zz}$  respectively.

As can be seen from the figures, the half contact lengths between the layer and half plane increase with the increase of the  $E_{xx}$  (modulus of elasticity in the x direction). The variation of  $E_{yy}$  and  $E_{zz}$  (modulus of elasticity in the y and z directions) does not affect the half contact lengths between the layer and the half plane. In addition, the contact stresses under the stamps are not affected by the changes in the modulus of elasticity  $E_{xx}$ ,  $E_{yy}$  and  $E_{zz}$ .

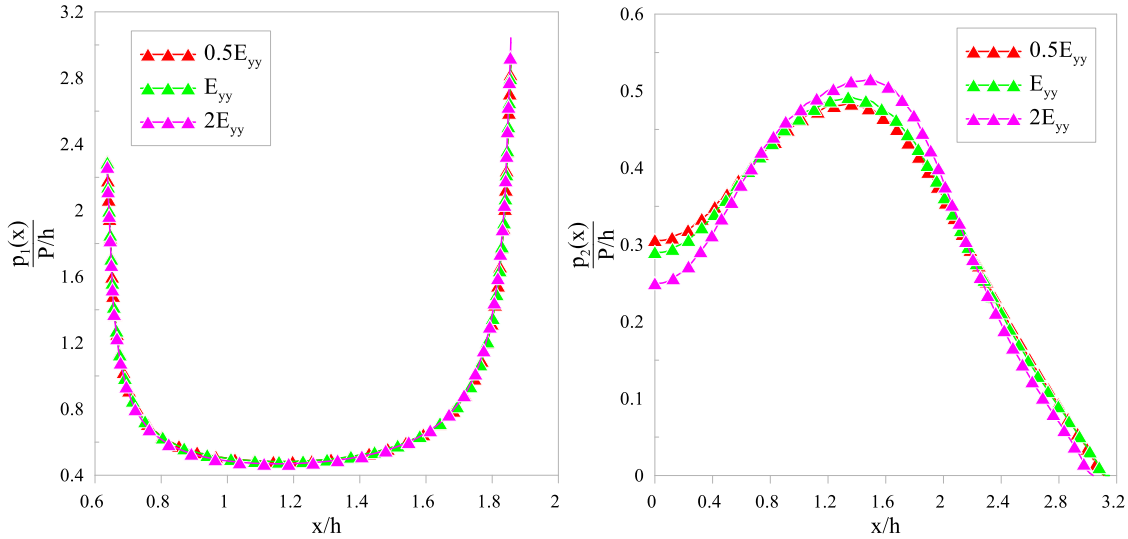


**Figure 6.** Variations of contact stress distributions under the stamp and between functionally graded orthotropic layer and half-plane by the  $E_{yy}$  ( $(b-a)/h=1.25$ ,  $(b+a)/(2h)=1.25$ ,  $\mu_2/C_{550}=2$ ,  $C_{top}/C_{bottom}=2$ ,  $\nu_2=0.25$ ,  $P/h=100$ , Material C).

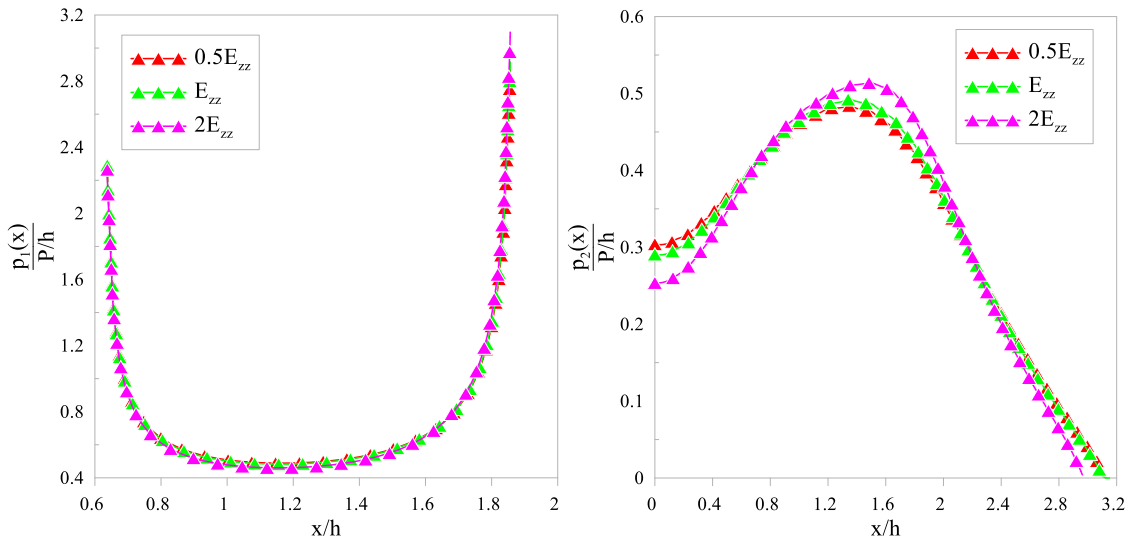


**Figure 7.** Variations of contact stress distributions under the stamp and between functionally graded orthotropic layer and half-plane by the  $E_{zz}$  ( $(b-a)/h=1.25$ ,  $(b+a)/(2h)=1.25$ ,  $\mu_2/C_{550}=2$ ,  $C_{top}/C_{bottom}=2$ ,  $\nu_2=0.25$ ,  $P/h=100$ , Material C).

Variations of contact stress distribution under the stamp and between the functionally graded orthotropic layer and half-plane by the different stamp distances from the y axis is shown in Figure 8. With the increasing stamp



distances from the y axis, the half contact lengths between the functionally graded orthotropic layer and half plane increase and the value of the contact stresses on the y axis decrease.

Finally, based of the comprasion of numerical values in the literature [7], difference with the finite element solution and the analytical solution is an acceptable range.

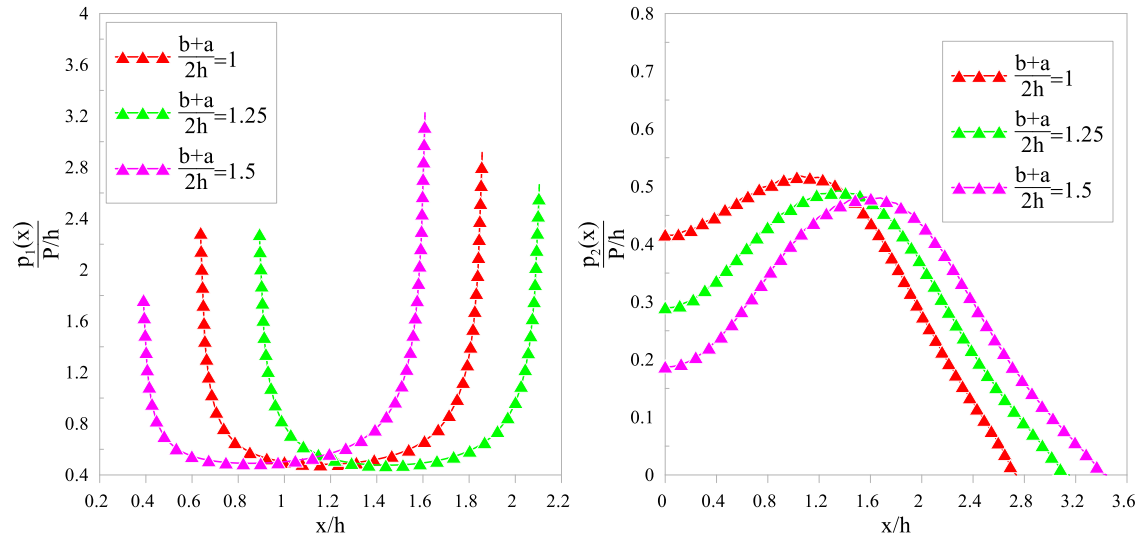


**Figure 8.** Variations of contact stress distributions under the stamp and between functionally graded orthotropic layer and half-plane by the different stamp distances  $((b+a)/(2h))$  from the symmetry axis  $((b-a)/h=1.25$  ,  $\mu_2 / C_{550} = 2$  ,  $C_{top} / C_{bottom} = 2$  ,  $\nu_2 = 0.25$  ,  $P/h = 100$  , Material C).

## References

- [1] Binidia, W. & Pindera, M., Frictionless contact of Layered Metal-Matrix and Polymer-matrix Composite Half-Planes, *Composite Science and Technology*, 50(1), 119-128.
- [2] Chen, P., Chen, S. & Peng, J., (2012), Frictional Contact of A Rigid Punch on An Arbitrarily Oriented Gradient Half-Plane, *Acta Mechanica*, 226, 4207-4221.
- [3] Çömez, İ., El-Borgi, S., Kahya, V. & Erdöl, R. (2016). Receding contact problem for two-layer functionally graded media intended by a rigid punch. *Acta Mechanica*, 227, 2493-2504.
- [4] Yilmaz, K. B., Çömez, İ., Guler M. A., Yildirim, B. & El-Borgi, S. (2018). Frictional receding contact problem for a graded bilayer system intended by a rigid punch. *International Journal of Mechanical Sciences*, 141, 127-142.
- [5] Yilmaz, K. B., Çömez, İ., Guler M. A. & Yildirim, B. (2019). Sliding frictional contact analysis of a monoclinic coating/isotropic substrate system. *Mechanics of Materials*, 137, 103132.
- [6] Karabulut P. M., Continuous and Discontinuous Contact Problem of A Functionally Graded Orthotrop Layer Lying On An Isotropic Layer Bonded to A Rigid Substrate, PD thesis, Karadeniz Technical University, Institute of Natural and Applied Sciences, 2021.
- [7] Karabulut P. M., Yaylacı, M., & Birinci, A., Fonksiyonel derecelendirilmiş tabaka ve yarım düzlem arasındaki sürtünmesiz ve ayrılmalı temas problemi, 20. Ulusal Mekanik Kongresi, Bursa, 2017, 196-204.



## Investigation of the Effects of Some Metals on Glutathione Reductase Activity Purified of from Rainbow Trout (*Oncorhynchus Mykiss*) Erythrocytes

**Ebru AKKEMİK<sup>1\*</sup>**, **Sevil KÖR<sup>2</sup>**, **Mehmet ÇİFTÇİ<sup>3</sup>**

<sup>1</sup>Faculty of Engineering, Food Engineering, Siirt University, Siirt, Türkiye

<sup>2</sup>Faculty of Medicine, Medical Biochemistry, Karadeniz Technical University, Trabzon, Türkiye

<sup>3</sup>Faculty of Veterinary, Basic Sciences, Bingöl University, Bingöl, Türkiye

### Abstract

The enzyme glutathione reductase (GR; \*E.C.1.6.4.2) was isolated from the erythrocytes of rainbow trout. GR enzyme was produced with a yield of 13.36 percent and a purification efficiency of 7135.2 EU/mg protein specific activity. SDS-PAGE was used to purity-check the enzyme after it had been purified. At a wavelength of 340 nm, enzyme activity was assessed spectrophotometrically using the Carlberg and Mannervik technique. All kinetic investigations and purification processes followed this technique. On the activity of the isolated enzyme, it was examined how certain metal ions ( $\text{Cu}^{2+}$ ,  $\text{Zn}^{2+}$ ,  $\text{Pb}^{2+}$ ,  $\text{Fe}^{2+}$ ,  $\text{Co}^{2+}$ ,  $\text{Mg}^{2+}$ ,  $\text{Cr}^{2+}$ , and  $\text{Al}^{3+}$ ) reacted *in vitro*. Metal ions that had an inhibitory impact have their  $\text{IC}_{50}$  values determined. To identify the kind of inhibition, Lineweaver-Burk plots were created, and the plot's  $K_i$  constants were extracted from it. The GR enzyme activity isolated from rainbow trout erythrocytes was found to be unaffected by  $\text{Al}^{3+}$  ion, whereas  $\text{Cr}^{2+}$  ion activates the enzyme.

**Keywords:** GR, Metal Ion, Inhibition, Erythrocyte

### 1. Introduction

Rainbow trout (*Oncorhynchus mykiss*), which belongs to the Salmonidae family, is a fish with high commercial value and consumption potential in the world and in our country, thanks to its taste and satiety among freshwater fish [1]. When these fish, which are consumed a lot due to their nutritive properties, are exposed to toxicity by xenobiotics, they engage their detoxification metabolism to tolerate it like all living organisms. However, sometimes the deficiency or inhibition of enzymes involved in detoxification metabolism disrupts the functioning of this system. Glutathione Reductase enzyme is required for the continuity of glutathione, which is the substrate of Glutathione S transferase, which is one of the phase II enzymes of detoxification metabolism [2]. In light of all these factors, we sought to investigate metals that are toxic to organzymes and induce bioaccumulation as well as to examine the harm these metals do to detoxification and metabolism from a new angle.

The glutathione reductase (GR) enzyme (EC 1.8.1.7) is a member of the disulfide oxidoreductase family that converts oxidized glutathione to its reduced form [3,4]. The mechanism by which the enzyme is catalyzed is schematic below (Figure 1).

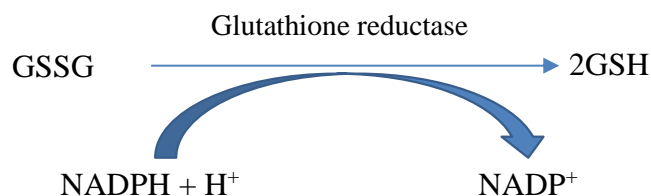


**Figure 1.** Catalysis mechanism of glutathione reductase enzyme [2]

\*Corresponding author. e-mail address: eakkemik@siirt.edu.tr

While GR converts oxidized glutathione to a reduced state, electrons from NADPH are not directly transferred to the disulfide bond of oxidized glutathione. They are first transferred to the tightly bound FAD, then transferred to oxidized glutathione by transfer to the disulfide bridge located between the two cysteines in the subunit [5-7]. This enzyme has been purified from numerous sources (fungi, spinach, wheat, corn, peas cyano bacteria, many mammalian tissues, characterized and amino acid sequence determined [3,6,8-13]. GR is a cytoplasmic and mitochondrial enzyme.

Because of the deleterious impacts of metals, water, an essential component of life, has an adverse impact on the universe. Since humans are at the top of the food chain, many metals over time accumulate in the environment, plants, and animals before reaching us. Depending on each metal's characteristics, different metals have different harmful effects [14-15]. In general, when heavy metals interact with organic substances, harmful consequences result. In order for biological molecules to carry out their duties, part of their qualities are lost, which leads to the death of the afflicted cells [14-15].

## **2. Materials and Methods**

### **2.1. Chemicals**

All compounds were analytical-grade and were bought from Sigma or Merck, Pharmacia.

### **2.2. Preparation of hemolysate**

Fish samples were taken from the Department of Aquaculture, Faculty of Agriculture, Atatürk University's rainbow trout farm. The caudal vein of the fish was taken for blood using a 10 mL plastic heparinized syringe (5 IU/mL). It was then put into tubes and centrifuged for 15 minutes at 3000 x g using a Hettich Micro 22 R refrigerator centrifuge. A drip was used to extract the plasma. The samples were centrifuged three times at a force of 3000 x g for 15 minutes to separate the supernatants after the package of red blood cells had been rinsed three times with KCl solution (0.16 M). The erythrocytes were centrifuged (+4°C, 13,000xg) for 30 minutes after being hemolyzed with 5 liters of ice-cold water. The precipitate was then thrown away. The supernatant was taken away [14].

### **2.3. Purification of glutathione reductase enzyme**

At 30-70 percent precipitation of ammonium sulfate, the enzyme was shown to precipitate [15]. The purification procedure was changed to fit the needs of our laboratory. The DEAE-Sephadex A50 anion exchange column (3 cm<sup>2</sup>x30 cm), was loaded with the enzyme solution. After the column had been cleaned with a buffer solution, elution was carried out using a linear gradient of 0-1.5 M KCl. At 340 nm, the eluted fractions were collected, and the enzyme activity was assessed. Enzyme-active tubes were joined. At 4°C, all purification processes were carried out. The affinity column was loaded with the previously obtained dialyzed enzyme solution, and the flow rate was set to 20 mL/h. A series of equilibrate buffer washes were performed on the column until the ultimate absorbance difference was 0.05. Elution solution was used to elute the enzyme at the end [15]. Final fractions were used to test the enzyme activity, and the tubes that had that activity were gathered. The temperature was maintained at +4°C during all processes [14, 15]. In the resulting solution, the protein was found with Bradford's technique [16]. To control enzyme purity was used by Laemmli's technique [17].

### **2.4. In vitro effects of metal ions**

The modified Carlberg and Mannervik technique was used to assess the glutathione reductase activity spectrophotometrically at 25°C [18,19]. Cu<sup>2+</sup> (0.01-0.2 mM), Zn<sup>2+</sup> (0.03-0.2 mM), Pb<sup>2+</sup> (0.1-0.55 mM), Fe<sup>2+</sup> (0.01-0.2 mM), Co<sup>2+</sup> (0.005-0.4 mM), and Mg<sup>2+</sup> (1.42-78.1 mM) were added to the reaction medium in order to study the effects of metal ions on trout erythrocyte GR. To get IC<sub>50</sub> values, plots of activity (percent) and metal ion concentration were employed. Lineweaver and Burk diagrams (1934) were produced using 1/V vs. 1/[S] observations, and the K<sub>i</sub> constant was calculated from these graphs [20].

### 3. Results and Discussion

Purification of glutathione reductase enzyme from rainbow trout erythrocytes was performed in four steps. By using two chromatographic techniques one after the other, GR enzyme was obtained with 7135.2 fold and 13.36% yield (Table 1). Ulusu and Tandoğan, using a method similar to our study, stated that they purified GR enzyme from bovine liver [21]. When the results were compared, rainbow trout erythrocyte GR was obtained with a higher purification coefficient. However, the yield is less. Tekman et al. purified GR enzyme from rainbow trout liver [15]. According to our study, it was purified with a lower purification coefficient.

**Table 1.** Purification steps of glutathione reductase enzyme

Purification stages	Total Protein (mg)	Total activity (EU)	Specific activity (EU/mg)	%Yield	Purification Coefficient
Hemolysate	1290.3	2.208	0.0017	100	1
Ammonium Sulfate Precipitation	299.28	0.384	0.0013	21.7	0.76
DEAE-Anion Exchange	13.248	1.62	0.122	73.36	71.76
2'5' ADP-Sepharose 4B	0.0243	0.295	12.13	13.36	7135.2

Inhibition type and  $K_i$  constants was determined as  $\text{Cu}^{2+}$   $0.008533 \pm 0.0031$  mM,  $\text{Fe}^{2+}$   $0.12800 \pm 0.03900$  mM,  $\text{Co}^{2+}$   $0.140333 \pm 0.0040$  mM,  $\text{Pb}^{2+}$   $0.154333 \pm 0.055$  mM,  $\text{Zn}^{2+}$   $0.049667 \pm 0.0055$  mM and  $\text{Mg}^{2+}$   $0.4993 \pm 0.071$  mM from the obtained graph (Table 2). It was determined that  $\text{Al}^{3+}$  ion did not show an inhibitory effect on the GR enzyme activity purified from rainbow trout erythrocytes, while  $\text{Cr}^{2+}$  ion activates the enzyme.

**Table 2.** Inhibitory effect of metal ions showing on glutathione reductase enzyme activity

Inhibitor	$K_i$ (mM)	Total activity (EU/mL)
$\text{Cu}^{2+}$	$0.008533 \pm 0.0031$	Uncompetitive
$\text{Fe}^{2+}$	$0.128 \pm 0.039$	Competitive
$\text{Co}^{2+}$	$0.140333 \pm 0.004$	Uncompetitive
$\text{Pb}^{2+}$	$0.15433 \pm 0.055$	Uncompetitive
$\text{Zn}^{2+}$	$0.049667 \pm 0.0055$	Competitive
$\text{Mg}^{2+}$	$0.498333 \pm 0.071$	Competitive

It has been reported that  $\text{Hg}^{2+}$ ,  $\text{Fe}^{3+}$ ,  $\text{Cd}^{2+}$ ,  $\text{Cu}^{2+}$ ,  $\text{Pb}^{2+}$ , and  $\text{Al}^{3+}$  ions have an inhibitory effect on GR activity purified from rainbow trout liver in vitro conditions [15]. The inhibitory effect of  $\text{Cu}^{2+}$ ,  $\text{Fe}^{3+}$ ,  $\text{Hg}^{2+}$ ,  $\text{Cd}^{2+}$ ,  $\text{Pb}^{2+}$ , and  $\text{Al}^{3+}$  metal ions on the activity of the enzyme glutathione reductase purified from human erythrocytes has been reported [14]. Although it was stated that it inhibited  $\text{Al}^{3+}$  in both studies, it did not show an inhibitory effect in our study. This is proof that the enzyme structure and its response to inhibitors differ from living thing to living thing and even from tissue to tissue. This is thought to be due to post-translational modifications.

The information gathered for this study was crucial in shedding light on the detrimental impact of metal ions in water and soil due to growing industry on the detoxification processes in living things. It is also a strong indication that an enzyme's sensitivity to an inhibitor might differ depending on the organism or tissue.

### Acknowledgment

This study was financially supported by TUBITAK, project no. 111T040. All experimental work was performed in the research laboratory of Atatürk University. The authors would like to thank all the supporters for their valuable contributions.

## References

- [1] Karaca İ, Pulatsü S, (2003) The Effect of Rainbow Trout (*Oncorhynchus mykiss* Walbaum, 1792) Cage Culture on Benthic Macrofauna in Kesikköprü Dam Lake\*, *Turk J Vet Anim Sci* 27, 1141-1146.
- [2] Csiszár, J., Horváth, E., Bela, K., Gallé, Á. (2016). Glutathione-Related Enzyme System: Glutathione Reductase (GR), Glutathione Transferases (GSTs) and Glutathione Peroxidases (GPXs). In: Gupta, D., Palma, J., Corpas, F. (eds) Redox State as a Central Regulator of Plant-Cell Stress Responses. *Springer, Cham*. [https://doi.org/10.1007/978-3-319-44081-1\\_7](https://doi.org/10.1007/978-3-319-44081-1_7)
- [3] Carlberg I, Mannervik B., (1981). Purification and Characterization of Glutathione Reductase from Calf Liver. an Improved Procedure for Affinity Chromatography *Chemistry*. 213(1), 77-85.
- [4] Rendon J. L., Calcagno, M., Mendoza-Hernandez, G. Ondarza, R. N., (1986). Purification, Properties And Oligomeric Structure of Glutathione Reductase from The Cyanobacterium *Spirulina Maxima*. *Archives Of Biochemistry And Biophysics*. 248(1), 215-223.
- [5] Siegel, R.L.K., Arscott, L.D., Janas, A.S., Schirmer, R.H., Williams, C.H., (1998). Role of Active Site Tyrosine Residues in Catalysis by Human Glutathione Reductase. *Biochemistry*. 37, 13968-13977.
- [6] Patel M. P., Marcinkeviciene, J. Blanchard, J. S., (1998) Enterococcus faecalis glutathione reductase: Purification, characterization and expression under normal and hyperbaric O<sub>2</sub> conditions. *FEMS Microbiology Letters*, 166, 155-163.
- [7] Iribarne F., Paulino, M., Tapia, O., (2000). Hybrid-Transfer Transition Structure As a Possible Unifying Redox Step for Describing The Branched Mechanism Of Glutathione Reductase. *Molecular-Electronic Antecedents. Theoretical Chemistry Accounts*, 103, 451-462.
- [8] Le Trang, N., Bhargava, K. K. and Cerami, A., (1983) Purification of Glutathione Reductase from Gerbil Liver in Two Steps. *Analytical Biochemistry*. 133, 94-99.
- [9] Acan N.L. and Tezcan E.F., (1989). Sheep Brain Glutathione Reductase: Purification and General Properties. *FEBS Letter*, 250, 1, 72-74.
- [10] McCallum M. J. Barrett, J., (1995) Purification and Properties of Glutathione Reductase from the Cestode *Moniezia Expanse*. *Int. J. Biochem. Cell. Biol., Chromatography B*. 684, 77- 97.
- [11] Jiang F., Hellmans, U., Stroga, E., Bergman, B., Mannervik, B., (1995) Cloning, Sequencing and Regulation of the Glutathione Reductase Gene from The Cyanobacterium *Anabaena PCC 7120*. *The Journal of Biological Chemistry*, 270(39), 22882-22889.
- [12] Mullineaux P., Enard C., Hellens R. Creissen G., Characterization Of Glutathione Reductase Gene And Its Genetic Locus From Pea (*Pisum Sativum L.*). *Planta*, 200, 186-194, (1996).
- [13] Lamotte F., Vianey-Liuaud, N., Duviau, M. P., Kobrehel, K., Glutathione Reductase In Wheat Grain. 1. Isolation And Characterization. *J. Agric. Food Chem.* 48, 4978-4983, (2000)
- [14] Coban A, Senturk M, Ciftci M And Kufrevioglu Ö.İ (2007) Effects Of Some Metal Ions On Human Erythrocyte Glutathione Reductase: An In Vitro Study, *Protein & Peptide Letters*, 14, 1027-1030.
- [15] Tekman B, Ozdemir H, Senturk M, Ciftci M (2008) Purification And Characterization Of Glutathione Reductase From Rainbow Trout (*Oncorhynchus Mykiss*) Liver And Inhibition Effects Of Metal Ions On Enzyme Activity. *Comp Biochem Physiol C*. 148, 117-121.
- [16] Bradford M.M., (1976) A Rapid And Sensitive Method For The Quantitation Of Microgram Quantities Of Protein Utilizing The Principle Of Protein-Dye Binding. *Analytical Biochemistry*, 72, 248-254.
- [17] Laemmli D.K., (1970) Cleavage Of Structural Proteins During In Assembly Of The Heat Of Bacteriophage T4. *Nature, London*, 227-680.
- [18] Carlberg I, Mannervik B., (1981) Purification And Characterization Of Glutathione Reductase From Calf Liver. An Improved Procedure For Affinity Chromatography *Chemistry*. 213(1), 77-85.
- [19] Carlberg, C., Mannervik B., (1985) Glutathione Reductase Assays. *Methods In Enzymology*, . Academic Press, Orlando, FL. 113 Pp 484-495.
- [20] Lineweaver H., Burk, D., (1934). The Determination Of Enzyme Dissociation Constants. *J. Am. Chem. Soc.* 57, 685.
- [21] Ulusu N.N., Tandoğan, B., (2007) Purification And Kinetic Properties Of Glutathione Reductase From Bovine Liver. *Mol Cell Biochem*, 303, 45-51.



## In Vitro Effects of Some Drugs on Glutathione Reductase Enzyme Purified from Sheep Spleen Tissue

Çiğdem ÇOBAN<sup>1</sup>, Mehmet ÇİFTÇİ<sup>2\*</sup>

<sup>1</sup>Solhan Healty Services Vocational School/Medical Services and Techniques, Bingöl Üniversitesi, Türkiye

<sup>2</sup>Faculty of Veterinary, Basic Sciences, Bingöl Üniversitesi, Türkiye

### Abstract

In this study, the effects of dexametopfen, meloxicam, phenylamidol HCl and hyoscine-N-butylbromide drugs on the enzyme Glutathione reductase (EC 1.8.1.7; GR, Glutathione: NADP<sup>+</sup> oxidoreductase), which is purified from sheep spleen tissue and which is the most important enzyme of antioxidant metabolism, was investigated. Firstly, GR enzyme was purified from sheep spleen tissue by ammonium sulfate precipitation between 20-70% and 2', 5' ADP-Sepharose 4B gel affinity chromatography with 44.61% yield and 1476,6 fold. The purity of the enzyme was checked by the SDS-PAGE method. In the next step, the effects of dexametopfen, meloxicam, phenylamidol HCl and hyoscine-N-butylbromide on the enzyme activity were investigated. Activity%-[I] and Lineweaver-Burk graphs were drawn to find the IC<sub>50</sub> value and K<sub>i</sub> constant for hyoscine-N-butylbromide, which showed an inhibitory effect. The IC<sub>50</sub> value of the drug hyoscine-N-butylbromide was calculated as 31,36 mM. In addition, the K<sub>i</sub> constant of this drug was 21.21±4.2 mM and the inhibition type was determined non-competitive. It was determined that dexametopfen, meloxicam, and phenylamidol HCl drugs did not have a significant activation or inhibition effect on the enzyme.

**Keywords:** Glutathione reductase, buscopan, inhibition

### 1. Introduction

Glutathione reductase (E.C. 1.8.1.7; GR), called NADP<sup>+</sup> oxidoreductase, is a very important enzyme that functions in the intracellular defense system by catalyzing the conversion of oxidized glutathione (GSSG) to reduced glutathione (GSH) [1]. The GR enzyme keeps the GSH/GSSG ratio, which is vital for the cell, at a certain level. In studies, this ratio is approximately 500/1 for erythrocyte cells, and a decrease in this ratio causes hemolysis [2]. Since the GSH molecule contains a large amount of -SH group in its structure, it has a protective antioxidant effect especially against free radicals. Free radicals that arise due to some factors such as harmful habits such as smoking, alcohol, and adequate and unbalanced nutrition that disrupt the biochemical order in the cell, especially the superoxide radical, are broken down into water and oxygen by the -SH group of the GSH molecule. Thus, metabolic order is provided in the cell [3, 4].

In order for the GR enzyme to react, it needs nicotinamide adenine dinucleotide phosphate (NADPH), which is supplied from the pentose phosphate pathway and functions in reducing biosynthesis events. The production of NADPH is produced by the enzyme glucose 6-phosphate dehydrogenase (G6PD), the first enzyme of the pentose phosphate pathway, in the presence of nicotinamide adenine dinucleotide (NAD<sup>+</sup>). The G6PD enzyme is an enzyme that synthesizes ribose phosphates, which are components of vital biomolecules such as DNA, FAD, RNA, ATP, CoA and NAD, along with the production of NADPH. The need for NADPH in the reaction catalyzed by the GR enzyme also reveals the relationship between G6PD and GR. Therefore, the inactivity of the G6PD enzyme causes a decrease in NADPH production. This situation also negatively affects the GR enzyme, and as a result, the formation of GSH may also be negatively affected [5, 6]. As a result, the reaction in which GSSG is converted to GSH with the use of NADPH to protect the cell against various types of oxidative stress is catalyzed by GR [7].

Numerous inhibition studies have been carried out on enzymes that function at key points in cell metabolism, such as the GR enzyme. Inhibitors are defined as substances that reduce or completely eliminate the activity of the enzyme. Many drugs and chemicals used for human, animal and plant health perform their functions by affecting the activities of enzymes and proteins in metabolism [5, 6, 8]. The inhibition effect of these chemicals on regulatory enzymes at important points of metabolism may allow the elimination of a disorder in that region. From this point of view, enzymes constitute an important field in pharmacological studies [9]. It is known that

\* Corresponding author. e-mail address: mciftci@bingol.edu.tr



the GR enzyme has been purified from many living tissues, its kinetic properties have been determined, and the effects of many drugs and chemical substances on enzyme activity have been investigated so far [10-12]. However, in the literature review, studies investigating the effects of dexketoprofen, meloxicam, phenylramidol HCl and hyoscine-N-butylbromide drugs related to the sheep spleen GR enzyme were not found.

Among these drugs, dexketoprofen is a drug with analgesic, anti-inflammatory and antipyretic effects, included in the anti-inflammatory drug group. It is widely used in the symptomatic treatment of mild to moderate pain such as musculoskeletal pain, toothache, postoperative pain. In addition, it binds to the plasma membrane at high rates (95% 98%) and has analgesic, antipyretic and anti-inflammatory effects. Meloxicam is a member of the enolic group of non-steroidal anti-inflammatory drugs. It has strong analgesic, antipyretic and ant rheumatic activity. Phenylramidol HCl is used as a pain reliever and muscle relax. Hyoscine-N-butylbromide is an anticholinergic drug that has both spasm-relieving and pain-relieving effects, and also helps to relax the digestive system. It is effective in relieving sudden and severe spasms in the muscles of the stomach, intestines, urinary bladder, urinary tract and bile ducts [13]. In this study, it was aimed to examine the effects of these drugs on GR activity.

## 2. Materials and Methods

### 2.1. Materials

The drugs used in the study were obtained from the pharmacy. 2', 5'-ADP-Sepharose 4B, NADPH, electrophoresis chemicals, GSSG, hydrochloric acid, sodium chloride, glycine, Tris, electrophoresis chemicals, protein standards, ammonium sulfate and other chemicals were obtained from Sigma-Aldrich Com. (St. Louis, MO) and Merck (Darmstadt, Germany).

### 2.2. Preparation of Homogenate

The sheep spleen tissue used in this study was obtained from the Combined Meat and Milk Institution of Bingöl according to the cold chain rules. 15 grams of tissue brought to the laboratory was taken and divided into small pieces and suspended in 45 mL of 50 mM  $\text{KH}_2\text{PO}_4$  (pH= 8.0) buffer. After the obtained suspension was centrifuged for 1 hour at 10,000xg and the precipitate was discarded and homogenate was formed [8, 10].

### 2.3. Ammonium Sulphate Precipitation and Dialysis

For the homogenate obtained from sheep spleen tissue, partial precipitation was performed with ammonium sulfate salt, which has a highly soluble feature in water, at 20-70% saturation concentrations. The obtained salty homogenates were centrifuged at 10,000xg for 15 minutes each time and the supernatant part was removed. The remaining precipitate was treated until dissolved with 50 mM  $\text{KH}_2\text{PO}_4$  (pH= 8.0) buffer and activity control for the enzyme was performed. Then, the enzyme solution was placed in dialysis bags and dialyzed with dialysis buffer (10 mM K-phosphate, 1 mM EDTA) adjusted to pH= 7.5 for 2 hours [8, 10, 14].

### 2.4. Enzyme Purification by 2', 5' ADP Sepharose-4B Affinity Chromatography

2', 5' ADP Sepharose-4B affinity chromatography was used to purify the enzyme sample, which was partially purified by ammonium sulfate precipitation. First, an affinity column was prepared. For a bed volume of 10 mL; The 2', 5'-ADP sepharose 4B gel was weighed 2 g dry. Afterwards, this gel was washed several times with 400 mL of distilled water to remove solids from the gel, while the gel was swollen. The air caused by swelling was removed by vacuuming using a water trumpet and the gel was suspended by adding equilibration buffer (50 mM  $\text{KH}_2\text{PO}_4$ /1 mM EDTA, 1mM DTT, pH: 6.0). The prepared gel was packed into a cooled column and waited for the gel to precipitate. The equilibration of the column was understood from the approximate equalization of the absorbance and pH of the eluate and buffer at 280 nm. 16 mL enzyme sample was applied to the prepared column. Then the column was washed with three separate wash solutions. 25 mL of each of the prepared washing solutions was used in turn. The column was first washed with 0.1 M K-acetate/0.1 M K-phosphate (pH=6) buffer. Then 0.1 M K-phosphate/0.1 M KCl (pH=7.85) buffer was used for washing and finally washed with 50 mM  $\text{KH}_2\text{PO}_4$ /1 mM EDTA (pH= 7) buffer. The washing process was followed in the

spectrophotometer and the absorbance values were determined to be approximately equal to the blank. After washing, the enzyme was eluted with elution buffer (50 mM  $\text{KH}_2\text{PO}_4$ /1 mM EDTA, 1mM GSH and 0.5 mM NADPH (pH= 7.3) [8, 10, 15-17]. Elutions were taken into 1.5 mL Eppendorf tubes and their activity values were checked. The enzyme samples we obtained were checked for purity by SDS-PAGE method.

## 2.5. Enzyme Activity Measurement

The activity of glutathione reductase enzyme was measured spectrophotometrically at 340 nm. This situation was determined by the decreasing amount of NADPH due to the oxidation of NADPH in the presence of GSSG [17].

## 2.6. Protein Determination

Quantitative protein amount was determined spectrophotometrically at 595 nm according to the Bradford method. Bovine serum albumin protein was used to draw the standard graph [18].

## 2.7. Enzyme Purity Control with SDS-PAGE

Purity control of the enzyme was carried out using 3-8% batch sodium dodecyl sulfate polyacrylamide gel electrophoresis (SDS-PAGE) according to the Laemmli method [19].

## 2.7. Kinetic Studies

The effects of deksketoprofen, meloxicam, phenylamidol HCl and hyoscine-N-butylbromide on enzyme activity were investigated in kinetic studies. Different concentrations of these drugs were taken and added to the cuvette medium. As a result of the activity measurements, experiments were made up to the highest possible inhibitor concentration, and the  $\text{IC}_{50}$  value was calculated by plotting the % Activity-[I] graph for hyoscine-N-butylbromide, which showed an inhibitory effect. In addition, in order to determine the  $K_i$  constant and inhibition type of this drug, preliminary experiments were carried out and five different substrate concentrations were determined, and measurements were made for each substrate concentration with three different inhibitor concentrations and Lineweaver-Burk plots were drawn [20].

# 3. Results and Discussion

## 3.1. Enzyme Purification

In this study, homogenate, ammonium sulfate precipitate and pure enzyme were purified 1476.6 times with a protein specific activity of 15.80 EU/mg and a yield of 44.61% from the standard graph used for the quantitative determination of proteins by Bradford method, and the results are shown in Table 1.

**Table 1.** Sheep spleen tissue GR enzyme purification steps

Purification steps	Total volume (mL)	Activity (EU/mL)	Protein (mg/mL)	Total protein (mg)	Total activity	Specific activity (EU/mg protein)	Yield %	Purification fold
Homogenate	25	0,581	52,59	1315	14,525	0,0110	100	1
Ammonium sulfate precipitation (20-70%)	16	0,697	64,57	1033	11,152	0,0107	76,78	0,972
2',5'-ADP Sepharose-4B affinity chromatography	10	0,648	0,041	0,41	6,48	15,80	44,61	1476,6



### 3.2. SDS-PAGE

SDS-PAGE was performed to determine the enzyme purity. The single band obtained on the gel is shown in Figure 1.

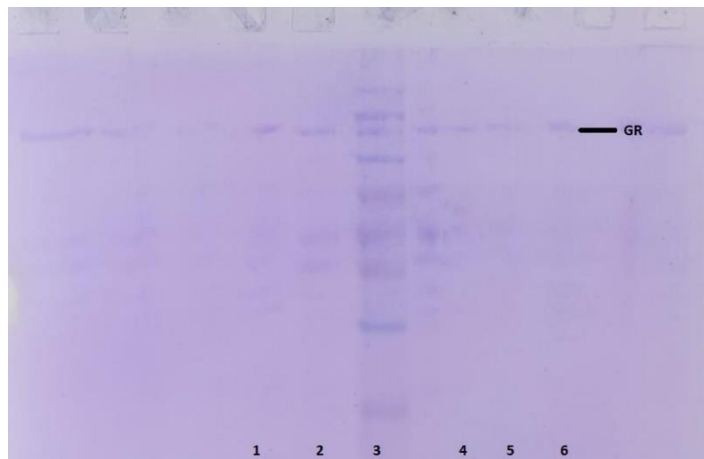


**Figure 1.** Lanes 4,5 and 6: Pure GR enzyme eluted from the affinity column. Lane 3: standard proteins (14kDa - 175 kDa).

### 3.3. Kinetic Studies

In kinetic studies, the effects of deksketoprofen, meloxicam, phenyramidol HCl and hyoscine-N-butylbromide drugs on GR enzyme activity at different concentrations were investigated. Among these drugs, deksketoprofen at 0.33, 0.66, 1.32, 1.98 and 2.64 mM concentrations, meloxicam at 0.028, 0.056 and 0.084 mM concentrations, phenyramidol HCl at 0.93, 1.86 and 2.79 mM concentrations and hyoscine-N-butylbromide concentrations of 0.227, 1.362, 2.27, 4.54, 9.08, 18.16, 24.97, 26.33, and 27.24 mM were used. The % Activity-[I] graph was drawn for hyoscine-N-butylbromide, which showed an inhibitory effect, and the  $IC_{50}$  value was calculated as 23.79 mM using the graph equation (Figure 2). In addition, Linevawer-Burk plot was drawn for the GR enzyme at 3 different inhibitors and 5 different substrate concentrations, and the  $K_i$  constant was determined as  $21.21 \pm 4.2$  mM and the inhibition type was non-competitive (Figure 3). It was determined that deksketoprofen, meloxicam and phenyramidol HCl drugs did not have a significant activation or inhibition effect on the enzyme.

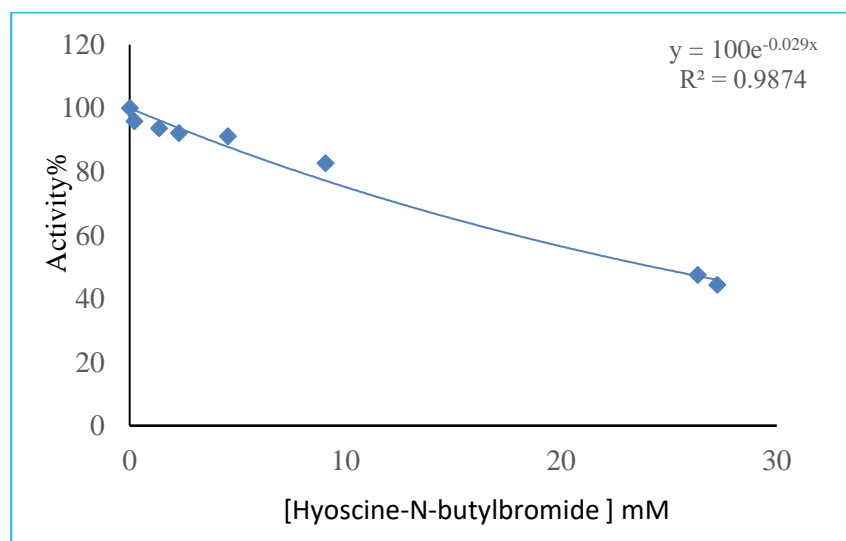


**Figure 2.** Effect of hyoscine-N-butylbromide on sheep spleen GR enzyme

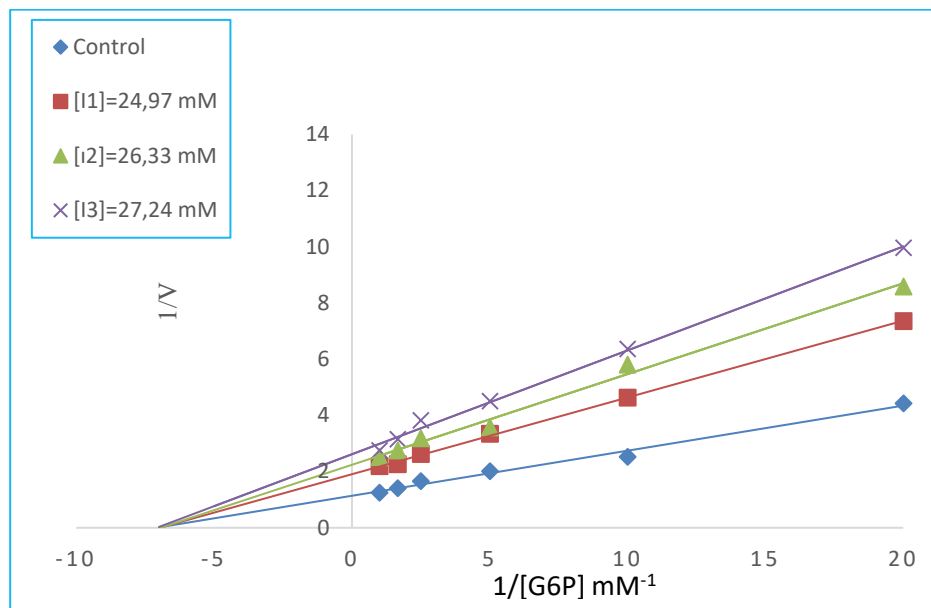


**Figure 3.** Lineweaver-Burk plot plotted for sheep spleen GR enzyme at 5 different substrates and 3 different hyoscine-N-butylbromide concentrations.

### 3.4. Discussion

The GR enzyme, which is involved in the intracellular defense system, belongs to the oxidoreductase enzyme group and catalyzes the conversion of GSSG to GSH. It is very important to keep the GSH/GSSG ratio at a certain level in metabolism. For example, this ratio is 500/1 in erythrocytes, and a decrease in this value leads to hemolysis [2]. In a study on antioxidants, the enzymes of antioxidant systems such as GR and G6PD decreased as a result of exposure of erythrocytes to oxidative stress for various reasons. The increase in malondialdehyde (MDA), an indicator of lipid peroxidation, determined this situation [21]. Radicals formed as a result of oxidative stress in the cell are eliminated by the regeneration and increase of the GSH molecule, which is the most important antioxidant system, and intracellular stress tolerance is provided [22].

In this study, the effects of deksketoprofen, meloxicam, phenylamidol HCl and hyoscine-N-butylbromide drugs on the enzyme were investigated by purifying the GR enzyme from sheep spleen tissue. In the purification of the enzyme, 20-70% ammonium sulfate precipitation was made in the homogenate prepared first [10]. Ammonium sulfate precipitation is important in terms of removing impurities from the enzyme sample and thus making the proteins more concentrated [23]. The enzyme sample obtained from the ammonium sulfate precipitation was applied to the 2', 5'-ADP Sepharose 4B affinity column and the enzyme with a specific activity of 15.80 EU/mg.protein was purified 1476.6-fold with a yield of 44.61%. In another purification performed on the sheep spleen GR enzyme, the enzyme was purified with a yield of 40.61% and 1564.8 times [10]. In addition, in another study, GR enzyme was purified 1654 times from rainbow trout liver with 2', 5'-ADP Sepharose-4B affinity chromatography with 41% yield [24]. In another study, GR enzyme was purified 1028 times from quail erythrocytes with 46.2% yield [12].

In the second phase of our study, the effects of deksketoprofen, meloxicam, phenylamidol HCl and hyoscine-N-butylbromide drugs, which are widely used in human and animal health, on the enzyme were investigated. When the study results were analyzed, it was observed that deksketoprofen, meloxicam and phenylamidol HCl did not have any activation or inhibition effects on enzyme activity. Hyoscine-N-butylbromide on the other hand, was found to have an inhibitory effect on the enzyme with an  $IC_{50}$  value of 23.79 mM. In addition, the  $K_i$  constant and inhibition type were determined in the 5 most suitable substrates, which were determined by the preliminary experiments, of this drug, which showed an inhibitory effect, first in the medium without inhibitor,

and then at 3 different fixed drug concentrations. According to this;  $K_i$  constant was  $21.21 \pm 4.2$  mM, inhibition type was determined without non-competition.

In the literature research, the GR enzyme was characterized by being purified from different tissues with the help of different chromatographic techniques, and it was determined that the effects of some drugs and organic compounds on the enzyme activity were investigated. In an inhibition study conducted by purifying the GR enzyme from human erythrocyte cells, the drugs diclofenac sodium, tenoxicam, etomidate, ketoprofen, lornoxicam, morphine and propofol were investigated on the enzyme. As a result, it was determined that propofol showed non-competitive inhibition, while the others showed competitive inhibition [25] (Şentürk et al., 2009).

In another study, it was determined that the GR enzyme purified from rat heart and lung tissues was inhibited by cefazolin, ceftazidime, cefuroxime furosemide, gentamicin, levofloxacin, methylprednisol, and teicoplanin [26]. In another study on sheep spleen tissue, the effects of some antibiotics and anti-inflammatory drugs on GR enzyme activity were investigated. It has been observed that ampicillin and gentamicin are non-competitive, while streptomycin sulfate, cefoperazone sodium and precort-lyo drugs inhibit the enzyme competitively [10]. In addition, the inhibitory effects of gentamicin sulfate, thiamphenicol, ofloxacin, levofloxacin, cefepime and cefazolin on sheep liver GR enzyme activity were investigated. It has been determined that ofloxacin, levofloxacin, cefepime and cefazolin antibiotics inhibit the enzyme semi-competitively [27].

In conclusion, inhibitors are of great importance for enzyme-treated approaches. In this study, it was determined that hyoscine-N-butylbromide inhibited the GR enzyme without competition. For this reason, it will be beneficial to be more careful with dose adjustments in the use of hyoscine-N-butylbromide.

## References

- [1] Taser, P., Ciftci, M. (2012). Purification and characterization of glutathione reductase from turkey liver. *Turkish Journal of Veterinary ve Animal Science*, 36(5), 546-553.
- [2] Keha, E., Küfrevioğlu, Ö.İ. (2010). Biyokimya, *Aktif Yayınevi*, Erzurum, s. 653.
- [3] Knapen, M.F., Zusterzeel, P.L., Peters, W.H., Steegers, E.A. (1999). Glutathione and glutathione-related enzymes in reproduction. *Eur. J. Obstet. Gynecol. Reprod. Biol.*, 82, 171-184.
- [4] Demir, H., Erat, M., Şakiroğlu, H. (2006). In vitro effects of some antibiotics on glutathione reductase obtained from chicken liver. *Turk. J. Vet. Anim. Sci.*, 30, 513-519.
- [5] Ciftci, M., Küfrevioğlu, OI, Gundogdu, M, Ozmen, I. (2000). Effects of some antibiotics on enzyme activity of glucose-6-phosphate dehydrogenase from human erythrocytes. *Pharmacological Research* 41(1), 109-113.
- [6] Sevki, A., Ciftci, M. (2012). Purification of rat kidney glucose 6 phosphate dehydrogenase, 6-phosphogluconate dehydrogenase, and glutathione reductase enzymes using 2', 5'-ADP sepharose 4B affinity in a single chromatography step. *Protein Expression and Purification*, 81(1), 1-4.
- [7] Montgomery, R., Conway, T.W., Spector, A.A., Chappell, D. (1996). Biochemistry a case-oriented Approach, Sixth edition. *Mosby*.
- [8] Çoban, Ç., Çiftci, M., (2022). Bazı ilaçların koyun dalak dokusundan saflaştırılan glukoz-6-fosfat dehidrogenaz enzimi üzerine *in vitro* etkileri. *Türk Doğa ve Fen Dergisi*, 11(1), 29-35.
- [9] Kose, L.P., Gulcin I., Ozdemir, H., Atasever, A., Alwasel S.H., Supuran, C.T. (2016). The effects of some avermectins on bovine carbonic anhydrase enzyme. *Journal of enzyme inhibition and medicinal chemistry*, 31(5), 773-778.
- [10] Çoban, Ç., 2022. Glutasyon redüktaz enziminin koyun dalak dokusundan saflaştırılması, karakterizasyonu ve bazı antibiyotiklerin enzim aktivitesi üzerine etkilerinin araştırılması *Doktora Tezi*, Bingöl Üniversitesi, Fen bilimleri Enstitüsü, Kimya Anabilim Dalı, s. 88.
- [11] Erat, M. (2002). İnsan ve sığır eritrosit glutasyon redüktaz enziminin saflaştırılması, bazı ilaç ve kimyasal maddelerin inhibisyon veya aktivasyon etkilerinin araştırılması. *Doktora tezi*, Atatürk Üniversitesi, Fen Bilimleri Enstitüsü, Kimya Anabilim Dalı, s.112-117.

- [12] Temel, Y., Bozkuş, T., Karagözoğlu, Y., Çiftci, M. (2017). Glutasyon redüktaz enziminin japon bildiricın (Coturnix coturnix japonica) eritrositlerinden saflaştırılması ve karakterizasyonu. *Journal of the Institute of Science and Technology*, 7(3),143-150.
- [13] Kayaalp, S.O. (2002), Rasyonel tedavi yönünden tıbbi farmakoloji.10. Baskı. *Hacettepe-TAŞ*, Kitabın muhtelif bölümleri.
- [14] Smith, L.L. (1987). Cholesterol autoxidation. *Chem. Phys. Lipids*, 44, 87-125.
- [15] Danner, J., Lenhoff, H.M., Heagy, W. (1977). Affinity chromatography of glutathione reductase: Bound by immobilized GSSG, eluted by NADPH. *Analytical Biochemistry*, (82),586-590.
- [16] Boggaram, V., Brobjer K.L., Mannervik, B. (1979). Purufication of glutathione reductase from porcine erythrocytes by the use of affinity chromatography on 2', 5'-ADP-Sepharose 4B and crisitalization of the enzyme. *Analytical Biochemistry*, 98, 335-340.
- [17] Carlberg, I., Mannervik, B. (1981). Purification and characterization of glutathione reductase from calf liver. An improved procedure for affinity chromatography on 2', 5'-ADP-Sepharose 4B. *Anal. Biochem.* 116, 531-536.
- [18] Bradford, M.M. (1976). A rapid and sensitive method for the quantitation of microgram quantities of protein utilizing the principle of protein dye binding. *Anal. Biochem.* 72(12), 248-254.
- [19] Laemmli, D.K., (1970). Cleavage of structural proteins during in assembly of the heat of bacteriophage T4. *Nature*, 227,680-685.
- [20] Lineweaver, H., Burk, D. (1934). The determination of enzyme dissociation constants. *J. Am. Chem. Soc.* 57, 658-666.
- [21] Stocks, J., Offerman, E.L., Modell, C.B., Dormandy, T.L. (1972). The susceptibility to autoxidation of human red cell lipids in health and disease. *Brit J Haematol*, 23, 713-724.
- [22] Hasanuzzaman, M., Hossain, MA., Silva, JAT., Fujita., M. (2012). Crop stress and its managemen. Perspectives and strategies. *Springer*, 261-315.
- [23] Ulusu, N.N., Tandogan, B. (2007). Purification and kinetic properties of glutathione reductase from bovine liver. *Mol Cell Biochem*, 303, 45-51.
- [24] Tekman, B., Ozdemir, H., Senturk, M., Ciftci, M. (2008). Purification and characterization of glutathione reductase from rainbow trout (*Oncorhynchus mykiss*) liver and inhibition effects of metal ions on enzyme activity. *Comparative Biochemistry and Physiology*, 148, 117-121.
- [25] Şentürk, M., Kufrevioglu, Ö.İ., Çiftci, M. (2009). Effects of some analgesic anaesthetic drugs on human erythrocyte glutathione reductase: An in vitro study. *J. Enz. Inh. Med. Chem.* 24(2), 420-424.
- [26] Adem, Ş. (2011). Sıçan kalp ve akciğer dokularından glukoz-6-fosfat dehidrogenaz, 6- fosfoglukonat dehidrogenaz, glutasyon redüktaz enzimlerinin saflaştırılması, karakterizasyonu, kotinin ve bazı ilaçların enzimlerin aktiviteleri üzerine etkilerinin incelenmesi. *Doktora Tezi*, Fen Bilimleri Enstitüsü, Erzurum.
- [27] Erat, M., Ciftci., M. (2003). İn vitro effects of some antibiotics on glutathione reductase from sheep liver. *Journal of Enzyme Inhibition and Medicinal Chemistry*. 18, 545-550.



# Design Multi Input Single Output DC to DC Converter for Mobile Devices

**Gözde GÜMÜŞ<sup>1,\*</sup>**, **Hakan GÜMÜŞ<sup>1</sup>**, **Okan GÜMÜŞ<sup>1</sup>**

<sup>1</sup>Graduate School of Natural and Applied Sciences, Department of Electrical and Electronics, Çankırı Karatekin University, Çankırı, Türkiye

## Abstract

In today's world. We have been able to find more than one way to generate energy. Also, humanity wants to store then use this energy. Based on this situation, we need to change our perspective on energy. Our electricity always falls short of consumption. So, we synthesize several generation methods. If we want to give an example, some plants have wind turbines and PV or PV and hydroelectric power plants. As you know turbines generate AC but PV systems generate DC. That can be a solution to energy shortage, but it can be not easy to transmit. On the other hand, this DC energy is using many areas but we haven't any good quality solution to store DC electricity. According to this, our work is about how to take different types of inputs and regulate energy for charging mobile devices. Regulating, methods are very different and they have also some methods. In this study, we are talking about multiple DC/DC converters. This study has Multiple input DC/DC converter topology. This type of converter has some production methods. Also, we are discussing some methods applications and their specification. In addition to this, we search about how to safely charge mobile devices.

**Keywords:** DC, AC, PV, Converter

## 1. Introduction

Smooth converting and transmission system is very important at these days. Cause of this reason, this study is researching methods about multiple input DC/DC converters. These are three main types of switching power supplies: boost, buck, and buck boost. The first is responsible for raising the input voltage, the second is responsible for lowering it and the. third is a mixture of the previous two. All these configurations work in a non-isolated way, that is, they share a common ground and the output voltage variation depends on the duty cycle applied to the switching component. [1] This time we worked with the voltage reducer (Buck), this configuration is commonly used because the output voltage is lower than the input voltage and its efficiency can reach very high values compared to the configuration. The simplest configuration is that of the voltage divider, which dissipates most of the energy as heat through the semiconductor devices. [2]

In Figure 1 you can see the circuit, which is composed of:

- A diode, this allows current to flow through the circuit when the switch is on.
- opened.
- A power switch which is usually an N-type Mosfet transistor.
- An inductance and a capacitor, which are responsible for filtering the output signal
- of the circuit.
- A resistor, which is the load of the output in the power stage [1].

## 2. Materials and Methods

In this part we are talking about the challenges for the developing circuit for mobile devices the first challenge is electricity type they should be all convert to DC. As you know we are using energy for mobile devices. Then how to charge mobile devices safely A converter with a buck-help design is used in one of the first isolated multi-input converters. The separation transformer's two components are designed to act as an inductor for the converter

\* Corresponding author. e-mail address: eem.gozdegumus@gmail.com

and to make absolute motions for certain data sources. This converter has three modes of operation. Switch S1 is on, S2 is off, and V1 charges the inductor L in the principal state. In the consequent state, S2 is on, S1 is off, and V2 charges the inductor, hence the inverse is true for switches.

Because there is no ability transfer from the data stage to the outcome stage during the underlying two modes, the pile is provided by the outcome capacitor. The two switches are off in the third working condition, and neither V1 nor V2 loads the inductor. Along these lines, the inductor passes limit on to the pile. For this converter, the outcome voltage,  $V_{out}$  is given as:

$$V_{out} = \frac{D_1}{N_1(1-D_1-D_2)} V_1 + \frac{D_2}{N_2(1-D_1-D_2)} V_2 \quad [3]$$

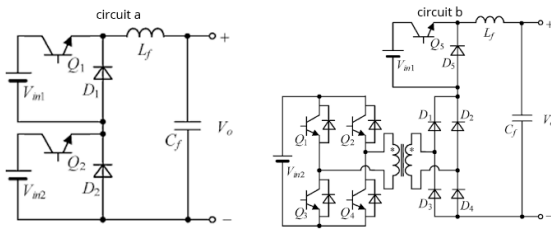


**Figure 1.** Multi-input full bridge converter [3] [4]

In this figure, you can clearly two circuits connected by pulsating current-source cell for generating energy. In these two circuits give ideas to multi input single output DC to DC converter. If I have to mention about pulsating current-source cell, simply it is pulsing energy to circuit with periodic square pulses outputs. As you see in circuit a there is two DC inputs. Also, we are talking deeply about AC and DC sources to circuit topology. if you need to compare our circuit to these two circuits. Circuit a is simply converting two DC sources to single output. In circuit b, there is one AC source which is called  $V_{in2}$ . This source is generating AC energy. Depend on this, we need to convert this electricity AC to DC.

### 3. Results and Discussion

Today's world had to use mobile devices for a glorified life. As you know we must to charge these devices. In that condition we have some methods. To give an example, using power banks, strong capacity Li-Ion batteries or using fast chargers.

If you are designing good quality chargers for mobile devices, you must notice to the features. Voltage and amperage values must be in accordance with the value specified in mobile devices. If any of these values is low, the device may be damaged due to low power supply. In addition, the minimum power requirement required by each mobile device differs. In order to prevent this, we saw that it would be appropriate to give 5V 2.1 Amps as a result of our research. In addition, it should be considered that the voltage and current value can be changed by adding a potentiometer to the output.

To design mobile charger you must know power supply. If we want to explain detailly, we must examine to schematic design for mobile charger.

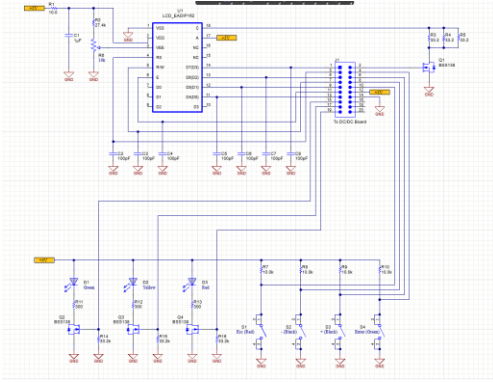


**Figure 2.** Reference design for mobile devices [5]

As you see in the Figure 3 you can clearly see the mobile charger reference design for our project. That is PMP8740. This component is using for industrial devices. This circuit has 2-kW AC/DC battery charger with %92 efficiency. That is the critical point because if we try to design a multiple input we must have a good efficiency. That efficiency value is about loss energy. Also, we have to design an efficiency circuit for a good engineering design. In addition, this circuit has 0V between 32V output voltage. If we are examining to output current, it has 62,5 maximum currents. If it is a qualified point to controlling with microcontroller. To finalize that it has 90 VAC between 264 VAC input voltage. Also, if we want to explain in order:

- 93.5% peak efficiency optimizes thermal management of the module
- Serial interface gives users the ability to easily parallel up to 10 hardware modules
- Two raw displays and four pushbuttons simplify configuration
- Pre-defined levels for li-ion, lead-acid and gel batteries
- Primary/Secondary or stand-alone configuration for battery charging or standard power supply unit

### 3.1. DESIGNING MULTIPLE INPUT DC/DC CONVERTER

Also, we must to examine to DC/DC converter topology for our studying. To understanding DC/DC converter we must look into this; DC-DC converters are widely used to generate an efficiently regulated voltage from a well-controlled or uncontrollable source to a load that may or may not be stable.

### 3.2. DC TO DC BUCK BOOST CONVERTER

Buck boost converters circuit, like other switched converters, are examined in two stages according to the conduction/off state of the switching element. First of all, we will examine the case where the switch is transmitting. When the switch is on, the circuit is divided into two parts. The first of these is the circuit formed by the source and the coil providing the input voltage, and the second is the circuit consisting of the load and the capacitor. These two circuits can be seen in detail in the figure below.



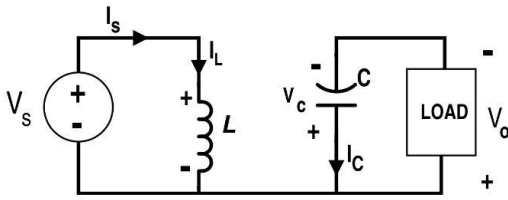


**Figure 3.** Initial State, Switching Element in Transmission

In switch transmission, the coil in the circuit is energized by the energy coming from the source. On the right side, the energy on the capacitor is transferred to the load. In this case, the D diode in the circuit is on. In direct current circuits, the average voltage of the coil and the average current of the capacitor are both zero., the voltage of the coil will be reverse induced and the current of the capacitor will flow in the opposite direction in the other when the switch is in the cut condition of the circuit.

In the second switch-off state of the circuit, the coil energized through the input source in the previous state discharges its energy on C and the load. The capacitor, which transfers its energy to the load in switch transmission, is re-energized with the energy coming from the coil in the second case. The circuit diagram of the second state, that is, when the switching element is in cut-off, is given in the figure below. In this case, since the input source will be completely disconnected from the circuit, the circuit is fed through the coil. In the circuit below, current flows through the D diode until the energy of the coil is depleted, and with this current, the capacitor and the load are fed.

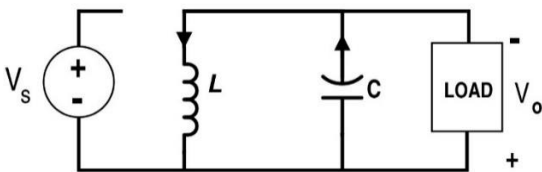


**Figure 4.** Second Case, Switching Element Cut-off

In the second (in the switch cut) state of the circuit, the coil energized over the input source in the previous state discharges its energy on C and the load. The capacitor, which transferred its energy to the load in the previous case (Key conduction), is re-energized with the energy coming from the coil in the second case. The circuit diagram of the second state, that is, when the switching element is in cut-off, is given in the figure below. In this case, since the input source will be completely disconnected from the circuit, the circuit is fed through the coil. In the circuit below, current flows through the D diode until the energy of the coil is depleted, and with this current, the capacitor and the load are fed.

Also, there are some DC/DC converter types they are

- Full Bridge
- Half Bridge
- Forward

These converter types their explanation does not quite cover the content of this thesis topic. About this topic we can analyze the DC converter design. As you can see in the Figure 5 the schematic of DC/DC converter. It is using UCC2813d-0. This component made by TI for wide input converters. As you see in the schematic the input of circuit has max input 250V 0.315A. Also, thanks to UCC2813d-0 we 12V 55mA output. This design can be holding the light this thesis.



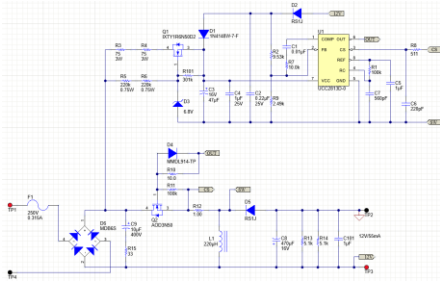


**Figure 5.** DC-DC converter schematic design [5]

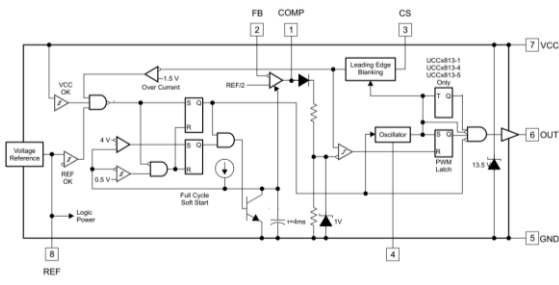


**Figure 6.** Block diagram of UCC2813d-0

Figure 6 is clearly showing the block diagram of UCC2813d-0. This diagram shows us how to work DC/DC converters work generally. In this diagram There is two voltage reference. Depend on that, this component regulating voltage using these references.

#### 4. Developed or Applied Approach

As we said before, different types of voltage inputs can be added to the diagram of the circuit to be established, and a power output will be obtained by regulating all of these voltages separately from each other. If we examine the input voltage part of the circuit to be made, I have realized that it will be risky for alternators producing direct current to operate on a single circuit. As a solution to this, the desired power will be obtained by using IGBT type MOSFETs instead of using ordinary quad diode gates, by providing the power regulation of the circuit in a controlled and safe manner. These features of the circuit here are similar to wide-input DC converters, but with a few differences. Another issue to be considered in the circuit planned to be designed is the different behavior of different types of voltages on the circuit. These behaviors cause factors such as temperature, noise and harmonics that we all know. In addition, the precaution we will take against the risk of alternating current jumping on the circuit will be to reduce this risk by placing transformers in safe places in the circuit. Another point to be considered while this electricity is regulated is that the output electricity is suitable for mobile devices. In order to ensure the compatibility condition, different phones, tablets and other similar smart devices used in today's world were examined and it was understood that an output of 5 volts and 2 amps would be suitable for almost all devices. In addition, it is aimed to move this circuit to the next level by using digital type current and voltage sensors in order to see the input and output voltages and detect possible problems. The reason for this type of sensors is to control the production of the input voltages of the circuit to be made and to prevent the circuit from being damaged. It is aimed to show in detail whether the power obtained by using 7-segment LEDs will be dangerous for the circuit and the device so that the sensors at the voltage input can clearly show data to the user. In addition, this excess power will be prevented by using mosfets in case of a possible overproduction, and there will be a manual switching system. These features will take the circuit to the next level while making it safe.

## 5. Results and Discussion

In this part, we will discuss the outputs of the circuit that decided to make it as a result of the researches. When you look at the circuit, it is a great difficulty to have more than one voltage type behind, but it is not a type of circuit made for the first time. When this difficulty is examined in general, it is seen that various restrictions and current dividers are used. When the diagram of the circuit we will make is examined, the voltage sensors that are planned to be used are digital, and each input and output power is controlled in isolation, as well as being able to be followed, which includes great differences and innovations. From another point of view, the battery control unit, which is designed to charge mobile devices appropriately, will be used as new type components. Transistors appear to be common in ordinary charge control circuits. This can be shown as another innovation. The controlled charging of the battery and the isolation of the battery's outgoing voltage also emphasize the importance of this control system once again.

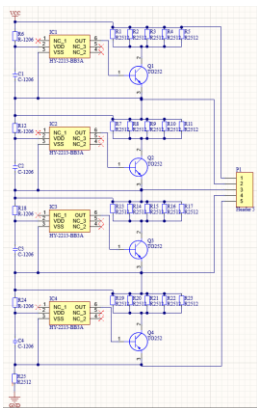


**Figure 7.** Battery management circuit (BMS)

Figure 7 clearly shows us how to charge a 4-cell battery. Unlike standard battery control units, the HY-2213 component is used. The suitability of the planned circuit for telephone batteries has been tested before and is shown in the datasheet of the product.

## References

- [1] Marzo, Understanding Buck Power Stages in Switchmode Power Supplies, T. Instruments, 1999 .
- [2] J. C. A. C.-P. A. E. A. a. R. G. C. Restrepo, "A noninverting buck-boost dc-dc switching converter with high efficiency and wide bandwidth," in *IEEE Transactions on Power Electronics*, vol. 26, September 2011, p. 2490 2503.
- [3] L. Y.-C. W. F.-Y. Chen Yaow-Ming, " Multi-input DC/DC converter based on the multiwinding transformer for renewable energy applications.," *IEEE Trans Ind Appl* , 2002, p. 38:1096–104.
- [4] A. L. a. J. A. P. L. Solero, "Design of multiple-input a dc dc power converter for hybrid vehicles," in *IEEE Trans. Power Electron.*, Oct. 2005., pp. vol. 20, no. 5,1007–1016.
- [5] [Online]. Available: <https://www.ti.com/tool/PMP8740> . [Accessed 04 20222].
- [6] E. A. v. S. Furbo, "Thermal destratification in small standart solar tanks due to mixing during tapping," in *Proceeding of ISES Solar Wolar Congress*, Jerusalem,Israel, 1999.



# Excision of Residual Cyst Associated with Odontoma from Ramus of Mandible: A Case Report

***Ramazan Serdar ESMER***<sup>1\*</sup> 

<sup>1</sup>Dentistry Faculty, Department of Oral and Maxillofacial Surgery, Çankırı Karatekin University, Çankırı, Türkiye

## Abstract

Residual cyst is in the group of inflammatory odontogenic cysts. These cysts originate from periapical granuloma and radicular cyst residues left after tooth extraction. They develop asymptotically, grow too large and cause bone defects and swelling in the jaw. Odontomas are classified as mixed odontogenic tumors. There are two types, compound and complex odontoma. It is the most common odontogenic tumor of the jaws. In this case report, enucleation of residual cyst associated with odontoma was reported from a 58-year-old male patient. At the same time, the pathogenesis, clinical and radiological features and differential diagnosis of residual cyst and odontoma are discussed.

**Keywords:** Residual Cyst, Odontoma, Enucleation

## 1. Introduction

Residual cysts are part of the group of inflammatory odontogenic cysts, one of the most common bone-destructive lesions affecting the jaws [1,2]. Inflammatory cysts are the most common cystic lesions on the jaws; they constitute 50-75% of all oral cysts [1-3]. Developmental odontogenic cysts and inflammatory odontogenic cysts are characterized by a slow growth and enlargement tendency, and although they are entities with benign biological behavior, they can reach significant sizes if not diagnosed in time and treated appropriately. Some cystic lesions of the jaws share similar clinical and radiographic features [1,2,3,7]. Diagnosis of odontogenic cysts usually requires a detailed analysis of clinical, radiographic and histopathological findings [3].

Odontomas are odontogenic tumors that are considered developmental anomalies resulting from the growth of differentiated epithelial and mesenchymal cells [3-6]. These tumors are composed of enamel and dentin and may also have variable amounts of cementum and pulp tissue. A compound odontoma forms an agglomeration of small tooth-like structures, while a complex odontoma forms an irregular mass in an irregular pattern [3-6].

In this case report, the treatment of the patient with these two entities is presented. In addition, general information about these two structures is discussed.

## 2. Case Report

A 58-year-old male patient was referred to our department by a general dentist. As a result of radiological and intraoral examination, a 3 cm diameter radiolucent lesion with smooth borders was diagnosed in the left mandibular corpus and ramus region (Figure 1). At the same time, a radiopaque round lesion 3-5 mm in diameter was observed at the mesial margins of this mass. A computed tomography image was requested for detailed examination of this asymptotically enlarged lesion. Computed tomography (CT) examination showed that; the bone around the lesion was highly fused and thinned the bone in the mandibular ramus and corpus region. The cyst is very close to the alveolar inferior canal. A surgical operation was planned for the treatment of the patient (Figure 2).

\* Corresponding author. e-mail address: raesmer@karatekin.edu.tr



**Figure 1.** Cystic lesion in left corpus and ramus.

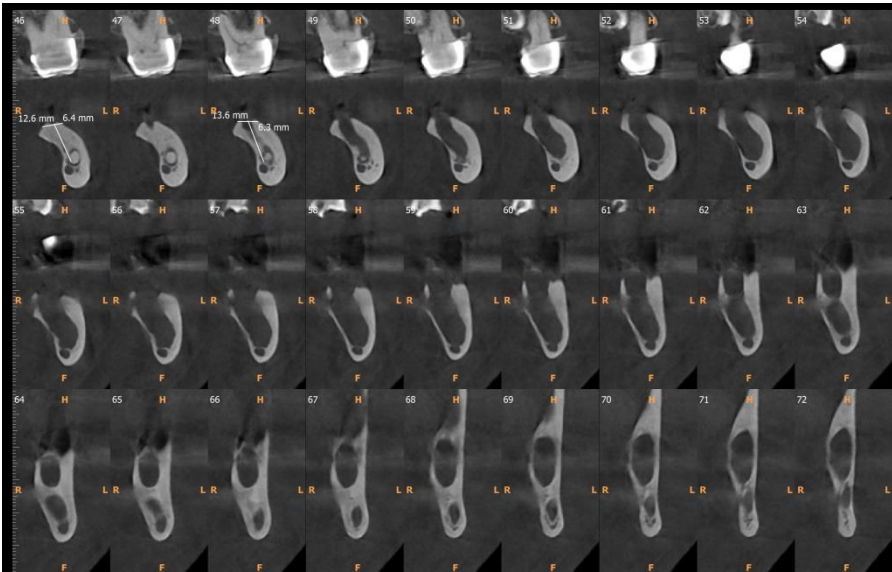


**Figure 2.** CT image of lesion.

On the day of the operation, the left mandible of the patient was anesthetized with local anesthesia. The operation area and the patient's face were treated with povidone iodine and the patient was covered with sterile drapes. The flap was opened with an envelope incision and the cystic area was exposed (Figure 3). The bone around the cyst was removed with bone burs and with the help of sharp curettes, first the fluid-filled cyst and then the 3-5 mm diameter odontoma were removed (Figure 4). The samples were sent to the pathology laboratory to make a complete diagnosis (Figure 5). Histopathologic examination revealed that the fluid-filled mass was a residual cyst and the hard tissue belonged to an odontoma. The 6-month follow-up radiograph showed that the operation site was completely ossified (Figure 6).



**Figure 1.** Expose of operation area



**Figure 4.** Removal of cyst.





**Figure 5.** Specimens prepared for histopathology.

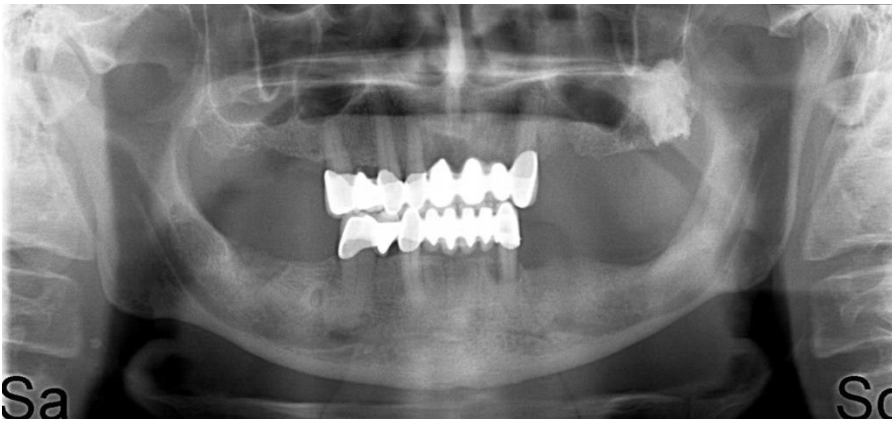


**Figure 6.** 6-months follow-up radiograph

### 3. Discussion

Residual cysts, as the name suggests, are not a special entity. It represents the remaining radicular cyst in the socket after tooth extraction. These cysts originate from malleses epithelial remnants [1]. Histologically, its lumen is lined by squamous epithelium [1,2]. Cholesterol crystals can be observed infrequently [3]. Residual cysts are seen in an edentulous area and do not show any relation to any teeth in clinical and radiological examination. [2,3,7]. This highly predictable radiological appearance has been noted in many studies[1,2,3]. These cysts may also cause bone resorption and compression of anatomical structures such as the inferior alveolar canal, maxillary sinus, and nasal cavity [3,5]. Differential diagnosis should be made with giant cell granulomas and benign and malignant lesions of the bone with a radiolucent appearance. It should be treated by enucleation. Routine follow-up radiographs should be taken during the recovery period [3].

Odontomas are the most common odontogenic tumors. Some prefer to use the definition of hamartoma for odontoma [3,5]. Radiographically, these tissues have a density comparable to normal tooth structure. have a distinct radiolucent rim that separates the lesion from the adjacent bone [5]. While most compound odontomas are seen in the maxilla anterior, complex odontomas are most commonly seen in the posterior mandible, especially in the third molar region [3]. Although it can be seen in any age range, it is most commonly diagnosed in the first and second decades. Histologically, the compound odontoma is usually contained within a connective tissue capsule. The lesion consists of anatomically distinct, small, well-formed or malformed teeth with enamel, dentin, pulp, and cementum. The complex odontoma lacks anatomical organization and is often interconnected in a cementum mass. It is also often surrounded by a thin connective tissue capsule [3,4,5].

Completely calcified complex or compound odontoma is biologically inert, does not grow [3]. Excision is not required if the clinical indication is safe and removal would serve no useful purpose. However, there are several reasons for excision of a lesion: (1) because of the patient's concern about the diagnosis when informed of the presence of the lesion; (2) to allow possible eruption of a tooth blocked by an odontoma in a clinically appropriate position; and (3) making a diagnosis between a complex odontoma and other radiographically opaque lesions, such as cementoblastoma, or large lesions containing a mixture of radiolucent and radiopaque areas that may represent an ossifying fibroma or an odontogenic neoplasm [3].

#### 4. Conclusion

In this case, two different structures requiring excision were seen together. The correct diagnosis and treatment of these two structures, which give clinical and radiological images in accordance with the definition in the literature, were made as a result of pathological research. In the literature the simultaneous occurrence of these two entities is rare hence this case is interesting.

#### Acknowledgment

Before surgery, the patient signed the consent form. This consent form informs the patient about the complications that may occur from surgery, and also obtains permission from the patient for case publication.

#### References

- [1] Erdoğan, Z. & Gulsun, B. (2019). Rezidüel Kist Enükleasyonu Sonrası İmplant Tedavisi: Bir Olgu Sunumu. *İzlek Akademik Dergi*, 2 (2), 101-109.
- [2] Sridevi, K., Nandan, S. R., Ratnakar, P., Srikrishna, K., & Vamsi Pavani, B. (2014). Residual cyst associated with calcifications in an elderly patient. *Journal of clinical and diagnostic research: JCDR*, 8(2), 246–249.
- [3] Fonseca, R. (2018). *Oral and Maxillofacial Surgery Volume 2*. 3<sup>rd</sup> ed. Missouri: Elsevier, 338-461.
- [4] Yadav, M., Godge, P., Meghana, S. M., & Kulkarni, S. R. (2012). Compound odontoma. *Contemporary clinical dentistry*, 3(Suppl 1), S13–S15.
- [5] Bilodeau, E. A., & Collins, B. M. (2017). Odontogenic Cysts and Neoplasms. *Surgical pathology clinics*, 10(1), 177–222. <https://doi.org/10.1016/j.path.2016.10.006>
- [6] Bordini, J., Jr, Contar, C. M., Sarot, J. R., Fernandes, A., & Machado, M. A. (2008). Multiple compound odontomas in the jaw: case report and analysis of the literature. *Journal of oral and maxillofacial surgery* 66(12), 2617–2620.
- [7] High AS, & Hirschmann PN. Age changes in residual radicular cysts. *J Oral Pathol*. 1986;15:524–28.



## Creatine Kinase Elevation in Covid-19 Patients on Statin

***Osamah AL-KILIDAR***<sup>1,\*</sup>, ***Volkan EYUPOGLU***<sup>2</sup>, ***Mahmood KHUDHAIR***<sup>3</sup>

<sup>1</sup> Department of Environment and Water, Directorate of Sciences and Technology, The Iraqi Ministry of Higher Education, Baghdad, Iraq

<sup>2</sup> Graduate School of Natural and Applied sciences, Department of Chemistry, Çankırı Karatekin University, Çankırı, Türkiye

<sup>3</sup> Department of Chemistry, Faculty of Medicine, Al Nahrain University The Iraqi Ministry of Health, Baghdad, Iraq

### Abstract

Recent studies have related the safety of statin drugs in COVID-19 patients, and its anti-inflammatory effect could reduce the severity of the infection and accelerate the recovery; while some case reports refer to rhabdomyolysis occurrence in COVID-19 patients, it is interesting that some of them were on statin therapy, this serious symptom considered an advanced adverse effect of statin drugs, in this study, we investigate the statin effect on creatine kinase in 140 patients, our cohort divided to four groups; 35 infected with Coronavirus on-statin, 35 infected not on statin, 35 not infected on-statin and 35 healthy Individuals as control, abbreviated to (A, B, C, and D) respectively, to compare their outcomes with each other. As a result, we can imply that statin has a highly significant effect on CK, with the p-value at 0.002. In group A, rhabdomyolysis was reported in two patients versus one case in group B.

**Keywords:** Covid-19, Rhabdomyolysis, Statin, Creatine kinase

### 1. Introduction

Since the World Health Organization (WHO) announced that the novel Coronavirus (COVID-19) had become a pandemic that endangers the whole world, causing acute respiratory distress syndrome (ARDS) [1], studying the effect of the virus on the body's biochemistry has become a necessity, to know and determine the reasons that lead to exacerbation disease more accurately, especially the study of complications and consequences that lead to an increase in mortality that is not only related to ARDS but also because of the comorbidities, the study of the association of this virus with the diseases and the accompanying medications has become mandatory.

Renal failure is among the severe consequences which restrict the medications required to relieve and treat the symptoms of viral infection, which puts therapists in a great challenge during the treatment period, particularly the COVID-19 severity seems to be related to older age and comorbidities; in particular, patients with pre-existing cardiovascular disease (CVD) are at high risk for adverse outcomes, and SARS-CoV2 infection is associated with common vascular and arrhythmic complications[1]. Thus, statins are considered one of the most important and best drugs that reduce cholesterol levels for primary or secondary prevention of cardiac disease[2].

On the other hand, this adverse effect may be accelerated with COVID-19 infection, particularly since many case reports have been published about myopathy and rhabdomyolysis during the infection period, which may be due to the penetration of the virus itself into skeletal muscle and hepatocytes, or it may be due to drug interactions that may occur during treatment also; these reports refer to patients admitted to the hospital with respiratory syndrome associated with COVID-19, their creatine kinase levels were exceeded upper limit of normal many times and developed Rhabdomyolysis, then they left after recovery with chronic kidney disease (CKD), noteworthy many of them were under statin therapy.[3,4]

Muscle weakness and elevated creatine kinase levels were also common with the progenitors of the novel coronavirus (SARS-CoV1 and MERS)[5]. Therefore, prescribing or continuing these medications in patients with Covid is under suspicion, and it has become necessary to investigate whether they cause a deterioration in patients' health.

\* Corresponding author. e-mail address: osama.alkileedar@outlook.com



This article aims to study the relation between Creatine Kinase (CK) and covid-19 by comparing CK levels in statin users with and without COVID-19 and studying the relation between rhabdomyolysis and statin treatment in covid-19 patients.

## 2. Materials and Methods

Samples were collected from the sixteenth of March to the tenth of May 2022 from Al-Shifa specialized Crisis Center / Baghdad, where isolation and treatment of COVID-19 patients for moderate and advanced cases since the beginning of the pandemic.

Patients were chosen after a study and review of 244 cases. A questionnaire was collected about; age, chronic diseases, muscle pain, statin use, exercise, smoking, and alcohol consumption. Cases that did not meet the objectives of this study were excluded. Where applied, 104 individual calibrated exclusions depending on comorbidities, medications used, drug allergy, all hepatic diseases, metabolic syndrome, or statin-related allergies were excluded.

Our cohort was divided into four groups as follows: A Covid patients on statins consist of 35 individuals, B covid patients not on statins consist of 35 individuals, C group represents 35 uninfected individuals on statins, and the D group contains 35 Individuals not infected nor using statins (healthy).

### 2.1. Study population

Our cohort was divided into four groups as follows: A Covid patients on statins consist of 35 individuals, B covid patients not on statins consist of 35 individuals, C group represents 35 uninfected individuals on statins, and the D group contains 35 Individuals not infected nor using statins (healthy).

### 2.2. Apparatus

RANDOX kit Creatine kinase N-acetyl-L-cysteine (CK-NAC) with serial number 487390 prepared and packaged in the United Kingdom (UK).

CK is characterized by instability due to oxidation at the active site, specifically in sulphydryl groups, leading to incorrect test results. Therefore, the best solution is to reactivate the enzyme by adding thiol compounds as N-acetyl-L-cysteine (NAC); the test system also includes adenosine-5'- monophosphate (AMP) in addition to didanosine pentaphosphate which inhibits the activity of myokinase, the determination of test depending on creatine phosphate and ADP, that characterized with greater sensitivity, addition to the ability to use small samples without blanks.

The reagents consist of R1a. which contains Imidazole buffer, glucose, Mg-acetate, and Ethylenediaminetetraacetic acid (EDTA).

R1b. consist of ADP, AMP, Diadenosine pentaphosphate, NADP, HK, G-6-PDH, N-acetylcysteine, and Creatine phosphate.

CK in the sample catalyzes the transforming of the phosphate group from creatine phosphate to ADP to forming creatine and ATP, which is catalyzed by hexokinase to react with glucose to form glucose-6-phosphate and ADP, then the glucose -6- phosphate reacts with NADP<sup>+</sup> with the presence of glucose -6- phosphate dehydrogenase as a catalyst to forming glucose-6- phosphate and NADPH + H<sup>+</sup>, The technique used for the measurement is UV method. The instruments and tools are listed in Table1 below.

**Table 1** Instruments and tools used in the current study

<i>NO</i>	<i>INSTRUMENT</i>	<i>SERIAL NO. COMPANY</i>	<i>ORIGIN</i>
1	CHEM-S1\ clinical semi-automated instrument	FL701534\ GENEX laboratories	USA
2	Medical laboratory centrifugation 5000 rpm	HIGHTOP	China
3	Gel tube (2.5mL)	AFCOVAC	Jordan
4	Disposable syringes	(5 mL)	China
5	Micropipettes (20-200 $\mu$ L), (100-1000 $\mu$ L), and (1-10 mL)	Slamed	Germany
6	Water bath	HH-2	China
7	Deep Freeze	GFL	Germany
8	Plain tube (5 mL)		China
9	pipette tips (1, 0.1, 0.01 mL)		China

### 2.3. Statistic

Statistical calculations were applied through SPSS software ® 23.0. with P-value  $\leq 0.05$  was considered the change as significant. The one-way ANOVA test has been implemented to compare the means of variants between and within groups. A t-test was used for multiple comparison tests across the p-value, showing significance and probability. The median, Q1, and Q3 were calculated for each group and each group variable. Then all groups were studied by distributing their data in one chart for each variable to show the difference in results, the extent of change, and the effect of statins and COVID-19 on creatine kinase and liver enzyme.

## 3. Results and Discussion

After our standards were applied, 70 / 244 COVID-19 patients were chosen, and their ages were between 40 and 83 years old. Their symptoms are almost the same ranging between cough, chest pain, myalgia, back pain, diarrhea, fatigue, and headache.

Group A consisted of 35 individuals under statin therapy for at least three months before being infected with COVID-19, and most were not doing any exercise. Reasons behind the use of statin in this group were diabetes, CAD, hypercholesterolemia, hypertension, and obesity. Mechanical ventilation was needed for most of them during their treatment duration in the hospital. The most frequent medications were; Favipiravir, Azithromycin, acetaminophen, Corticosteroids, and vitamin C.

Correspondingly, 35 individuals were not under any statin therapy, but they at the same condition as the first group; diabetes, hypercholesterolemia, hypertension, and obesity had a presence in this group as well; it is noteworthy that seven patients were under statin therapy and they discontinued due to muscles pain. And they considered group B.

Whereas the third group, C (35 patients), were not infected with COVID-19 and had been vaccinated against novel coronavirus, they were under statin therapy for at least three months before enrolling in our cohort.

The last group was the control (group D) which consisted of 35 healthy individuals, never been infected with COVID\_19 or treated with statin. Characteristics of admitted cohort and classification into four groups are shown in Table 2 next.

### 3.1. Creatine Kinase (CK)

After analyzing data with ANOVA one-way test, as shown in Table 3, the results confirm a variance between groups. The alternative hypothesis is accepted due to the significant p-value of 0.0021. The F statistic is greater than F critical value (F crit). SS shows the sum of squares quantifies between and within groups, which quantifies the variability within and between groups of interest.

**Table 2** Characteristics and classification of the admitted cohort into four groups

	<b>GROUP A</b> <i>N=35</i>	<b>GROUP B</b> <i>N=35</i>	<b>GROUP C</b> <i>N=35</i>	<b>GROUP D</b> <i>N=35</i>
Reang of age	40 - 83	43 - 82	45 - 75	41 - 68
Male	54% (n=19)	54% (n=19)	48% (n=17)	57% (n=20)
Female	46% (n=16)	46% (n=16)	51% (n=18)	43% (n=15)
ATORVASTATIN (ATV) 20mg	39% (n=14)	Non	57% (n=20)	Non
Atorvastatin (ATV) 40mg	20% (n=7)	Non	3% (n=1)	Non
ROSUVASTATIN (RTV) 20 mg	34% (n=12)	Non	31% (n=11)	Non
Rosuvastatin (RTV) 40 mg	9% (n=3)	Non	9% (n=3)	Non
Simvastatin (SVT) 80 mg.	3% (n=1)	Non	Non	Non
Diabetes	26% (n=9)	17% (n=6)	60% (n=21)	Non
Coronary artery disease (CAD)	14% (n=5)	Non	26% (n=9)	Non
Hypercholesterolemia	63% (n=22)	35% (n=7)	83% (n=29)	Non
Hypertension	77% (n=27)	91% (n=32)	69% (n=24)	Non
Obesity	83% (n=29)	29% (n=10)	51% (n=18)	37% (n=13)

**Table 3** CK-ANOVA test results

<b>SOURCE OF VARIATION</b>	<b>SS</b>	<b>df</b>	<b>MS</b>	<b>F</b>	<b>P-value</b>	<b>F crit</b>
Between Groups	778190.5	3	259396.8	5.15193	0.0021	2.671178
Within Groups	6847525	136	50349.45			
Total	7625716	139				

The variance shows the average of the squared differences from the mean, and it is greater in group A the average and Sum (total of values) as well; the count shows the number of data points in each group and is equal in all groups and as shown in Table 4 below.

**Table 4** CK-NOVA test summary

<b>GROUPS</b>	<b>COUNT</b>	<b>SUM</b>	<b>AVERAGE</b>	<b>VARIANCE</b>
A	35	10024	286.4	121968.5
B	35	7843	224	69592.37
C	35	5229	149.4	7060.071
D	35	3122	89.2	2776.871

Then the multiple comparisons test was applied to compare groups and determines the most affected group. The median shows a greater value at 149 in group A, and the p-value at 0.002 indicates the highest risk and is considered highly significant. Also, Q3 was 305 in group A, which means 75% of individuals had CK levels more minor than this value, which is compatible with Dashti-Khavidaki and Khalili [6] in their hypothesis that statin may induce myotoxicity in COVID-19 patients, also corresponding with Castiglione et al. [7] in their opinion that the use of statin with antiviral drugs could increase myotoxicity.

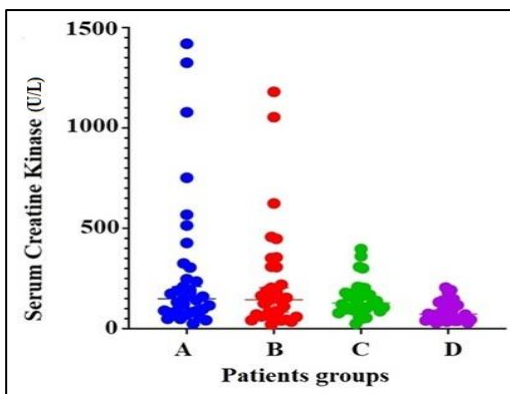
The B group (COVID not on statin) also shows a significant p-value of 0.016. Q3 shows 307.5, as listed in Table 5 below.

31% (n=11) among group B had abnormal CK values, and 5.7% (n=2) had the greatest level of CK at 1180, 1054 U/L (up to 6 fold ULN); the therapists had to do dialysis on one of them because of the high levels of serum potassium, creatinine, and urinary albumin with a dark urine color, which indicates rhabdomyolysis occurrence, this is consistent with the outcomes of Haroun et al. [4] which showed that elevated CK and rhabdomyolysis they were common consequences among COVID-19 patients.

The C group (statin) shows a significant p-value versus the D group at 0.02, where the greatest CK 397 U/L is 2.85% (n=1). Whereas A versus B and C show non-significant values, and B versus C cohort individuals are distributed among groups as shown in Figure 1 below.

**Table 5** Comparative CK results in all cohort

CK	A	B	C	D
Median	149	144	128	72.5
25% Q1	82	64.25	97	44.25
75% Q3	305	307.5	177	134
Multiple comparisons test	Value-P			
A vs. B	>0.999			
A vs. C	>0.999			
A vs. D	0.002			
B vs. C	>0.999			
B vs. D	0.016			
C vs. D	0.020			

**Figure 1.** Distribution of cohort groups according to CK results

In group A, the CK results obtained for 35 patients were; a mild increase up to 325 U/l in 13.8% (n=5), three under AVT 20 mg/day, and two under AVT 40 mg/day. The moderate increase in 8.3% (n=3) of them (less than three times the ULN, up to 568 U/L), which considered statin-related myotoxicity (SRM) stage 2 due to their symptoms, and more than the ULN reached approximately seven times in 8.3% (n=3) patients (up to 1325 U/L) which considered SRM at stage 3. All of them were treated with 40 mg/day (AVT and RVT) except for the three mentioned above with 20 mg/day statins.

While it exceeded seven times the ULN (1435 U/L) in 2.7% (n=1) SRM 3 according to CK concentration, was on SVT 80 mg. Noteworthy classification of Alfirevic et al. [8] shows that the stages of SRM listed previously in table 2.2 were used due to the presence of statins in all individuals in group A and the appearance of symptoms of muscle injury. This use came to clarify the convergence and not to assert that statins are the only cause of muscle injury here.

Furthermore, the rest of the group, 63.8% (n=23) within the normal range, were under statin 20 mg/day. The clinicians decided that two patients had to be transferred to the dialysis unit due to the appearance of renal failure symptoms, where elevating was reported in serum potassium, creatinine, and urinary albumin with a very dark urine color. However, urinary myoglobin was not examined, the previous biomarkers were sufficient to indicate that rhabdomyolysis already occurs, and that was confirmed by their CK levels (1325 U/l and 1435 U/l) which were not performed by the hospital and were conducted for the purpose of this study while the patients were already in the hospital. These two cases were related to males ages 72 and 81 years old who were admitted with cough, chest pain, and fever. Then they were diagnosed with SARS-CoV2 due to a positive rtPCR swab. After review of their data case in the hospital, the clinician's initial assessment; of diabetes type 2, atherosclerosis, and a cardiac catheterization had been done previously to one of them, and both were under treatment with ATV 40 mg, SVT 80 mg, metformin, metoprolol, and Plavix, the most effective medications described in-hospital are Favipiravir, Paracetamol, and Azithromycin. However, this outcome seems to be consistent with Chan et al. [9] in terms of the occurrence of rhabdomyolysis during the infection period and compatible with Suwanwongse and Shabarek [10] in rhabdomyolysis occurrence with a statin user.

Also, these outcomes may correspond with the results of Hougaard Christensen et al. [11] due to the high possibility of drug interaction between azithromycin and statins, especially there is a high dose of simvastatin, which concentration rises to 5 times the ULN, and atorvastatin, rises to 4 times the ULN in the presence of azithromycin, in addition to the antiviral effect, where two types of CYP inhibitors are combined lead to inadequate metabolism of statins and an increase in their circulation concentration, which increases the statin exposure of skeletal muscles even after discontinuing statins, the half-life of some statins considered long, especially ATV, which lasts up to 80 hours.

In the questionnaire presented to individuals in group A or their companions, 38% of them (n = 15) answered that fatigue and back pain were the first symptoms of the disease that they felt. The initial diagnosis of the therapists indicated that 25% (n = 9) who were admitted to the hospital had muscle pain, back pain, and general weakness, in addition to the common symptoms of COVID-19. Therefore, these results may reconcile with the report of Chan et al. [9]

Regarding fatigue and elevated CK as one of the initial symptoms of infection. Compared with the B group (Covid not on statin), the p-value was non-significant and the C group (statins). However, when comparing these last two groups with the D group, it changed to significant, and this indicates that statins and COVID-19 cause elevation of CK, but in heterogeneous patterns and related to clinical and pharmacological factors, while the more elevated was partial with the A group (COVID with statin) significantly with patients whose treated with high doses of statins and that appear clearly in the patients' distribution which shown in figure 1.

However, these findings differ from Castiglione et al. [7] hypothesis that statin use in hospitalized COVID-19 patients had a positive effect on symptom improvement and shorter recovery time through its anti-inflammatory effect by upregulation of angiotensin-converting enzyme 2, which is the main pathway of the virus, in order to use statin as a low-cost drug in low-income countries, where our results showed the statin plays a role as an additional factor that accelerates the occurrence of muscle damage, especially with high doses that led to the consequences of renal injury.

Myopathy and even rhabdomyolysis occurred with group B and at a higher frequency in numeral and severity in group A. These data indicate that these complications occur due to novel coronavirus disease and are exacerbated by the presence of statin, especially at higher doses. It may be due to mitochondrial dysfunction caused by statins; the impairment of energy transfer leads to accelerated muscle breakdown when viral infection depletes skeletal muscle energy. This is exacerbated by using drugs that increase the exposure of the skeletal muscles to statins by inhibiting CYP pathways and raising their concentration in blood circulation. Therefore, the use of statins with COVID-19 patients should be limited to the presence of the risk of heart attack, atherosclerotic cardiovascular disease, or diabetes, with monitoring of CK levels and avoiding high doses of statins, where the reconsideration of the benefits of using statins in coronavirus patients is required due to the consequences that may be occurred.

## References

- [1] "Coronavirus", [https://www.who.int/health-topics/coronavirus#tab=tab\\_1](https://www.who.int/health-topics/coronavirus#tab=tab_1) (2022).
- [2] Downs, J. R., Clearfield, M., Weis, S., Whitney, E., Shapiro, D. R., Beere, P. A., Langendorfer, A., Stein, E. A., Kruyer, W., and Gotto, A. M., "Primary Prevention of Acute Coronary Events With Lovastatin in Men and Women With Average Cholesterol Levels: Results of AFCAPS/TexCAPS", *JAMA*, 279 (20): 1615–1622 (1998).
- [3] Khosla, S. G., Nysten, E. S., and Khosla, R., "Rhabdomyolysis in Patients Hospitalized With COVID-19 Infection: Five Case Series", *Journal Of Investigative Medicine High Impact Case Reports*, 8: (2020).
- [4] Haroun, M. W., Dieiev, V., Kang, J., Barbi, M., Marashi Nia, S. F., Gabr, M., Eman, G., Kajita, G., and Swedish, K., "Rhabdomyolysis in COVID-19 Patients: A Retrospective Observational Study", *Cureus*, 13 (1): (2021).
- [5] Lee, N., David Hui, M. ., Alan Wu, M. ., Paul Chan, M. D., Peter Cameron, M. ., Gavin M. Joynt, M. ., Anil Ahuja, M. ., Yung, M. Y., and Leung, M. ., "A Major Outbreak of Severe Acute Respiratory Syndrome in Hong Kong", *The New England Journal Of Medicine*, 348: 1986–94 (2003).
- [6] Dashti-Khavidaki, S. and Khalili, H., "Considerations for Statin Therapy in Patients with COVID-19", *Pharmacotherapy*, 40 (5): 484–486 (2020).

- [7] Castiglione, V., Chiriaco, M., Emdin, M., Taddei, S., and Vergaro, G., "Statin therapy in COVID-19 infection", *European Heart Journal - Cardiovascular Pharmacotherapy*, 6 (4): 258–259 (2020).
- [8] Alfirevic, A., Neely, D., Armitage, J., Chinoy, H., Cooper, R. G., Laaksonen, R., Carr, D. F., Bloch, K. M., Fahy, J., Hanson, A., Yue, Q. Y., Wadelius, M., Maitland-Van Der Zee, A. H., Voora, D., Psaty, B. M., Palmer, C. N. A., and Pirmohamed, M., .
- [9] Chan, K. H., Farouji, I., Abu Hanoud, A., and Slim, J., "Weakness and elevated creatinine kinase as the initial presentation of coronavirus disease 2019 (COVID-19)", *American Journal Of Emergency Medicine*, 38 (7): 1548.e1-1548.e3 (2020).
- [10] Suwanwongse, K. and Shabarek, N., "Rhabdomyolysis as a Presentation of 2019 Novel Coronavirus Disease", *Cureus*, 12 (4): (2020).
- [11] Hougaard Christensen, M. M., Bruun Haastrup, M., Øhlenschläger, T., Esbech, P., Arnspang Pedersen, S., Bach Dunvald, A. C., Bjerregaard Stage, T., Pilsgaard Henriksen, D., and Thestrup Pedersen, A. J., .



## Examining the Relationship Between Quality of Life and Physical Activity, Exercise Perception in Middle Adulthood

**Meltem YAZICI GÜLAY** 

*Faculty of Health Sciences, Department of Occupational Therapy, Çankırı Karatekin University, Çankırı, Türkiye*

### Abstract

Adulthood is examined as young, middle and advanced adulthood. Middle adulthood is a period in which the social roles, productivity and coping skills of individuals between the ages of 40-50 are high and their life habits are stereotyped [1,2]. Examining the quality of life, physical activity levels and exercise perceptions of middle-aged individuals will provide important information in the creation of a healthy elderly population [3]. For this purpose, the relationship between middle-aged individuals' quality of life, physical activity levels and exercise perceptions was examined. This study was conducted as a pilot study of a comprehensive study with the participation of 20 people (10 women and 10 men) between the ages of 40-50. Data were collected using personal information form, World Health Organization Quality of Life Scale-Bref Form (WHOQOL-BREF), International Physical Activity Questionnaire short form (IPAQ-SF), Exercise Benefits/Barriers Scale. Spearman Correlation Analysis was used to examine the relationship between WHOQOL-BREF and Exercise Benefits/Barriers scales and IPAQ-SF in data that were not normally distributed. The Mann-Whitney U test was used to determine whether the investigated parameters differed between the genders. First, the general demographic characteristics of the participants included in the study were determined (43.2±10.3 years, 169.9±0.9cm and 69.3±11.9 kg). According to the correlation analysis, it was observed that there was no linear relationship between the physical activity levels of middle-aged individuals and their exercise perceptions and quality of life ( $p>0.05$ ). Similarly, no difference was found between these parameters investigated between male and female individuals ( $p>0.05$ ). The study was conducted with a low sample and individuals who take an active role in daily life and have moderate physical activity. Participants may be physically active due to their life roles, uncorrelated to their perceptions of exercise. Therefore, the results may also be uncorrelated to quality of life.

**Keywords:** *Perception of Exercise, Physical Activity, Middle Adulthood, Quality of Life*

### 1. Introduction

Adulthood has been studied as young, middle and advanced adulthood since the beginning of the twentieth century. Young adulthood between the ages of 20-30, middle adulthood between the ages of 40-50 and the ages of 50 and above are called advanced adulthood [1,2]. Middle age period; It refers to a stage in which the social roles, productivity and coping skills of individuals are high, and their life habits become stereotyped, and it constitutes the pre-old age period [3]. It is known that many chronic diseases and quality of life in old age are related to lifestyle in youth and adulthood [4, 5]. For healthy aging, it is important to prevent the development of chronic diseases, to establish and maintain a healthy lifestyle [5]. Today, the world population is aging due to the prolongation of life expectancy and the decrease in birth rates. It is reported that especially developing countries will be more affected by this situation [6]. While the total population growth rate in Turkey was 13.7‰ in 2013, the increase rate of the elderly population is approximately 3 times (‰36.2) of this (TÜİK 2014). it is predicted that the elderly population will increase by 201% [7]. For this reason, in our country, the State Planning Organization, the Ministry of Family, Labor and Social Services, the Ministry of Health and many institutions and organizations have carried out studies on healthy and active aging, elderly health and care [8-10]. Today, researches are carried out in different fields to determine the needs related to aging and to carry out supportive studies. The quality of life of individuals can be increased by adopting regular physical activities and an active lifestyle. According to national and international public health recommendations, regular physical activities for all age groups should be at least 30 minutes every day of the week or several days of the week. should be planned at a moderate level [11]. In this study, it is aimed to obtain information that will contribute to

\* Corresponding author. e-mail address: meltemyazici@karatekin.edu.tr

this process by investigating the quality of life, physical activity levels and exercise perceptions of middle-aged individuals before the old age period.

## 2. Materials and Methods

### 2.1. Assessments

**2.1.1. Personal Information Form:** Height and weight information of individuals were recorded and Body Mass Index (BMI) was calculated. Job statuses are recorded.

**2.1.2. World Health Organization Quality of Life Questionnaire Short Form (WHOQOL-BREF):** It was developed by the World Health Organization (WHO) to measure the health-related quality of life of individuals between the ages of 18-65 [12]. Its Turkish validity and reliability were demonstrated by Eser et al. [13]. The WHOQOL-BREF scale is the abbreviated form of the scale consisting of 100 questions. The scale consists of 4 domains: physical, psychological, social relations and environmental domains. Each section was calculated out of 100 points.

**2.1.3. International Physical Activity Questionnaire short form (IPAQ-SF):** Craig et al. (2003) to determine the physical activity levels of participants between the ages of 15-65 [14]. The Turkish validity and reliability study of the scale was carried out by Öztürk (2005) [15]. MET values were calculated in the evaluation of all activities. Physical activity levels are classified as physically inactive (<600 MET-min/week), low physical activity level (600–3000 MET-min/week), and adequate physical activity level (> 3000 MET-min/week) [14].

**2.1.4. Exercise Benefits/Barriers Scale (EBBS):** The EBBS was applied to identify exercise-related barriers and facilitators for individuals' perceptions of exercise [16]. This scale composed of a 14-item barrier scale and a 29-item benefit scale. The lowest score of the benefits scale is 29 while the highest score is 116. A high score indicates positive exercise perception. The score range of the barriers scale is between 14 and 56 points. High scores from the barriers scale indicate that individuals have perceived barriers to exercise [16].

**Statistically Analysis:** Descriptive analyses were performed using mean Standard deviation and median-quartiles for non-normally distributed continuous variables. Spearman Correlation Analysis was used to examine the relationship between WHOQOL-BREF and Exercise Benefits/Barriers scales and IPAQ-SF in data that were not normally distributed. The Mann-Whitney U test was used to determine whether the investigated parameters differed between the genders.

## 3. Results and Discussion

It was found that the mean age of the individuals was  $43.2 \pm 10.3$ , and the BMI was within the normal range ( $24.03 \pm 3.61$ ). In general, it was found that the quality of life of the individuals was moderate ( $52.50 \pm 16.52$ ), their physical activity levels were high ( $5739.05 \pm 9776.25$ ), and their Positive Exercise perceptions ( $92.00 \pm 13.84$ ) were found to be at moderate levels. The results are shown in Table 1.

**Table 1.** Descriptive Analysis

Parametres	M	IQR(25-75)	X $\pm$ SD
Age (years)	45.00	40 - 48	43.2 $\pm$ 10.3
BMI (kg/m <sup>2</sup> )	23.52	21.32 - 26.09	24.03 $\pm$ 3.61
WHOQOL BREF	50	40 - 71	52,50 $\pm$ 16.52
IPAQ-SF	2209.50	1311- 4858	5739.05 $\pm$ 9776.25
EBBS-Barrier	32	29 - 35	32.22 $\pm$ 5.44
EBBS-Benefit	62	55 - 67	60.31 $\pm$ 11.06
EBBS Total Score	97	76-105	92,00 $\pm$ 13,84

X = Mean, SD = Standard Deviation, M = Median, IQR = Interquartile Range, BMI = Body Mass Index, WHOQOL-BREF= World Health Organization Quality of Life Questionnaire Short Form, IPAQ-SF=International Physical Activity Questionnaire short form, EBBS= Exercise Benefits/Barriers Scale.



The relationships between the evaluation parameters are shown in Table 2. No correlation was found between general evaluation parameters ( $p>0.005$ ). There was only a relationship between EBSS Total Score and the subgroups of the scale ( $p=0.036$ ,  $p<0.001$ ; respectively).

**Table 2.** Examining the relationships between variables

Assesments		WHOQOL BREF	IPAQ-SF	EBBS- Barrier	EBBS- Benefit	EBSS Total Score
BMI (kg/m <sup>2</sup> )	r	.028	.195	.244	-.037	-.155
	p	.907	.409	.315	.880	.528
WHOQOL BREF	r		-.003	-.124	.109	.243
	p		.989	.612	.656	.316
IPAQ-SF	r			.436	-.075	.206
	p			.062	.760	.397
EBBS-Barrier	r				.032	.484*
	p				.897	<b>.036</b>
EBBS-Benefit	r					.786**
	p					<b>.000</b>

$p<0.05$ ; X = Mean, SD = Standard Deviation, M = Median, IQR = Interquartile Range, BMI = Body Mass Index, WHOQOL-BREF= World Health Organization Quality of Life Questionnaire Short Form, IPAQ-SF=International Physical Activity Questionnaire short form, EBBS= Exercise Benefits/Barriers Scale.

The comparison of the evaluation parameters by gender is shown in Table 3. According to Table 3, no difference was found between men and women in terms of quality of life, physical activity level, and exercise perception ( $p>0.05$ ).

**Table 3.** Comparison of assessments by gender

Assesments	Women		Men		Mann Whitney U
	<b>M, IQR (25-75)</b>	<b>X±SD</b>	<b>M, IQR (25-75)</b>	<b>X±SD</b>	p
WHOQOL BREF	50, (37.50-56.25)	48.75±18.11	50, (46.87-75.00)	56.25±14.73	.377
IPAQ-SF	1818, (1080-2883)	2098.90±1422.41	2971.50, (1876-13205)	9379±13049	.131
EBBS-Barrier	32, (26,75-35.50)	32.00±7.11	32, (30-36)	32.44±3.09	.712
EBBS-Benefit	57, (49-67)	56.80±14.11	65, (60-67)	64.22±4.32	.119
EBBS Total Score	89, (77,75-100.50)	87.80±17.33	96 , (91-103)	96.66±6.80	.220

$p<0.05$ ; X = Mean, SD = Standard Deviation, M = Median, IQR = Interquartile Range, BMI = Body Mass Index, WHOQOL-BREF= World Health Organization Quality of Life Questionnaire Short Form, IPAQ-SF=International Physical Activity Questionnaire short form, EBBS= Exercise Benefits/Barriers Scale.

According to the research results of the Turkish Statistical Institute (TUIK, 2014), it is seen that 27.8% (73.2%) of the individuals in the 31-50 age group do not exercise [18]. To see the protective and improving effect of physical activity on health, together with daily activities; It is possible with planned, repetitive and regular physical activity. This type of physical activity can also be called exercise [19,20]. At least 150 minutes of moderate-intensity exercise per week is recommended for every adult individual. It is preferred that these exercises consist of endurance activities such as walking, jogging, cycling or swimming that involve large muscle masses, each exercise session should be at least 10 minutes and spread over at least 3-5 days a week [4,19]. The physical activity level of the study sample is over 3000 METs, which indicates that the individuals in the sample are active. Of the individuals in the study, 10 men and 4 women are active professionals. 6

Women do not have a profession, but it is seen that all individuals have an active lifestyle during the day. The fact that the physical activity levels of the individuals in our study were different from the TUIK data may be related to the weak universe representation of our study group. At the same time, the period between the ages of 40-50 is a narrow age range in which the psychological, social and physical health levels of individuals are high. Examining the research in different age ranges is important in terms of revealing different results. The small sample size of the study is the most important limitation of the study, which also affects the research results.

Regular physical activities are effective in developing and maintaining a person's physical, mental, intellectual, social and environmental well-being. Regular physical activity is the most effective and cheapest medicine for prevention of heart diseases, obesity, high blood pressure, diabetes, osteoporosis and some types of cancer. Physical activity increases the quality of life by making the person feel more energetic, more lively, active and peaceful [20,21]. Therefore, in our study, the relationships between quality of life and physical activity levels were investigated. In order to examine the subject in more detail and to reveal the results related to healthy aging, making these evaluations in the young old and middle-aged processes may reveal important results. The most important reason for the lack of a relationship between the evaluation parameters may be the low sample size.

There are studies showing that men have higher quality of life and physical activity levels [22]. This situation can be associated with physical activity levels in some studies. In this study, however, no difference was found between the physical activity levels of women and men, and similarly, the lack of difference between their quality of life and exercise perceptions suggests that this may be due to the fact that the sample was made between male and female individuals with similar life habits.

The establishment of a healthy aging process and the development of healthy life behaviors are important for healthy aging and old age. Improving the level of physical activity is a priority among health policies and one of the approaches known to be effective in the prevention and control of chronic diseases [22, 23]. For this reason, research on lifestyle, physical activity and quality of life in old age and pre-senile is important issues. Based on what this preliminary study showed, the next basic study will be planned by keeping the sample age range wider and examining the lifestyles.

## Acknowledgement

This study is the preliminary study of a comprehensive research comparing the processes of adulthood and old age. It does not receive any financial support.

## References

- [1] Santrock, J. W. (2010). *Life-Span Development*, 13th ed. McGraw-Hill.
- [2] Boyd, D. Bee, H. (2014). *Lifespan development*. 7 th ed. Pearson
- [3] Ulusoy-Özcan, Y. (2020). Investigation of the perceptions of middle age people on their age periods. *Electronic Journal of Social Sciences*, 19(74), 587-601.
- [4] Zhang S, Wei C, Harada K, Ueda K, Fukumoto K, Matsuo H, Minamoto K, Nishikawa T, Araki E, Ueda A (2013) Relationship between lifestyle and lifestyle-related factors in a rural–urban population of Japan. *Environmental health and preventive medicine* 18:267–274
- [5] Zheng X, Xue Y, Dong F, Shi L, Xiao S, Zhang J, Xue B, Qian Y, Zhu H, Man Q, Zhang C (2022) The association between health-promoting-lifestyles, and socioeconomic, family relationships, social support, health-related quality of life among older adults in china: a cross sectional study. *Health and Quality of Life Outcomes* 20
- [6] Samancı-Tekin, Ç, Kara F. (2018) Dünyada ve Türkiye’de Yaşlılık. *Journal of International Scientific Researches* 3:219–229 . doi: 10.21733/ibad.370584.
- [7] Kinsella K, He W (2009) US Census Bureau, international population reports. Washington, DC: US Census Bureau.
- [8] Devlet Planlama Teşkilatı (2007-2013), Dokuzuncu Kalkınma Planı (2007). pp. 10-11.
- [9] T.C. Aile, Çalışma ve Sosyal Hizmetler Bakanlığı, 2019-23 Stratejik Plan. (2019), p. 2-6, acshb\_2019-2023-

stratejik-plan.pdf

- [10] Kalkınma Bakanlığı (2019). Yaşlanma özel ihtisas komisyonu raporu. On Birinci Kalkınma Planı (2019-2023). pp. 167-168 Ankara.
- [11] The World Health Report 2010
- [12] Group W (1998) Development of the World Health Organization WHOQOL-BREF quality of life assessment. *Psychological medicine* 28:551–558
- [13] Eser E, Aydemir Ö, Cengiz Özyurt B, Akar A, Deveci, Serol; Eser S, Ayık C (2018) Psychometric Properties of the Turkish Version of the World Health Organization Quality of Life Instrument for People with Intellectual and Physical Disabilities (WHOQOL-DIS-TR). *Türk Psikiyatri Dergisi* 29:
- [14] Craig CL, Marshall AL, Sjöström M, Bauman AE, Booth ML, Ainsworth BE, Pratt M, Ekelund U, Yngve A, Sallis JF, Oja P (2003) International physical activity questionnaire: 12-country reliability and validity. *Medicine and science in sports and exercise* 35:1381–1395 . doi: 10.1249/01.MSS.0000078924.61453.FB
- [15] Öztürk, M. The Validity and Reliability of the International Physical Activity Questionnaire and Determination of Physical Activity Levels in University Education Students. Master Thesis. Hacettepe University Institute of Health Sciences, Ankara, 2005.
- [16] Sechrist KR, Walker SN, Pender NJ (1987) Development and psychometric evaluation of the exercise benefits/barriers scale. *Res Nurs Health* 10(6):357–365.
- [17] Ortabag, T., Ceylan, T., Akyuz, A., Bebis H. (2010) The validity and reliability of the exercise benefits / barriers scale for turkish military nursing students. *Military G, Academy.* 32:55–70
- [18] TÜİK., (2014), *Türkiye İstatistik Kurumu, İstatistiklerle Yaşlılar, 2013*, Sayı: 16057 <https://data.tuik.gov.tr/Bulten/Index?p=İstatistiklerle-Yaşlılar-2014-18620>
- [19] T.C. Sağlık Bakanlığı, Türkiye Halk Sağlığı Kurumu (2014) Türkiye Fiziksel Aktivite Rehberi
- [20] Zheng X, Xue Y, Dong F, Shi L, Xiao S, Zhang J, Xue B, Qian Y, Zhu H, Man Q, Zhang C (2022) The association between health-promoting-lifestyles, and socioeconomic, family relationships, social support, health-related quality of life among older adults in china: a cross sectional study. *Health and Quality of Life Outcomes* 20:1–8 . doi: 10.1186/s12955-022-01968-0
- [21] Izquierdo M, Duque G, Morley JE (2021) Physical activity guidelines for older people: knowledge gaps and future directions. *The Lancet Healthy Longevity* 2:e380–e383
- [22] Rejeski WJ, Focht BC (2002) Aging and physical disability: on integrating group and individual counseling with the promotion of physical activity. *Exercise and sport sciences reviews* 30:166–170
- [23] Genç A, Şener Ü, Karabacak H, Üçok K (2011) Kadın ve Erkek Genç Erişkinler Arasında Fiziksel Aktivite ve Yaşam Kalitesi Farklılıklarının Araştırılması. *Kocatepe Tıp Dergisi* 3:145–150.



# Electrochemical Detection of Dopamine Using a Simple Redox Cycling-Based Device

**Mustafa SEN**<sup>1</sup> 

<sup>1</sup>Faculty of Engineering and Architecture, Department of Biomedical Engineering, Izmir Kâtip Çelebi University, İzmir, Turkey

## Abstract

Here, a dual ITO microchip was fabricated for highly sensitive detection of dopamine (DA) based on redox-cycling. The ITO electrodes with 3×3 mm working areas were made via photolithography and dry etching processes. The microchip was obtained by first aligning the working areas of two ITO electrodes to overlap and then fixing them in that position using a double-sided tape, which also formed a sealed microchannel between the ITO electrodes for test solution delivery. The ITO electrodes and microchips were electrochemically characterized using EIS, cyclic voltammetry and chronoamperometry. Compared to a single ITO electrode in a microchannel, the microchip had a significantly higher signal due to redox cycling. The microchip was lastly used for the detection of DA at varying concentrations. According to the results, the microchip had an LOD of 0.15 µM in a linear detection region of 0.1 to 50 µM. The microchip requires less than 1 µl of solution to complete the analysis and has great potential to be applied for immunosensing.

**Keywords:** Redox-cycling, Dopamine, ITO microchip, Electrochemical measurement, Microfabrication

## 1. Introduction

Dopamine (DA) is a neurotransmitter that plays an important role in the cardiovascular and central nervous systems. Therefore, high DA levels indicate cardiotoxicity leading to rapid heartbeat, hypertension and heart failure. On the contrary, low DA levels in the central nervous system are seen as the main cause of various neurological diseases such as Parkinson's disease, schizophrenia, Alzheimer's disease, stress and depression [1]. Therefore, it is clear that DA measurements are necessary to understand its biological functions and related biological processes/mechanisms. Currently, there is a growing interest in developing specific and low-cost biosensors that take advantage of the ease with which DA is oxidized on an electrode surface. In addition, the biosensors should be able to provide a sensitive response in the appropriate concentration range (0.01–1 µM for a healthy individual and in the nanomolar range for patients with Parkinson's disease) [2]. In this study, sensitive detection of DA was performed with a dual ITO microchip that can amplify the signal based on redox cycling. The 3×3 mm working areas of two ITO microchips were designed to overlap with the help of double-sided tape, and a dual ITO microchip was created with a microchannel. The applicability of the dual ITO microchip as a biosensor was analyzed using different concentrations of DA solution.

## 2. Materials and Methods

### 2.1. Apparatus

DA hydrochloride (SigmaAldrich, USA), phosphate buffered saline (PBS - 0.01 M phosphate buffer, 0.0027 M KCl and 0.137 M NaCl, pH 7.4 at 25 °C), potassium ferricyanide (K<sub>3</sub>Fe(CN)<sub>6</sub>) (Sigma-Aldrich, USA), potassium ferrocyanide (K<sub>4</sub>Fe(CN)<sub>6</sub>) (Sigma-Aldrich, USA), ferrocenemethanol (FcCH<sub>2</sub>OH) (Sigma-Aldrich, USA), Multi-potentiostat (µStat-i 400 (Bi)potentiostat/Galvanostat/Impedance Analyzer (EIS), DropSens Metrohm, Switzerland)

### 2.2. ITO microfabrication

Microchips were produced from indium tin oxide (ITO) films using the “ion-beam etching” process. Firstly, the surfaces of ITO coated glass substrates (slides) were cleaned with the help of distilled water and acetone. Next, cleaned ITO-coated glasses were placed in the “Spin-Coater” device and coated with “AZ5214E” (MicroChemicals, Germany) positive/reversal photoresist to cover the entire surface. The coating process was

\* Corresponding author. e-mail address: mustafa.sen@ikcu.edu.tr

carried out at 2000 rpm for 60 s. Afterwards, the slides covered with photoresist were kept in an oven set at 90 °C for 30 minutes to ensure the polymerization (pre-baking) of the photoresist. A lithography mask with the desired design was used to transfer the patterns to the microchip. Briefly, the patterns on the mask were exposed to UV light via a UV mask aligner and transferred onto photoresist-coated slides [3]. An alkaline developer was used to remove the areas exposed to UV light. Afterward, etching process was carried out with the help of "ion beam etching" device with 30 sccm Argon gas for 1 hour using the parameters 750 V, 49 W, 0.05 A and the sample holder was rotated at an angle of 22.5°.

### 2.3. Electrochemical characterization with electrochemical impedance spectroscopy (EIS)

EIS measurements of ITO microchip were performed in 50 mM  $[\text{Fe}(\text{CN})_6]^{3-/4-}$  + 0.1 M KCl solution. Impedance spectra were recorded at open circuit potential with a 10 mV amplitude signal in the frequency range of 10 Hz to 10 kHz [4,5].  $R_{ct}$  values were calculated with fit and simulation option in AUTOLAB 302 Nova 2.1.5 software using Randles circuit model.

### 2.4. Redox-cycling

The 3×3 mm working areas of two ITO microchips were aligned to overlap and then fixed using a double-sided tape to form a sealed microchannel. Electrochemical characterization of the dual ITO microchip was carried out using cyclic voltammetry (CV) and chronoamperometry. Briefly, the microchannel was first filled with 200 μM DA and 0.1 mM  $\text{FcCH}_2\text{OH}$ , respectively [6]. Then the generator electrode was scanned from 0 V to +0.35 V (vs. Ag/AgCl) at a scanning rate of 0.05 V/s, while the collector electrode was fixed at 0 V (vs. Ag/AgCl) in a dual mode measurement where redox cycling was induced. The applicability of the dual ITO microchip was demonstrated with DA solutions at different concentrations (0, 0.01, 0.05, 0.1, 0.5, 1, 10, 50, 100 μM). Basically, the generator and collector electrodes were set at +0.35 V and 0 V (vs. Ag/AgCl) for 50 s and the oxidation and reduction currents at 50 s were used to obtain a calibration curve. The limit of detection (LOD) was calculated based on three replicates using the following equation:  $\text{LOD} = 3.3 \times (\text{standard deviation of the calibration curve/slope of the calibration curve})$ [7,8]. All electrochemical experiments were performed using a multi-potentiostat.

## 3. Results and Discussion

### 3.1. Electrochemical characterization

Using the proposed fabrication method, the 3×3 mm working areas of two ITO microchips were successfully and correctly overlapped using a double-sided tape and a microchannel was formed for test solution delivery. In other words, the fabrication of a dual ITO microchip was realized using a simple fabrication procedure without using laborious and precise alignment processes. The electrochemical behavior of a single ITO was analyzed by CV using 0.1 mM  $\text{FcCH}_2\text{OH}$  and 200 μM DA, as shown in Figure 1a-b. The CV curves as expected confirmed the electrochemical detection of  $\text{FcCH}_2\text{OH}$  and DA. As can be seen in the Nyquist plot of ITO, the  $R_{ct}$  value was measured to be 590 Ω (Figure 1c).

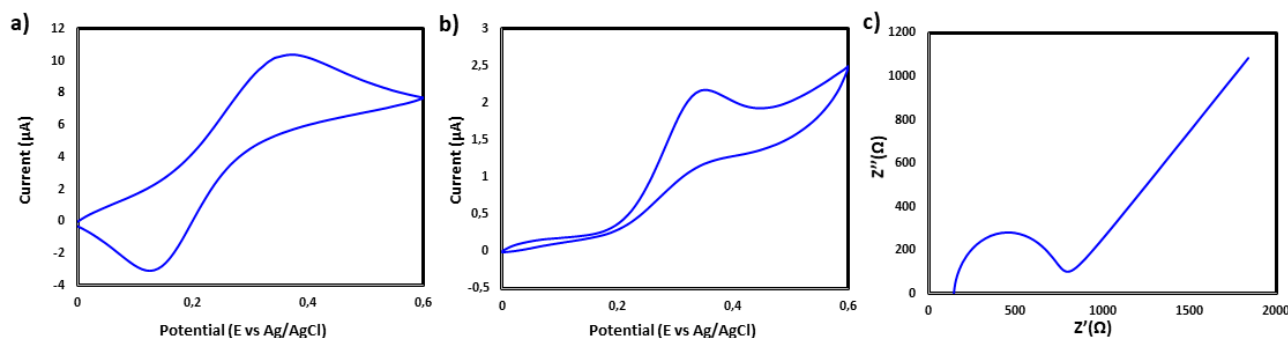


**Figure 1.** CV curves of bare ITO recorded in 0.1 mM  $\text{FcCH}_2\text{OH}$  (a) CV curves of bare ITO recorded in 200 μM DA (b) EIS curves of bare SPCE (c)

In dual-mode chronoamperometry, redox-cycling capacity of a dual ITO microchip was studied by first setting the potential of both the generator and collector electrodes first at +0.35V (vs. Ag/AgCl) and then +0.35 and 0 V (vs. Ag/AgCl), respectively (Figure 2a). When the two electrodes were set at +0.35V (vs. Ag/AgCl), both electrodes oxidize and consume FcCH<sub>2</sub>OH in the microchannel, resulting a low current (0.08  $\mu$ A). However, when the generator and collectors were set at +0.35 and 0 V (vs. Ag/AgCl), respectively, the generator electrode oxidizes FcCH<sub>2</sub>OH to FcCH<sub>2</sub>OH<sup>+</sup> which is then reduced back to FcCH<sub>2</sub>OH by the collector electrode. Thus, a redox-cycling is induced, resulting a much higher current (3.1  $\mu$ A). Figure 2b shows the behavior of dual-mode CV curves at different scanning rates in 0.1 mM FcCH<sub>2</sub>OH.

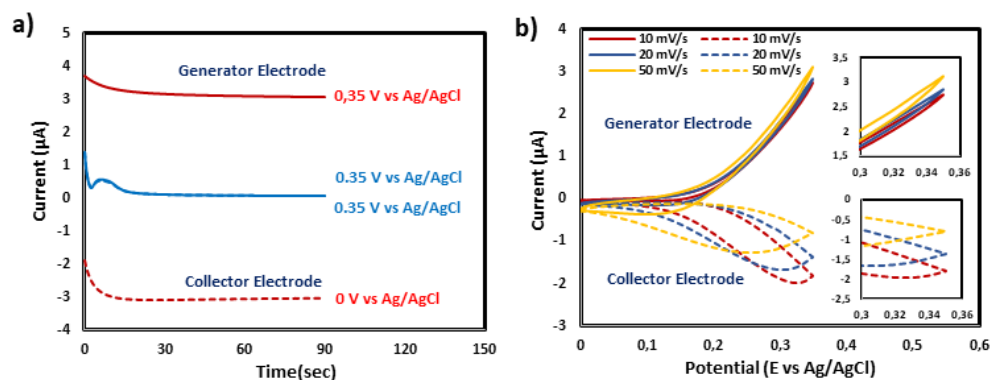


**Figure 2.** Dual mode chronoamperometry from dual ITO in 0.1 mM FcCH<sub>2</sub>OH at different potential (a) dual mode cyclic voltammograms from dual ITO in 0.1 mM FcCH<sub>2</sub>OH at different scan rates (b).

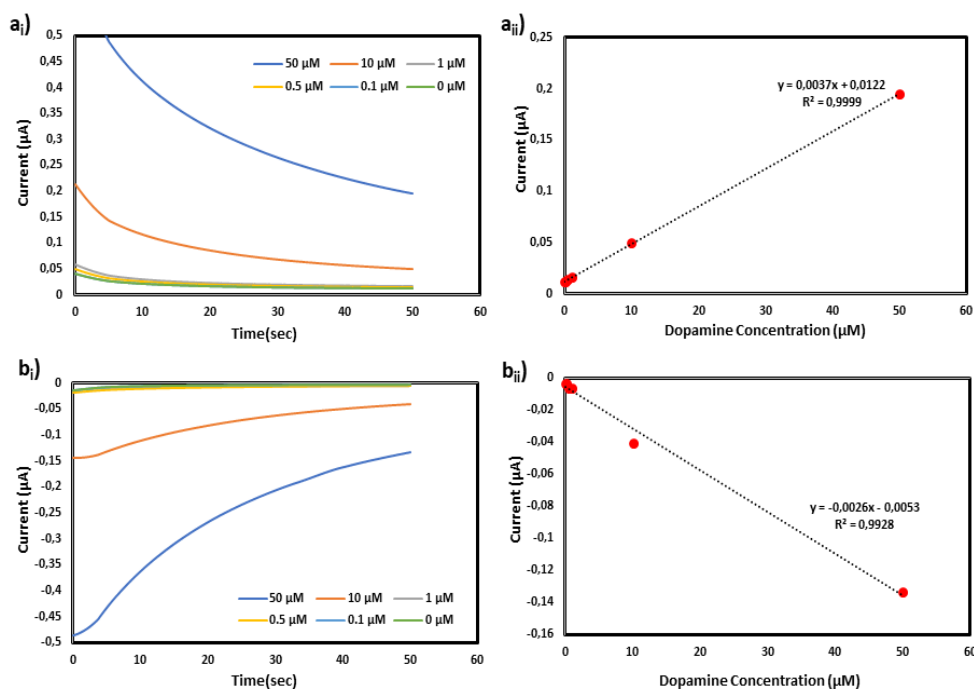


**Figure 3.** Chronoamperometric curves obtained in PBS with varying concentration of DA (0, 0.1, 0.5, 1, 10 and 50  $\mu$ M) oxidation curve (a<sub>i</sub>) reduction curve (b<sub>i</sub>) and a calibration curve obtained based on the last oxidation current (a<sub>ii</sub>) and a calibration curve obtained based on the last reduction current (b<sub>ii</sub>).

### 3.2. Electrochemical detection of DA

The performance of the dual ITO microchip for the detection of DA was evaluated in dual mode. Basically, the potentials of generator and collector electrodes were set at +0.35 and 0 V (vs. Ag/AgCl), respectively, as described above. As the DA is oxidized to DA quinone (DAQ) by the generator electrode, DAQ then diffuses to the collector electrode surface where it is reduced back to DA, resulting signal amplification and a higher current. Figure a<sub>i</sub>-b<sub>i</sub> show the oxidation and reduction-based chronoamperometric responses obtained in DA solutions at varying concentrations, respectively. In both cases, the currents at 120s were used to obtain calibration curves

(Figure a<sub>ii</sub>-b<sub>ii</sub>). The both calibration curves had an  $R^2$  value greater than 0.99. The LOD values for the generator and collector electrodes were calculated to be 0.15 and 1.46  $\mu\text{M}$ , respectively. The microchip requires less than 1  $\mu\text{l}$  of solution for analysis and can be applied for immunosensing with enzymes producing molecules that can be electrochemically cycled between two electrodes.

## Acknowledgment

This research was supported by the scientific research projects coordination unit of Izmir Katip Celebi University (Project Nos. 2022-ÖDL-MÜMF-0007 and 2021-GAP-MÜMF-0055).

## References

- [1] Klein, M. O., Battagello, D. S., Cardoso, A. R., Hauser, D. N., Bittencourt, J. C., & Correa, R. G. (2019). Dopamine: functions, signaling, and association with neurological diseases. *Cellular and Molecular Neurobiology*, 39, 31–59.
- [2] Lakard, S., Pavel, I. A., & Lakard, B. (2021). Electrochemical biosensing of dopamine neurotransmitter: A review. *Biosensors*, 11, 179.
- [3] Şen, M., Ino, K., Ramón-Azcón, J., Shiku, H., & Matsue, T. (2013). Cell pairing using a dielectrophoresis-based device with interdigitated array electrodes. *Lab on a Chip*, 13, 3650-3652.
- [4] Seven, F., Gölce, T., & Şen, M. (2020). Nanoporous carbon-fiber microelectrodes for sensitive detection of  $\text{H}_2\text{O}_2$  and dopamine. *Journal of Electroanalytical Chemistry*, 864, 114104.
- [5] Şen, M. (2019). Using electropolymerization-based doping for the electroaddressable functionalization of a multi-electrode array probe for nucleic acid detection. *Analytical Sciences*, 35, 565–569.
- [6] Şen, M., Ino, K., Shiku, H. & Matsue, T. (2012). Accumulation and detection of secreted proteins from single cells for reporter gene assays using a local redox cycling-based electrochemical (LRC-EC) chip device. *Lab on a Chip*, 12, 4328-4335.
- [7] Mercan, Ö. B., Kılıç, V., & Şen, M. (2021). Machine learning-based colorimetric determination of glucose in artificial saliva with different reagents using a smartphone coupled  $\mu\text{PAD}$ . *Sensors and Actuators B: Chemical*, 329, 129037.
- [8] Şen, M., Azizi, E., Avcı, İ., Aykaç, A., Ensarioğlu, K., Ok, İ., Yavuz, G. F., & Güneş, F. (2022). Screen printed carbon electrodes modified with 3D nanostructured materials for bioanalysis. *Electroanalysis*, 34, 1-10.





## The Investigation of The Inhibitory Potentials of Some Polyphenols for Acetylcholinesterase Activity

Alyaa Sabri AL-MAMOORI<sup>1</sup> , Şevki ADEM<sup>1\*</sup>

<sup>1</sup> Graduate School of Natural and Applied Sciences, Department of Chemistry, Çankırı Karatekin University, Çankırı, Türkiye

### Abstract

This investigation primarily focuses on the AChE enzyme. In many cholinergic pathways, acetylcholinesterase is used in the central and peripheral nervous systems to quickly hydrolyze the neurotransmitter acetylcholine to stop impulse transmission. Accumulation of acetylcholine, excessive stimulation of nicotinic and muscarinic receptors, and trouble with neurotransmission are all effects of enzyme inactivation. Acetylcholinesterase inhibitors are used as appropriate medications and toxins because they interact with the enzyme as their primary target. Therefore, investigating the potential of polyphenols to prevent AChE was the primary aim of this research. Molecular docking studies were performed and 3 compounds were tested to determine their inhibition potential against the cholinesterase (AChE) enzyme. Results from in vitro and in silico experiments suggested that the compounds could function as AChE inhibitors. "(2R,3S)-3,5,7-tris(benzyloxy)-2-(3,4-bis(benzyloxy)phenyl) chromane" compound showed adequate drug-like properties and potent inhibitory properties against the enzyme, with IC<sub>50</sub> values of 13.59 µM, "(E)-3,5-bis(benzyloxy)-2-(3-(3,4,5-tris(benzyloxy)phenyl)allyl)phenol" compound exhibited inhibitory activity against the enzyme as well, with IC<sub>50</sub> values of 15.07 µM and "(2R,3S)-5,7-bis(benzyloxy)-2-(3,4,5-tris(benzyloxy)phenyl)chroman-3-ol" compound with IC<sub>50</sub> values of 15.75 µM, the substance exhibited inhibitory properties against the enzyme. Additionally, the Swissadem and pkCSM web servers scanned all compounds' predictive qualities for drug similarity using ADMET estimations, where the molecules' theoretically calculated properties and the absorption, distribution, metabolism, and elimination were all calculated. The three compounds mentioned above-demonstrated no-toxicity potential (AMES toxicity). The data metal complexes did not exhibit ADMET properties, which could cause serious adverse effects in humans.

**Keywords:** Acetylcholinesterase, Metal Complex, Molecular docking, ADMET, Alzheimer's

### 1. Introduction

A class of medications known as cholinesterase inhibitors increases the amount and duration of ACh in the CNS and PNS by preventing the conversion of acetate and choline from acetylcholine (ACh). The uses of acetylcholinesterase inhibitors are numerous. Treatment for neurological diseases such as Alzheimer's, Parkinson's, and Lewy body dementia is where they are most frequently used. ACh-producing cells are destroyed by a number of the physiological mechanisms underlying these degenerative diseases, which also decrease cholinergic transmission in various brain regions. ChEIs inhibitors reduce the rate of ACh breakdown and thereby maintain the ACh level by inhibiting AChE activity [1]. A cholinergic enzyme known as AChE is mainly in muscles and nerves and detected in postsynaptic neuromuscular junctions. Acetylcholine (ACh), a naturally occurring neurotransmitter, is rapidly hydrolyzed or degraded into choline and acetic acid [3]. The main function of AChE is to halt synaptic transmission and signalling, which stops ACh from spreading and activating nearby receptors. AChE, an essential component of pesticides and nerve agents, is inhibited by organophosphates. Because of their numerous uses, including anticonvulsant, centigrade, antioxidant, antifungal, anticancer, anti-inflammatory activity and corrosion inhibition, Schiff base metal complexes have drawn received a lot of attention recently. In coordination chemistry, the azomethine functional group (C=N) is a significant donor. The well-studied class of coordination chemistry known as Schiff bases-complexes, which have a distinctive configuration, structural variability, and sensitivity to molecular environments, is derived from substituted salicylaldehydes and various aromatic amines. Interesting biological activities are exhibited by Schiff base complexes with primary amines produced from salicylaldehydes and their components that include the N2O, N2S, NO2, or NOS donor sets [6]. AChE inhibitors have shown clinical success in treating Alzheimer's disease.

\* Corresponding author. e-mail address: sevkiadem@karatekin.edu.tr



Due to a number of issues with the currently available medications, novel cholinesterase inhibitors must be developed. Characteristics of the Schiff base and its Pt (II) and Pd (II) complexes for the pancreatic cholesterol esterase (CEase) and (AChE/BChE) enzymes using the Molegro Virtual Docker software [4]. In the present study, we look into possible metal ion complexes that could inhibit AChE and use molecular docking to look into the interactions that different compounds listed in Protein Data Bank (PDB), a collection of inhibitor derivatives with the highest affinity, had when inhibiting AChE. This is among the most widely used computational methods in medication development using the structure [5]. To find the most effective AChE inhibitors, a computational model for predicting Absorption, Distribution, Metabolism, Excretion, and Toxicity (ADME/Tox) is being developed. These actions might aid in the creation of more potent disease treatments. Alzheimer's medication [2].

## 2. Materials and Methods

The solutions that were used, by dissolving 0.6057 g (5 mmol) of tris in 90 mL of distilled water, 1 M Tris-HCl (pH = 8.0) was created. The pH was raised to 8.0 using an HCl solution. After that, water was added to bring the entire capacity to 50 mL. Also 15 mM ATChI: 14 mg of ATChI was obtained, then dissolved with water. Water was added to the volume to make it 5 mL. In addition 6 mM "5, 5'-ditiyobis-(2- nitro- benzoic acid)" DTNB Solution: 11.2 mg of "5,5'-ditiyobis-(2- nitro- benzoic acid)" was obtained, then dissolved with water. Water was added to the volume to make it 5 mL. In order to create stock solutions for inhibitors, the substances were dissolved in the DMSO at a 1 mg/mL concentration. The solutions used for activity measurement. Table 1 provides a list of the elements used to measure activity.

**Table 1.** Measurement of AChE enzyme activity procedure

Matter	Control Cuvette	Sample Cuvette
Stock Solution	Volume (μL)	Volume( μL)
Tris-HCl (1 M)	50	50
5,5'-ditiyobis-(2- nitro- benzoic acid) (DTNB)	60	60
Distilled water	100	100
Sample of enzyme	10	10
For ten minutes, incubation		
ATChI	25	25

The main hydrolase acetylcholinesterase was used in this study. Molegro Virtual Docker Tools were used to prepare human AChE's crystal structure PDB (ID): 4EY7, which were found in the Protein Data Bank (PDB) in a PDB file format, It is a centralized global database of knowledge about the three-dimensional (3D) structures of big biological compounds, such as proteins and nucleic acids (<https://www.rcsb.org/structure/4EY7>) and prepared for molecular docking. The docking area was chosen at X: -13.97, Y: -43.97, Z: 27.83 coordination centre and an area of 15 Å for docking. For each ligand, the programme was set to make 10 docking attempts and energy minimization. Using "BIOVIA Discovery Studio Visualizer v20.1.0.19295 (DSV, 2020)", the search space was assigned for the required molecular docking.

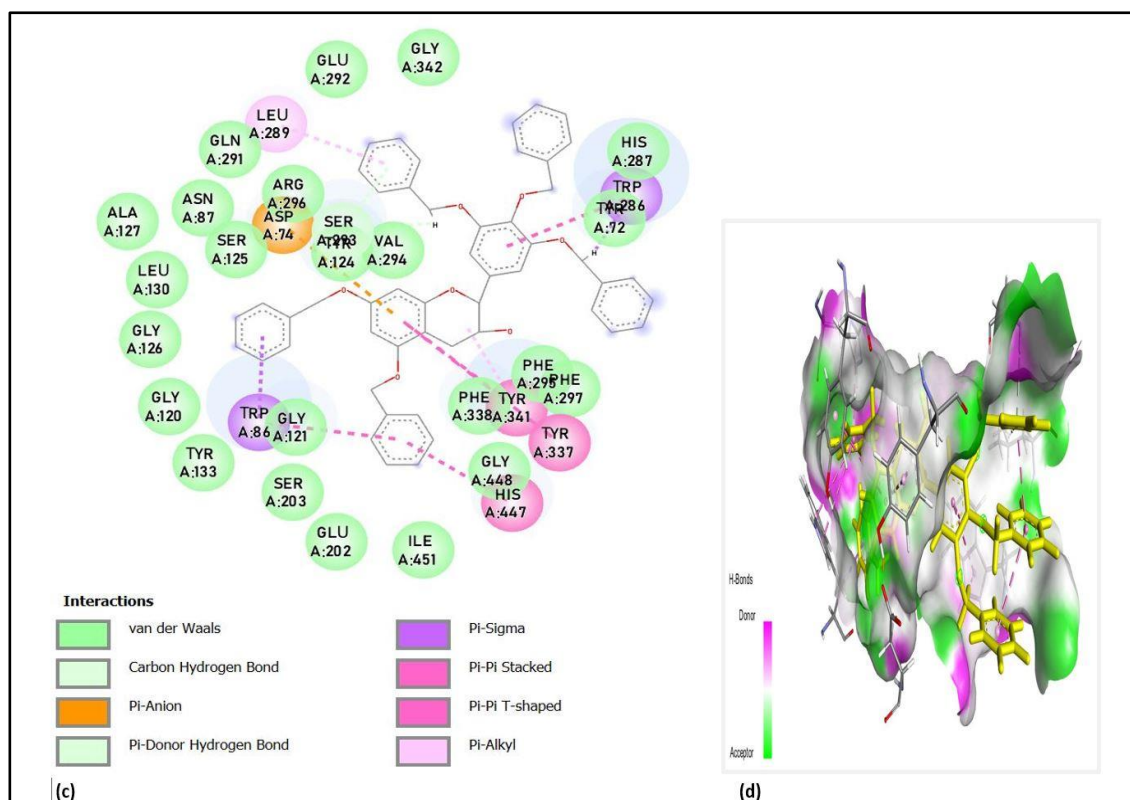
## 3. Results and Discussion

Results from in vitro and in silico experiments suggested that the compounds could function as AChE inhibitors. (+) Pentabenzylated catechin "(2R,3S)-3,5,7-tris(benzyloxy)-2-(3,4-bis(benzyloxy)phenyl)chromane" compound, IA – 123"(E)-3,5-bis(benzyloxy)-2-(3-(3,4,5-tris(benzyloxy)phenyl)allyl)phenol" compound, IA–169–2"(2R,3S)-5,7-bis(benzyloxy)-2-(3,4,5tris(benzyloxy)phenyl)chroman-3-ol" compound, Table 2 displays the in silico and in vitro outcomes.

**Table 2.** Compounds' effects on the activity of the AChE enzyme

Ligand	IC <sub>50</sub> values	MolDock Score	Rerank Score	Interaction	HBond
IA – 169 - 2	15.75	-242.963	-167.862	-263.686	0
(+) Pentabenzylated catechin	13.59	-220.272	45.7092	-247.543	-1.27932
IA - 123	15.07	-210.803	78.9668	-229.643	1.32075

Eight different types of interaction were observed for IA – 169 - AChE complex forming a "Pi-Donor hydrogen bond" and a "carbon-hydrogen bond" with residue SRE 293(A). It involved one or more Pi-Alkyl interactions with LEU 289(A) and TYR 341(A). It formed "Pi-Pi Stacked" and "Pi-Pi T-stacked" bonds with TYR 447(A), TRP 286(A) and HIS 447(A). It formed one Pi-Anion bond with SER 74(A) and Pi-Sigma with TRP 286(A) and 86(A), the remaining residues forming a weak Van der Waals interacting with the ligand were PHE 297(A), PHE 295(A), PHE 338(A), GLY 448(A), ILE 451(A), GLU 202(A), SER 203(A), GLY 121(A), TYR 133(A), GLY 120(A), GLY 126(A), LEU 130(A), ALA 127(A), SER 125(A), ASN 87(A), VAL 294(A), SER 293(A), ARG 296(A), GLN 291(A), GLU 292(A), GLY 342(A), HIS 287(A) and TYR 72(A). Figure 1 shows the amino acids that bind the AChE active site, as well as the patterns of interaction

**Figure 1.** (c, d): 2D and 3D representation of IA – 169 -2 compound with the active region of AChE.

IA – 169 – 2-compound demonstrated inhibition against the AChE enzyme using a 15.75 micromolar IC<sub>50</sub> value. Per cent of activity – [IA – 169 - 2] diagram was provided in Figure 2. According to the docking results, IA – 169 – 2 – AChE-complex measured the binding energy of -242.963 kcal/mol (MolDock score).

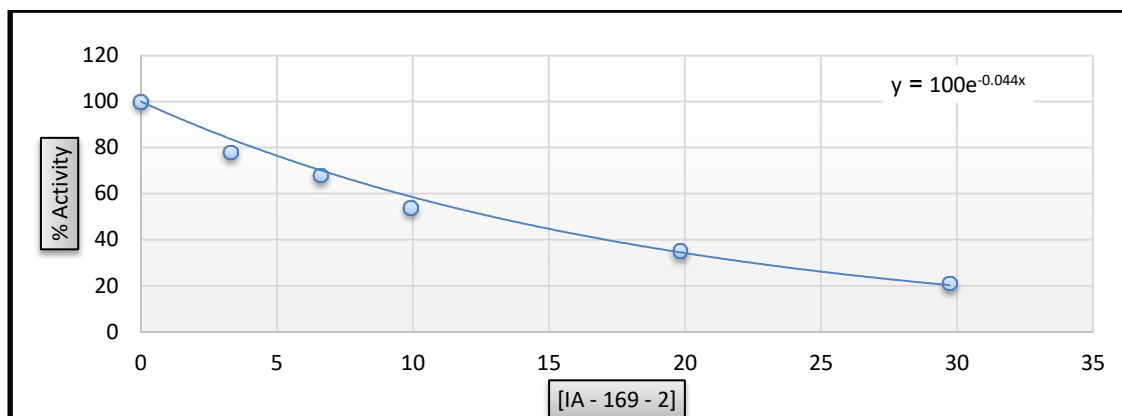


**Figure 2.** IA – 169 -2 compound % activity – [IA – 169 - 2] graph AChE enzyme activity.

Ten different types of interaction were observed for (+) Pentabenzylated catechin -AChE complex involving 4 Pi-donor hydrogen interactions with PHE 338(A), TYR 124(A), ASP 74(A) and TRP 86(A) and 3 carbon-hydrogen bonds interactions with TYR 124(A), ASP 74(A) and PHE 295(A). It formed 3 unfavourable bumps 1 bond interacted with GLN 71(A) and 2 bonds interacted with TRP 86(A). It formed one Pi-Anion bond interaction with ASP 74(A), and 4 Pi-Alkyl bond interactions with ALA 127(A), LEU 130(A), PRO 88(A), and VAL 294(A). It formed 4 "Pi-Pi Stacked", "Pi-Pi T-shaped" and "Amide-Pi Stacked" bonds 2 bonds interacted with TRP 86(A), 1 bond interacted with GLY 120(A) and TRP 286(A), which involved 1 bond Pi-Sigma with VAL 294(A), the remaining residues forming a weak Van der Waals interacting with the ligand were ASN 89(A), VAL 68(A), GLY 126(A), ASN 87(A), VAL 73(A), TYR 72(A), PHE 338(A), SER 293(A), PHE 297(A), ARG 296(A), LEU 76(A), THR 75(A), TYR 133(A), ILE 451(A), GLU 202(A), SER 203(A), GLY 121(A) and HIS 447(A). Figure 3 shows the amino acids that bind the AChE active site, as well as the patterns of interaction.

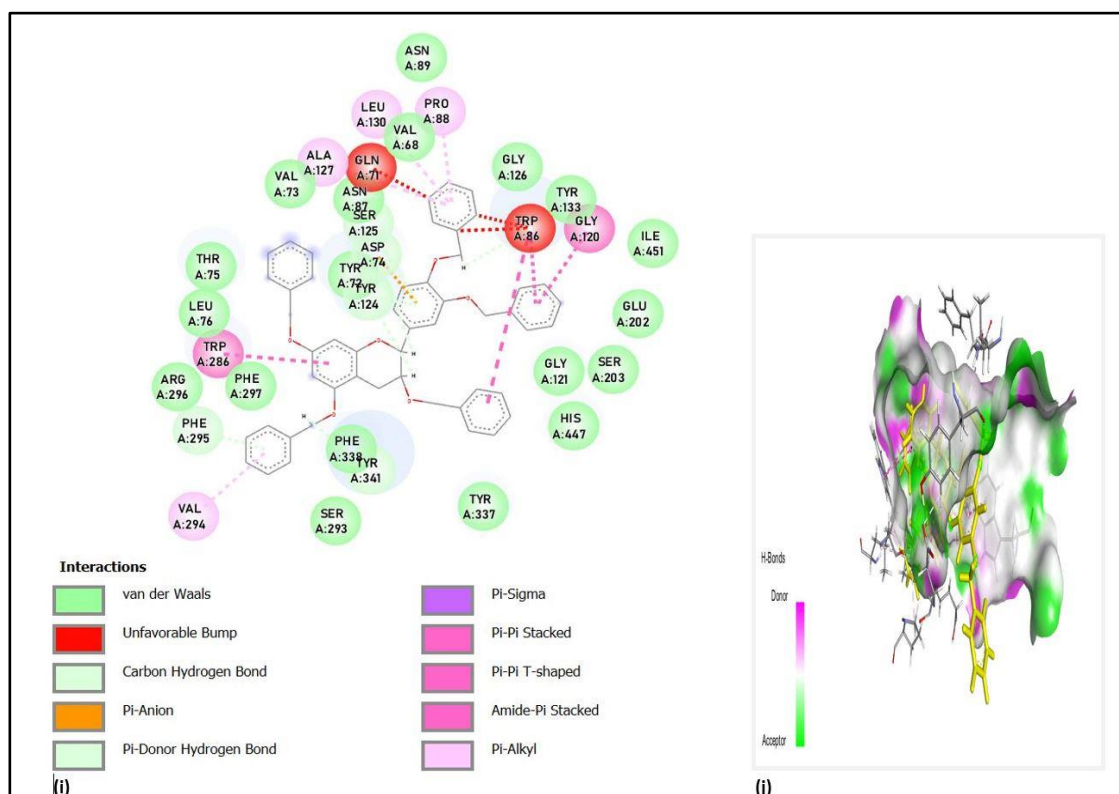


**Figure 3.** (i, j): 2D and 3D representation of (+) Pentabenzylated catechin compound with the binding site of AChE.

(+) Pentabenzylated catechin-compound demonstrated inhibition against the AChE enzyme using a 13.59 micromolar  $IC_{50}$  value. Per cent of activity – [(+) Pentabenzylated catechin] a diagram was shown in Figure 4. According to the docking results, (+) Pentabenzylated catechin – AChE-complex measured the binding energy of -220.272 kcal/mol (MolDock score).

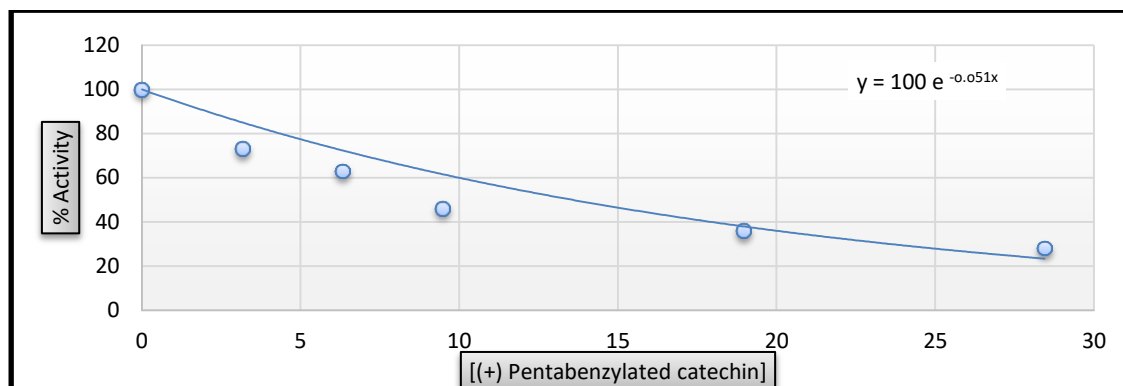


**Figure 4.** (+) Pentabenzylated catechin compound % activity – [(+) Pentabenzylated catechin] graph AChE enzyme activity.

Ten different types of interaction were observed for IA – 123 - AChE complex involving 2 carbon-hydrogen bonds that interacted with TYR 341(A) and ASN 87(A). It formed 6 unfavourable bumps 2 bonds interacted with TRP 86(A) and 4 bonds interacted with TYR 124(A). It formed one Pi-Anion bond that interacted with ASP 74(A), and 3 Pi-Alkyl bonds interacted with LEU 76(A), TYR 72(A), and TYR 341(A). It formed 4 Pi-Pi Stacked, Pi-Pi T-shaped bonds 2 bonds interacted with TYR 341(A), 1 bond interacted with TRP 286(A) and 1 bond interacted with TRP 124(A), the remaining residues forming a weak Van der Waals interacting with the ligand were THR 75(A), LEU 339(A), VAL 340(A), PHE 346(A), ALA 343(A), PRO 344(A), GLY 342(A), VAL 2949(A), PHE 295(A), ARG 296(A), SER 293(A), LEU 289(A), PHE 297(A), PHE 338(A), GLN 71(A), GLY 126(A), VAL 73(A), PRO 88(A), SER 125(A), GLY 121(A), GLY 122(A), SER 203(A), and HIS 447(A). Figure 5 shows the amino acids that bind the AChE active site, as well as the patterns of interaction.

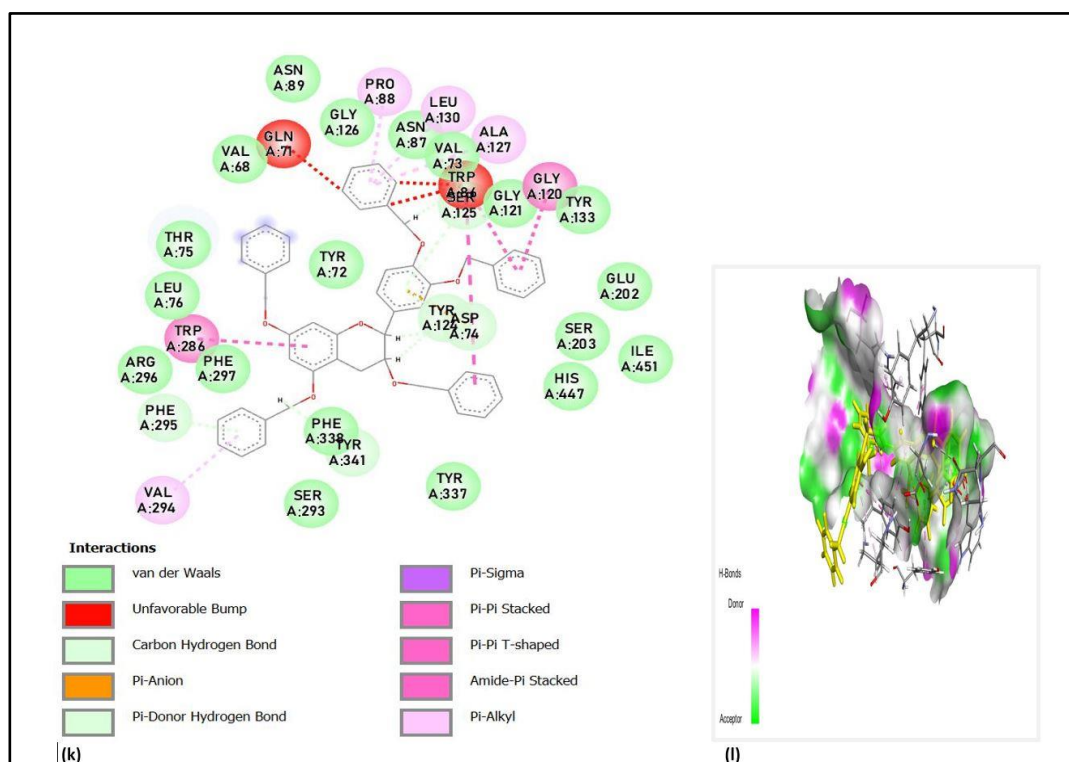


**Figure 5.** (k, l): 2D and 3D representation of IA – 123 compound with the active region of AChE.

IA – 123 compound exhibited inhibitory effects against the AChE enzyme with a 15.07 micromolar  $IC_{50}$  value. Per cent of activity – [IA – 123] diagram was shown in Figure 6. According to the docking results, IA – 123 – AChE-complex measured the binding energy of -210.803 kcal/mol (MolDock score).

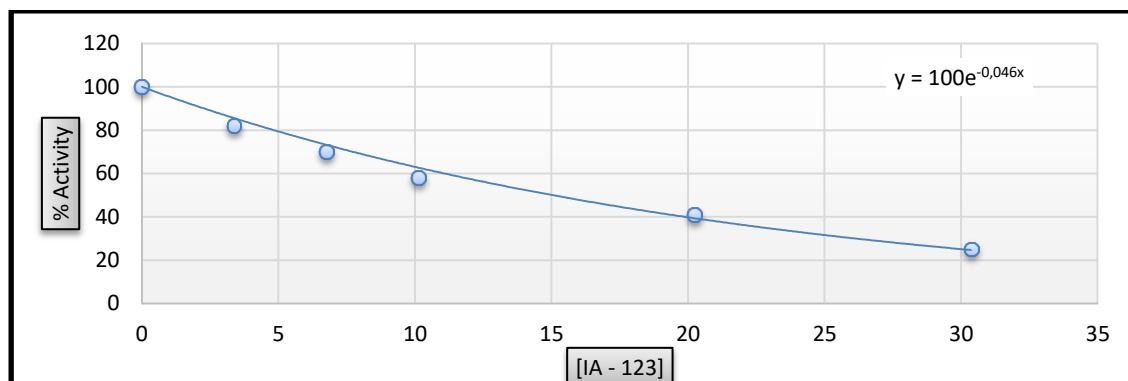


**Figure 6.** IA – 123 compound % activity – [IA – 123] graph AChE enzyme activity.

## Conclusions

In this study, three agents were investigated for their ability to inhibit the cholinesterase (AChE) enzyme using molecular docking experiments. Results from in vitro and in silico experiments suggested that the compounds could function as AChE inhibitors. . (+) Pentabenzylated catechin, IA – 123 and IA-169-2 with  $IC_{50}$  values of 13.59  $\mu$ M 15.07  $\mu$ M and 15.75  $\mu$ M respectively. They failed the ability to pass the blood-brain barrier (BBB), but are anticipated to be absorbed by the digestive system and are not a substrate for the majority of cytochrome enzymes. They were crucially free of false-positive PAINS screening warnings, which allowed us to concentrate on the inappropriate targets and delete them. Additionally, the Swissadem and pkCSM web servers scanned all compounds' predictive qualities for drug similarity using ADMET estimations, where the molecules' theoretically calculated properties and the absorption, distribution, metabolism, and elimination were all calculated. The interaction depended heavily on hydrogen bonds and hydrophobic interactions. The three compounds mentioned above-demonstrated no-toxicity potential (AMES toxicity). However, before these molecules could be used as effective AD agents, more thorough in vivo research must be done.

## References

- [1] Colovic, M. B., Krstic, D. Z., Lazarevic-Pasti, T. D., Bondzic, A. M. and Vasic, V. M. 2013. Acetylcholinesterase inhibitors: pharmacology and toxicology. *Current Neuropharmacology.*, 11: 315–335.
- [2] Merzoug, A., Boucherit, H., Khaled, R., Chefiri, A., Chikhi, A. and Bensegueni, A. 2021. Molecular docking study of the acetylcholinesterase inhibition. *Curr. Issues Pharm. Med. Sci.*, 34: 20–27.
- [3] McHardy, S. F., Wang, H.-Y. L., McCowen, S. V and Valdez, M. C. 2017. Recent advances in acetylcholinesterase inhibitors and reactivators: an update on the patent literature 2012-2015. *Expert Opinion on Therapeutic Patents.*, 27: 455–476.
- [4] Şahin, Ö., Özmen Özdemir, Ü., Seferoğlu, N., Adem, Ş. and Seferoğlu, Z. 2020. Synthesis, characterization, molecular docking and in vitro screening of new metal complexes with coumarin Schiff base as anticholine esterase and antipancreatic cholesterol esterase agents. *Journal of Biomolecular Structure and Dynamics.*, 1–15.
- [5] Stahura, F. L. and Bajorath, J. 2004. Virtual screening methods that complement HTS. *Combinatorial Chemistry & High Throughput Screening.*, 7: 259–269.
- [6] Turan, N., BİNGÖL, M., Savci, A., Kocpinar, E. F. and Colak, N. 2021. Synthesis, structural studies and antioxidant activities of M (II) complexes with NOS donor schiff base ligand. *Sigma Journal of Engineering and Natural Sciences.*, 39: 279–289.





# Relationship Between Growth Hormone And Juvenile Idiopathic Arthritis in Iraqi Patients

*Basim Dheyauldeen Hussein ALHAYALI<sup>1</sup> \* , Hakan ÇOLAK<sup>2</sup> *

<sup>1</sup>Chemistry of Department, Çankırı Karatekin University, Türkiye

## Abstract

The current study aims to investigate the link between kids' growth hormones and juvenile idiopathic arthritis, it has included two groups of children less than 18 years, 25 children, the patient's group who suffered from JIA, and the other (25 Childs) were healthy control. In this work, some parameters were selected such as; age, Hb, AST, ALT, Urea, Creatinine, ESR, WBC, and height. All these selected parameters were measured in both patient children with idiopathic juvenile arthritis and healthy control. Mean and standard deviation of age, Hb, AST, ALT, Urea, and WBC in patients were more than in the control group, but creatinine, ESR, and Height in patients were less than in the control group. Also, the results of this study showed a negative relationship between JIA represented by ESR level in patients and growth hormone represented by Height with the predictive equation of linear relationship as  $(-0.0486x + 15.349)$ . The study concluded that there is a relationship between GH and JIA in children.

**Keywords:** *Inflammatory markers, Tumor necrosis factor- $\alpha$ , Interleukin-6, Obesity*

## 1. Introduction

Children with JIA should have annual slit-lamp eye examinations, as recommended by their physicians, when left untreated, chronic anterior uveitis may cause irreversible vision loss [1]. Systemic juvenile idiopathic arthritis is characterized by extra-articular manifestations in young patients, such as fever, rash, enlarged lymph nodes, enlarged liver or spleen, serositis, and anemia [2].

JIA is a long-term condition that, if left untreated, can lead to catastrophic problems. Complications have been reduced and results have improved as a result of regular follow-up and new treatments. Inflammation can harm the joint, cartilage, and bone if it is not managed. These JIA problems have become far less common as a result of contemporary therapy [3].

Because of the widespread nature of the damage caused by JIA, some children may suffer a general slowing of their development [4]. It's possible that the sickness itself, together with the treatments for it, especially corticosteroids, are to blame for this. Inflamed main joints (such the knee) may lead to unexplained, temporary differences in limb length (i.e. one arm or leg is slightly longer than the other) [5].

JIA can be difficult to diagnose, in part because joint discomfort in children is so frequent and might be caused by a variety of things other than JIA [6]. Arthritis is characterized by joint swelling, which is sometimes – but not always – accompanied by discomfort. Another common symptom is joint stiffness, which is most noticeable in the morning and improves with activity [7].

A doctor may order imaging tests to rule out more serious conditions including a fracture, cancer, infection, or congenital abnormality when a patient complains of joint discomfort and swelling. Sometimes aspirating fluid from the joint and analyzing it might aid in diagnosis. This test helps rule out potential infectious causes of arthritis [8].

## 2. Materials and Methods

Alanine aminotransferase (ALT), aspartate aminotransferase (AST), and creatinine (Cr) are inflammatory factors involved in liver and kidney function (ESR). The serum samples were kept in the freezer at a temperature of 30 degrees Celsius. The Abbott Architect C16000 analyzer was used for photometric assays of

\* Corresponding author. e-mail address: basimalhayali82@gmail.com

biochemicals in the blood, including urea and creatinine (Abbott Diagnostics, Illinois, USA). Abbott Cell DynRuby analyzer was used for white blood cell and hemoglobin (Hb) hematological testing (Abbott Diagnostics, Illinois, USA). Outpatient clinic patients ages 4 to 18 at Balad General Hospital ( IRAQ ) . were evaluated for the rheumatological disorder juvenile idiopathic arthritis (JIA) using the most recent criteria from the International League Against Rheumatism (ILAR). A patient's eligibility was contingent on their having regular contact with both parents. According to the Institutional Review Boards of both universities, permission was obtained to conduct the research.

### 3. Results and Discussion

In this work, some parameters including age, Hb, AST, ALT, Urea, Creatinin, ESR, WBC, and height were measured in patient children with idiopathic juvenile arthritis and a healthy control group to detect the relationship between arthritis disease and growth hormones. All these results and comparisons for the selected parameters are shown in Figure 1, it can be concluded from these this Figure that the high differentiate between the groups led to indicate it is significant to use it to detect this kind of diseases.

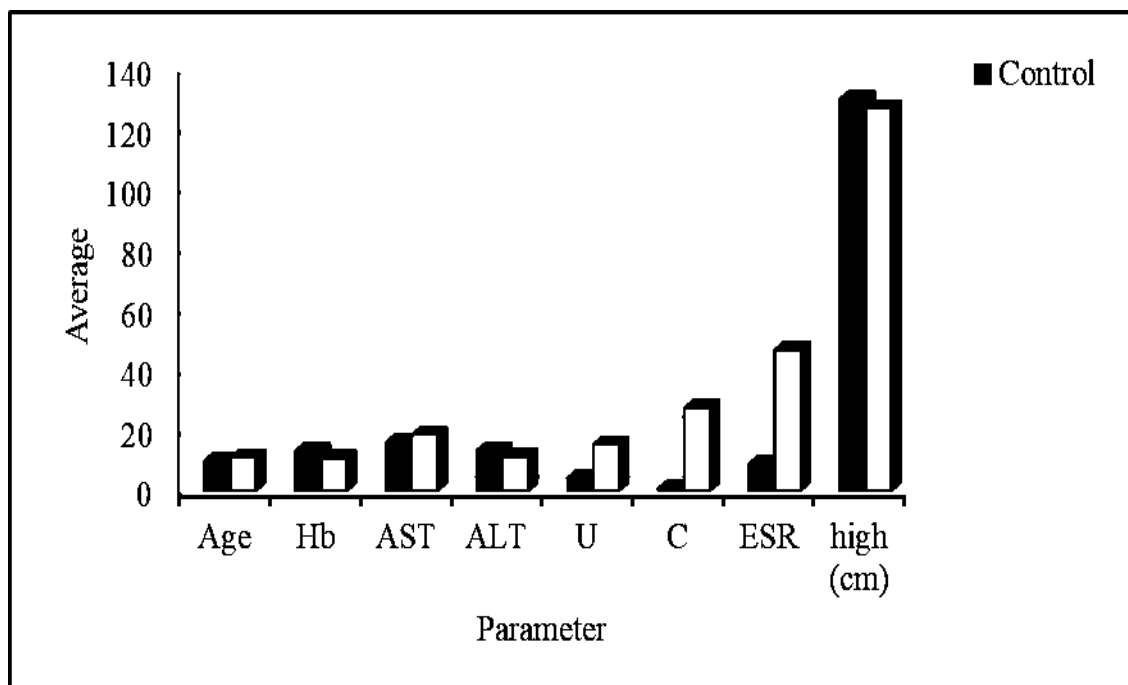


**Figure 1.** Mean and standard deviation of the selected parameters

Long-term effects of JIA include growth stunting and postponement of puberty in affected patients. Although these children suffer chronic growth impairment throughout the active stages of their illness, some do exhibit "catch-up" growth after disease activity or GCs doses are reduced. Although there are now more treatment options available, 10%-20% of people with severe types of the condition continue to demonstrate growth retardation, leading to short final stature.

### Acknowledgment

In this study, the financial support was provided by the Author. All experimental works were conducted in Balad General Hospital (IRAQ) . The author would like to thank all supporters due to their precious contributions.

## References

- [1] Hamdulay, S. S., Glynne, S. J. and Keat, A. 2006. When is arthritis reactive? *Postgraduate medical journal.*, 82(969): 446–453.
- [2] Giancane, G., Consolaro, A., Lanni, S., Davì, S., Schiappapietra, B. and Ravelli, A. 2016. Juvenile idiopathic arthritis: diagnosis and treatment. *Rheumatology and therapy.*, 3(2): 187-207.
- [3] Foster, H.; Rapley, T. and May, C. 2009. "Juvenile idiopathic arthritis: improved outcome requires improved access to care". *Rheumatology.*, 49 (3): 401–403.
- [4] Ringold, S., Angeles-Han, S. T., Beukelman, T., Lovell, D., Cuello, C. A., Becker, M. L. and Reston, J. 2019. American College of Rheumatology/Arthritis Foundation guideline for the treatment of juvenile idiopathic arthritis: therapeutic approaches for non-systemic polyarthritis, sacroiliitis, and enthesitis. *Arthritis care & research.*, 71(6): 717-734.
- [5] Torreggiani, S., Torcoletti, M., Campos-Xavier, B., Baldo, F., Agostoni, C., Superti-Furga, A. and Filocamo, G. 2019. Progressive pseudorheumatoid dysplasia: a rare childhood disease. *Rheumatology international.*, 39(3): 441-452.
- [6] Lundberg, V. 2020. Children with juvenile idiopathic arthritis: Health-related quality of life and participation in healthcare encounters, Doctoral dissertation, UmeåUniversitet, 72 page, Sweden.
- [7] Yunus, M., Masi, A. T., Calabro, J. J., Miller, K. A. and Feigenbaum, S. L. 1981. Primary fibromyalgia (fibrositis): clinical study of 50 patients with matched normal controls. In *Seminars in arthritis and rheumatism*, WB Saunders, pp. 151-171, USA
- [8] Kim, K. H. and Kim, D. S. 2010. Juvenile idiopathic arthritis: Diagnosis and differential diagnosis. *Korean journal of paediatrics.*, 53(11): 931-935.





## Effect of Parameters on the Calcium Sulfate Crystallization

**Ghassan MUTTAR JASSEM JASSEM**<sup>1</sup> , **Muhammed Bora AKIN**<sup>2\*</sup>

<sup>1</sup> The Ministry of Industry and Minerals, General Company for Engineering Industries, Nassiriyh, Iraq

<sup>2</sup> Faculty of Engineering, Department of Chemical Engineering, Çankırı Karatekin University, Çankırı, Türkiye

### Abstract

Calcium sulfate, together with its hydrates, has a wide application area, especially in construction, medicine, cosmetics and ceramics [1].  $\text{CaSO}_4$  – the water system has six stages, with four phases at room temperature: calcium sulfate dihydrate ( $\text{CaSO}_4 \cdot 2\text{H}_2\text{O}$ ), calcium sulfate hemihydrate ( $\alpha\text{-CaSO}_4 \cdot 1/2\text{H}_2\text{O}$  and  $\beta\text{-CaSO}_4 \cdot 1/2\text{H}_2\text{O}$ ),  $\gamma\text{-CaSO}_4$  and  $\beta\text{-CaSO}_4$ .  $\alpha\text{-CaSO}_4$  exists only above 1180 °C and transforms into  $\beta\text{-CaSO}_4$  at lower temperatures (40-1180 °C) [2].  $\text{CaSO}_4$  is used as a desiccant, pigment and paper filler in its anhydrous form [3]. Hemihydrate (bazanite) is used in gypsum board production [4], as a bone filler [5], and has been investigated as a drug delivery system [6].  $\text{CaSO}_4 \cdot 2\text{H}_2\text{O}$  is also used in gypsum board production [7, 8], Portland cement [9], food production [10, 11], surgical and It is used as a setting retarder in the manufacture of dental molds and in the manufacture of toothpaste [12, 13]. Calcium sulfate crystals are obtained as a result of the reaction of calcium chloride and sodium sulfate solutions mixed by changing various parameters. The morphological and dimensional properties of the obtained calcium sulfate crystals are revealed by XRD, SEM and BET analyses. (This study was made from MSc thesis of the first ranked student.)

**Keywords:**  $\text{CaSO}_4$ , Calcium sulfate, Crystallization, Bassanite

## 1. Introduction

Calcium sulfate occurs in three crystalline forms with different levels of hydration  $\text{CaSO}_4 \cdot 2\text{H}_2\text{O}$  (Gypsum),  $\text{CaSO}_4 \cdot 0.5\text{H}_2\text{O}$  (Bassanite), and  $\text{CaSO}_4$  (Anhydride). The conversion of  $\text{CaSO}_4 \cdot 1/2\text{H}_2\text{O}$  to  $\text{CaSO}_4 \cdot 2\text{H}_2\text{O}$  is of great industrial importance as the reaction behind the production of plasterboard in sheet form and, in particular, the placement of medical plasters.  $\text{CaSO}_4 \cdot 2\text{H}_2\text{O}$  is used as a material for orthopedic plasters, as allergic reactions are very rare. It is also included in foods and cosmetics as a binder and/or stabilizer. Calcium sulfate ( $\text{CaSO}_4$ ) is a white solid that is slightly soluble in water, which preserves the physical properties of food and cosmetics and keeps the mixture evenly. It is shown with the code E516 within the E-numbers (food additive code numbers) determined by the European Union [14]. It is used as a binder in gypsum board and gypsum blocks in the construction industry. It has also found a lot of application in dry mortar applications such as plaster in the sector. Gypsum, also known by the name "Plaster of Paris", has been used in medicine for femoral etc. casting support for over 100 years in the treatment of different fractures [15].  $\text{CaSO}_4$  occurs in nature in three crystalline forms with varying levels of hydration:  $\text{CaSO}_4 \cdot 2\text{H}_2\text{O}$  (gypsum),  $\text{CaSO}_4 \cdot 0.5\text{H}_2\text{O}$  (bassanite), and  $\text{CaSO}_4$  (anhydride) [16].

In this study, the effect of changing the concentration of reagents on the formation of calcium sulfate compound ( $\text{CaSO}_4$ ) crystals from the reaction of calcium chloride ( $\text{CaCl}_2$ ) with sodium sulfate ( $\text{Na}_2\text{SO}_4$ ) was investigated using different concentrations of reacting compounds. XRD, SEM and BET analyzes of the reaction products were used to investigate the effect of the concentrations on the crystals obtained at the end of the reaction. Although changes in crystal size was observed with increasing reactant concentration, change in crystal morphology was not observed.

## 2. Materials and Methods

The reactants used in the experiments to synthesize calcium sulfate were chosen as calcium chloride dihydrate (ACS reagent >99%) and sodium sulfate (ACS reagent >99.5%). Solutions were prepared using reactants by mixing Type II water produced from Merck Millipore. All experiments carried out in aqueous media. Reactant concentrations are equamolar and concentrations of 0.04, 0.05, 0.06, 0.07, and 0.08 M were studied in experiment.

\* Corresponding author. e-mail address: mbakin@karatekin.edu.tr

The reactions were carried out in a 1 L jacketed glass-lid reactor and the temperature was kept constant at 30°C during the experiments. A mechanical mixer (IKA Eurostar 20) was used in the experiments and the mixing speed was set as 300 rpm. The residue, which is filtered and dried after washing was dried in a vacuum oven at 80 °C about 12 hours. XRD, SEM and BET analyzes of the obtained powder were made. X-ray diffraction Bruker D8 Discover instrument was used in the investigation of the powder materials. Scans were conducted to select the 2Theta range with respect to approximate patterns found for CaSO<sub>4</sub> from the International Centre for Diffraction Data (ICDD) database. The 2Theta values were between 13° to 90°. SEM analyzes were performed using Carl Zeiss Sigma 300 VP field emission scanning electron microscope. BET specific surface analyzes were performed using the Quantachrome Nova Touch LX<sup>4</sup> instrument.

### 3. Results and Discussion

XRD analyses show that the materials produced in all experiments consist of calcium sulfate in the form of Bassanite. Crystal morphology was monoclinic. Three type of Bassanite form was seen in XRD analyses: Calcium Sulfate(VI) 0.67-hydrate – Alpha, Calcium Sulfate Hydrate (1/1/0.6), and Calcium Sulfate Hemihydrate. Table 1 summarizes properties of these forms. Synthesized material with equimolar reactant concentration of 0.06 M has all the three type of Bassanite forms. Figure 1 shows XRD analysis of this condition.

**Table 1.** Properties of the Bassanite Crystals

Reference Code	Chemical Name	Chemical Formula	Calculated Density (g/cm <sup>3</sup> )	Volume of Cell (10 <sup>6</sup> pm <sup>3</sup> )
98-001-1607	Calcium Sulfate(VI) 0.67-hydrate - Alpha	Ca(SO <sub>4</sub> ) (H <sub>2</sub> O) <sub>0.67</sub>	2.80	1055.96
98-003-4677	Calcium Sulfate Hemihydrate	Ca(SO <sub>4</sub> ) (H <sub>2</sub> O) <sub>0.5</sub>	2.73	1058.07
98-002-8108	Calcium Sulfate Hydrate (1/1/0.6)	Ca(SO <sub>4</sub> ) (H <sub>2</sub> O) <sub>0.6</sub>	2.76	529.88

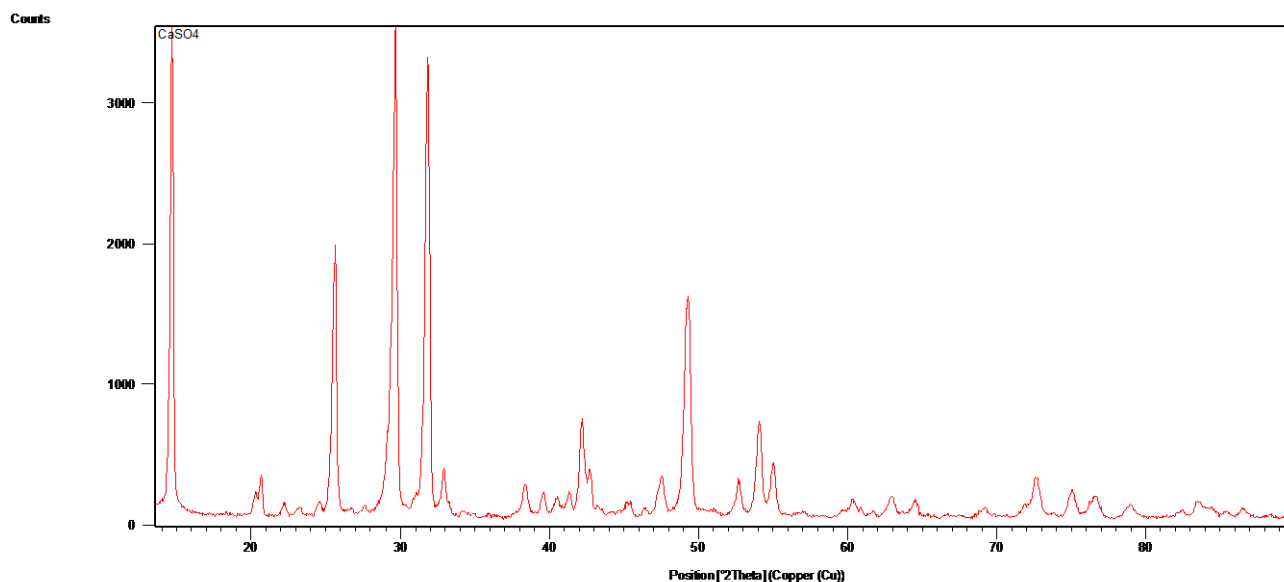


**Figure 1.** XRD analysis of synthesized material with equimolar reactant concentration of 0.06 M.

Figure 2 shows the morphology of products under different concentration conditions. Column-shaped and plate-like morphology are seen at 0.04 M concentration and the dimensions are quite high in both crystal types. Even if the morphology of the products is similar, the content of column-shaped products changes with increasing concentration. When the concentration is 0.06 M, there are more products in the form of plate-like, and the short column-shaped products with less content is smaller, and some needle-like crystal formed. When the concentration increased to 0.07, the content of needle-like products increased, but its length was short, and some

plate-like crystals existed. When the concentration is further increased to 0.08, the content of plate-like decreased and the number of needle-like crystals increased. The concentration has a certain regulating effect on the crystal morphology of calcium sulfate hemihydrate, and the crystal size is smaller when the concentration is 0.08 M. In addition, when the initial concentration was tuned 0.08 M, the crystals, has needle-like morphology was appeared to be about 1  $\mu\text{m}$  in width. Similar to this formation is also seen in the literature [17]. As a result of the BET specific surface analysis, it was determined that the BET surface area of this material was 38.7  $\text{m}^2/\text{g}$ .

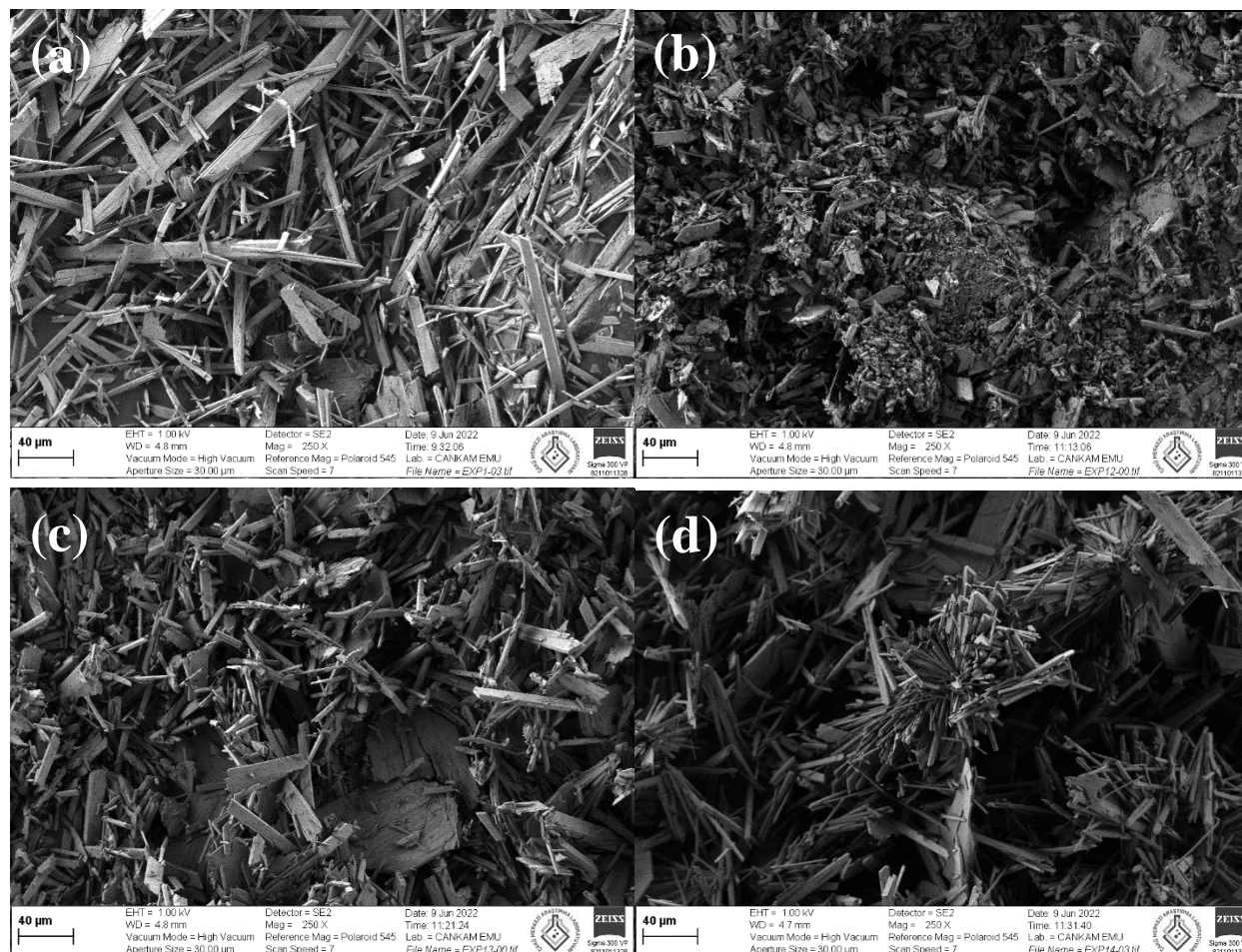


**Figure 2.** SEM micrographs showing the morphology of products under different concentration (a) 0.04 M; (b) 0.06 M; (c) 0.07 M; (d) 0.08 M.

#### 4. Conclusion

In this study, calcium sulfate hemihydrate crystals were synthesized by a rapid reaction using calcium chloride ( $\text{CaCl}_2$ ) and sodium sulfate ( $\text{Na}_2\text{SO}_4$ ) solutions, and the synthesized crystals were characterized SEM and XRD. Experiments were carried out at  $30^\circ\text{C}$ , at a stirring speed of 300 rpm. In experiments, reactant solutions were equimolar and kept between 0.04 and 0.08 M values. Analyzes of the materials showed that  $\text{CaSO}_4 \cdot 1/2\text{H}_2\text{O}$  is obtained. Moreover, a change in crystal size is observed with the increase in the concentration of reactants.

#### Acknowledgement

In this study, the authors declare that there is no conflict of interest and thank to Çankırı Karatekin University, Chemical Engineering Department for the laboratory provided.



## References

- [1] Tritschler, U., Van Driessche, A. E. S., Kempter, A., Kellermeier, M., & Cölfen, H. (2015). Controlling the Selective Formation of Calcium Sulfate Polymorphs at Room Temperature. *Angewandte Chemie International Edition*, 54(13), 4083–4086.
- [2] Zhang, H. B. T.-B. M. in C. E. (Ed.). (2011). 6 - Building Mortar. In *Woodhead Publishing Series in Civil and Structural Engineering* (pp. 150–423). Woodhead Publishing.
- [3] Kim, D. H., Jenkins, B. M., & Oh, J. H. (2011). Gypsum scale reduction and collection from drainage water in solar concentration. *Desalination*, 265(1–3), 140–147.
- [4] Mélinge, Y., Lanos, C., Nguyen, K. S., Daiguebonne, C., Guillou, O., & Freslon, S. (2010). One-Dimensional-Time Study of the Dehydration of Plasterboards Under Standard Fire Condition (ISO 834): Thermo-Chemical Analysis. *Journal of Fire Sciences*, 29(4), 299–316.
- [5] Fu, L., Xia, W., Mellgren, T., Moge, M., & Engqvist, H. (2017). Preparation of High Percentage  $\alpha$ -Calcium Sulfate Hemihydrate via a Hydrothermal Method. *Journal of Biomaterials and Nanobiotechnology*, 08(01), 36–49.
- [6] Parker, A. C., Smith, J. K., Courtney, H. S., & Haggard, W. O. (2011). Evaluation of two sources of calcium sulfate for a local drug delivery system: a pilot study. In *Clinical orthopaedics and related research* (Vol. 469, Issue 11, pp. 3008–3015).
- [7] Crescenzo, P., Gennaro, M., & Gaetano, M. (2016). Mechanical Properties of Plasterboards: Experimental Tests and Statistical Analysis. *Journal of Materials in Civil Engineering*, 28(11), 4016129.
- [8] Thomas, G. (2002). Thermal properties of gypsum plasterboard at high temperatures. *Fire and Materials*, 26(1), 37–45.
- [9] Artioli, G., & Bullard, J. W. (2013). Cement hydration: the role of adsorption and crystal growth. *Crystal Research and Technology*, 48(10), 903–918.
- [10] Jayasena, V., Tah, W., & Nasar-Abbas, S. M. (2014). Effect of coagulant type and concentration on the yield and quality of soy-lupin tofu. *Quality Assurance and Safety of Crops & Foods*, 6, 159–166.
- [11] Tsai, S.-J., Lan, C. Y., Kao, C. S., & Chen, S. C. (1981). Studies on the Yield and Quality Characteristics of Tofu. *Journal of Food Science*, 46(6), 1734–1737.
- [12] Darvell, B. W. (2018). Chapter 2 - Gypsum Materials. In B. W. B. T.-M. S. for D. (Tenth E. Darvell (Ed.), *Woodhead Publishing Series in Biomaterials* (pp. 40–69). Woodhead Publishing.
- [13] López-Delgado, A., López-Andrés, S., Padilla, I., Alvarez, M., Galindo, R., & José Vázquez, A. (2014). Dehydration of Gypsum Rock by Solar Energy: Preliminary Study. *Geomaterials*, 04(03), 82–91.
- [14] Stawski, T., van Driessche, A., Ossorio, M. et al. (2016). Formation of calcium sulfate through the aggregation of sub-3 nanometre primary species. *Nat Commun* 7, 11177.
- [15] Austin RT. (1983). Treatment of broken legs before and after the introduction of gypsum. *Injury*. 14(5):389-94
- [16] [https://pubchem.ncbi.nlm.nih.gov/compound/calcium\\_sulfate#section=Food-Additives-and-Ingredients](https://pubchem.ncbi.nlm.nih.gov/compound/calcium_sulfate#section=Food-Additives-and-Ingredients) Access Date: 07.07.2022.
- [17] Fukugaichi S, Matsue N. (2018). One-Step Synthesis of Calcium Sulfate Hemihydrate Nanofibers from Calcite at Room Temperature. *ACS Omega*. 3, 2820–4.



## Investigation of the Photovoltaic, Structural, Electronic and Spectroscopic Properties of Some Molecules Containing Dimethylaniline

Melike AYAZ , Burcu ORTATEPE , Bekir YURDUGUZEL , E. Burak YURDAKUL ,  
Yusuf ERDOĞDU 

Science Faculty, Department of Physics, Gazi University, 06400, Teknikokullar, Ankara, TURKEY

### Abstract

In this work, the conformational analysis, ground state structure, non-linear optical properties and photovoltaic parameters of some molecules containing dimethylaniline have been calculated by Density Functional Theory (DFT) and time dependent DFT (TD-DFT) computations. Initially, conformational analysis was carried out to determine the most stable structure. Conformational space was scanned using Merck Molecular Force Field (MMFF) method. The conformers derived from conformational space analysis have been optimized by B3LYP/6-31G(d,p) level of theory. Subsequently, B3LYP/6-311G(d,p) quantum calculations were performed to optimize the geometries and electronic, structural, non-linear optical and photovoltaic properties of the title molecules. The title molecules could be used as sensitizers for dye sensitized solar cell (DSSC) applications. Therefore, the theoretical results have presented that TD-DFT calculations using the B3LYP with the polarized split-valence 6-311G(d,p) basis sets and the polarizable continuum model (PCM) were satisfactorily capable of predicting the excitation energies, the absorption and the emission spectra of the molecules. The HOMO and LUMO energy levels of these dyes can confirm a positive effect on the process of electron injection and dye regeneration. Essential parameters in close connection with including light-harvesting efficiency (LHE), injection driving force ( $\Delta G^{\text{inject}}$ ) and total reorganization energy ( $\lambda_{\text{total}}$ ) were examined.

**Keywords:** DSSC, Dimethylaniline, DFT, Photovoltaic parameters, Electronic properties

### 1. Introduction

The dimethylaniline or dimethylphenylamine is an organic compound that is formed by a benzene ring with an amino group substituted with two methyl groups. Its chemical formula is  $C_8H_{11}N$ . N, N-Dimethylaniline is a pale yellow to brown oily liquid with the characteristic odor of amines. It is a basic compound and reacts with nitrous acid to form a nitroso compound. When exposed to air it turns brown. N,N-Dimethylaniline is used as an intermediate in the manufacture of dyes and other substances (1). High-level conjugated polyene dyes with vibrant colors have been forthcoming as promising organic dyes for the DSSC since 2003. By combining the bis-N,N-dimethylaniline (DMA) electron donor, the CAA acceptor and various linkers, satisfactory performance can be achieved with high absorption in the visible region. (2).

DSSCs has many benefits than previous generations, such as low cost and flexibility. The search for original, extremely effective and inexpensive DSSCs is in progress (2). DSSC is made up of a dye, conductive transparent glass, a film of nanocrystalline semiconductors, electrolyte, and counter electrodes. The molecular structure of the dye is one of the most effective factors in controlling the efficiency of DSSCs. (2). Dyes are responsible for the absorption of solar radiation and the transfer of charge (CT) from the semiconductor to the electrolyte. The excited electron is injected into semiconductor electrode while the oxidized dye is regenerated by the electrolyte which in turn captures electrons from the counter electrode to complete the circuit (2).

In this paper, the researchers comprise the theoretical results of a systematic study of conformational analysis, molecular structure, UV-Vis spectra and photovoltaic parameters of the novel dye compounds containing a dimethylaniline ring by Density Functional Theory (DFT).

### 2. Computational Details

The quantum mechanical calculations of the novel dye compounds containing a dimethylaniline ring have been utilized by the Gaussian 09 software (3). The B3LYP functional was used in geometry optimizations,

\* Corresponding author. e-mail address: melike.ayaz@hotmail.com

spectroscopic, electronic and some photophysical properties of the dye molecules with 6-311G(d,p) basis set (4) (5) (6).

The ground ( $E^{\text{dye}}$ ) and excited ( $E^{\text{dye*}}$ ) state oxidation potentials, electron injection free energy ( $\Delta G^{\text{inject}}$ ) (7) (8) (9), the light-harvesting efficiency (LHE) (10) and lifetime associated with the oscillator strength ( $f$ ) of dye molecules at the maximum absorption of the dyes were predicted by means of B3LYP/6-311G(d,p) level of theory. In addition, Ionization potential (IP), electron affinity (EA) and global hardness ( $\eta$ ) were calculated using the functional and basis set mentioned in the preceding sentence (11). The  $E^{\text{dye}}$ ,  $E^{\text{dye*}}$ ,  $\Delta G^{\text{inject}}$ , LHE,  $\tau$ , IP, EA and  $\eta$  were calculated using the following equations.

$$\begin{aligned} E^{\text{dye}} &= -E_{\text{HOMO}} \\ E^{\text{dye*}} &= E^{\text{dye}} - E_{\text{exc}} \\ \Delta G^{\text{inject}} &= E^{\text{dye*}} - E_{\text{CB}} \\ \text{LHE} &= 1 - 10^{-f} \\ \tau &= \frac{1.499}{fE^2} \\ \text{IP} &= E(\text{optimized cation}) - E(\text{optimized neutral}) \\ \text{EA} &= E(\text{optimized neutral}) - E(\text{optimized anion}) \\ \eta &= \frac{\text{IP} - \text{EA}}{2} \end{aligned}$$

The time dependent density functional theory (TD-DFT) calculations were performed to determine the absorption properties of the dye molecules. The B3LYP functionals combined with the 6-311G(d,p) basis set was used to simulate the UV-Vis absorption spectra. TD-DFT calculation of the dyes was predicted by DFT theory within 0-700 nm range in DMSO solvent using the conductor-like polarizable continuum model (C-PCM).

Here we also discuss the calculation of some transport coefficients entering into the Marcus model for transport which is valid in the hopping regime (12). Within this study, we calculated the molecular reorganization energies defined by the following expressions. We confine our study to molecular reorganisation energy calculations, which are defined by the following term, using the four-point method. (13) (14). The calculated  $\Lambda_{\text{total}}$  is the sum of the electron ( $\Lambda_e$ ) and hole ( $\Lambda_h$ ) reorganization energies. The  $\Lambda_e$ ,  $\Lambda_h$ , and  $\Lambda_{\text{total}}$  were calculated using the following equations.

$$\begin{aligned} \Lambda_e &= (E_n^- - E_a) + (E_a^0 - E_n) \\ \Lambda_h &= (E_n^+ - E_c) + (E_c^0 - E_n) \\ \Lambda_{\text{total}} &= \Lambda_e + \Lambda_h \end{aligned}$$

where  $E_n$  is the optimized energy of the neutral case;  $E_c$  is the optimized energy of the cationic case;  $E_a$  is the optimized energy of the anionic case.  $E_n^+$  ( $E_n^-$ ) is the single point energies of the cation (anion) without change in their neutral geometry, and  $E_c^0$  ( $E_a^0$ ) is the single point energies of the neutral case without change in cationic (anionic) geometries.

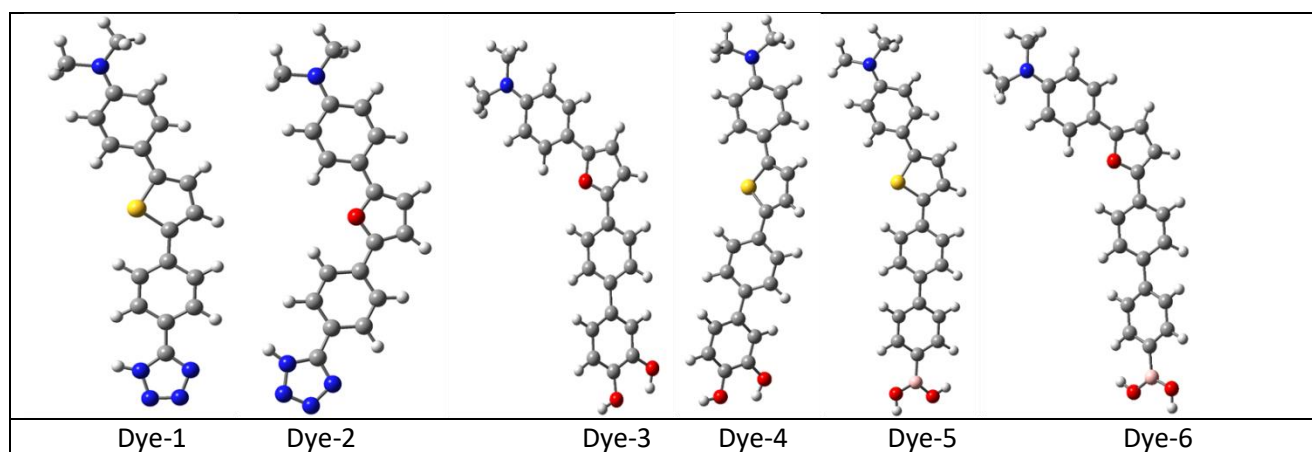
### 3. Results and Discussion

#### 3.1. Conformational Analysis

The conformational distribution of the dye molecules was obtained by scanning the potential energy surface. These calculations were performed through Spartan 08 program (15). Conformational analysis calculations were made using the Merck Molecular Force Field (MMFF) method. All possible conformers were obtained to determine the state geometries. Then, the geometry optimization calculations were made by using of the Gaussian 09 program. Conformational analysis result of dye molecules tabulated in Table 1. The most stable molecular geometries of dye molecule illustrated in Figure 1.

**Table 1.** Conformational analysis results of dye molecules.

Dye-1				Dye-5			
	Rel. Energy (k.cal.mol <sup>-1</sup> )	Optimized Energy (a.u.)	Population (298 K)/%		Rel. Energy (k.cal.mol <sup>-1</sup> )	Optimized Energy (a.u.)	Population (298 K)/%
<b>Conformer-1</b>	<b>0.000</b>	-1406.18426583	37.64	<b>Conformer-1</b>	<b>0.000</b>	-1556.20359835	26.62
Conformer-2	0.012	-1406.18424595	36.88	Conformer-2	0.019	-1556.20356798	25.78
Conformer-3	0.231	-1406.18389771	25.48	Conformer-3	0.035	-1556.20354333	25.10
Dye-2				Conformer-4	0.129	-1556.20339296	21.42
	Rel. Energy (k.cal.mol <sup>-1</sup> )	Optimized Energy (a.u.)	Population (298 K)/%	Conformer-5	2.221	-1556.20005935	0.63
<b>Conformer-1</b>	<b>0.000</b>	-1083.21360758	54.503	Conformer-6	2.744	-1556.19922520	0.26
Conformer-2	0.107	-1083.21343737	45.497	Conformer-7	2.923	-1556.19894015	0.19
Dye-3				Dye-6			
	Rel. Energy (k.cal.mol <sup>-1</sup> )	Optimized Energy (a.u.)	Population (298 K)/%		Rel. Energy (k.cal.mol <sup>-1</sup> )	Optimized Energy (a.u.)	Population (298 K)/%
<b>Conformer-1</b>	<b>0.000</b>	-1207.64908584	37.31	<b>Conformer-1</b>	<b>0.000</b>	-1233.23255080	96.01
Conformer-2	0.021	-1207.64905249	36.01	Conformer-2	2.263	-1233.22894395	2.11
Conformer-3	0.202	-1207.64876411	26.53	Conformer-3	2.727	-1233.22820474	0.96
Conformer-4	3.705	-1207.64318184	0.07	Conformer-4	2.755	-1233.22816092	0.92
Conformer-5	4.158	-1207.64245986	0.03				
Conformer-6	4.174	-1207.64243441	0.03				
Dye-4							
	Rel. Energy (k.cal.mol <sup>-1</sup> )	Optimized Energy (a.u.)	Population (298 K)/%				
<b>Conformer-1</b>	<b>0.000</b>	-1530.62025950	15.45				
Conformer-2	0.021	-1530.62022580	14.91				
Conformer-3	0.053	-1530.62017509	14.13				
Conformer-4	0.065	-1530.62015656	13.84				
Conformer-5	0.206	-1530.61993196	10.91				
Conformer-6	0.223	-1530.61990397	10.60				
Conformer-7	0.245	-1530.61986948	10.22				
Conformer-8	0.262	-1530.61984130	9.93				
Conformer-9	4.226	-1530.61352528	0.01				
Conformer-10	4.352	-1530.61332402	0.01				

**Figure 1.** Optimized molecular structure of dye molecules.

### 3.2. Some Electronic Properties

The energies of the highest occupied molecular orbital (HOMO), the lowest unoccupied molecular orbital (LUMO), dye regeneration driving force ( $(E_{I_3^-/I^-} - E_{HOMO})$ , ionization potential (IP), electron affinity (EA), absolute hardness ( $\eta$ ) of the ground state of the dye molecules were predicted by B3LYP/6-311G(d,p). HOMO-LUMO plot of dye molecules were given in Figure 2. As seen in Table 2, the HOMO ( $E_{HOMO}$ ) energies of the most stable geometries were calculated as -5.199 eV (Dye-1), -5.116 (Dye-2), -4.968 eV (Dye-3), -5.118 (Dye-4), -5.016 (Dye-5) and -4.998 (Dye-6). LUMO energies of the dye molecules were calculated as -2.099 eV (Dye-1), -1.946 (Dye-2), -1.553 eV (Dye-3), -1.636 (Dye-4), -1.601 (Dye-5) and -1.739 (Dye-6). The LUMO energy level of the dyes are much higher than that of TiO<sub>2</sub> conduction band edge (about -4.0 eV). It is

seen that the LUMO level for dyes is higher than the conduction band of TiO<sub>2</sub>. This is an important condition indicating that electron transfer from the dye to the semiconductor will occur. The HOMO of dyes are lower than that of  $I_3^-/I^-$  (about -4.8 eV). For this reason, these electron-losing dye molecules can regain their original form by taking electrons from the electrolyte. As a result, it can be expressed as being energetically permitted to electron injection and regeneration. This indicates that the dye is a molecule that can be used in the application of DSSCs.

The dye regeneration driving force ( $E_{I_3^-/I^-} - E_{HOMO}$ ) were predicted as 0.399 eV (Dye-1), 0.316 eV (Dye-2), 0.168 eV (Dye-3), 0.318 eV (Dye-4), 0.216 eV (Dye-5) and 0.198 eV (Dye-6) by using B3LYP/6-311G(d,p) level of theory. The greater the driving force for dye regeneration will result in higher performance of this dye in DSSC. Thus, Dye-1 molecule favorably act as an excellent sensitizer for DSSC applications.

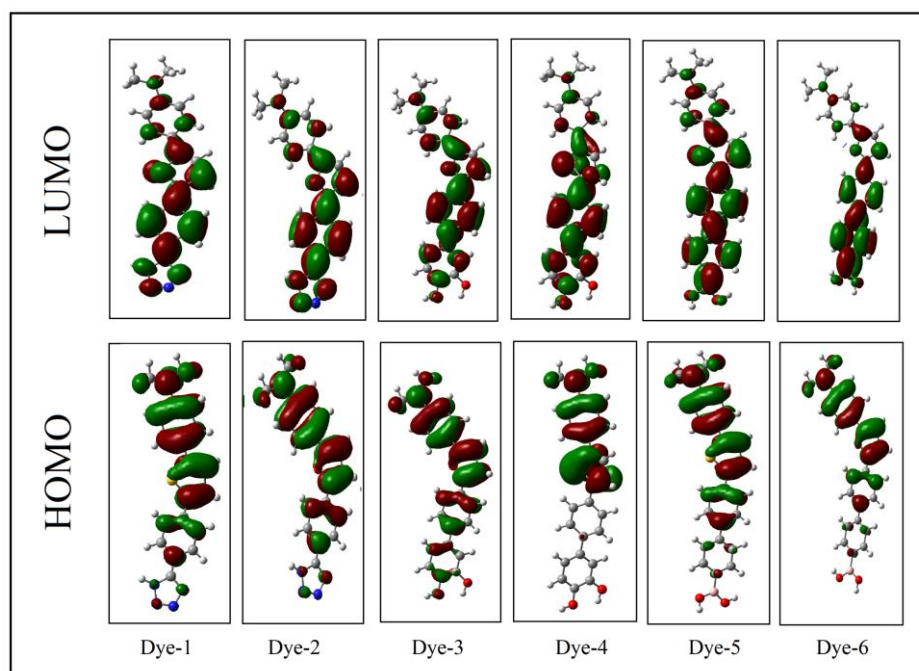


**Figure 2.** HOMO-LUMO plot of the dye molecules.

**Table 2.** The calculated UV-Vis, electronic and photovoltaic parameters of dye molecules.

	Wavelength $\lambda$ (nm)	Excitation energies (eV)	Oscillator strengths (f)	Excited state
Dye-1	2.7502	450.82	0.9667	HOMO $\rightarrow$ LUMO
Dye-2	2.7082	457.82	1.0018	HOMO $\rightarrow$ LUMO
Dye-3	3.0243	409.96	1.3381	HOMO $\rightarrow$ LUMO
Dye-4	3.0718	403.62	1.3232	HOMO $\rightarrow$ LUMO
Dye-5	2.9424	421.37	1.1513	HOMO $\rightarrow$ LUMO
Dye-6	2.8902	428.98	1.1779	HOMO $\rightarrow$ LUMO
	$E^{dye}$ (eV)	$E^{dye*}$ (eV)	$\Delta G^{inject}$ (eV)	LHE
Dye-1	5.199	2.449	-1.551	89.2
Dye-2	5.116	2.407	-1.593	90.0
Dye-3	4.968	1.944	-2.056	95.4
Dye-4	5.118	2.046	-1.954	95.2
Dye-5	5.016	2.073	-1.927	92.9
Dye-6	4.998	2.108	-1.892	93.4
	$E_{HOMO}$ (eV)	$E_{LUMO}$ (eV)	$E_{H-L}$ (eV)	$(E_{I_3^-/I^-} - E_{HOMO})$
Dye-1	-5.199	-2.099	3.101	0.399
Dye-2	-5.116	-1.946	3.170	0.316
Dye-3	-4.968	-1.553	3.416	0.168
Dye-4	-5.118	-1.636	3.482	0.318
Dye-5	-5.016	-1.601	3.415	0.216
Dye-6	-4.998	-1.739	3.259	0.198
	IP (eV)	EA (eV)	$\eta$ (eV)	



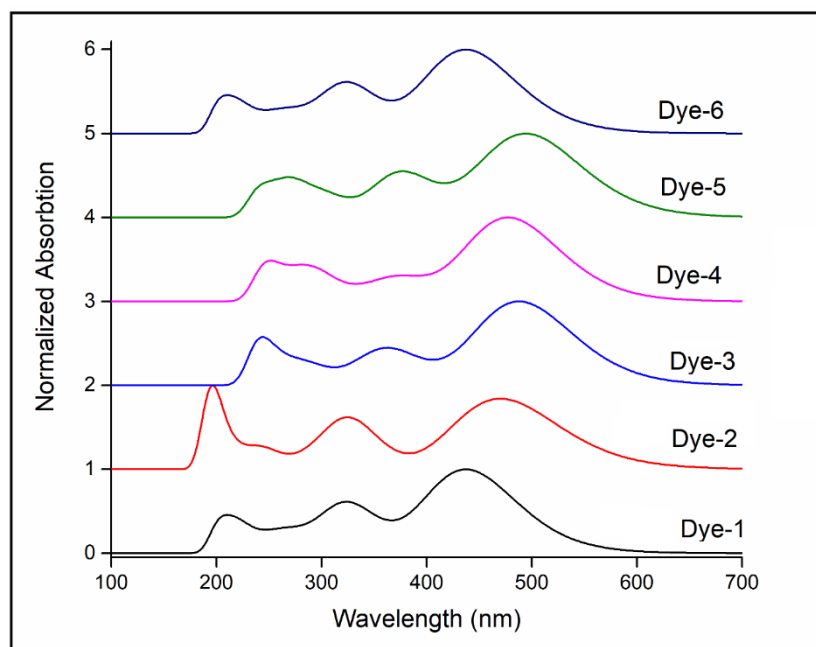
**Table 2.** The calculated UV-Vis, electronic and photovoltaic parameters of dye molecules. (Continued)

Dye-1	6.362	0.949	2.707	
Dye-2	6.294	0.780	2.757	
Dye-3	5.831	0.297	2.767	
Dye-4	5.915	0.482	2.717	
Dye-5	6.050	0.713	2.669	
Dye-6	5.964	0.576	2.694	
	$\Lambda_e$ (eV)	$\Lambda_h$ (eV)	$\Lambda_{total}$ (eV)	$\tau$ (ns)
Dye-1	0.422	0.328	0.751	3.15
Dye-2	0.327	0.256	0.582	3.14
Dye-3	0.554	0.303	0.857	1.88
Dye-4	0.650	0.385	1.035	1.85
Dye-5	0.518	0.380	0.898	2.31
Dye-6	0.443	0.290	0.733	2.34

As shown in Table 2, for the studied dyes, the IP values increase in the following order: Dye-3<Dye-4<Dye-6<Dye-5<Dye-2<Dye-1 showing that Dye-3 attained the lowest IP value, which indicates that it is easier to release electrons and create holes in Dye-3. Nevertheless, the values of EA decrease in the following order: Dye-1> Dye-2> Dye-5> Dye-6> Dye-4> Dye-3, suggesting that Dye-1 undertakes a faster rate of injecting electron directly to the TiO<sub>2</sub> semiconductor conduction band.

### 3.3. UV-Vis Spectra and Photovoltaic Parameters

The theoretical and experimental UV-Vis spectra of dye molecules have been indicated in Figure 3. The maximum absorption wavelengths ( $\lambda_{max}$ ), theoretical electronic excitation energies, oscillator strength and molecular orbital contributions were determined from the calculated UV-Vis spectra. The theoretical and experimental UV-Vis spectral data were collected in Table 2.

**Figure 3.** The predicted UV-Vis spectra of the dye molecules

As seen in Figure 3 and Table 3, it was observed that the dye molecules absorb in the visible region in the DMSO solvent. Therefore, it can be stated that the dyes can be used as a photosensitizer for DSSC. The dyes displays theoretically absorption maxima at 450 nm (Dye-1), 457 nm (Dye-2), 409 nm (Dye-3), 403 nm (Dye-4), 421 nm (Dye-5) and 428 nm (Dye-6). HOMO→LUMO electronic transitions (with 60-70% configuration)

contribute to the  $\lambda_{\max}$  for the dyes. In order to obtain a high  $J_{sc}$ , the light harvesting efficiency (LHE) of dyes should be as large as possible. In the present work, LHE were determined in the 89 % and 95% region by DFT.

In Table 2, electronic injection free energy ( $\Delta G^{\text{inject}}$ ) is an important parameter in investigating the electrochemical properties of excited dyes. The electron injection efficiency of the injected electrons in the semiconductor from the excited state is related to  $\Phi_{\text{inj}}$  and this could be affected the short-circuit current density  $J_{sc}$ . In the present study, it reveals that the dye molecules have a negative  $\Delta G^{\text{inject}}$  value in the order of -1.551 eV (Dye-1) > -1.593 eV (Dye-2) > -2.056 eV (Dye3) > -1.954 eV (Dye-4) > -1.927 eV (Dye-5) > -1.892 eV (Dye-6). This means that the excited state energy levels are above the CB of the semiconductor. Hence, it indicates an injection of electrons from the excited dye to the CB of  $\text{TiO}_2$ .

Table 2 notes that the reorganization energies for the hole transport ( $\Lambda_h$ ) of the dyes are lower than that of the electron ( $\Lambda_e$ ). According to the values of the hole and electron reorganization energies listed in Table 2, the small total reorganization energy value confirms a more effective hole-charge separation. For the studied dyes, Dye-2 has the lowest total reorganization energy, which reflects that it has the most favorable charge-transport properties and the least degree of charge recombination.

## Acknowledgement

We thanks to Dr. Ömer DERELİ for Spartan 08 software.

## References

1. Dimethylaniline: structure, properties, synthesis, uses. (warbletoncouncil.org). 2022.
2. A El-Meligy, N Koga, S Iuchi, K Yoshida, K Hirao, A H. Mangood, A M. El-Nahas. Journal of Photochemistry and Photobiology A: Chemistry. 367, (2018) 332-346 <https://doi.org/10.1016/j.jphotochem.2018.08.036>
3. M. J. Frisch, et al. Gaussian 16, Revision B.01, Gaussian, Inc., Wallingford CT. 2016.
4. Becke, A. D. Density-functional exchange-energy approximation with correct asymptotic behavior. Phys Rev A. 1988; 38. doi:10.1103/PhysRevA.38.3098.
5. Becke, A. D. The role of exact exchange. J. Chem. Phys. 98, 1993. doi:10.1063/1.464913
6. C. Lee, W. Yang, R. G. Parr. Development of the Colle-Salvetti correlation- energy formula into a functional of the electron density. Phys. Rev. B37 (1988), 785–789. doi:10.1103/PhysRevB.37.785
7. R. Katoh, A. Furube, T. Yoshihara, K. Hara, G. Fujihashi, S. Takano, S. Murata, H. Arakawa, and M. Tachiya. J. Phys. Chem. 2004 ; 108(15) 4818–4822. <https://doi.org/10.1021/jp031260g>
8. T. Marinado, K. Nonomura, J. Nissfolk, M. K. Karlsson, D. P. Hagberg, L. Sun, S. Mori, and A. Hagfeldt. Langmuir 26, 2009. (4), 2592–2598.
9. Pearson, R. G. Inorg. Chem. 1988; 27,(4) 734–740.
10. Nalwa, H. S. Handbook of Advanced Electronic and Photonic Materials and Devices: Semiconductors. Cambridge : vol. 1, Academic Press, 2001.
11. Y. Erdogdu, S. Erkoc. Jnl. of Comp. & Theo. Nano., 2012; 9. 837–850. <https://doi.org/10.1166/jctn.2012.2105>.
12. Marcus, R. A. The Journal of Chemical Physics 24. 1956; (5) 979-989. <https://doi.org/10.1063/1.1742724>
13. Berlin Y A et.al, The Journal of Physical Chemistry A, J. Phys. Chem. A 2003, 107, 19, 3970–3980. <https://doi.org/10.1021/jp034225i>
14. M, Rosso K M and Dupuis. Theoretical Chemistry Accounts. 2006; (116): 124-136. <https://doi.org/10.1007/s00214-005-0016-x>
15. Spartan 08, Wavefunction Inc. USA : Irvine. 2008; CA 92612.



## Study of the Association of Genes and Proteins of Resistance to Multiple Drugs with Molecular Markers in Patients with Acute Leukaemia

***Hayder Hatem Abdulwahhab AL-DOORI*** \* 

*Department of Biology, Molecular Biology, Erzincan Binali Yıldırım University, Türkiye*

### Abstract

The study of thesis the association of genes and proteins of resistance compilations of evidence obtained in this study are patients with AL (n=75) who did not go into remission (n=56/75) after induction chemotherapy had a higher median age than patients who went into remission (n=19/75); the median survival of patients with AML, B-ALL and T-ALL were three months, 25 months and five months, respectively; the median survival of APL patients (n=19) was greater than 60 months; FMS3-DIT (5.8%) and LACTATE DEHYDROGENASE3-D835 (8.4%) mutations were rare; the JAK2V617F mutation was not detected in any patient; only six subjects expressed survivin (9.4%); the expression profile of MDR genes and proteins in AL patients was heterogeneous. In cases of AL, ABCB1 expression and LDH activity were positively correlated, the presence of the CD34 marker was associated with the highest transcription of abcc1, and the highest transcription of *lrp* was associated with the absence of the marker CD56 and with the absence of survivin transcription, In AML carriers (n=28/75), abcc1 transcription and patient age were positively correlated, and the absence of survivin transcription was associated with higher *lrp* transcription and in patients diagnosed with APL (n=19/75), abcc1 and LRP expressions were positively correlated with the percentage of leukemic promyelocytes at diagnosis, and ABCC1 expression was positively correlated with LDH activity and in ALL-B cases (n=19/75), ABCB1 and abcc1 expressions correlated positively with LDH activity, ABCC1 expression was negatively correlated with leukocyte count at diagnosis, and LRP expression was positively correlated with the number of leukocytes at diagnosis and was associated with the presence of TL-2.2. In T-ALL cases (n=7/75), *abcb1* transcription and leukocyte count were positively correlated; higher LRP expression was associated with the diagnosis of AML, Patients diagnosed with AL and AML who did not go into remission after induction therapy.

**Keywords:** *Genes and proteins of resistance, Multiple drugs, Molecular markers, Acute leukaemia*

### 1. Introduction

All malignant leukaemia's are defined by the uncontrolled proliferation, survival and aberrant differentiation of hematopoietic cells in the bone marrow (BM) that eventually spread to other organ systems [1].

There are many stages of tumorigenesis, each of which represents a genetic mutation that impacts a cell. In order for a cell to bypass normal cell growth and homeostasis, each successive genetic mutation provides the cell with a new advantage over regular cells [2]. As a result, a normal cell gradually transforms into a cancerous cell. Scientists believe there are four fundamental changes in cell physiology that reveal themselves in different ways in leukaemia genotypes and together define the disease's uncontrollable growth and spread. Self-sufficiency, insensitivity, apoptosis avoidance and unrestricted replication are all aspects that contribute to a cell's ability to thrive. Reprogramming of energy metabolism and evasion of immune system destruction by T and B lymphocytes, macrophages, and natural killer cells have recently been linked to cancer aetiology [3].

A somatic mutation in a primordial cell (the stem cell) is the cause of leukemic transformation, which can occur at various stages of lymphoid or myeloid precursor development, making it a diverse disease from a biological and morphological perspective [4]. Acute and chronic lymphoid and myeloid leukemias can be distinguished in this way. ALs are characterized by the accumulation of immature cells (blasts) unable to differentiate due to a maturation block. When this maturational block occurs in the myeloid lineage, it gives rise to acute myeloid leukemias (AMLs) and, when it affects the lymphoid lineage, it causes acute lymphoid leukemias (ALLs) [5]. In some rare cases, two populations of blasts from different lineages may coexist, or existing blasts may have specific markers from more than one lineage. Historically, there is a difficulty in how to define this type of acute leukemia of mixed phenotype (ALMP), but, currently, it is accepted the denomination of Bilineal Acute Leukemia for the first case and Acute Biphenotypic Leukemia (ABL) for the second situation [6].

\* Corresponding author. e-mail address: hayderhatam82@gmail.com

## 2. Materials and Methods

### 2.1. Apparatus

All reagents for cell culture, molecular biology assays and DNA extraction were purchased from Sigma Aldrich. The RNA extraction kit was purchased from Thermo Fisher and the Ficoll-Hypaque (density 1077 g/m<sup>3</sup>) from Thermo Fisher. Anti-CD34 and anti-CD45 monoclonal antibodies were purchased from Thermo Fisher Scientific; anti-ABCB1 and anti-ABCC1, from Thermo Fisher Scientific; anti-LRP, from Millipore; and the Alexa Fluor 488, from Thermo Fisher Scientific. The fixation and permeabilization kit were purchased from Thermo Fisher Scientific (USA) [7].

## 3. Results and Discussion

### Detection of Gene Transcription of *abcb1*, *abcc1*, *lrp* AND survivin BY Semi quantitative RT-PCR

The evaluation of gene transcription of resistance proteins was performed using the semiquantitative RT-PCR technique. The oligonucleotide primers or primers pairs (Table 1) used to assess the transcription of *abcb1*, *abcc1*, *lrp* and *survivin* were previously described by Tomiyasu, et al. (2012) and glyceraldehyde-3-phosphate dehydrogenase (GAPDH) transcription was used for band normalization [8]

Table 1 – Sequence of primers for the detection of *abcb1*, *abcc1*, *lrp* and *survivin*.

Gene	Sequência	product size
<i>abcb1</i>	5'–CCGCAAGTTTACCTGCAGG–3'	157bp
	5'–GCTCCTAACTTCTGAGGTTCA–3'	
<i>abcc1</i>	5'–TGGGGGACTGTCACGAAT–3'	260bp
	5'–AGGCCGAATATGACTTCCC–3'	
<i>lrp</i>	5'–GTCGGGCAGCTCGTCGGTGTCTG–3'	240bp
	5'–GCCTGGGTCTGTCTCTTGCCTTGG–3'	
<i>survivin</i>	5'–GCATCCTGGACTTCTCAACACC–3'	393bp
	5'–CCCATGGAGCTGCATCAGCCA–3'	
<i>GAPDH</i>	5'–CCCGTCTTCGAGAAACCATGA–3'	330bp
	5'–TCTGGGATGTATGAGGCAGG–3'	

After collection, the samples were divided into three parts (Figure 1). One part was used for RNA extraction, for the synthesis of complementary DNA (cDNA) and for semiquantitative RT-PCR assays. In cases where there was an indication at the time of diagnosis of a specific subtype of AL with cytogenetic alterations, the cDNA synthesized at this stage was also used to perform the search for the following translocations: TL-1, TL-2, TL-3 [t(15;17)(q22;q21)] and TL-4. The second part of the sample was used to perform the protein expression assays by flow cytometry and the third part for DNA extraction and the performance of assays to identify the presence of mutations in the FMS3 gene and in the JAK2 gene [9].

After collection, part of the sample was used for RNA extraction, complementary DNA (cDNA) synthesis, semiquantitative RT-PCR assays and, when indicated, the investigation of t(8;21)(q22) translocations, TL-2,

TL-3 and TL-4. A second part of the sample was used for flow cytometry assays and another part for DNA extraction and the research for the presence of mutations in the FMS3 gene and in the JAK2 gene. TCLE – Free and Informed Consent Term [10].

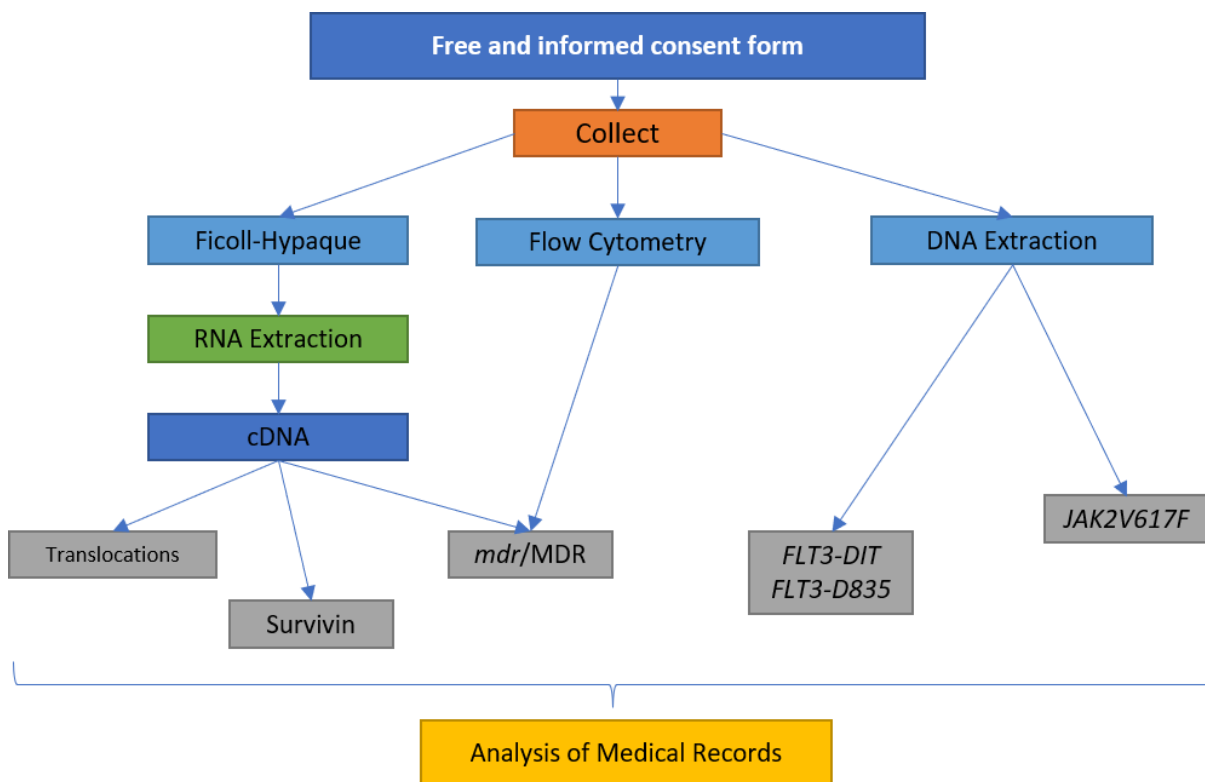


**Figure 1.** Processing flowchart of peripheral blood or bone marrow samples [11].

In addition to molecular biology and flow cytometry assays, a search was performed on medical records to obtain clinical data and other laboratory data from patients. The following data were collected from the medical records: age, WBC and LDH levels at diagnosis, gender, immunophenotype, karyotype, final diagnosis, occurrence of deaths and presence or absence of MRD after induction therapy. The absence of MRD was considered to be the occurrence of complete hematological remission, that is, the presence of 5% or less of blasts in the OM, reestablishment of normal hematopoiesis (return to normal values of hemoglobin, leukometry, differential leukocyte count and platelet count). and absence of extramedullary disease after induction therapy [12].

All reactions were prepared with a final volume of 50  $\mu$ L. PCR reactions with primers for *abcb1* and *lrp* were performed. The samples were initially denatured at 94 °C for 5 minutes and then subjected to the ideal reaction conditions for each pair of primers. At the end of the PCR cycles, a final extension was performed at 72°C for 10 minutes [13]. The ideal reaction conditions and the number of cycles used were established in previous tests carried out at the Laboratory of Experimental Oncology and Hemopathies (LOEH) so that the PCR ended in the exponential phase of the amplification. The PCR products were electrophoresed in 2% agarose gel at 100 volts for 30 minutes and stained with ethidium bromide. The bands were visualized in a transilluminator (HOEFER-MacroVue UV-20) under UV light of 320 nm (Figure 2) and photographed with the gel photo-documentation system (DOC-PRINT®, Biosystems). The size of the fragments was estimated by comparison with the 50 bp molecular size marker.

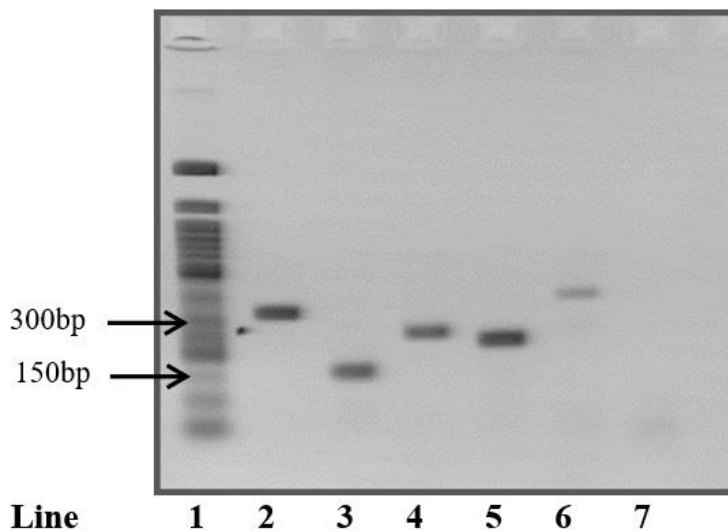


**Figure 2.** Representative 2% agarose gel of polymerase chain reaction (PCR) positive controls for detection of *abcb1* (K562-LUCENA), *abcc1* (Jurkat), *lrp* (Jurkat) and survivin (K562). [Line 1 – Molecular size marker 50 bp; Line 2 – PCR product with primers for *gapdh* (330 bp); Line 3 – PCR product with primers for *abcb1* (157 bp); Line 4 – PCR product with primers for *abcc1* (260 bp); Line 5 – PCR product with primers for *lrp* (240 bp); Line 6 – PCR product with survivin primers (393 bp); Line 7 – Negative control with water.]

The mean intensity of each band was assessed by the digital analysis program. The intensity of the *abcb1*, *abcc1*, *lrp* and survivin gene bands was divided by the intensity of the *gapdh* normalizing gene. Results were reported in the form of relative transcription.

### Acknowledgement

In this study, the financial support was provided by The Scientific and Technological Research Council of Turkey (TUBITAK), Project No. 217612502. All experimental works were conducted in Erzincan Binali Yıldırım University, Turkey Research Laboratory. The author would like to thanks to all supporters due to their precious contributions.



### References

- [1] Abdulsalam, Abbas. (2010). Laboratory diagnosis of acute leukemia in Iraq, the available options. Turkish Journal of Hematology. 27. 10.5152/tjh.2010.59.
- [2] Alyaqubi, Kifah & AL-Faisal, A. & Almothaffar, Ali & Tobal, Khalid. (2014). Assessment of Multidrug Resistance Gene (MDR1) Expression in Acute Myeloid Leukemia.. IJAR.. 2. 375-383.
- [3] Mjali, Ahmed & Hasan Jaleel Al-Shammari, Haider & Abbas, Nareen & Azeez, Zahraa & Abbas, Saja. (2019). Leukemia Epidemiology in Karbala province of Iraq. Asian Pacific Journal of Cancer Care. 4. 135-139. 10.31557/apjcc.2019.4.4.135-139.
- [4] Biteau B, Hochmuth CE, Jasper H. Maintaining tissue homeostasis: dynamic control of somatic stem cell activity. Cell Stem Cell. 2011 Nov 4;9(5):402-11. doi: 10.1016/j.stem.2011.10.004. PMID: 22056138; PMCID: PMC3212030.
- [5] Ferlay J, Ervik M, Lam F, Colombet M, Mery L, Piñeros M, et al. Global Cancer Observatory: Cancer Today. Lyon: International Agency for Research on Cancer; 2020 (<https://gco.iarc.fr/today>, accessed February 2021).
- [6] Carrillo, Olarte & Ramos-Peñafiel, Christian & Peralta, E & Fuller, E & Ipiña, J & Centeno, Federico & Garrido, Efraín & Jaloma, J & Vargas, K & Martínez Tovar, Adolfo. (2016). Clinical significance of the ABCB1 and ABCG2 gene expression levels in acute lymphoblastic leukemia. Hematology (Amsterdam, Netherlands). 22. 1-6. 10.1080/10245332.2016.1265780.
- [7] Maroofi, Farzad & Amini, Sabrieh & Roshani, Daem & Ghaderi, Bayazid & Abdi, Mohammad. (2015). Different frequencies and effects of ABCB1 T3435C polymorphism on clinical and laboratory features of B cell chronic lymphocytic leukemia in Kurdish patients. Tumor Biology. 10.1007/s13277-014-2914-9.
- [8] Tomiyasu, Hirotaka & Watanabe, Manabu & Goto-Koshino, Yuko & Fujino, Yasuhito & Ohno, Koichi & Sugano, Sumio & Tsujimoto, Hajime. (2012). Regulation of the expression of ABCB1 and LRP genes by

- MAPK/ERK pathway and its role in the generation of side population cells in canine lymphoma cell lines.. *Leukemia & lymphoma*. 54. 10.3109/10428194.2012.751529.
- [9] James, William & Grech, Victor. (2017). A review of the established and suspected causes of variations in human sex ratio at birth. *Early Human Development*. 109. 10.1016/j.earlhumdev.2017.03.002.
- [10] Liu, TC & Lin, Hsiu-Fen & Chen, TP & Chang, JG. (2002). Polymorphism analysis of CYP3A5 in myeloid leukemia. *Oncology Reports*. 9. 327-329.
- [11] Kumar CC. Genetic abnormalities and challenges in the treatment of acute myeloid leukemia. *Genes Cancer*. 2011 Feb;2(2):95-107. doi: 10.1177/1947601911408076. PMID: 21779483; PMCID: PMC3111245.
- [12] Miladpoor, Behnoosh & Shokouhi, Amireh & Shirdel, Abbas & entezari heravi, Reza & Banihashem, Abdollah & Esmaily, Habibollah & Khedri, Azam & Behravan, Javad. (2009). Association of Acute Lymphoblastic Leukemia and MDR1 Gene Polymorphism in an Ethnic Iranian Population. *Iranian journal of blood and cancer. SIDIRANIAN JOURNAL OF BLOOD AND CANCER* | Volume 1, Number 2 ,63-66
- [13] Rafiq, Sabika & Raza, Muhammad & Younas, Mehwish & Naeem, Fariha & Adeeb, Romisha & Iqbal, Javed & Anwar, Pervez & Sajid, Umara & Manzoor, Hafiza. (2018). Molecular Targets of Curcumin and Future Therapeutic Role in Leukemia. *Journal of Biosciences and Medicines*. 06. 33-50. 10.4236/jbm.2018.64003.



# The Effect of Material Preference on Engine Performance in Otto Cycle Engine

Nilay AKDENİZ ACAR<sup>1</sup>, \* , Emre ARABACI<sup>2</sup> ,

<sup>1</sup>Alaplı Vocational School of H. Education, Dept. of Machinery and Metal Tech., Zonguldak Bülent Ecevit Uni., Zonguldak, Türkiye

<sup>2</sup>Faculty of Technology, Department of Automotive Engineering, Pamukkale University, Denizli, Türkiye

## Abstract

Internal combustion engines are used in the automotive industry, construction, agriculture and energy sectors. These internal combustion engines have been in development for over 150 years. However, the thermodynamic cycles of internal combustion engines are among the main topics of thermodynamics textbooks. In this study, Otto cycle, which is the thermodynamic equivalent of spark ignition engines, has been analyzed from a different perspective. For the Otto cycle, the performance evaluation was made by using the melting points of various materials as the maximum temperature value. Thus, the effect of material selection on specific net work and mean effective pressure for an Otto cycle engine was investigated. It has also been shown that the optimum compression ratio of the engine can be determined depending on the material selection. It is foreseen that the results obtained in this study are guiding especially for engine designers.

**Keywords:** Otto cycle engine, Engine material, Performance

## 1. Introduction

Performance analysis using thermodynamic cycles for internal combustion engines that we have been using for more than 150 years is very instructive in terms of determining the design parameters. Engines in use today are classified as compression-ignition or spark-ignition, and both are widely used. It is possible to find many studies on the thermodynamic cycles of these engines in the literature. It is possible to list some of the works as follows. Gonca et al. [1] examined different cycles comparatively in their study. Chen et al. [2] examined the effect of specific heat changes on performance in the irreversible Otto cycle in their study. Yuan et al. [3] optimized the thermodynamic cycles for two finite dimensional reservoirs in their study. Ge et al. [4] investigated the optimal piston movement configuration in an otto cycle engine according to the maximum ecological function. Ozdemir et al. [5] examined the effect of average piston speed and residual gas ratio on performance for the irreversible otto cycle.

In this study, the effect of material selection on engine performance in Otto cycle engines was investigated theoretically. As it is known, Otto-cycle engines are engines in which the heat input is constant. As a general thermodynamic approach, thermal efficiency is presented only as a function of compression ratio. However, with the compression ratio, the in-cylinder pressure and temperature also increase. In addition, the maximum in-cylinder temperature varies according to the compression ratio as well as the input heat. In addition to these conditions described, a performance evaluation was made by limiting the maximum temperature of the cycle. Specific net work and mean effective pressure parameters were used for performance evaluation.

## 2. Materials and Methods

In this study, a model was created on the air standard Otto cycle (Figure 1). Thermodynamic relations are created for this model [6-8]. Irreversibility is ignored in the model. The following equations are used for thermal efficiency and specific net work.

$$\eta_{th} = \frac{w_{net}}{q_{in}} = \frac{q_{in} - |q_{out}|}{q_{in}} = 1 - \frac{1}{\varepsilon^{k-1}} \quad (1)$$

\* Corresponding author. e-mail address: nakdeniz@beun.edu.tr



$$w_{\text{net}} = q_{\text{in}} - |q_{\text{out}}| = c_v(T_3 - T_2 - T_4 + T_1) \quad (2)$$

$$T_4 = \frac{T_3}{\varepsilon^{k-1}} = \frac{T_1 T_3}{T_2} \quad (3)$$

Figure 1 shows the P-v and T-s diagrams for the Otto cycle.

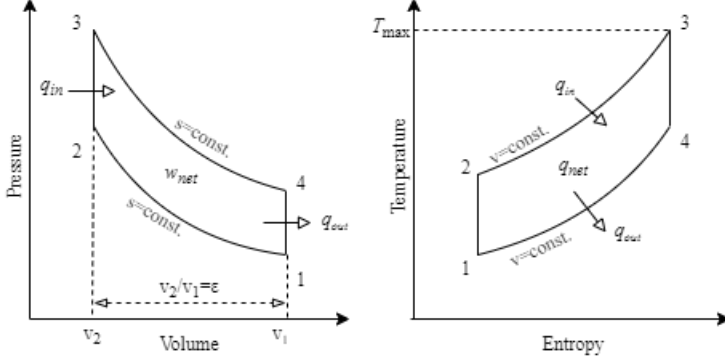


**Figure 1.** P-v and T-s diagram for Otto cycle

The following equations are used for specific net work optimization:

$$\frac{dw_{\text{net}}}{dT_{2s}} = c_v \left( -1 + \frac{T_1 T_3}{T_2^2} \right) = 0 \quad (4)$$

$$T_{2,\text{opt}} = \sqrt{T_1 T_3} = T_{4,\text{opt}} \quad (5)$$

$$\varepsilon_{\text{opt}} = \sqrt[k-1]{\frac{T_3}{T_1}} = \sqrt[k-1]{\tau} \quad (6)$$

$$w_{\text{net,max}} = c_v T_1 (\sqrt{\tau} - 1)^2 \quad (7)$$

The following equations are used for the mean effective pressure optimization:

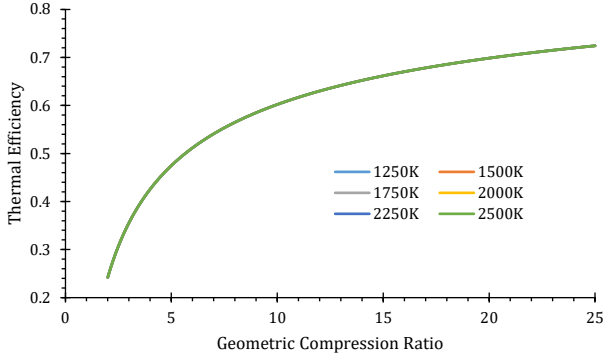
$$\frac{dp_{\text{me}}}{dT_2} = (k-1)(T_1 T_3 - T_2^2) \left( \frac{T_2}{T_1} \right)^{\frac{1}{k-1}} - T_1 [(k-2)T_3 + T_2] - T_2 (T_3 - kT_2) = 0 \quad (8)$$

$$\frac{dp_{\text{me}}}{d\varepsilon} = \varepsilon(k-1)(\tau + \varepsilon^{2k-2}) - (k-2)\tau - (\tau+1)\varepsilon^{k-1} + k\varepsilon^{2k-2} = 0 \quad (9)$$

Using the equations presented here, the maximum specific net work and maximum mean effective pressure can be determined. Here, the cycle maximum temperature is used as a performance limiter. The melting point of the engine building material selected as the cycle maximum temperature was used. Alumina (2345K), Titanium (1943K), Carbon-Steel (1813K), Cast Iron (1477K) were used as possible engine materials for this study [9]. For this reason, the range of 1250K-2500K was used as the maximum temperature in the calculations. In addition, a range of 2-25 is used for the compression ratio. In addition, it is assumed that  $T_1 = 300$  K,  $P_1 = 100$  kPa,  $c_v = 0.718$  kJ/kgK,  $k = 1.4$ .

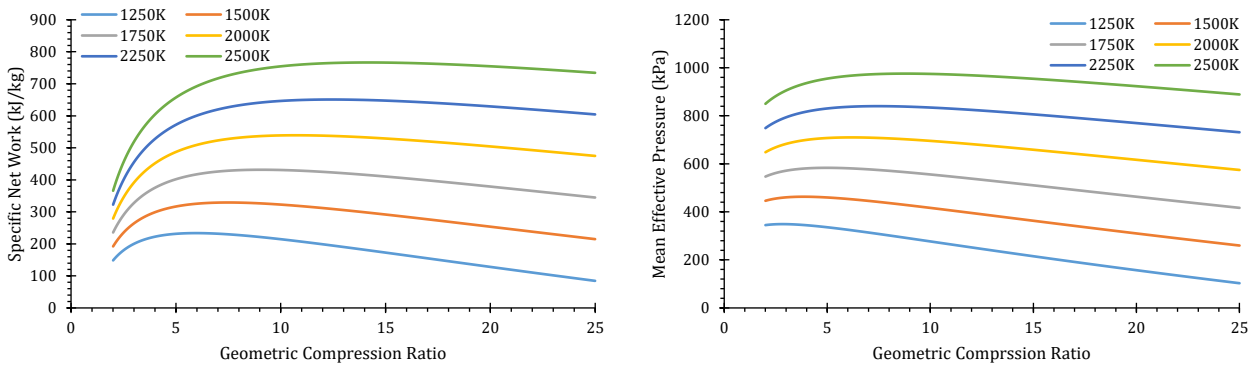
### 3. Results and Discussion

Figure 2 shows the variation of the thermal efficiency depending on the compression ratio. Here all the lines overlap. Because thermal efficiency is only a function of compression ratio. As can be seen, the higher the compression ratio, the higher the thermal efficiency.



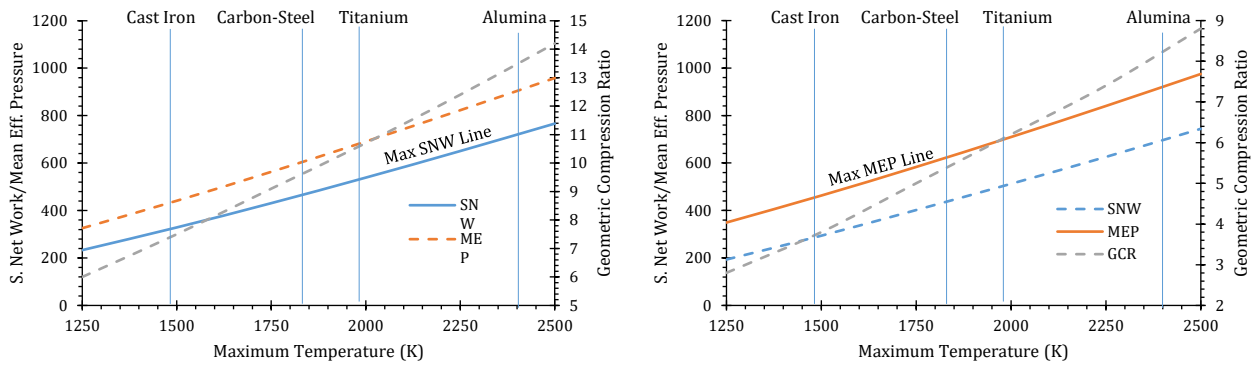
**Figure 2.** Variation of thermal efficiency with compression ratio

Figure 3 shows the variation of the specific net work and the mean effective pressure depending on the compression ratio. As can be seen, as the maximum temperature increases, the specific net work and mean effective pressure increase. However, both the specific net work and the mean effective pressure are maximum for only one compression ratio.



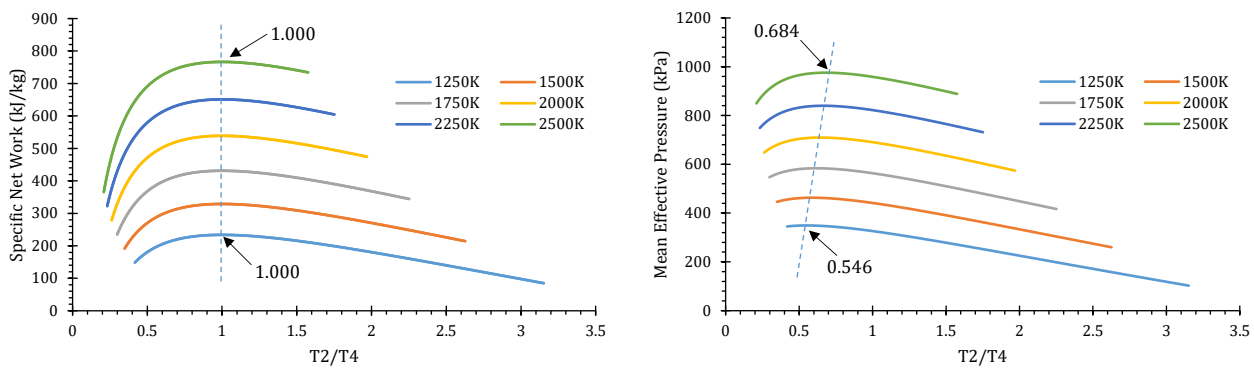
**Figure 3.** Variation of specific net work and mean effective pressure with compression ratio

Figure 4 shows the variation of the specific net work and the mean effective pressure with respect to the maximum temperature. In addition, the graphs show the variation of geometric compression ratio depending on the maximum temperature. Compression ratio values in cases where the specific net work and mean effective pressure are maximum were evaluated. In addition, the materials used for this paper are also labeled on the graphics. As can be seen, when materials with higher melting points are preferred, the engine can be operated at higher compression ratios.



**Figure 4.** Variation of specific net work and mean effective pressure with maximum temperature

Figure 5 shows the variation of specific net work and average effective pressure with respect to  $T_2/T_4$ . Here,  $T_2/T_4$  temperature required for maximum specific net work and mean effective pressure is an important parameter. According to Eq. 5, it is stated that  $T_2 = T_4$  should be in order for the specific net work to be maximum. This is also shown in Figure 5. For the maximum value of the mean effective pressure, as the  $T_3$  temperature is increased, the  $T_2/T_4$  temperature should also be increased. However, even when the maximum pressure is doubled, the  $T_2/T_4$  value increases by 25%.



**Figure 5.** Variation of specific net work and mean effective pressure with respect to  $T_2/T_4$

In this study, the effect of material selection on specific net work and mean effective pressure for an Otto cycle engine was investigated. It has also been shown that the optimum compression ratio of the engine can be determined depending on the material selection. It is foreseen that the results obtained in this study are guiding especially for engine designers.

## Acknowledgment

No financial support was received from any institution or organization for this study.

## References

- [1] Gonca, G. (2016). Comparative performance analyses of irreversible OMCE (Otto Miller cycle engine)-DiMCE (Diesel miller cycle engine)-DMCE (Dual Miller cycle engine). *Energy*, 109, 152-159.
- [2] Ge, Y., Chen, L., & Qin, X. (2018). Effect of specific heat variations on irreversible Otto cycle performance. *International Journal of Heat and Mass Transfer*, 122, 403-409.
- [3] Yuan, H., Ma, Y. H., & Sun, C. P. (2022). Optimizing thermodynamic cycles with two finite-sized reservoirs. *Physical Review E*, 105(2), L022101.

- [4] Ge, Y., Chen, L., & Feng, H. (2022). Optimal piston motion configuration for irreversible Otto cycle heat engine with maximum ecological function objective. *Energy Reports*, 8, 2875-2887.
- [5] Özdemir, A. O., Kılıç, B., Arabacı, E., & Orman, R. Ç. (2018). Effect of mean piston speed and residual gas fraction on performance of a four-stroke irreversible Otto cycle engine. *Scientific Journal of Mehmet Akif Ersoy University*, 1(1), 6-12.
- [6] Kanoğlu, M., Çengel, Y. A., & Cimbala, J. M. (2020). *Fundamentals and applications of renewable energy*. McGraw-Hill Education.
- [7] Babu, V. (2019). *Fundamentals of Engineering Thermodynamics*. CRC Press.
- [8] Borgnakke, C. (2022). *Fundamentals of thermodynamics*. John Wiley & Sons.
- [9] Palaci, Y., & Gonca, G. (2020). The effects of different engine material properties on the performance of a diesel engine at maximum combustion temperatures. *Thermal Science*, 24(1 Part A), 183-191.



## Evaluation of Some Biological Parameters and Trace Elements in Prostatic Tumors among Iraqi Patients with DMII

Usama Salman Mahdy AL-AZZAWI<sup>1</sup> \* , Volkan EYÜPOĞLU<sup>1</sup>

<sup>1</sup>Chemistry Department, Çankırı Karatekin University, Türkiye

### Abstract

Among the challenges facing doctors in advanced prostate, cancer management is that it is developing quickly, which requires research in rapid ways to predict its development. Our goal in this study is to define some liver tests (Alp), Chlo, PSA, and TPA tests, focus on some trace elements in men with prostate and type 2 diabetes and discover the linear relationship between the specified tracking elements that were estimated between cases. The kidney fears tests were not mentioned in this study, but the levels of uric acid were significantly affected. There was clear importance of liver enzymes, whose levels were clearly affected, and there was a link between them and PSA in prostate cancer patients. The vowed elements did not have great influence, especially magnesium and selenium, on the contrary, zinc had a great statistical and clinical importance in this study. In general, during this study, the necessary parameters will be identified as good indicators for prostate cancer patients and DMII at the same time.

**Keywords:** Prostatic tumors, Trace elements, DMII, PSA, TPA

### 1. Introduction

Prostate cancer is the 6<sup>th</sup> most widely spread type of cancer in the world, the 2nd most common type in men, and the most widely spread type of cancer in men in Europe, the US, and parts of Asia [1]. The number of newly diagnosed cases was 513,000 patients in the year 2000, whereas it became 1.1 million patients in the year 2012. This means that there is an increased number of cases of prostate cancer in the past 10 years. The good news is that a large number of patients survive after many years post diagnosing, which refers to the fact that systems of cancer registration include only the two ends of the disease spectrum and are not adequate enough for determining the actual disease burden [2].

Prostate cancer is a multifactorial disease, and its exact etiology is not clear yet. It has been suggested that genetic causes as well as environmental and lifestyle factors play a role in developing prostate cancer. In addition to these genetic and lifestyle factors Prostate cancer is a multifactorial disease, and the exact etiology is not clear yet [3].

It has been suggested that genetic causes as well as environmental and lifestyle factors play a role in developing prostate cancer. In addition to these genetic and lifestyle factors, variation in prostate cancer occurrences and mortality rates across the different parts of the world can be attributed to healthcare differences in cancer screening and registration also the commonly accepted factors of risk are age, ethnicity, and family history of PC [4].

Heavy metals are rather dense ones that have potential toxicity, particularly in environmental contexts. They are obtained naturally from the crust of the earth and become concentrated due to human activities. Heavy metals can enter human tissues through diet, inhalation, and manual handling. Another possible source of contamination of heavy metals is absorbed by skin contact, for instance from contact with soil [5]. The toxic heavy metals can bioaccumulate in the human body as they are difficult to be metabolized. Those metals may bind to and interfere with the functioning of vital cellular elements [6]. It was proven that some trace elements play an important part in the biology of cancer; on the other hand, there still remains a gap in the understanding of the correlation between the functions and initiation of the trace elements, advancement, and inhibition of carcinogenic procedure in the prostate gland [7].

\* Corresponding author. e-mail address: [osa12281@gmail.com](mailto:osa12281@gmail.com)

Therefore, trace element analysis is important in the tissues of the human body. It can be of importance for the identification of differences in trace elements homeostasis between two common illnesses of the aging prostate which is the benign prostatic hyperplasia (BPH) and prostate cancer (PCa) [8]. due to the fact that both of those conditions have varying histopathology and clinical behavior, various metabolic alterations have to be accounted for those pathologic procedures [9].

## 2. Materials and Methods

A total of 140 cases have participated in this research and were divided to 2 groups. The first one included 100 male patients aged between 44 - 75 years, this group was patients with prostate tumors and DMII. The second group included 40 healthy men that have normal prostate glands and without any previous history of any systemic diseases, Figure 3.1 shows the groups of current medical investigation.

I. Group A: 100 with prostate tumors & DMII (patients groups).

II. Group B: 40 without prostate tumors & DMII (control group).

For the calculations of hemoglobin A1c (HbA1c) in patients' blood, it can use the below Equation.

$$\text{HbA1c (\%)} = R_{\text{unknown}} / R_{\text{standard}} \times \text{Standard concentration}$$

For calculations glucose levels, see below Equation.

Glucose oxidase



Peroxidase



for the calculation the Calcium levels in patient's blood it can be use below Equation.

$$\text{Total Calcium (mg / dL)} = A_{\text{sample}} / A_{\text{standard}} \times C_{\text{standard}}$$

## 3. Results and Discussion

A total of 140 cases participated in this research and were divided into two groups. The first male patients between the ages of 30 and 75 were included, and this group (100 patients) represented the group of patients with prostate and DMII tumors. The second group included 40 healthy men who have a natural prostate gland without any previous date of any systemic diseases.

All these results and comparisons for the selected parameters are shown in Figure 1, it can be concluded from this Figure that the high differentiation between the groups led to indicate it is significant to use age and RBS to detect this kind of disease.

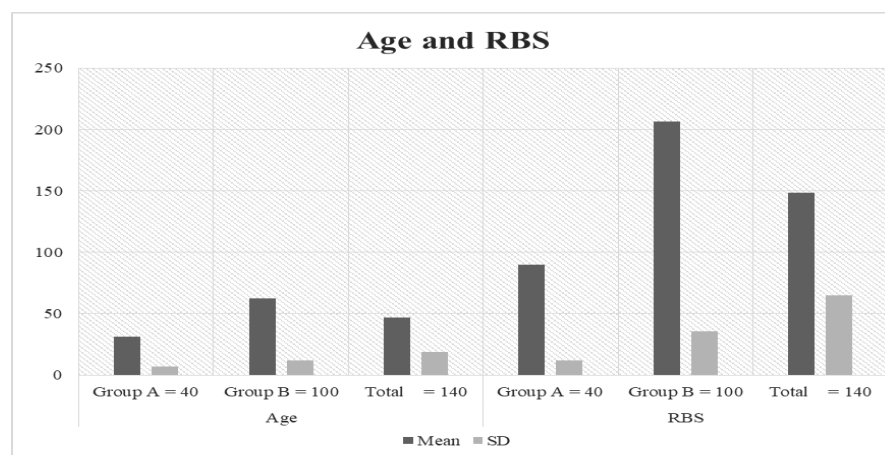


**Figure 1.** The mean and SD of age and RBS for the studied groups

Among the challenges facing doctors in advanced prostate, cancer management is that it is developing quickly, which requires research in rapid ways to predict or predict a rapid development. The results of the study indicated that with the progress of age, stainlessness increases with prostate cancer, and the complications of the treatment increase.

### Acknowledgement

In this study, the financial support was provided by the Author. All experimental works were conducted in Diyala Hospital Laboratory. The author would like to thanks to all supporters due to their precious contributions.

### References

- [1] Asare, G. A., Ngala, R. A., Afriyie, D., Adjei, S., Nyarko, A., Anang-Quartey, Y. and Mossanda, K. 2017. Calcium-Magnesium imbalance implicated in benign prostatic hyperplasia and restoration by a phytotherapeutic drug–*Croton membranaceus* Müll. Arg. BMC Complementary And Alternative Medicine, 17(1), 1-8.
- [2] Kumar, R. J., Barqawi, A. B., & Crawford, E. D. 2004. Epidemiology of prostate cancer. Business Briefing: US Oncology Review, 1-6.
- [3] Hope, T., Goodman, J., Allen, I. Meta-analysis of 68Ga-PSMA-11 PET accuracy for the detection of prostate cancer validated by histology. J Nucl Med 2019; 6600: 786.
- [4] Ali, H. M., Qater, A. N. A. K. and Selman, M. O. 2019. Effect of Some Heavy Metals on Testosterone Hormone in Infertile Men. Journal of University of Babylon for Pure and Applied Sciences, 27(6): 368-377.
- [5] Qu, C; Ma, Z; Yang, J; Lie, Y; Bi, J; Huang, L . 2014. Human Exposure Pathways of Heavy Metal in a Lead-Zinc Mining Area". In Asrari, E. Heavy Metal Contamination of Water and Soil: Analysis, assessment, and remediation strategies. Apple Academic Press. Pp 129–156.
- [6] Fendler, W., Calais, J., Eiber, M. 2019. Assessment of 68Ga-PSMA-11 PET accuracy in localizing recurrent prostate cancer: a prospective single arm trial. JAMA Oncol 2019 (epub Mar 28).
- [7] Calais, J., Ceci, F., Eiber, M. 2019. 18F-fluciclovine PETCT and 68Ga-PSMA-11 PET-CT in patients with early biochemical recurrence after prostatectomy: a prospective, single-centre, single arm, comparative imaging trial. Lancet Oncol 2019; 20:1286.
- [8] Banas, A., Kwiatek, W. M., Banas, K. 2010. Correlation of concentrations of selected trace elements with Gleason grade of prostate tissues. J. Biol. Inorg. Chem., 15: 1147-55.
- [9] Radwan, N., Phillips, R., Ross, A., Rowe, S. P., Gorin, M. A., Antonarakis, E. S. and Tran, P. T. (2017). A phase II randomized trial of Observation versus stereotactic ablative Radiation for OLigometastatic prostate CancEr (ORIOLE). BMC cancer, 17(1), 1-9.



# Improved Speed and Torque Efficiency for DTC Controlled Asynchronous Machine Using Fuzzy Switching Algorithm

**Goksu GOREL<sup>1,\*</sup>**, **Wahib HILOUAN MOHAMED<sup>2</sup>**

<sup>1</sup> Institute of science, Faculty of Engineering, Department of Electrical and Electronics, Çankırı Karatekin University, Çankırı, Türkiye

<sup>2</sup> Institute of science, Faculty of Engineering, Department of Electrical and Electronics, Çankırı Karatekin University, Çankırı, Türkiye

## Abstract

A vector form of control called direct torque control is based on stator flux and torque. Takashi invented it in the middle of the 1980s. Control of the primary components of an asynchronous machine, particularly the stator flux and electromagnetic torque, is possible by direct selection of the inverter's output voltage vectors. These choices are done in a manner that keeps both values inside a hysteresis band. Through the use of two regulators, the PI controller and fuzzy logic, this study aims to reduce torque ripple while also accomplishing motor speed control. To determine which performs better, comparisons will be made [1] [2] [3] [4] [5]. The results will be shown by using Matlab/Simulink at the end of the article, and a discussion will be made by comparing those two regulator.

**Keywords:** Asynchronous machine, direct torque control, fuzzy logic, pi regülâtör

## 1. Introduction

The asynchronous machine is the most widely used machine for achieving speed variations. It has a default unlike the DC machine, in which the power supply causes the same current to create the flux and the torque, by causing a flux variations obtained by the torque variations.

The DTC is the most efficient, straightforward, and accurate method of torque control for IM drives. With the exception of stator resistance, it is widely known for being tolerant to changes in motor parameters. The drive performance may suffer if the parameters speed, or loads are changed because the majority do not provide the quickest torque response [6]. Speed management is one of the most crucial components of an IM drive and must be handled skillfully. Researchers have been working on kind solutions to help DTC perform well for decades. Our study is focusing on applied direct torque control on the induction machine while using fuzzy logic controller, and PI regulator. Then seeing the difference between them and the performance they can afford.

## 2. Materials and Methods

### 2.1. Direct torque control method

Direct Torque Control (DTC) has replaced previous methods, particularly Field Oriented Control, more and more in the industry. The DTC estimates the stator flux and torque of the motor using stator current measurements without the use of electromechanical sensors.

Direct torque control has gained popularity due to its quick dynamic torque feedback and easy control structures. In contrast to other control systems, the direct torque control approach still has a number of drawbacks. The most prominent of these is excessive torque ripple, which can lead to problems with motor performance [7].

In order to control the electro-magnetic torque and stator flux, a voltage inverter is switched using a control sequence that must be determined. Hysteresis controllers are in charge of regulating the system's state while taking electromagnetic torque and the amplitude of the stator fluctuation into account.

\* Corresponding author. e-mail address: goksugorel@karatekin.edu.tr



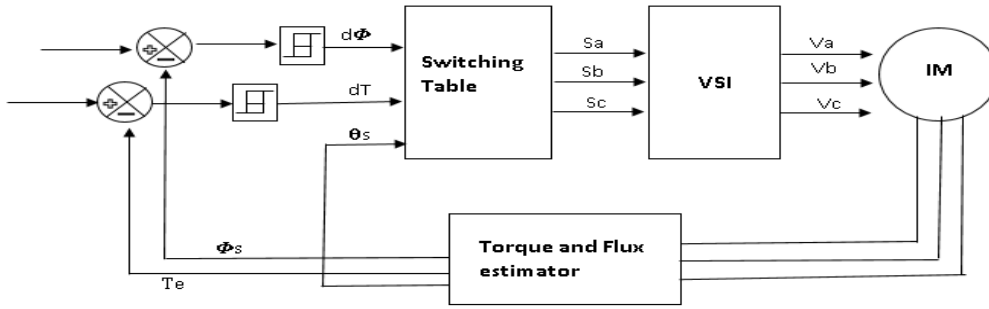


**Figure 1.** The conventional structure of direct torque control.

Seven possible points in the phase plane, or eight sequences of the voltage vector at the inverter output, are reachable by the inverter (a two-level inverter). The following figure 2 can be used to demonstrate direct control of the conventional torque of a three-phase asynchronous machine:

The inverter's purpose is to convert a DC voltage  $E$  (provided by a rectifier or another DC supply) into three simple AC voltages noted  $V_{an}$ ,  $V_{bn}$ , and  $V_{cn}$  that are given to the motor as a three-phase system with variable frequency and amplitude. The logical  $S_a$ ,  $S_b$ ,  $S_c$  operate the converter. The voltage vector  $V_s$  can have two null vectors ( $V_0$  and  $V_7$ ) and six non-null vectors, as shown in Figure 2, when the converter's various states are combined.

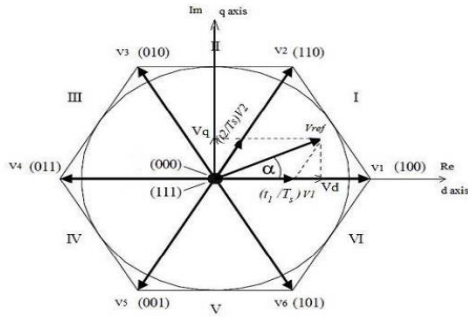


**Figure 2.** Voltage vector  $V_s$  based on switching states

The following equation is a representation of the voltage vector:

$$V_s = \sqrt{\frac{2}{3}} * E(S_a + a * S_b + a^2 * S_c) \quad (1)$$

The following equation is a representation of the voltage vector:

There are six zones within the ( $s$ ) movement area, with  $i=[1;6]$ .

One of the eight voltage vectors given below can be utilized to control the flux and torque while it is inside a zone  $i$  [8].

When  $V(i+1)$  is selected,  $(\Phi_s)$  and  $(\Gamma_{em})$  rise.

If  $V(i-1)$  is selected,  $(\Phi_s)$  rises and  $(\Gamma_{em})$  decreases.

If  $V(i+2)$  is selected, both  $(\Phi_s)$  and  $(\Gamma_{em})$  increase.

If  $V(i-2)$  is selected,  $(\Phi_s)$  and  $(\Gamma_{em})$  decrease as well.

If  $V_0$  and  $V_7$  are selected, the rotation of the stator flux is halted and a sharp reduction in  $(\Gamma_{em})$  is demonstrated while still taking into consideration the fact that the stator value is unaltered.

At the beginning of the region, the vectors  $V_i$  and  $V_{(i+3)}$  are not used because the flux component is very strong with a zero torque in the middle of the zone. At the end of the zone, the direction of the torque or flux evolution is the opposite.

The voltage vector at the inverter's output is calculated from the torque and flux differences, as well as the position of the vector  $F_s$ , in relation to their reference. A flux estimator in modulus and position is needed along with a torque estimator.

### 2.1.1 Stator Flux and Torque Estimation

The flux is shown as follows using the equation from the stator reference:

$$\Phi_s = \int_0^t (V_s - R_s * I_s) dt \quad (2)$$

The stator current is measured while the stator voltage depends on the state of the switches (Sa, Sb, Sc), and the DC link voltage E. Projecting on the two axes  $\alpha$  and  $\beta$ , we will obtain the two components of the estimated stator flux vector:

$$\Phi_{s\alpha} = \int_0^t (V_{s\alpha} - R_s * I_{s\alpha}) dt \quad (3)$$

$$\Phi_{s\beta} = \int_0^t (V_{s\beta} - R_s * I_{s\beta}) dt \quad (4)$$

When we use Concordia's transformation, we get:

$$V_{s\alpha} = \sqrt{\frac{2}{3}} * E * (s_a - \frac{1}{2}(s_b + s_c)) \quad (5)$$

$$V_{s\beta} = \sqrt{\frac{1}{2}} * E * (s_b - s_c) \quad (6)$$

$$V_s = V_{s\alpha} + jV_{s\beta} \quad (7)$$

Similar to how the currents  $I_s$  and  $I_s$  are produced from the measurement of the machine's true currents  $I_{sa}$ ,  $I_{sb}$ , and  $I_{sc}$  ( $I_{sa}+I_{sb}+I_{sc}=0$ ), we also get the following results after performing the CONCORDIA transformation:

$$I_{s\alpha} = \sqrt{\frac{2}{3}} * I_{sa} \quad (8)$$

$$I_{s\beta} = \sqrt{\frac{1}{2}} * (I_{sb} - I_{sc}) \quad (9)$$

$$I_s = I_{s\alpha} + jI_{s\beta} \quad (10)$$

From the two flux components in frame -, the estimated stator flux's angle and amplitude are calculated as follows:

$$\Phi_s = \sqrt{\Phi_{s\alpha}^2 + \Phi_{s\beta}^2} \quad (11)$$

$$\theta_s = \text{atan}\left(\frac{\Phi_{s\alpha}}{\Phi_{s\beta}}\right) \quad (12)$$

The measured currents and estimated fluxes can be used to estimate the electromagnetic torque, which can be represented as follows:

$$Te = \frac{3}{2}p * (\Phi_{s\alpha} I_{s\beta} - \Phi_{s\beta} I_{s\alpha}) \quad (13)$$

### 2.1.2 Stator Flux and Torque Hysteresis Comparator

This corrector is used to maintain the end of the stator flux vector in a circular band. The error between the reference flux and the estimated flux is injected into the two-level hysteresis controller. It generates at its output the variable  $\Phi_{flux}$  which indicates whether the amplitude should be increased or decreased.

The electromagnetic torque can be positive or negative depending on the direction of rotation of the machine. It is possible to propose two solutions (two-level or three-level corrector) The two-stage corrector allows controlling in one sense of rotation only [9].

### 2.1.4 Switching Table

The state of the Boolean variables at the output of the two flux correctors, the electromagnetic torque, and the sector providing the information on the position of the flux vector are taken into account when creating the switching table.

**Table 1.** Switching table.

Flux	Torque	S1	S2	S3	S4	S5	S6
$d\Phi=1$	$dT=-1$	V3	V4	5	V6	V1	V2
	$dT=0$	V0	V7	V0	V7	V0	V7
	$dT=1$	V5	V6	V1	V2	V3	V4
$d\Phi=0$	$dT=-1$	V2	V3	V4	V5	V6	V1
	$dT=0$	V7	V0	V7	V0	V7	V0
	$dT=1$	V6	V1	V2	V3	V4	V5

### 2.2 Speed Controllers

Pid controller is widely used in industries to regulate pressure, temperature, speed, flow, e.g. Subordinate mode improves the model system's soundness and allows for an increase in gain  $K_p$ . In the actual world, the PID controller seems to be a very effective approach to a variety of control problems [10] [11].

The mathematical form of this controller can be described as follows:

$$U(t) = K_p e(t) + K_i \int_0^t e(\tau) d\tau + K_d \frac{de(t)}{dt} \quad (14)$$

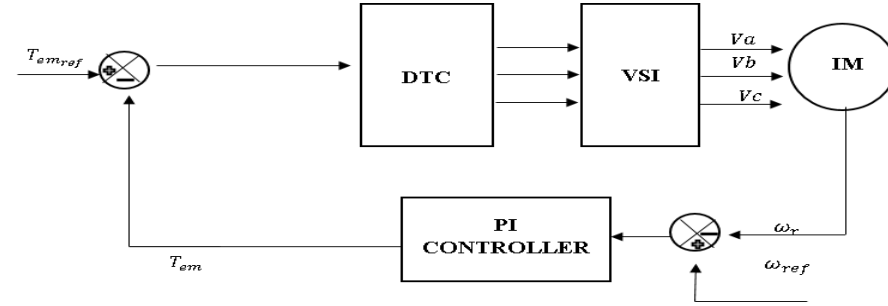


**Figure 3.** The design of PI speed controller.

The fuzzy logic controller (FLC) does not deal with a well-defined mathematical relationship. Instead, it uses inferences with several rules, based on linguistic variables. In this section, we will present the general procedure of designing a fuzzily-controlled computer system [9].

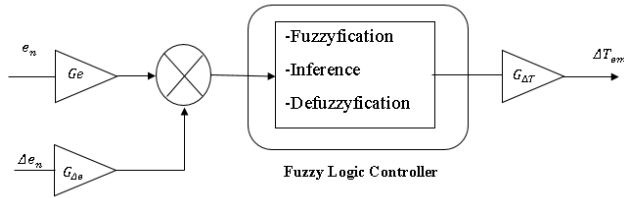


**Figure 4.** The design of Fuzzy logic speed controller.

The variables that reflect the error, its speed change, and the change in output can be normalised in the manner shown below:

$$e_n = \frac{e}{G_e} \quad (15)$$

$$\Delta e_n = \frac{\Delta e}{G_{de}} \quad (16)$$

$$\Delta T_{em} = \frac{\Delta T_{em}}{G_{\Delta T}} \quad (17)$$

### 3. Results and Discussion

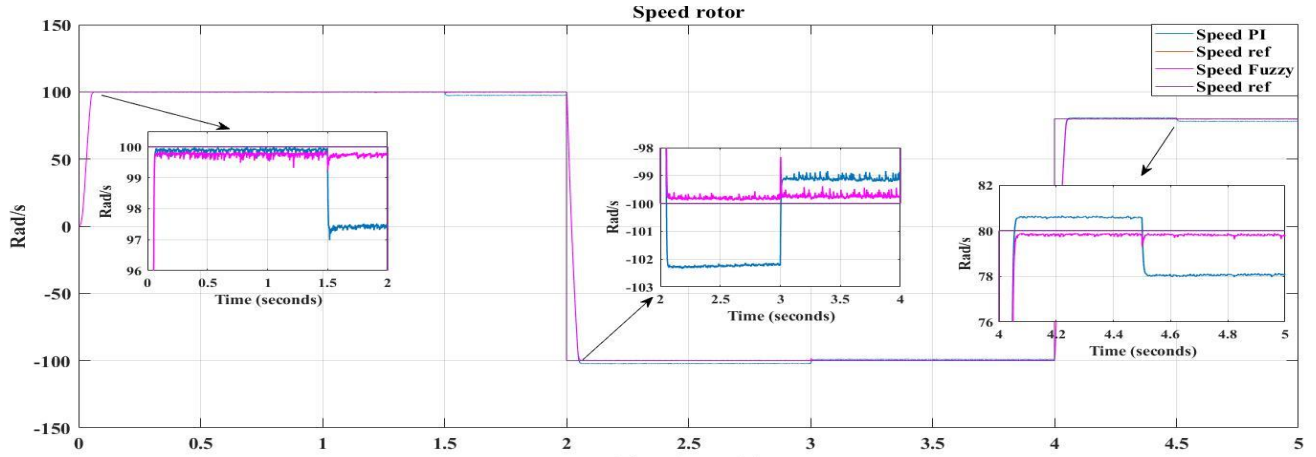


Figure 5 Rotor speed's response.

Both methods showed excellent response at start-up, but when the speed reference was changed, the fuzzy logic showed excellent performance not only in tracking the reference point but also when a change in torque reference was modified, it also showed excellent response, as you can see in the figure. In terms of efficiency and responsiveness, the fuzzy logic clearly outperforms the PI regulator.

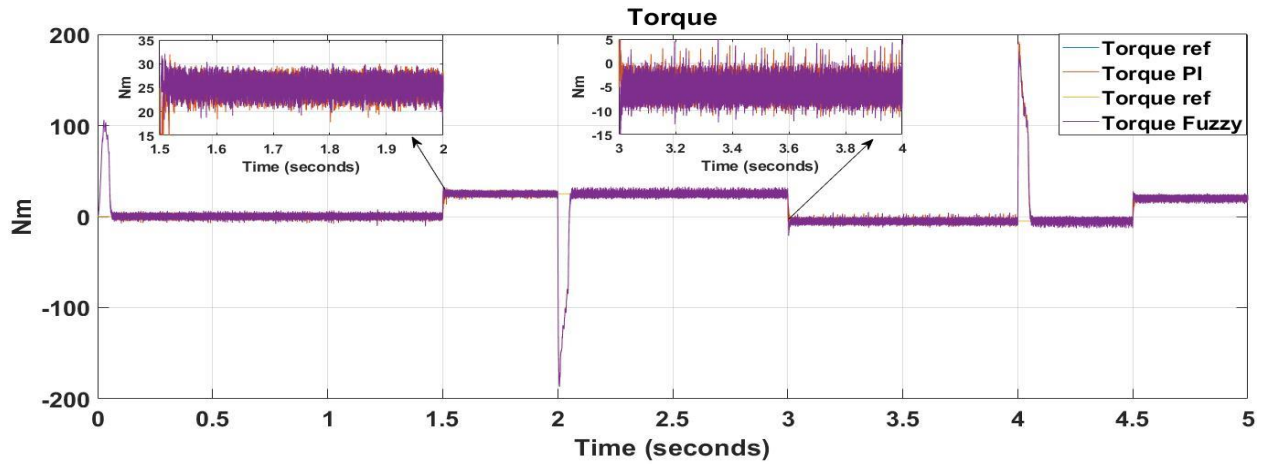


Figure 6 Torque's result.

At  $t = 1.5$  s to  $t = 2$  s, The fuzzy logic method has slightly reduced the torque ripple in contrast to the PI regulator, as shown in the figure. However, both of them shows a slight ripple when the torque becomes negative.

#### 3.1 Conclusion

In conclusion, by directly choosing the output voltage vectors of the inverter from a switching table, the primary asynchronous machine characteristics, notably the stator flux and the electromagnetic torque, are controlled. These decisions are taken in order to keep both quantities within a hysteresis band that is within the bounds of their reference values.

In addition, After comparing these two controllers, it is found that fuzzy logic provides better efficiency and reference point tracking than the Pi controller when the speed reference is changed.

## References

- [1] Korkmaz, F., Cakir, M. F. and Topaloglu, I. (2012). Fuzzy based stator flux optimizer design for direct torque control. arXiv preprint arXiv:1212.0160.
- [2] Farah, N., Talib, H. N. and Isa, Z. (2021). Fuzzy membership functions tuning for speed controller of induction motor drive: Performance improvement. *Indonesian Journal of Electrical Engineering and Computer Science*, 23(3), 1258-1270.
- [3] Patel, C., Rajeevan, P. P. and Kazmierkowski, M. P. (2011). Fast direct torque control of an open-end induction motor drive using 12-sided polygonal voltage space vectors. *IEEE Transactions on Power Electronics*, 27(1), 400-410.
- [4] Korkmaz, F., Topaloğlu, İ., and Mamur, H. (2015). Fuzzy logic based direct torque control of induction motor with space vector modulation. arXiv preprint arXiv:1508.01345.
- [5] El-Shimy, M. E., and Zaid, S. A. (2016). Fuzzy PID controller for fast direct torque control of induction motor drives. *Journal of Electrical Systems*, 12(4), 687-700.
- [6] Yordanova, S. (2015). Intelligent approaches to real time level control. *International Journal of Intelligent Systems and Applications*, 7(10), 19.
- [7] Farah, N., Talib, H. N. and Isa, Z. (2021). Fuzzy membership functions tuning for speed controller of induction motor drive: Performance improvement. *Indonesian Journal of Electrical Engineering and Computer Science*, 23(3), 1258-1270.
- [8] Cheok, A. D., and Fukuda, Y. (2002). A new torque and flux control method for switched reluctance motor drives. *IEEE Transactions on Power Electronics*, 17(4), 543-557.
- [9] Chikhi, A., Chikhi, K., and Belkacem, S. (2010). Induction Motor Direct Torque Control–Fuzzy Logic Contribution. *IU-Journal of Electrical & Electronics Engineering*, 10(2), 1207-1212.
- [10] Aggarwal, A., Rai, J. N., and Kandpal, M. (2015). Comparative Study of Speed Control of Induction Motor Using PI and Fuzzy Logic Controller. *IOSR Journal of Electrical and Electronics Engineering (IOSR-JEEE)*, 10(2), 43-52.
- [11] Abdullah, A. N., and Ali, M. H. (2020). Direct torque control of IM using PID controller. *International Journal of Electrical and Computer Engineering*, 10(1), 617.



# Study Change in Liver Enzymes and Hepcidin Hormone as a Possible Risk Factor to Juvenile Idiopathic Arthritis

Zeyad Abdulkareem Jumaah ALBYATI<sup>1,\*</sup>, Saliha ALYAR<sup>2</sup>

<sup>1</sup>Chemistry, Çankırı Karatekin University, Türkiye

<sup>2</sup>Ministry of Health, Iraq

## Abstract

As the principal hormone responsible for maintaining healthy iron levels, hepcidin has gained widespread attention in recent years. AST, ALT, hepcidin, ALP, hemoglobin, white blood cell count, erythrocyte sedimentation rate (ESR), and reluctance to bind sulfate were measured in patients with idiopathic juvenile arthritis (JIA) and healthy controls (RBS). The ages of rheumatoid arthritis patients and non-diseased controls were comparable. The average age of JIA patients was significantly higher than that of the controls. No significant differences were seen between patients with JIA and healthy controls in terms of AST levels. The researchers observed no significant differences in AL between individuals with JIA and healthy controls. Individuals with JIA have considerably higher ALP levels compared to the general population. Those with JIA exhibited considerably greater levels of ALP than the controls.

**Keywords:** Juvenile idiopathic arthritis, Hepcidin hormone, AST, ALP, ALT

## 1. Introduction

Hepcidin has recently been discovered to have a crucial role in regulating iron metabolism (Ganz 2003). Reduced iron absorption from food occurs as a result of hepcidin's ability to prevent iron from being released from the liver and from the macrophage, where iron is stored. Hepcidin acts on ferroportin to inhibit its iron transfer activity. One hepcidin receptor, ferroportin, is responsible for iron export in vertebrates (Donovan et al. 2005). Hepcidin-injected mice exhibited significantly lower blood iron levels one hour later. While a single dose of hepcidin is typically eliminated from plasma within a few hours, its effects may last for up to 72 hours. This amount of time is probably necessary for the body to produce enough new hepcidin receptor ferroportin. An increase in hepcidin synthesis is seen during periods of infection and inflammation (Rivera et al. 2005).

Hepcidin is a liver-made antimicrobial peptide that was originally isolated from human urine and serum (Krause et al. 2000, Park et al. 2001). Interleukin (IL)-6 stimulates the production of this type II acute phase protein (Nemeth et al. 2003, Wrighting and Andrews 2006). Hepcidin is a cytokine that is more common under conditions of inflammation, anemia, and hypoxia (Nicolas et al. 2002). Hepcidin not only acts as a negative iron-regulating hormone, but also as an inflammatory mediator by binding to ferroportin and causing its internalization and destruction (De Domenico et al. 2007, Geerts et al. 2012, Nemeth et al. 2004b). Because of its intricate relationship with inflammatory cytokines and iron metabolism, hepcidin has been singled out as a key mediator of ACD (Ganz 2003, Means 2004).

## 2. Materials and Methods

Tests for a variety of liver enzymes—including AST, ALT, and ALP—were run on a sysmex analyzer in accordance with the manufacturer's protocols and under conventional laboratory circumstances.

Serum levels of biochemicals such random blood sugar (RBS) were tested using a sysmex analyzer in accordance with the manufacturer's guidelines and under controlled laboratory settings.

\* Corresponding author. e-mail address: ziyadkarim49@gmail.com

All of the hematological tests used in this research followed industry standards and were performed in a clean room. WBC and ESR estimates are among the assays measured.

### 3. Results and Discussion

In this work, some parameters including age, AST, ALT, Hepcidin, ALP, Hb, WBC, ESR, and RBS, Patients with idiopathic juvenile arthritis (JIA) and healthy controls had their ages and weights taken, to detect the relationship between arthritis disease and hepcidin hormone. All these results and comparisons for the selected parameters are shown in Figure 1, it can be concluded from these this Figure that the high differentiate between the groups led to indicate it is significant to use it to detect this kind of diseases.

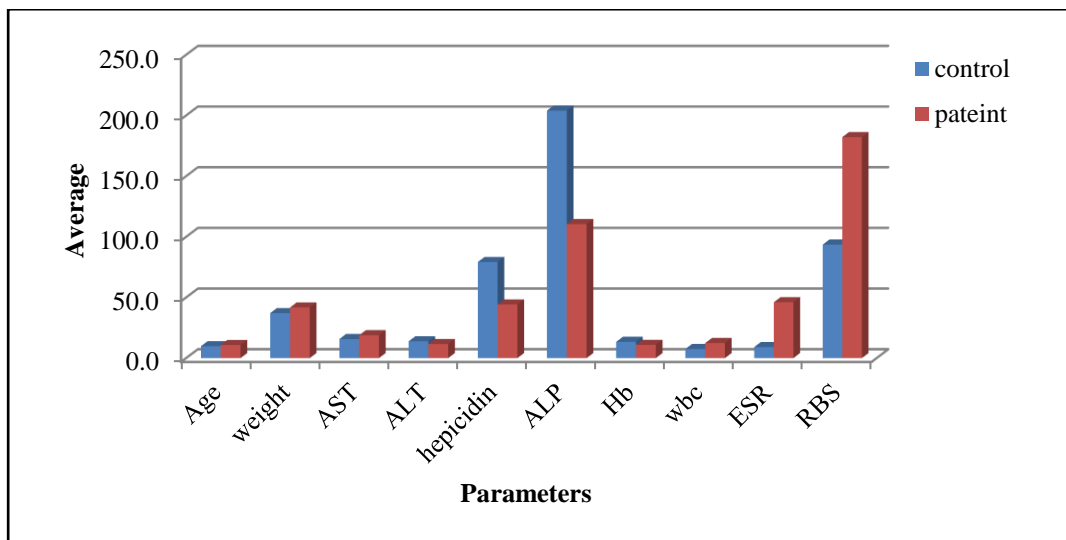


**Figure1:**All metrics were compared between the control and patient groups

In humans, the HAMP gene codes for the hepcidin protein. The hormone hepcidin is essential in controlling how much iron animals absorb. Iron absorption is blocked by macrophages and liver cells that become iron-receptive when hepcidin levels are excessively high, as they are during inflammation. Common causes of anemia include inadequate serum iron levels. Hemochromatosis, also known as iron overload, develops when the body does not produce enough of the hormone hepcidin, leading to an increase in the absorption of iron from the intestines and a proportional increase in the release of iron from iron stores through ferroportin (Ganz 2003).

### Acknowledgment

In this study, we found no association between age and hepcidin in either JIA patients or controls. Liver enzyme levels, notably ALT and AST, are frequently checked in human blood.

This study could not detect any correlation between ESR or RA and hepcidin levels in the blood.

This study found no association between serum hepcidin levels and RA activity. The use of hepcidin levels in clinical practice to evaluate RA patients' disease activity seems to be premature at this time.

## References

- [1] Ganz, T. 2003. Heparidin, a key regulator of iron metabolism and mediator of anemia of inflammation. *Blood.*, 102(3): 783-788.
- [2] Krause, A., Neitz, S., Magert, H.J., Schulz, A., Forssmann, W.G., Schulz-Knappe, P. and Adermann, K. 2000. LEAP-1, a novel highly disulfide-bonded human peptide, exhibits antimicrobial activity. *FEBS Lett.*, 480 (2-3):147-150.
- [3] Park CH, Valore EV, Waring AJ and Ganz T. 2001. Heparidin, a urinary antimicrobial peptide synthesized in the liver. *J Biol Chem.*, 276(11):7806–7810.
- [4] Nemeth E, Valore EV, Territo M, Schiller G, Lichtenstein A. and Ganz T. 2003. Heparidin, a putative mediator of anemia of inflammation, is a type II acute-phase protein. *Blood.*, 101(7):2461–2463.
- [5] Wrighting, D. M. and Andrews, N. C. 2006. Interleukin-6 induces heparidin expression through STAT3. *Blood.*, 108(9): 3204-3209.
- [6] Nicolas G, Chauvet C, Viatte L, Danan JL, Bigard X, Devaux I, Beaumont C, Kahn A. and Vaulont S. 2002. The gene encoding the iron regulatory peptide heparidin is regulated by anemia, hypoxia, and inflammation. *J Clin Invest.*, 110(7):1037–1044.
- [7] De Domenico I, Ward DM, Langelier C, Vaughn MB, Nemeth E, Sundquist WI, Ganz T, Musci G, Kaplan J. 2007. The molecular mechanism of heparidin-mediated ferroportin down-regulation. *Mol Biol Cell.*, 18(7):2569–2578.
- [8] Geerts, I., Vermeersch, P. and Joosten, E. 2012. Evaluation of the first commercial heparidin ELISA for the differential diagnosis of anemia of chronic disease and iron deficiency anemia in hospitalized geriatric patients. *International Scholarly Research Notices.*, (2012):1-4.
- [9] Nemeth, E., Rivera, S., Gabayan, V., Keller, C., Taudorf, S., Pedersen, B. K. and Ganz, T. 2004. IL-6 mediates hypoferremia of inflammation by inducing the synthesis of the iron regulatory hormone heparidin. *The Journal of clinical investigation.*, 113(9): 1271-1276.
- [10] Ganz, T. 2003. Heparidin, a key regulator of iron metabolism and mediator of anemia of inflammation. *Blood.*, 102(3): 783-788.
- [11] Means RT Jr. 2004. Heparidin and anaemia. *Blood Rev.*, 18(4):219–225.





## The Relationship Between Growth Differentiation Factor-15 And Testosterone Hormone Level in Prostate Cancer Patients

**Saif Abdalaziz Meteab BANIDAHIR<sup>1,\*</sup>**, **Ayşe ŞAHİNYAĞLIOĞLU<sup>2</sup>**, **Maysaa Jalal MAJEED<sup>3</sup>**

<sup>1</sup>Çankırı Karatekin University, Faculty of Science and Arts, Department of Chemistry, Çankırı, Türkiye

<sup>2</sup>Amasya University, Faculty of Science and Arts, Department of Chemistry, Amasya, Türkiye

<sup>3</sup>University of Baghdad, Faculty of Medicine, Department of Biochemistry, Baghdad, Iraq

### Abstract

Prostate cancer (PCa) is a common non-skin malignancy disease that frequently causes death males and the burden of this cancer continuously elevating in many countries and especially Asian. Hence the need to find prognostic markers to predict aggressiveness, patients' outcome, and efficacy of treatment are raising. Samples were recruited from the department of Oncology of AL-Ramadi teaching hospital and Haditha general hospital of AL\_Anbar - IRAQ. A total of 100 male patients were recruited from December 2019 to November 2020. All patients received after clinically and laboratory diagnoses. Patients was 70 person while the control groups 30 subject. Serum growth differentiation factor 15 (GDF-15), prostate specific antigen (PSA), total serum testosterone, follicle-stimulating hormone (FSH) and C-reactive protein (CRP) were assayed by BioTek Elisa and Roche Cobas c 311. In Serum PCa patients with continuously disease progression were Levels of GDF-15 elevated. There was a significant increase PSA levels with prostate cancer patients with old injury but observed a trend to tiny depression in levels of serum total Testosterone and FSH. Concerning to the Pearson Scale there were positive significantly ( $P < 0.0023$ ) correlated between serum GDF-15 with Prostate-specific antigen (PSA) levels. In addition, there were a positive significantly ( $P < 0.002$ ) correlated to the duration of the disease with the level of C-reactive protein (CRP) in serum. In our conclusion, a strong correlation was observed between increasing (GDF-15), PSA and body mass index (BMI) with PCa risk. Also, Prostate cancer patients was related to depress FSH and total testosterone levels. The present thesis reinforce the use of GDF-15 and PSA examinations as prognostic biomarkers in PCa and in determining disease progression.

**Keywords:** Prostate Cancer, GDF-15, Total Testosterone, PSA, FSH, Roche Cobas c 311

### 1. Introduction

Cancer is a disease that affects the way cells in the body divided. Healthy tissue cells divide in an orderly fashion. However, this process may cause in the cells to form double tumor or malfunction in growth. The tumors are benign or malignant. Malignant tumors are cancerous and may spread to other areas of the body [1]. Prostate cancer (PCa) is the most common form of non-skin malignancy diagnosed in many countries. Accounting for nearly 25% of the total number of male cancer diagnoses in 2014. It is estimated that by 2020 PCa will become the most common form of cancer [2]. Worldwide, more than 913,000 men were diagnosed with PCa in 2008, with two-thirds of these male living in different world's locations. Today, in the majority of Western European countries, the United States, Australia, and New Zealand, prostate cancer is the most frequently diagnosed form of male specific cancer [3]. Previous research has shown that Growth Differentiation Factor-15 has the potential to be used as a diagnostic marker for a wide range of disorders, including several types of cancer. In order to develop adequate reference ranges for GDF-15 so that it can serve as a clinically meaningful biomarker, it is necessary to evaluate the severity of the disease and the disease risk strata. GDF-15 is useful for a variety of clinical applications, including ordinary clinical practice, clinical measurement, and it can even help the therapeutic administration of medications. The amount of GDF-15 can be utilized to not only offer diagnostic and diagnostic information, but it can also be used to make clinical judgments about specific disorders. GDF-15 can be used as a single mark or multi-mark approach with another individual mark. There is currently insufficient information about the pathophysiology of GDF-15 in certain diseases that are highly likely to result in death, such as prostate cancer and other types of cancer [4]. One of the cytokines that is released in reaction to stress is called GDF-15. In both normal and pathological situations, it is highly expressed in vascular smooth muscle cells, cardiomyocytes, adipocytes, macrophages, and endothelial cells. It is also substantially expressed in macrophages. Additionally, the GDF-15 ratio increases in response to tissue injury

\* Corresponding author. e-mail address: saifabud@googlemail.com

and inflammation [5]. From this point, The Aims of this study to provide new data and information about the relationship between GDF15, PSA, and Testosterone for finding new biomarkers and improve prognostic of prostatic cancer that will help in choose a suitable way of therapeutics and improve the management of prostate cancer patients in Iraq. This project will be useful as one of the few ones in this area.

## 2. Materials and Methods

### 2.1. Design of Study

The study was take the analytical cross- sectional designed. The samples collected at the beginning of the study were 140 patients depending on the data of the study but 70 patients were selected after making sure of the preliminary analyzes in order service of researches aim. Blood samples were collected from control and patients group in the morning at 08:00 a.m - 01:00 p.m. Using a disposable syringe, the blood was withdrawn from the vein (5 mL). The samples were put into disposable tubes with a gel that facilitated serum separation. Blood keep in the gel tubes allowed to clot at 37° C approximately at ten - fifteen minutes and then centerifuged at 2000 RPM for five - ten mintues then the serum was stored at (-20° C) untile analysis (Prostate Specific antigen, C-reactive protein, Growth differentiation factor-15 (GDF-15), Total Testosterone hormone and Follicle stimulating hormone).

### 2.2. Subject

The subjects of the study divided into two groups. All subjects are male and range in age from 35 - 90 year. The study was based one 100 Samples.

Patient group: Consist from 70 patient, these 70 people diagnosed with prostate cancer, all of them are of the gender of men, with ages ranging from 40 to 90 years. PSA values of most patients > 4 ng/ml in order service of researchers aim.

Control group: Consist from 30 healthy male with age range (35 - 90 years). The PSA values of most patients are < 4 ng/ml.

### 2.3. Apparatus and Biochmical kits

All the apparatus and material that used in this study listed in Table 1 and Table 2.

**Table 1.** Materials and Kits that used

Apparatus	Ref.	Company	Origin
Prostate Specific Antigen (PSA) kit	52030	Human Diagnostica mbH	Germany
Growth Differentiation Factor 15 (GDF15) kit	H0150F038	MyBioSource	USA
C reactive protein (CRP) kit	0004956842190c501V11.0	Roche Diagnostics GmbH	Germany
Testosterone Hor. kit	S010	VEDALAB	France
Follicle stimulating Hormone (FSH) kit	100269	Monobid	USA

**Table 2.** Apparatuses that are used and the companies supplied them and their origin

Apparatus	SN	Company	Origin
Elisa ELx800	257381	BioTek	U S A
Cobas c 311 Automated Chemistry Analyzer	19R0-09	Roche	Germany
Centrifuge C- 12000	6M 1810968	Xinkang	China
Water bath	L513.0977	Memmert	Germany
Refrigerator	100269	Bosch	Germany

### 3. Results and Discussion

#### 3.1. Age with Prostate cancer

In the studies was results patients and controls for Age ( $64.4 \pm 10.9$  year;  $49.3 \pm 8.02$  year) respectively, This results was a statistically significant (\*P 0.011) at  $P < 0.05$ , as shown in Table 3. The study concluded that prostate cancer gradually increased with age. In previous studies, Age is considered to be the biggest risk factor for prostate cancer. Understandably, this disease has become one of the biggest public health problems [6]. This result is also in agreement with our study.

**Table 3.** Comparison of Clinical characteristic between patients and control in Age, BMI

Parameters	Mean $\pm$ SD	
	Age (year)	BMI (kg/m <sup>2</sup> )
Patients group	$64.45 \pm 10.97$	$24.93 \pm 4.03$
Control group	$59.33 \pm 8.01$	$28.49 \pm 4.04$
T-test	4.413 *	1.747 **
P-value	0.0233	0.0001
* ( $P \leq 0.05$ ), ** ( $P \leq 0.01$ ).		

#### 3.2. BMI with Prostate Cancer

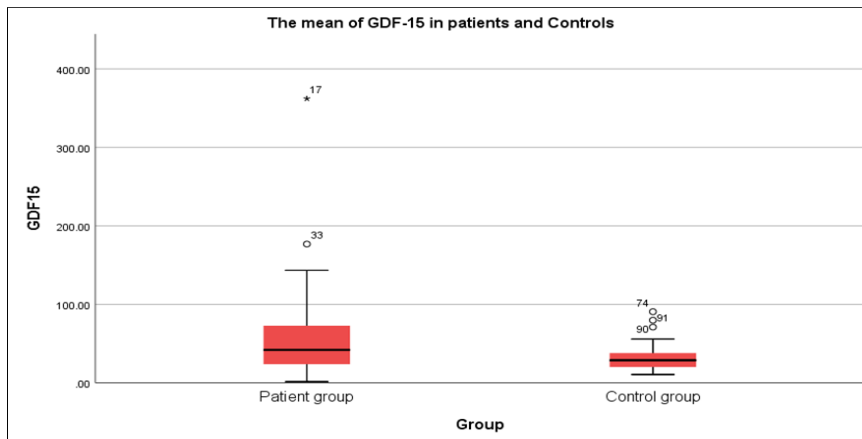
In the weight was patients and controls results ( $24.93 \pm 4.03$  kg/m<sup>2</sup>;  $28.49 \pm 4.04$  kg/m<sup>2</sup>) respectively, this results was highly significant statistical (\*P 0.0001) at  $P < 0.05$ , as shown in Table 3. Obesity is a risk factor for the development of aggressive prostate cancer, according to the majority of published studies [7]. Some previous studies revealed after following up to 15 year for obese people that baseline obesity was associated with prostate volume and with the rate of change in PSA [8]. While other studies provide opposite results regarding local or overall prostate cancer risk [9]. It is possible that the inverse association between obesity and a diagnosis of prostate cancer is at least partially due to detection bias, which is caused by large prostate sizes and hemodilution in obese men. This bias may explain why obesity is associated with a lower risk of being diagnosed with prostate cancer. This bias may explain why obese men have a lower risk of being diagnosed with prostate cancer [8]. As well, Dickerman et al., supported our research. Weight loss and obesity were found to be associated with an increased risk of prostate cancer. According to the findings of Dickerman and colleagues, there is a correlation between weight gain over a long period of time and an increased risk of mortality from prostate cancer (2017) [10].

#### 3.2. GDF15

In our study, serum GDF15 levels were significantly higher in the patient group than in the control group. The mean of GDF15 (mg/dl) was has a significant difference between groups, the results was ( $53.8 \pm 50.8$  mg/dl;  $33.4 \pm 19.3$  mg/dl, respectively) (\*P 0.0352) at  $P < 0.05$ , as shown in Table 4 and Figure 1. GDF-15 concentrations have frequently been found to be elevated during the progression of various types of cancer, including gastric, ovarian, prostate, and breast cancers [11, 12]. In spite of the fact that the GDF-15 expression profile has been adequately described in a wide variety of cancers, a comprehensive investigation into its specific role in the development of prostate tumors is still required. Our study supported with presented studies. The presented data indicated that serum GDF15 levels were significantly higher in patients with metastasized cancer (Pca) who had a rapid disease progression [13]. Welsh et al. discovered that metastatic prostate cancer patients had significantly higher serum GDF15 levels than normal controls [14]. Another prior study found that metastatic prostate cancer expressed less GDF15 than main prostate cancer when gene expression data was compared from over 1,000 samples of primary prostate cancer and 200 samples of metastatic prostate cancer. GDF15 in the primary tumor lower levels are associated with prostate cancer patients [15].

**Table 4.** Comparison between patients and control in C.R.P, PSA and GDF15

Parameters	Mean $\pm$ SD		
	S.C.R.P (nmol/L )	S. PSA (ng/ml )	S.GDF15 (mg/dl)
Patients Group	92.57 $\pm$ 79.30	38.92 $\pm$ 33.21	53.85 $\pm$ 50.88
Control Group	12.96 $\pm$ 30.95	2.19 $\pm$ 5.78	33.35 $\pm$ 19.27
T-test	29.72 **	12.107 **	19.041 *
P. value	0.0001	0.0001	0.0352
* (P $\leq$ 0.05), ** (P $\leq$ 0.01).			

**Figure 1.** The percentage difference in GDF-15 levels between the patient and control groups.

### 3.3. PSA

The PSA results of patients and controls were ( $38.9 \pm 33.1$  ng/ml;  $2.19 \pm 5.78$  ng/ml , respectively) this results was a significant statistical ( \*P 0.0001 ) at P < 0.05, as shown in Table 4. and Figure 2. Other findings from a major multicenter study showed that the total serum PSA use for prostate biopsy is greater than 4 ng/mL [16]. While serum PSA is a sensitive indicator of prostate cancer early detection, its specificity is limited by elevated levels in benign prostate disease [17]. These studies supported our study. In another study, PSA levels decreased in prostate cancer [18]. PSA concentration in some patient's have come down due to receive some drugs such as abiraterone and degarelix and these treatment will reduces the production of androgens in the body that can promote the growth of a prostate gland tumor. Suggesting the influence of both testosterone and FSH on PSA levels [18].

### 3.4. Serum CRP

The CRP results of patient and control were ( $92.6 \pm 79.3$  nmol/L;  $12.9 \pm 30.9$  nmol/L) respectively. The results was a significant statistical (\* P 0.001) at P. value <0.05, as displayed in Table 4. and Figure 2. Elevated serum CRP levels before treatment in PCa patients are closely related to bad prognosis [19]. CRP levels decreased in prostate cancer patients that received treatment [20]. CRP is a readily measurable biomarker that has the potential to detection the progress of the patient's condition deterioration or improvement [21]. As well as in our study showed a highly positive correlation between CRP with duration of disease ( $r=0.421^{***}$ , P 0.002 respectively), as shown in Table 4.4 by used Pearson Correlation Analysis. This shows that there is a close relationship between CRP concentration and progression of disease in PCa patient. In some of the previous studies, CRP levels have been shown to be related to worse PCa patient outcomes [22].

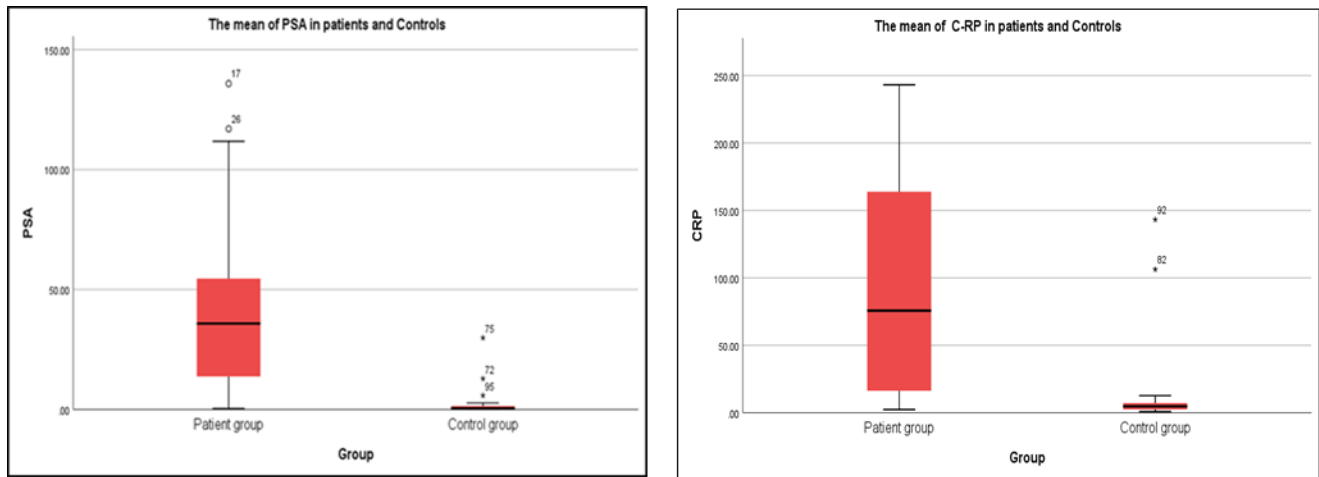


**Figure 2.** The percentage difference in PSA and CRP levels between the patient and control groups.

### 3.5. Serum Testosterone and Serum FSH with Prostate Cancer

The testosterone results of patients and controls were ( $5.72 \pm 3.63$  ng/ml;  $4.37 \pm 2.28$  ng/ml) respectively. The results were a non-significant statistical (\* P 0.064 ) at P value  $< 0.05$ , as displayed in Table 5 and Figure 3. The studies are consistent with the report which reported that serum testosterone has not related with the incidence of prostate cancer [23]. However, some studies contradicted our findings that high TT serum levels are associated with high-risk disease in PCa patients. Endogenous TT should be considered as a biological marker for assessing EAU PCA risk classes [24]. Internal prostatic milieu levels are not accurately reflected by serum testosterone levels [25]. On the other hand, if testosterone levels are to be considered in the etiology of prostate cancer, they should be measured and interpreted chronically over a period of years using multiple measurements [26]. While the FSH results was in patients and controls ( $4.79 \pm 5.47$  mIU/ml;  $2.89 \pm 3.40$  mIU/ml) respectively, this results was a non-significant statistical (\* P 0.082 ) at P. value  $< 0.05$ , as displayed in Table 5 and Figure 3. Previously, researchers have discovered that Follicle Stimulating Hormone (FSH) is an important component in the natural history for progression of PCa [18]. The result shown don't supported our study. Because, FSH concentration may be related to tumor size, revealing that there is a correlation before treatment. Most of the PCa patients in this study had undergone to different treatment methods, one of these methods used is medication which originally work to reduce some hormones that help in the growth of cancer cells may be the cause of this noticeable decrease in FSH and Testosterone hormone. Catarinicchia et al., revealed in one of the experiment worked that some medication such as abiraterone and degarelix lead to decrease levels of FSH and Testosterone in PCa patient [18]. Whereas a recent study established that postoperative FSH levels were significantly lower. Also, FSH levels decreased after radical prostatectomy [27]. However, additional research is required to fully understand the differences in FSH concentration between patients who have received treatment and those who have not.

**Table 5.** Comparison between patients and control in Hormones level

Parameters	Mean $\pm$ SD	
	S. Testosterone (ng/ml )	S. FSH (mIU/ml)
Patients Group	$5.72 \pm 3.63$	$4.79 \pm 5.47$
Control Group	$4.37 \pm 2.28$	$2.89 \pm 3.40$
T-test	1.427 NS	2.146 NS
P-value	0.0641	0.0820
NS: Non-Significant.		

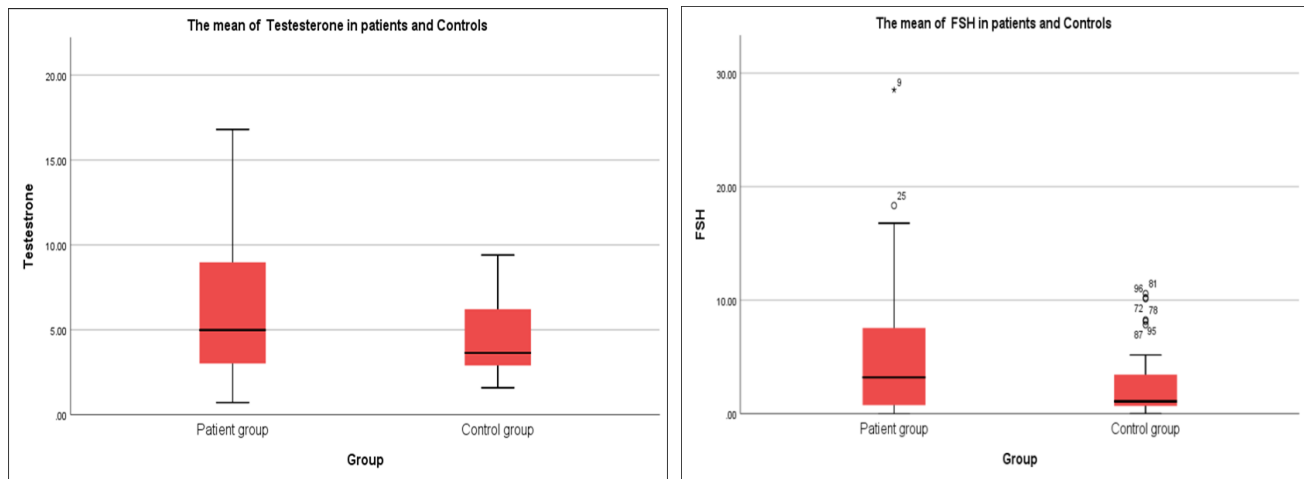


**Figure 3.** The percentage difference in Testosterone and FSH levels between the patient group and healthy groups.

### Acknowledgement

God the AL-mighty be thanked for assisting me in my studies and providing me with the ability to complete my thesis. I'd like to express my heartfelt appreciation to my supervisor, Prof. Dr. Ayşe ŞAHİN YAĞLIOĞLU, for her guidance and encouragement throughout the course of writing my thesis. Her inestimable commentary on the thesis chapters enriches the entire work and her words always encourage me to work hard. This thesis is the fruit of my collaboration with my supervisor, Prof. Dr. Ayşe ŞAHİN YAĞLIOĞLU. Once again I thank her sincerely and appreciate her. My deep thanks go to the Chemistry Department Head and to all of the Department's teachers. Additionally, I would like to express my gratitude to secondary supervisor Prof. Dr. Maysaa Jalal MAJEED for assisting me in revising and editing my thesis. I goes my special love and thanks to my dear wife and my children for being with me every step of the way and for sharing my good and bad day.

### References

- [1] Beilin, J., Harewood, L., Frydenberg, M., Mameghan, H., Martyres, R. F., Farish, S. J. and Zajac, J. D. 2001. A case-control study of the androgen receptor gene CAG repeat polymorphism in Australian prostate carcinoma subjects. *Cancer*, 92(4), 941-949.
- [2] National Institute of Health and Care Excellence. (2014). Prostate cancer: diagnosis and treatment. Available at <https://www.nice.org.uk/guidance/cg175>. Retrieved April 15, 2021.
- [3] Ferlay, J., Parkin, D. M. and Steliarova-Foucher, E. 2010. Estimates of cancer incidence and mortality in Europe in 2008. *European journal of cancer*, 46(4), 765-781.
- [4] Li, J., Yang, L., Qin, W., Zhang, G., Yuan, J. and Wang, F. 2013. Adaptive induction of growth differentiation factor 15 attenuates endothelial cell apoptosis in response to high glucose stimulus. *PloS one*, 8(6), e65549.
- [5] National Cancer Institute, Surveillance Epidemiology and End Results. Cancer of the Corpus and Uterus, Adela, R. and Banerjee, S. K. 2015. GDF-15 as a target and biomarker for diabetes and cardiovascular diseases: a translational prospective. *Journal of diabetes research*, 3-12.
- [6] Syrigos, K. N., Karapanagiotou, E. and Harrington, K. J. 2005. Prostate cancer in the elderly. *Anticancer research*, 25(6C), 4527-4533.
- [7] Choi, J. B., Myong, J. P., Lee, Y., Kim, I., Kim, J. H., Hong, S. H. and Ha, U. S. 2020. Does increased body mass index lead to elevated prostate cancer risk? It depends on waist circumference. *BMC cancer*, 20(1), 575-589.
- [8] Wallner, L. P., Morgenstern, H., McGree, M. E., Jacobson, D. J., St Sauver, J. L., Jacobsen, S. J. and Sarma, A. V. 2011. The effects of body mass index on changes in prostate-specific antigen levels and prostate volume over 15 years of follow-up: implications for prostate cancer detection. *Cancer epidemiology, biomarkers & prevention: a publication of the American Association for Cancer Research, cosponsored by the American Society of Preventive Oncology*, 20(3), 501-508.

- [9] Gong, Z., Neuhouser, M. L., Goodman, P. J., Albanes, D., Chi, C., Hsing, A. W., Lippman, S. M., Platz, E. A., Pollak, M. N., Thompson, I. M. and Kristal, A. R. 2006. Obesity, diabetes, and risk of prostate cancer: results from the prostate cancer prevention trial. *Cancer epidemiology, biomarkers & prevention : a publication of the American Association for Cancer Research, cosponsored by the American Society of Preventive Oncology*, 15(10), 1977–1983.
- [10] Dickerman, B. A., Ahearn, T. U., Giovannucci, E., Stampfer, M. J., Nguyen, P. L., Mucci, L. A. and Wilson, K. M. 2017. Weight change, obesity and risk of prostate cancer progression among men with clinically localized prostate cancer. *International journal of cancer*, 141(5), 933–944.
- [11] Bauskin, A. R., Brown, D. A., Kuffner, T., Johnen, H., Luo, X. W., Hunter, M. and Breit, S. N. 2006. Role of macrophage inhibitory cytokine-1 in tumorigenesis and diagnosis of cancer. *Cancer research*, 66(10), 4983–4986.
- [12] Baek, K. E., Yoon, S. R., Kim, J. T., Kim, K. S., Kang, S. H., Yang, Y., Lim, J. S., Choi, I., Nam, M. S., Yoon, M. and Lee, H. G. 2009. Upregulation and secretion of macrophage inhibitory cytokine-1 (MIC-1) in gastric cancers. *Clinica chimica acta; international journal of clinical chemistry*, 401(1-2), 128–133.
- [13] Winand, F. J., Boegemann, M., Gallitz, I., Hertle, L., Semjonow, A., Eveslage, M. and Steinbicker, A. U. 2014. GDF15 and Hepcidin as prognostic factors in patients with prostate Cancer. *Journal of Molecular Biomarkers and Diagnosis*, 5(6), 1–9.
- [14] Welsh, J. B., Sapinoso, L. M., Kern, S. G., Brown, D. A., Liu, T., Bauskin, A. R., Ward, R. L., Hawkins, N. J., Quinn, D. I., Russell, P. J., Sutherland, R. L., Breit, S. N., Moskaluk, C. A., Frierson, H. F., Jr, and Hampton, G. M. 2003. Large-scale delineation of secreted protein biomarkers overexpressed in cancer tissue and serum. *Proceedings of the National Academy of Sciences of the United States of America*, 100(6), 3410–3415.
- [15] Zhang, W., Hu, C., Wang, X., Bai, S., Cao, S., Kobelski, M., Lambert, J. R., Gu, J. and Zhan, Y. 2019. Role of GDF15 in methylseleninic acid-mediated inhibition of cell proliferation and induction of apoptosis in prostate cancer cells. *PloS one*, 14(9), e0222812.
- [16] Catalona, W. J., Richie, J. P., Ahmann, F. R., Hudson, M. A., Scardino, P. T., Flanigan, R. C., DeKernion, J. B., Ratliff, T. L., Kavoussi, L. R., Dalkin, B. L., Waters, W. B., MacFarlane, M. T. and Southwick, P. C. 1994. Comparison of digital rectal examination and serum prostate specific antigen in the early detection of prostate cancer: results of a multicenter clinical trial of 6,630 men. *The Journal of urology*, 151(5), 1283–1290.
- [17] Oesterling J. E. 1991. Prostate specific antigen: a critical assessment of the most useful tumor marker for adenocarcinoma of the prostate. *The Journal of urology*, 145(5), 907–923.
- [18] Catarinichia, S. and Crawford, E. D. 2016. The Role of FSH in Prostate Cancer: A Case Report. *Urology case reports*, 7, 23–25.
- [19] Wu, D., Wang, X., Shi, G., Sun, H. and Ge, G. 2021. Prognostic and clinical significance of modified glasgow prognostic score in pancreatic cancer: a meta-analysis of 4,629 patients. *Aging (Albany NY)*, 13(1), 1410.
- [20] Margel, D., Ber, Y., Peer, A., Shavit-Grievink, L., Pinthus, J. H., Witberg, G., Baniel, J., Kedar, D. and Rosenbaum, E. 2021. Cardiac biomarkers in patients with prostate cancer and cardiovascular disease receiving gonadotrophin releasing hormone agonist vs antagonist. *Prostate cancer and prostatic diseases*, 24(1), 177–185.
- [21] Prins, R. C., Rademacher, B. L., Mongoue-Tchokote, S., Alumkal, J. J., Graff, J. N., Eilers, K. M. and Beer, T. M. 2012. C-reactive protein as an adverse prognostic marker for men with castration-resistant prostate cancer (CRPC): confirmatory results. *Urologic oncology*, 30(1), 33–37.
- [22] Beer, T. M., Lalani, A. S., Lee, S., Mori, M., Eilers, K. M., Curd, J. G. and Chi, K. N. 2008. C-reactive protein as a prognostic marker for men with androgen-independent prostate cancer: results from the ASCENT trial. *Cancer: Interdisciplinary International Journal of the American Cancer Society*, 112(11), 2377–2383.
- [23] Chen, C., Weiss, N. S., Stanczyk, F. Z., Lewis, S. K., DiTommaso, D., Etzioni, R. and Goodman, G. E. 2003. Endogenous sex hormones and prostate cancer risk: a case-control study nested within the Carotene and Retinol Efficacy Trial. *Cancer Epidemiology Biomarkers and Prevention*, 12(12), 1410–1416.
- [24] Tafuri, A., Sebben, M., Shakir, A., Pirozzi, M., Processali, T., Rizzetto, R., Amigoni, N., Brunelli, M., Migliorini, F., Siracusano, S., Cerruto, M. A., Artibani, W., Antonelli, A. and Porcaro, A. B. 2020. Endogenous testosterone mirrors prostate cancer aggressiveness: correlation between basal testosterone serum levels and prostate cancer European Urology Association clinical risk classes in a large cohort of

- Caucasian patients. *International urology and nephrology*, 52(7), 1261–1269.
- [25] Tafuri, A., Sebben, M., Shakir, A., Pirozzi, M., Processali, T., Rizzetto, R., Amigoni, N., Brunelli, M., Migliorini, F., Siracusano, S., Cerruto, M. A., Artibani, W., Antonelli, A. and Porcaro, A. B. 2020. Endogenous testosterone mirrors prostate cancer aggressiveness: correlation between basal testosterone serum levels and prostate cancer European Urology Association clinical risk classes in a large cohort of Caucasian patients. *International urology and nephrology*, 52(7), 1261–1269.
- [26] Loughlin K. R. 2016. The testosterone conundrum: The putative relationship between testosterone levels and prostate cancer. *Urologic oncology*, 34(11), 482–482
- [27] Choi, S. Y., Chi, B. H., Lee, W., Lim, B., You, D. and Kim, C. S. 2020. Luteinizing Hormone Levels Relate to the Unfavorable Pathology of Prostate Cancer. *Journal of clinical medicine*, 9(5), 1281.





## Role of Transcription Factor 7 like RS7903146 and RS12255372 Gene Polymorphisms and Selective Biochemical Tests in Type II Iraqi Diabetic Patients

**Hayder DHYAA<sup>1,\*</sup>** , **Volkan EYÜPOĞLU<sup>2</sup>** , **Ahmed ABBAS<sup>3</sup>** 

<sup>1</sup> B. Sc. Medical Lab., College of Health and Medical Technology, Middle Technical University, Baghdad, Iraq

<sup>2</sup> Department of Chemistry, Çankırı Karatekin University, Çankırı, Türkiye

<sup>3</sup> Medical Laboratory Technology / College of Medicine, Alforat Alawsat Technical University, Najaf, Iraq

### Abstract

Recent studies have related to see whether the TCF7L2 gene polymorphisms rs7903146 (C/T) and rs12255372 (G/T) are linked to the risk of developing T2DM in the Iraqi population. In this study, biochemical and genetic parameters. Real-time PCR was used to genotype the samples. In both patients and controls, the frequency of genotypes, alleles, anthropometric measurements, glycemia, and glycated hemoglobin (HbA1c) was measured. As result, The TCF7L2 SNPs rs7903146 and rs12255372 had genotyping success rates of 98.55 and 97.42 percent, respectively. For both SNPs, the allele and genotype frequencies were in Hardy-Weinberg equilibrium. Between patients and controls, the genotype and allele frequencies for (TCF7L2 SNP rs7903146) allele were not substantially different. The frequency of the (rs7903146 T) allele in the controls was 29 percent, whereas it was 28 percent in the patients (P = 0.61). The TCF7L2 SNP rs12255372 genotypic and allelic frequencies did not vary substantially between patients and controls. In controls, (rs12255372 T) allele frequency was 21%, but in patients, it was 27% (P = 0.42).

**Keywords:** Type 2 diabetes, Genetic association, Transcription factor 7-like 2 (TCF7L2), Polymorphism

### 1. Introduction

Hyperglycemia is the primary symptom of type 2 diabetes, which is a metabolic illness with several contributing factors. Inadequate insulin production or resistance to insulin that has been secreted both play critical roles in the pathogenesis of type two diabetes (1,2). In addition to this, it may lead to a number of consequences, the most common of which are cardiovascular and endothelial illnesses (3,4). An examination of the whole genome indicated that numerous genes have a role in the etiology of type two diabetes (5). In particular, the transcription factor (7-like 2), or TCF7L2, gene is recognized as the best potential gene involved in everything from the impairment of insulin synthesis to the development of type 2 diabetes (5). The transcription factor 7 like 2 (TCF7L2) gene is an essential component of the Wnt signaling pathway. It is an entero-endocrine transcription factor that is located on chromosome 10q (6). Following this, stimulation of Wnt catenin promotes the assembly of -catenin with BCL9, which is then followed by translocation, into the nucleus and the formation of an active form with (TCF7L2) (7).

### 2. Materials and Methods

**2.1. Materials:** Primers (rs7903146, rs 12255372), 100 bp DNA ladder, 50 bp DNA lader, Restriction enzymes (RsaI enzyme, 2U Tsp509I enzyme).

**2.2. Methods:** Genomic DNA extraction  
Genomic DNA Profiling  
RFLP-PCR Technique

\* Corresponding author. e-mail address: haedar19@yahoo.com

PCR master mix preparation  
PCR Program

### 3. Result and discussion

#### 3.1 The Genotype and allele frequencies of the (TCF7L2 SNPs rs7903146) gene polymorphism

There was no discernible difference between the patients and the controls with regard to the genotype or allele frequencies for (TCF7L2 SNP rs7903146 allele). In the healthy control, the frequency of the (rs7903146) T allele was 28 percent, whereas in the sick population, it was only 29 percent. The rs7903146 C allele frequency for the controls was 72 %, whereas it was 71% in the patients ( $P = 0.61$ ). The frequencies of the T/T, C/C, and C/T genotypes were 54, 36, and 10 percent, respectively, for the controls, while the rates were 49, 44, and 7 percent, straight, for the patients ( $P = 0.30$ ). (Table 1).

**Table 1.** Genotype and allele frequencies of the (TCF7L2 SNPs rs7903146) gene polymorphism in with diabetic patients and healthy control group

TCF7L2 SNPs rs7903146	PATIENTS (N=100)	HEALTHY (N=100)	P.VALUE
Genotypes	-	-	-
CC	49(49%)	54(54%)	0.32
CT	44(44%)	36(36%)	
TT	7(7%)	10(10%)	
Alleles	-	-	-
C	142(71%)	144(72)	0.61
T	58(29%)	56(28%)	
P = <0.05, N= Number of persons			

#### 3.2 The Genotype and allele frequencies of the(TCF7L2 SNPs Rs 12255372) polymorphism

In terms of genotypic and allelic frequencies for the TCF7L2 SNP rs12255372, there was no significant difference between patients and controls. The frequency of the rs12255372 T allele was 21 percent in the control group, but it was 27 percent in the sick group ( $P = 0.42$ ). The frequency of the rs12255372 G allele was 79 percent in the normal group, and it was 73 percent in the patient group ( $P = 0.51$ ). The T/T, G/G, and G/T genotype frequencies were, respectively, 63, 32, and 5% for the controls. However, they were, respectively, 52, 42, and 6% for the patients ( $P = 0.31$ ); this indicates that the T/T, G/T, and G/G genotype frequencies were significantly lower in the patients. (Table 2).

**Table 2.** Genotype and allele frequencies of the(TCF7L2 SNPs Rs 12255372 polymorphism in with diabetic patients and healthy control group

<b>TCF7L2 SNPs Rs 12255372 gene</b>	<b>PATIENTS (N=100)</b>	<b>HEALTHY (N=100)</b>	<b>P.VALUE</b>
Genotypes	-	-	-
GG	52 (52%)	63 (63%)	0.31
GT	42 (42%)	32 (32%)	0.31
TT	6 (6%)	5 (5%)	0.31
+Alleles	-	-	-
G	146 (73%)	158 (79%)	0.51
T	54 (27%)	42 (21%)	0.42
P = <0.05, N= Number of persons			

#### 4. Conclusion

This is the first study to investigate at the TCF7L2 SNPs rs7903146 and rs12255372 in Type 2 Diabetes patients from a racially mixed community in Iraq. The results that are given here are just incomplete. Despite the fact that allele frequencies and the genotype in the patient groups as well as the control group, were equal ( $P > 0.05$ ) for each variants, the patient group had a significantly higher frequency of both variations, Given the limited number of people that participated in the study, we cannot say for certain that the results we obtained are accurate, because we cannot rule out the possibility that our findings are skewed due to the small sample size. Alternately, such results might be ascribed to unique ethnic effects due to the fact that the majority of the previously reported connections were established in research with populations that were mostly European.

#### References

- [1] Lin, Y. and Sun, Z. 2010. Current views on type 2 diabetes. *The Journal of endocrinology*, 204(1): 1.
- [2] Kyrou, I. and Kumar, S. 2010. Weight management in overweight and obese patients with type 2 diabetes mellitus. *The British Journal of Diabetes and Vascular Disease*, 10(6): 274-283.
- [3] Ali, R., Mzayek, F., Rastam, S., Fouad, F. M., O'Flaherty, M., Capewell, S. and Maziak, W. 2013. Forecasting future prevalence of type 2 diabetes mellitus in Syria. *BMC Public Health*, 13(1): 1-7.
- [4] DeSouza, C. and Fonseca, V. 2009. Therapeutic targets to reduce cardiovascular disease in type 2 diabetes. *Nature Reviews Drug Discovery*, 8(5): 361-367.
- [5] Elbein, S. C. 2009. Genetics factors contributing to type 2 diabetes across ethnicities. *Journal of diabetes science and technology*, 3(4): 685-689.
- [6] Castrop, J., van Norren, K. and Clevers, H. 1992. A gene family of HMG-box transcription factors with homology to TCF-1. *Nucleic acids research*, 20(3): 611.
- [7] Yi, F., Brubaker, P. L. and Jin, T. 2005. TCF-4 mediates cell type-specific regulation of proglucagon gene expression by  $\beta$ -catenin and glycogen synthase kinase-3 $\beta$ . *Journal of Biological Chemistry*, 280(2): 1457-1464.



# Lung Opacity Classification with Convolutional Neural Network

Yunus KÖKVER<sup>1</sup> \* 

<sup>1</sup> Elmadag Vocational School, Computer Technologies Department, Ankara University, Ankara, Turkey

## Abstract

On chest radiographs, the term of lung opacity refers to one or more areas where the normally darker lung appears more opaque or hazy. Lung opacity is usually benign and resolves spontaneously without complications in patients with short-term disease. In this study, a prediction process is performed by classifying chest x-ray images obtained from a public dataset with deep learning methods in order to help physicians in the diagnosis of the disease and to enable physicians to pay more attention to these areas before the disease passes to the pneumonia stage. The classical Convolutional Neural Network (CNN) model is preferred for the classification process. The CNN model is able to classify the dataset categorised as Normal and Lung Opacity with an accuracy rate of 92.93%.

**Keywords:** Lung opacity, Deep learning, CNN, Disease classification

## 1. Introduction

Opacity represents any area on a chest radiograph that is whiter than it should be. The term of lung opacity on chest radiographs refers to one or more areas where the normally darker (air-filled) lung appears more opaque, hazy or cloudy [1]. Lung opacities are not homogeneous and do not have a clear center or clear boundaries. Therefore, it is difficult to separate them from the whole image and segment them properly. Lung opacity is generally benign and resolves spontaneously without any complications in patients [2–5].

Nowadays, artificial intelligence technologies have come of age with the development of deep learning methods, and as in many fields, it has become an area of interest for researchers in health technologies, where physicians can be used in the diagnosis of many diseases [6]. It is known that large datasets are highly effective in the success of deep learning studies [7].

In this study, the Convolutional Neural Network model, which is one of the deep learning techniques proven in the literature and frequently used in the biomedical field, is used to classify normal and lung opacity of images from a dataset.

In the second part of the study, literature studies, in the third part, materials and methods, in the fourth part, research findings related to this study are given, and in the last part, the results obtained within the scope of the study are shared.

## 2. Related Studies

Senan et al. used two deep learning models, ResNet-50 and AlexNet, to classify the images they collected from many sources. Each mesh was used to classify images with four classes (lung opacity, viral pneumonia, COVID-19 and normal) and two classes (normal and COVID-19) [8].

In another study, Li et al. proposed a model they named Cov-Net for the detection of radiological images with four classes (lung opacity, covid19, viral pneumonia and normal). The asymmetric convolution method was used for the correct determination of the classes [9].

Mergen et al. used deep learning methods to detect lung opacity. Multi-scale deep reinforcement learning technique was used to detect anatomical landmarks. [10].

Sirazitdinov et al., on the other hand, designed an ensemble model consisting of two CNNs, RetinaNet and Mask R-CNN, to automatically detect lung opacity and other pneumonias [11].

\* Corresponding author. e-mail address: ykokver@ankara.edu.tr

### 3. Materials and Methods

#### 3.1. Dataset

The dataset, which was compiled from various sources and public datasets, is used from the relevant link. All explanations about the dataset and labels can be downloaded from the related link (<https://github.com/turkfuat/covid19-multiclass>).

The available dataset is divided into training and testing subsets to develop and tune the classification algorithms. Then, data augmentation methods are applied to the images. Each dataset consists of two separate classes, Normal and Lung Opacity. In total, 22000 images are allocated for training data and 2431 images are allocated for testing data.

#### 3.2. Convolutional Neural Network (CNN) Model

CNNs are a class of Deep Neural Networks that can recognise and classify certain features from pictures and are widely used to analyse visual images [12]. It has applications in video and image recognition, classification of image, segmentation of image, analysis of medical image, interfaces of brain-computer, processing of natural language, etc. [13–16].

Figure 1 represents the architecture of the classical CNN network model.

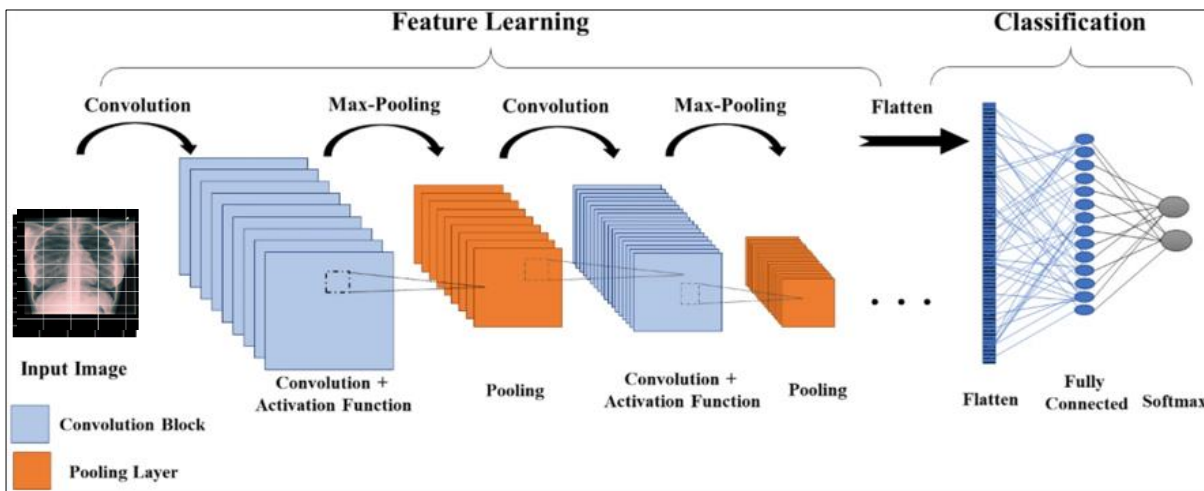


**Figure 1.** Architecture of Classical CNN network model

### 4. Results and Discussion

In this study, the classical CNN network model is designed as a deep learning model. Adam is used for the optimisation process and ReLU and Softmax functions are used for the activation function. The graph of training and validation loss values and training and validation accuracy values as a result of the algorithm is presented in Figure 2.

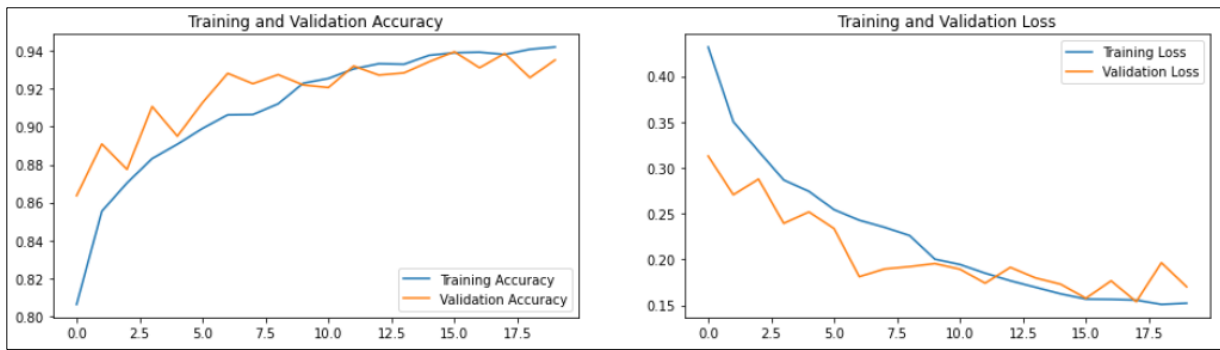


**Figure 2.** Accuracy and loss graph after training process

In the classification process consisting of two classes, an accuracy of 92.93% is obtained. Accuracy, Recall, Precision and F1 Score metrics are used for measure the performance of the algorithm.

The confusion matrix of the result values is presented in Figure 3 and the Precision, Recall and F1 Score values calculated according to this confusion matrix are presented in Table 1.

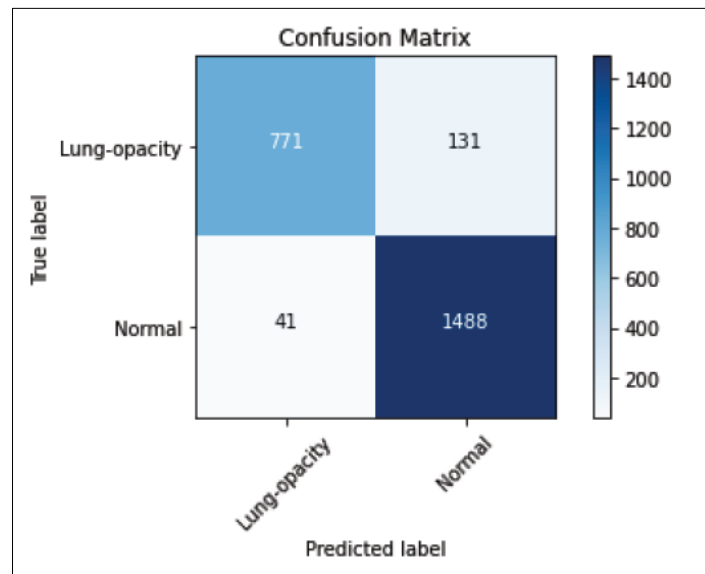


**Figure 3.** Confusion matrix according to the result of CNN model

**Table 1.** CNN architecture performance metrics

	Precision	Recall	F1-Score
<b>Lung-opacity</b>	0.95	0.85	0.90
<b>Normal</b>	0.92	0.97	0.95
<b>Accuracy(avg)</b>	0.9293		

## 5. Conclusion

In this study, convolutional neural network model, which is one of the deep learning methods, is applied on images consisting of lung opacity and normal categories using a publicly available dataset and the images are correctly classified with a success rate of 92.93%. CNN can be recommended instead of classical machine learning algorithms in the detection of lung opacity disease. Accuracy rates can be raised by increasing the number of epochs, making updates in the selection of hyperparameters and the design of the network structure. In future studies, it is planned to create an ensemble model by using more classifier models and to diagnose three-classes, four-classes and five-classes diseases.

## References

- [1] W. Herring, *Learning radiology: recognizing the basics*. Elsevier Health Sciences, 2019.
- [2] Zahavi, G. What are lung opacities? Kaggle (2018). Available at: <https://www.kaggle.com/zahaviguy/what-are-lung-opacities>.
- [3] J. J. Arenas-Jiménez, J. M. Plasencia-Martínez, and E. García-Garrigós, ‘When pneumonia is not COVID-19. Radiologia [Internet]. 2021; 63 (2): 180-92’.
- [4] W. Kim *et al.*, ‘Utility of a deep learning algorithm for detection of reticular opacity on chest radiography in patients with interstitial lung disease’, *Am. J. Roentgenol.*, vol. 218, no. 4, pp. 642–650, 2022.
- [5] M. Zhu *et al.*, ‘A computerized tomography-based radiomic model for assessing the invasiveness of lung adenocarcinoma manifesting as ground-glass opacity nodules’, *Respir. Res.*, vol. 23, no. 1, pp. 1–11, 2022.
- [6] H. M. Ünver, Y. Kökver, E. Duman, and O. A. Erdem, ‘Statistical edge detection and circular hough transform for Optic disk localization’, *Appl. Sci.*, 2019, doi: 10.3390/app9020350.
- [7] F. Türk, M. Lüy, and N. Barışçı, ‘Kidney and renal tumor segmentation using a hybrid V-Net-Based model’, *Mathematics*, vol. 8, no. 10, p. 1772, 2020.
- [8] E. M. Senan, A. Alzahrani, M. Y. Alzahrani, N. Alsharif, and T. H. H. Aldhyani, ‘Automated diagnosis of chest X-ray for early detection of COVID-19 disease’, *Comput. Math. Methods Med.*, vol. 2021, 2021.
- [9] H. Li, N. Zeng, P. Wu, and K. Clawson, ‘Cov-Net: A computer-aided diagnosis method for recognizing COVID-19 from chest X-ray images via machine vision’, *Expert Syst. Appl.*, vol. 207, p. 118029, 2022.
- [10] V. Mergen *et al.*, ‘Deep learning for automatic quantification of lung abnormalities in COVID-19 patients: First experience and correlation with clinical parameters’, *Eur. J. Radiol. Open*, vol. 7, p. 100272, 2020.
- [11] I. Sirazitdinov, M. Kholiavchenko, T. Mustafaev, Y. Yixuan, R. Kuleev, and B. Ibragimov, ‘Deep neural network ensemble for pneumonia localization from a large-scale chest x-ray database’, *Comput. Electr. Eng.*, vol. 78, pp. 388–399, 2019.
- [12] M. V Valueva, N. N. Nagornov, P. A. Lyakhov, G. V Valuev, and N. I. Chervyakov, ‘Application of the residue number system to reduce hardware costs of the convolutional neural network implementation’, *Math. Comput. Simul.*, vol. 177, pp. 232–243, 2020.
- [13] A. Tsantekidis, N. Passalis, A. Tefas, J. Kannianen, M. Gabbouj, and A. Iosifidis, ‘Forecasting stock prices from the limit order book using convolutional neural networks’, in *2017 IEEE 19th conference on business informatics (CBI)*, 2017, vol. 1, pp. 7–12.
- [14] A. Van den Oord, S. Dieleman, and B. Schrauwen, ‘Deep content-based music recommendation’, *Adv. Neural Inf. Process. Syst.*, vol. 26, 2013.
- [15] O. Avilov, S. Rimbert, A. Popov, and L. Bougrain, ‘Deep learning techniques to improve intraoperative awareness detection from electroencephalographic signals’, in *2020 42nd Annual International Conference of the IEEE Engineering in Medicine & Biology Society (EMBC)*, 2020, pp. 142–145.
- [16] R. Collobert and J. Weston, ‘A unified architecture for natural language processing: Deep neural networks with multitask learning’, in *Proceedings of the 25th international conference on Machine learning*, 2008, pp. 160–167.



## The Inhibition Effects Investigation of Metal Complexes with Coumarin Schiff Base on 6PGD Activity

**Nadia Murshed ABED<sup>1,\*</sup>**, **Ümmühan Özdemir ÖZMEN<sup>2</sup>**, **Şevki ADEM<sup>1</sup>**, **Volkan EYÜPOĞLU<sup>1</sup>**

<sup>1</sup>Department of Chemistry, Çankırı Karatekin University, Çankırı, Türkiye

<sup>2</sup>Department of Chemistry, Gazi University, Ankara, Türkiye

### Abstract

This work is focused on the 6PGD enzyme. Without 6PGD, cancer cells are unable to thrive or spread. The beginning or course of cancer is not affected by a 6PGD shortage of less than one percent. Delaying or stopping cell growth and division may have a detrimental effect on the development of cells. Definition of cancer based on glucometabolism Cancer cells depend on 6PGD to produce NADPH and DNA. When SIRT2 is activated, it reduces NADPH production as well as DNA synthesis. In this research, 10 different compounds were tested for their inhibitory effects on the 6PGD enzyme.. OPP enzymes are now being considered as prospective therapeutic targets because of their close ties to tumor metabolism. The importance of 6-Phosphogluconate dehydrogenase (6PGD), PPP's third oxidative decarboxylase, in carcinogenesis and redox homeostasis has been well shown in recent years. 6PGD upregulation enhances cancer cells' proliferative and metastatic capacity by providing them with a metabolic and defense edge. In this work, we used spectrophotometric techniques to examine the impact of several Schiff bases and their complexes on 6PGD activity in vitro. The Molegro Virtual Docker program was also used to assess probable attachment patterns. Inhibition of the 6PGD enzyme by Pt3TbCTS. With a docking score of -212.732 on MolDock, this interaction was poorly matched. Hydrogen bonds were formed between Ser480 and Pt3TbCTS in the enzyme's three-dimensional interaction map

**Keywords:** Inhibition, Metal complexes, Coumarin, Schiff base, 6PGD

### 1. Introduction

Mutations in DNA, epigenetic alterations, malfunctioning enzymes, and misaligned signaling pathways all contribute to the multifaceted hyperproliferative nature of cancer (Vander *et al.* 2017). With an average of 1,670 deaths per day in the United States in 2018, cancer has overtaken heart disease and stroke as the most prevalent cause of death in the country's health care system. The fatal weapon's weight Illness is expected to rise in the next years. Six basic physiological alterations that are often recognized as cancer hallmarks may be used to describe cancer biology. Refusing to be stimulated by angiogenesis and other apoptotic processes and resisting the spread of invasion and metastasis by anti-growth signals is a learned ability. Cancerous cell populations have certain properties (Sarraz *et al.* 2018). They must learn these six key skills before they may conquer their environment. Take control of your own destinies The metabolic rewiring has been documented recently. a novel characteristic of cancer. Metabolism rewired is a phrase used to describe a person's capacity to increase their metabolic flow by various alterations to their metabolic and signaling systems. Because cancer cells rely on the glycolytic process rather than the more efficient and effective oxidative route, this metabolically changed state profile is one of the most essential elements of this metabolically altered state profile (Liberti and Locasale 2016). Here, the issue of why cancer cells adopt these less successful routes is at stake. Cancer cells' malignant activity is controlled by a combination of reprogrammed pathways and metabolic activities. Components of macromolecules such as protein structure and energy production (ATP), redox regulators (NADPH), and reducible enzymes. There may be a link between these metabolic intermediates and cancer cell proliferation. Why are malignant cells able to consume more glucose?. Tumors get their nutrition from a multitude of places. Carbohydrate, amino acid, and other metabolic pathways that branch out from the primary glycolytic route. Overexpression of lipid metabolism in cancer cells has been shown (Cho *et al.* 2018). There are two primary branches to the pentose phosphate pathway: The glycolytic cascade is the initial step in the process. It serves as an intermediary. structure and NADPH in the growth of cancer cells NADPH homeostasis plays a critical role in cancer cells' capacity to flourish in the presence of ROS and metabolic stress, as shown

\* Corresponding author. E-mail address: nadiamurshed10@gmail.com



by many longitudinal lines of evidence. NADPH homeostasis is thereby being rewired in the organism. An intriguing advance is the use of ROS-induced cell oxidation in cancer treatment NADPH is synthesized in the third phase of the PPP as a consequence of the conversion of 6-phosphogluconate to ribulose by 6PGD. In humans, the expression of 6PGD has increased in many malignancies. In the battle against deadly illnesses like cancer, a focus on 6PGD might be beneficial. This review has made an attempt to provide new insights on the history, characteristics, and participation of 6PGD in cancer in this enzyme. 6PGD has also been linked to metastasis in research. Chemoresistance, medication resistance, and 6PGD as an inhibitor, as well as cancer biomarker studies in the future (Lin *et al.* 2015).

## 2. Materials and Methods

This approach may be used to measure enzyme activity: The reaction with NADP<sup>+</sup> shows that 6-phosphogluconate dehydrogenase is responsible for the reduction of 6-phosphogluconate. During the enzymatic process, NADPH is formed. NADPH is well-known for its ability to absorb light with a wavelength of 340 nm. The increase in NADPH at 340 nm was utilized to measure the activity of the enzyme (Beutler 1971). In order to assess activity, a 96-well microplate was used. Components of activity measurement are listed in Table 1.

**Table 1.** The 6PGD enzyme activity testing procedure

	The cuvette must be regulated	Cuvettes for testing
A ready supply of	Volume (μL)	Volume (μL)
1 M Tris-HCl	50	50
2 mM NADP <sup>+</sup>	20	20
D.W	100	100
Enzyme	10	10
<i>An incubation period of ten minutes</i>		
6 mM 6PGA	-	20

N-benzylindole derivatives were shown to be very strong inhibitors and activators of enzymes in this study. In the reaction medium, the substrate concentrations (G6P and 6PGA) were 6.25, 15.30, 62.5, and 90 M with or without inhibitor. As illustrated in Figure 1, three fixed dosages of N-benzoylindole derivatives were added to the reaction medium, which resulted in a total reaction volume of 1 mL. The G6P/6PGA IC<sub>50</sub> value was calculated by determining the activity of G6P/6PGA at various inhibitor doses. Enzyme activity was found to be 100 percent in the absence of any chemicals. Plots of enzyme activity percentage vs compound concentration were used to establish the IC<sub>50</sub> values (concentrations that reduce enzyme activity by 50%).

This analysis was based on the crystal structure of 6PGD (PDB code: 5UQ9). In BIOVIA Discovery Studio 2017 R2 (DS) software, the NADP<sup>+</sup> binding site as soon as it was positioned in the area. There is van der Waals contact, electrostatic connection as well as hydrogen bond interaction when the ligand binds to the receptor.

## 3. Results and Discussion

An investigation into the inhibitory effects of three different substances on the 6PGD enzyme was conducted. Table 2 displays the in vitro and in silico results.

**Table 2.** Compounds' impact on enzyme 6PGD activity

Name	Ligand	IC <sub>50</sub> values μM	MolDock Score	Rerank Score	HBond
Pt(3TbCTS) <sub>2</sub>	Unknown 1_9	16.91	-212.732	-82.2137	-2.53156
Pt(5MCTS) <sub>2</sub>	Unknown 1_8	20.09	-199.994	-150.161	-2.04248
Pt(3MeOCTS) <sub>2</sub>	Unknown 1_7	17.68	-190.794	-118.784	-4.14846

The 6PGD enzyme was inhibited by the Pt3TbCTS molecule. Figure 4.3 displays Pt3TbCTS graphs, whereas Figure 1 displays 3D interaction maps. MolDock's docking score was -212.732 out of 100. According to the enzyme's 3D interaction map, Ser480 amino acids interacted through hydrogen bonds with Pt3TbCTS. Figure 2 shows the existence of hydrogen bonds, which are shown by the light green lines in the diagram.

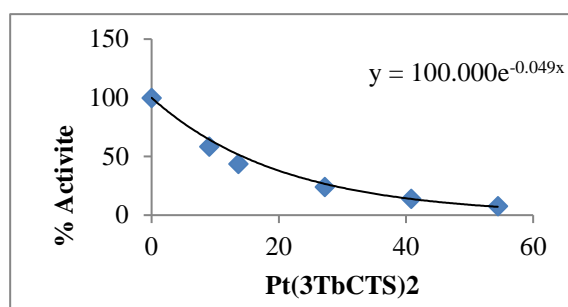


**Figure 1.** Chemical activity percentage [Pt3TbCTS] – [Pt3TbCTS] graph 6PGD enzyme

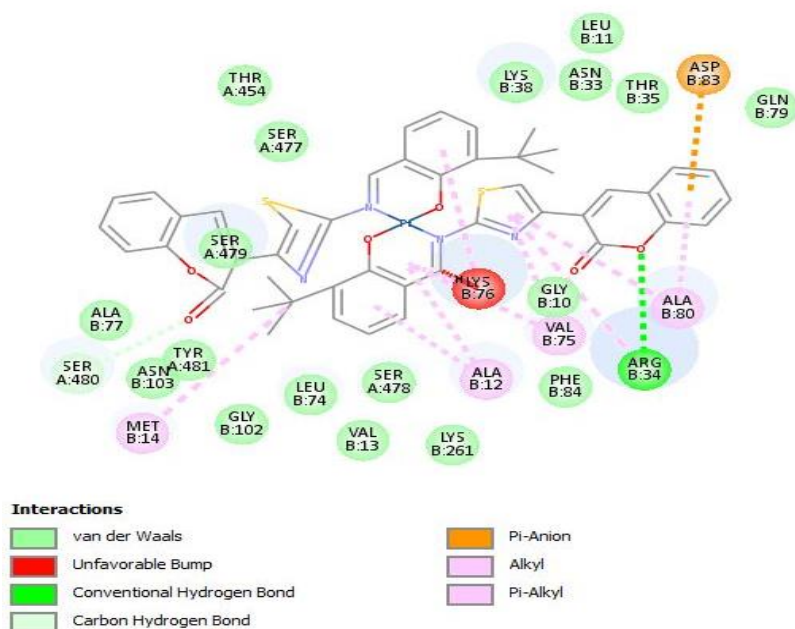


**Figure 2.** Pt3TbCTS and 6PGD's active area interact

The 6PGD enzyme was inhibited by the Pt(5MCTS)<sub>2</sub> molecule. Figure 3 showed Pt(5MCTS)<sub>2</sub> graphs, whereas Figure 4 depicted 3D interactions maps. MolDock scored -199.994 out of 100 in the docking results. The enzyme's 3D interaction map shows that Asn 103 amino acids connected with Pt(5MCTS)<sub>2</sub> through hydrogen bonds. Light green lines in Figure 4.6 indicate the presence of hydrogen bonding.

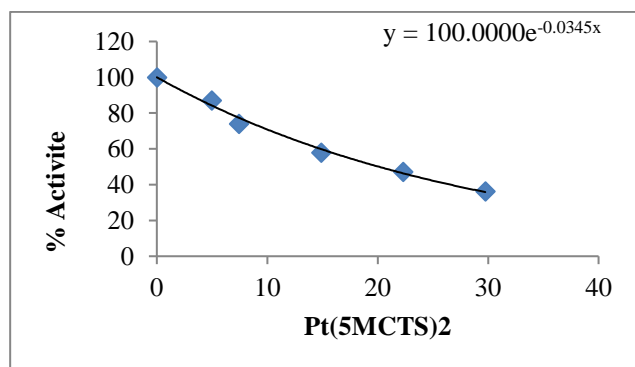


**Figure 3.** Chemical activity percentage [Pt(5MCTS)<sub>2</sub>] – [Pt(5MCTS)<sub>2</sub>] graph 6PGD enzyme

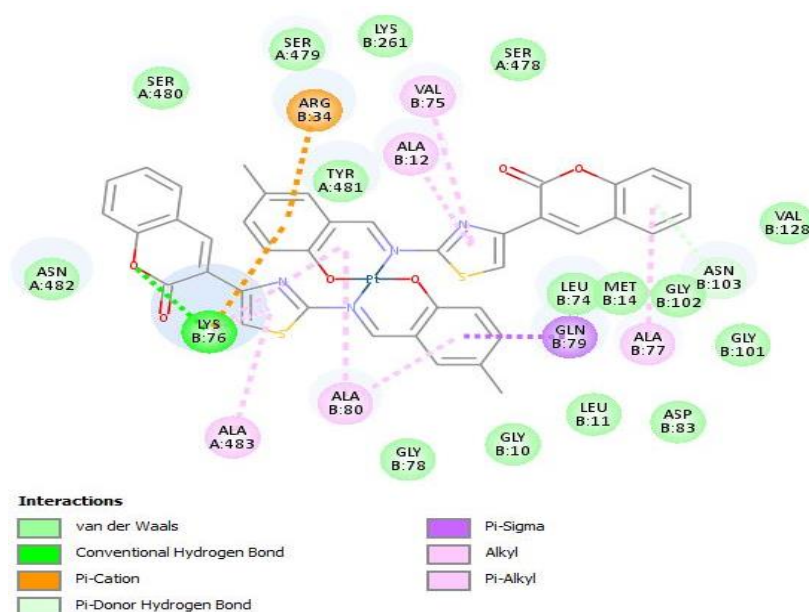


**Figure 4.** Pt(5MCTS)<sub>2</sub> and 6PGD's active area interact

The 6PGD enzyme was inhibited by the Pt(3MeOCTS)<sub>2</sub> molecule. Figure 5 showed Pt(3MeOCTS)<sub>2</sub> graphs, whereas Figure 6 depicted 3D interactions maps. MolDock docked with a score of -190.794 out of 100. According to the enzyme's 3D interaction map, Asn33 and Lys 76 amino acids interacted through hydrogen bonds with Pt(3MeOCTS)<sub>2</sub>. Figure 4.8 shows the existence of hydrogen bonds, which are shown by the light green lines in the diagram.

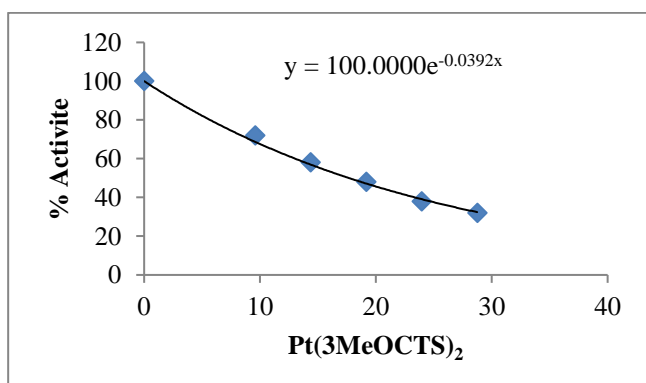


**Figure 5.** Chemical activity percentage [Pt(3MeOCTS)<sub>2</sub>] – [Pt(3MeOCTS)<sub>2</sub>] graph 6PGD enzyme

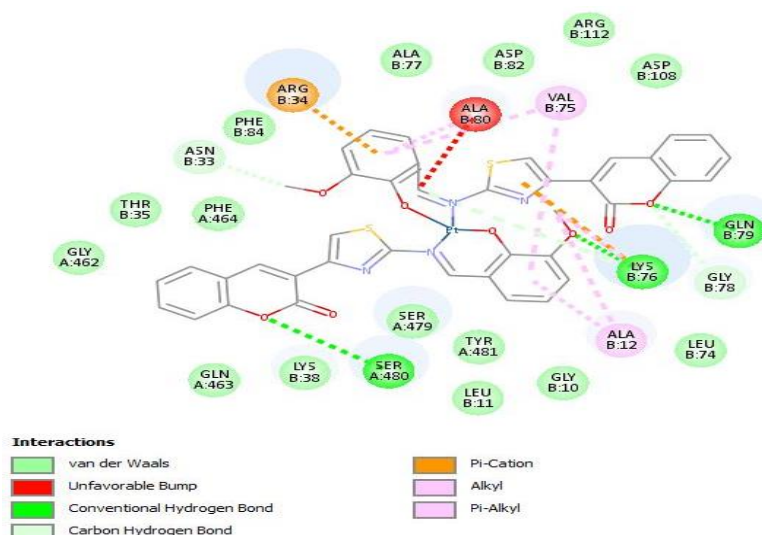


**Figure 6.** Pt(3MeOCTS)<sub>2</sub> and 6PGD's active area interact

#### 4. Conclusion

Recent studies have identified this new biological molecule, 6PGD as a promising cancer treatment target. The proliferation, survival, and metastasis of tumor cells may be boosted by 6PGD's reprogrammed tumor bioenergetics, according to several studies. In addition, overexpression of 6PGD leads to the development of chemoresistance in cancer cells. The mechanism of chemo-drug resistance has yet to be discovered, though. Is the elevated phosphorylation of 6PGD due to EGFR-mediated EGFR activation a factor in chemoresistance? Is it possible that 6PGD-mediated alterations in the expression of p53 contribute to cancer cell resistance? Future research should focus on this. Future studies should concentrate on 6PGD's nonenzymatic and protein–protein interactions in order to create and ensure the effectiveness of new inhibitors of 6PGD. Nonenzymatic actions of 6PGD are crucial to the cell's regular functioning, but how substantial are they? PGAM1 has been shown to interact with 6PGD, thus we should think about how these two metabolic pathways are intertwined. Existing 6PGD inhibitor biosafety profiles and side effects, as well as metabolic-dependent toxicity, must be explored. The utilization of 6PGD as a therapeutic target requires more research. That's why we need to keep an eye out for new avenues of research in order to get a complete understanding of the function of 6PGD in cancer progression.

#### References

- [1] Vander Heiden, M. G. and Berardinis, R. J. 2017. Understanding the intersections between metabolism and cancer biology. *Cell.*, 168(4): 657-669.
- [2] Sarfraz, I., Rasul, A., Hussain, G., Hussain, S. M., Ahmad, M., Nageen, B. and Ali, M. 2018. Malic enzyme 2 as a potential therapeutic drug target for cancer. *IUBMB life.*, 70(11): 1076-1083.
- [3] Liberti, M. V. and Locasale, J. W. 2016. The Warburg effect: how does it benefit cancer cells. *Trends in biochemical sciences.*, 41(3): 211-218.
- [4] Cho, E. S., Cha, Y. H., Kim, H. S., Kim, N. H. and Yook, J. I. 2018. The pentose phosphate pathway as a potential target for cancer therapy. *Biomolecules and therapeutics.*, 26(1): 29.
- [5] Lin, R., Elf, S., Shan, C., Kang, H. B., Ji, Q., Zhou, L. and Chen, J. 2015. 6-Phosphogluconate dehydrogenase links oxidative PPP, lipogenesis and tumour growth by inhibiting LKB1–AMPK signalling. *Nature cell biology.*, 17(11): 1484-1496.



# Investigation of Effect of the Parameters on Calcium Carbonate Crystallization

Ghassan AHMED HUSSEIN HUSSEIN<sup>1</sup> , Muhammed Bora AKIN<sup>2\*</sup>

<sup>1</sup> North Oil Refineries / Biji, Ministry of Oil, Iraq

<sup>2</sup> Faculty of Engineering, Department of Chemical Engineering, Çankırı Karatekin University, Çankırı, Türkiye

## Abstract

The properties of  $\text{CaCO}_3$  are particularly important in industrial applications, particularly in crystal structure, whiteness, chemical purity, specific surface area, particle size distribution, and morphology. Therefore, it is important to understand and control the formation of different  $\text{CaCO}_3$  crystal types formed during crystallization, which has attracted increasing research attention recently [1]. As far as is known, various physicochemical factors responsible for the process, such as temperature [2], solvent type [3], pH [4] and initial supersaturation [5] lead to the phase transformation of  $\text{CaCO}_3$ . In the presence of barium, strontium and magnesium ions [6,7], graphene oxide [8], bovine serum albumin and polydopamine [9], selenic acid, arsenic acid and silicic acid [10] and various amino acid species [11,12],  $\text{CaCO}_3$  morphology has changed. In this study,  $\text{CaCO}_3$  crystals are synthesized with the mixing calcium chloride and sodium sulfate solutions. It was observed that the morphological properties of the  $\text{CaCO}_3$  crystals changed, which were analyzed by SEM, XRD and BET. (This study was made from the thesis work of the first ranked student.)

**Keywords:**  $\text{CaCO}_3$ , Calcium carbonate, Crystallization, Additive

## 1. Introduction

Calcium carbonate is a kind of chemical compound popularly known as limestone. Its formula is  $\text{CaCO}_3$ . This compound is found mostly in rocks, pearls, shells of microorganism and eggs in nature. Calcite in rhombohedral crystal morphology is the most stable and abundant material on the earth crust. Aragonite, with a needle-like crystalline morphology, is metastable under ambient pressure and temperature without structural defects. Vaterite, the most unstable form of hexagonal calcium carbonate, can gradually recrystallize to form calcite when in contact with water [13].

Traditionally,  $\text{CaCO}_3$  has many different usage areas. Additionally, materials produced by morphology and size control find their place in industrial applications in electronics, cosmetics, pigments, ceramics and medicine. The biomineralization process of naturally occurring  $\text{CaCO}_3$  was inspired by its low temperature, inexpensive and controllable nature. In scientific studies for  $\text{CaCO}_3$  synthesis, most of the production processes are hydrothermal processes. In  $\text{CaCO}_3$  production, various parameters such as solvent, additives and surfactants are known to have a significant effect on morphology and size [14].

In this study,  $\text{CaCO}_3$  crystals were synthesized by hydrothermal process using  $\text{CaCl}_2$  and  $\text{Na}_2\text{CO}_3$  solutions. The size and morphological properties of the synthesized  $\text{CaCO}_3$  crystals were characterized by SEM, XRD and BET.

## 2. Materials and Methods

The reactants used in the experiments to synthesize calcium carbonate were chosen as calcium chloride dihydrate (ACS reagent >99%) and sodium carbonate (ACS reagent >99.5%). Solutions were prepared using reactants using Type II water produced from Merck Millipore. Initial reactant concentrations are equimolar and concentration were kept 0.1 M in each experiment. The reactions were carried out in a 1 L jacketed glass-lid reactor and the temperature was kept constant at 25°C during the experiments. A magnetic stirrer (Heidolph MR Hei Tech) was used in the experiments and the mixing speed was set as 400 rpm. In experiments using additives, the additive concentration was changed between 0.01 and 0.05. The precipitate, which is filtered and dried after washing was dried in a vacuum oven at 80 °C about 12 hours. XRD, SEM and BET analyzes of the

\* Corresponding author. e-mail address: mbakin@karatekin.edu.tr

obtained powder were made. X-ray diffraction Bruker D8 Discover instrument was used in the investigation of the powder materials. It was understood that Calcite and Vaterite were synthesized in the comparison of the scan results made with the International Center for Diffraction Data (ICDD) database. 2Theta values ranged from 5° to 90° in XRD analysis scans. SEM analyzes were performed using Carl Zeiss Sigma 300 VP field emission scanning electron microscope. The Brunauer–Emmett–Teller (BET) method was used to determine the specific surface area of the synthesized materials. BET specific surface analyzes were performed using the Quantachrome Nova Touch LX4 instrument. Before BET specific surface area measurements, degas treatment was performed at 80 °C for 10 h. Measurements were taken with a multi-point isotherm. BET method is commonly applied to calculate the specific surface area on the basis of nitrogen adsorption isotherm measurements at 77K.

### 3. Results and Discussion

The peak values obtained in XRD analyzes were examined, and as a result of this examination, it was determined that calcium carbonate crystals were formed in the form of calcite and vaterite minerals. It was observed that vaterite was not formed in the experiment performed without additives, and all the synthesized material was calcite. With the experiments using 0.01 M additive, the vaterite form begins to appear next to the calcite form. In XRD analyzes, the peaks of the vaterite form appear next to the calcite peaks with the experiments using 0.01, 0.02 and 0.05 M additives. When the peak lengths are examined in the presence of 0.02 M additive, it is seen that the vaterite form becomes dominant over the calcite form. It was found that this situation changed in the presence of 0.05 M additive and the calcite form became dominant again in this additive concentration. Figure 1 shows XRD analyses of the synthesized materials with and without additive.

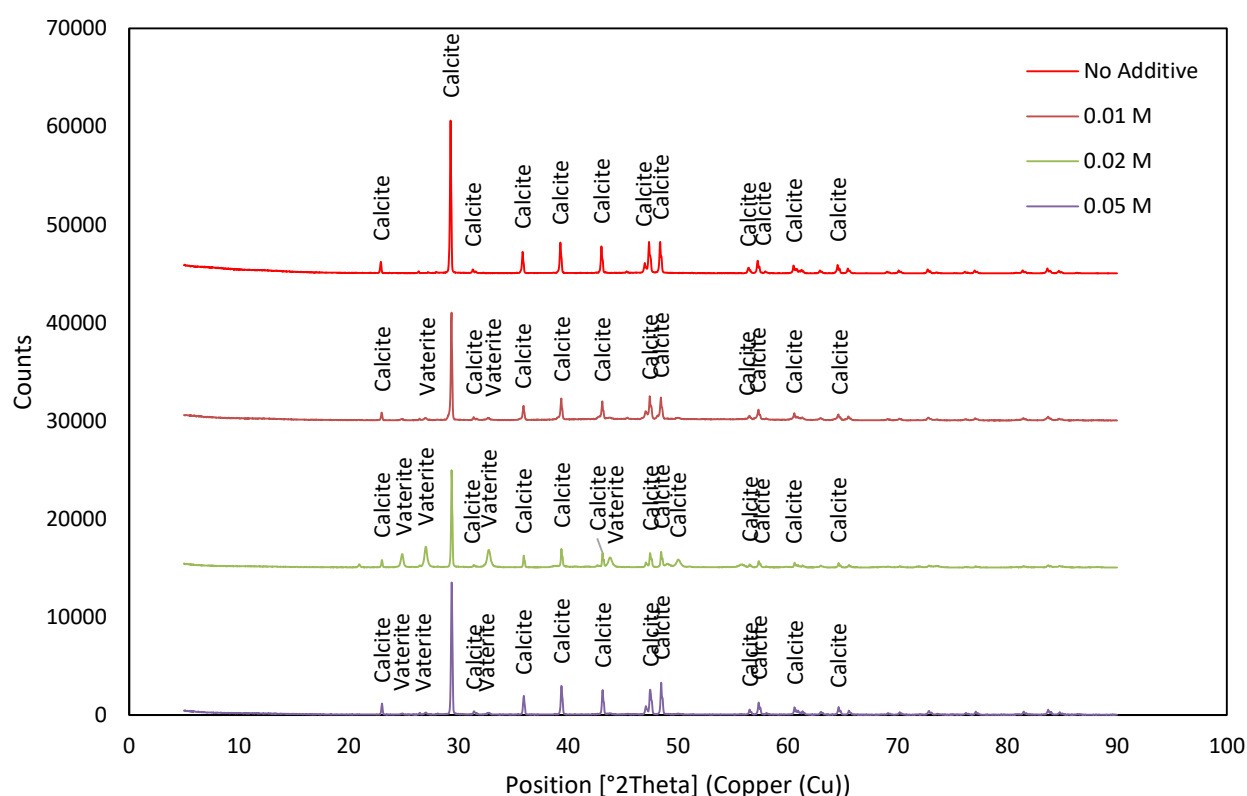


**Figure 1.** XRD analyses of the synthesized materials in the presence of additive (a) No additive, (b) 0.01 M, (c) 0.02 M, (d) 0.05 M.

As a result of the comparison made from the ICDD database for synthesized materials, it is seen that peaks of the calcite match JCPDS 98-006-0995 and the vaterite peaks match JCPDS 98-000-6034. Table 1 summarizes the patterns that match the peaks detected in the XRD analyzes of the synthesized materials.



**Table 1.** XRD analyses of the synthesized crystals

Experiment Code	Additive Amount (M)	Chemical Name	ICDD Pattern Codes
E1	0	Calcite	98-006-0995
E2	0.01	Calcite / Vaterite	98-006-0995 / 98-000-6034
E3	0.02	Calcite / Vaterite	98-006-0995 / 98-000-6034
E4	0.05	Calcite / Vaterite	98-006-0995 / 98-000-6034

SEM microphotographs were examined to support the XRD analysis results and to obtain information about the crystal size. In the result of investigation of the SEM micro-photographs, it was seen that completely agglomerated calcite crystals were formed in the experiments carried out without additives under the aforementioned conditions (Figure 2a). The average length of the edges of the agglomerated calcite crystals is around 15  $\mu\text{m}$ . Vaterite formations found in XRD analysis in the presence of additive are confirmed by SEM analysis (Figure 2b, 2c, 2d). Although it is seen that the vaterite crystals are spherical and approximately 12  $\mu\text{m}$  in diameter when viewed at 500X magnification (Figure 2b, 2c), it is understood that these spheres are composed of nano-sized spherical crystals at higher magnifications such as 10,000X (Figure 2d).

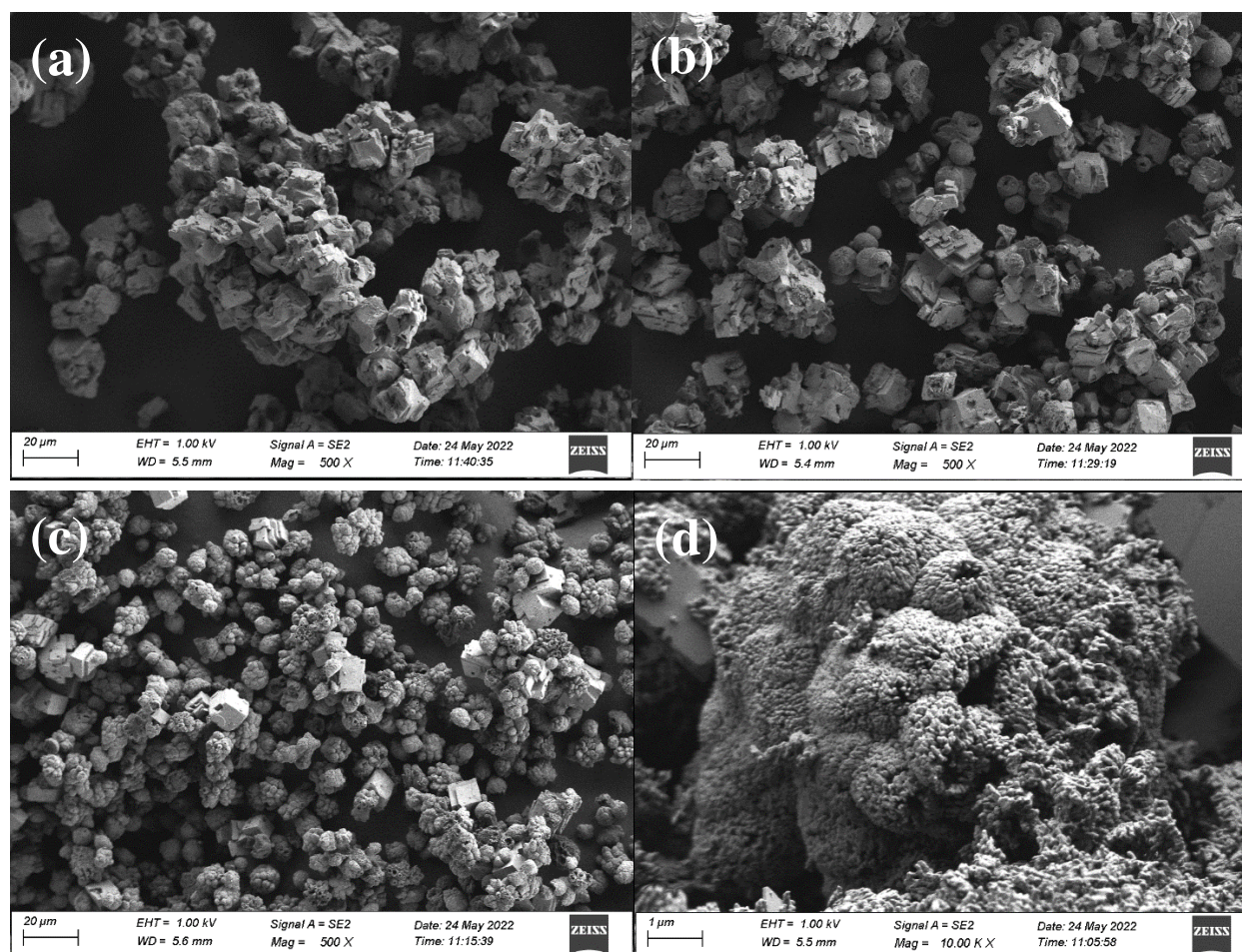


**Figure 2.** SEM micrographs showing the morphology of products in the presence of additive (a) No additive; (b) 0.01 M; (c) 0.02 M; (d) 0.05 M.

The BET specific surface area value increases with the increase in the amount of additive due to the nano-sized vaterite crystals synthesized in the presence of additives (Figure 3).

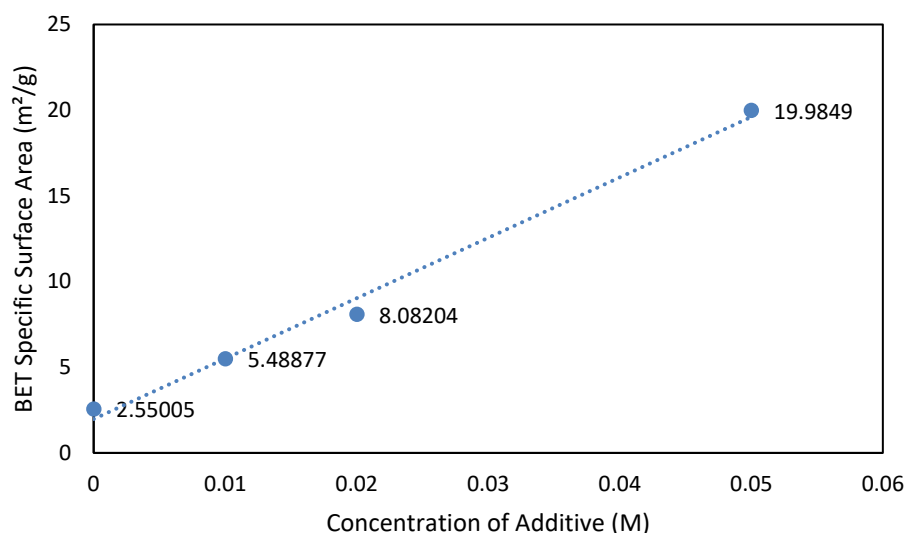


**Figure 3.** Plot of BET specific surface area with additive concentration

#### 4. Conclusion

In this study, calcium carbonate was synthesized using calcium chloride ( $\text{CaCl}_2$ ) and sodium carbonate ( $\text{Na}_2\text{CO}_3$ ) solutions in the presence of propionic acid as additive, and the synthesized crystals were characterized SEM and XRD. Experiments were carried out at  $25^\circ\text{C}$ , at a stirring speed of 400 rpm. In experiments, reactant solutions were equimolar and kept 0.1 M value. Analyzes of the materials showed that vaterite and calcite are obtained. Moreover, a change in crystal size and morphology are observed with the increase in the concentration of additive. Nano-sized spherical vaterite crystals was synthesized. It was also determined that the BET specific surface area increased with the increase of nano-sized vaterite crystals in parallel with the increase in additives.

#### Acknowledgement

In this study, the authors declare that there is no conflict of interest and would like to thank Çankırı Karatekin University, Department of Chemical Engineering for their support of the laboratory studies.

#### References

- [1] Carteret, C., Dandeu, A., Moussaoui, S., Muhr, H., Humbert, B., & Plasari, E. (2009). Polymorphism Studied by Lattice Phonon Raman Spectroscopy and Statistical Mixture Analysis Method. Application to Calcium Carbonate Polymorphs during Batch Crystallization. *Crystal Growth & Design*, 9(2), 807–812.
- [2] Kitamura, M. (2002). Controlling factor of polymorphism in crystallization process. *Journal of Crystal Growth*, 237–239, 2205–2214.
- [3] Flaten, E. M., Seiersten, M., & Andreassen, J. P. (2009). Polymorphism and morphology of calcium carbonate precipitated in mixed solvents of ethylene glycol and water. *Journal of Crystal Growth*, 311(13), 3533–3538.
- [4] Hu, Y.-B., Wolthers, M., Wolf-Gladrow, D. A., & Nehrke, G. (2015). Effect of pH and Phosphate on Calcium Carbonate Polymorphs Precipitated at near-Freezing Temperature. *Crystal Growth & Design*, 15(4), 1596–1601.
- [5] Kim, W.-S., Hirasawa, I., & Kim, W.-S. (2004). Polymorphic Change of Calcium Carbonate during Reaction Crystallization in a Batch Reactor. *Industrial & Engineering Chemistry Research*, 43(11), 2650–2657.
- [6] Sanjiv Raj, K., Devi, N., & Subramanian, V. K. (2020). Effect of barium and strontium ions on the morphology and polymorphism of  $\text{CaCO}_3$ . *Chemical Physics Letters*, 750(January).
- [7] Yao, Q., Wang, Y., Zhang, Y., Li, H., & Zhou, G. (2019). A biomimetic experimental study of magnesium



- ion mineralization in Mg-enriched aragonite. *Science China Earth Sciences*, 62(10), 1619–1629.
- [8] Zheng, D., Yang, H., Yu, F., Zhang, B., & Cui, H. (2019). Effect of graphene oxide on the crystallization of calcium carbonate by C3S carbonation. *Materials*, 12(13), 1–10.
  - [9] Vidallon, M. L. P., Yu, F., & Teo, B. M. (2020). Controlling the Size and Polymorphism of Calcium Carbonate Hybrid Particles Using Natural Biopolymers. *Crystal Growth & Design*, 20(2), 645–652.
  - [10] Kawano, M., & Maeda, T. (2020). Impact of selenite, arsenate, and silicate oxyanions on the polymorphism and precipitation rate of calcium carbonate minerals in solutions with  $Mg^{2+}$  ions. In *Journal of Crystal Growth* (Vol. 535).
  - [11] Polat, S., Özalp, T. N., & Sayan, P. (2021). Polymorphic phase change of calcium carbonate with glutamic acid as an additive. *Journal of the Turkish Chemical Society, Section A: Chemistry*, 8(1), 117–124.
  - [12] Štajner, L., Kontrec, J., Njegić Džakula, B., Maltar-Strmečki, N., Plodinec, M., Lyons, D. M., & Kralj, D. (2018). The effect of different amino acids on spontaneous precipitation of calcium carbonate polymorphs. *Journal of Crystal Growth*, 486, 71–81.
  - [13] Hammad, S., Mingli, C., Muhammad, M. K., Mehran, K., Muhammad, M. K., Ali, R. (2020). Preparation and applications of calcium carbonate whisker with a special focus on construction materials, *Construction and Building Materials*, 236, 117613.
  - [14] Zhao, Z., Zhang, L., Dai, H., Du, Y., Meng, X., Zhang, R., Liu, Y., Deng, J., (2011). Surfactant-assisted solvo- or hydrothermal fabrication and characterization of high-surface-area porous calcium carbonate with multiple morphologies, *Microporous and Mesoporous Materials*, 138, 191–199